

ABSTRACT

Title: CRITICAL BEHAVIOR OF LONG SPAN
CELLULAR BEAMS IN FIRE

Darlene Rini, Master of Science, 2006

Directed by: James A. Milke, Associate Professor, Department
of Fire Protection Engineering

This paper presents an investigation of the structural response of a long span cellular beam with varying section geometries while subject to various temperature-time curves. This type of beam is under investigation, in part, because of its increased use in long span building construction and its unique thermal response when protected with intumescent coatings; but more importantly, to provide an increased understanding into how these beams affect the surrounding structure in fire conditions.

A nonlinear, finite element computational analysis of a steel-frame composite structure incorporating a long span cellular beam with a composite deck was examined to investigate local buckling behavior, midspan displacements, and connection forces of the long span cellular beam, and to compare the results with a similar I-shaped member with no web openings.

This study appears to indicate that long span cellular beams exposed to fire experience two buckling events prior to undergoing large displacement behavior and catenary action. In addition, global and local response of these beams is largely controlled by local web stiffness particularly in pre-buckling behavior.

CRITICAL BEHAVIOR OF LONG SPAN CELLULAR BEAMS IN FIRE

By

Darlene T. Rini

Thesis submitted to the Faculty of the Graduate School of the
University of Maryland, College Park, in partial fulfillment
of the requirements for the degree of
Master of Science
2006

Advisory Committee:
Professor James A. Milke, Chair
Professor Jose Torero, Co-Advisor
Professor Fred Mowrer
Professor Ricardo Medina

© Copyright by
Darlene Rini
2006

Acknowledgments

This work is supported by Ove Arup & Partners. I want to thank the Associate Director of ArupFire in London Dr. Barbara Lane, as well as, the Building Specialties Director of the Americas Mr. James R. Quiter for their support and encouragement. I want to express my gratitude to Dr. Jose Torero and Dr. James A. Milke, my advisors, for their guidance, support and countless time to help me to complete this work. I would also like to thank, Dr. Fred Mowrer for his endless guidance, support and encouragement.

I would also like to give special thanks to Dr. Ricardo Medina, I really appreciated your support. A special thanks to Dr. Asif Usmani, Allan Jowsey and all the other people and graduate students at the University of Edinburgh for expanding my knowledge and who without which could not have made this possible.

I would also like to thank all the staff and graduate students in the Fire Protection Engineering Department at the University of Maryland for deepening my understanding of fire protection engineering and being a daily support group, especially to Sean O'Rourke, Sam Hu, Yi Wang, and Peter Veloo.

Finally, I would like to thank my friends and family for their encouragement and support always to give me the strength and confidence in myself to complete my dreams.

TABLE OF CONTENTS

| | |
|--|------------|
| ACKNOWLEDGMENTS | ii |
| TABLE OF CONTENTS | iii |
| LIST OF FIGURES | v |
| CHAPTER 1: INTRODUCTION | 1 |
| 1.1 Overview | 1 |
| 1.2 Literature Review | 4 |
| 3.1.1 Background of Cellular Beams | 4 |
| 3.1.2 Early Tests and Data on Cellular Beams | 5 |
| 1.3 Research Objectives | 12 |
| 1.4 Outline of thesis chapters | 13 |
| CHAPTER 2: FUNDAMENTALS OF STRUCTURAL FIRE ANALYSIS | 15 |
| 2.1 Dynamics of Building Fires | 17 |
| 2.2 Temperature Effects On Structural Materials | 19 |
| 2.2.1 Steel | 19 |
| 2.2.2 Concrete | 29 |
| 2.3 Thermo-Mechanical Response | 43 |
| 2.3.1 Pure Thermal expansion | 45 |
| 2.3.2 Pure Thermal bowing | 56 |
| 2.3.3 Deflections | 61 |
| 2.3.4 Combinations of thermal expansion and thermal bowing | 63 |
| 2.3.5 Membrane action | 68 |
| CHAPTER 3: METHODOLOGY – CELLULAR BEAM STUDY | 70 |
| 3.1 Overview | 70 |
| 3.2 Solver Used | 70 |
| 3.3 Model Background | 71 |
| 3.4 Fire and Heat Transfer Models | 72 |
| 3.4.1 Analysis Fire Models | 72 |
| 3.4.2 Major Assumptions | 75 |
| 3.4.3 Heat Transfer Model for Steelwork | 77 |
| 3.4.4 Heat Transfer Model for Concrete | 82 |

| | |
|---|----------------|
| 3.5 Structural Model – Input Data | 86 |
| 3.5.1 Base Model Geometry | 86 |
| 3.5.2 Cases for Analysis | 89 |
| 3.5.3 Material Properties | 93 |
| 3.5.4 FEM Element type and Meshing | 93 |
| 3.5.5 Boundary Conditions | 93 |
| 3.5.6 Ambient Loading | 94 |
| 3.5.7 Thermal Loading | 94 |
| CHAPTER 4: RESULTS AND DISCUSSION | 109 |
| 4.1 Overview | 109 |
| 4.2 Results and Discussion | 110 |
| 4.2.1 Cellular Beam Model Analysis | 111 |
| 4.2.2 Solid Beam Model | 121 |
| 4.2.3 Scenario I Parametric Study | 125 |
| 4.2.4 Scenario II – Parametric Study | 157 |
| 4.2.5 Scenario III – Parametric Study | 163 |
| 4.3 Summary of Results and General Observations | 166 |
| 4.3.1 General Buckling Behavior | 166 |
| 4.3.2 Cellular Beam Axial Forces And Midspan Displacements | 170 |
| 4.3.3 Affect of Various Heating Curves and Thermal Profiles | 176 |
| CHAPTER 5: CONCLUSIONS | 178 |
| APPENDIX A: HEAT TRANSFER CALCULATIONS | 180 |
| APPENDIX B: STRUCTURAL DESIGN SHEETS (FABSEC) | 207 |
| APPENDIX C: SAMPLE INPUT FILE (UPON REQUEST) | 236 |
| APPENDIX D: ABAQUS STRUCTURAL FIRE ANALYSIS DATA FOR EACH CASE STUDY | 237 |
| REFERENCES | 334 |

LIST OF FIGURES

| | |
|---|----|
| Figure 1 - Typical long span design using cellular beams. (image from Westok Ltd.)..... | 2 |
| Figure 2 - (left) Cellular beam manufactured from cutting and expanding a standard universal beam (Westok). (right) Cellular beam fabricated from steel plates cut and welded (Fabsec Ltd.)..... | 5 |
| Figure 3 - General arrangement of Fabsec Beam Test 1 – 3. | 7 |
| Figure 4 - Central deflection of the beams in the Fabsec fire tests. | 7 |
| Figure 5 - (top left) Shear failure in beam test 1. (top right) Vierendeel buckling in beam test 2. (left) Overall buckling in beam test 3. (photos courtesy: Fabsec Ltd.)..... | 8 |
| Figure 6 - General arrangement for Fabsec Tests 4 & 5..... | 9 |
| Figure 7 - (left) Web-post buckling failure Fabsec Beam #4. (right) Web crushing failure Fabsec Beam #5.. | 9 |
| Figure 8 - General arrangement of unprotected cellular beams tests (Westok)..... | 10 |
| Figure 9 - Summary of data on ratio of web-post temperatures to bottom flange temperatures for protected cellular beams (Fabsec, Westok and SCI design curve). Image courtesy: SCI Document RT983 | 12 |
| Figure 10 - Specific heat of steel at elevated temperatures (EC3:1995)..... | 21 |
| Figure 11 - Thermal conductivity of steel at elevated temperatures (EC3:1995)..... | 22 |
| Figure 12 - Thermal strain of steel at elevated temperatures (EC3:1995)..... | 23 |
| Figure 13 - Creep strain figure from Buchanan | 24 |
| Figure 14 - Stress-strain relationships for steel at elevated temperatures. (Buchanan) | 25 |
| Figure 15 - Stress-strain relationships for steel at elevated temperatures (EC3:1995)..... | 27 |
| Figure 16 - Relative mechanical properties at elevated temperatures in comparison to ambient conditions. (Buchanan) | 29 |
| Figure 17 - Collapsed textile factory in Alexandria, Egypt (BBC News, 2000) | 30 |
| Figure 18 - Katrantzos Department Building in Athens, Greece, After 1980 Fire (Papaioanmoa, 1986) | 31 |
| Figure 19 – Thermal conductivity of varying types of concrete (Reproduced from EC2, 1993) | 33 |
| Figure 20 – Specific heat of concrete (Reproduced from EC2, 1993.)..... | 34 |
| Figure 21 - Thermal elongation for siliceous and calcaerous concrete at elevated temperatures (EC2:1993) | 36 |
| Figure 22 – Total deformation in different concretes during heating (Reproduced from Schneider (1988))..... | 37 |
| Figure 23 – Creep in concrete one day after loading at 10% of the initial strength (Reproduced from Khoury and Sullivan (1988))...... | 38 |
| Figure 24 - Stress-strain relationships for concrete at elevated temperatures (EC 2, 1993) | 39 |
| Figure 25- Reduction in compressive strength with temperature (Reproduced from Schneider (1988))...... | 39 |
| Figure 26 - Design values for reduction of compressive temperature (Reproduced from EC2, 1993). | 40 |
| Figure 27 -Relative strength of concrete from ambient conditions. (EC2, 1993)..... | 41 |

| | |
|---|----|
| Figure 28 -Relative tensile strength of concrete to ambient strength conditions as a function of temperature..... | 42 |
| Figure 29 - Design values for reduction of modulus of elasticity with temperature. (Reproduced from Buchanan)..... | 43 |
| Figure 30 - Thermal expansion of simply supported beam with no axial restraint. | 46 |
| Figure 31 - Compressive force P arising in a rigidly restrained beam..... | 47 |
| Figure 32 -Buckling of an axially restrained beam subjected to uniform heating..... | 49 |
| Figure 33 - Deflection of axially restrained elastic beams subjected to heating: (top) Single beam, (bottom) three beams of varying slenderness. Reproduced from Usmani 2001). | 50 |
| Figure 34 - Forces in an axially restrained elastic beam subjected to heating: (top) axial forces, and (bottom) moments. (Reproduced from Usmani 2001). | 51 |
| Figure 35 - Deflections in an axially restrained elastic-plastic beam. Reproduced from Usmani 2001)..... | 52 |
| Figure 36 - Axial forces in an axially restrained elastic-plastic beam. Reproduced from Usmani 2001)..... | 53 |
| Figure 37 - Defelctions in a restrained beam with reducing elastic stiffness. (Reproduced from Usmani 2001). | 53 |
| Figure 38 - Axial forces in a restrained beam with reducing elastic stiffness. (Reproduced from Usmani 2001). | 54 |
| Figure 39 - Heating of beam with finite axial restraint. (Reproduced from Usmani 2001). | 55 |
| Figure 40 -Buckling temperatures for thermal expansion against finite lateral restraint. (Usmani 2001) | 56 |
| Figure 41 - Simply supported beam subjected to uniform thermal gradient | 57 |
| Figure 42 -Laterally restrained beam subjected to a uniform thermal gradient..... | 59 |
| Figure 43 - Beam with finite rotational restraint with a uniform thermal gradient. (Usmani 2001). | 60 |
| Figure 44 - Combined thermal expansion and bowing in a fully fixed beam. (Usmani, 2001). | 64 |
| Figure 46 - Temperature deflection responses for combinations of ε_T and ε_ϕ (Usmani, 2001) | 67 |
| Figure 47 - Structural model rendered in ABAQUS (slab is removed for clarity)..... | 72 |
| Figure 48 - The generalized exponential time temperature curve is plotted with varying rates of heating against the ISO 834 standard fire curve. | 74 |
| Figure 49 - Examined gas compartment time-temperature curves | 75 |
| Figure 50 - Slab temperatures from standard fire case | 83 |
| Figure 51 - Slab temperatures from case 1 fire..... | 84 |
| Figure 52 - Slab temperatures from case 2 fire..... | 84 |
| Figure 53 - Slab temperatures from case 3 fire..... | 85 |
| Figure 54 - Slab temperatures from case 4 fire..... | 85 |
| Figure 55 -Slab temperatures from case 5 fire..... | 86 |
| Figure 56 - Cellular beam geometry | 87 |
| Figure 57 - Base cellular beam model geometry | 88 |

| | |
|---|-----|
| Figure 58 - Protected and Unprotected steel time temperature curves for Scenario I. The standard fire curve (ISO 834), representing the gas phase temperatures, is plotted for reference..... | 96 |
| Figure 59 - Temperatures through depth of concrete (Scenario I)..... | 97 |
| Figure 60 - Steel Temperatures given a generalized time temperature curve with $T_{max}=1200^{\circ}\text{C}$ and the rate of heating parameter = 0.005. | 98 |
| Figure 61- Steel Temperatures given a generalized time temperature curve with $T_{max}=1000^{\circ}\text{C}$ and the rate of heating parameter = 0.005. | 99 |
| Figure 62 - Steel Temperatures given a generalized time temperature curve with $T_{max}=800^{\circ}\text{C}$ and the rate of heating parameter = 0.005. | 99 |
| Figure 63 - Steel Temperatures given a generalized time temperature curve with $T_{max}=1000^{\circ}\text{C}$ and the rate of heating parameter = 0.0015. | 100 |
| Figure 64 - Steel Temperatures given a generalized time temperature curve with $T_{max}=1000^{\circ}\text{C}$ and the rate of heating parameter = 0.0007. | 100 |
| Figure 65 - Temperatures through depth of slab (Case 1) | 101 |
| Figure 66 - Temperatures through concrete slab (Case 2)..... | 102 |
| Figure 67 - Temperatures through concrete slab (Case 3)..... | 102 |
| Figure 68 - Temperatures through concrete slab (Case 4)..... | 103 |
| Figure 69 - Temperatures through concrete slab (Case 5)..... | 103 |
| Figure 70 - Steel Temperatures for the top flange, web, bottom flange of the cellular beam section given a standard fire exposure, the top curves are for unprotected and the bottom are for protected..... | 105 |
| Figure 71 - Temperatures for concrete slab in Scenario III tests | 106 |
| Figure 72 - Protected Steel Temperatures for bottom flange and web from Bailey/Westok Ltd. | 107 |
| Figure 73 - Protected Steel Temperatures for the top flange, web, bottom flange of the cellular beam section obtained from FABSEC..... | 107 |
| Figure 74 - Envelope of time-temperature curves investigated in this report..... | 108 |
| Figure 75 - Base cellular beam model (image from Abaqus)..... | 112 |
| Figure 76 - Vertical displacement of "base" cellular beam model after loading. | 113 |
| Figure 77 - Vertical Displacement and Deformation of base model after the 2-hour fire exposure. | 114 |
| Figure 78 - Lateral torsional buckling of cellular beam at the end of the simulation.... | 114 |
| Figure 80 – At $t=1030\text{s}$, stress concentrations spreading from the supports. Web posts are buckling and the beam is undergoing lateral torsional buckling. ($T=542^{\circ}\text{C}$) | 117 |
| Figure 81 - Midspan displacement of cellular beam with time | 118 |
| Figure 82 - Midspan displacement of cellular beam with temperature. | 118 |
| Figure 83 - Axial force in cellular beam as a function of temperature. | 119 |
| Figure 84 - Axial forces at different locations in Cardington steel beam test. [Usmani,] Ref.33..... | 120 |
| Figure 85 - Solid beam model..... | 121 |
| Figure 86 - Bottom flange buckling in solid beam model. | 123 |
| Figure 87 - Endpost, web post, and bottom flange buckling in cellular beam model ($t = 700\text{s}$, $T=350-400^{\circ}\text{C}$) | 123 |
| Figure 88 - Axial force vs. temperature of solid beam and base cellular beam models. | 124 |
| Figure 89 - Midspan displacement vs. time for solid and cellular beam models..... | 124 |

| | |
|--|-----|
| Figure 90 - Midspan displacement vs. Temperature comparison of solid beam and cellular beam..... | 125 |
| Figure 92 - Axial forces vs. Temperature of cellular beams with varying web opening diameters..... | 129 |
| Figure 93 - Midspan displacement of cellular beams with varying web opening diameters vs. time..... | 129 |
| Figure 94 - Displacement vs. Temperature for various web opening diameters | 130 |
| Figure 95 - Web post buckling evident in 500 mm diameter case. This occurred at 250 °C. | 130 |
| Figure 96 - Bottom flange yielding and end post buckling initiating in 150 mm diameter case. This occurred at ~ 350 °C | 131 |
| Figure 97 – End post length case study. End posts tested include:..... | 132 |
| Figure 98 - Axial forces vs. temperature for varying end post lengths..... | 133 |
| Figure 99 - Displacement vs. time for varying end post lengths | 134 |
| Figure 100 - Displacement vs. Temperature for varying endpost lengths..... | 136 |
| Figure 101 - Asymmetric web post buckling and lateral torsional buckling of 1400 mm endpost test..... | 136 |
| Figure 102 – Number of web openings case study. No. of openings include: | 137 |
| Figure 103 - Axial forces vs temperature for varying number of web openings..... | 140 |
| Figure 104 - Displacement vs. time for varying # of holes | 140 |
| Figure 105 - Displacement vs. temperature for varying # of holes | 141 |
| Figure 106 - Deformations of case with 28 web openings | 141 |
| Figure 107 - Vary web thickness study (8mm, 12 mm, 20mm) | 142 |
| Figure 108 - Axial forces vs Temperature for varying web thickness..... | 144 |
| Figure 109 - Displacement vs. Time for varying web thicknesses | 144 |
| Figure 110 - Displacement vs. Temp for varying web thicknesses | 145 |
| Figure 111 - Bottom flange yielding of 20 mm web thickness beam..... | 145 |
| Figure 112 - Web post buckling behavior in 8 mm web thickness case..... | 146 |
| Figure 113 - Varied flange thickness study (12 mm, 24 mm, and 48 mm) | 147 |
| Figure 114 - Axial forces vs. temperature | 148 |
| Figure 115 - Displacement vs. time | 149 |
| Figure 116 - Displacement vs. temp | 149 |
| Figure 117 - Bottom flange buckling in thin flange | 150 |
| Figure 118 - Web buckling in thick flange case | 150 |
| Figure 119 - Vary bottom flange thickness. (270 mm, 370 mm, and 470 mm) | 152 |
| Figure 120 - Axial force vs temperature for varying bottom flange width..... | 152 |
| Figure 121 - Displacement vs. Time for varying bottom flange thicknesses | 153 |
| Figure 122 - Displacement vs. Temp for varying bottom flange thicknesses | 153 |
| Figure 123 - Varying Span Lengths tested. | 155 |
| Figure 124 - Displacement vs time for varying spans | 156 |
| Figure 125 - Displacement vs. Temp for varying spans | 156 |
| Figure 126 - Heating curves tested in this scenario | 158 |
| Figure 127 - Displacement vs. Time for various heat rates and maximum temperature fires. | 159 |
| Figure 128 - Displacement vs. temperature for various heating curves. | 160 |
| Figure 129 - Axial forces vs. temperature for varying fire scenarios | 161 |

| | |
|---|-----|
| Figure 130 - Buckling of web near supports observed in Case 1, 3,4 and 5..... | 162 |
| Figure 131 - Endpost and bottom flange buckling in Case 2..... | 162 |
| Figure 132 - Midspan deflection vs. time for beams with web temperatures hotter than the flanges..... | 164 |
| Figure 133 - Midspan deflection vs. temperature for beams with web temperatures hotter than the flanges. | 165 |
| Figure 134 – Axial forces vs. temperature for beams with web temperatures hotter than the flanges. | 165 |
| Figure 135 - Modes of behavior of cellular beams at fire limit state..... | 169 |
| Figure 136 - Connection forces of cellular beams with various web opening diameters | 173 |
| Figure 137 - Connection forces for cellular beams with various web thicknesses..... | 173 |
| Figure 138 - Displacement versus temperature for varying web thicknesses..... | 174 |
| Figure 139 - Displacement versus temperature for varying bottom flange widths..... | 175 |

Chapter 1: Introduction

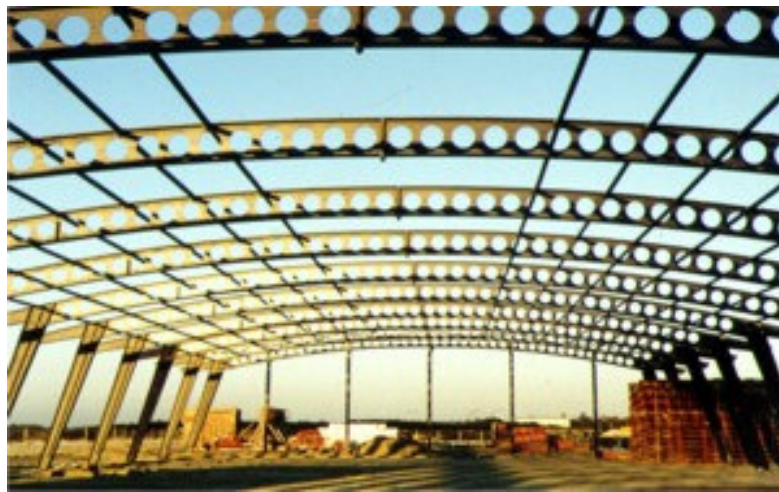
1.1 Overview

Historically, analysis of the performance of steel and composite structures in fire has primarily been based on the structural and thermal response of a single element under a prescribed standard time-temperature curve [1]. However, little work has been conducted to determine how the structural fire response of individual elements affect the surrounding structure. Due to the limitations and costs associated with traditional fire performance methods and tests, engineers and researchers have been relying more heavily on computer modeling. Advances in this technology, particularly with the use of computational fluid dynamics and finite element packages for fire applications, has enabled more reliable insight into the global and local response of structures to realistic fire scenarios. These methods of analysis are becoming increasingly important as modern construction continues to push the envelope of design, geometry, space, size and materials. One such advance in modern construction has been the increased demand for large open spaces.

In recent years, the use of cellular steel beams has become increasingly popular in building design primarily to achieve longer spans and to reduce overall building height and steel weight costs. A cellular beam, as seen in Figure 1, is typically a wide flange beam with regular circular openings. Unlike castellated beams, cellular beams have more flexibility in opening pitch, diameters and location [2]. These beams offer the flexibility offer multiple internal floor configurations, as well as, a reduction in construction cost by minimizing the number of columns and structural

walls (See Figure 1). In addition, the web openings enable the reduction in overall building height by allowing building services (mechanical, electrical, plumbing etc.) to pass within the structural depth of the beam as opposed to being hung from the bottom of the elements. These added benefits make cellular beams an efficient and cost-effective material for modern building construction.

Figure 1 - Typical long span design using cellular beams. (image from Westok Ltd.)



While it is evident that cellular beams offer tremendous advantages – longer spans, reduced construction costs, etc – their reduced shear capacity as a result of the web openings and Vierendeel effects make them more susceptible to shear failure and lateral torsional buckling under ambient conditions, let alone under fire conditions. Like any other structural beam element, cellular beams are required to achieve a certain level of fire-resistance depending on the building's construction type, occupancy, level of active and passive protection systems, and exposure to external fire loads. This fire resistance has historically been assessed using single element tests, where a single beam element is evaluated under the standard fire curve [3]. However, it is difficult to extrapolate this structural test performance to real fire scenarios and building geometries where loading conditions, continuity,

end conditions and local beam geometry markedly affect structural performance. In addition, typical compartments limit beam sizes to 4 meter spans, which may not predict the performance of cellular beams in long span applications.

Further compounding the issue are the results from recent tests on cellular beams. In these tests conducted independently by cellular beam manufacturers (Fabsec and Westok), Colin Bailey and the Steel Construction Institute (SCI), the web of the beams between the holes (commonly referred to as the web-post) experienced higher than expected temperatures [4, 5, 6, 7]. As evident from the studies, the temperature distributions through the cross-section of cellular beams is not fully understood, let alone the structural performance of this beam type in a range of structural applications and geometries. The higher web temperatures may be a result of the failure of the intumescent coatings around the web openings, the small length scale of the web opening thickness, or the airflow characteristics of the testing chamber. This makes the task of providing a level of fire-resistance with any degree of confidence difficult.

Predictive models and analysis tools are necessary to evaluate structural fire characteristics (structural performance and solid phase temperatures), coupled with fire models to predict realistic gas temperatures. Developments in computational fluid dynamics (CFD) modeling and finite element modeling (FEM) make it possible to simulate the gas behavior of fires and structural fire performance with a high degree of fidelity. However, before these tools can be used effectively for structural fire analysis, the mechanics and physics involved in the behavior of structures to fire must be clearly understood.

Empirical data based on a few experiments [4-7], can be used as preliminary predictive models; however, they have a limited range of validity and are weakly dependent on many effects that may influence the structural behavior of the cellular beams to fire. This paper, through a parametric study using the finite element model ABAQUS [8], attempts to better understand the structural behavior of cellular beams under a wide range of time-temperature exposures, temperature distributions and structural geometries. While full-scale tests were not conducted to validate the parametric study, ABAQUS 6-5.4 is a well validated finite element program used for a wide-variety of structural engineering problems and applications.

1.2 Literature Review

3.1.1 *Background of Cellular Beams*

Cellular beams were introduced into the steel construction industry in 1987, by the steel manufacturer Westok (Ltd) [10]. These beams are the successor of the castellated beam which was developed in the early 1950's. These types of beams have been used in over 3500 projects in over twenty countries and their primary use has been in secondary floor beams to achieve long spans and service integration. They are also used as roof beams beyond the range of portal frame construction, curved roofs, tapered members, gable columns and wind-posts.[2] Full-scale destructive tests have been conducted to verify structural integrity and design criteria at Bradford University in 1988, Leeds University in 1995 and the University of Manchester Institute of Science and Technology in 2000, with the supervision of the Steel Construction Institute (SCI) in the UK.[2]

Cellular beams are currently manufactured by two processes. Like its predecessor the castellated beam, a cellular beam can be manufactured as an expanded member achieved by welding together the two halves of a universal beam (or wide flange beam) with a variety of specified opening configurations. This enables the cellular beam to be up to 1.6 times deeper than the parent solid beam. In the other manufacturing process, the cellular beams are fabricated as built-up members from steel plates using automated plate cutting and welding techniques. The flange plates are welded to the webs using a double-sided process in which a thin wire submerged arc creates a 7 mm fillet weld in a single pass. Butt welds are used to achieve the desired lengths and flame cutting is used to achieve the required width of the plates and the openings. [11]

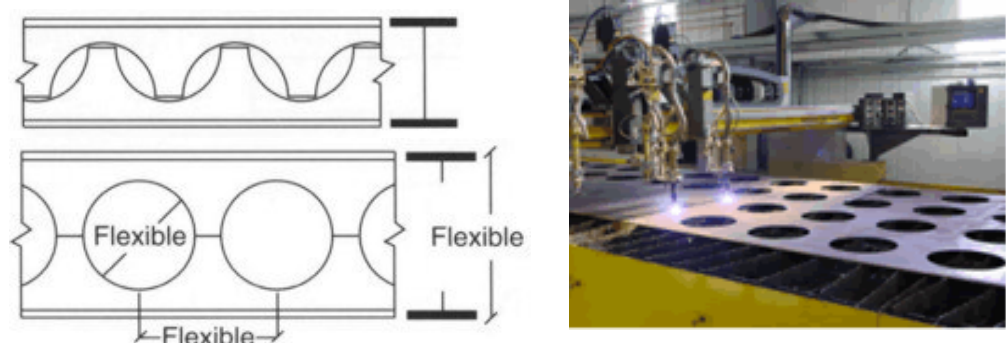


Figure 2 - (left) Cellular beam manufactured from cutting and expanding a standard universal beam (Westok). (right) Cellular beam fabricated from steel plates cut and welded (Fabsec Ltd.)

3.1.2 Early Tests and Data on Cellular Beams

Limited experimental work has been conducted to characterize the heat transfer characteristics and structural performance of cellular beams in fire conditions [4-7]. Much of the early work was conducted by the Steel Construction Institute (SCI) in conjunction with the Association for Specialist

Fire Protection and the Fire Test Study Group on castellated beams and was extended to cover cellular beams. This work is proprietary and has largely been done in the UK, where the market size for cellular beams has significantly increased in recent years to approximately 30,000 tonnes [2]. Based on these preliminary tests, beams with webs openings, including castellated beams, cellular beams with circular web openings, and beams with multiple openings of varying size and shape have traditionally been fire protected using the guidance given by *Fire Protection for Structural Steel in Buildings*, commonly referred to as the “Yellow Book”. This guide was based on the limited tests conducted by SCI which studied loaded castellated beams protected with a thick, insulating, spray applied, fire protection materials, but was extended to cover cellular beams. [12]

In recent years, several tests have been conducted on cellular beams by Fabsec Ltd, Westok Ltd and Ameron International.[4-7] In the Fabsec study, five loaded fire resistance tests were conducted on protected composite cellular beams at Warrington Fire Research Center (WFRC), along with a number of unloaded, protected short sections tested at WFRC and W & J Leight’s test furnace.[11] The 4.2m cellular composite beams were loaded and tested for a 120-min fire exposure with Firetex FB120 intumescent coatings. Figure 3 is a schematic drawing of the general test layout for tests 1-3. All three tests had similar parameters; however, test 2 incorporated rectangular openings as opposed to circular openings, and test 3 incorporated slightly larger circular openings with ring stiffeners. As seen in Figure 4, the beams failed due to excessive deflections between 117 minutes to 135 minutes. While global failure was indicated by runaway

deflections, the failure mechanisms differed. Table 1 indicates the failure mechanism observed for each test; Figure 5 illustrates the observed failure.

Figure 3 - General arrangement of Fabsec Beam Test 1 – 3.

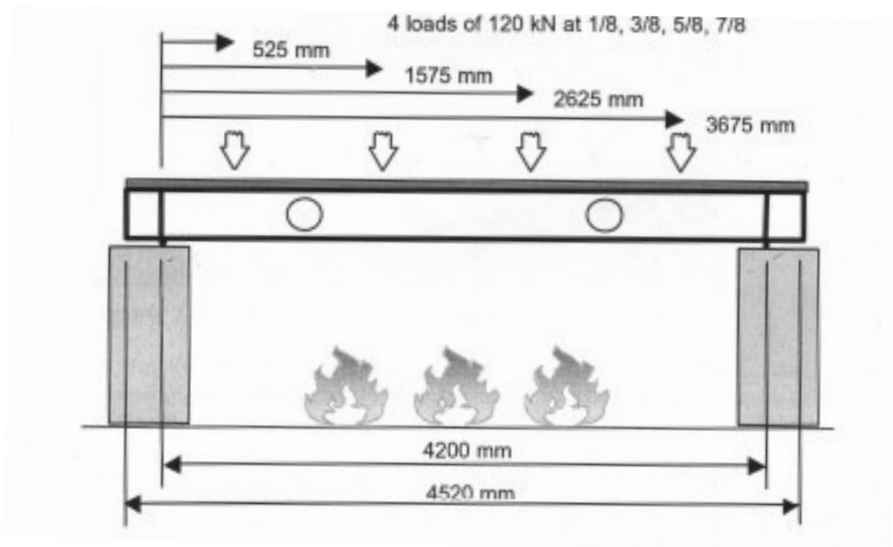
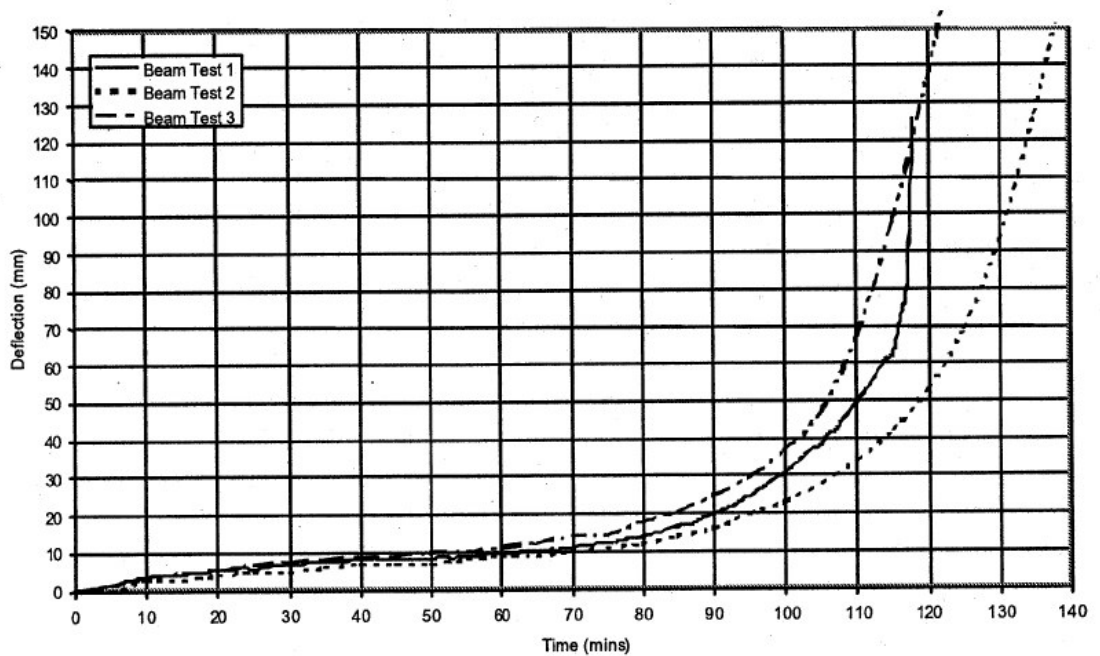


Figure 4 - Central deflection of the beams in the Fabsec fire tests.



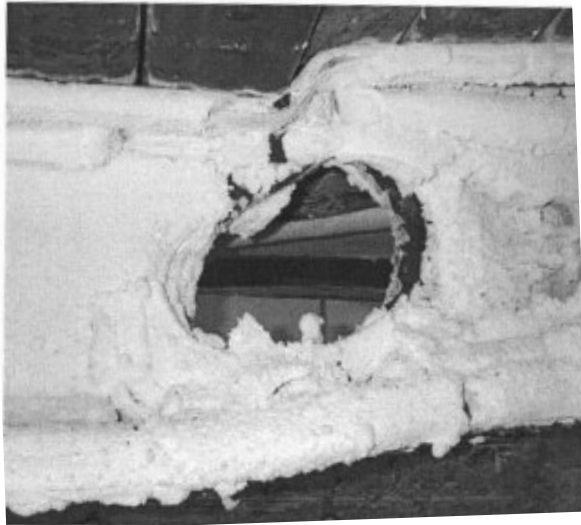


Figure 5 - (top left) Shear failure in beam test 1. (top right) Vierendeel buckling in beam test 2. (left) Overall buckling in beam test 3. (photos courtesy: Fabsec Ltd.)

Table 1: Failure Mechanisms for Beam Tests 1 -3 (reproduced from Fabsec Design Guide)

| Beam Test | Failure Mechanism |
|-----------|--|
| 1 | Shear Failure at opening |
| 2 | Vierendeel Bending (local failure around openings due to transferring of shear forces) |
| 3 | Overall bending (test reached deflection limit of $L/30$) |

Figure 6 illustrates the general set-up for Tests 4 and 5. In these tests, the web post size and affect of thinner intumescent coatings was evaluated. In Test 4, the beam failed after 57 minutes due to the buckling of the narrower web-post. Test 5 was similar to test 4 but with a thinner coating. Test 5 failed at 47 minutes due to web crushing. Figure 7 illustrates the observed failure mechanisms for each test.

Figure 6 - General arrangement for Fabsec Tests 4 & 5

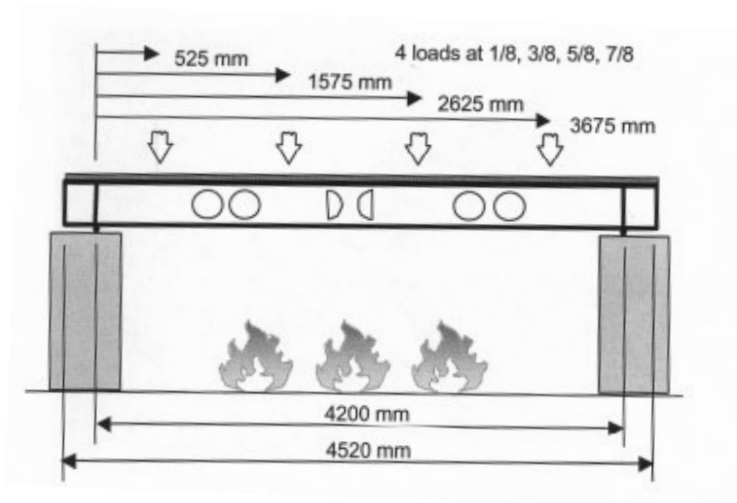
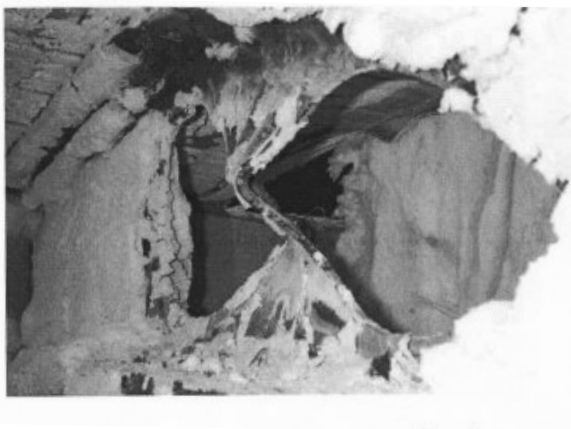


Figure 7 - (left) Web-post buckling failure Fabsec Beam #4. (right) Web crushing failure Fabsec Beam #5..



In the Westok and Ameron International study, a series of unloaded tests were conducted on unprotected and protected beams, and compared with a similar solid beam. The focus of these tests was on the temperature distribution in the cellular beams, particularly around the web openings. These temperatures were compared relative to the temperatures observed in a solid beam section. Figure 8 illustrates a typical test setup. These tests were conducted on beam elements of approximately 1m in length and were not studied for structural behavior.

Figure 8 - General arrangement of unprotected cellular beams tests (Westok).



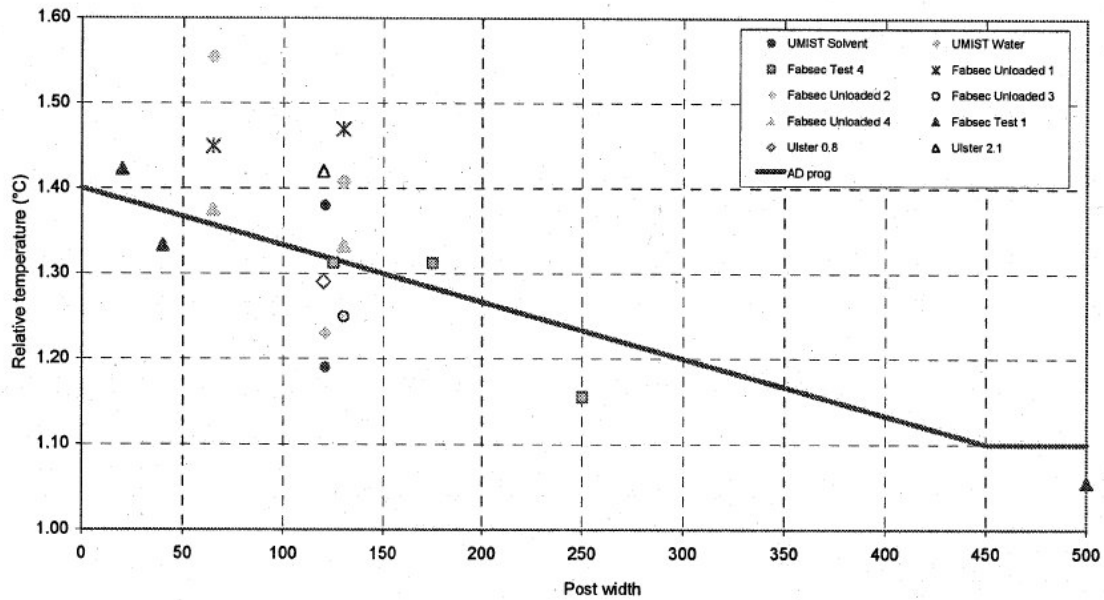
The results from both studies indicate that greater than expected temperatures were observed in the web-post of cellular beams in comparison to the flange temperatures. However, there does not appear to be any evidence suggesting that the web posts of unprotected cellular beams heat at a faster rate than an identical solid beam of similar

dimensions [4]. This is likely due to the fact that the exposed surfaces for the cellular beam is not much different than that of a solid beam of the same size. That is, the additional surfaces created by adding a web opening, is comparable to the area of the web taken away from the solid web. For unprotected cellular beams, as with solid beams, the web appears to be approximately 5% greater than the adjacent web.

In protected cellular beams, the ratio between web-post temperature and adjacent flange temperatures appears to be significantly higher. Figure 9 shows the ratio of web-post temperature to adjacent flange temperature for the relevant Fabsec and Westok tests. The Fabsec tests are expressed in terms of buckling temperature and average bottom flange temperature, and the Westok tests are expressed as average web post temperatures and bottom flange temperature. These ratios are also plotted with the design value assumed by SCI. As seen in the figure, the ratio between the web-post and bottom flange temperature increases as web-post length decreases. While this data seems to indicate a substantial increase in web-post temperatures of cellular beams of up to 40%, the results may be misleading. In both Fabsec and Westok tests, the intumescent coatings began to detach and develop cracks around the openings. The performance of the intumescent coatings may be the cause of the significant temperature differences.

Figure 9 - Summary of data on ratio of web-post temperatures to bottom flange temperatures for protected cellular beams (Fabsec, Westok and SCI design curve).

Image courtesy: SCI Document RT983



1.3 Research Objectives

This paper, through a parametric study using the finite element code ABAQUS, attempts to contribute to the understanding of the global behavior of long span cellular beams under fire conditions and to appreciate the controlling mechanisms that lead to local failure and possibly runaway failure. The process of this study included:

- Investigation of the sensitivity of section geometry on the structural behavior of long span cellular beams exposed to a standard fire
- Investigation on whether varying the heating rate or maximum temperature plays a significant role on structural response of these beam types

- Investigation on whether increased web temperatures observed in recent fire tests significantly affect the structural fire behavior of long span cellular beams.

1.4 Outline of thesis chapters

Chapter 2

Fundamentals of Structural Fire Analysis

This section provides a background to the basic important understanding of structural fire analysis with respect to the dynamics of building fires, temperature effects on structural materials and thermo-mechanics.

Chapter 3

Methodology – Cellular Beam Study

The model to be used for the analyses is described in detail, including geometry, material behavior, thermal loading, and output to be expected.

Chapter 4

Analysis and Interpretation of Results

Presentation and analysis of the results is given in this chapter. Each model is presented and compared with other models within the parametric group. Each group is then compared against the base models (cellular beam and solid beam models). The analysis focuses on the initial failure mechanism, displacements, stress concentrations and forces that affect the behavior of the cellular beam in question. Analysis of the supporting frame is not included.

Chapter 5

Conclusions and further work

This chapter summarizes the results of the analyses as discussed previously and states the conclusions of the study. Also included are suggestions for additional work to be undertaken.

Chapter 2: Fundamentals of Structural Fire Analysis

In performing a structural fire engineering assessment, it is of interest to explore the expected fire scenarios, thermal response of the structural elements, and the mechanical or structural response of the structural system or building component. Developments in computational fluid dynamics (CFD) and finite element methods (FEM) have made it possible to simulate the continuous phase behavior of fires and the mechanical response of a structure with a high degree of reliability, respectively. In the fire analysis, it is important to understand the dynamics of building fires insofar as they influence the expected fire exposure scenarios. This will be briefly discussed in Section 2.1.

In the structural fire analysis, as noted by Buchanan [13], the methods of assessment are essentially similar to the analysis techniques used during ambient condition design. That is, the methods to determine the deformations and internal forces induced by the applied loads are conceptually the same. However, the main differences at the time of fire, as highlighted by Buchanan are as follows:

- Reduced applied loads
- Thermally induced internal forces
- Reduced strengths of materials
- Reduced cross-section areas by charring and spalling
- Deflections are less critical
- Different failure mechanisms dominate

These factors manifest themselves differently depending on the materials used in construction and the types of boundary conditions. Historically, it was believed that the

thermal effects on material properties dominated the global behavior of the structure. However, with the increase in research and understanding of thermo-mechanics, the role of boundary conditions appears to play a more significant role in structural response to fire.

Much of this recent work on understanding the behavior of structures under fire conditions has been conducted by Usmani et al at the University of Edinburgh in Scotland, who participated in the “Cardington tests” [14] sponsored by British Steel PLC (now CORUS) following the 1990 Broadgate fire in London [15]. Their analysis of the Cardington tests provides new insights into the response of structures to fire, particularly with respect to elongation and thermal curvature. As noted by Usmani, et al.[16]:

“Behavior of composite structures in fire has long been understood to be dominated by the effects of strength loss caused by thermal degradation, and that large deflections and runaway resulting from the action of imposed loading on a ‘weakened’ structure. Thus ‘strength’ and ‘loads’ are quite generally believed to be the key factors determining structural response (fundamentally no different from ambient behavior). The new understanding ... is that composite framed structures of the type tested at Cardington possess enormous reserves of strength through adopting large displacement configurations. Furthermore, it is the thermally induced forces and displacements, and not material degradation that govern structural response in fire.”

Usmani, et al., lay down some of the most important and fundamental principles that govern the behavior of composite frame structures in fire. Section 2.2 will address the

thermal effects on material properties, and Section 2.3 will discuss thermo-mechanics. Among these, the performance criteria are crucial to providing the objectives for the desired structural performance. However, there is currently no general performance criteria established in the U.S., with limited guidance in Europe. Furthermore, large scale testing data on the global response of structures to fire is limited. Development of a general understanding of the global response of cellular beams to fire will be the focus of this study. The structural response will be sensitive to the fire exposure, beam geometry, support conditions, loading, and material response.

2.1 Dynamics of Building Fires

In order to assess structural performance in fire, it is necessary to understand the thermal boundary conditions to which the structure will be subjected. This exposure depends on a number of factors, including those identified in the ASTM E119 fire resistance test standard [17], and as listed below:

1. Fuel load—amount and type;
2. Distribution of the fuel load;
3. Specific surface characteristics of the fuel load;
4. Ventilation, as determined by the size and shape of openings;
5. Geometry of the fire compartment—size and shape;
6. Thermal characteristics of the enclosure boundaries;
7. Relative humidity of the atmosphere.

In buildings, the confinement effects give rise to four stages of enclosure fires, which are defined by Mowrer [18] as:

- Fire plume / ceiling jet period

- Enclosure smoke filling period
- Preflashover vented period
- Postflashover vented period

In the post-flashover or “fully developed” fire virtually all exposed fuel surfaces have ignited during the flashover process. In this period, the burning rate within the enclosure is usually regulated by the rate of air flow into the enclosure rather than by the rate of fuel released from the burning surfaces. During this stage of the fire, the gas temperatures and radiant heat fluxes in the enclosure are typically at their highest and can be assumed to be uniform throughout the enclosure. [Buchanan: 61] The temperature, however, varies at any given time and depends on the balance between the heat released and the heat lost.

As mentioned before, developments in CFD have made it possible to characterize the gas phase temperatures in a compartment with high fidelity. Post-flashover temperatures can be determined; however, in order to conduct a structural fire analysis solid phase temperatures are required. Despite the advances in CFD and FEM packages, there is still a disconnect between the gas phase temperatures calculated in CFD models and the solid phase temperatures required for the structural analysis. While it is relatively simple to model the expected fire scenarios and model the structural response of a system separately, it is difficult to streamline the transition from the gas phase temperature outputs from CFD to the solid phase input temperatures for the structural assessment.

The following sections of this report will address the effects of solid phase temperatures on the material and mechanical properties of structural systems.

Section 3.3 will discuss how the disconnect between the gas phase temperatures and solid phase temperatures is resolved.

2.2 Temperature Effects On Structural Materials

In this study, a long span cellular beam is evaluated in a composite steel and concrete structural bay. While the cellular beam is the focus of the paper, the concrete aspects of the system significantly influence the overall response of the structural system. Therefore, the material properties of both steel and concrete are presented in this section.

2.2.1 Steel

When steel is exposed to fire, the steel temperatures increase resulting in the reduction of the strength and stiffness of the steel. This material response to fire can lead to possible deformations and failure, depending on the applied loads, temperature profile, and support conditions. The increase in steel temperatures depends on the severity of the fire, the section factor (area of exposed steel) and the amount and type of applied fire protection materials.

In general, unprotected steel structures perform poorly in fires relative to other structural materials such as concrete, gypsum, and timber. This poor performance can be partly attributed to the thinner elements used, the higher thermal conductivity of steel and high thermal expansion.[13] Despite the vulnerability of steel as a material, steel structures have historically performed well structurally in fire scenarios, in particular protected steel structures (i.e. First Interstate Bank [19], One Meridian Plaza [20], Cardington tests [14], Broadgate fires [15], Mercantile Credit Insurance Building [21] etc); that is there has only been one reported structural steel building collapse where fire

was the main cause (World Trade Center 7, 2001) and two partial collapses [21].

The main material properties affected by fire, as they relate to structural behavior, will be discussed further in this chapter.

2.2.1.1 Thermal Properties

Density

The density of steel does not vary much with temperature and can be assumed constant at 7850 kg/m³.

Specific Heat

The specific heat of steel varies according to temperature as shown in Figure 10, reproduced from Eurocode 3, 1995 [22]. For simple calculations, the specific heat c_a can be taken as 600 J/kg-K. However, it is more accurate to use the following equations (1), where $\theta_{a,t}$ is the steel temperature in degrees Celsius:

$$c_a(\theta_{a,t}) := \begin{cases} 425 + 7.73 \cdot 10^{-1} \cdot \theta_{a,t} - 1.69 \cdot 10^{-3} \cdot (\theta_{a,t})^2 + 2.22 \cdot 10^{-6} \cdot \theta_{a,t}^3 & \text{if } \theta_{a,t} < 600 \\ \left(666 + \frac{13002}{738 - \theta_{a,t}} \right) & \text{if } 600 \leq \theta_{a,t} < 735 \\ \left(545 + \frac{17820}{\theta_{a,t} - 731} \right) & \text{if } 735 \leq \theta_{a,t} < 900 \\ 650 & \text{if } 900 \leq \theta_{a,t} \leq 1200 \end{cases} \quad (1)$$

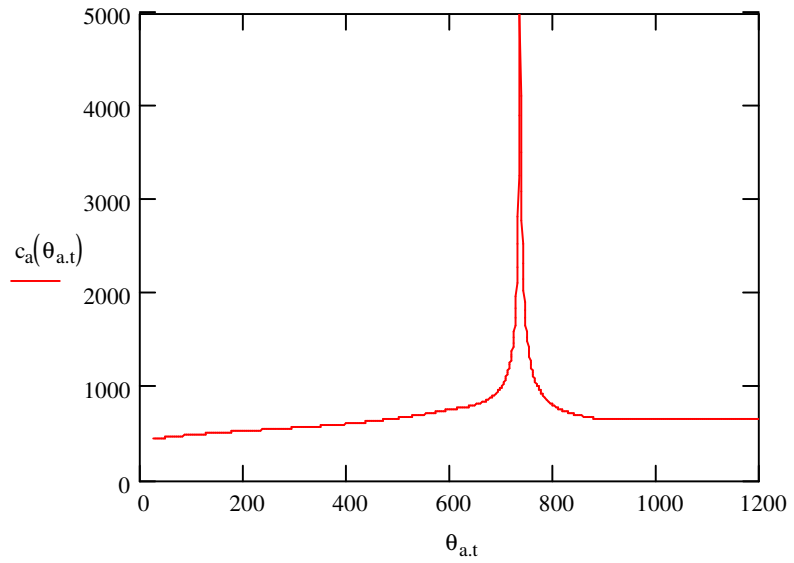


Figure 10 - Specific heat of steel at elevated temperatures (EC3:1995)

Thermal conductivity

The thermal conductivity of steel varies according the temperature as shown in Figure 11, reproduced from EC 3, 1995. For simple calculations, the thermal conductivity λ_a can be taken as 45 W/m-K. However, for more complex calculations, the following equations can be used, where $\theta_{a,t}$ is the steel temperature in degrees Celsius, and λ_a is in W/m-K.

Thermal Conductivity:

$$\lambda_a(\theta_{a,t}) := \begin{cases} (54 - 3.33 \cdot 10^{-2} \cdot \theta_{a,t}) & \text{if } \theta_{a,t} < 800 \\ 27.3 & \text{if } 800 \leq \theta_{a,t} \leq 1200 \end{cases} \quad (2)$$

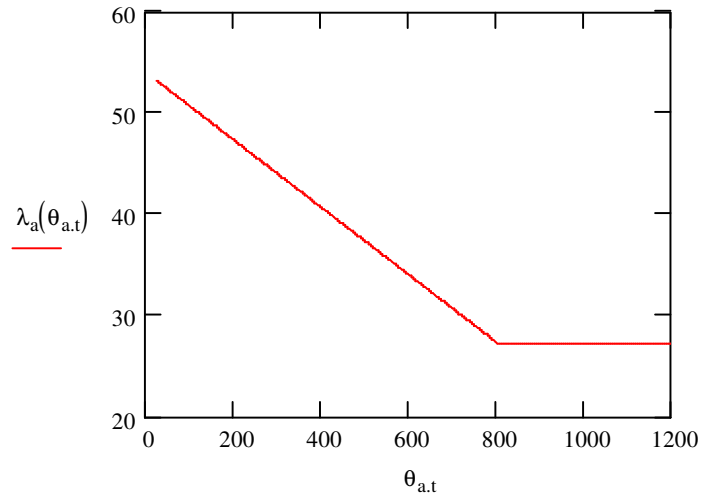


Figure 11 - Thermal conductivity of steel at elevated temperatures (EC3:1995)

2.2.1.2 Mechanical Properties

2.2.1.2.1 Thermal strain

Thermal strain is the well-known phenomenon that occurs when most materials are heated. At room temperature, the coefficient of thermal expansion for steel can be taken as $14.0 \times 10^{-6} / ^\circ\text{C}$ from Eurocode 3 (1995). At higher temperatures, the coefficient increases, resulting in the thermal strain as seen in Figure 12, reproduced from the Eurocodes (EC3:1-2, 1995).

$$\varepsilon_T(\theta_{a,t}) := \begin{cases} 1.2 \cdot 10^{-5} \cdot \theta_{a,t} + 0.4 \cdot 10^{-8} \cdot (\theta_{a,t})^2 - 2.416 \cdot 10^{-4} & \text{if } 20 \leq \theta_{a,t} < 750 \\ 1.1 \cdot 10^{-2} & \text{if } 750 \leq \theta_{a,t} < 860 \\ (2 \cdot 10^{-5}) \cdot \theta_{a,t} - 6.2 \cdot 10^{-3} & \text{if } 860 \leq \theta_{a,t} < 1200 \end{cases} \quad (3)$$

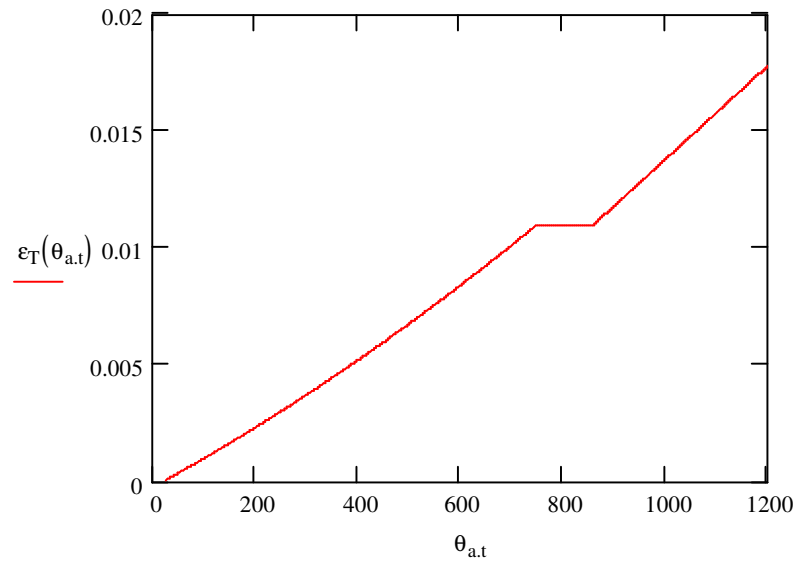


Figure 12 - Thermal strain of steel at elevated temperatures (EC3:1995)

2.2.1.2.2 Creep Strain

At ambient temperatures, creep plays a relatively insignificant role in structural steel performance. However, from tests conducted by Poh (1996), Kirby and Preston (1988)[13] creep is shown to become very important at temperatures over 400°C or 500°C. As seen in Figure 13 creep is not only dependent on temperature but also on the stress level of the element.

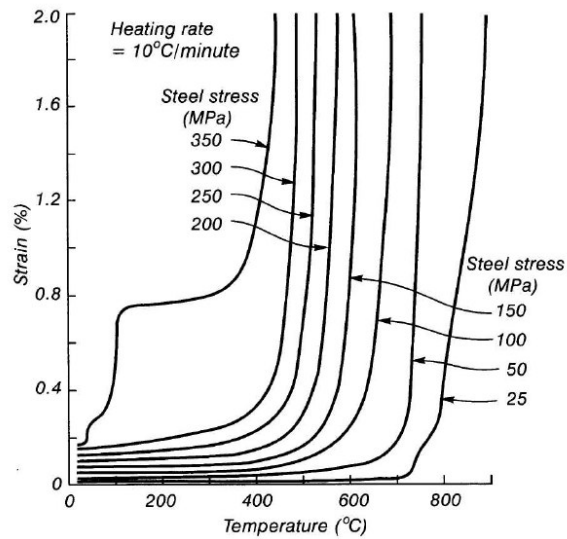


Figure 13 - Creep strain figure from Buchanan

As noted by Buchanan, the importance of creep deformations in fire-exposed structures, while significant, is often not explicitly included in computer based fire design processes. It is typically assumed that the stress-strain relationships are “effective “and are implicitly capturing the deformations from creep during the fire exposure (EC3, 1995).

2.2.1.2.3 Yield Strength

At higher temperatures, the yield strength decreases, while the ultimate tensile strength increases slightly at moderate temperatures, before decreasing at higher temperatures. Typical stress-strain relationships for structural steel at elevated temperatures are show in Figure 14. As seen in the figure, the well-defined yield strength at ambient

temperatures tends to disappear at elevated temperatures. Similar relationships are available for prestressing steel, but are not presented here in this report.

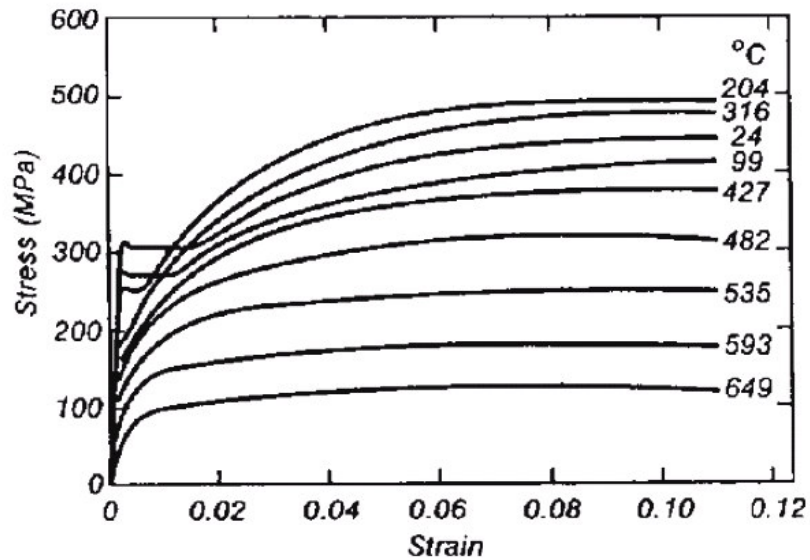


Figure 14 - Stress-strain relationships for steel at elevated temperatures. (Buchanan)

The structural Eurocode for steel (EC3, 1995) has more detailed expressions, with equations for the stress-strain relationship of various steels and a table of reduction factors for steel at elevated temperatures. The reduction factors are relative to the appropriate value at 20°C, and are as follows:

- Relative effective yield strength: $k_{y,\theta} = f_{y,\theta} / f_y$
- Relative proportional limit: $k_{p,\theta} = f_{p,\theta} / f_y$
- Relative Elastic modulus: $k_{E,\theta} = E_{a,t} / E_a$

The reduction values in Table 2 are then used to determine the stress-strain relationships supplied in Figure 15. These

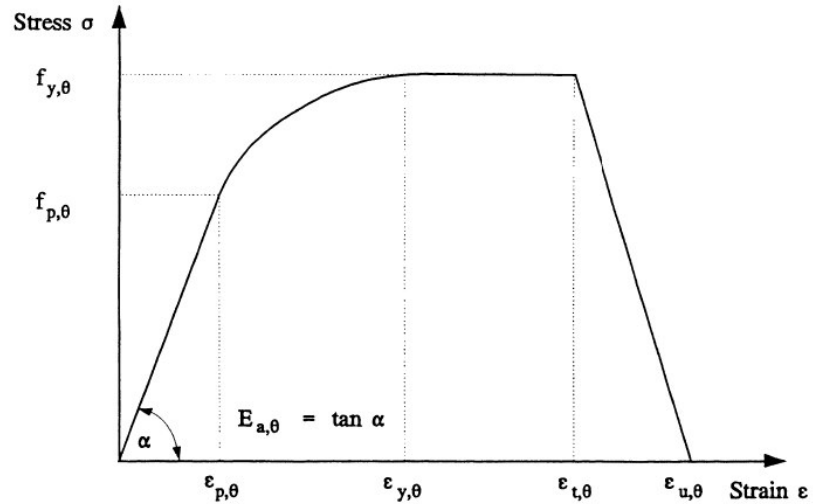
relationships and ultimately affect the tension, compression, moment and shear capacity of a structural element.

Table 2: Reduction factors for stress strain relationships for steel at elevated temperatures. (EC3, 1995)

| Steel temperature θ_a | Reduction factors at temperature θ_a relative to the value of f_y or E_a at 20 °C | | | |
|--|--|---|--|--|
| | Reduction factor (relative to f_y) for effective yield strength | Modified factor (relative to f_y) for satisfying deformation criteria | Reduction factor (relative to f_y) for proportional limit | Reduction factor (relative to E_a) for the slope of the linear elastic range |
| | $k_{y,\theta} = f_{y,\theta}/f_y$ | $k_{x,\theta} = f_{x,\theta}/f_y$ | $k_{p,\theta} = f_{p,\theta}/f_y$ | $k_{E,\theta} = E_{a,\theta}/E_a$ |
| 20 °C | 1,000 | 1,000 | 1,000 | 1,000 |
| 100 °C | 1,000 | 1,000 | 1,000 | 1,000 |
| 200 °C | 1,000 | 0,922 | 0,807 | 0,900 |
| 300 °C | 1,000 | 0,845 | 0,613 | 0,800 |
| 400 °C | 1,000 | 0,770 | 0,420 | 0,700 |
| 500 °C | 0,780 | 0,615 | 0,360 | 0,600 |
| 600 °C | 0,470 | 0,354 | 0,180 | 0,310 |
| 700 °C | 0,230 | 0,167 | 0,075 | 0,130 |
| 800 °C | 0,110 | 0,087 | 0,050 | 0,090 |
| 900 °C | 0,060 | 0,051 | 0,0375 | 0,0675 |
| 1000 °C | 0,040 | 0,034 | 0,0250 | 0,0450 |
| 1100 °C | 0,020 | 0,017 | 0,0125 | 0,0225 |
| 1200 °C | 0,000 | 0,000 | 0,0000 | 0,0000 |
| NOTE: For intermediate values of the steel temperature, linear interpolation may be used. | | | | |

Figure 15 - Stress-strain relationships for steel at elevated temperatures (EC3:1995)

| Strain range | Stress σ | Tangent modulus |
|---|---|---|
| $\varepsilon \leq \varepsilon_{p,\theta}$ | $\varepsilon E_{a,\theta}$ | $E_{a,\theta}$ |
| $\varepsilon_{p,\theta} < \varepsilon < \varepsilon_{y,\theta}$ | $f_{p,\theta} - c + (b/a)[a^2 - (\varepsilon_{y,\theta} - \varepsilon)^2]^{0,5}$ | $\frac{b(\varepsilon_{y,\theta} - \varepsilon)}{a[a^2 - (\varepsilon_{y,\theta} - \varepsilon)^2]^{0,5}}$ |
| $\varepsilon_{y,\theta} \leq \varepsilon \leq \varepsilon_{t,\theta}$ | $f_{y,\theta}$ | 0 |
| $\varepsilon_{t,\theta} < \varepsilon < \varepsilon_{u,\theta}$ | $f_{y,\theta} \left[1 - (\varepsilon - \varepsilon_{t,\theta}) / (\varepsilon_{u,\theta} - \varepsilon_{t,\theta}) \right]$ | - |
| $\varepsilon = \varepsilon_{u,\theta}$ | 0,00 | - |
| Parameters | $\varepsilon_{p,\theta} = f_{p,\theta} / E_{a,\theta}$ $\varepsilon_{y,\theta} = 0,02$ $\varepsilon_{t,\theta} = 0,15$ $\varepsilon_{u,\theta} = 0,20$ | |
| Functions | $a^2 = (\varepsilon_{y,\theta} - \varepsilon_{p,\theta})(\varepsilon_{y,\theta} - \varepsilon_{p,\theta} + c/E_{a,\theta})$ $b^2 = c(\varepsilon_{y,\theta} - \varepsilon_{p,\theta})E_{a,\theta} + c^2$ $c = \frac{(f_{y,\theta} - f_{p,\theta})^2}{(\varepsilon_{y,\theta} - \varepsilon_{p,\theta})E_{a,\theta} - 2(f_{y,\theta} - f_{p,\theta})}$ | |



Key:

- $f_{y,\theta}$ is the effective yield strength;
- $f_{p,\theta}$ is the proportional limit;
- $E_{a,\theta}$ is the slope of the linear elastic range;
- $\varepsilon_{p,\theta}$ is the strain at the proportional limit;
- $\varepsilon_{y,\theta}$ is the yield strain;
- $\varepsilon_{t,\theta}$ is the limiting strain for yield strength;
- $\varepsilon_{u,\theta}$ is the ultimate strain.

Alternatively, the Eurocode 3 provides an approximate curve for the reduction in yield strength and is given by:

$$k_{y,T} = [0.9674(1 + \exp[(T - 482)/39.13])]^{-1/3.833} \quad (4)$$

In general, steel retains strength and stiffness approximately equal to 50 percent of its strength and stiffness at ambient conditions at a temperature of 593 °C. At 704 °C, steel retains about 20 percent strength and stiffness and loses all strength at approximately 1,204 °C.

In some cases, it is convenient to represent the variation of yield strength, modulus or elasticity, and proportional limit as a function of temperature and as a fraction relative to the steel strength at ambient temperature, as shown in Figure 16 and Table 2. In this figure, it is interesting to note that the modulus of elasticity reduces more quickly than the yield strength as temperature increases. This plays a significant role in how a structural system behaves at elevated temperatures and predicting the failure mechanism. That is, this figure suggests that the stiffness of the structural element will be the limiting factor in the performance of the system. This may result in increased deflections and deformations as temperatures increase.

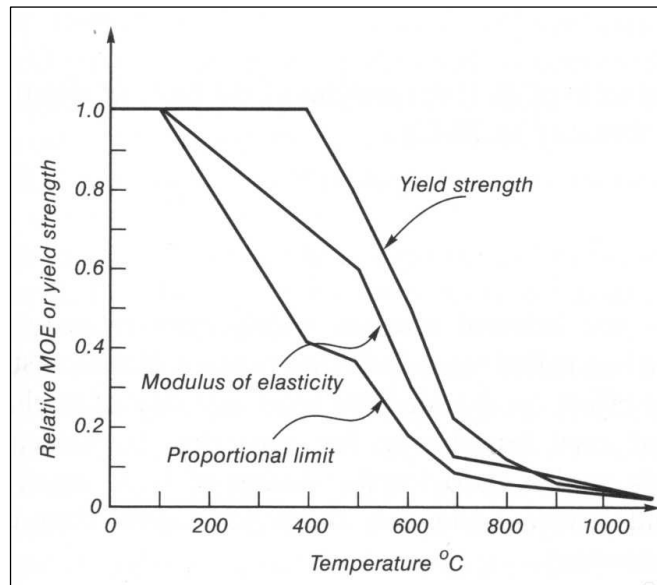


Figure 16 - Relative mechanical properties at elevated temperatures in comparison to ambient conditions. (Buchanan)

2.2.1.2.4 Modulus of Elasticity

As eluded to in the above section, the modulus of elasticity decreases with increasing temperatures. The reduction in modulus shows the same trend as the reduction in yield strength; however, the modulus tends to reduce at a slightly more rapid rate (See Figure 16). Table 2 and Figure 15 from the Eurocode can be used for design purposes in determining the temperature history of the elastic modulus.

2.2.2 Concrete

Concrete is non-combustible and has a low thermal conductivity. In addition, the cement paste undergoes an endothermic reaction when heated as the embedded water changes phase. This reaction helps reduce the temperature rise in fire-exposed concrete structures in the early stages of the

fire. However, this reaction can also lead to spalling, which will cause the core of the concrete element to heat faster. If spalling is limited, then the cover concrete tends to protect the inner core of the structural element and insulate the reinforcing steel from higher temperatures. In this way, the concrete structure is able to maintain load bearing capacity for longer duration fires.



Figure 17 - Collapsed textile factory in Alexandria, Egypt (BBC News, 2000)

The global performance of concrete structures, as with steel, is dependent on several factors: the applied loads, the elevated temperatures of the concrete and reinforcing steel, the mechanical properties of both materials, and support conditions. While catastrophic failures for reinforced concrete structures in fire are rare, some occasionally occur (e.g. Papaioannou, 1986, Berto and Tomina, 1988, Alexandria Egypt, 2000) [21]. A NIST (National Institute of Standards and Technology) survey of 22 fire collapsed buildings since 1970 indicated

that 7 of these buildings were of reinforced concrete construction (one being the Pentagon) [23].



Figure 18 - Katrantzos Department Building in Athens, Greece, After 1980 Fire (Papaioanmoa, 1986)

The main material properties affected by fire, as they relate to structural behavior, will be discussed further in this chapter.

2.2.2.1 Physical Process

Spalling

The loss of cover in fire conditions is one of the more difficult phenomena to characterize and predict in concrete structures. This

event plays a critical role in a concrete structure's ability to withstand a thermal assault. In some cases, the spalling of the cover concrete is related to type of aggregate or to thermal stresses near corners; however, according to Buchanan it is more often connected to the response of the cement paste.

In general, most spalling occurs when water vapor within the concrete microstructure is driven off from the cement paste during heating. The changing of phase of the embedded water creates high pore pressures in the concrete matrix and produces tensile stresses in excess of the tensile strength of the concrete. Experiments from Malhotra (1984) and Phan (1996) have shown that concrete is more susceptible to spalling as a result of high moisture content, rapid rates of heating, slender members, and high concrete stresses. In addition, high strength concrete tends to be more vulnerable to spalling than normal strength concrete due to the reduced porosity, which inhibits the diffusion of the water vapor through the concrete. [24, 25]

2.2.2.2 Thermal Properties

2.2.2.2.1 Density

When concrete is heated to 100°C, the density of most concretes reduces by up to 100 kg/m³ from the evaporation of the free water. This event, however, has little effect on thermal response. As the temperature increases, the density of the concrete undergoes minor changes, except for

calcareous aggregate concrete that decomposes above 800°C (Buchanan).

2.2.2.2.2 Thermal Conductivity

The thermal conductivity of concrete changes with temperature, as seen in Figure 19 [26]. This property varies with temperature and depends on the aggregate, moisture content, and mix proportions of the concrete (Schneider, 1988). Approximate values for design purposes are 1.6 W/m-K for siliceous concrete, 1.3 W/m-K for calcareous aggregate concrete, and 0.8 W/m-K for lightweight concrete. (Eurocode 2, 1993) [26].

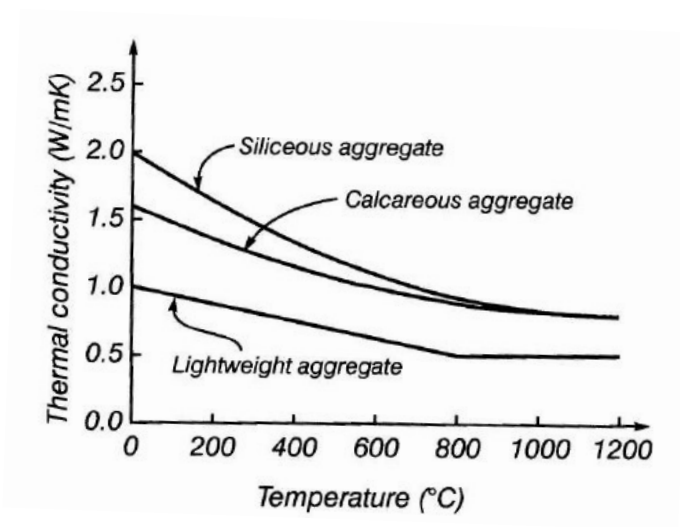


Figure 19 – Thermal conductivity of varying types of concrete (Reproduced from EC2, 1993)

2.2.2.2.3 Specific Heat

The specific heat of concrete also varies broadly with temperature and depends on the moisture content. Figure 20, from Eurocode 2 1993 (EC2:1993), illustrates the design values. The peak between 100°C and 200°C takes into consideration water evaporation during the heating process. Approximation for design purposes are: 1000 J/kg-K for siliceous and limestone aggregates, and 840 J/kg-K for lightweight concrete from EC2 1993 [26].

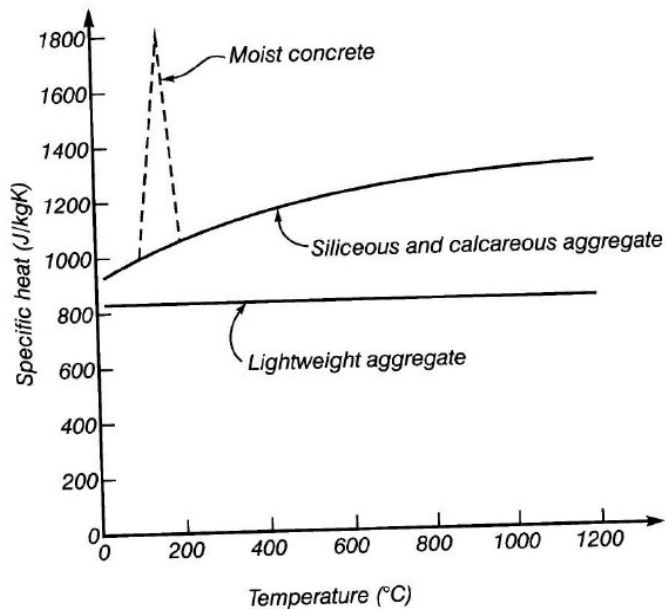


Figure 20 – Specific heat of concrete (Reproduced from EC2, 1993.)

2.2.2.3 Mechanical Properties

The deformation of concrete at elevated temperatures is slightly more complex than that of steel, due to the inclusion of transient strain. According to Buchanan, the deformation of concrete can be described by the total strain ϵ consisting of four components:

$$\varepsilon = \varepsilon_{th}(T) + \varepsilon_{\sigma}(\sigma, T) + \varepsilon_{cr}(\sigma, T, t) + \varepsilon_{tr}(\sigma, T) \quad [5]$$

Where $\varepsilon_{th}(T)$ is the thermal strain as a function of temperature, $\varepsilon_{\sigma}(\sigma, T)$ is the stress related strain, $\varepsilon_{cr}(\sigma, T, t)$ is the creep strain, and $\varepsilon_{tr}(\sigma, T)$ is the transient strain. Creep strain and transient strain are closely linked. Creep is typically measured in tests in which the load is kept constant and the deformations over time are measured. Transient creep occurs when the specimen is subjected to an initial load, then the temperatures are increased at a constant rate while the load is maintained. These strains are also discussed by Anderberg 1976, Schneider 1988 and Khoury et al. 1985).

2.2.2.3.1 Thermal Strain

The thermal strain of concrete varies with temperature. Figure 21 from Eurocode 2 illustrates the variation of the thermal elongation with temperatures. Expressions for these strains (ε_c) are as follows for siliceous and calcareous aggregates:

Siliceous aggregates:

$$\varepsilon_c(\theta) = -1,8 \times 10^{-4} + 9 \times 10^{-6}\theta + 2,3 \times 10^{-11}\theta^3 \quad \text{for } 20^\circ\text{C} \leq \theta \leq 700^\circ\text{C}$$

$$\varepsilon_c(\theta) = 14 \times 10^{-3} \quad \text{for } 700^\circ\text{C} < \theta \leq 1200^\circ\text{C}$$

Calcareous aggregates:

$$\varepsilon_c(\theta) = -1,2 \times 10^{-4} + 6 \times 10^{-6}\theta + 1,4 \times 10^{-11}\theta^3 \quad \text{for } 20^\circ\text{C} \leq \theta \leq 805^\circ\text{C}$$

$$\varepsilon_c(\theta) = 12 \times 10^{-3} \quad \text{for } 805^\circ\text{C} < \theta \leq 1200^\circ\text{C}$$

Where θ is the concrete temperature ($^\circ\text{C}$).

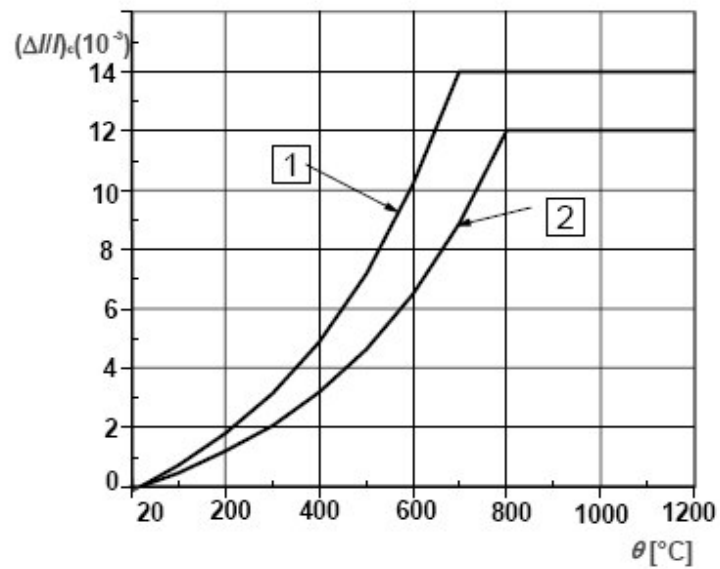


Figure 21 - Thermal elongation for siliceous and calcaerous concrete at elevated temperatures (EC2:1993)

Where Curve 1 is for siliceous concrete and Curve 2 is for calcareous concrete. These above expressions include both shrinkage and thermal strain effects.

2.2.2.3.2 Creep Strain and Transient Strain

Like structural steel, concrete experiences creep strain; however, concrete also undergoes transient strains. These two strains are closely linked and are often coupled

in experiments. Figure 22 from Schneider (1988) [27] are of tests conducted on concrete specimens that were heated under load and show the combination of strain components described above.

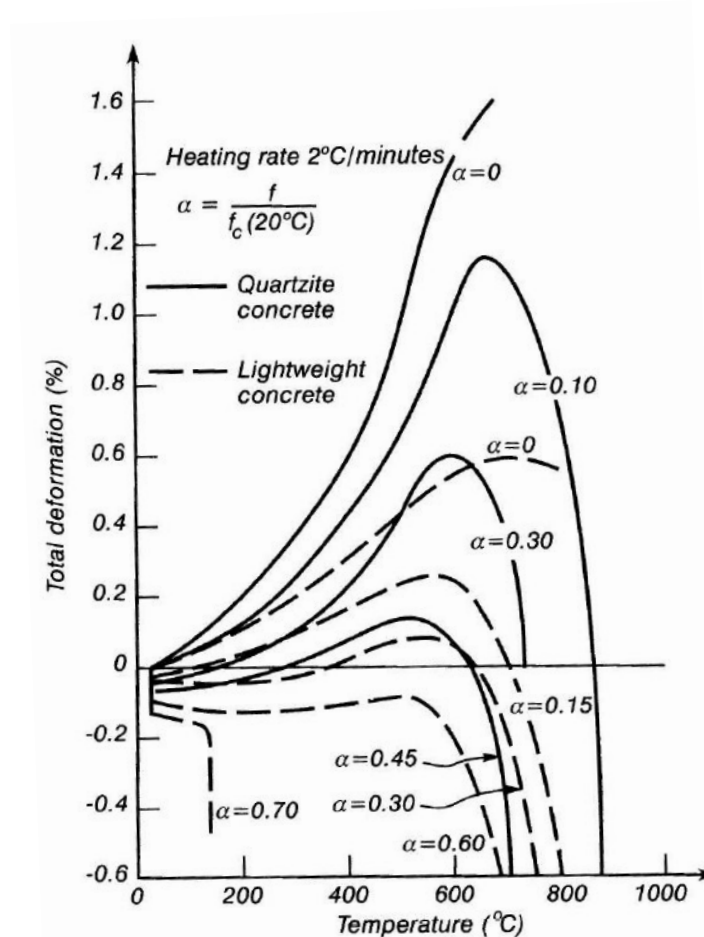


Figure 22 – Total deformation in different concretes during heating (Reproduced from Schneider (1988))

Measurements of creep strains are illustrated in Figure 23 for gravel concrete, lightweight concrete, and cement paste. These tests were conducted by Khoury et al. (1985) [28], which capture both creep and transient strains.

Transient strains occur during the first time heating of concrete under load at around 600C.

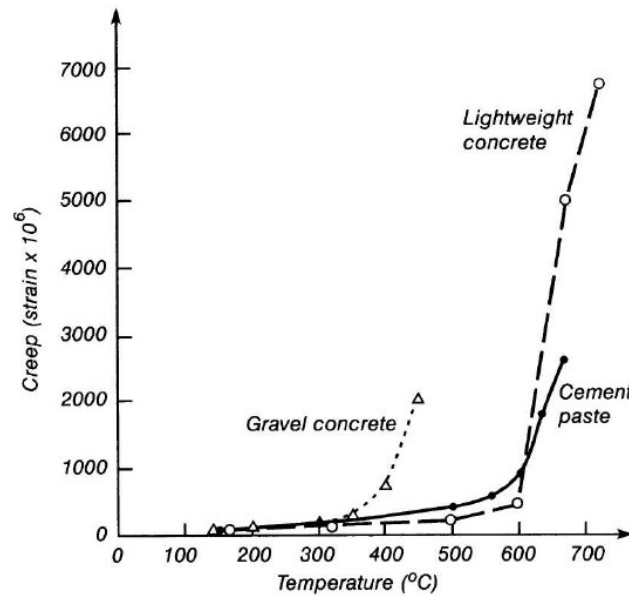


Figure 23 – Creep in concrete one day after loading at 10% of the initial strength (Reproduced from Khoury and Sullivan (1988)).

2.2.2.3.3 Stress-Related Strain

2.2.2.3.3.1 Yield Strength

Typical stress-strain curves of normal weight concrete at elevated temperatures can be seen in Figure 24. As seen in the figure, the ultimate compressive strength of concrete drops at higher temperatures, while the strain at peak stress increases. This reduction in compressive strength can also be seen in Figure 25. produced from tests conducted by Schneider [27]. For well-confined concrete, no specific studies have been conducted to determine if confined concrete has

enhanced strength and ductility at elevated temperatures as it does at ambient conditions [13, 27].

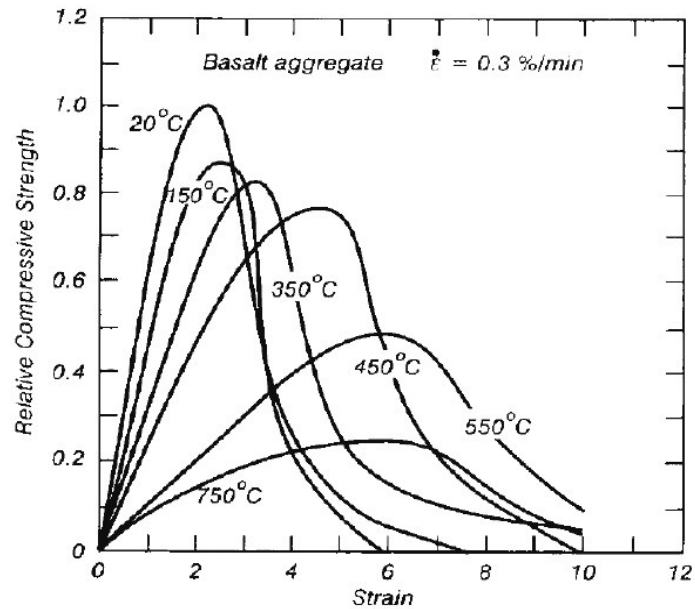


Figure 24 - Stress-strain relationships for concrete at elevated temperatures (EC 2, 1993)

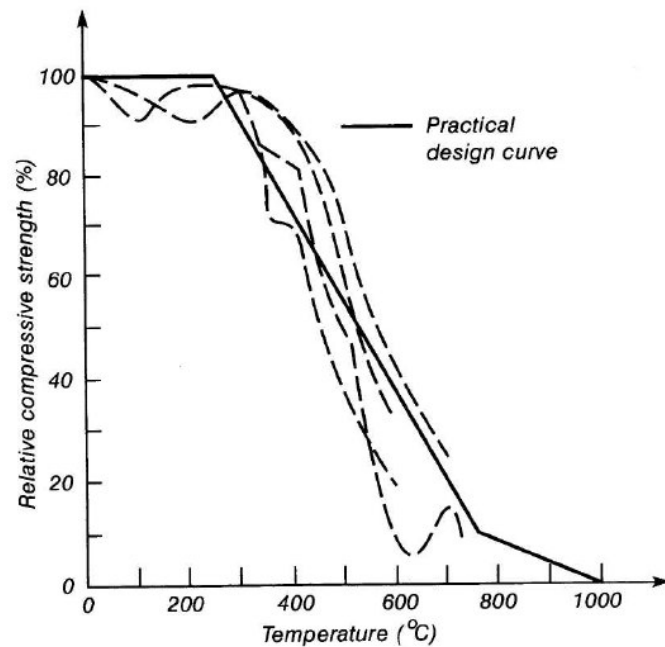


Figure 25- Reduction in compressive strength with temperature (Reproduced from Schneider (1988).)

For the compressive strength at elevated temperatures simple expressions can be used such as expressions 6 and 7 from BS 8110 (BSI, 1985)[29]:

For normal weight concrete :

$$\frac{f_c(T)}{f_c(20^\circ C)} = 1.0 \quad \text{for } T < 350^\circ C \quad (6)$$

$$\frac{f_c(T)}{f_c(20^\circ C)} = (910 - T)/560 \quad \text{for } T > 350^\circ C$$

For light weight concrete :

$$\frac{f_c(T)}{f_c(20^\circ C)} = 1.0 \quad \text{for } T < 500^\circ C \quad (7)$$

$$\frac{f_c(T)}{f_c(20^\circ C)} = (1000 - T)/500 \quad \text{for } T > 500^\circ C$$

These expressions can be seen in the following figure.

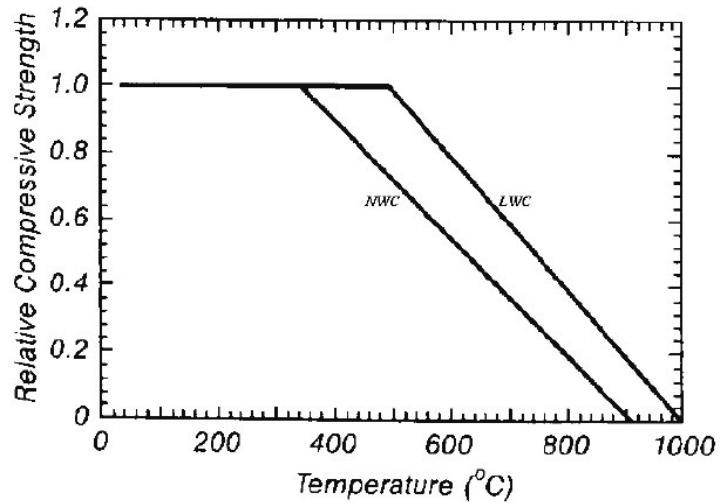


Figure 26 - Design values for reduction of compressive temperature (Reproduced from EC2, 1993).

Alternatively, for more complex simulations, equations in the Eurocodes (EC2, 1993) can be used and as seen in Figure 27.

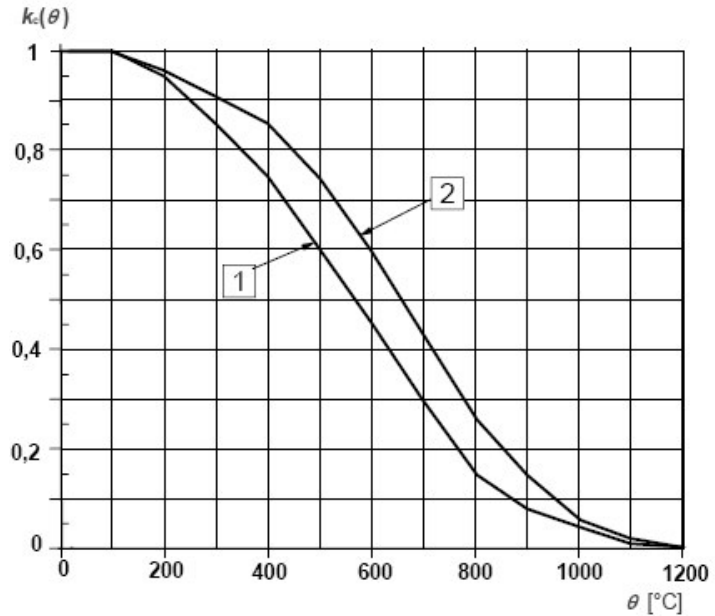


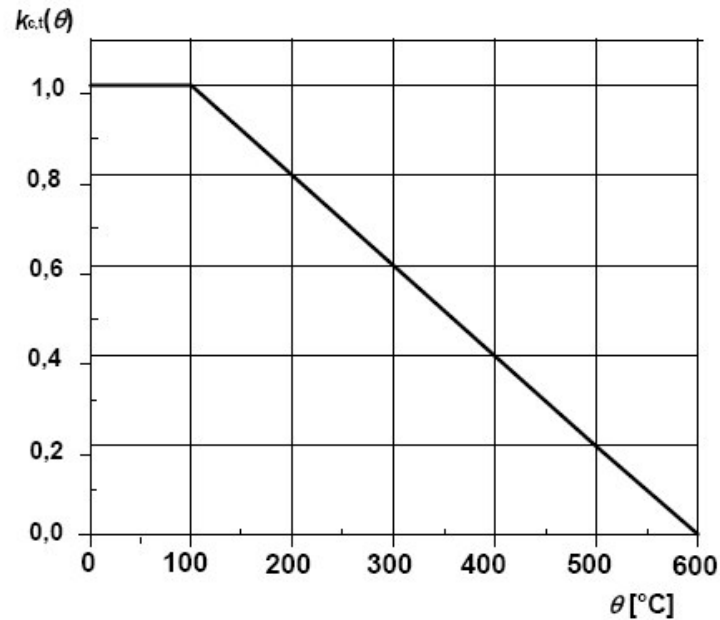
Figure 27 -Relative strength of concrete from ambient conditions. (EC2, 1993)

For design purposes, the tensile strength of concrete can be assumed to be zero. Alternatively, Eurocode 2 and Eurocode 4 give the expressions 8 for tensile strength f_t :

$$\frac{f_t(T)}{f_t(20^\circ C)} = 1.0 \quad 20^\circ C \leq T \leq 100^\circ C \quad (8)$$

$$\frac{f_t(T)}{f_t(20^\circ C)} = 1.0 - 1.0(T - 100)/500 \quad \text{for } 100^\circ C < T \leq 600^\circ C$$

Figure 28 -Relative tensile strength of concrete to ambient strength conditions as a function of temperature.



While EC 2 and EC 4 provide strength reduction factors for concrete tensile capacity, little information is available on the elastic behavior and strain limits.

2.2.2.3.3.2 Modulus of Elasticity

As seen in the stress-strain diagrams in Figure 24-28, the modulus of elasticity also decreases with increasing temperature. The following equations from BS 8110 (1985), provides a simplification of the modulus of elasticity at elevated temperatures:

$$\frac{E(T)}{E(20^{\circ}C)} = 1.0 \quad \text{for } T \leq 150^{\circ}C \quad (9)$$

$$\frac{E(T)}{E(20^{\circ}C)} = (700 - T)/550 \quad \text{for } T > 150^{\circ}C$$

This simplification can be applied to lightweight, normal weight, and high strength concretes. More complex expressions are available in Eurocode 2, 2005. As seen Figure 29 from Buchanan [13], the modulus of elasticity reaches zero before the strength of concrete reaches zero. Due to this disconnect, Inwood (1999) has proposed an extension (which appears in the dotted line) [30].

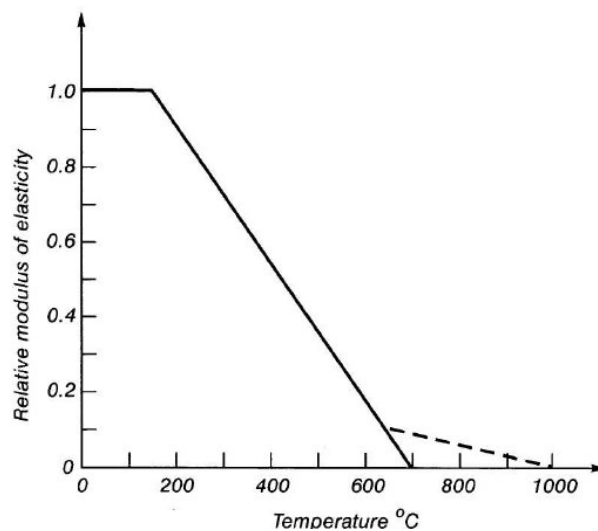


Figure 29 - Design values for reduction of modulus of elasticity with temperature. (Reproduced from Buchanan)

2.3 Thermo-Mechanical Response

In recent years, a great deal of research has been conducted to understand the mechanics of global structural behavior under fire conditions. This research strongly indicates that material degradation has less of a role than the thermally induced mechanical forces from boundary conditions that occur in a structure under fire conditions. As mentioned earlier, Usmani, et al. [16] have laid the ground work for the most fundamental principles that govern the response of structures in fire. The

most basic of these principles is:

$$\varepsilon_{total} = \varepsilon_{thermal} + \varepsilon_{mechanical} \quad (10)$$

where, ε_{total} is the total strain that governs the deformed shape of the structure,
 $\varepsilon_{mechanical}$ is the strain related to the stress state, and
 $\varepsilon_{thermal}$ is the strain caused by thermal exposure

So, when a structural element is thermally unrestrained with no externally applied mechanical loads, the total strain on the structure is only a function of the thermal strain. That is,

$$\varepsilon_{total} = \varepsilon_{thermal} \quad (11)$$

In this case the axial expansion or thermal curvature (“bowing”) only depends on the thermal strains. On the other hand, when a structural element is fully restrained with no externally applied mechanical loads, the basic equation appears as:

$$0 = \varepsilon_{thermal} + \varepsilon_{mechanical} \quad (12)$$

where, $\varepsilon_{thermal}$ are the strains caused by thermal loads, and
 $\varepsilon_{mechanical}$ are the mechanical induced strains caused
when thermal elongation is inhibited by
the fully restrained boundary conditions

As indicated by the above equations and suggested by Usmani et al [16], the most critical factor in the real response of a structure to heating is the manner in which it responds to the thermal strains induced during fire conditions. These thermal strains can produce thermal expansion leading to the elongation of the structural element (under an average centrodial temperature rise), and/or a thermal curvature in which

the hotter lower surfaces expand more than the cooler upper surfaces (under a thermal gradient through the section depth) that leads to “thermal bowing” and may lead to large displacements. Depending on the element boundary conditions, the structure may undergo any number of responses – expansive displacements, thermal curvature, and/or a combination of both – all of which can lead to large lateral and/or axial displacements and increased stress states. These structural responses, as mentioned before, are highly dependent upon the element boundary conditions and the element’s cross-sectional thermal state. Therefore, different structural responses can be expected given certain end restraints and cross-sectional thermal profiles. The following sections will develop these concepts in greater detail.

2.3.1 Pure Thermal expansion

For most structural materials, when a uniform temperature rise is applied to a material a thermal expansion strain, ε_T , is induced. This strain is given by:

$$\varepsilon_T = \alpha \Delta T \quad (13)$$

2.3.1.1 Thermal expansion with no axial restraint

If the uniform temperature rise, ΔT , is applied to a simply supported beam along its length, L , with no axial restraint, the beam will expand axially, as illustrated in Figure 30. This axial expansion, ΔL , is given by:

$$\Delta L = L \alpha \Delta T \quad (14)$$

where α is the coefficient of thermal expansion for the material and ΔT is the temperature rise above ambient.

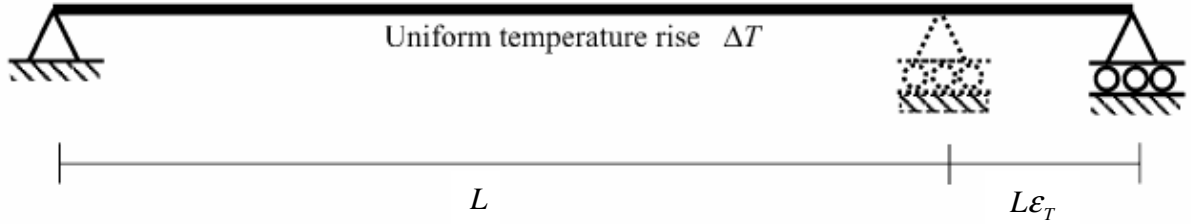


Figure 30 - Thermal expansion of simply supported beam with no axial restraint.

Therefore the total strain is equal to the thermal strain, $\epsilon_{total} = \epsilon_{thermal}$, which indicates that the element has a zero stress state. Note: Only mechanical strains can produce stresses.

2.3.1.2 Thermal expansion against rigid lateral restraint

In most structural applications, beams are laterally restrained and not free to elongate. In this case, when a laterally restrained beam is heated uniformly along its length, the total strain is equal to zero, as indicated by Equation 12. Due to the restrained end conditions, the thermally induced strain, $\epsilon_{thermal}$, is counter-acted by an equal and opposite mechanical strain $\epsilon_{mechanical}$ such that $\epsilon_{thermal} = -\epsilon_{mechanical}$. Unlike the prior example, the beam is unable to expand freely inducing a uniform mechanical strain, ϵ_{mech} , resulting in

an axial stress equal to $E\epsilon_{mech}$. This stress is associated with a compressive force, P , as seen in Figure 31, with a magnitude given by:

$$P = EA\epsilon_{mechanical} = -EA\epsilon_{thermal} = -EA\alpha\Delta T \quad (15)$$

where, E is the modulus of elasticity and A is the cross-sectional area of the beam. See Section 2.2 for material properties as a function of temperature.

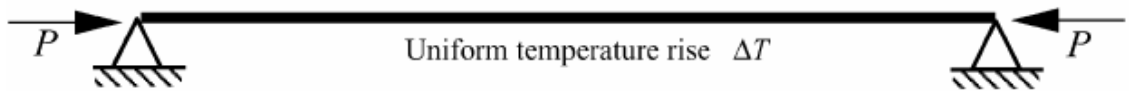


Figure 31 - Compressive force P arising in a rigidly restrained beam.

This compressive force, if large enough, can lead to structural failure of the element, either by yielding of the cross-section or buckling. As in ambient structural analysis, these failure thresholds are dependent upon the slenderness of the beam or element.

1. For relatively slender beams, the elastic limit state will typically be yielding of the member before buckling. The time at which yielding occurs can be determined by calculating the stress state of the section and comparing it with the yield stress of the material. The stress state is determined by : $\sigma = E\alpha\Delta T$ (16)

Or more precisely, with the inclusion of material degradation as a function of temperature:

$$\sigma = E(T)\alpha(T)\Delta T \quad (17)$$

This stress state can then be compared with the yield stress of the material with temperature degradation considered.

2. For stocky beams, the elastic limit state will typically be buckling before yielding. The critical Euler buckling load for a beam or column as in Figure 31 is:

$$P_{cr} = \frac{-\pi^2 E(T)I}{L^2} \quad (18)$$

where the elastic modulus changes as a function of temperature. This equation can be equated to the restraining force P as described in equation 15 $-(EA\alpha\Delta T)$. This expression is valid for other end-restraint conditions provided L is considered as the effective length of the structural member.

If the critical buckling load is reached in a beam element and the temperature further rises, the total restraining force will remain constant provided the material is elastic and there is no material degradation.

As the temperature rises, the thermal strains increase and the beam deflects further as in Figure 32.

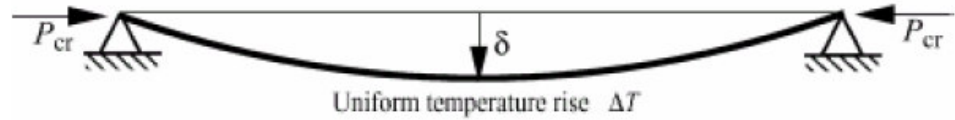


Figure 32 -Buckling of an axially restrained beam subjected to uniform heating.

In purely elastic slender restrained beams, a pre-buckling and post-buckling response can be seen in the axial load, deflection and moment time histories. Figures 33 and 34, reproduced from Rotter et al [31], illustrate this pre-buckling/post-buckling behavior in the deflection, axial force and moment time histories. In these figures a uniformly distributed load is imposed on a beam, which results in an initial displacement and increasing axial force. Once buckling occurs, the midspan moment continues to rise consisting mostly of $P\text{-}\delta$ moment produced by the axial restraint force times the midspan deflection.

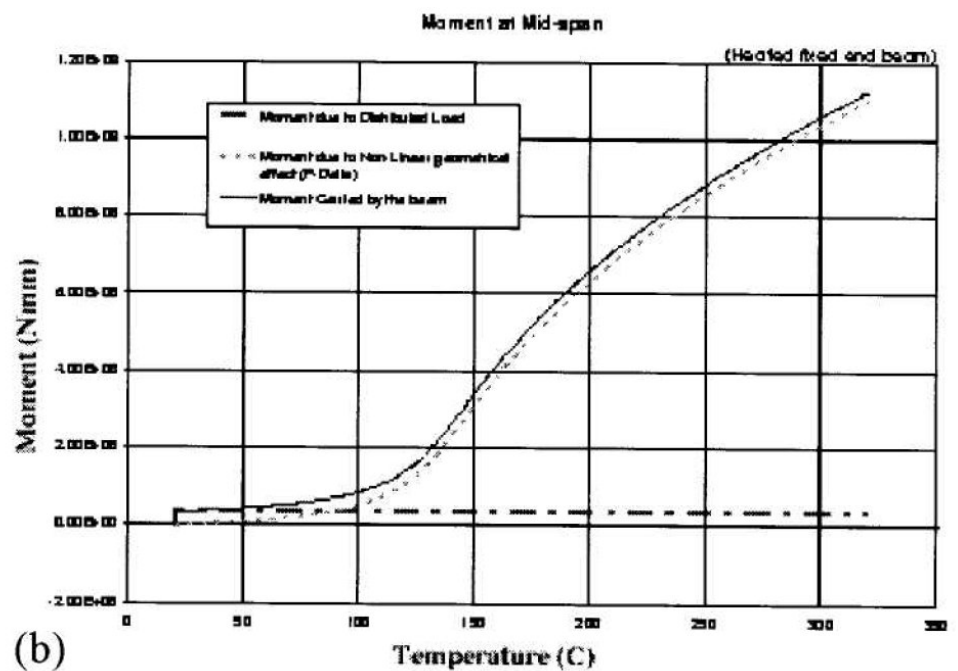
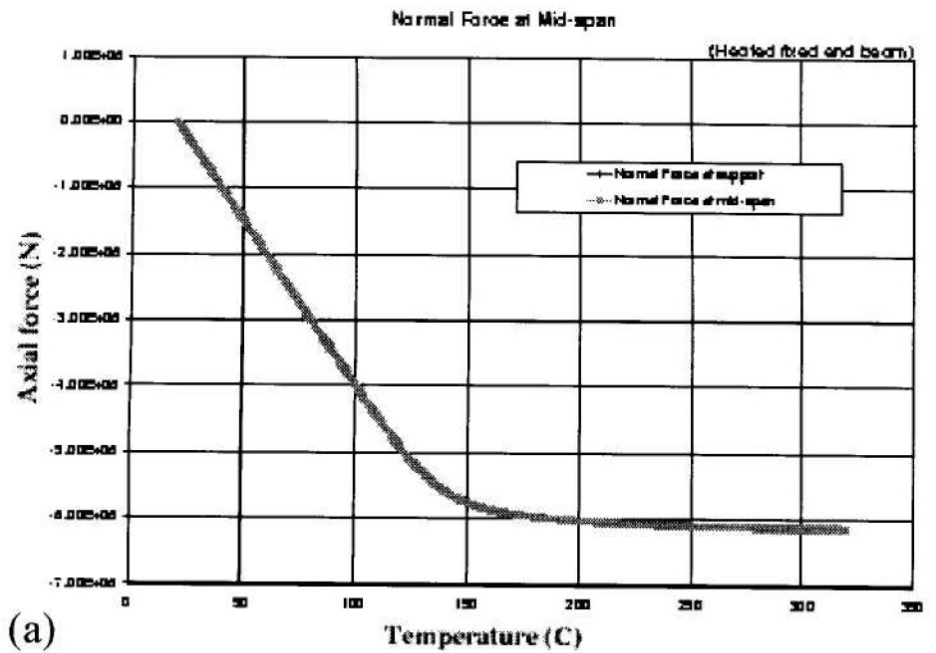


Figure 34 - Forces in an axially restrained elastic beam subjected to heating: (top) axial forces, and (bottom) moments. (Reproduced from Usmani 2001).

If the beam is elastic perfectly plastic, then the deflections and axial force vary as in Figure 35 and Figure 36. If the properties are elastic but undergo uniform temperature degradation, then the element behaves as in Figure 37 and Figure 38. Ultimately, from these figures the real response of composite beams subjected to restrained thermal expansion will be a combination of the response presented here. This behavior can be seen in Sanad et al [32]. As can be seen in the figures above, the reduction in stiffness of the material properties by heating reduces the magnitude of the axial compression force in restrained beam elements. When the material reaches its yield value, there is a more rapid reduction in the restraining force with a corresponding rise in deflections due to $P-\delta$.

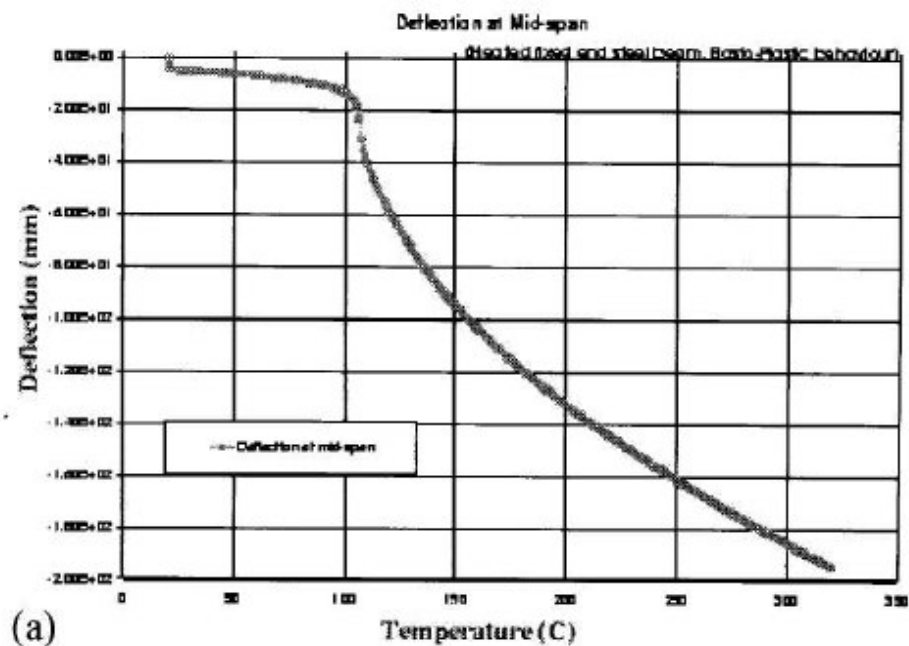


Figure 35 - Deflections in an axially restrained elastic-plastic beam. Reproduced from Usmani 2001).

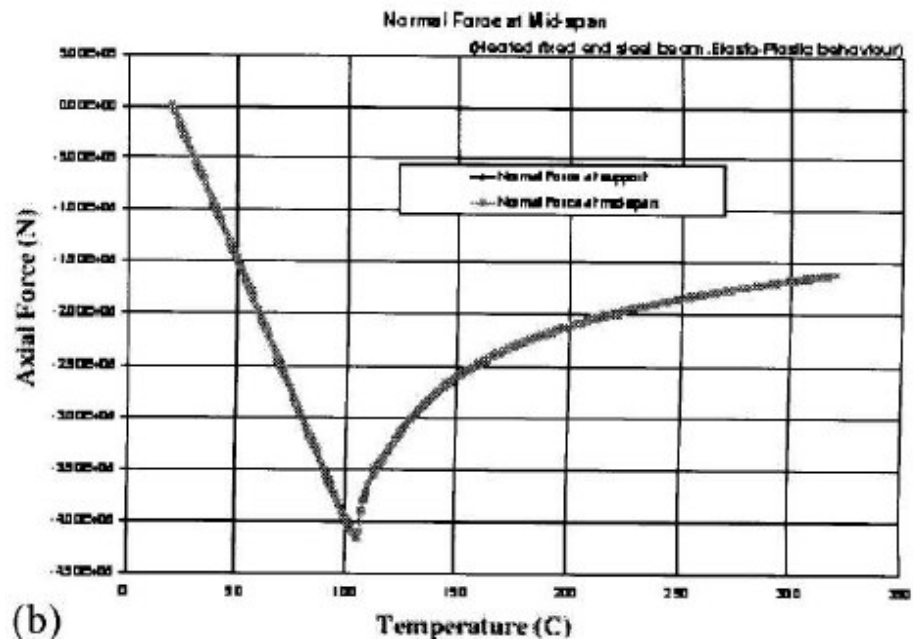


Figure 36 - Axial forces in an axially restrained elastic-plastic beam. Reproduced from Usmani 2001).

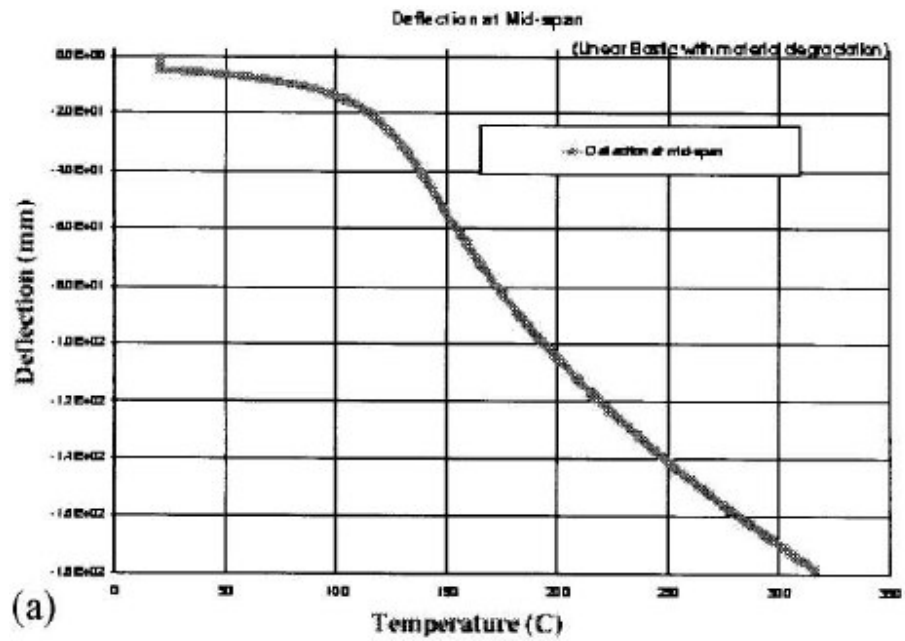


Figure 37 - Deflections in a restrained beam with reducing elastic stiffness. (Reproduced from Usmani 2001).

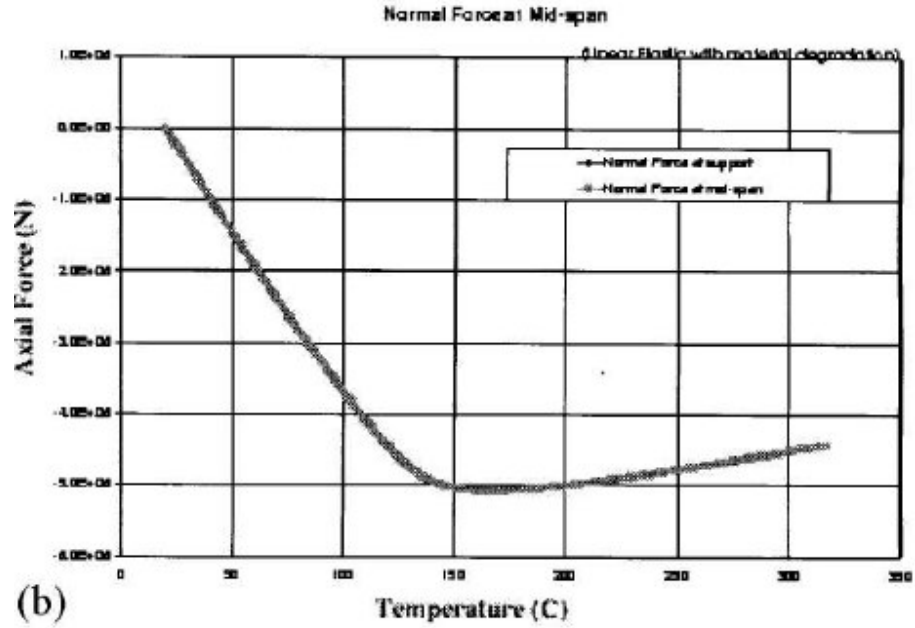


Figure 38 - Axial forces in a restrained beam with reducing elastic stiffness. (Reproduced from Usmani 2001).

2.3.1.3 Thermal expansion against finite lateral restraint

In realistic structures perfectly rigid end conditions do not exist. A partial restrained beam can be represented by a translational spring stiffness k_t . The compressive axial stress developed by thermal expansion is then expressed by:

$$\sigma_T = \frac{E\alpha\Delta T}{a + \frac{EA}{k_t L}} \quad (19)$$

And the critical buckling temperature is now given by:

$$\Delta T_{cr} = \frac{\pi^2}{\alpha\lambda^2} \left(1 + \frac{EA}{k_t L} \right) \quad (20)$$

From equation (11) it can be seen that in structures with translational restraint of stiffnesses (k_t) comparable to the axial stiffness of the member (EA/L), the buckling and post-buckling phenomena should occur at moderate fire temperatures. Figure 40 illustrates the critical buckling temperature plotted against element slenderness ratios with restraint stiffness varying from $\frac{EA}{L}$ (stiffness comparable to axial stiffness) to ∞ (infinitely rigid supports). From the results it is clear that for slender elements the effect of end restraint on buckling is less critical, however, the likelihood of buckling in these elements is very likely in typical fires where temperatures can easily exceed 100°C and the axial stiffness reduces due to heating.

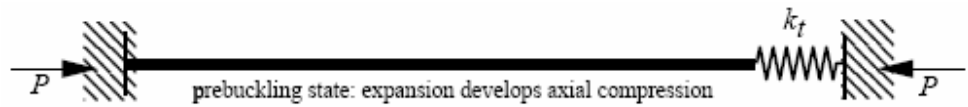


Figure 39 - Heating of beam with finite axial restraint. (Reproduced from Usmani 2001).

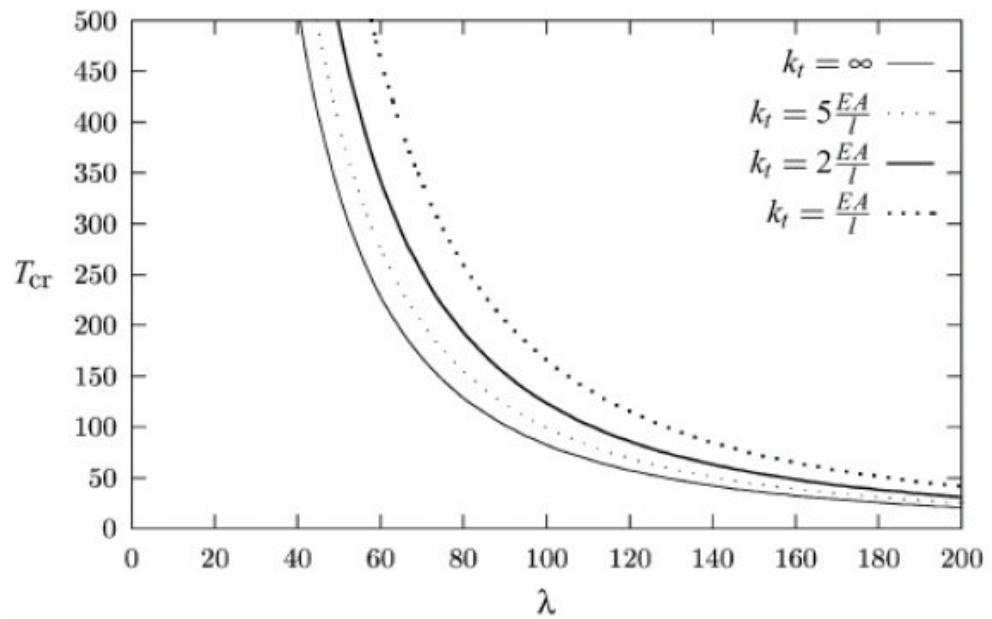


Figure 40 -Buckling temperatures for thermal expansion against finite lateral restraint. (Usmani 2001)

2.3.2 Pure Thermal bowing

In realistic fire scenarios and building geometries, structural elements do not typically experience a uniform temperature rise. The temperature distribution within the structural elements is contingent on several factors, some of which include: material properties, geometry, construction and design (i.e. insulation). For example, concrete beams/slabs and masonry walls can be subjected to very high temperature gradients due to their low conductivities. This thermal characteristic causes the exposed surfaces to be at a much greater temperature than the surfaces on the unexposed side of the compartment. The hotter inner surfaces, ultimately, expand more than the cooler outer surfaces, and is called *thermal bowing*.

This effect is one of the main causes of deformations in concrete and masonry structures and can play a more significant role in composite building

construction, where large temperatures differences can occur due to the varying materials used in the composite system. In composite beams/slabs assemblies, the differences in temperatures of the steel joist and the slab can lead to significant thermal bowing particularly in the early stages of the fire where the steel retains most of it strength.

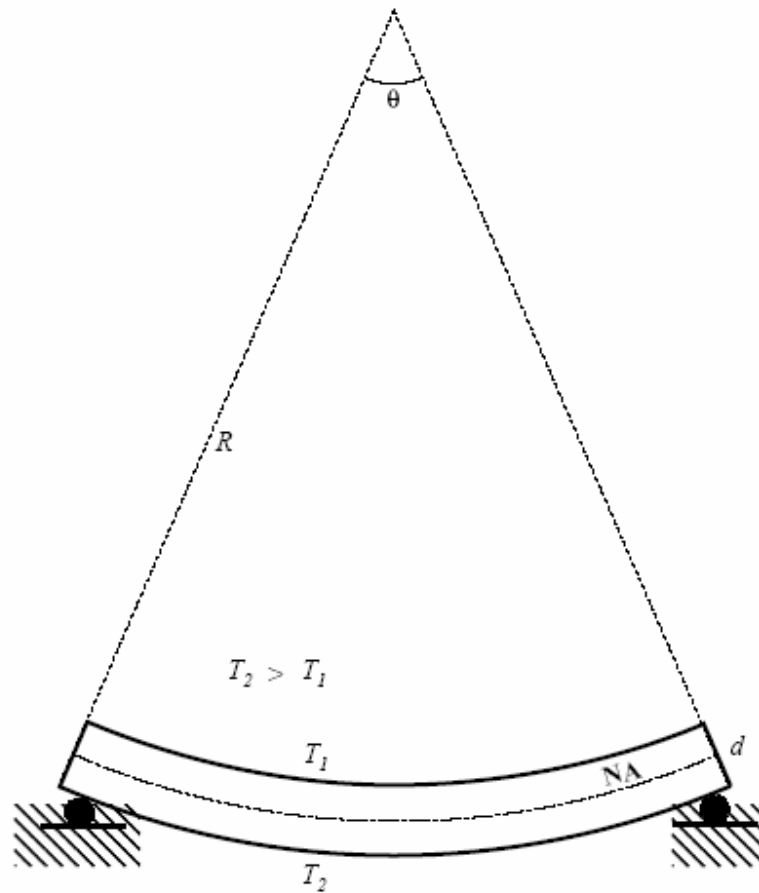


Figure 41 - Simply supported beam subjected to uniform thermal gradient

2.3.2.1 Thermal bowing in simply supported beam (no rotational restraint)

As noted by Usmani et al [16], relationships can be derived for thermal bowing. Figure 41 illustrates a beam subjected to a uniform temperature gradient through its depth (d) along its whole length (L).

Assuming simply supported end conditions, the following relationships can be derived:

1. Assuming a linear temperature distribution, the thermal gradient ($T_{,y}$) over the depth can be described as:

$$T_{,y} = \frac{T_2 - T_1}{d} \quad (21)$$

2. Assuming a linear temperature profile through the depth of the section, the new lengths of the top and bottom can be described in terms of a constant thermal expansion and angle of curvature, as follows:

$$\begin{aligned} L_1 &= R\theta = L_o + \alpha(T_1 - T_o) \\ L_2 &= (R + d)\theta = L_o + \alpha(T_2 - T_o) \end{aligned} \quad (22)$$

where, L_o is the original length of the element, T_o is the original temperature, R is the radius of curvature, θ is the arc angle of the beam and α is the coefficient of thermal expansion. By evaluating the difference in the two lengths, the angle of curvature can be described as:

$$\begin{aligned} L_2 - L_1 &= d \cdot \theta = \alpha(T_2 - T_1) \\ \theta &= \frac{\alpha(T_2 - T_1)}{d} = \alpha T_{,y} \end{aligned} \quad (23)$$

3. Due to this curvature, the horizontal distance between the ends of the beam will reduce. If this reduction is interpreted as a contraction strain, ε_θ , then the value of the strain can be determined as follows:

$$\varepsilon_\theta = 1 - \frac{\sin\left(\frac{L\theta}{2}\right)}{\left(\frac{L\theta}{2}\right)} \quad (24)$$

2.3.2.2 Thermal bowing in laterally and/or rotationally restrained beams

In the case of a laterally restrained beam, a uniform thermal gradient $T_{,y}$ will result in a thermally induced tensile force at the supports (Figure 42), as opposed to, a compressive force in the case of a uniform temperature rise on the same beam (Figure 31).. This effect is a result of the restrained end conditions against the contraction strain (ε_θ) induced by the thermal gradient.

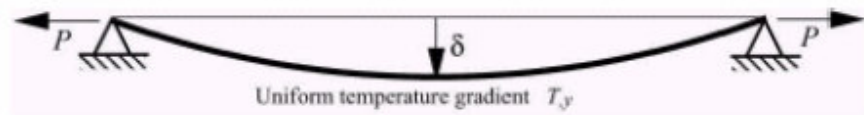


Figure 42 -Laterally restrained beam subjected to a uniform thermal gradient

For a fixed end beam subjected to a uniform temperature gradient, the uniform thermal curvature $\theta = \alpha T_{,y}$ described for the simply supported beam, will now be counteracted by the support moments. In this case, the fixed end beam remains 'straight' with a constant moment of $M = EI \phi$ along its length.

Ultimately, the effect of boundary conditions is critical in determining the response of a structural member to thermal actions. If a structural member is unrestrained, then the thermal strains will be manifested as displacements; if the member is restrained by end conditions, then the thermal strains will result in stresses.

2.3.2.3 Thermal bowing in finite lateral restraint

As discussed earlier for laterally restrained systems, perfect rotational restraint is not realistic or easily achievable in typical building construction. Figure 43 illustrates a beam that is rotationally restrained by rotational springs of stiffness k_r . In this case, the restraining moment in the springs, as described by Usmani et al, as a result of a uniform thermal gradient can be found to be:

$$M_k = \frac{EI\alpha T_{,y}}{\left(1 + \frac{2EI}{k_r L}\right)} \quad (25)$$

This equation suggests that if the rotational restraint stiffness is equal to the rotational stiffness of the beam (EI/L) then the moment it attracts will be about a third of a fixed support moment.

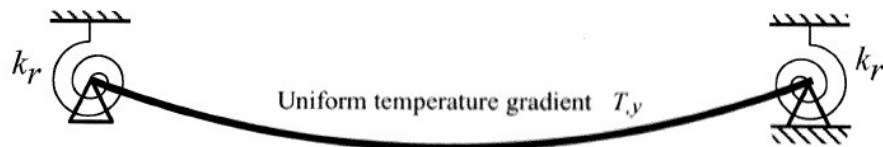


Figure 43 - Beam with finite rotational restraint with a uniform thermal gradient. (Usmani 2001).

2.3.3 Deflections

One of the most compelling aspects of structural fire response is the large deflections that the structure undergoes as it is heated. Under ambient conditions, large deflections are typically associated with the loss of strength or stiffness. However, in the case of fire, the relation between section state and deflections is not so simple. While thermal expansion and thermal bowing result in large deflections, the element's stress states subjected to varying degrees of these two mechanisms is not unique for a given deflection. In addition, there are a large range of stress states that can exist depending on the temperature distribution, material properties and restraint conditions [16].

In typical construction where structural members are restrained from elongating, the main cause of large deflections under fire conditions is due to the structure attempting to accommodate the additional length generated by thermal expansion.

2.3.3.1 Simply supported beams with uniform temperature profile

For slender beams with a uniform temperature profile and restrained against lateral translation (Figure 32), the deflection can be approximated by:

$$\delta = \frac{2L}{\pi} \sqrt{\epsilon_{tot} + \frac{\epsilon_{tot}^2}{2}} \quad (26)$$

This approximation, as presented by Usmani et al [16], uses the sine curve of length $L(1+\epsilon_{tot})$ where the total strain of the system (ϵ_{tot}), is only comprised of thermal axial strain caused by thermal expansion ($\epsilon_a = \alpha\Delta T$).

2.3.3.2 Simply supported beams with uniform thermal gradient

For simply supported slender beams under a uniform thermal gradient, the deflection tends to be limited by the tensile P- δ effects that restrain the curvature imposed by the thermal gradient. Structural response is ultimately determined by the axial-bending (P-M) interaction of the element. In this case, the same approximation used above for deflection can be used; however, the total strain on the system (ϵ_{tot}) is now comprised of axial strain from thermal expansion ($\epsilon_a = \alpha\Delta T$) and strain from thermal bowing ($-\kappa_z y$). That is for 2-D analysis:

$$\epsilon_{tot} = \epsilon_a - \kappa_z y \quad (27)$$

In fire scenarios, the total strain tends to be dominated by the strain from thermal curvature causing a tensile force on the member. This total strain is related to force by:

$$\epsilon_{tot} = \frac{P}{EA} \quad (28)$$

After determining the deflection of the system using the sine curve approximation, the tensile force can then be determined from equation 2:

$$P_t = \left(\sqrt{\frac{1}{2} \left(\frac{\pi \delta}{L} \right)^2} + 1 - 1 \right) EA \quad (29)$$

Alternatively, the deflection can be determined using Euler-Bernoulli beam theory. For simply supported beams with no axial restraint and subjected to a uniform curvature (ϕ), deflection is as follows:

$$\frac{d^2 y}{dx^2} = \phi \quad (30)$$

For simply supported beams with lateral restraint, the deflection equation will be the same except with the addition of the tensile force causing a moment P_y over the length of the beam:

$$\frac{d^2 y}{dx^2} = \phi - \frac{P_y}{EI} \quad (31)$$

The solution to this equation, as presented by Usmani et al [16], is:

$$y(x) = -\frac{\phi}{k^2} \left(\frac{\cosh kl - 1}{\sinh kl} \sinh kx - \cosh kx + 1 \right) \quad (32)$$

2.3.4 Combinations of thermal expansion and thermal bowing

In previous sections, thermal elongation and thermal bowing were discussed in isolation. However, in realistic structures, a combination of these mechanisms will exist. For composite frame structures, the composite action of the steel joists, framing into an interior column, with a continuous slab,

produces conditions similar to a fully fixed system as shown in Figure 44. In this case, the beam is restrained both in rotation and translation.

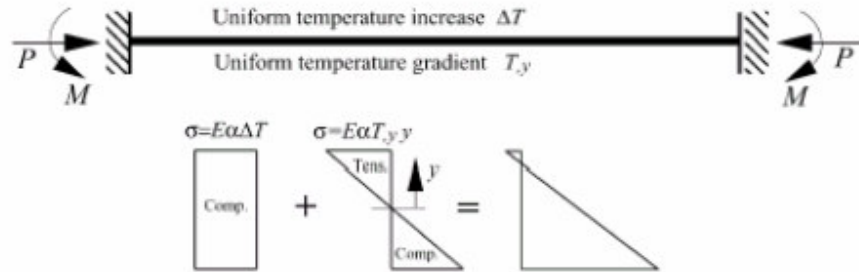


Figure 44 - Combined thermal expansion and bowing in a fully fixed beam. (Usmani, 2001).

If this type of beam is subjected to a mean temperature rise and a through depth thermal gradient, then the beam will experience a uniform compressive force due to the restrained thermal expansion, and a uniform moment as a result of the thermal gradient. As seen, in Figure 44, the bottom of the beam will experience high compressive forces while the top of the beam can experience anywhere from significant compressive forces to significant tensile forces.

The scenario described above was witnessed in the Cardington [33] tests and other fires [14]. Due to the high compressive forces in the bottom of the beam, local buckling of the bottom flanges occurred early in the fires. This inevitably changed the end restraints from fully-fixed to pinned which was indicated by the change in stresses at the ends of the beams. This resulted in the relief of the negative moment by the newly formed hinges leading to large rotations at the supports coupled with large deflections at midspan. Because this behavior tends to happen early in the fire, Usmani et al. [16] suggest that

composite beams under fire loading behave similar to simply supported beams with lateral restraint.

Due to local buckling phenomena of the bottom flange, the following section will discuss the combination of thermal expansion and thermal bowing with regards to laterally restrained beams – the system that dominates structural behavior in composite structures.

2.3.4.1 Combination of thermal expansion and thermal bowing – lateral restrained beams

As discussed in previous sections, two opposite stress regimes can occur depending on the thermal regime applied; that is, thermal expansion can lead to compressive forces, where as, bowing results in tensile forces. The main parameter governing these stress states are the average temperature rise (ΔT) and an average equivalent thermal gradient ($T_{,y}$). A procedure for determining these parameters in beams is given by Usmani [16]

In a study conducted by Usmani et al [16], the effective strain (ϵ_{eff}) of a beam element for different values of thermal gradient was plotted against the mean temperature as it increased from 0°C to 400°C. Figure 45 illustrates the results from this study, in which the effective strain is the strain state of the element considering strains from both thermal expansion (which produces positive strain) and

thermal bowing (which produces negative strain) in laterally restrained beams. This effective strain is calculated as follows:

$$\varepsilon_{eff} = \varepsilon_T - \varepsilon_\phi \quad (33)$$

where, ε_T is the thermal expansion strain; and
 ε_ϕ is the thermal bowing strain;

As seen in the Figure, even at a low thermal gradient of 5°C/mm the effect of thermal bowing appears to dominate the behavior of the beam element early in the fire. This thermal gradient is low for realistic fire scenarios in which the thermal gradients tend to be greater, as seen in the 2-D analysis conducted on a concrete slab in this report. Steel, on the other hand, has a high thermal conductivity and typically had thermal expansion dominating the response.

Figure 46 is a summary of the main types of deflection responses in laterally restrained beams exposed to fire conditions with varying degrees of thermal expansion and thermal bowing. For example,

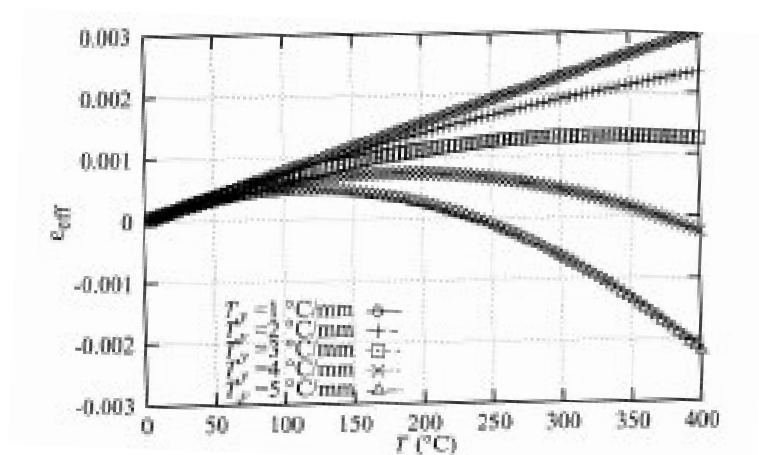


Figure 45 - Effective expansion strains (Reproduced from Usmani [16])

when there is only thermal expansion (ϵ_T), the beam undergoes distinct pre-/post-buckling regions and has the lowest deflection response. If the beam is dominated by thermal bowing strains (ϵ_ϕ), then the structural response history of the beam will be dominated by tensile forces and large displacements. See Reference [16] for more details.

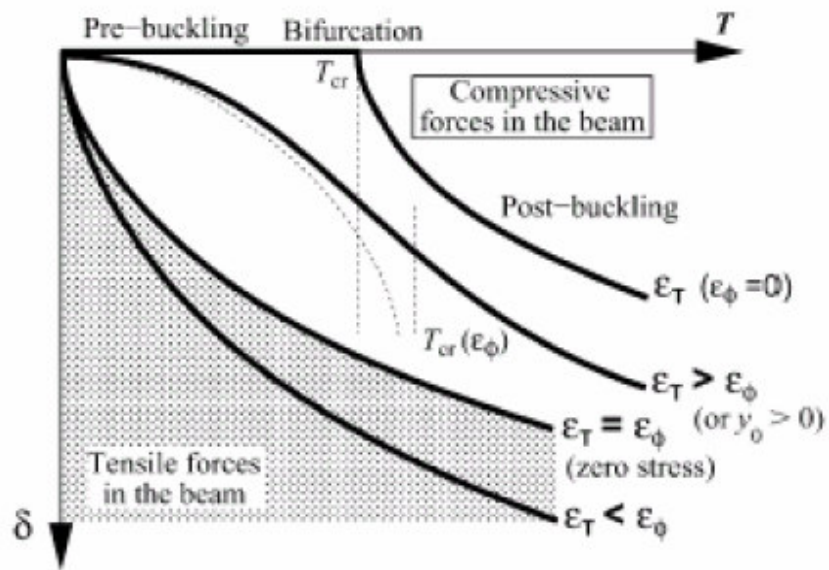


Figure 46 - Temperature deflection responses for combinations of ϵ_T and ϵ_ϕ (Usmani, 2001)

In the above sections, the effects of the relative axial and flexural stiffnesses of the beams are not explicitly considered. The actual response of the beam, as in ambient conditions, is highly dependent upon the relative values of axial and flexural stiffness of the beam. A slender beam has low flexural stiffness and cannot overcome the tensile axial stiffness and develop curvature as much as a stocky

beam. Therefore, bowing deflection will be much lower in slender beams than in stocky composite beams.

2.3.5 Membrane action

In a number of investigations and studies [16],[34-37] composite structures exposed to real fires experienced no collapse or failure. This behavior can largely be attributed to the compressive and tensile membrane action of concrete slabs, which can ultimately prolong the structural stability of a building during fire events.

While composite members in steel framed buildings are designed for flexure, they have considerably more load-carrying capacity due to the “arching” or compressive membrane action of the concrete decks that are laterally restrained. This additional capacity can be as much as 2 to 10 times that predicted by the yield line theory [35]. However, what is interesting to note is that these slabs do not have to be fully restrained in order to develop membrane forces. As indicated by Guice [37], restraint against lateral movement is sufficient to develop tensile stresses with large deflections in reinforced concrete slabs.

While lateral restraint alone can increase load bearing capacity of concrete slabs, the substantial increases in capacity are typically seen with restraint in both translation and rotation.[36]

Chapter 3: Methodology – Cellular Beam Study

3.1 Overview

As mentioned in Chapter 1, the primary goal of this study is to develop an understanding of the global behavior of long span cellular beams under fire conditions and to appreciate the controlling mechanisms that lead to local failure and possibly runaway failure. Using the finite element software, ABAQUS, this study will investigate the sensitivity of varying cellular beam characteristics (i.e. web post size, hole diameter, end post size, span, number of holes, etc.), varying compartment temperatures, and varying temperature profiles with respect to global response. Achieving the primary goal consisted of a three step process:

- Evaluation of the expected fire exposure conditions (i.e., gas temperatures) to which structural elements are subjected as a function of time;
- Evaluation of the thermal response of protection materials and structural elements to the fire exposure conditions;
- Analysis of the structural response of the structure to the thermal conditions developing in the structural elements.

3.2 Solver Used

An ABAQUS implicit solver was used for all model runs [8]. The ABAQUS standard Newton-Raphson implicit solver was used to capture the global response of each cellular beam simulation. As with any finite element analysis, the choice between using the implicit and explicit solver is dependent upon the problem and the efficiency in which the problem can be solved. Due to the small size of the

proposed model, the implicit solver was chosen due to its efficiency in computation costs (i.e. time), despite the convergence problems from contact and/or material complexities. Where time permitted, the explicit solver was used to determine additional post-buckling behavior, large displacement behavior and failure mechanisms. The explicit solver was not used as the main ABAQUS solver due to the computational costs (i.e. time). For the basic structural system described in the proceeding section (and later referred to as the “base” model), the explicit solver was necessary particularly to capture the complete behavior of the system for the duration of the simulation.

The results obtained from the implicit analysis matched the explicit analysis up until the point that the implicit model was stopped; therefore, the use of the explicit solver is proposed to be reasonable, and will not be discussed any further here.

3.3 Model Background

The structural system modeled in this study consisted of a single, interior bay incorporating one long span cellular beam (18m), two supporting columns, 2 edge beams (5m), 2 half-bay cellular beams (9m) and a corresponding 5 m wide concrete slab that was continuous over the supports (See Figure 47).

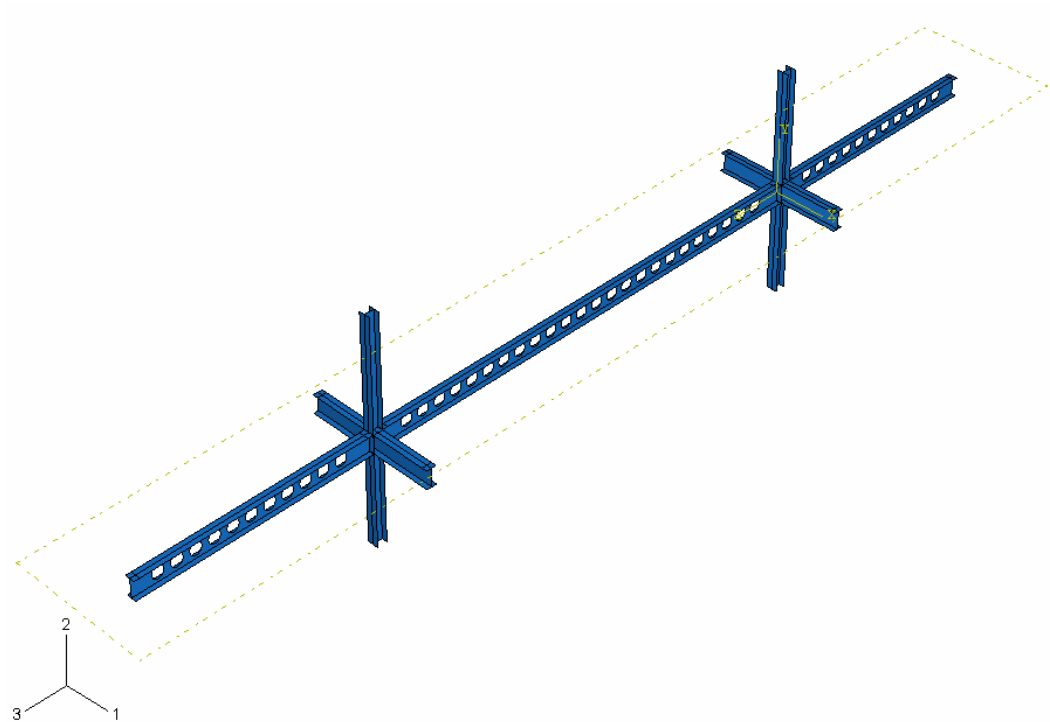


Figure 47 - Structural model rendered in ABAQUS (slab is removed for clarity)

This model included as much of a realistic long span structure while small enough to run in a reasonable time, allowing for a detailed parametric study. In addition, the focus of the study is on the structural performance of the cellular beam, and so, the supporting frame elements are intended to provide a realistic environment where continuity, load transfer, support conditions, heat transfer, and restraint contribute to the performance of the beam. Future work could include different support conditions (i.e. exterior bay or corner bay) for a more detailed analysis.

3.4 Fire and Heat Transfer Models

3.4.1 Analysis Fire Models

Due to the limited fire test data available for cellular beams, particularly in long span applications, a more generalized approach was used for the analysis fire models. For a preliminary study, the heating phase of the fire

was only considered. Given this constraint, several heating conditions were created for this analysis based on two general fire curves: the standard fire (ISO 834) [3] and a generalized exponential curve. The ISO 834 curve is represented as follows:

$$T(t) = 345 \log \left(8 \cdot \frac{t}{60} + 1 \right) + T_o \quad (34)$$

The generalized exponential curve suggested by Usmani et al [38] is given by:

$$T(t) = T_o + (T_{\max} - T_o)(1 - e^{-\alpha t}) \quad (35)$$

where, T_{\max} is the maximum compartment temperature, T_o is the initial or ambient temperature, α is an arbitrary ‘rate of heating’ parameter and t represents the time over which the model is analyzed. This curve provides a temperature-time relationship representing a post-flashover compartment fire, for input to the heat transfer analysis. In this form, the artificially generated “rate of heating” term coupled with the T_{\max} term is used to provide a sensitivity analysis that can capture an envelope of different fires or different levels of insulation, as indicated by Usmani et al [38]. Figure 48 illustrates how the rate of heating term (α) can be varied to achieve a wide range of fire scenarios. Similarly, the T_{\max} term can be varied to achieve hotter fires.

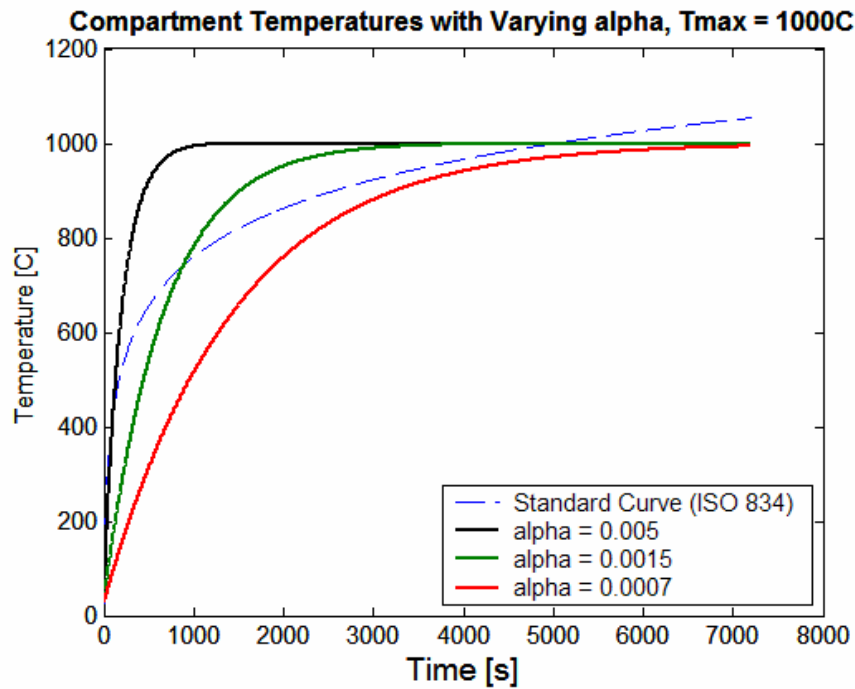


Figure 48 - The generalized exponential time temperature curve is plotted with varying rates of heating against the ISO 834 standard fire curve.

While heat-flux vs. time curves are a more appropriate measure for determining the energy input into the structure, the use of equation (35) is a justified approach for doing a parametric study for a significant range of heat fluxes and rates of change of heat flux. These temperature time curves should not be taken as representations of realistic fires, but just a mechanism to assign in a systematic manner different heating conditions. In this way, numerous fire scenarios can be analyzed without formally resolving the gas phase temperature and solid phase temperature disconnect [38].

Figure 48 illustrates the gas compartment temperatures examined in this study. These compartment time-temperature curves provide a wide range of heating rates and maximum temperature fires. A range of T_{\max} (1200°C, 1000°C, and 800°C) and a range of heating rates (0.005, 0.0015, 0.0007)

were used in this study. The variations of the generalized exponential time temperature curve appear to envelope the standard fire curve, and are therefore assumed reasonable.

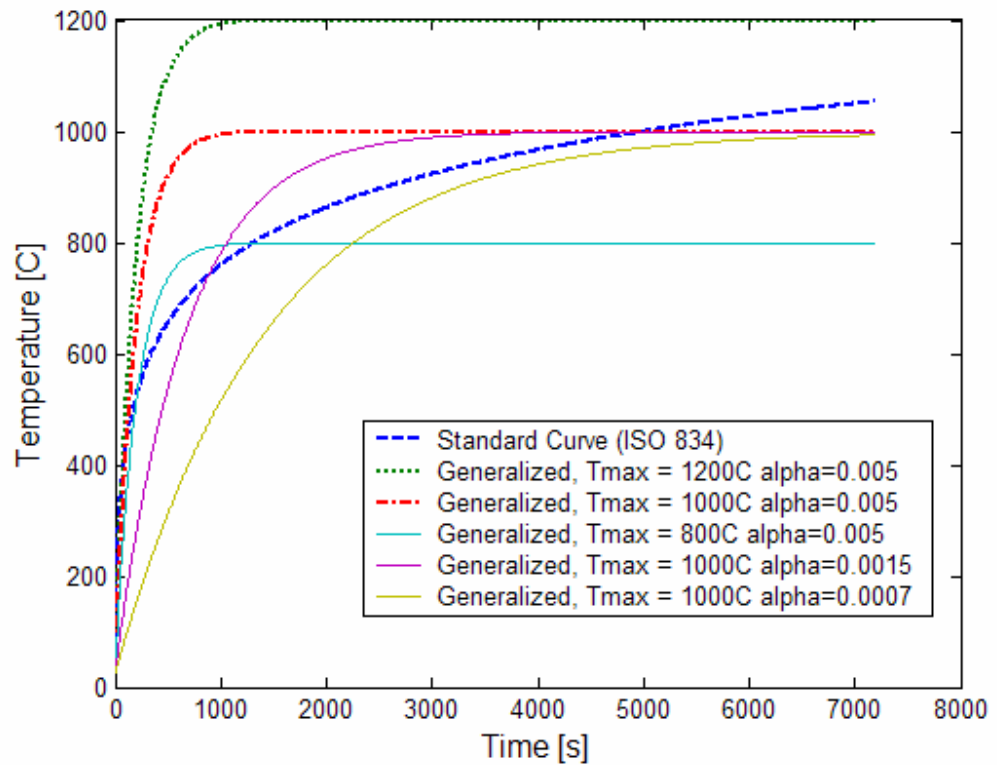


Figure 49 - Examined gas compartment time-temperature curves

3.4.2 Major Assumptions

In this study, a 2-hour fire exposure was assumed in a single structural bay. Therefore, the cellular beam, edge beams and bottom half of the columns were assigned time-temperature curves based on the Eurocode 3 (1995) heat transfer models for protected and unprotected steelwork [9]. For the composite deck, a 1-D heat transfer analysis was conducted for each design fire to determine the temperature profile over the depth of the slab. The remainder of the structure was assigned ambient conditions of 25° C.

Initially, the standard fire and generalized time-temperature curves described earlier were going to be applied to the cellular beam models directly, with minor adjustments to the parameters to capture protected and unprotected time-temperature curves. However, in considering the inclusion of the supporting structural frame and their major role in the performance of the cellular beam, it was decided to use the heat transfer assumptions for protected and unprotected steelwork stipulated in Eurocode 3:1995 [9] to determine solid phase time-temperature curves of the unprotected cellular beam and the protected supporting steel elements.

While the Eurocode 3 heat transfer model may not be entirely valid, separate solid phase time-temperature curves for the cellular beam, in question, and the remaining structure are necessary to ensure that the surrounding structural elements were not the limiting factor in the behavior of the cellular beam, in question. Essentially, assigning the entire structure to a single solid phase time-temperature curve would have biased the structural performance of the cellular beam; and as mentioned previously, the purpose of the supporting frame is to provide realistic boundary conditions. In a later study, a more detailed heat transfer analysis should be conducted and coupled with the structural fire analysis.

In addition, the columns were assumed to be uniformly heated along the length with no thermal gradient across the depth, as would be experienced in a fully developed fire. If the columns were located in an external bay of the structure, a thermal gradient across the depth in addition to a reduced

temperature profile would have been more appropriate. Also, the exposed beam elements were assumed uniformly heated along the length and depth (except in Scenario III) due to the high thermal conductivity of steel. While a thermal gradient is likely to occur across the depth of the steel beams in an actual building fire, this approach has generally been accepted in practice to simplify the analysis and is representative of a mean temperature rise in the structure. The thermal gradient, that occurs in a real building fire, is typically captured by modeling the slab with the actual thermal gradient.

For the structural elements in the system, heat transfer analyses were conducted on the elements separately. So, the bottom of the concrete slab will have a different time-temperature curve than the top of the steel beam. This method of analysis approximates the actual heat transfer that will occur in a building fire, and is the accepted industry approximation for this complex analysis.

3.4.3 Heat Transfer Model for Steelwork

As discussed earlier, the heat transfer model presented in Eurocode 3, 1995 [9] was used to determine the solid phase time temperature curves for the “unprotected” cellular beam and the “protected” supporting elements from the design curves described above. The assumptions made by Eurocode 3 are not discussed in this paper; however, the equations used to determine the relative time temperature curves for the cellular beam and surrounding elements are reproduced below for convenience.

Both the standard fire curve (ISO 834) and generalized exponential curves in Figure 48 were used to calculate the solid phase temperatures of the protected and unprotected steel members using Equation 4.21 and 4.22 of Eurocode 3 Part 1-2, respectively. These equations are reproduced below, for reference. See Appendix for details.

Unprotected steel:

$$\text{Equation 4.21: } \Delta\theta_{a,t} = \frac{\frac{A_p}{V}}{c_a \cdot \rho_a} \cdot q_{\text{net}3} \cdot \Delta t \quad (36)$$

Protected steel:

$$\text{Equation 4.22: } \Delta\theta_{a,t} = \frac{\lambda_p \cdot \frac{A_p}{V}}{d_p \cdot c_a \cdot \rho_a} \cdot \frac{(\theta_{g,t} - \theta_{a,t})}{\left(1 + \frac{\phi}{3}\right)} \cdot \Delta t - \left(e^{\frac{\phi}{10}} - 1\right) \cdot \Delta\theta_{g,t} \quad (37)$$

$$\text{with } \phi = \frac{c_p \cdot \rho_p}{c_a \cdot \rho_a} \cdot d_p \cdot \frac{A_p}{V}$$

where: $\frac{A_p}{V}$ is the section factor for steel members insulated by FP materials

A_p is the appropriate area of FP material per unit length of member

c_a is the specific heat of steel [J/kgK]

c_p is the specific heat of the fire protection material [J/kgK]

d_p is the thickness of the fire protection material [m]

Δt is the time interval [s]

$\theta_{a,t}$ is the steel temperature at time t;

$\theta_{g,t}$ is the ambient gas temperature at time t;

$\Delta\theta_{g,t}$ is the increase of the ambient gas temperature during the time interval Δt

λ_p is the thermal conductivity of the fire protection material [W/mK]

ρ_a is the unit mass of steel [kg/m³]

ρ_p is the unit mass of the fire protection material [kg/m³]

q_{net3} is the net heat flux per unit area [W/m²]

The parameters used for this heat transfer model are provided in Table 3. The material properties of steel were varied as a function of temperature as described in Section 2.2 of this report. The H_p/A values represent the section factors of the steel elements. Note: The fire duration is a 2-hour fire and the initial temperature of the study is assumed at 25°C. The material properties for the fire protection materials are for a generic cementitious spray-applied fire protection material [39]. These properties are used to determine the amount (thickness) of protection material to simulate

intumescent paint behavior. This method is typically used in industry to determine the heat transfer for protected steelwork. These material values are reported in Table 4.

Table 3 : Heat Transfer input data for steel.

| VARIABLE | STRUCTURAL STEEL ELEMENTS | | |
|------------------------------------|---------------------------|---------|---------|
| | Beams | | Columns |
| | cellular | solid | |
| To (C) | 25 | 25 | 25 |
| dt (s) | 5 | 5 | 5 |
| Total section H_p/A (m^{-1}) | 96.843 | 104.119 | 53.7 |
| Top Flange H_p/A (m^{-1}) | 45.721 | 46.059 | N/A |
| Web H_p/A (m^{-1}) | 166.67 | 222.222 | N/A |
| Bottom Flange H_p/A (m^{-1}) | 87.387 | 87.725 | N/A |

Table 4: Fire protection material properties (39)

| Fire Protection Properties | Values |
|---|--------|
| Thickness of Protection, d_p (m) | 0.02 |
| Specific Heat, c_p (J/kg-K) | 900 |
| Density, ρ_p (kg/m^3) | 700 |
| Thermal conductivity, λ_p (W/m-K) | 0.1 |

The net heat flux calculation from the Eurocodes [40] is determined by considering thermal radiation and convection from and to the fire environment. The net heat flux is determined from equations 38 reproduced below from ENV 1991-2-2:1995 [40]:

$$\dot{h}_{net,d} = \gamma_{n,c} \cdot \dot{h}_{net,c} + \gamma_{n,r} \cdot \dot{h}_{net,r} \quad [\text{W/m}^2] \quad (38)$$

where :

$\dot{h}_{net,c}$ is the net convective heat flux

$\dot{h}_{net,r}$ is the net radiative heat flux

$\gamma_{n,c}$ is a factor to account for different national types of tests [1,0]

$\gamma_{n,r}$ is equal to [1,0] as $\gamma_{n,c}$

The convective heat flux is determined from equation 6:

$$\dot{h}_{net,c} = \alpha_c (T_g - T_s) \quad [\text{W/m}^2] \quad (39)$$

where :

α_c is the heat transfer coefficient [$\text{W/m}^2\text{K}$]

T_g is the gas temperature [C]

T_s is the surface temperature of the member [C]

The radiative heat flux is determined from equation 7:

$$\dot{h}_{net,r} = \Phi \cdot \epsilon_{res} \cdot 5.67 \cdot 10^{-8} (T_g^4 - T_s^4) \quad [\text{W/m}^2] \quad (40)$$

where :

ϵ_{res} is the resultant emissivity [see below]

Φ is the configuration factor

T_g is the gas temperature [C]

T_s is the surface temperature of the member [C]

$5.67 \cdot 10^{-8}$ is the Stefan Boltzmann constant [$\text{W/m}^2\text{K}^4$]

$$\epsilon_{res} = \epsilon_f \cdot \epsilon_m$$

ϵ_m is the emissivity related to the fire compartment, usually 0.8

ϵ_f is the emissivity related to the surface material, usually 0.7

These equations were applied to the standard fire curve and the generalized exponential curves described earlier. Due to assumptions stated before, these equations were also applied to the generalized time-temperature curves. Further work should be conducted to validate the use of these equations in other applications. Table 5 includes the parameters used in the net heat flux calculations.

Table 5: Heat Flux Calculations Variables (ENV 1991:2-2:2001)

| Heat Flux Variables | Values |
|--|-----------------------|
| Configuration factor, Φ | 1 |
| Resultant emissivity, ϵ_{res} | 0.56 |
| Heat transfer coefficient, α_c | 25 W/m ² K |
| Factor $\gamma_{n,c}$ | 1 |
| Factor $\gamma_{n,r}$ | 1 |

3.4.4 Heat Transfer Model for Concrete

In all the analysis models, the concrete slab has a realistic temperature distribution applied through its depth rather than using a mean temperature/gradient system. This is done by applying individual time-temperature curves to 5 different points through the depth of the slab (top, bottom, and 1/4 points). The time temperature distributions used in this analysis were taken from a 1D heat transfer analysis, based on the input gas temperature curves described in Figure 49.

The slab used in the heat transfer analysis was 3000 mm in length with an effective depth of 120 mm and a density of 2250 kg/m³. The input thermal

properties were those described in Section 2.2 of this report. In the ABAQUS model, a convective heat loss on the unexposed side and exposed side were assumed to be $10 \text{ W/m}^2\text{K}$ and $25 \text{ W/m}^2\text{K}$, respectively from Eurocode 1 Part 1-2 (1995). Radiation was also considered with emissivities of 0.1 and 0.8 for the unexposed and exposed sides, respectively.

The following figures illustrate the time-temperature curves for five (5) equally spaced points through the depth of the slab. Figure 50 is for the standard fire and Figures 51-55 are for the generalized exponential time temperature exposures seen in Figure 49. In the input data section for thermal loading, the concrete temperature profiles were divided into three heating time steps to simplify the thermal profiles through the depth of the slab.

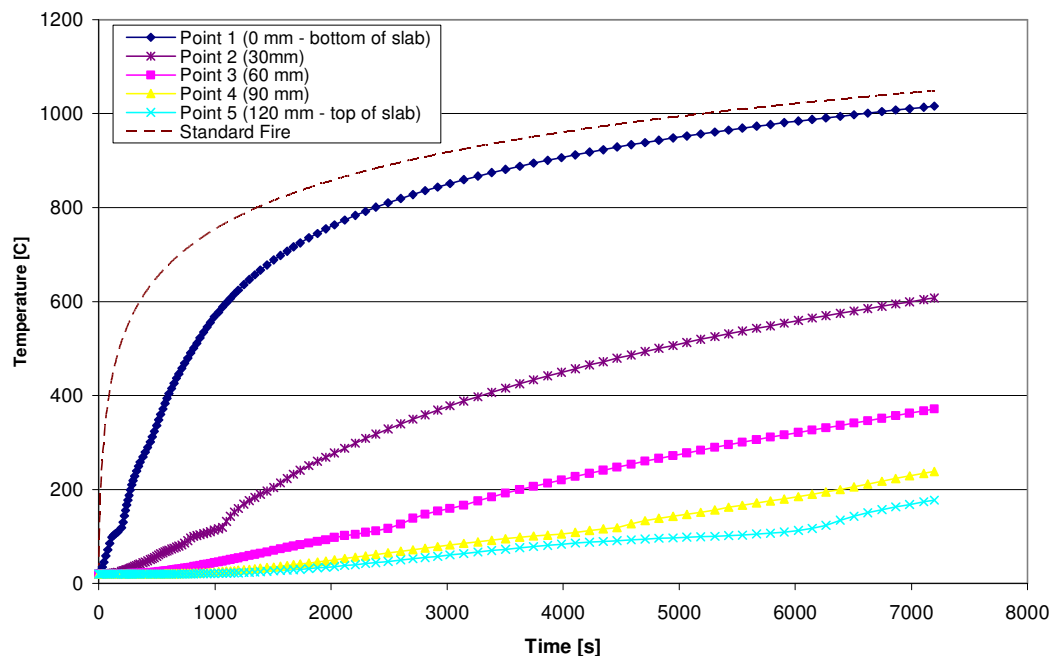


Figure 50 - Slab temperatures from standard fire case

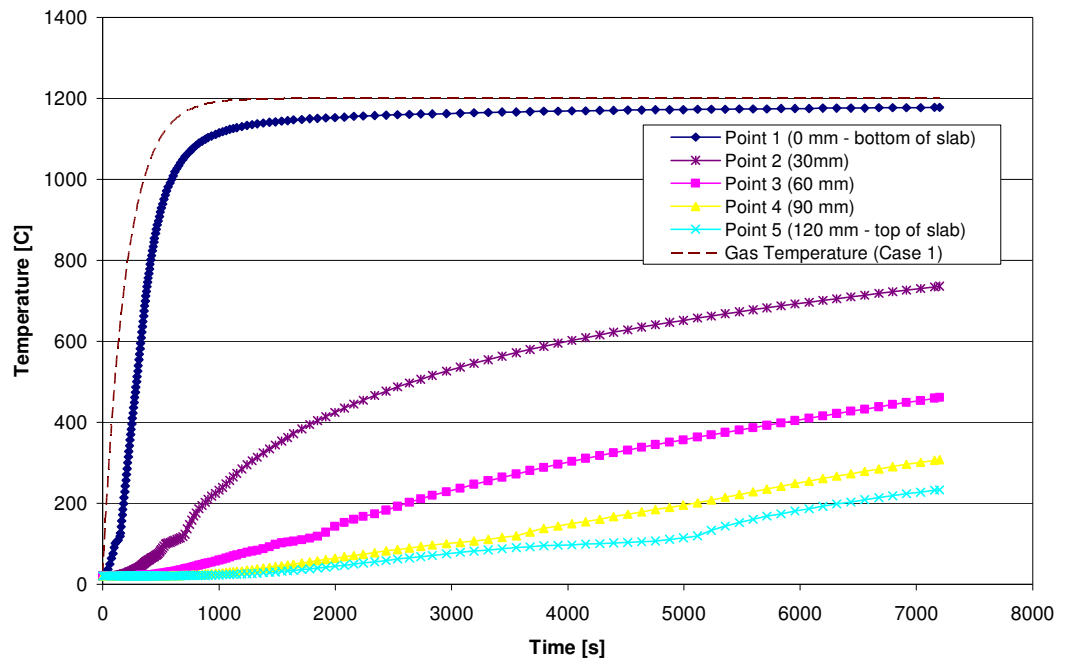


Figure 51 - Slab temperatures from case 1 fire

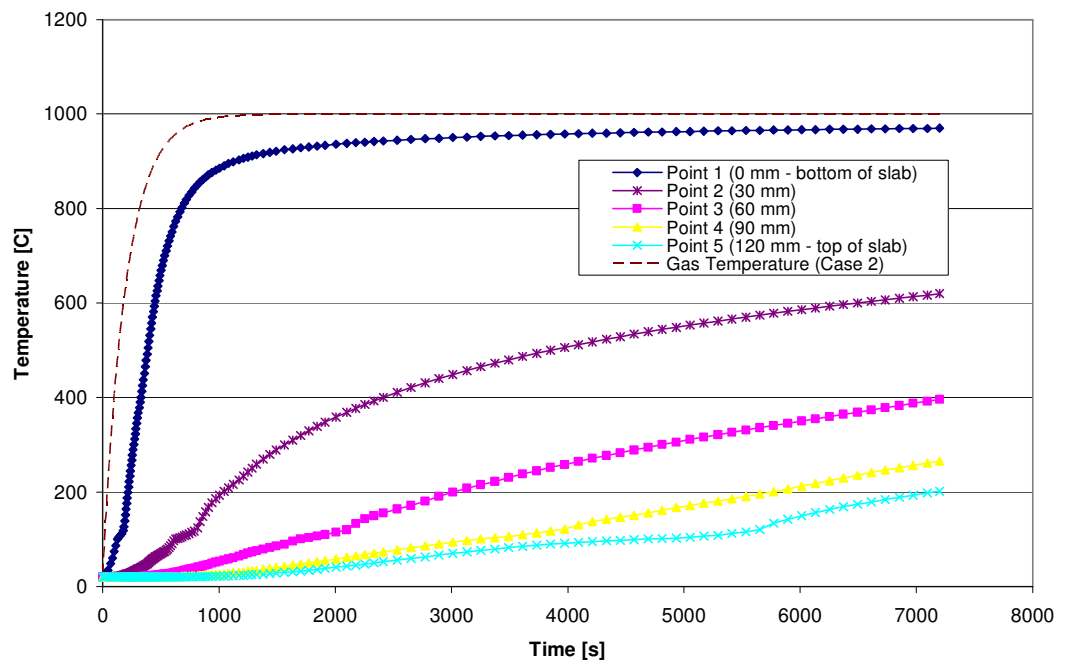


Figure 52 - Slab temperatures from case 2 fire

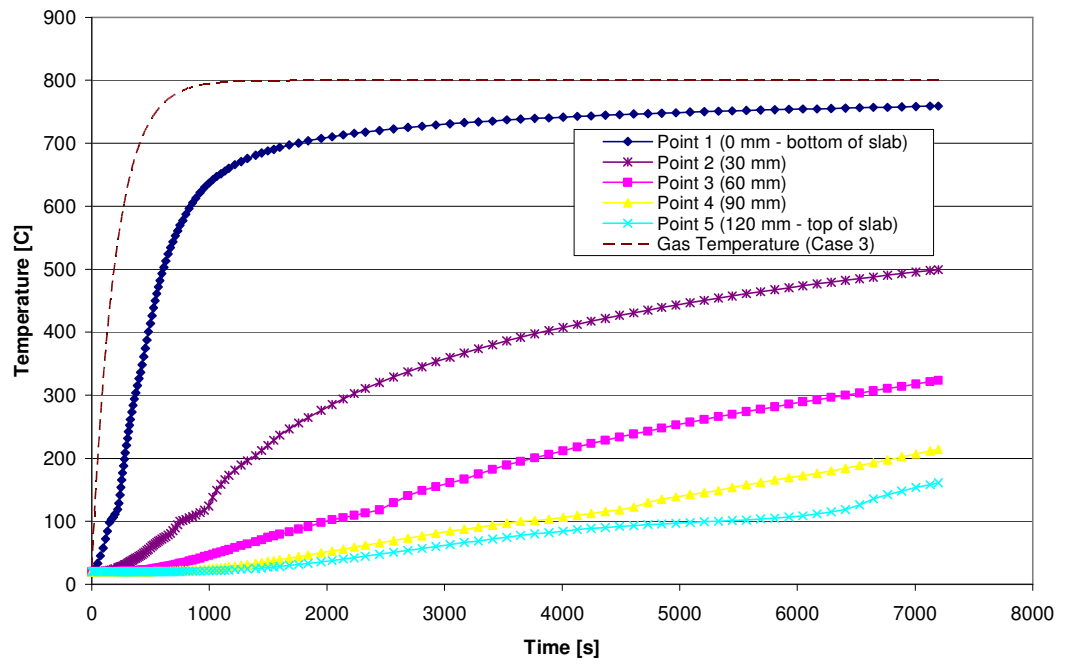


Figure 53 - Slab temperatures from case 3 fire

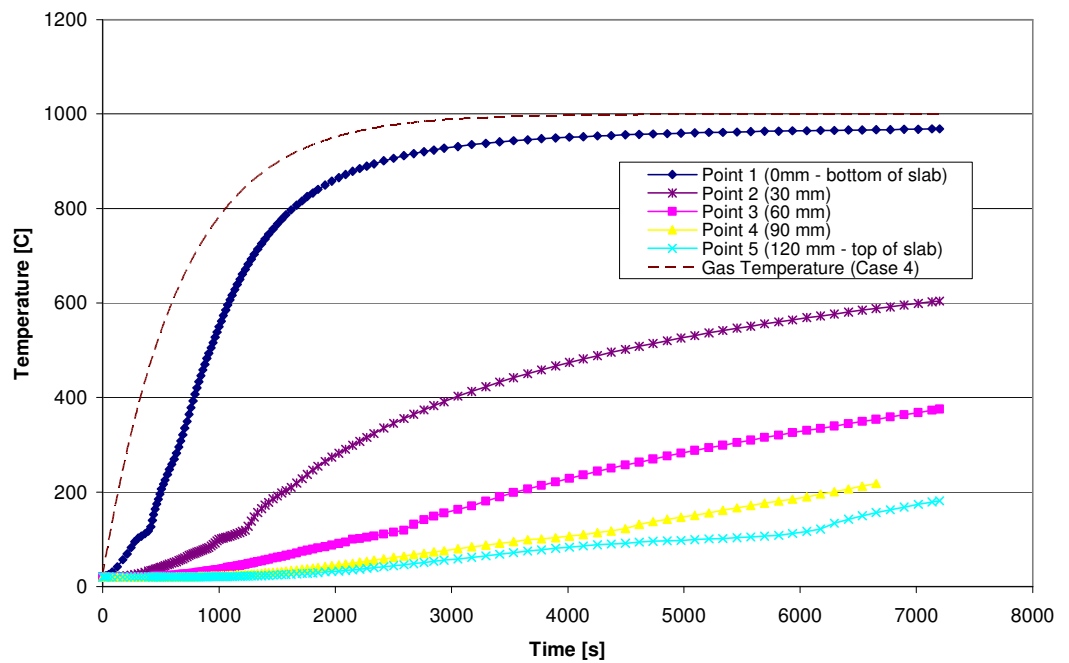


Figure 54 - Slab temperatures from case 4 fire

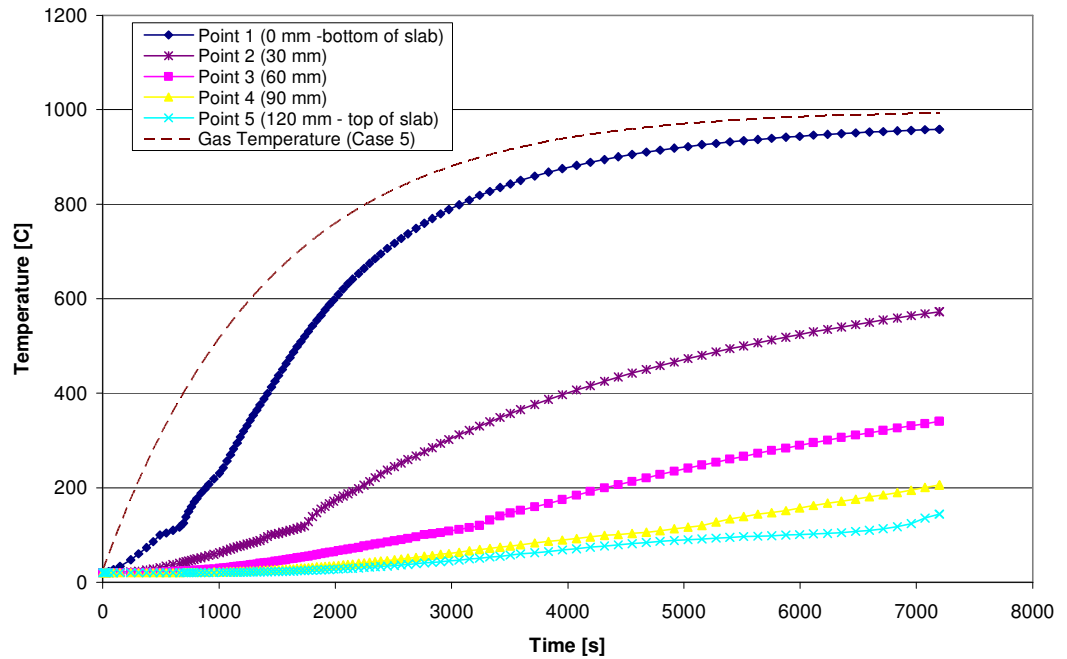


Figure 55 -Slab temperatures from case 5 fire

3.5 Structural Model – Input Data

3.5.1 Base Model Geometry

The “base” model consisted of a single, long span cellular beam with supporting frame elements (i.e. columns, edge beams etc.). The cellular beam is 18m in length and is a 690mm x 370mm/370mm x 179.9 kg/m 355MPa steel member designed using FBEAM [41], a structural analysis tool developed by FABSEC [41], to optimize and design cellular beam for ambient and fire conditions. The details of this beam are as follows and can be seen in the Figure 56:

| Scenario | Span | Depth of Member | Bottom Flange Width | Web Thickness | Flange Thickness | No. of Holes | Hole Diameter | Web Post Size | End Post Size |
|------------|-------|-----------------|---------------------|---------------|------------------|--------------|---------------|---------------|---------------|
| | [mm] | [mm] | [mm] | [mm] | [mm] | | [mm] | [mm] | [mm] |
| Base Model | 18000 | 690 | 370 | 12 | 24 | 24 | 450 | 295 | 900 |

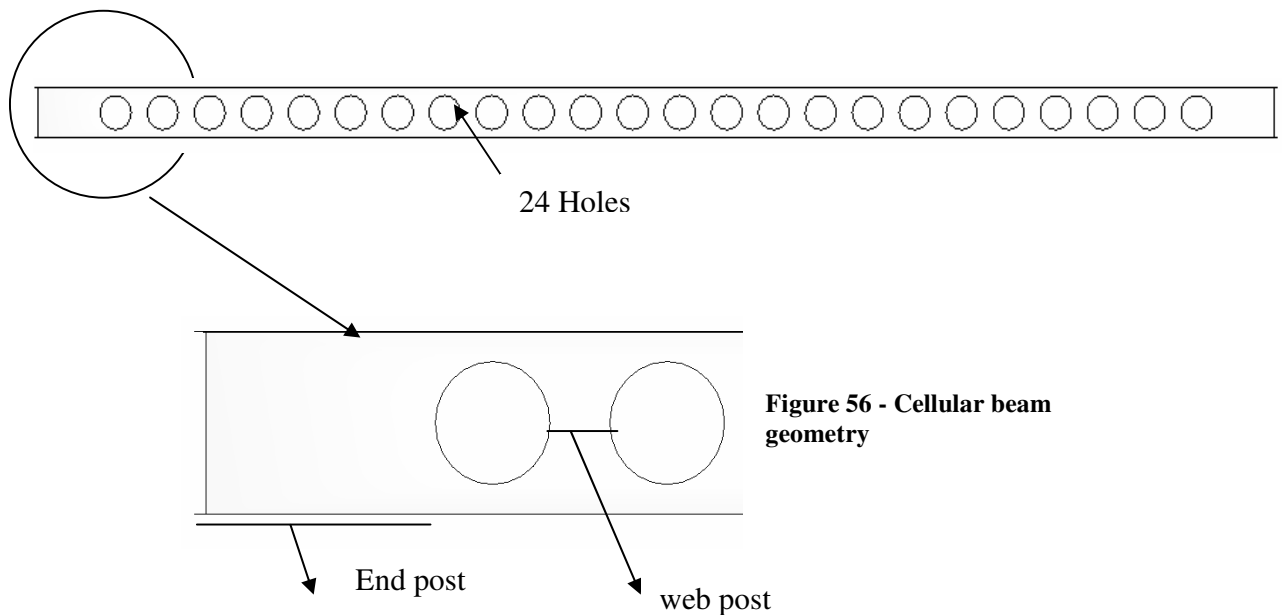


Figure 56 - Cellular beam geometry

The supporting edge beams, as indicated in Figure 57, are 5 m in length and are 670 mm / 370mm/370 mm x 183.4 kg/m S355 MPa steel member. The half-bay cellular beams have the same characteristics as the main, long span cellular beam but are 9m in length. The columns are universal columns, UC 356 x 406x 467 [42]. The columns were modeled as continuous over two stories, with a length of 8000m.

The concrete deck is continuous over the edge beams and extends the length of the model [36872 mm = 18000mm (cellular beam span) + (2) 436mm (column lengths) + (2) 9000mm (half-bay lengths)]. The slab is modeled as a two-way slab, 130mm thick slab of normal weight C40

(40MPa) concrete with reinforcement explicitly included as welded wire fabric with 6 mm bars at 200 mm pitch running in both direction. One layer was provided in both the top and bottom of the slab with 30mm of cover.

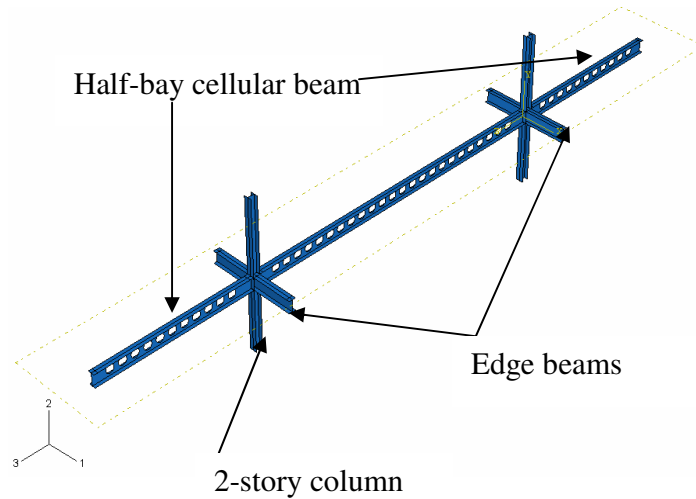


Figure 57 - Base cellular beam model geometry

In addition to the “base” cellular beam model, a solid beam model was also created for comparison. This model had the same geometric and material characteristics as the cellular beam model, with the exception of a solid, long span beam. This beam is also 18m in length and is a 670 mm x 370mm/370mm x 183.4 kg/m 355 MPa steel member designed using FBEAM, a structural analysis tool developed by FABSEC [41].

Table 1A is a summary of the structural members investigated. See Appendix for load calculations and design sheets used to determine the member sizes. All structural members were designed using the design guides and governing structural codes (BS 5950, EC3:1995, EC2:1995 and EC 4:1995).

Table 1A: Structural members used in analysis

| STRUCTURAL ELEMENT | DESCRIPTION | DESIGN REFERENCE |
|--------------------|--|---------------------------------------|
| Beams | (depth x flange width/bottom flange width) | |
| Cellular | 670 x 370/370 | FBEAM (See Appendix for calculations) |
| Solid | 690 x 370/370 | |
| Edge | 690 x 370/370 | |
| Column | UC 356x406x467 | BS 5950 Part 1 |
| Slab | 130 mm two-way slab | EC 2 (1995) |

3.5.2 Cases for Analysis

This section outlines how the “base” cellular beam model was varied during the analysis. Three (3) basic scenarios were examined for this study and are listed in Table 1. In Scenario I, several parameters of the “base” cellular beam model were varied and included: hole diameter, end post size, number of holes, web thickness, flange thickness, bottom flange width, span and span. The models of Scenario I were exposed to the standard fire curve that was applied to the structural elements uniformly across the depths and lengths.

Table 1: Brief outline of analyses conducted in structural fire model

| Scenario | Fire Exposure | Structural System | Thermal Distribution |
|----------|------------------------------|-------------------|---|
| I | Standard Fire | Varied | Uniform |
| II | General Curve | Single system | Uniform |
| III | Standard Fire + Test Data | Single system | Gradient across depth; uniform along length |

In Scenario II, the “base” cellular beam model was then exposed to a generalized exponential time-temperature curve (described earlier), from which five (5) different fire exposures were applied. In this scenario, the generalized fire curve was applied to the structural elements uniformly across the depths and lengths.

In Scenario III, the “base” cellular beam model was exposed to the standard fire curve. However, in this case, the fire exposure was varied over the depth of the cellular beam based on the thermal profiles observed by the early work conducted by Fabsec Ltd. and Westok Ltd. (described in Chapter 1). In this scenario, solid phase temperature profiles were calculated separately for the bottom flange, web and top flange. (See Fire Scenarios section for more detail)

All three scenarios, discussed in further detail in §3.5.7.1, were conducted on the simple structural bay illustrated in Figure 47, with the central long-span cellular beam element being the emphasis of this report. Table 2 shows the testing matrix used in the analyses of the base model in greater detail. Note: Case h in Scenario I was discarded. Since the model consisted of an internal bay, loading the columns more would not have affected the structural response of the cellular beam. In this study, the column plays an insignificant role.

Table 2: Test Matrix

| Scenario | Case | Implicit/ Explicit | Fire Exposure Standard Fire - SF Generalized Fire - G | Uniform (U) or Thermal Gradient | Hole Diameter [mm] | End Post Size [mm] | No. of Holes | Web Thickness [mm] | Flange Thickness [mm] | Bottom Flange Width [mm] | Span [mm] | Column Load [N/mm] |
|------------|------|-----------------------|---|--|--------------------------|-----------------------------|--------------------|--------------------------|-----------------------------|-----------------------------------|--------------|--------------------------|
| Base Model | | I | SF | U | 450 | 900 | 24 | 12 | 24 | 370 | 18000 | 7.9 |
| Solid Beam | | I | SF | U | n/a | n/a | o | 9 | 24 | 370 | 18000 | 7.9 |
| I | a | I | SF | U | 150 | 900 | 24 | 12 | 24 | 370 | 18000 | 7.9 |
| | | E | SF | U | 150 | 900 | 24 | 12 | 24 | 370 | 18000 | 7.9 |
| | | I | SF | U | 300 | 900 | 24 | 12 | 24 | 370 | 18000 | 7.9 |
| | | I | SF | U | 500 | 900 | 24 | 12 | 24 | 370 | 18000 | 7.9 |
| | b | I | SF | U | 450 | 100 | 24 | 12 | 24 | 370 | 18000 | 7.9 |
| | | I | SF | U | 450 | 400 | 24 | 12 | 24 | 370 | 18000 | 7.9 |
| | | I | SF | U | 450 | 1400 | 24 | 12 | 24 | 370 | 18000 | 7.9 |
| | | E | SF | U | 450 | 1400 | 24 | 12 | 24 | 370 | 18000 | 7.9 |
| | c | I | SF | U | 450 | 900 | 12 | 12 | 24 | 370 | 18000 | 7.9 |
| | | I | SF | U | 450 | 900 | 30 | 12 | 24 | 370 | 18000 | 7.9 |
| | | E | SF | U | 450 | 900 | 30 | 12 | 24 | 370 | 18000 | 7.9 |
| | d | I | SF | U | 450 | 900 | 24 | 8 | 24 | 370 | 18000 | 7.9 |
| | | E | SF | U | 450 | 900 | 24 | 8 | 24 | 370 | 18000 | 7.9 |
| | | I | SF | U | 450 | 900 | 24 | 20 | 24 | 370 | 18000 | 7.9 |
| | e | I | SF | U | 450 | 900 | 24 | 12 | 12 | 370 | 18000 | 7.9 |
| | | I | SF | U | 450 | 900 | 24 | 12 | 48 | 370 | 18000 | 7.9 |
| | | E | SF | U | 450 | 900 | 24 | 12 | 48 | 370 | 18000 | 7.9 |
| | f | I | SF | U | 450 | 900 | 24 | 12 | 24 | 270 | 18000 | 7.9 |
| | | E | SF | U | 450 | 900 | 24 | 12 | 24 | 270 | 18000 | 7.9 |
| | | I | SF | U | 450 | 900 | 24 | 12 | 24 | 470 | 18000 | 7.9 |
| | g | I | SF | U | 450 | 900 | 24 | 12 | 24 | 370 | 6150 | 7.9 |
| | | I | SF | U | 450 | 900 | 24 | 12 | 24 | 370 | 12000 | 7.9 |

| | h | I | SF | | U | 450 | 900 | 24 | 12 | 24 | 370 | 18000 | 9.085 |
|------|---|---|--------|--------|--------------------------------|-----|-----|----|----|----|-----|-------|-------|
| | | I | SF | | U | 450 | 900 | 24 | 12 | 24 | 370 | 18000 | 10.27 |
| II | 1 | I | Tmax | α | U | 450 | 900 | 24 | 12 | 24 | 370 | 18000 | 7.9 |
| | | | G | | | | | | | | | | |
| | | | 1200 | 0.005 | | | | | | | | | |
| | 2 | I | G | | U | 450 | 900 | 24 | 12 | 24 | 370 | 18000 | 7.9 |
| | | | 1000 | 0.005 | | | | | | | | | |
| | 3 | I | G | | U | 450 | 900 | 24 | 12 | 24 | 370 | 18000 | 7.9 |
| | | | 800 | 0.005 | | | | | | | | | |
| | 4 | I | G | | U | 450 | 900 | 24 | 12 | 24 | 370 | 18000 | 7.9 |
| | | | 1000 | 0.0015 | | | | | | | | | |
| | 5 | I | G | | U | 450 | 900 | 24 | 12 | 24 | 370 | 18000 | 7.9 |
| 1000 | | | 0.0007 | | | | | | | | | | |
| III | 1 | I | SF | | Thermal Gradient - Protected | 450 | 900 | 24 | 12 | 24 | 370 | 18000 | 7.9 |
| | 2 | I | SF | | Thermal Gradient - Unprotected | 450 | 900 | 24 | 12 | 24 | 370 | 18000 | 7.9 |

3.5.3 *Material Properties*

In this study, the properties of both steel and concrete varied with temperature and were described in detail in Section 2.2. The values input into ABAQUS were the design values stipulated in Eurocode 2: 1993 [26] and Eurocode 3:1995 [9] for concrete and steel structures, respectively.

3.5.4 *FEM Element type and Meshing*

The element type used for all members of the analyses is a 4-node double curved general purpose shell, termed S4. This comprises 4 integration points within each element allowing increased accuracy in results.

All the element meshes in the model except the columns were generated by ABAQUS at a fineness of 300 mm. The column mesh had a resolution of 100 mm. These resolutions were chosen based on efficiency in computation time but not at the expense of the accuracy of the results.

3.5.5 *Boundary Conditions*

All the beams in the model were connected continuously along the web to the columns, which were oriented in strong axis bending for the long span cellular/solid beam. In addition, the top surfaces of the beams also were tied to bottom of the concrete slab.

Symmetry boundary conditions were applied to the edges of the slab, edge beams and half-bay cellular beams; that is, the elements were restricted from translating along their main axis and rotating laterally. The columns

were assumed fully-fixed at the base, with the tops of the columns free to translate vertically, while restricted from rotating about the vertical axis.

3.5.6 Ambient Loading

The dead and live loads were factored in accordance with the structural Eurocodes (EC1:1994, EC2:1995, EC3:1995). For ambient conditions, the solid and cellular beams were designed using the follow load combination:

$$1.4 \text{ Dead Load} + 1.6 \text{ Live Load}$$

For fire conditions, the loads were factored in accordance with BS 5950 Part 8(2004) [43] for office buildings as follows:

$$1.0 \text{ Dead Load} + 1.0 \text{ Permanent Imposed Load} + 0.5 \text{ Non-Permanent Imposed Load}$$

Typical loads were applied to the structure, and are as follows:

$$\text{Dead Load (DL)} = 3.0 \text{ kN/m}^2$$

$$\text{Live Load (LL)} = 4 \text{ kN/m}^2$$

The loads applied in the fire limit state are:

$$(3.0 \times 1) + (0.5 \times 4) = 5 \text{ kN/m}^2$$

Because this bay could potential be located anywhere within a building and at any floor level, the columns were assumed to be loaded to 50% of their ambient capacity from the floors above. According to BS 5950 [42], a UC 356 x 406 x 467 has an axial load capacity of 19,100 kN. Half of this load was applied to the tops of the columns.

3.5.7 Thermal Loading

The methods for determining the solid phase time-temperature curves for the steel and concrete slab in the models were explained in detail in

Section 3.4. This section illustrates the time-temperature curves that were input in the ABAQUS structural analysis models for each scenario. As mentioned in the thermal assumptions section, this study consisted of a 2-hour fire exposure in a single structural bay. Therefore, the cellular beam, edge beams and bottom half of the columns had thermal loadings. The cellular beam was considered “unprotected” while the columns and edge beams were “protected”. By applying “unprotected” steel temperatures to the cellular beam, failure will occur sooner in the beam. In this way, the structural fire performance of the beam can be assessed more readily. Section 3.4.7.1 describes the time-temperature curves for Scenario I; Section 3.4.7.2, for Scenario II; and Section 3.4.7.3, for Scenario III.

3.5.7.1 Scenario I

3.5.7.1.1 Steel Time-Temperature Curves

In Scenario I, the standard fire curve (ISO 834) was used to calculate the solid phase temperatures of the protected and unprotected steel members using Equation 4.21 and 4.22 of Eurocode 3 Part 1-2, respectively. These solid phase time-temperature curves were applied uniformly across the length and depth of the members

As illustrated in Figure 58, the solid phase time-temperature curves for each structural element given their level of protection is provided. These curves are plotted against the assumed compartment time temperature curve. Given this standard fire exposure, a parametric study was then conducted on the

structural characteristics of the cellular beam (number of holes, web post thickness, end post thickness, size of hole, etc.) and how these parameters affect local and global behavior of the system.

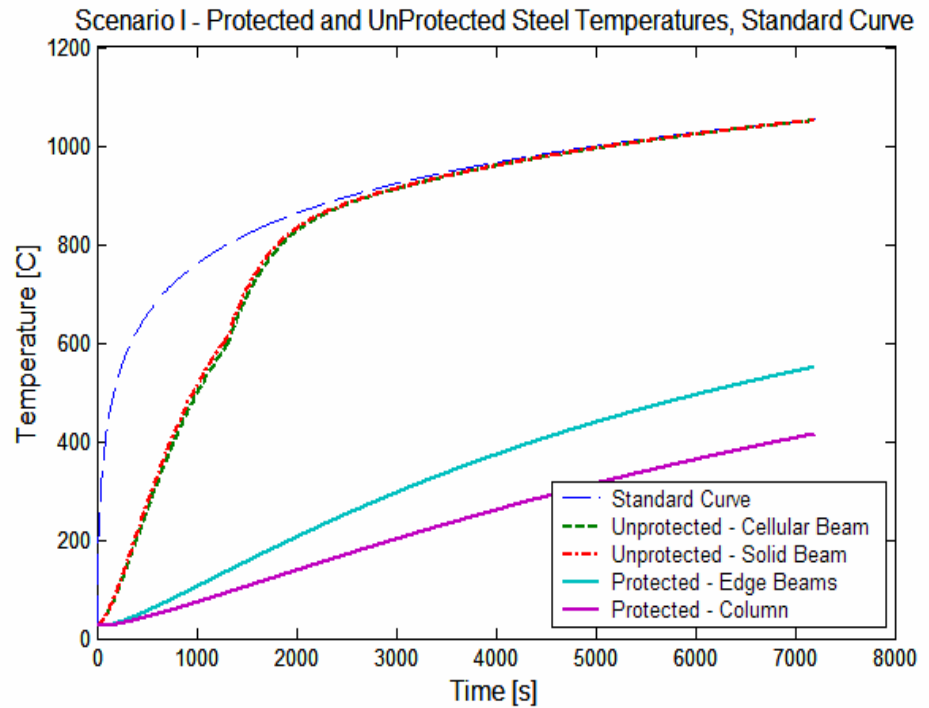


Figure 58 - Protected and Unprotected steel time temperature curves for Scenario I. The standard fire curve (ISO 834), representing the gas phase temperatures, is plotted for reference.

3.5.7.1.2 Concrete

As mentioned in the fire scenario section of this report, the concrete slab was modeled with a thermal gradient through the depth of the section at five equally-spaced points. The time-temperature curves from the heat transfer analysis for Scenario I were simplified as illustrated in Figure 59.

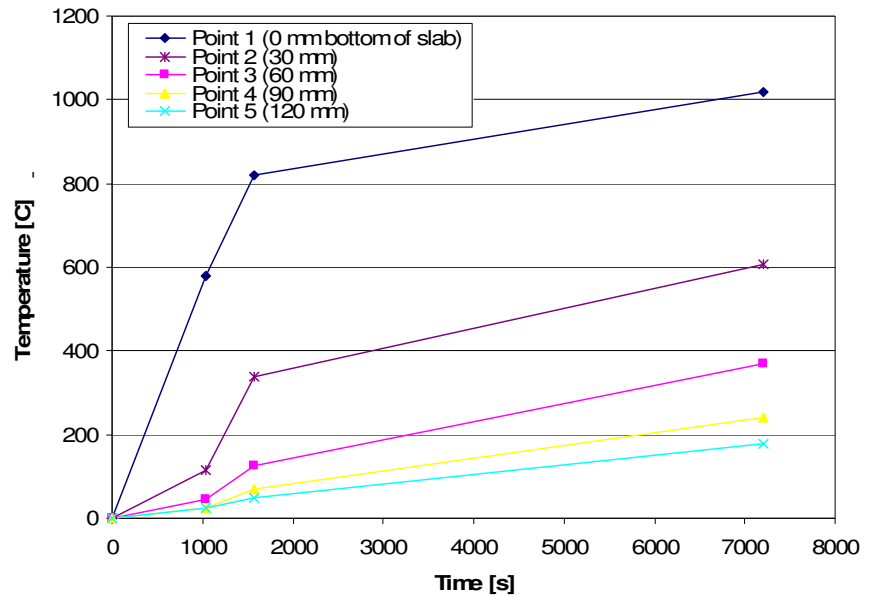


Figure 59 - Temperatures through depth of concrete (Scenario I)

3.5.7.2 Scenario II

In Scenario II, the generalized exponential time-temperature curve described in Equation 35 was used to artificially capture a range of gas temperatures that may result from varying heat fluxes and rates of heating. By adjusting the T_{\max} and α terms in Equation 35, an envelope of time-temperature curves were produced and applied to the “base” cellular beam model, where the standard fire curve was used as the benchmark (See Figure 49).

3.5.7.2.1 Steel Time-Temperature Curves

A total of five (5) generalized exponential time temperature curves were created. Similar to a standard and hydrocarbon fire, the generalized curves were used to calculate the solid phase temperatures of the protected and unprotected steel members

using Equation 4.21 and 4.22 of Eurocode 3 Part 1-2, respectively.

These solid phase time-temperature curves were applied uniformly across the length and depth of the members.

Table 6 summarizes the five (5) cases studied in this scenario.

Table 6: Input Parameters for generalized time-temperature curve

| Case | Generalized Exponential Time-Temperature Curves | |
|------|---|----------|
| | Tmax [C] | α |
| 1 | 1200 | 0.005 |
| 2 | 1000 | 0.005 |
| 3 | 800 | 0.005 |
| 4 | 1000 | 0.0015 |
| 5 | 1000 | 0.0007 |

Figures 60-64, illustrate the assumed time temperature profiles for each structural member given one of the above compartment time-temperature curves.

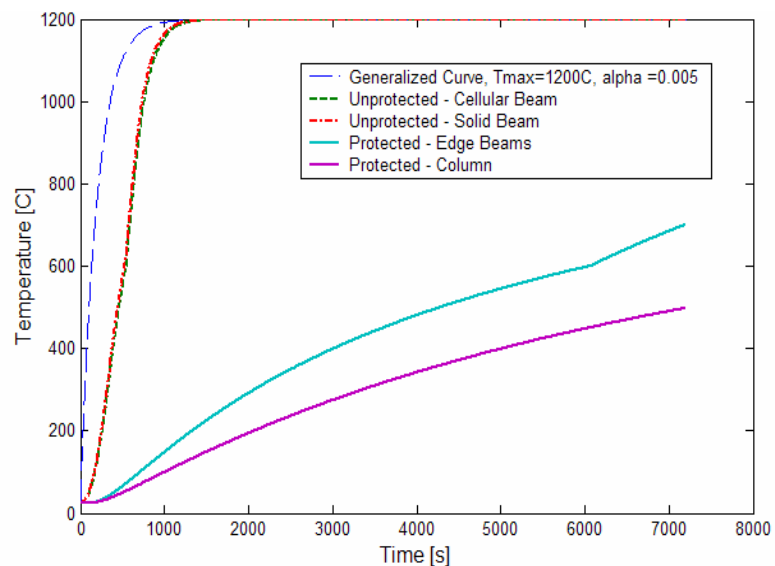


Figure 60 - Steel Temperatures given a generalized time temperature curve with $T_{max} = 1200^{\circ}\text{C}$ and the rate of heating parameter = 0.005.

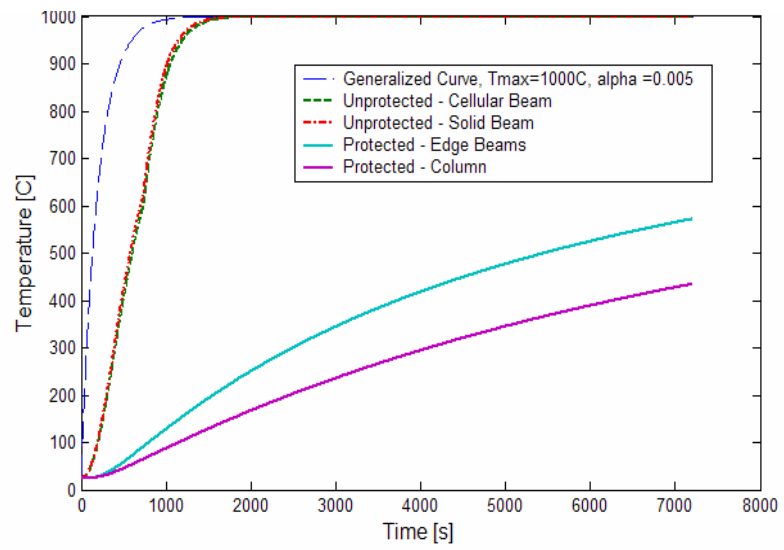


Figure 61- Steel Temperatures given a generalized time temperature curve with $T_{\max} = 1000^{\circ}\text{C}$ and the rate of heating parameter = 0.005.

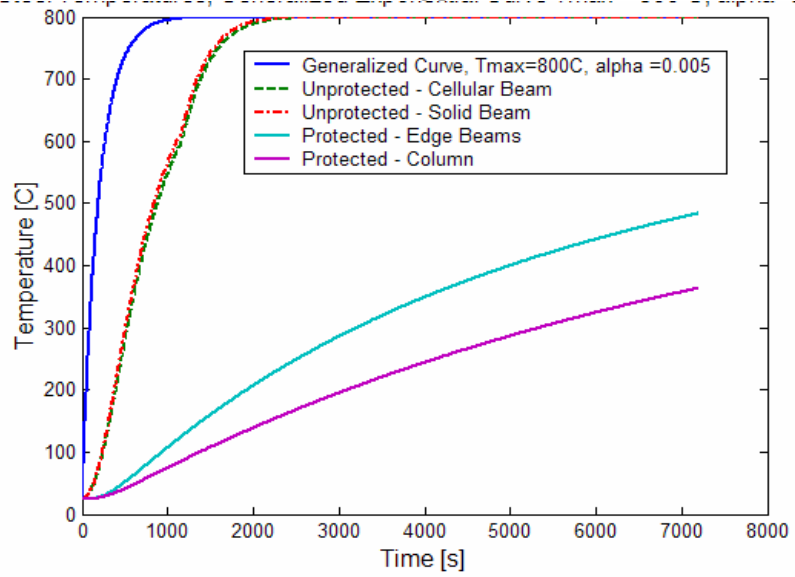


Figure 62 - Steel Temperatures given a generalized time temperature curve with $T_{\max} = 800^{\circ}\text{C}$ and the rate of heating parameter = 0.005.

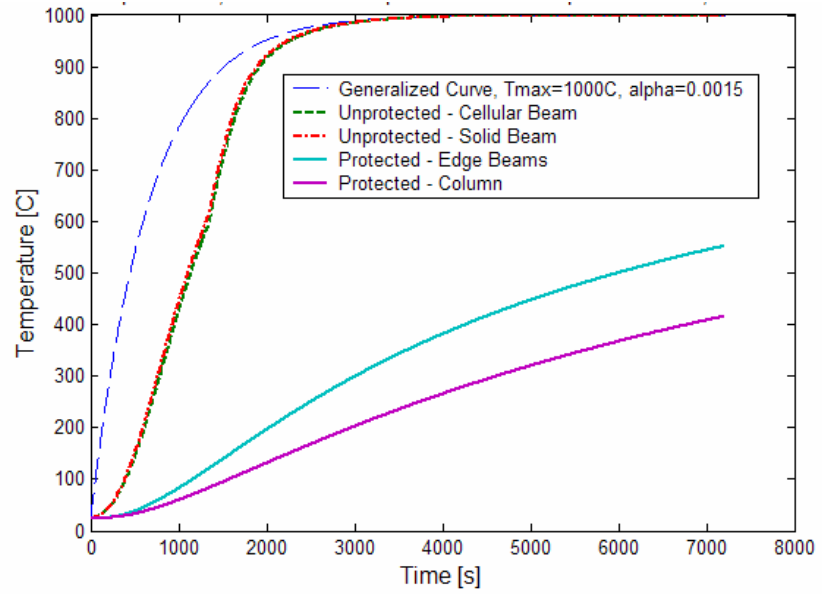


Figure 63 - Steel Temperatures given a generalized time temperature curve with $T_{\max} = 1000^{\circ}\text{C}$ and the rate of heating parameter = 0.0015.

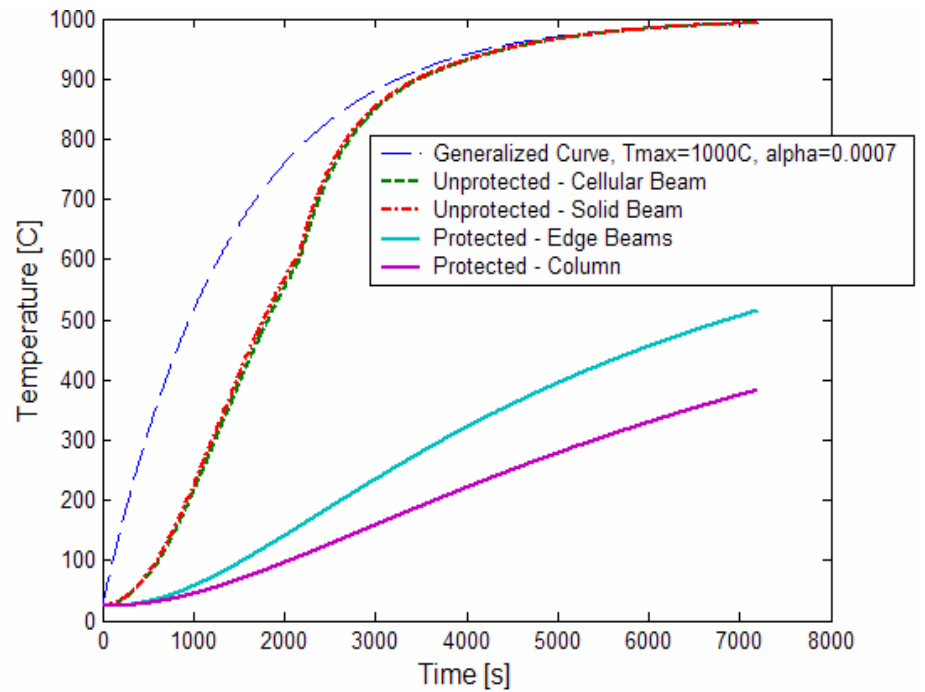


Figure 64 - Steel Temperatures given a generalized time temperature curve with $T_{\max} = 1000^{\circ}\text{C}$ and the rate of heating parameter = 0.0007.

3.5.7.2.2 Concrete Time-Temperature Curves

The time-temperature curves from the heat transfer analysis for Scenario II were simplified as illustrated in Figure 65-69 for each generalized exponential time temperature case.

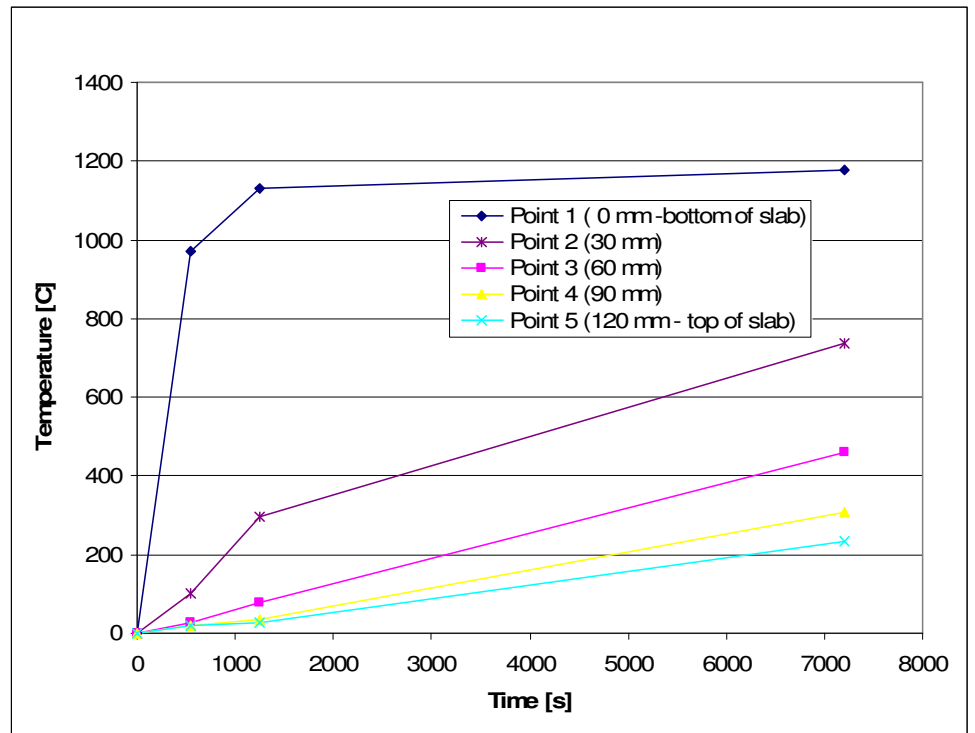


Figure 65 - Temperatures through depth of slab (Case 1)

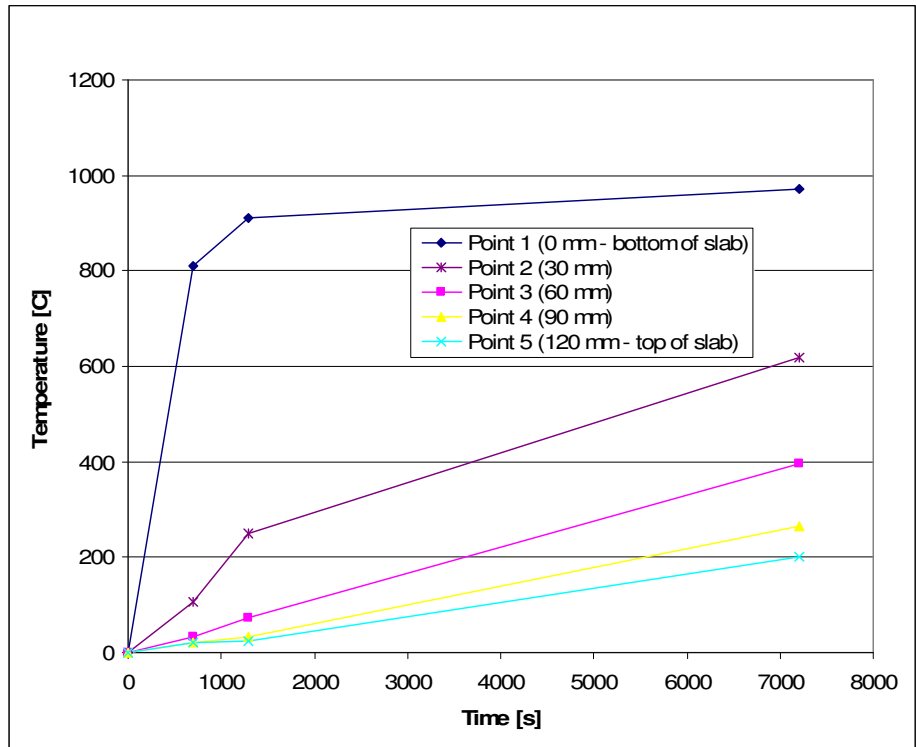


Figure 66 - Temperatures through concrete slab (Case 2)

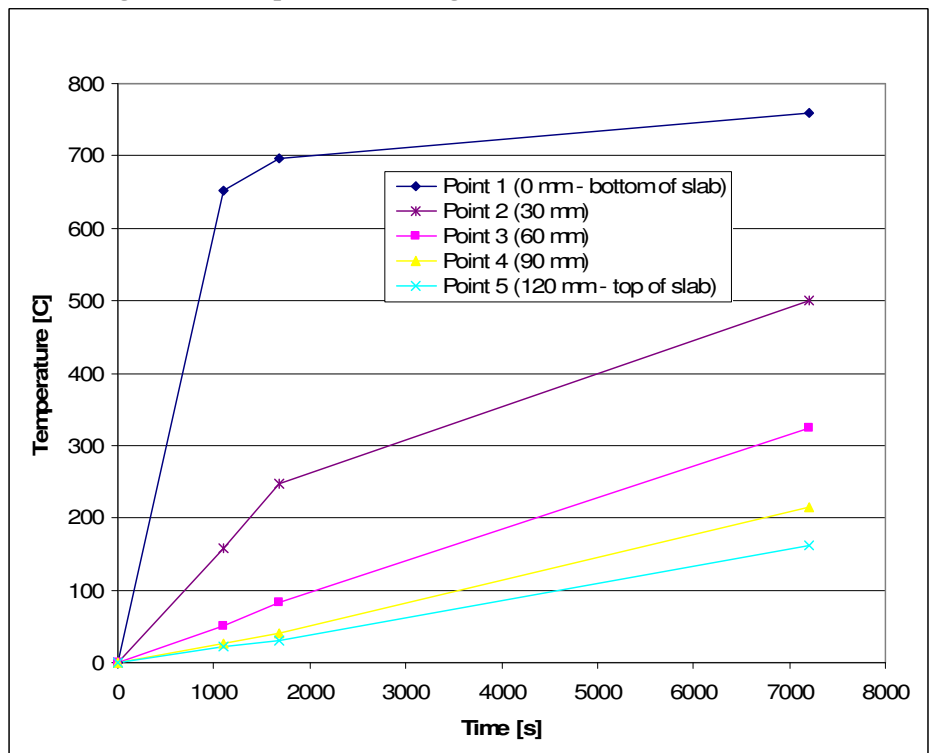


Figure 67 - Temperatures through concrete slab (Case 3)

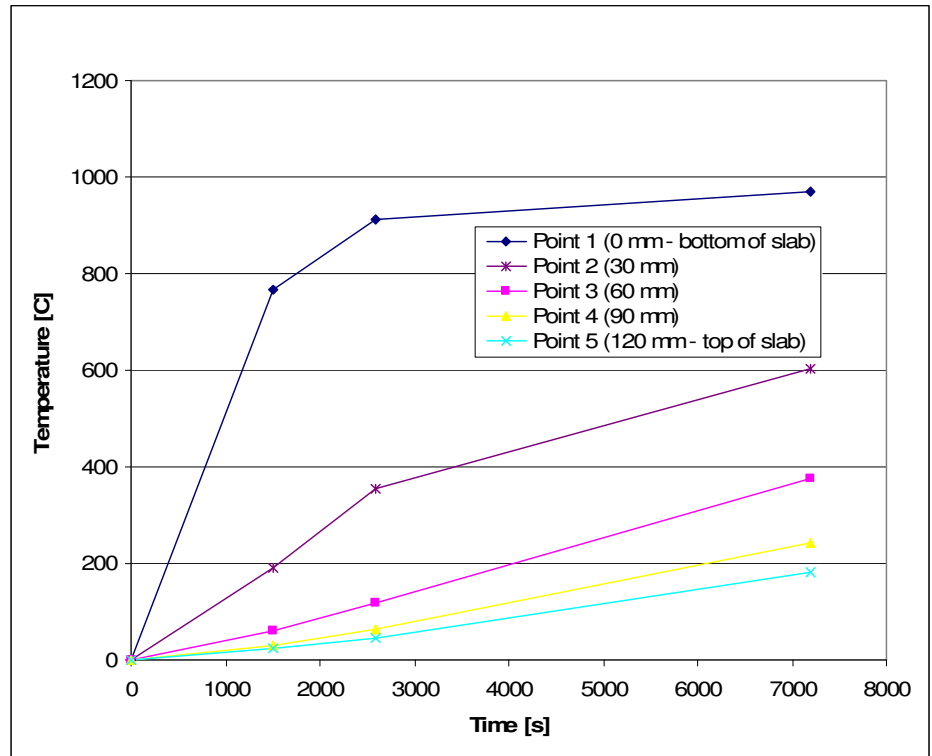


Figure 68 - Temperatures through concrete slab (Case 4)

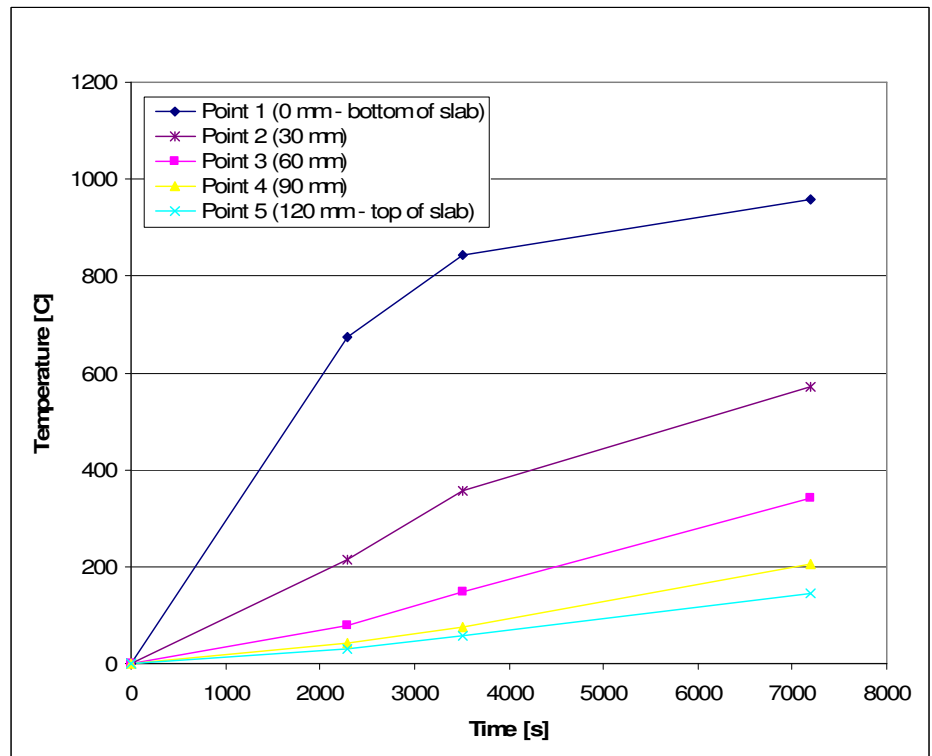


Figure 69 - Temperatures through concrete slab (Case 5)

3.5.7.3 Scenario III

In Scenario III, the test findings from FABSEC Ltd. , Westok Ltd., and SCI were analyzed. As discussed in Chapter 1, the early fire tests on protected cellular beams indicated [4] that the web of the beams between the holes (commonly termed the web-post) heats up more quickly than expected in some cases by 100°C more than the bottom flange. This phenomenon was also witnessed in unprotected beams but to a lesser extent. To simulate these time-temperature differences between the web and flange, the solid-phase time-temperature curves were determined using the section factors of the flanges and webs separately. Essentially, the same calculations described in Section 3.4 were performed with the exception of using the individual H_p/A values for the webs and flanges, as opposed, to the total H_p/A value for the entire section.

The standard fire curve was used for the gas compartment temperatures. (See Table 3 for the section factors used for the webs and flanges). Two cases were analyzed in this section – one for protected cellular beams and one for unprotected cellular beam.

3.5.7.3.1 Steel Time Temperature Curves

Figure 70 illustrates the solid phase time temperature curves for the protected and unprotected cases in Scenario III.

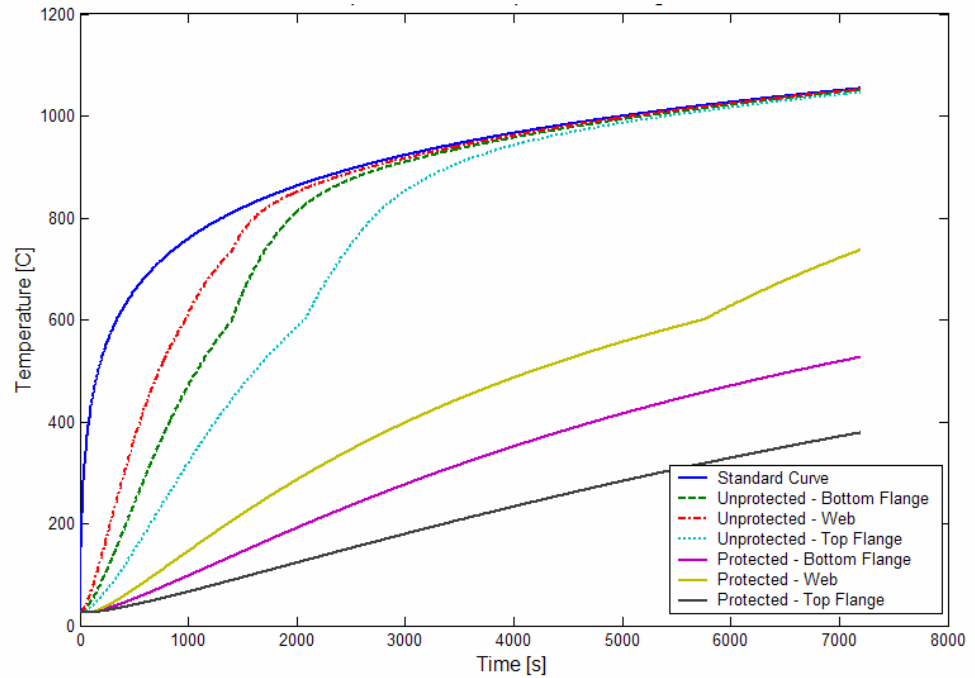


Figure 70 - Steel Temperatures for the top flange, web, bottom flange of the cellular beam section given a standard fire exposure, the top curves are for unprotected and the bottom are for protected.

3.5.7.3.2 Concrete Time Temperature Curves

In Scenario III, the concrete slab temperatures are the same as in Scenario I. The gas compartment temperatures are from the standard time-temperature curve, and therefore, the heat transfer analysis is the same. As with the other cases, the temperature distributions were simplified (See Figure 71).

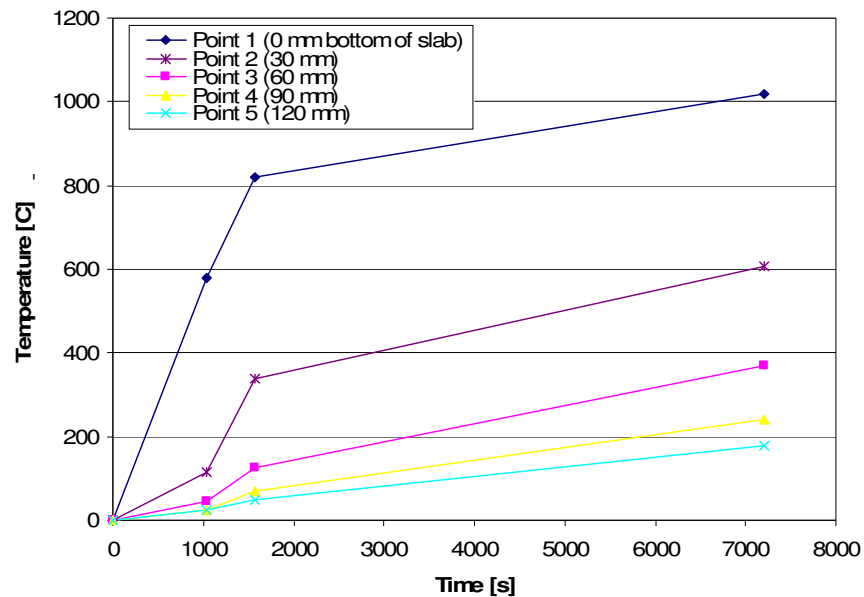


Figure 71 - Temperatures for concrete slab in Scenario III tests

ADDITIONAL COMMENTS

Although the results from Bailey/Westok and Fabsec Ltd will not be explicitly tested in this report, the envelope of time-temperature profiles will be analyzed to cover both ends of the spectrum. Figure 72 is a reproduction of the data presented by Bailey for protected cellular beams; and, Figure 73 reports the temperatures output by Fabsec’s cellular beam software (FBEAM) at 30s, 60s, 90s, and 120s. The temperatures provided by FBEAM are interpolated from the limited test data conducted in the fire tests, discussed in Chapter 1. These data points were outputted by the software program for the “base” cellular beam in this study.

Figure 74 illustrates the wide range of time-temperature curves analyzed in this report. While the exact test data was not

incorporated into the analysis, as can be seen in Figure 74, the FABSEC and Bailey curves appear to fall well within the bounds of the temperature-time curves that were investigated. This seems to be a reasonable assumption.

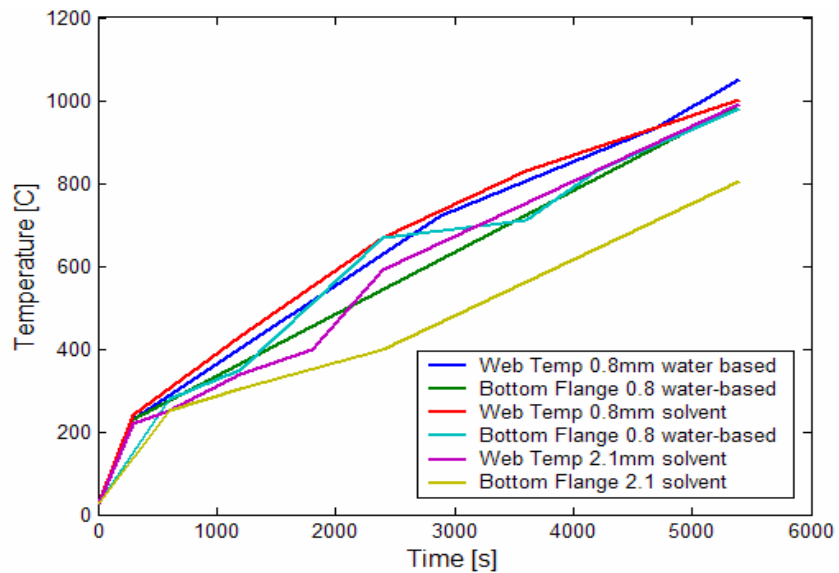


Figure 72 - Protected Steel Temperatures for bottom flange and web from Bailey/Westok Ltd.

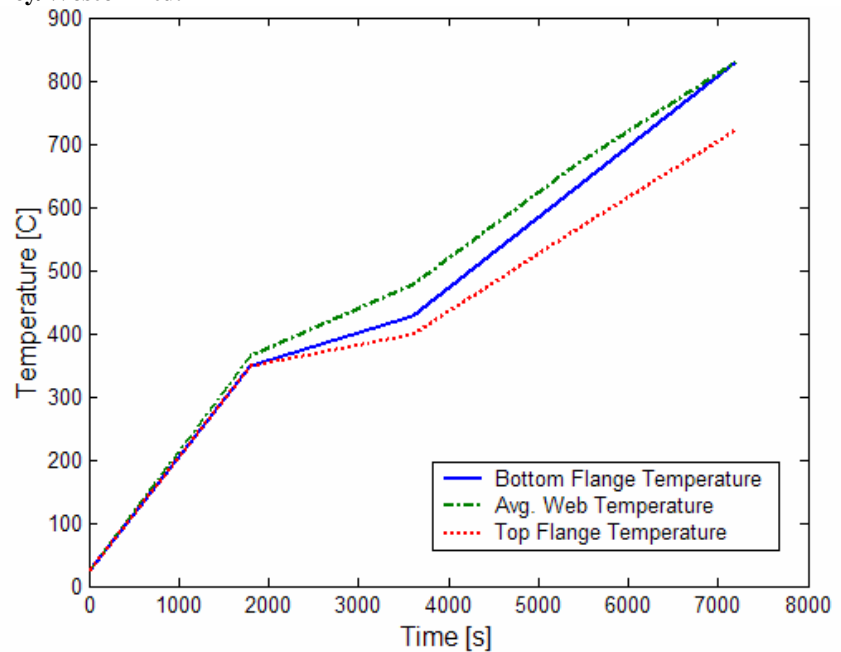


Figure 73 - Protected Steel Temperatures for the top flange, web, bottom flange of the cellular beam section obtained from FABSEC.

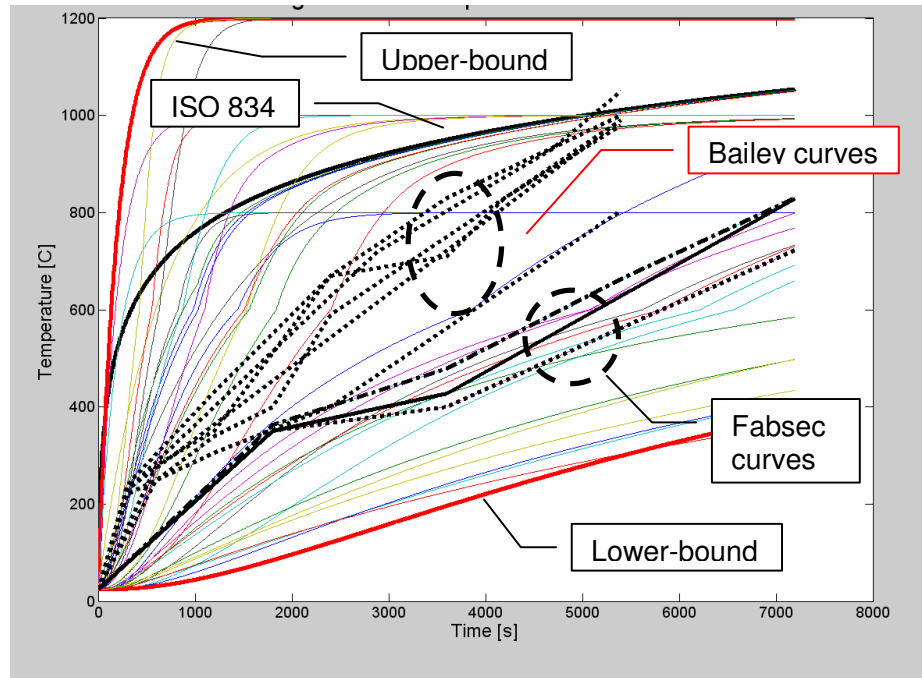


Figure 74 - Envelope of time-temperature curves investigated in this report.

Chapter 4: Results and Discussion

4.1 Overview

The structural fire analysis conducted in this study is an uncoupled model, which means that the solid phase temperatures are calculated in a separate heat transfer analysis independent of the mechanical analysis. But in a fully coupled model, the calculated solid phase temperatures would be continuously updated and calculated based on the state of the fire and the gas phase temperatures. Nevertheless, the structural fire analysis conducted in this study reveals interesting insight into the structural response of cellular beams; it provides a sense of how these structural elements behave and which parameters play a more critical role in the response.

The cellular beam structural model is evaluated from several perspectives in this study to determine its sensitivity to several parameters. The displacements, deformations, connection forces, and stress concentrations of each case study are compared with the base cellular beam model and a solid beam mode. These details will indicate the effects varying parameters have only on global response and also local response of the cellular beam. This study will also reveal insight into the role of the surrounding structure to the response of the cellular beam, in question. As mentioned before, traditional structural tests are conducted on single elements, which markedly underestimate the reserved capacity of the structure as a continuous system. Support conditions, continuity, load transfer and structural redundancy that exist in typical structures are often neglected in historical structural fire analysis methods.

4.2 Results and Discussion

A summary of the models analyzed in this study are provided in Table 8 below. This table includes the distinguishing parameter studied, type of analysis method, simulation time, and if convergence was reached. Refer to Table 2: Test Matrix for more details regarding the beam characteristics.

As seen in Table 8, most of the analyses examined are conducted using the implicit solver in ABAQUS. Although most of the analyses do not go to completion, local failure mechanisms and general structural behavior is still observed. The lack of convergence in the implicit models are typically indicative of abrupt changes in the structure and/or material complexities. That is, any rapid changes in geometry or material properties.

Section 4.2.1 will discuss the results of the cases analyzed in Scenario I. The structural response of the “base” cellular beam model and solid beam model will be discussed in detail. Structural responses that are unique to the base models will be highlighted. For more specific details on each individual tests, refer to the Appendix. Section 4.2.2 will discuss the results of Scenario II; and Section 4.2.3 will detail the results of Scenario III.

Table 8: Computational results of the analyses

| Scenario | Case | Parameter Tested | Implicit/ Explicit | Analysis Time [s] | Converge / No Conv |
|------------|-------|---|-----------------------|-------------------------|--------------------------|
| Base Model | A | | I | 2010 | NC |
| Base Model | | | E | 7200 | C |
| Solid Beam | B | | I | 7200 | C |
| I | a.1 | hole diameter = 150mm | I | 1918 | NC |
| | a.2 | hole diameter = 300mm | I | 1966 | NC |
| | a.3 | hole diameter = 500mm | I | 7200 | C |
| | b.1 | end post = 100mm | I | 1790 | NC |
| | b.2 | end post = 400mm | I | 7200 | C |
| | b.3 | endpost = 1400mm | I | 1030 | NC |
| | b.3DE | endpost = 1400mm | E | 7200 | C |
| | c.1 | # of holes = 12 | I | 2000 | C |
| | c.2 | # of holes = 28 | I | 7200 | NC |
| | d.1 | web thickness = 8mm | I | 1828 | NC |
| | d.2 | web thickness = 20mm | I | 2046 | NC |
| | e.1 | flange thickness = 12mm | I | 7200 | C |
| | e.2 | flange thickness = 48mm | I | 1633 | NC |
| | f.1 | bottom flange width = 270mm | I | 1990 | NC |
| | f.2 | bottom flange width = 470mm | I | 1991 | NC |
| | g.1 | span = 6150mm | I | 7200 | C |
| | g.2 | span = 12000mm | I | 7200 | C |
| II | 1 | Tmax = 1200C, a = 0.005 | I | 1635 | NC |
| | 2 | Tmax = 1000C, a = 0.005 | I | 7200 | C |
| | 3 | Tmax = 800C, a = 0.005 | I | 1098 | NC |
| | 4 | Tmax = 1000, a = 0.0015 | I | 2008 | NC |
| | 5 | Tmax = 1000, a = 0.0007 | I | 2295 | NC |
| III | 1 | Increased web temperature (protected) | | 4380 | NC |
| | 2 | Increased web temperature (unprotected) | | 1030 | NC |

4.2.1 Cellular Beam Model Analysis

The “base” cellular beam model was used as the reference case throughout the study. It is described in detail in section 3.5.1. The geometric variables of the model (hole diameter, end post length, number of holes, web

thickness, flange thickness, bottom flange width, and span length) are presented and discussed independently.

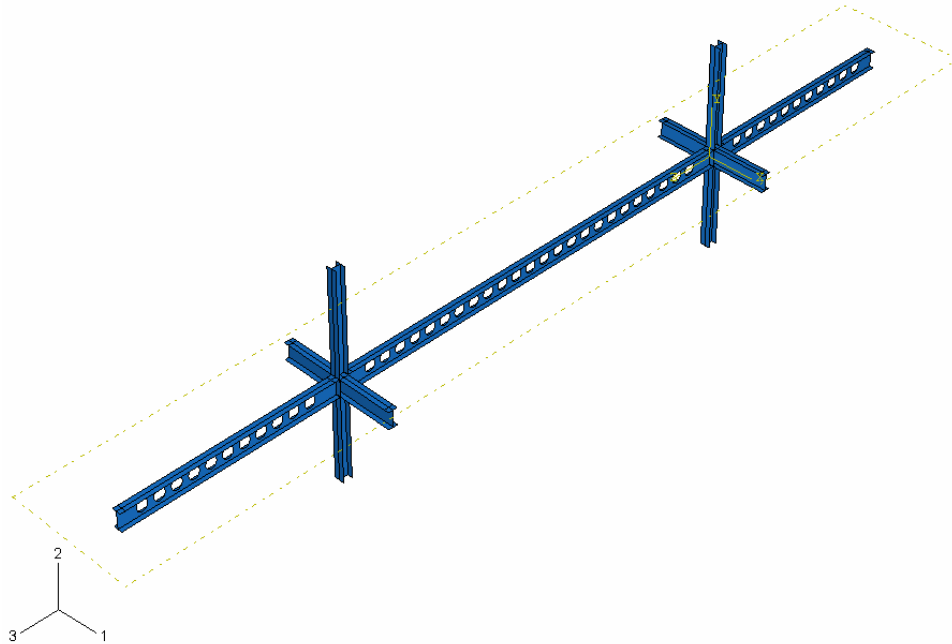


Figure 75 - Base cellular beam model (image from Abaqus)

Figures 76 and 77 show the displacement of the entire structural system after loading and after the 2-hour fire exposure, along with the corresponding deformation of the cellular beam at the final stage. At the end of the fire simulation, the cellular beam has undergone significant lateral torsional buckling, as seen in Figure 78. Snap shots of the deforming beam over time can be seen in Table 9, and provide insight into the mechanisms that initiate local failure of the beam. In addition Table10, illustrates the Von Mises stresses over time highlighting significant times in which the stress concentrations indicate local failures, particularly the 1st failure mechanism. As indicated and seen in Table 9 and 10, the initiating failure mechanism appears to be the buckling of the

web post. Figure 79 is an enlarged image of the end-post at the initiation of buckling failure (at $t=515s$ and $t=536s$). This appears to occur at 515s with a steel temperature of 319C. After this point, the stress concentrations spread into the length of the beam from the end supports; the web posts near the end supports begin to buckle in succession leading to significant lateral torsional buckling (Figure 80). After 2600s, additional lateral torsional buckling is minimal and the beam appears to displace in catenary action.

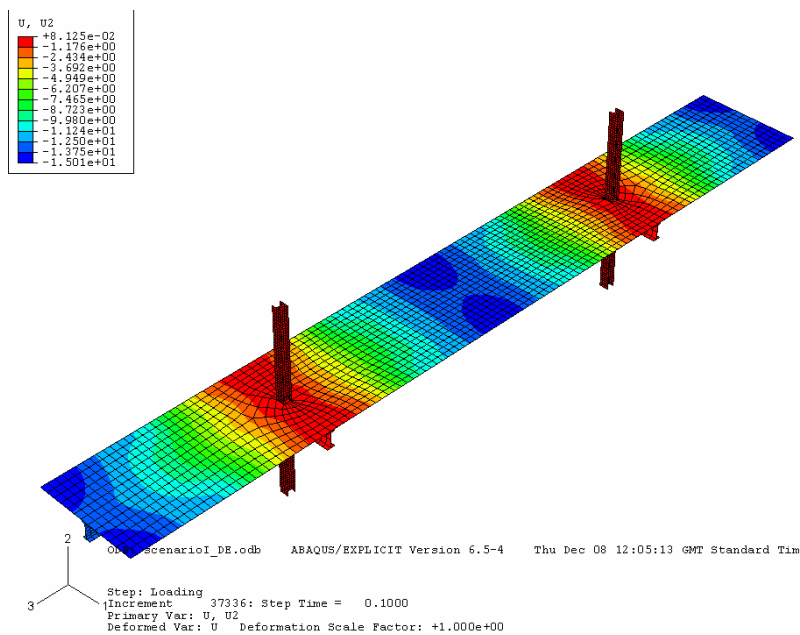


Figure 76 - Vertical displacement of "base" cellular beam model after loading.

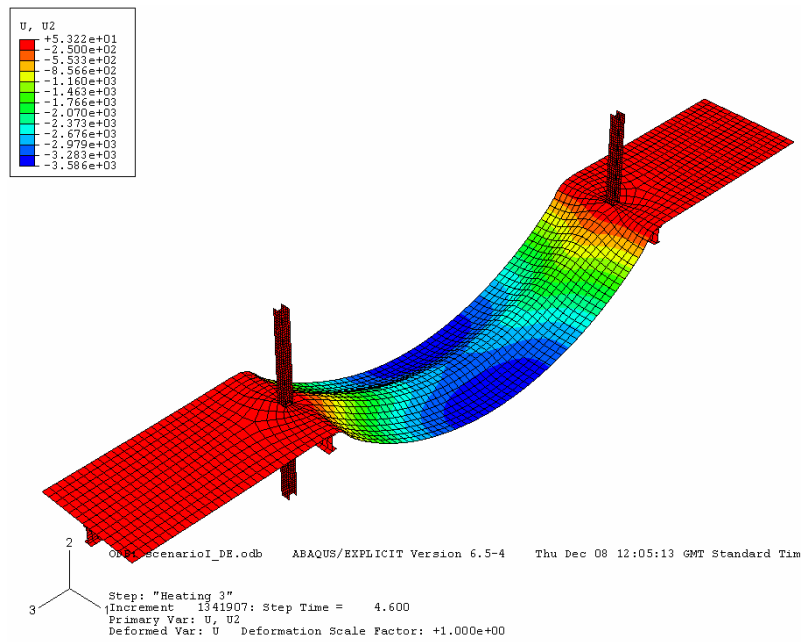


Figure 77 - Vertical Displacement and Deformation of base model after the 2-hour fire exposure.

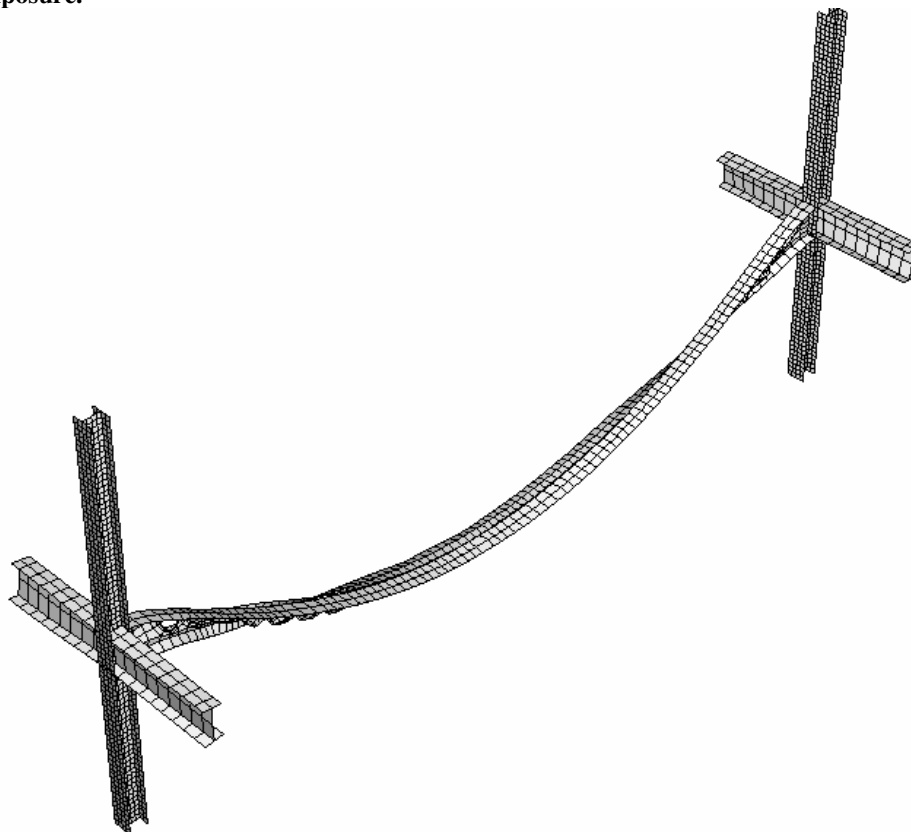


Figure 78 - Lateral torsional buckling of cellular beam at the end of the simulation.

Table 9: Deformations Time History of “Base” Cellular Beam Model

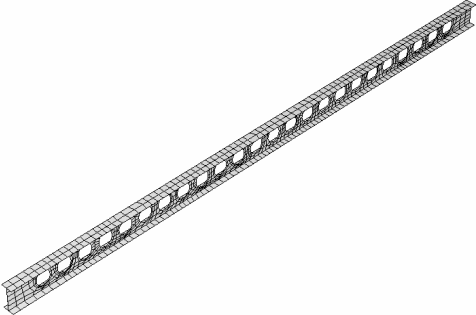
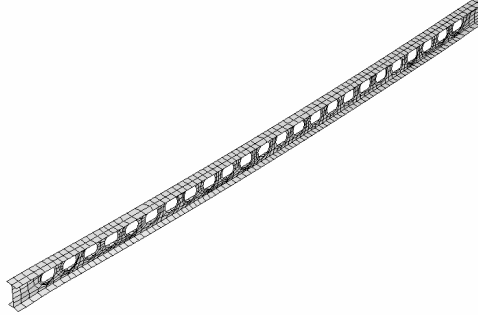
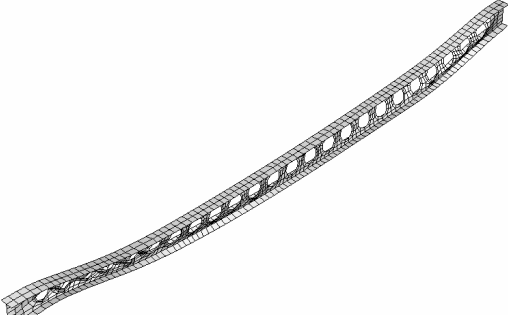
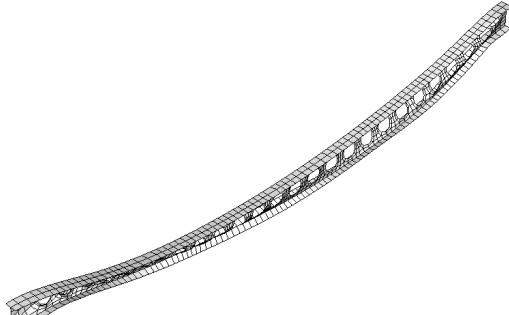
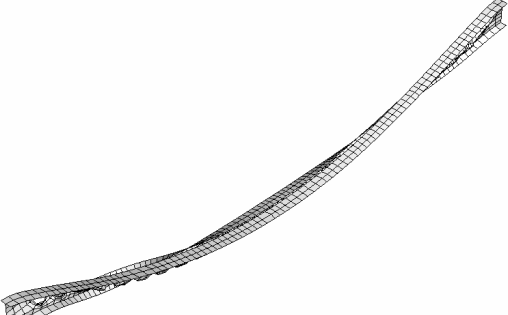
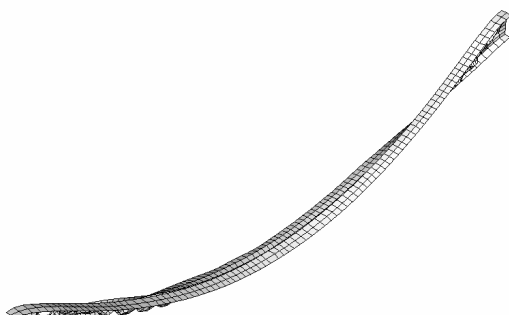
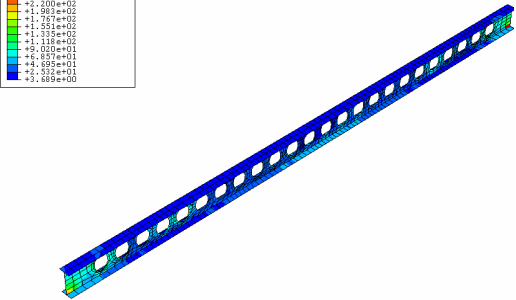
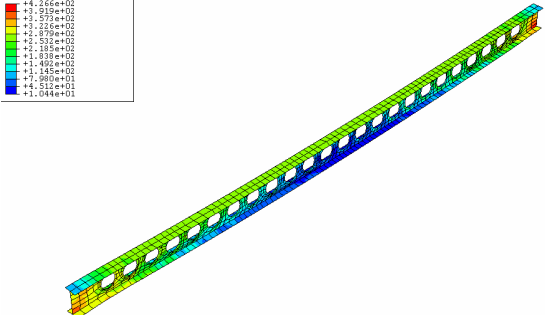
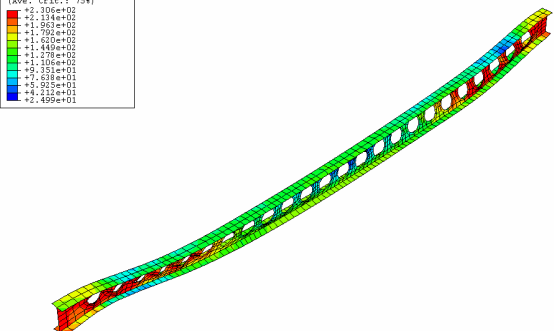
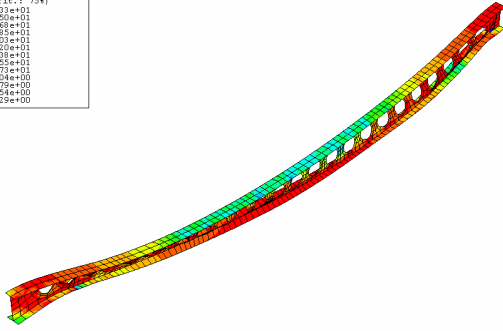
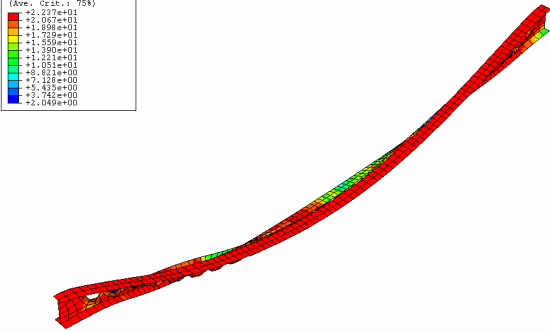
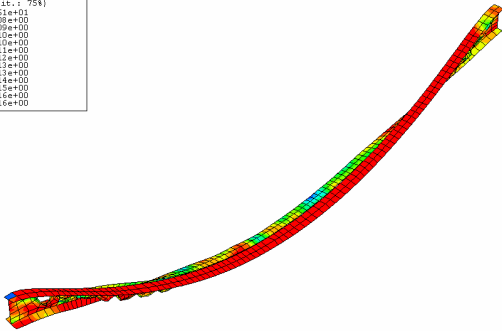
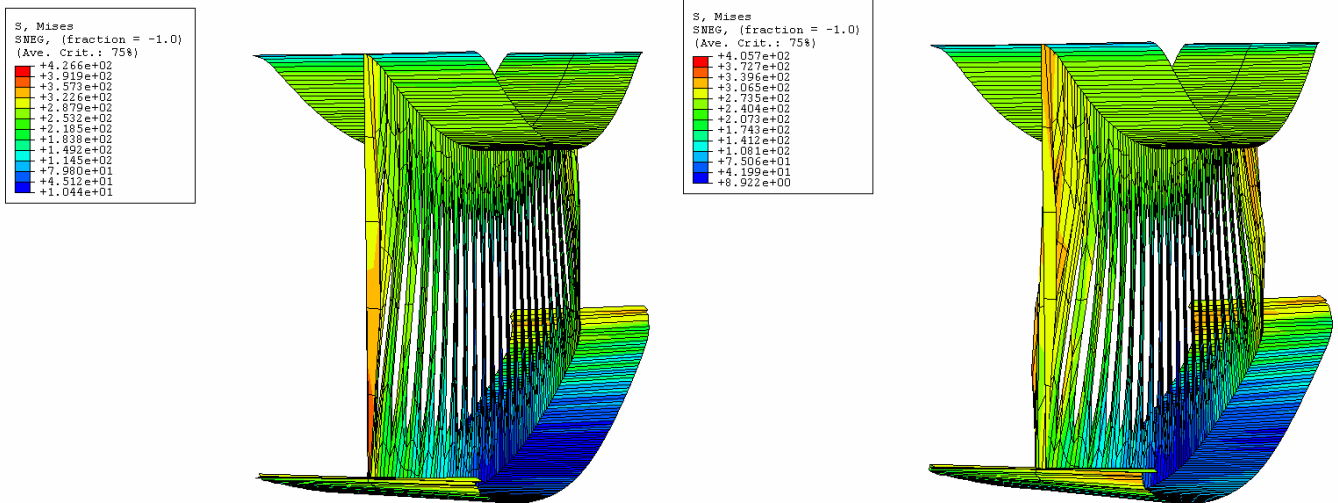
| | |
|--|---|
|  <p>Time = 0 sec, Temp = 25 C, Localized stress concentrations at bottom of beam at end supports</p> |  <p>Time = 515 sec, Web Temp = 319 C Bottom flange starts to lateral displace; end post appears to be buckling. Lateral torsional buckling is initiated. Stress concentrations are near the supports. Web posts near the support are starting to buckle</p> |
|  <p>Time = 1030 sec, Temp = 542C Significant lateral torsional buckling. After last slide, web posts began to buckle rapidly. Bottom flange appears to be buckling too. High stress concentrations at supports</p> |  <p>Time = 1867 sec, Temp = 821 C As the stress concentrations spread along the web of the beam, more web posts buckle. Significant web and flange buckling. Significant lateral torsional buckling and displacement.</p> |
|  <p>Time = 2600 sec, Temp = 894 C Stress concentrations throughout the length of the beam. Significant lateral torsional buckling.</p> |  <p>Time = 7200 sec, Temp = 1051C Stress concentrations throughout beam. No increase in lateral torsional buckling. Catenary action witnessed. No global failure of system. End of simulation.</p> |

Table 9: Von Mises Stress Time History of “Base” Cellular Beam Model

| | |
|--|---|
| <div><p>S, Mises SRES, (fraction = -1.0) (Ave. Crit.: 75%)</p></div> <p>Time = 0 sec, Temp = 25 C, Localized stress concentrations at bottom of beam at end supports</p> | <div><p>S, Mises SRES, (fraction = -1.0) (Ave. Crit.: 75%)</p></div> <p>Time = 515 sec, Web Temp = 319 C Bottom flange starts to lateral displace; end post appears to be buckling. Lateral torsional buckling is initiated. Stress concentrations are near the supports. Web posts near the support are starting to buckle</p> |
| <div><p>S, Mises SRES, (fraction = -1.0) (Ave. Crit.: 75%)</p></div> <p>Time = 1030 sec, Temp = 542C Significant lateral torsional buckling. After last slide, web posts began to buckle rapidly. Bottom flange appears to be buckling too. High stress concentrations at supports</p> | <div><p>S, Mises SRES, (fraction = -1.0) (Ave. Crit.: 75%)</p></div> <p>Time = 1867 sec, Temp = 821 C As the stress concentrations spread along the web of the beam, more web posts buckle. Significant web and flange buckling. Significant lateral torsional buckling and displacement.</p> |
| <div><p>S, Mises SRES, (fraction = -1.0) (Ave. Crit.: 75%)</p></div> <p>Time = 2600 sec, Temp = 894 C Stress concentrations throughout the length of the beam. Significant lateral torsional buckling.</p> | <div><p>S, Mises SRES, (fraction = -1.0) (Ave. Crit.: 75%)</p></div> <p>Time = 7200 sec, Temp = 1051C Stress concentrations throughout beam. No increase in lateral torsional buckling. Catenary action witnessed. No global failure of system. End of simulation.</p> |



2
1

Figure 79 – At 515s, end post buckling of base cellular beam model. This appears to be the initiating failure mechanism. (Note: T = 319C) (Right) At 536s, the web posts near the support begin to buckle.

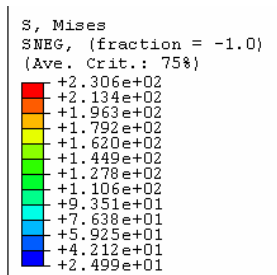


Figure 80 – At t=1030s, stress concentrations spreading from the supports. Web posts are buckling and the beam is undergoing lateral torsional buckling. (T=542C)

After this ultimate buckling event, deflection begins to grow at a higher rate which is also supported by the displacement-time curve and displacement-temperature curves (Figures 81 and 82). In addition, this event seems to be

coupled with the steel beam reaching its ultimate axial capacity, which is occurring around 350C.

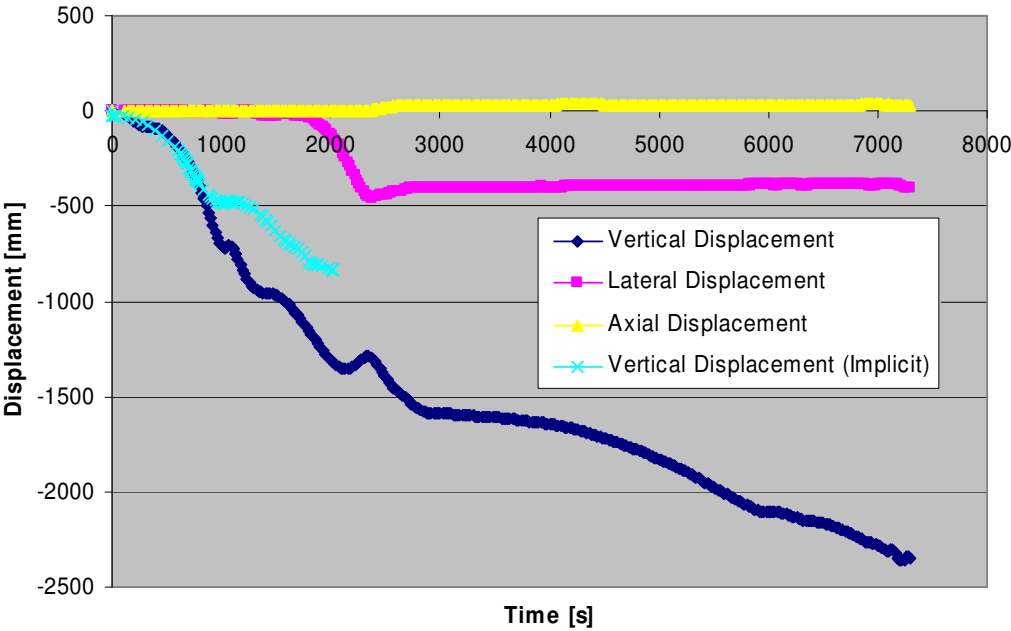


Figure 81 - Midspan displacement of cellular beam with time

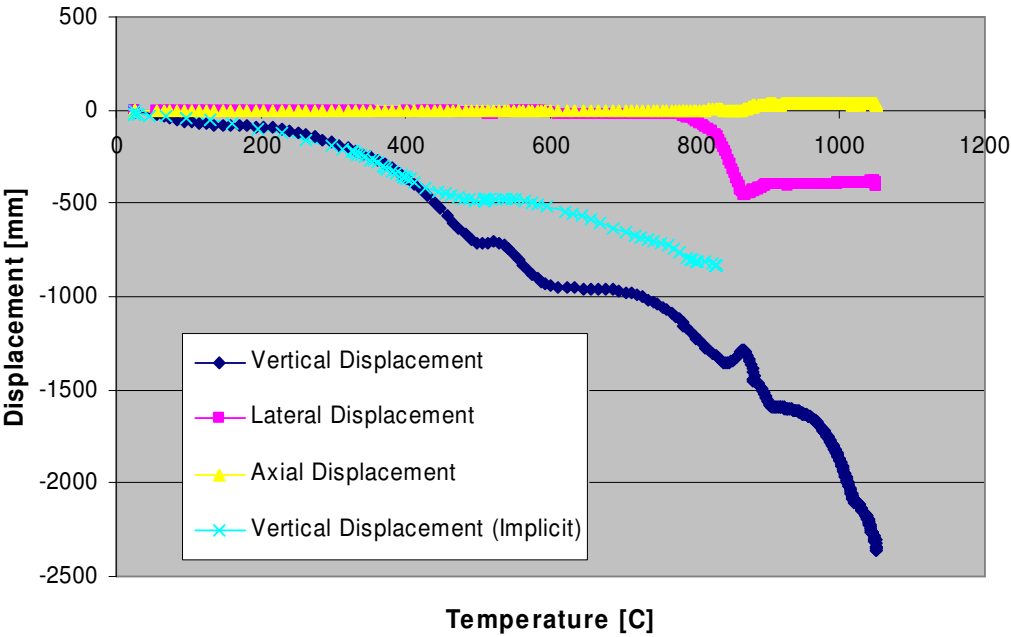


Figure 82 - Midspan displacement of cellular beam with temperature.

Figure 83 shows the axial forces at various points along the height of the heated steel beam, all of which begin to decline as the steel strength and stiffness degrades from heating.

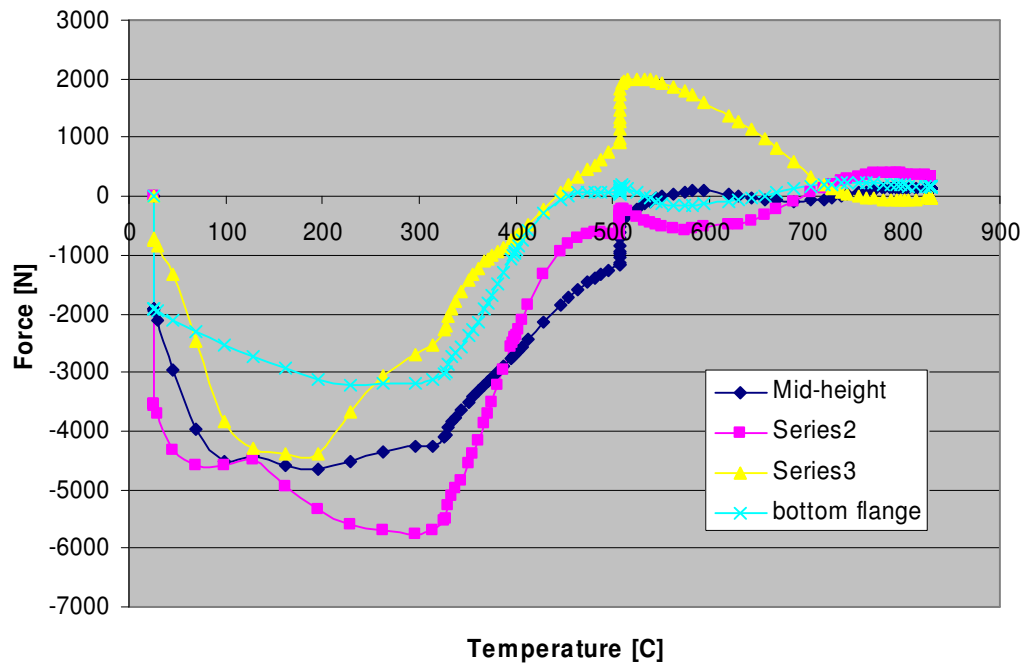


Figure 83 - Axial force in cellular beam as a function of temperature.

In the paper by Usmani and Lamont [33], an initial local buckling event of the lower flange is described as being one of the first structural events to occur in steel beams with composite decks. This study examined the event in detail by considering a secondary beam from the Cardington restrained beam tests. From the analysis, the stress in the bottom flange at 150°C was calculated as 573 MPa which was clearly over the yield stress of the steel (318 MPa). The analysis in this paper would suggest that the initial local buckling event would occur at around 120°C and was clearly evident by the reduction in axial forces (Figure 84) and a significant increase in deflection rate.[33]

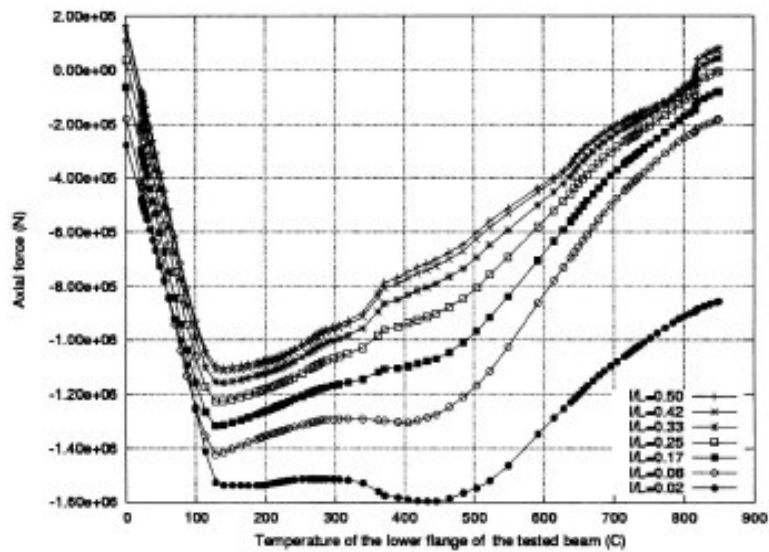


Figure 84 - Axial forces at different locations in Cardington steel beam test.
[Usmani,] Ref.33

This local buckling behavior appears to be evident in the base cellular beam model and is suggested by the force-temperature history in Figure 83, where a “kink” occurs even before 100 °C. The yielding of bottom flange may be occurring at an earlier time in the fire in the cellular beam model than the temperature suggested by Usmani [33] because the holes in the cellular beam may be increasing the local compressive forces in comparison to a solid beam.

However, this behavior is not visible in the deformation/stress time history analysis, or in the displacement temperature history. In these figures, there does not appear to be a significant increase in displacements after the initial yielding event. The second major event, the buckling of the web-post, appears to be the more significant event that leads to increased deflection rates and ultimately significant P-delta moments.

In terms of global failure of the system, the deflections appear to be increasing rapidly with very small increases in temperature, as seen in Figure 82. This phenomena of runaway displacement is an indication that global structural failure is occurring.

4.2.2 Solid Beam Model

In addition to the base cellular beam model, the solid beam model was used throughout the study for comparison. The solid beam model was analyzed in a similar fashion to the cellular beam model analysis, as presented above. For brevity the detailed deformations, displacements, and stress concentration snap-shots are provided in Appendix D. This section will highlight the main differences observed between the two models.

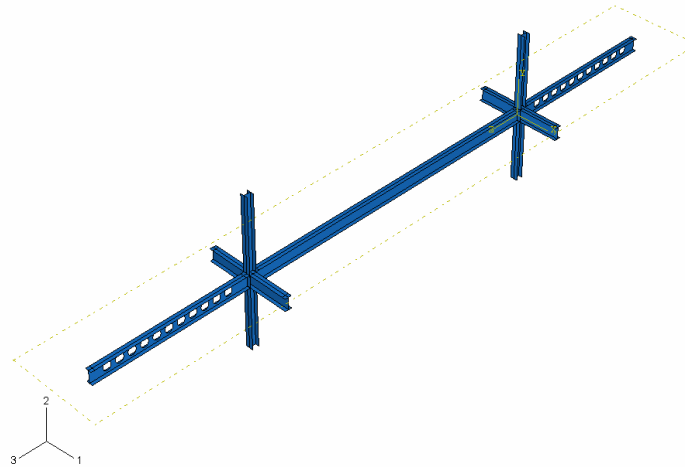


Figure 85 - Solid beam model

In analyzing, the failure mechanisms of the solid beam model in comparison with the base cellular beam model, the solid beam model does not appear to have a distant first local yielding event described by Usmani [33] of the bottom flange. At around 100 – 150 °C, the solid beam

is continuing to have increased compression axial forces as seen in Figure 88 with no increased displacement rates visible in Figures 89 and 90. Also, the magnitude of the axial forces in the early stages of the fire are substantially less than those in the cellular beam. These factors maybe suggesting that there is not a significant compression force localizing at the bottom flange and causing a sudden buckling of that section, as was the case with the cellular beam. This may be a result of the increased depth (690mm) of the solid beam relative to the beams tested in the Cardington tests which may be causing the axial forces to be distributed more evenly in the web and bottom flange. With respect to the cellular beam, the solid beam has the full depth of its web to transfer forces, reducing the likelihood of force localization.

As with the cellular beam model, the significant increases in displacement appear to occur at a second buckling event around 350 °C. For the solid beam, the second event appears to be the buckling of the bottom flange near the support and is a more gradual failure mechanism than that experienced in typical composite beam fire tests.

Figure 86 , taken at $t = 790$ s, illustrates that the high stress concentrations are located near the support and that the bottom flange of the beam is yielding, evident by the lateral torsional buckling.

As seen in Figure 87, the cellular beam model has substantial web post buckling, end post buckling, and bottom flange buckling. This snap-shot is approximately 700 s into the fire exposure.

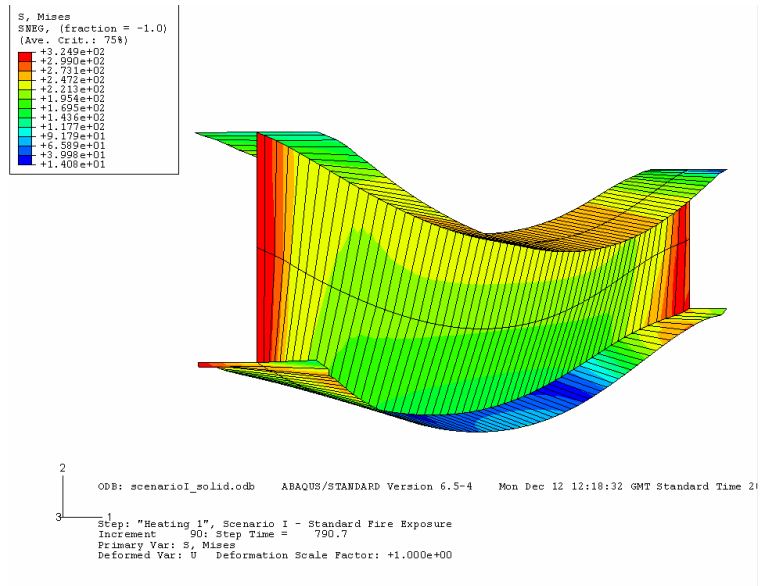


Figure 86 - Bottom flange buckling in solid beam model.

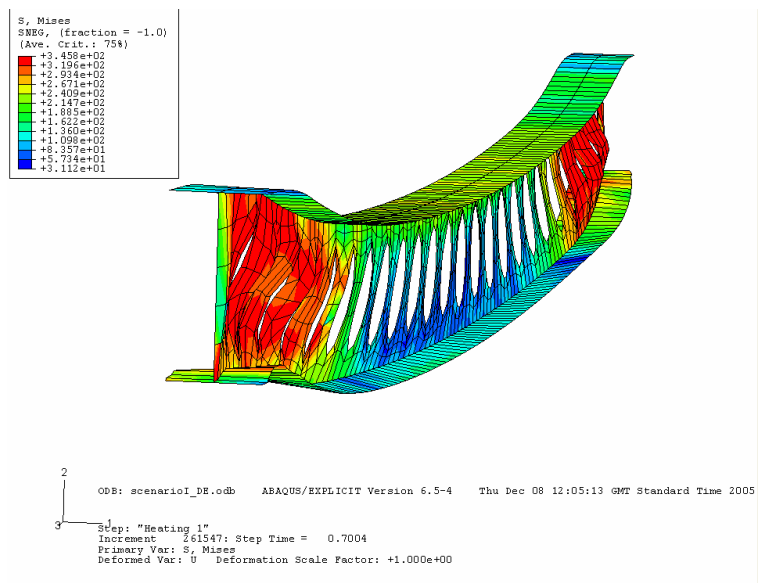


Figure 87 - Endpost, web post, and bottom flange buckling in cellular beam model (t = 700s, T=350-400 °C)

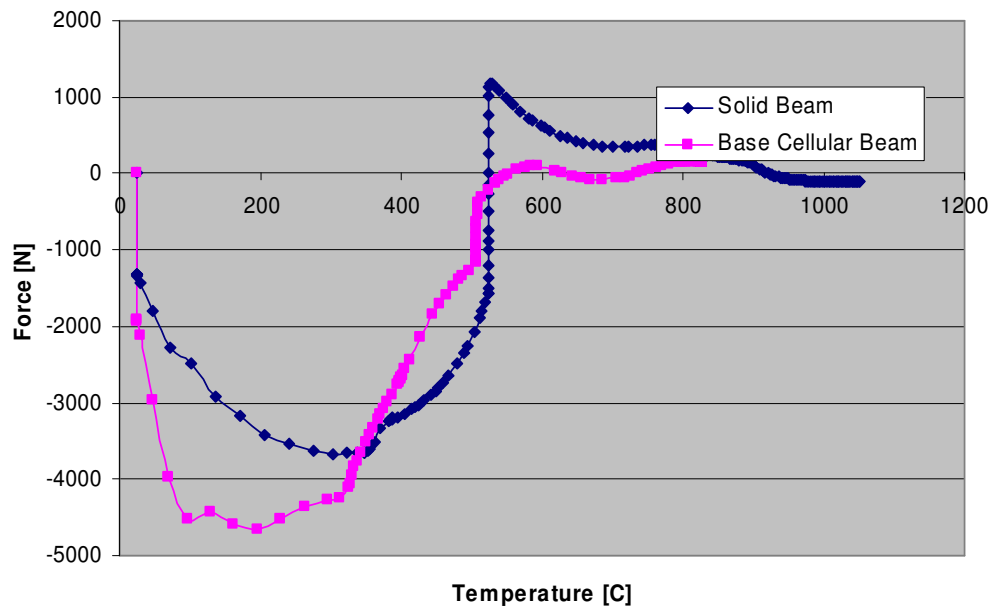


Figure 88 - Axial force vs. temperature of solid beam and base cellular beam models.

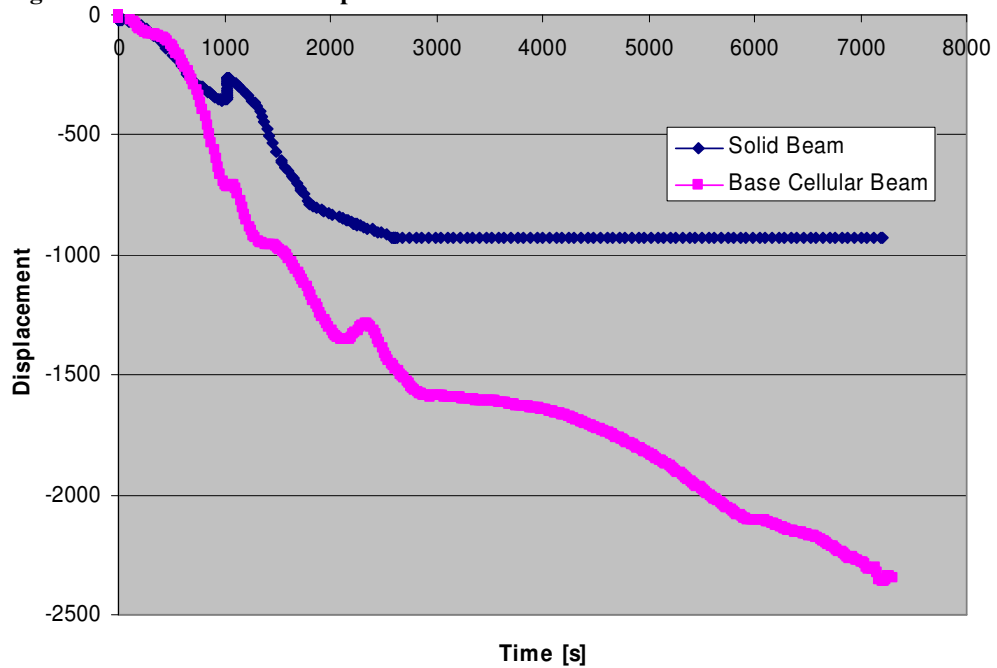


Figure 89 - Midspan displacement vs. time for solid and cellular beam models

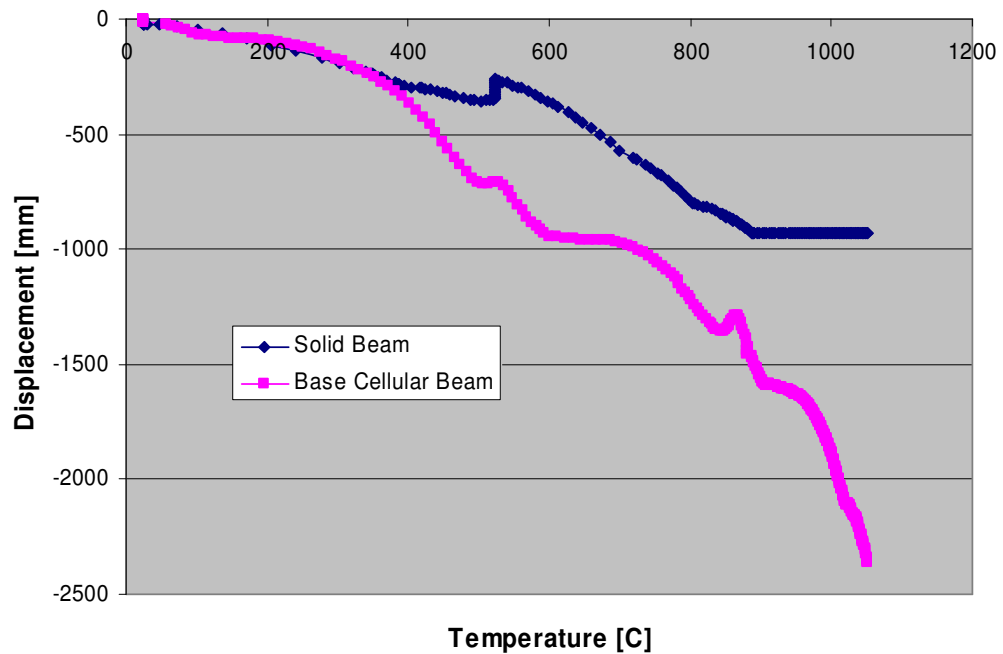


Figure 90 - Midspan displacement vs. Temperature comparison of solid beam and cellular beam.

Overall, the solid beam appears to behave relatively better than the base cellular beam model. Because there is a delay in the buckling/yielding, the structure appears to be more stable – less displacements, lower displacement rates and less localization of forces – which may limit the likelihood of a sudden global failure.

4.2.3 Scenario I Parametric Study

The variables in this scenario were web opening diameters, end post length, number of holes, web thickness, flange thickness, bottom flange width, and span length. Each variable was analyzed similar to that conducted in the base cellular beam model and solid beam model. Each variable is presented and discussed independently. Case specific results

will be discussed in the following sections. General observations common to all tests will be discussed in the summary section.

4.2.3.1 Vary Diameter of Holes

In this case study, various web hole diameters were studied. The sizes tested were 150 mm, 300 mm and 500 mm. The base cellular beam model had web opening diameters of 450 mm. All other aspects of the structural system and geometry were maintained. However, in order to keep the end post length and number of holes, the web post lengths were adjusted to accommodate the new diameters. The web post lengths were 548 mm, 391 mm, and 183 mm of the 150 mm diameter case, 300 mm and 500 mm case respectively. The base model had a web post length of 235 mm. Refer to Table 8 and Appendix D for details of the analysis. Figure 91 is a visual representation of each case analyzed.

Figure 91 - Web hole diameter case study. Web holes tested include: 150mm, 200mm, 300mm, and 500mm

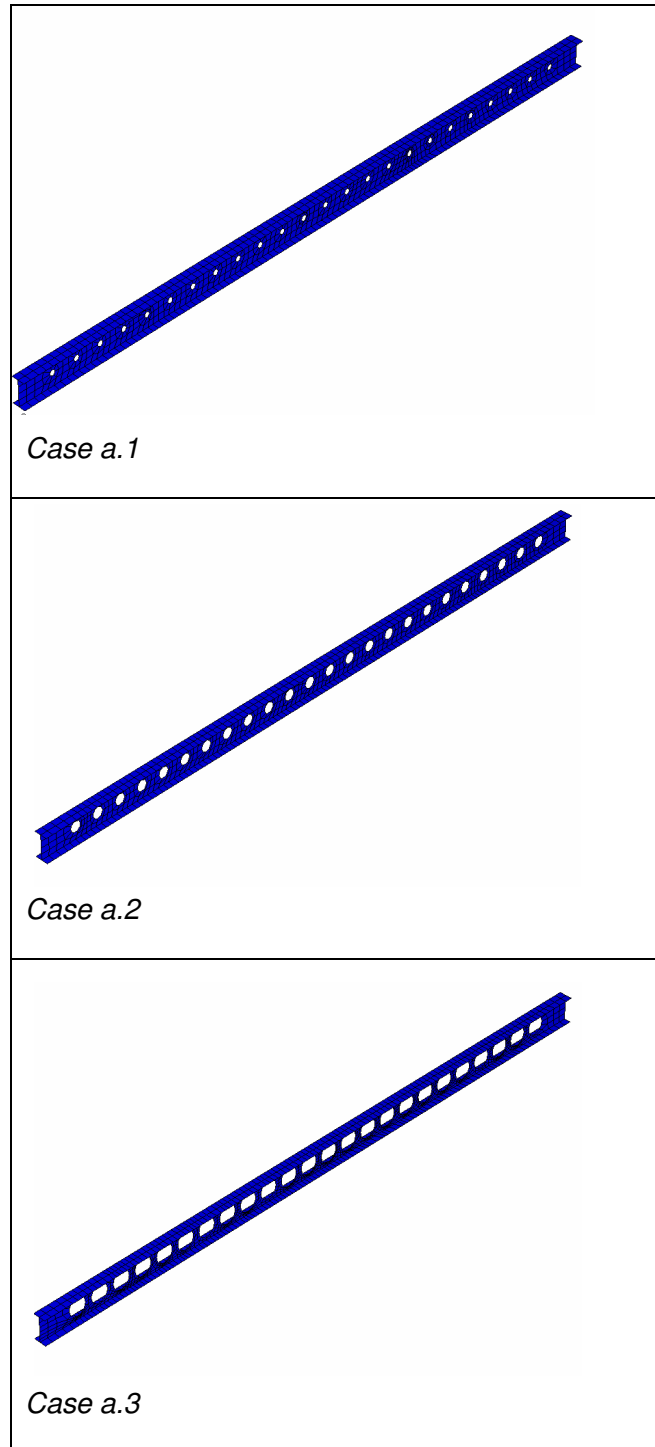


Figure 92 shows that web hole diameter does not have an effect on axial forces until the web opening becomes too large at 500 mm. All the diameters have similar axial force behavior until the axial forces began reversing at around 300 °C, which coincides with the second buckling event described earlier. After this event, the 500 mm case rapidly changes from compression to tension. This may suggest that large diameter openings in webs, once local buckling has occurred, will immediately go into catenary action or have a sudden failure. Global structural failure, however, is not evident in Figures 93 and 94 for the 500 mm diameter case.

Figure 94 shows the vertical displacement for various web opening diameters over time. It can be seen that diameter does not affect the displacement of the beam up to around 380 °C, apart from the 500 mm case which displaces much sooner at 250 °C. The differences in displacement after this point may be a result of the mechanism of failure (i.e. the second buckling failure mode). The 150 mm, 300 mm, and solid beam models all had similar failure mechanisms in that they had bottom flange yielding at similar temperatures (~350 °C), as seen in Figure 95. The 500 mm and 450 mm (base model) cases had web-post buckling as the dominant failure mechanism as seen in Figure 96. In addition, the main buckling event for the 500 mm case occurred at 250 °C. This may be an explanation for the displacement behavior seen in Figure 94.

Also, in Figure 94 the 500 mm does not appear to experience runaway displacement throughout the duration of the simulation. This case involves the largest diameter holes and therefore is the weakest beam for this case

study. As such, it is reasonable to assume that the cases with smaller diameter holes will not experience runaway displacement as well. However, explicit models should be conducted to verify this assumption.

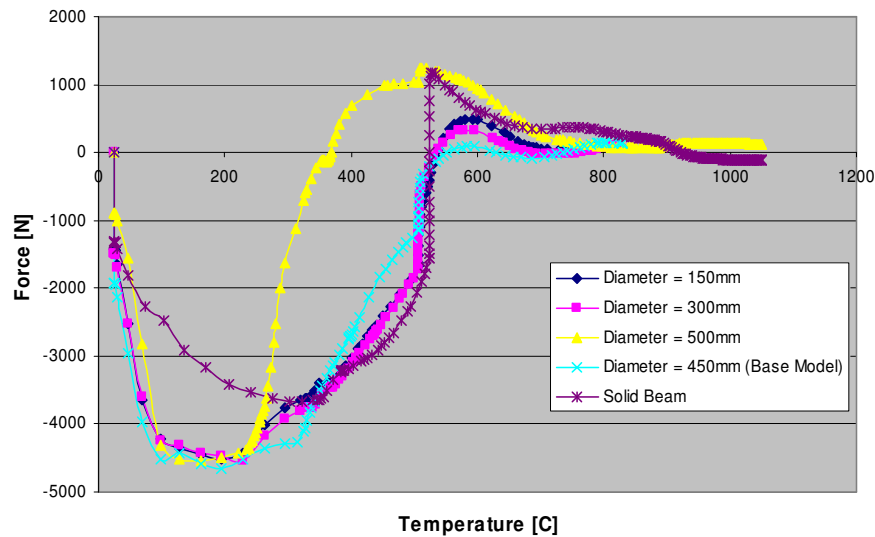


Figure 92 - Axial forces vs. Temperature of cellular beams with varying web opening diameters.

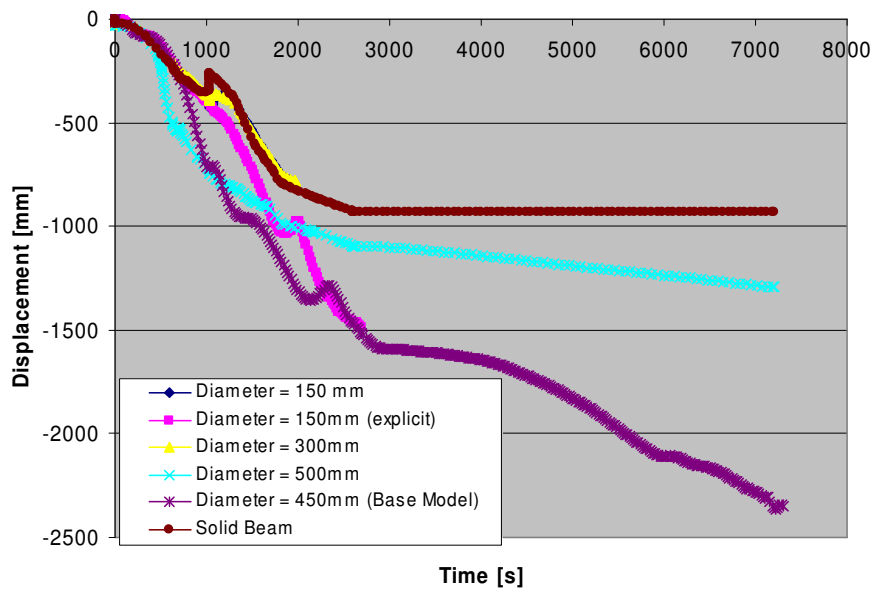


Figure 93 - Midspan displacement of cellular beams with varying web opening diameters vs. time

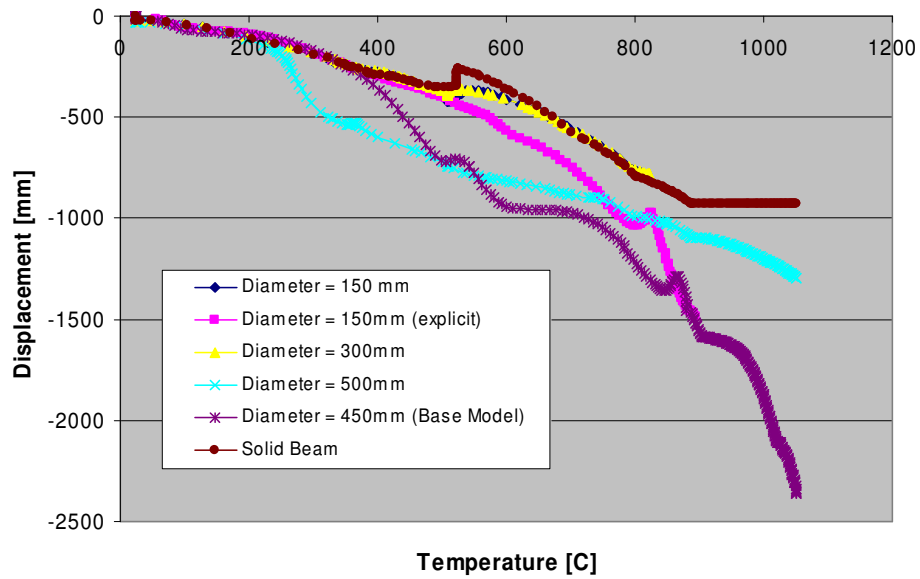


Figure 94 - Displacement vs. Temperature for various web opening diameters

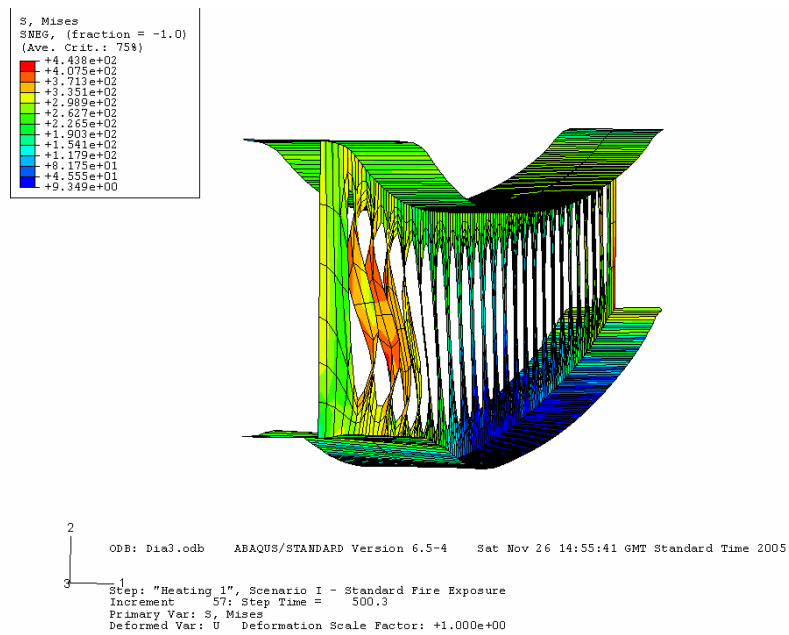


Figure 95 - Web post buckling evident in 500 mm diameter case. This occurred at 250 °C.

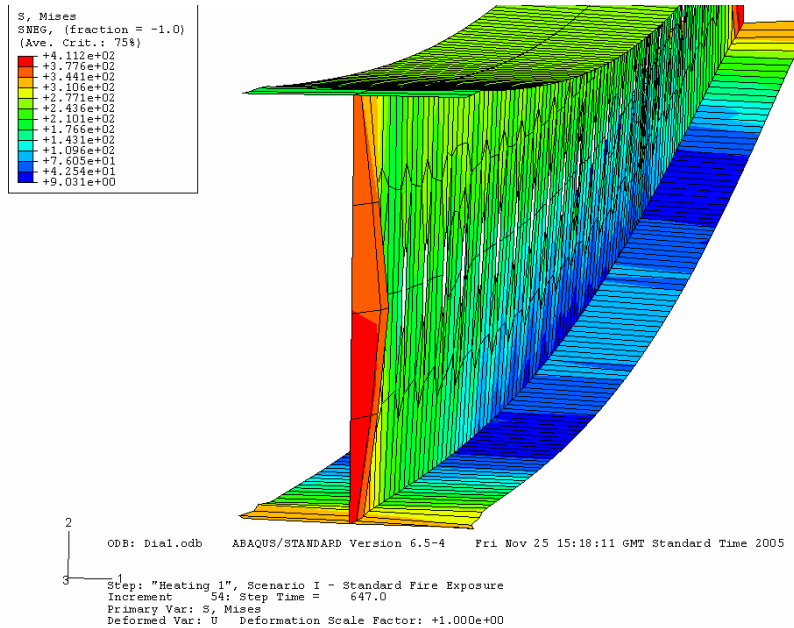


Figure 96 - Bottom flange yielding and end post buckling initiating in 150 mm diameter case. This occurred at ~ 350 °C

4.2.3.2 Vary End Post Length

In this case study, various end post lengths were examined. The end post, as commonly referred to, is the distance from the end of the beam to the edge of the first web opening. The sizes tested were 100 mm, 400 mm and 1400 mm. The base cellular beam model had an end post distance of 900 mm. All other aspects of the structural system and geometry were maintained. However, in order to keep the original hole diameter and number of holes, the web post lengths were adjusted to accommodate the new end post lengths. All three trials were run using implicit analysis. Refer to Table 8 and Appendix D for details of the analysis. Figure Y is a visual representation of each case analyzed.

**Figure 97 – End post length case study. End posts tested include:
100mm, 400mm, 900mm, and 1400mm**

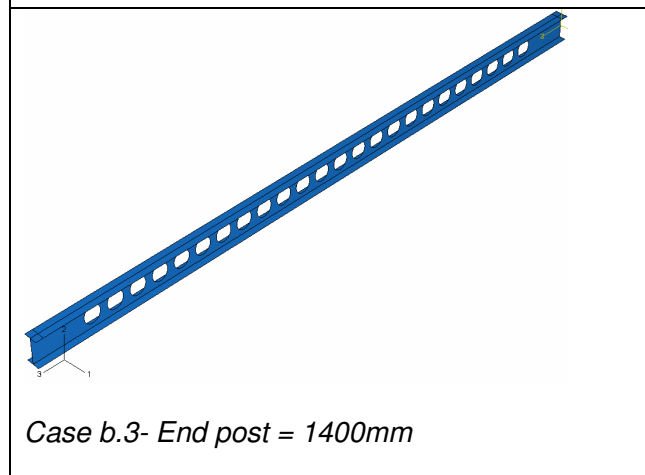
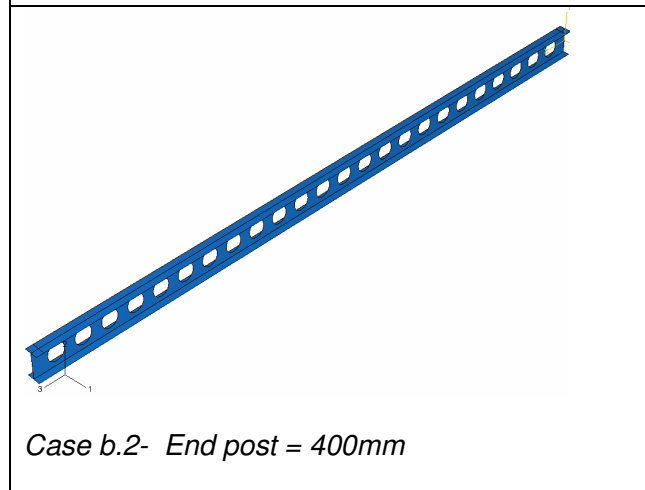
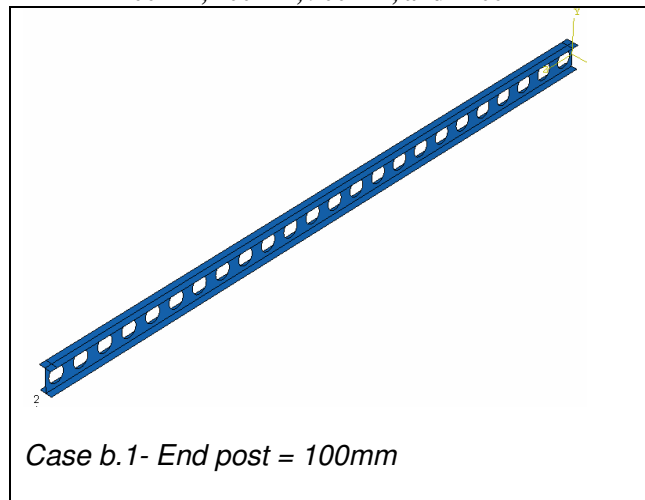


Figure 98 shows that increasing the end post length results in greater axial forces at the mid-height of the support with temperature. An end post length of 100mm induces an axial compressive force of approximately 2kN, while an end post length of 1400mm, an axial force of 4.5kN is seen. This is most likely a result of the forces being taken at the mid-height of the web, where the axial forces would be low for beams with holes near the support. The tensile and compressive forces would mostly be transferred to the support through the flanges. As the end post increases to 900 mm and 1400 mm the forces appear to be similar, until the solid beam case. Further study would need to be conducted to determine if a more efficient force distribution in the solid beam is the discrepancy in the forces.

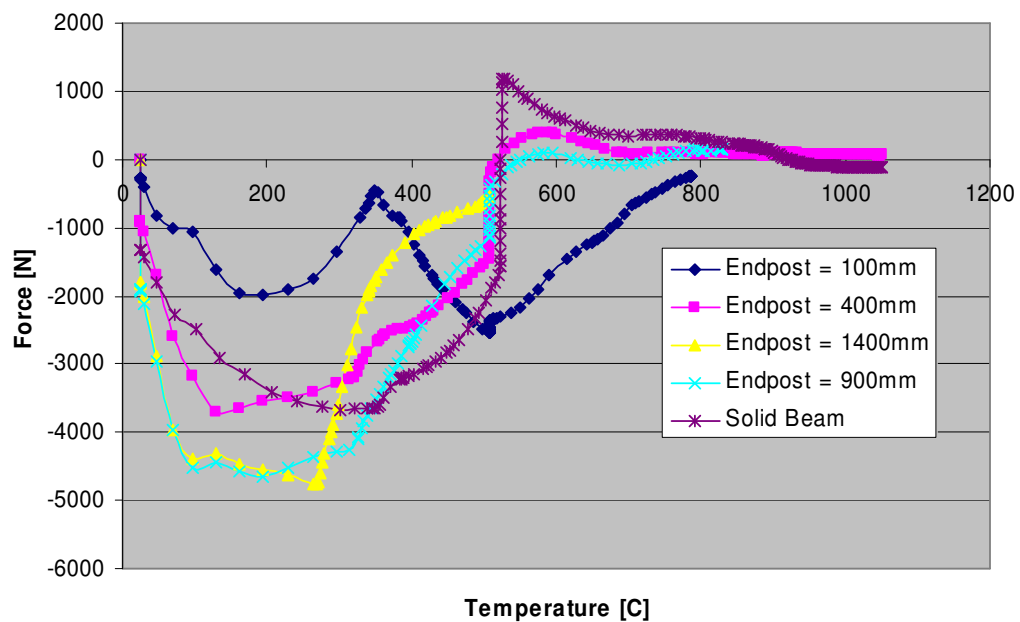


Figure 98 - Axial forces vs. temperature for varying end post lengths

It is interesting to note in Figure 98 that the 400 mm end post test appears to indicate the first local buckling event described by Usmani

[33]; whereas, the other cases appear to have two buckling events. (See Summary Section for further discussion.)

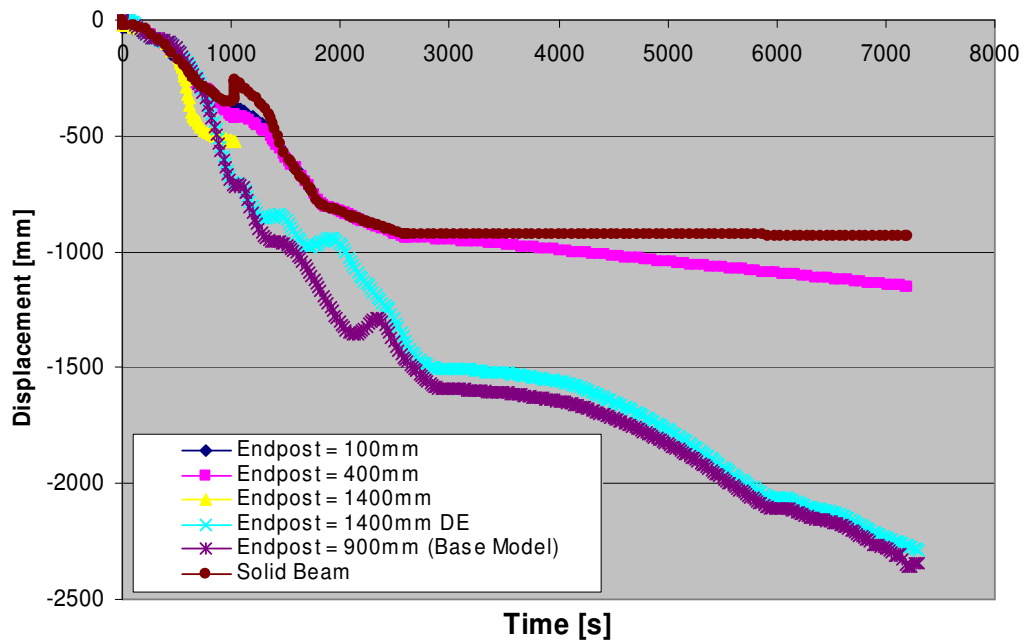


Figure 99 - Displacement vs. time for varying end post lengths

Figures 99 and 100 appear to indicate that smaller end posts result in lower displacements over time, as well as, lower displacements with respect to temperature. However, in analyzing the deformations, stresses and buckling behavior of the beams, the correlation between end post length and displacement behavior is misleading. The smaller end posts had buckling of the bottom flange similar to the solid beam tests; the larger end posts, had web-post buckling behavior. These failure mechanisms and the associated displacements also occurred in the previous variable study. Table 9 shows the web-posts for the various tests, the mode of failure and relative displacement. It can be seen that there is a strong correlation between web post size, type of failure mechanism and the resulting displacements.

Table 9: Type of failure mechanism and web-post length

| Scenario | Case | Parameter Tested | Type of Failure Mechanism | Web post Length | Relative Displacement |
|----------|------|-----------------------|---------------------------|-----------------|-----------------------|
| I | a.1 | hole diameter = 150mm | bottom flange yielding | 548 | Less |
| | a.2 | hole diameter = 300mm | bottom flange yielding | 391 | Less |
| | base | hole diameter = 450mm | web post buckling | 235 | Larger |
| | a.3 | hole diameter = 500mm | web post buckling | 183 | Larger |
| | b.1 | endpost = 100mm | bottom flange yielding | 304 | Less |
| | b.2 | endpost = 400mm | bottom flange yielding | 278 | Less |
| | Base | endpost = 400mm | web post buckling | 235 | Larger |
| | b.3 | endpost = 1400mm | web post buckling | 191 | Larger |

From Figures 98, 99, and 100 the effect of end post length does not appear to be clearly defined. Additional studies should be conducted to better determine the effects of end post length on beam response where they are not coupled with the web post thickness. End post length may play a significant role where shear is high near the supports.

An interesting failure mechanism was observed in the explicit model of the 1400 mm end post case. As seen in Figure 101, the cellular beam experienced some asymmetric web post buckling and lateral torsional buckling.

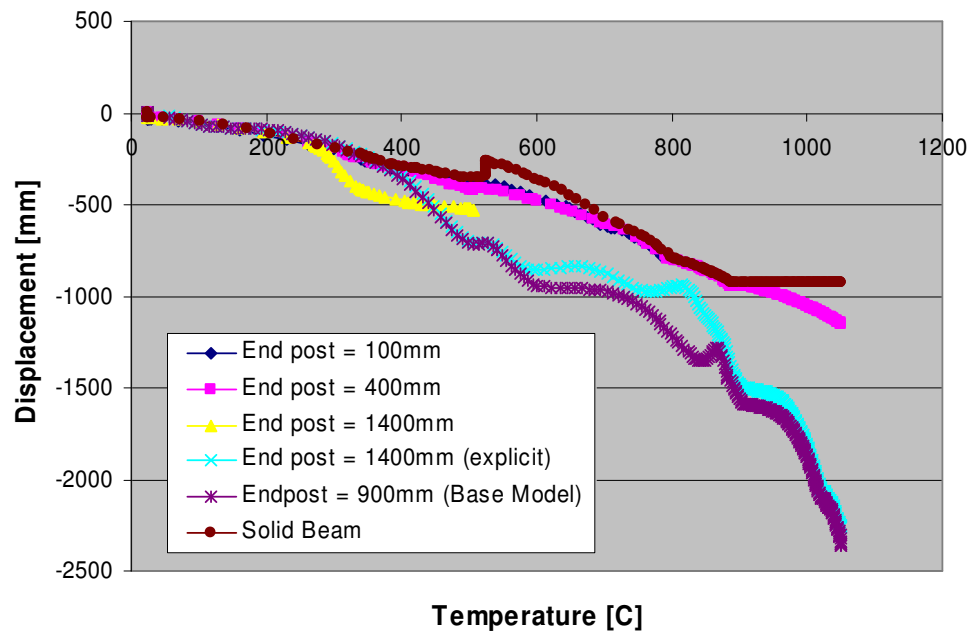


Figure 100 - Displacement vs. Temperature for varying endpost lengths.

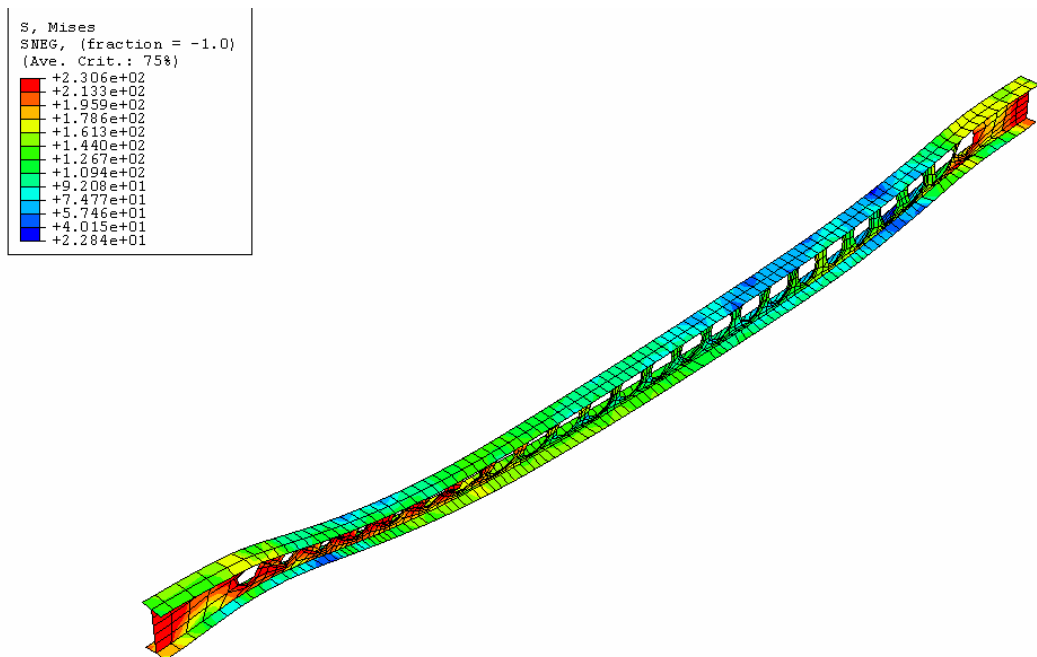


Figure 101 - Asymmetric web post buckling and lateral torsional buckling of 1400 mm endpost test.

4.2.3.3 Vary Number of Holes

In this case study, the number of holes along the length of the beam was studied. The number of holes tested was 12 and 28 holes. The base cellular beam model had 24 holes. All other aspects of the structural system and geometry were maintained. However, in order to keep the original hole diameter and end post length, the web post lengths were adjusted to accommodate the new opening count. Refer to Table 8 and Appendix D for details of the analysis. Figure 102 is a visual representation of each case analyzed.

**Figure 102 – Number of web openings case study. No. of openings include:
0, 12, 24, 28**

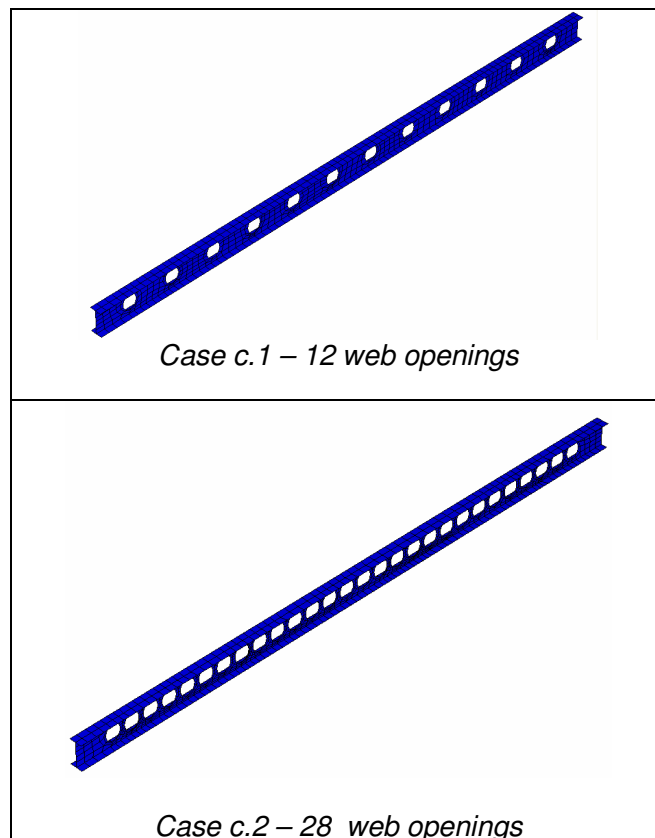


Figure 103 suggests that the number of web openings does not have an effect on axial forces during pre-buckling behavior. However, in post-buckling the effect of the number of holes is more evident. During post buckling, the beams with an increased number of holes have reduced axial stiffness and therefore increase in deflections and unload rapidly. The difference in axial force after the local buckling event, described earlier, is also associated with the failure mechanism. Similar to the previous two cases, the variation of this parameter was coupled with the web post lengths.

Table 10 is an update of Table 9 and indicates the web post lengths and observed failure mechanism. From these results, it can be seen that the increase in holes and the decrease in web-post length leads to web post buckling failure and ultimately larger displacements than beams with larger web posts. By increasing the number of holes and subsequently decreasing the web post size, you not only reduce the horizontal shear capacity of the beam, but also, decreasing the moment capacity and flexural stiffness of the section. This behavior is evident in Figure 104 and 105, as well as Figure 109.

Aside from the web post sizes, Figure 105 seems to indicate that increasing the number of holes results in greater deflection in the initial stages of the fire exposure. Because of the reduced flexural and axial stiffness of these beams, the displacements should be larger both in pre-buckling and post-buckling regimes. It is therefore reasonable to assume that this will continue in later stages of the fire. The base model appears to be experiencing runaway displacement; and being the more conservative model, it may be

reasonable to assume that the 28 hole case will have runaway failure as well.

An explicit model for both the 12 and 28 hole case should be run to validate this theory.

Table 10: Failure mechanisms and web post lengths (updated)

| Scenario | Case | Parameter Tested | Type of Failure Mechanism | Web post Length | Relative Displacement |
|----------|------|-----------------------|---------------------------|-----------------|-----------------------|
| I | a.1 | hole diameter = 150mm | bottom flange yielding | 548 | Less |
| | a.2 | hole diameter = 300mm | bottom flange yielding | 391 | Less |
| | Base | hole diameter = 450mm | web post buckling | 235 | Larger |
| | a.3 | hole diameter = 500mm | web post buckling | 183 | Larger |
| | b.1 | endpost = 100mm | bottom flange yielding | 304 | Less |
| | b.2 | endpost = 400mm | bottom flange yielding | 278 | Less |
| | base | endpost = 900mm | web post buckling | 235 | Larger |
| | b.3 | endpost = 1400mm | web post buckling | 191 | Larger |
| | c.1 | # of holes = 12 | bottom flange yielding | 982 | Less |
| | base | # of holes = 24 | web post buckling | 235 | Larger |
| | c.2 | # of holes= 28 | web post buckling | 133 | Larger |

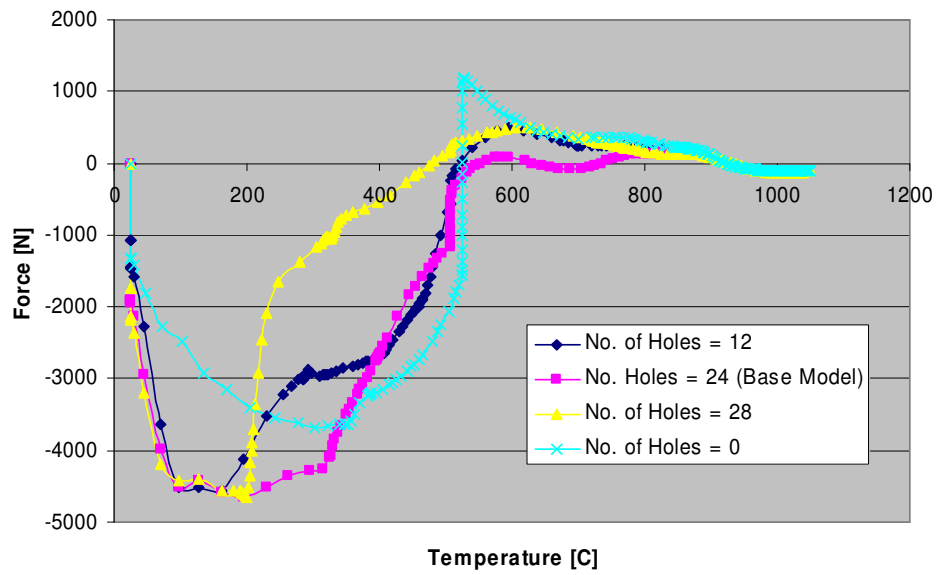


Figure 103 - Axial forces vs temperature for varying number of web openings.

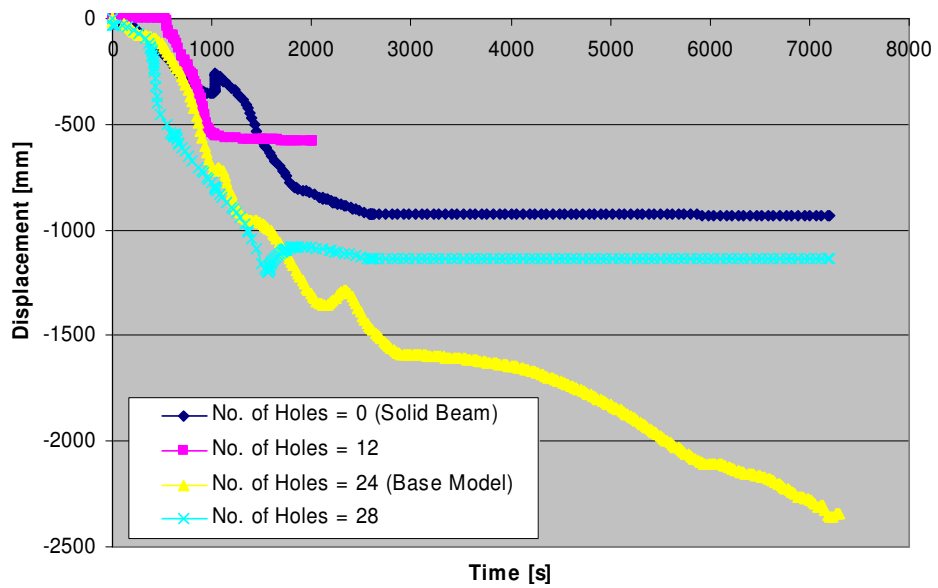


Figure 104 - Displacement vs. time for varying # of holes

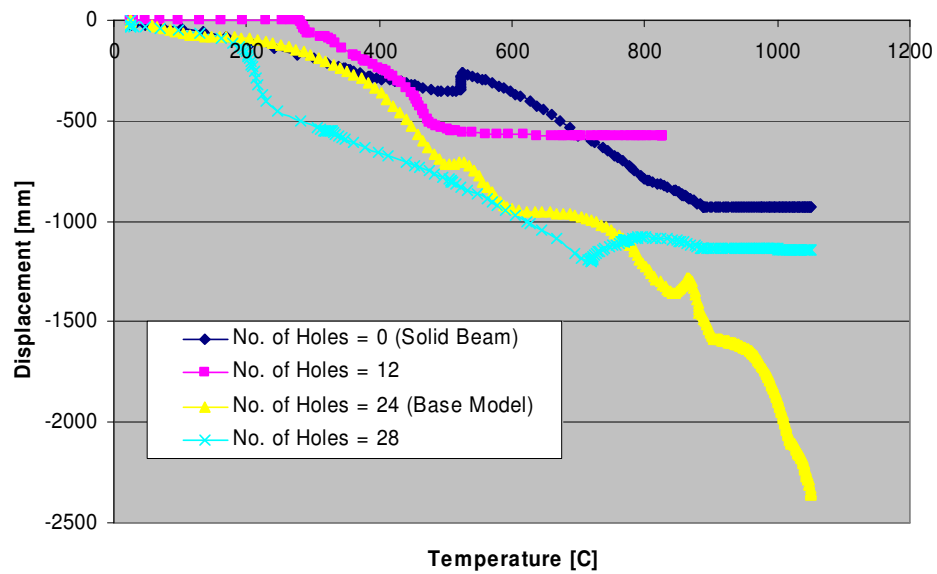


Figure 105 - Displacement vs. temperature for varying # of holes

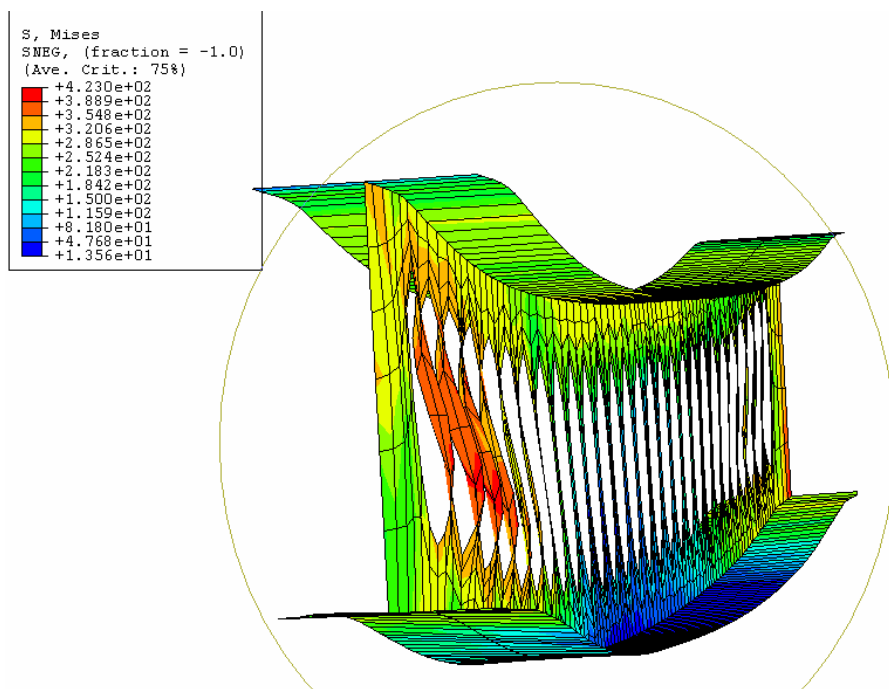


Figure 106 - Deformations of case with 28 web openings

4.2.3.4 Vary Web Thickness

In this case study, the thickness of the web was studied. The web thicknesses tested included: 8 mm and 20 mm. The base cellular beam model had a web thickness of 12 mm. All other aspects of the structural system and geometry were maintained. In addition, the time-temperature curve for these beams were maintained despite the change in mass of each beam. Refer to Table 8 and Appendix D for details of the analysis. Figure 107 is a visual representation of each case analyzed.

Figure 107 - Vary web thickness study (8mm, 12 mm, 20mm)

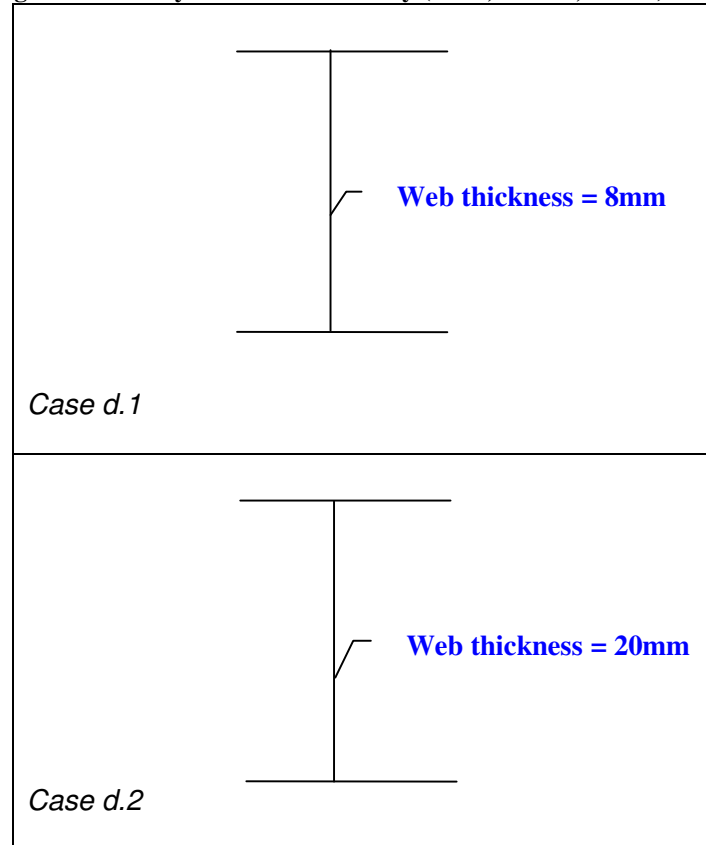


Figure 108 shows the change in axial force at the support of the beam for increasing temperature. By increasing the web thickness from 8 mm to 20 mm the axial forces on the column increased from 2 kN to 8 kN.

This should be expected, because by increasing the web the flexural stiffness of the beam should increase, providing better pre-buckling behavior. Since these cellular beams are dominated by lateral torsional buckling increases in web thickness should post-pone web buckling. Flexural moment capacity should also increase. By increasing the stiffness of the member, this will inevitably attract more forces as the beam will continue to expand against the column. This increase in forces could over stress the supporting columns and surrounding structure. However, the thinner webs are buckling at lower temperatures and are therefore unloading sooner.

The increase in web thickness should also increase post-buckling behavior due to the increase in axial stiffness (EA), which can be seen by the delay of the forces from transferring from axial compressive forces into catenary action. Although, the displacement-time or displacement-temperature curves (Figures 109 and 110) do not illustrate the post-buckling benefit, it is reasonable to assume that this will occur. Additional explicit models should be run to verify this assumption.

Note, Figures 111 and 112 show the difference in buckling behavior between the 20mm web and the 8mm web. As expected, the thinner web experienced web-post buckling and the thicker web had bottom flange yielding.

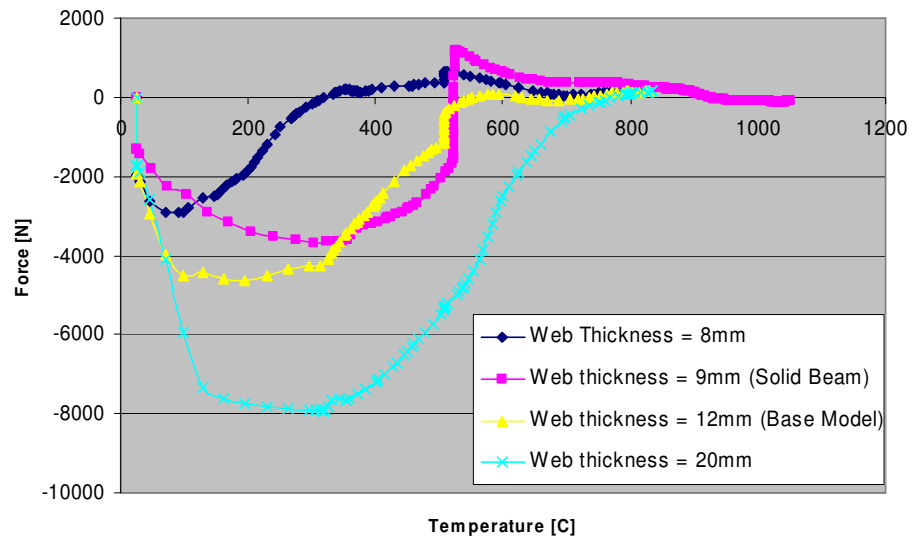


Figure 108 - Axial forces vs Temperature for varying web thickness

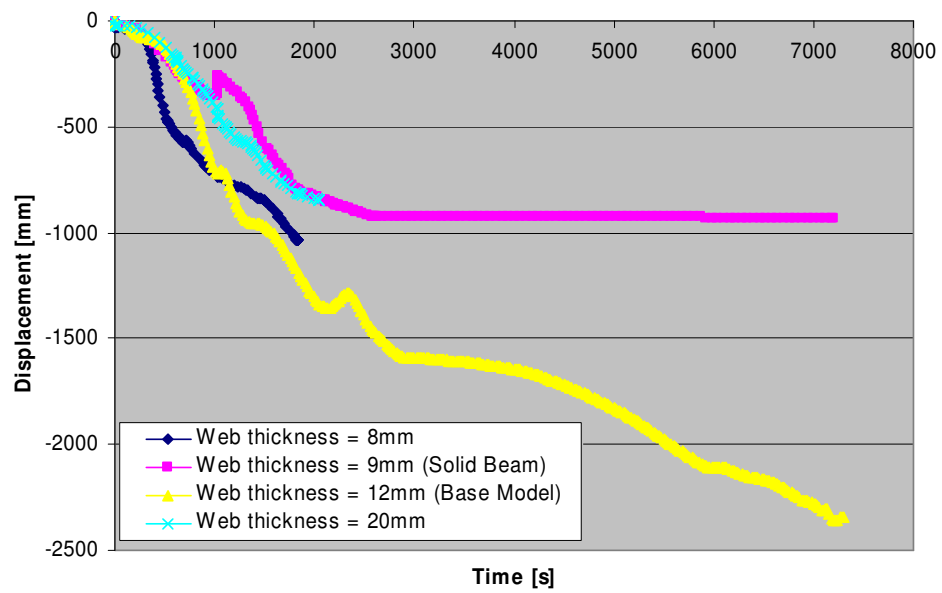


Figure 109 - Displacement vs. Time for varying web thicknesses

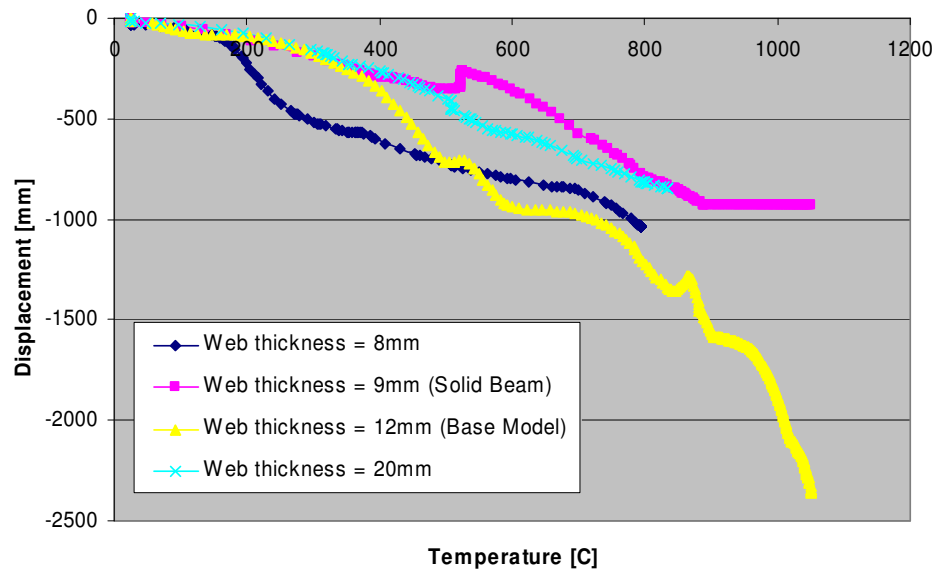


Figure 110 - Displacement vs. Temp for varying web thicknesses

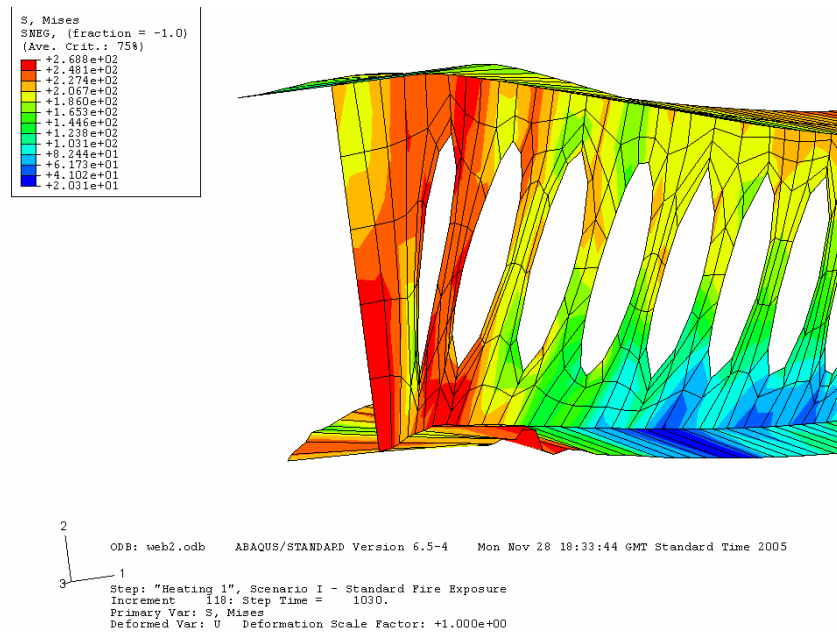


Figure 111 - Bottom flange yielding of 20 mm web thickness beam.

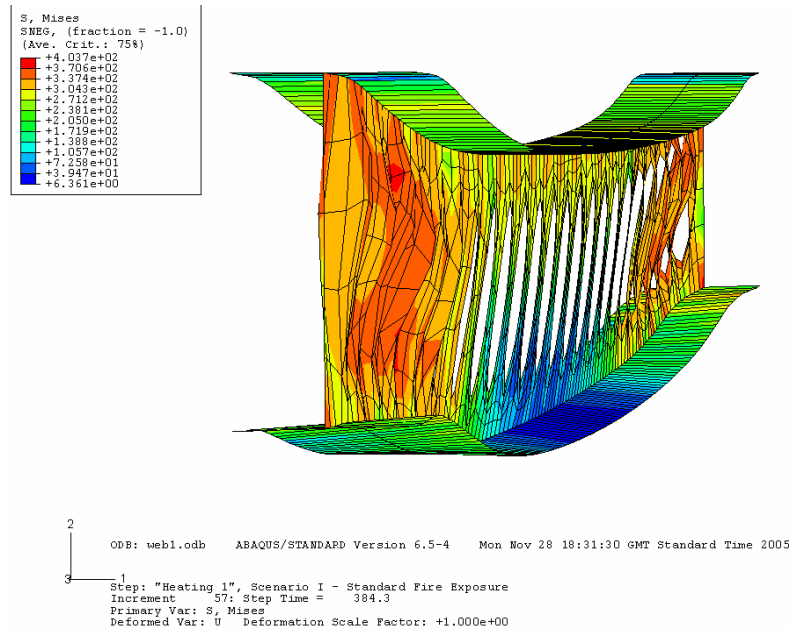
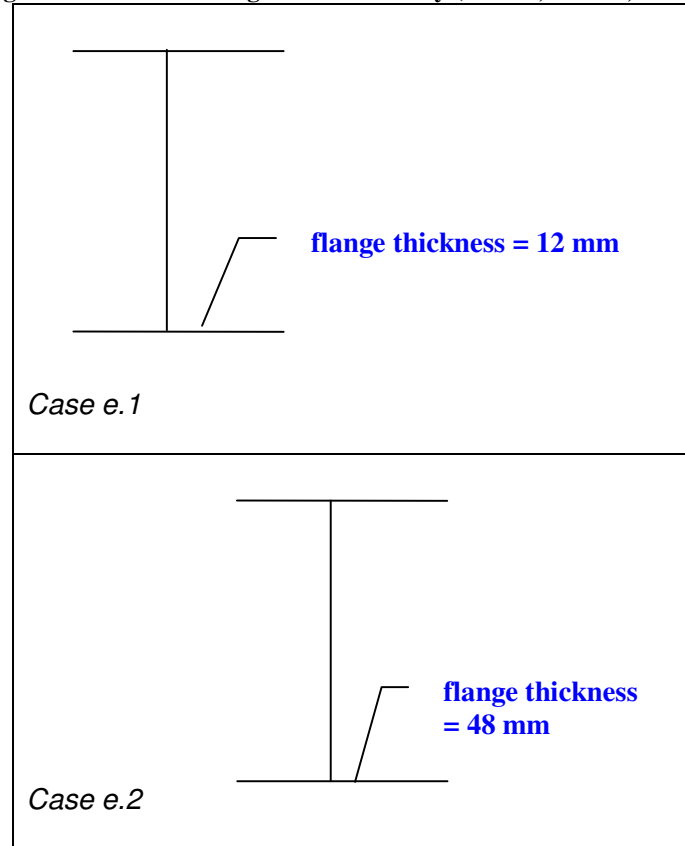


Figure 112 - Web post buckling behavior in 8 mm web thickness case.

4.2.3.5 Case e – Vary Flange Thickness

In this case study, the thickness of the flange was studied. The flange thicknesses tested included: 12 mm and 48 mm. The base cellular beam model had a flange thickness of 12 mm. All other aspects of the structural system and geometry were maintained. In addition, the time-temperature curve for the cellular beams in this case was not altered, despite the change in mass due to the changing flange thicknesses. Both trials were run using implicit analysis. Figure 113 is a visual representation of each case analyzed. Refer to Table 8 and Appendix D for more details of analysis.

Figure 113 - Varied flange thickness study (12 mm, 24 mm, and 48 mm)



As mentioned before, the dominant mode of failure for long span cellular beams appears to be lateral torsional buckling of the web. Therefore, the increase in flange thickness should not have an effect on pre-buckling behavior. As evident in Figure 114, the behavior of the axial forces in pre-buckling are all similar. However, in the post-buckling regime, the effect of flange thickness is more apparent. By increasing the flange thickness, the axial stiffness and axial capacity increase. This could provide added benefits in the post-buckling regime where the increased axial stiffness should provide more benefits in catenary action. This behavior is not evident in the displacement graphs (Figure 115, and 116) and should be verified in an explicit

model.

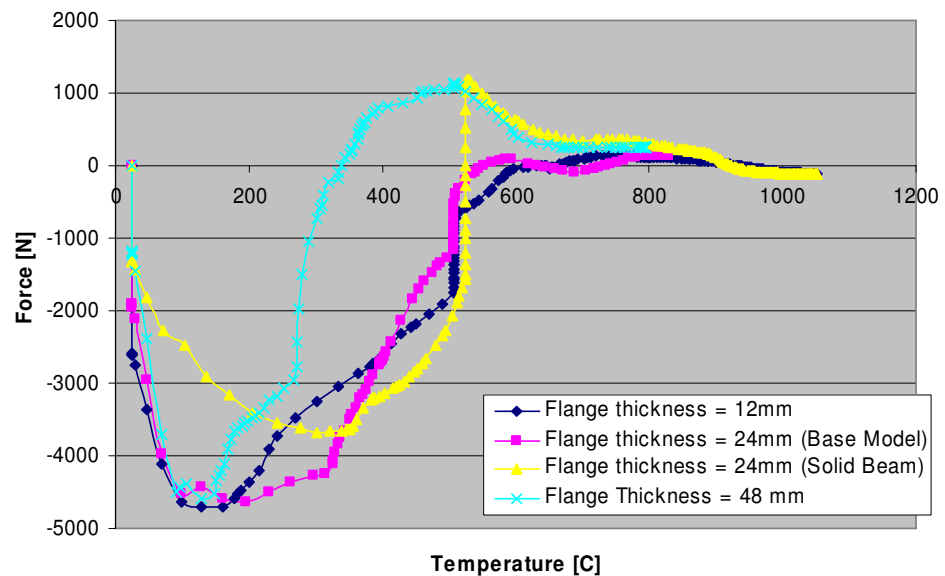


Figure 114 - Axial forces vs. temperature

It is interesting to note that the thickest flange (48 mm) quickly unloaded after initial buckling failure. This may be a result of the web-post buckling behavior that would be expected for increased flange thickness (See Figure 118). The web-post failure may have caused this rapid reduction in axial compressive forces, resulting in catenary action sooner than the other beams in this case. This local buckling, however, is not indicative of structural failure of the global system. Further investigation is needed in the post-buckling region to determine if stability is maintained. It is also interesting to see that as the flange thickness is decreased to 12 mm, the web-post buckling behavior seen in the base model changes to bottom flange yielding (See Figure 117).

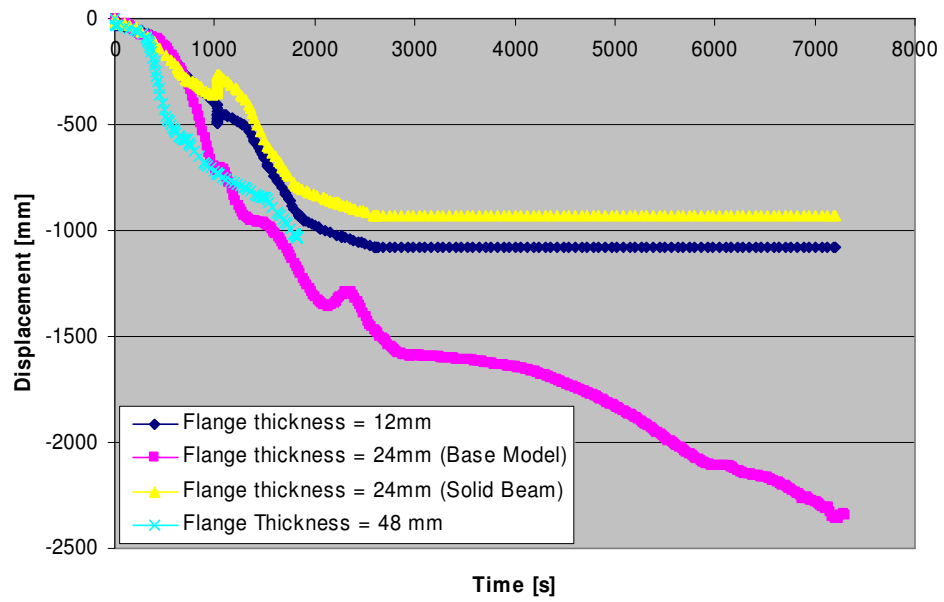


Figure 115 - Displacement vs. time

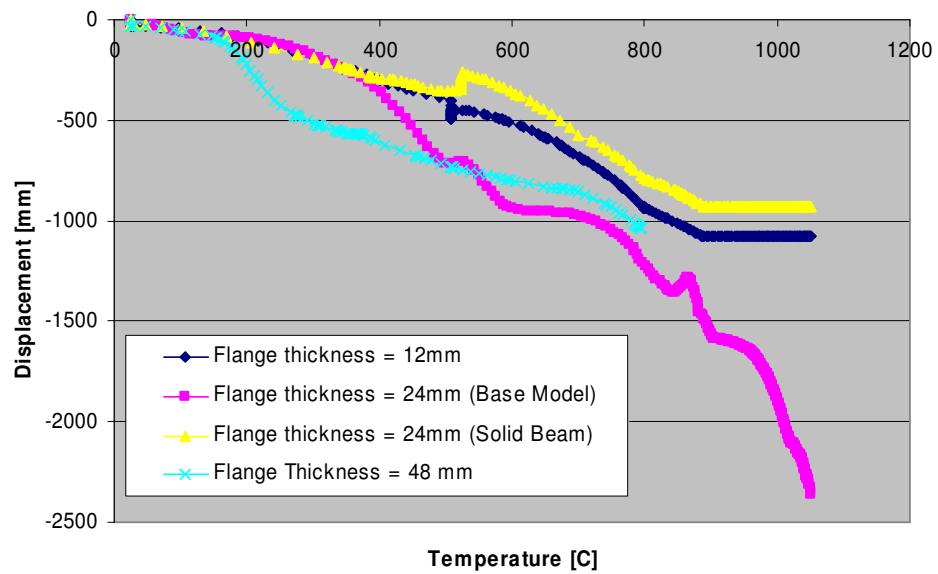


Figure 116 - Displacement vs. temp

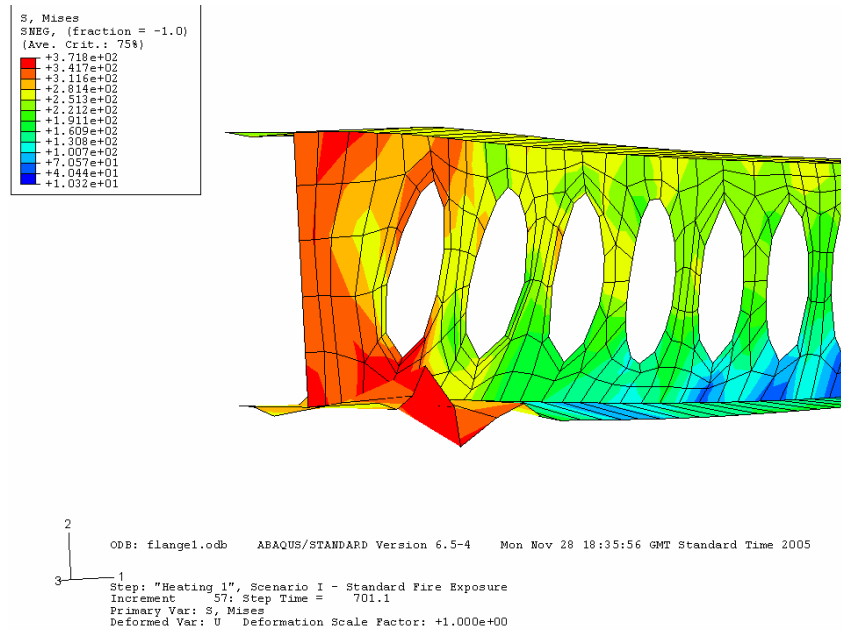


Figure 117 - Bottom flange buckling in thin flange

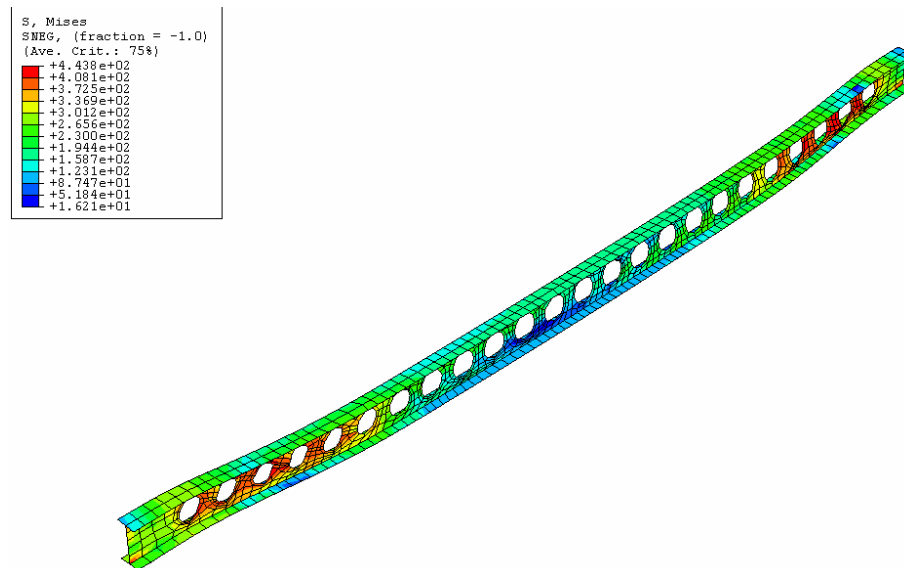


Figure 118 - Web buckling in thick flange case

4.2.3.6 Vary Bottom Flange Width

In this case study, the width of the bottom flange was studied. The bottom flange widths tested included: 270 mm and 470 mm. The base

cellular beam model had a flange width of 370mm. All other aspects of the structural system and geometry were maintained. Both trials were run using implicit analysis. Figure 119 is a visual representation of each case analyzed.

Similar to the previous case, the increase in bottom flange width should not have an effect on pre-buckling behavior given the “base” models web-post buckling mode of failure. By increasing the bottom flange width, the flexural capacity and flexural stiffness should increase, which would affect pre-buckling behavior. However, in the “base” cellular beam model, the beam buckling is due to web-post buckling which is a local web stiffness issue around the openings. Therefore, an increase in bottom flange width would provide no major benefit in this respect. This is evident in the following axial-temperature, displacement-time, and displacement-temperature curves.

On the other hand, an increase in flange width should increase post-buckling behavior due to the increase in axial stiffness and capacity (as was the case in the previous example). This added benefit is not evident from the implicit models and should be verified with explicit models. In addition, the failure modes for the bottom flange thickness were similar to the results of the previous case.

Figure 119 - Vary bottom flange thickness. (270 mm, 370 mm, and 470 mm)

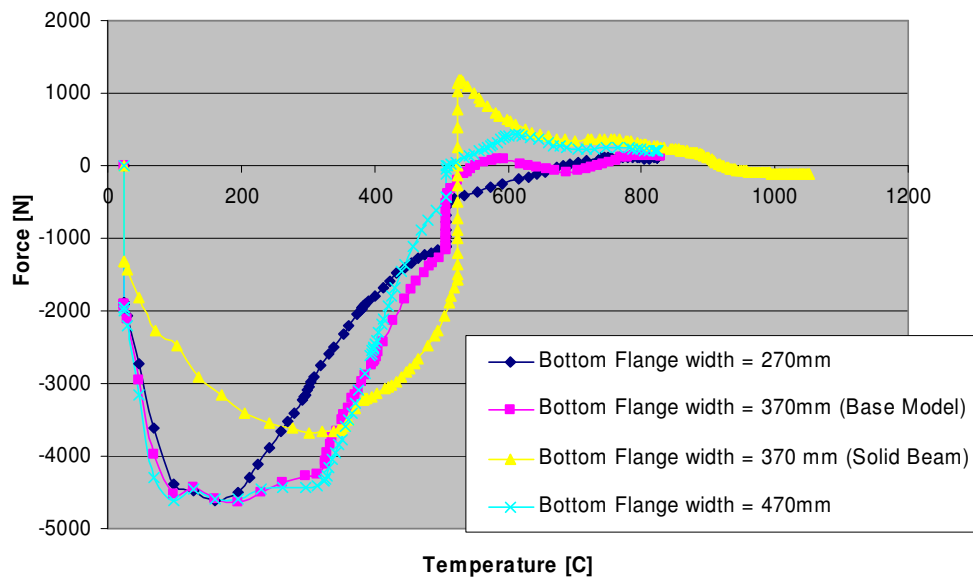
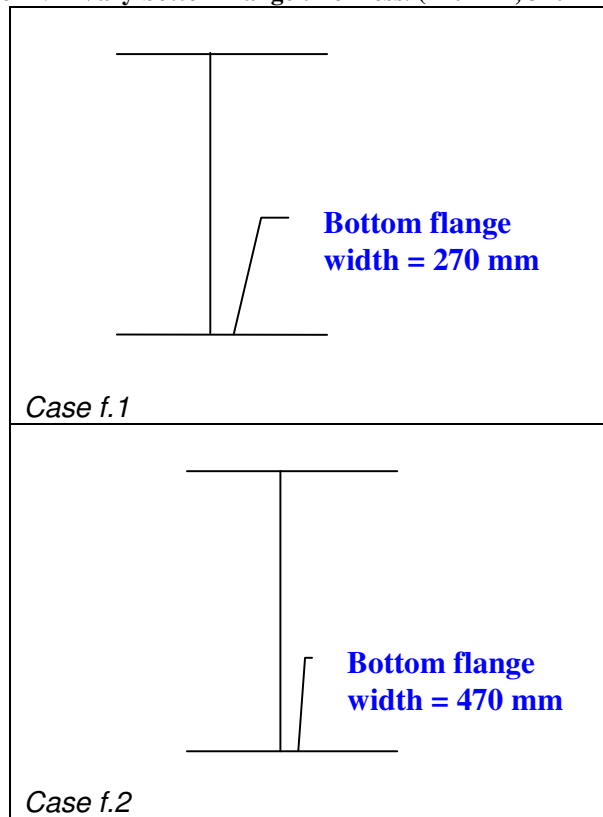


Figure 120 - Axial force vs temperature for varying bottom flange width

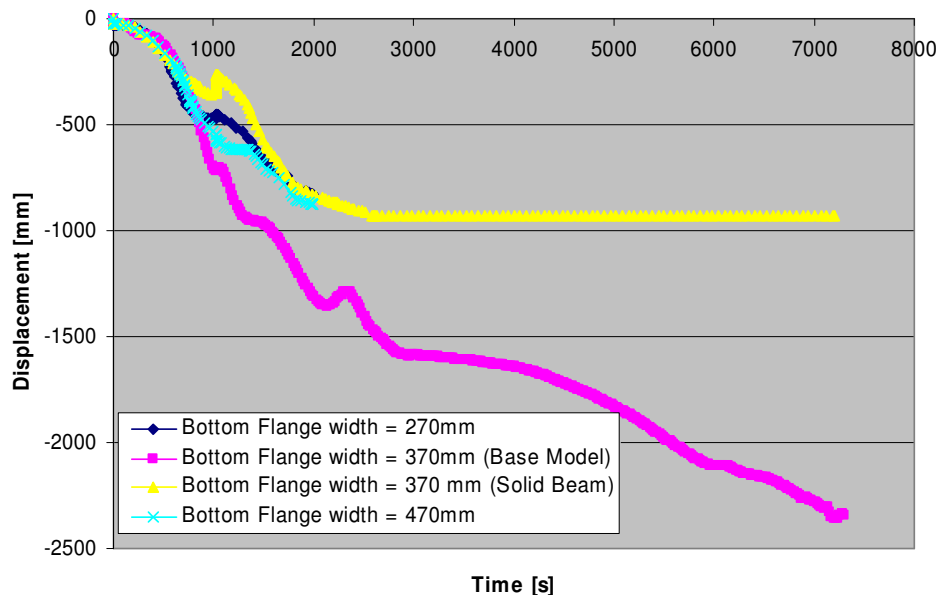


Figure 121 - Displacement vs. Time for varying bottom flange thicknesses

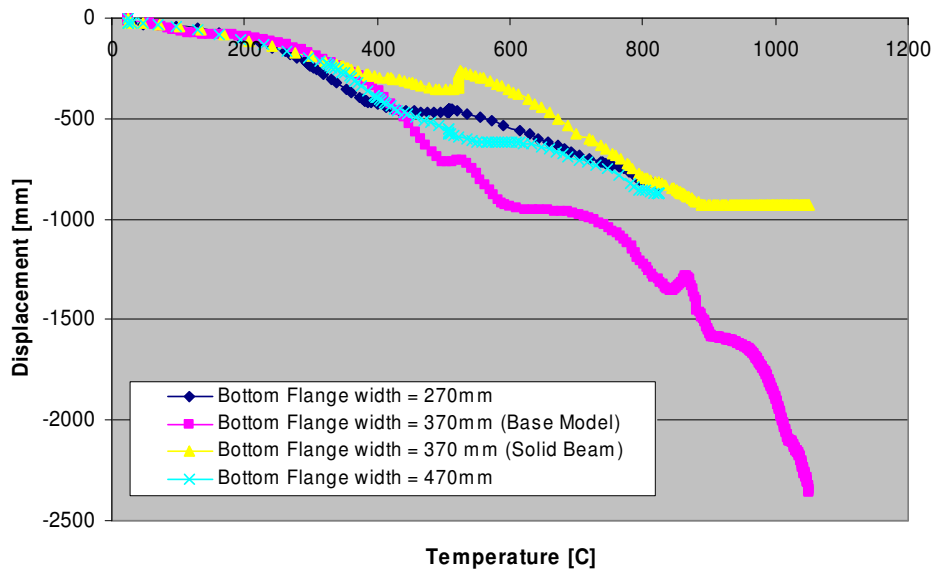


Figure 122 - Displacement vs. Temp for varying bottom flange thicknesses

4.2.3.7 Vary Span

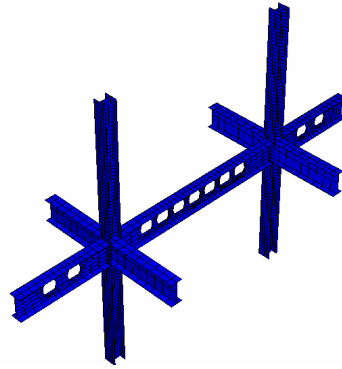
In this case study, the span of the cellular beam was studied. The span lengths tested included: 6150 mm (~20 ft) and 12000 mm (~39 ft). The

base cellular beam model had a span of 18000 m (~59 ft). Both trials were run using implicit analysis. Figure 123 is a visual representation of each case analyzed.

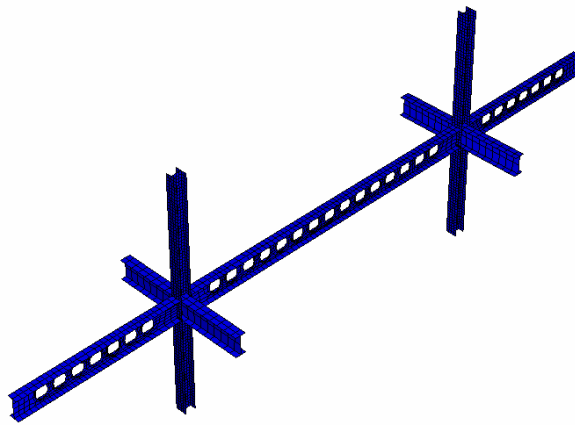
Figures 124 and 125 illustrate the displacements of the various span beams with respect to time and temperature, respectively. As would be expected, increasing span length would increase displacements. The shorter span case has the same section as the longer span member. Therefore, the shorter span will no longer be governed by flexural behavior, resulting in reduced deflections and reduced susceptibility to thermal bowing. This is evident in Figure 126 where buckling is delayed in the shorter spans and the axial forces are lower. In addition, post-buckling capacity should also increase due to the higher capacity of the over-sized beam in the shorter spans tested.

Additional studies should be conducted on shorter spans with the suitable beam size for that application. The variables in this test should be examined to observe differences in local and global structural response.

Figure 123 - Varying Span Lengths tested.



Case g.1 – Span = 6150 mm



Case g.2 – Span = 12000 mm

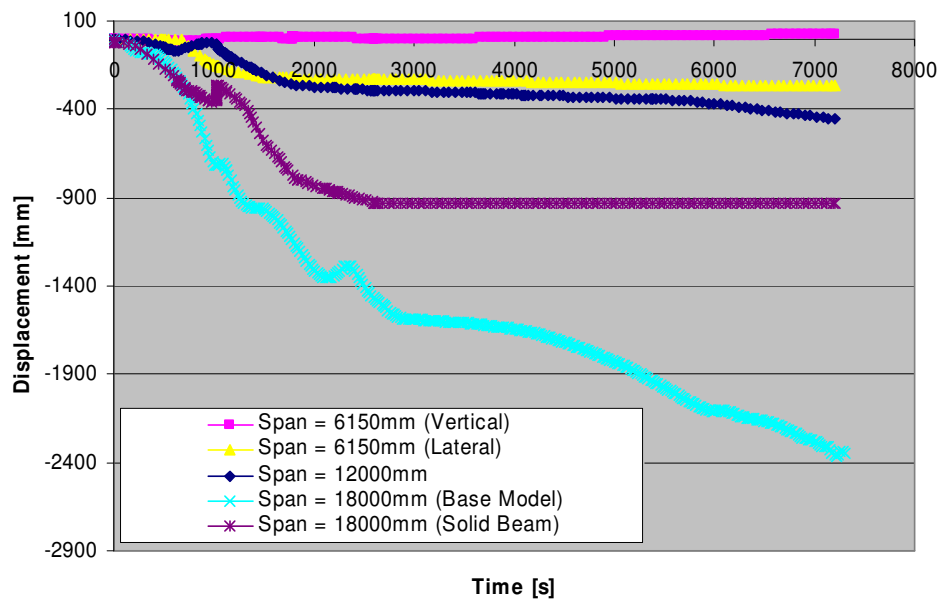


Figure 124 - Displacement vs time for varying spans

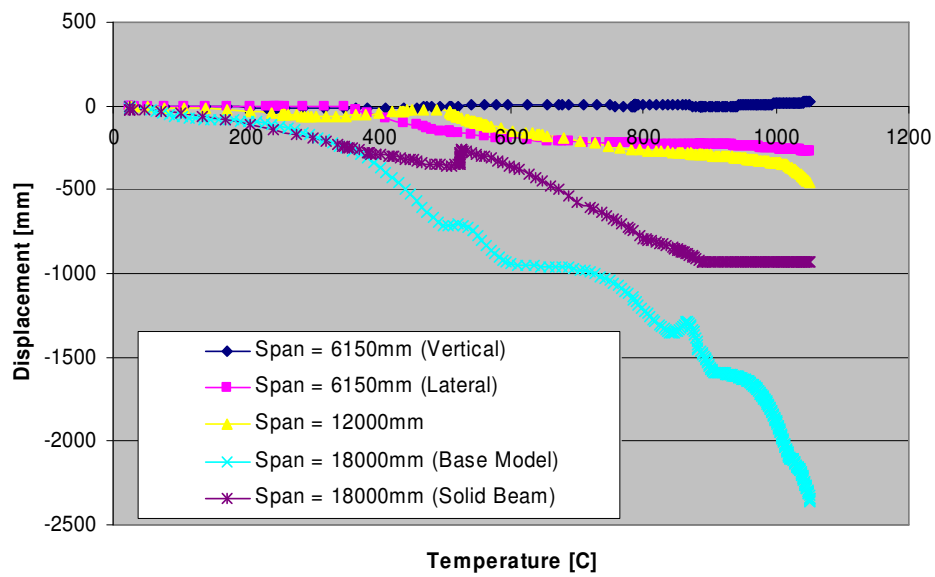
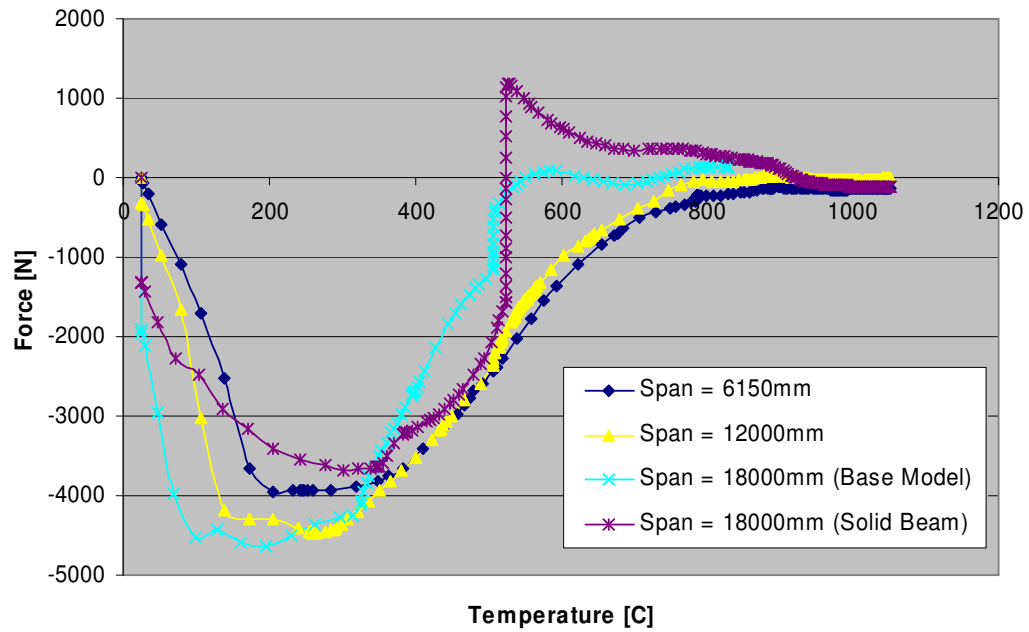


Figure 125 - Displacement vs. Temp for varying spans



4.2.4 Scenario II – Parametric Study

The variable in this scenario was the thermal exposure which was applied to the “base” cellular beam model. Five heating scenarios were created from the generalized exponential time temperature curve:

$$T(t) = T_o + (T_{\max} - T_o)(1 - e^{-\alpha t}).$$

Each case was analyzed similarly to analysis conducted in the base cellular beam model and solid beam model.

Figure 126 are the curves tested and is provided for reference.

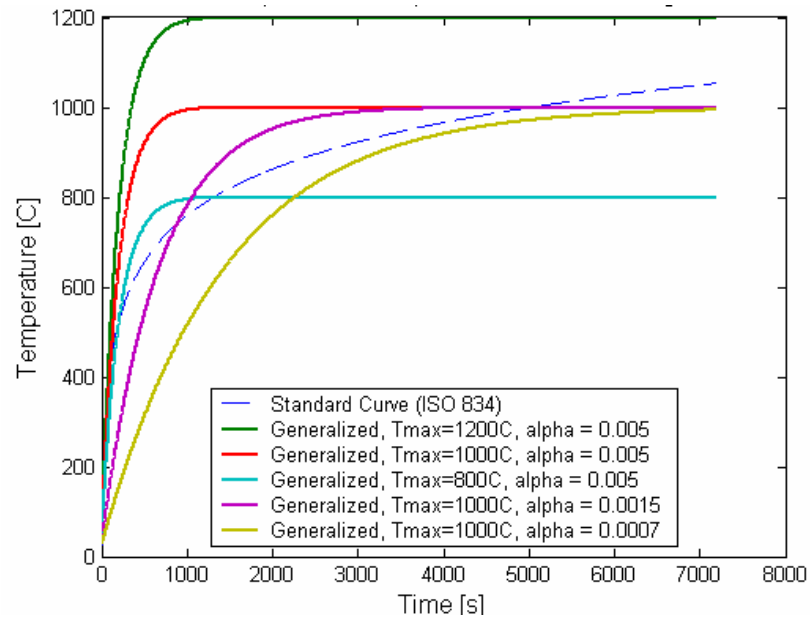


Figure 126 - Heating curves tested in this scenario

Figure 127 shows the displacement change in mid-span displacement with time. The Case 2 model appears to not increase in displacement with time after around 1030s. This same phenomenon occurs in the solid beam model and may be indicative of an error in the model. However, the data prior to this event may still be useful.

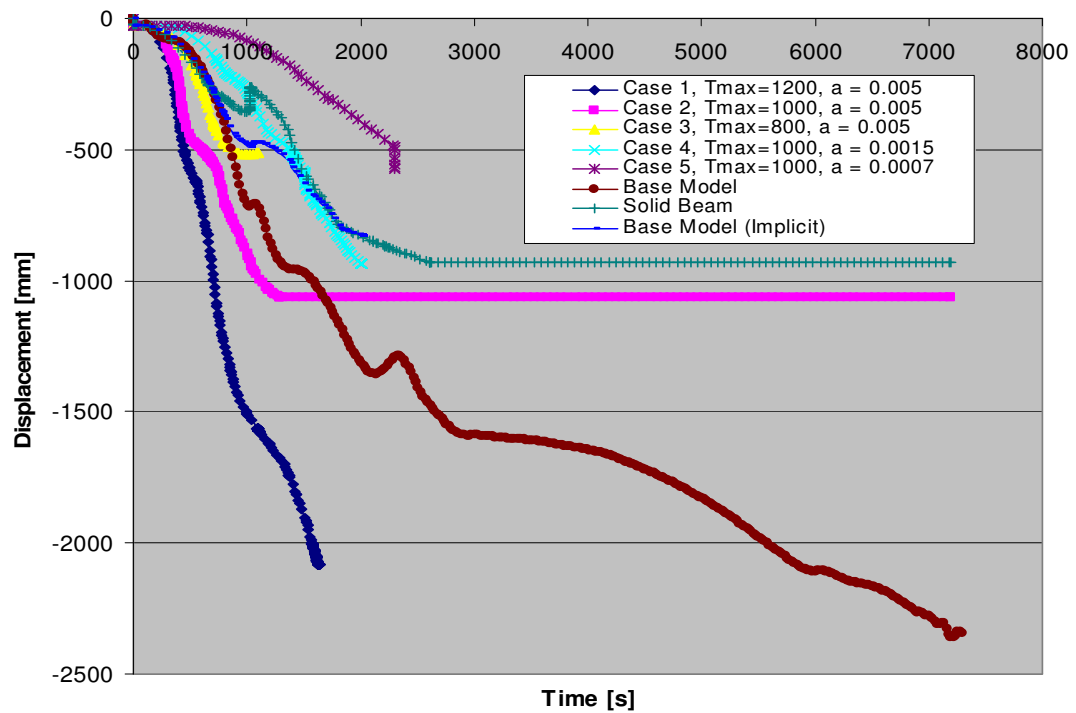


Figure 127 - Displacement vs. Time for various heat rates and maximum temperature fires.

In Figure 127, Case 1 appears to have an extremely high rate of deflection. The fire curve for this model is similar to a hydrocarbon fire, which heats up fast and to a high temperature. In this figure and in Figure 128, the Case 1 model appears to be having runaway deflection at 1635 s (27.25 min). At the end of the simulation, the Case 1 fire scenario induces a deflection of 2.1 m, while a deflection of 274 mm is seen for the Case 5 fire at that same time. However, in Figure 128 the displacements of each case are plotted against temperature. It appears that the displacement behavior of the cellular beam is a function of the temperature and not of the fire scenarios tested. It is interesting to note that the explicit model of the “base” cellular beam (where the standard ISO834 curve was used) does not collapse around the other heating

curves studied. However, the implicit model of the same beam appears to follow the other curves. Additional tests should be conducted to determine this discrepancy.

In addition, there does appear to be some slight differences in the displacement in the post-buckling regime, which occurred around 350°C, as seen in Figure 128 and in the axial force vs. temperature plot (Figure 129.) In analyzing the deformation and stress concentration animations, all the Cases 1, 3, 4, and 5 had buckling occur in the end post near the support (Figure 130). Case 2 appeared to have bottom flange yielding prior to web post buckling that initiated the ultimate buckling event (Figure 131).

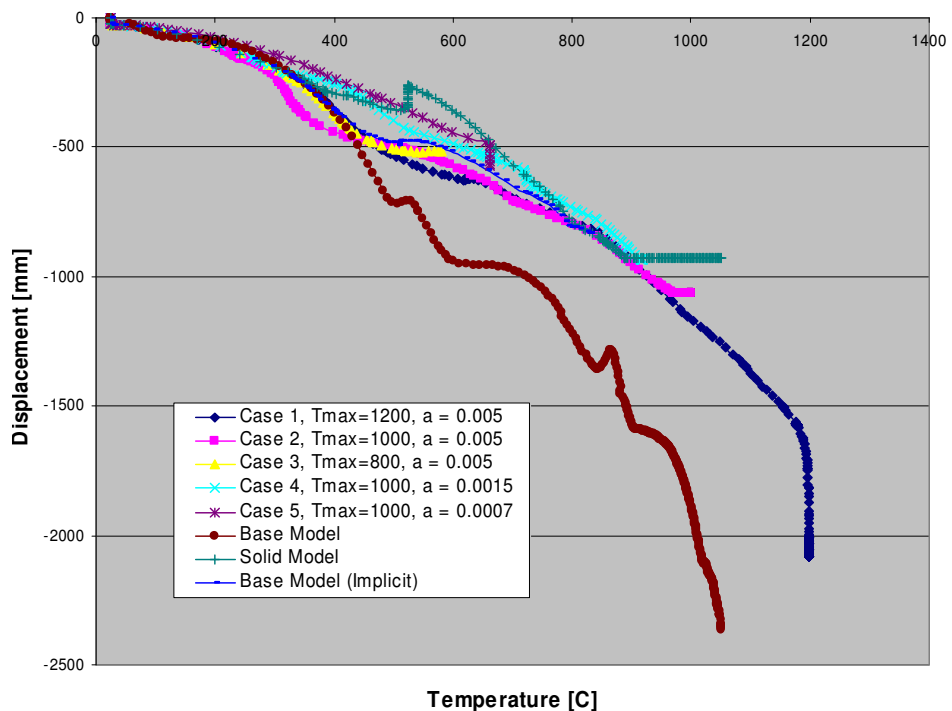


Figure 128 - Displacement vs. temperature for various heating curves.

This behavior may explain the slight difference in the displacement of the Case 2 beam immediately after buckling. It is interesting to note that in observing the failure mode in the explicit base model versus the implicit base model the modes were different. The implicit model appeared to fail similar to Cases 1, 3, 4 and 5; whereas, the explicit model failed in web post buckling. The difference in local buckling modes may be a result of the dynamic effects that are captured in the explicit analysis and not in the implicit model.

Figure 129 shows that there is no significant difference in the axial forces within the pre-buckling phase. In the post-buckling regime, there are slight differences, but all the fire scenarios appear to follow the same trend.

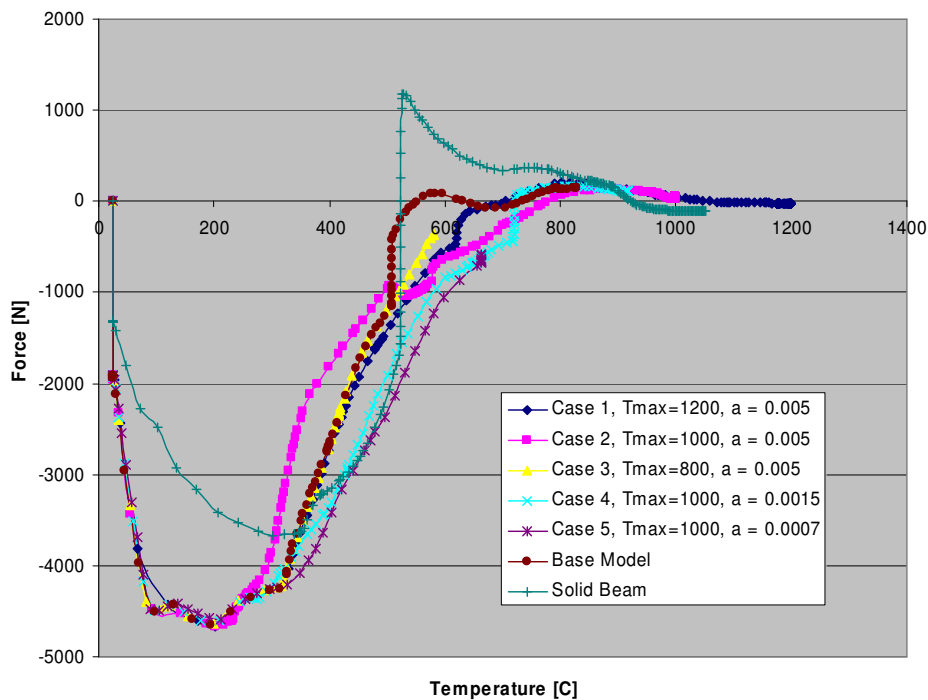


Figure 129 - Axial forces vs. temperature for varying fire scenarios

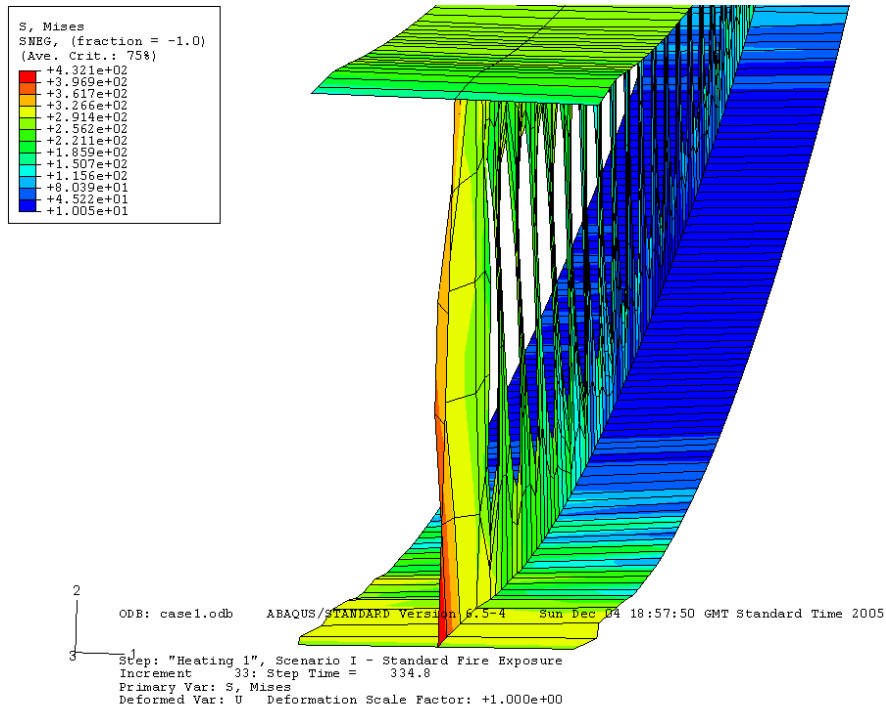


Figure 130 - Buckling of web near supports observed in Case 1, 3,4 and 5.

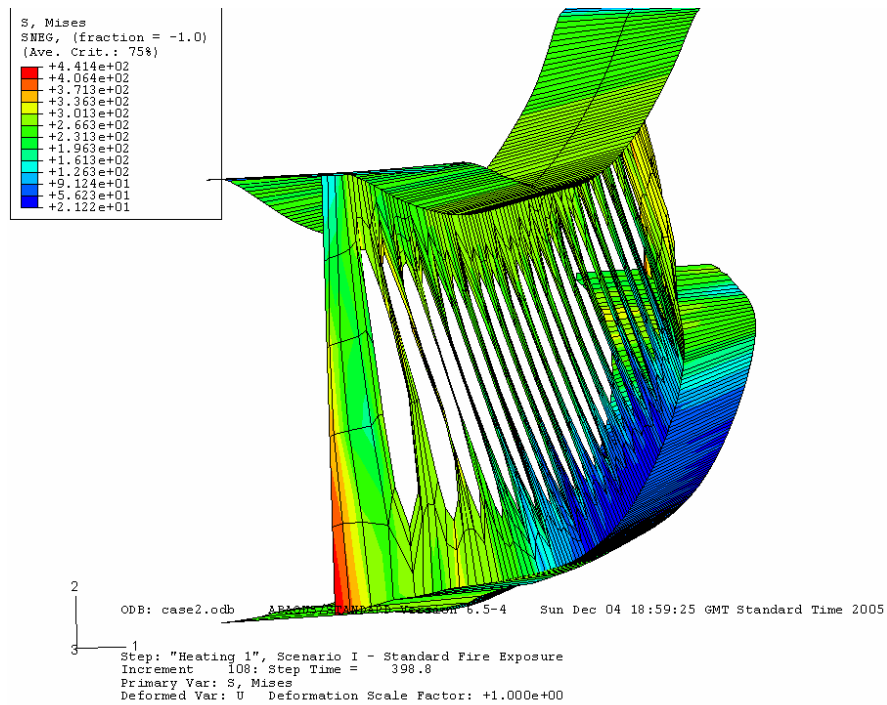


Figure 131 - Endpost and bottom flange buckling in Case 2

4.2.5 Scenario III – Parametric Study

In this scenario, two cases were analyzed and were based on experimental observations conducted in earlier cellular beam studies that indicating higher than expected web temperatures in cellular beams. Therefore, two cases (protected and unprotected) were studied in which the web temperatures were hotter than the flange temperatures.

Figures 132 and Figures 133 illustrate the midspan deflection of the cellular beam over time and temperature, respectively. Figure 132 suggests that the hotter web temperatures for unprotected cellular beams do not affect the displacement rate or the displacement with respect to temperature. This is also evident in Figure 133 for the axial forces with temperature. The “unprotected” hotter web temperature case has similar pre-buckling and post-buckling behavior to the base model where the temperatures were uniform across the depth of the section.

For the “protected” hotter web temperature case, the displacement rate of the beam is lower than the base model; however, this is a function of the temperature (as seen in Figure 133). Similarly to the unprotected case, the pre-buckling behavior is also similar. However, there is a slight difference in the post-buckling behavior observed in Figure 133. This case appears to unload at a faster rate than base model and the “unprotected” model, initially. This may be a result of differences in the axial capacity of the protected beam versus the unprotected cases, at these temperatures. Axial stiffness and capacity are critical factors in the post-buckling behavior of the beam. The temperature differences between the web and flanges in

the “protected” case were higher than in the “unprotected” case. This difference may explain the initial difference in post-buckling behavior, where the axial forces are declining as the steel strength and stiffness degrade with heating. Near the end of the simulation, all the curves appear to follow the same trend.

Also, the displacement curves do not appear to indicate runaway failure of this system.

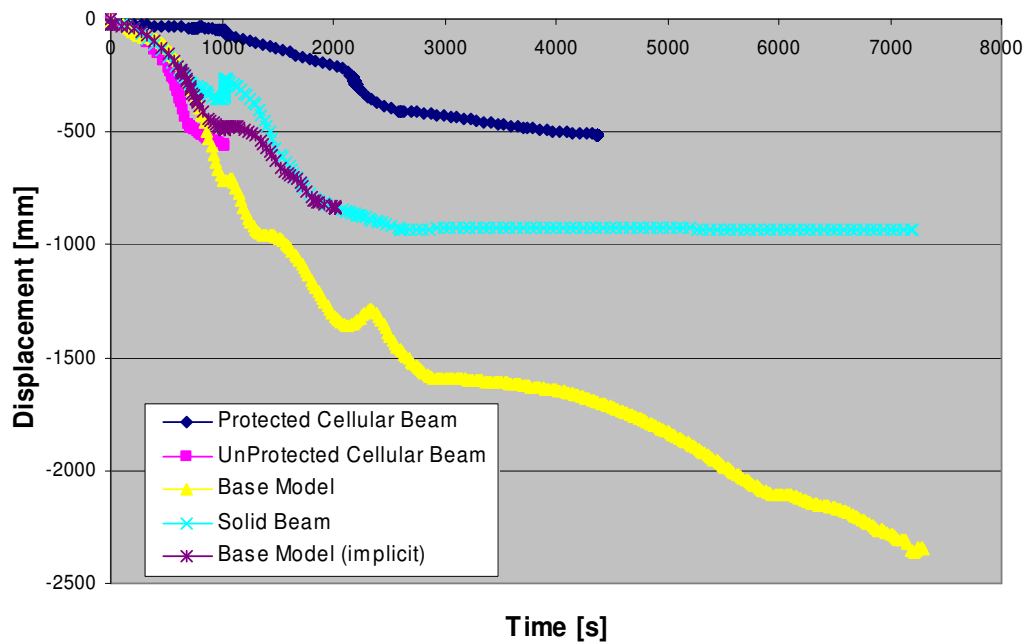


Figure 132 - Midspan deflection vs. time for beams with web temperatures hotter than the flanges.

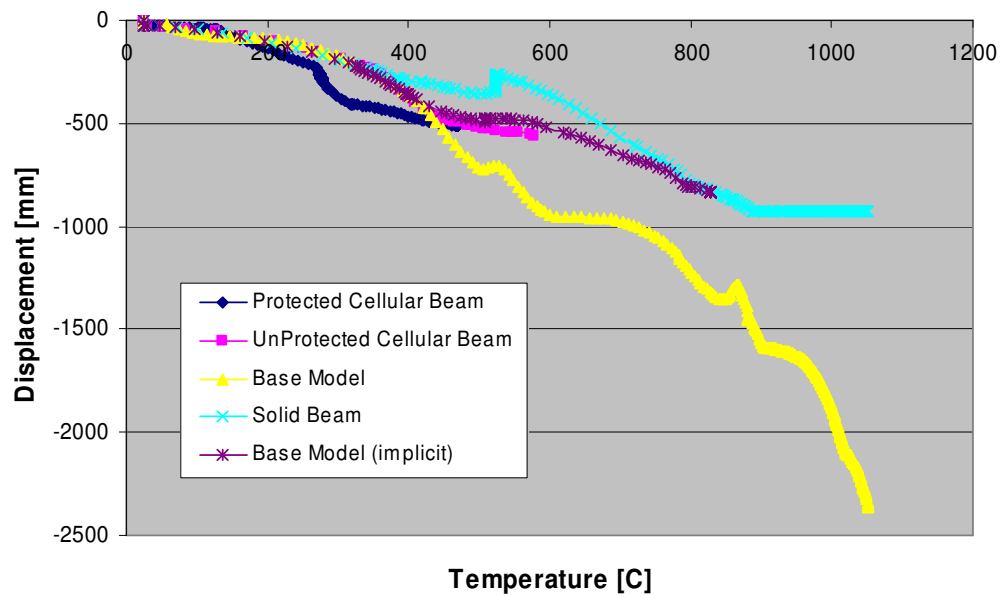


Figure 133 - Midspan deflection vs. temperature for beams with web temperatures hotter than the flanges.

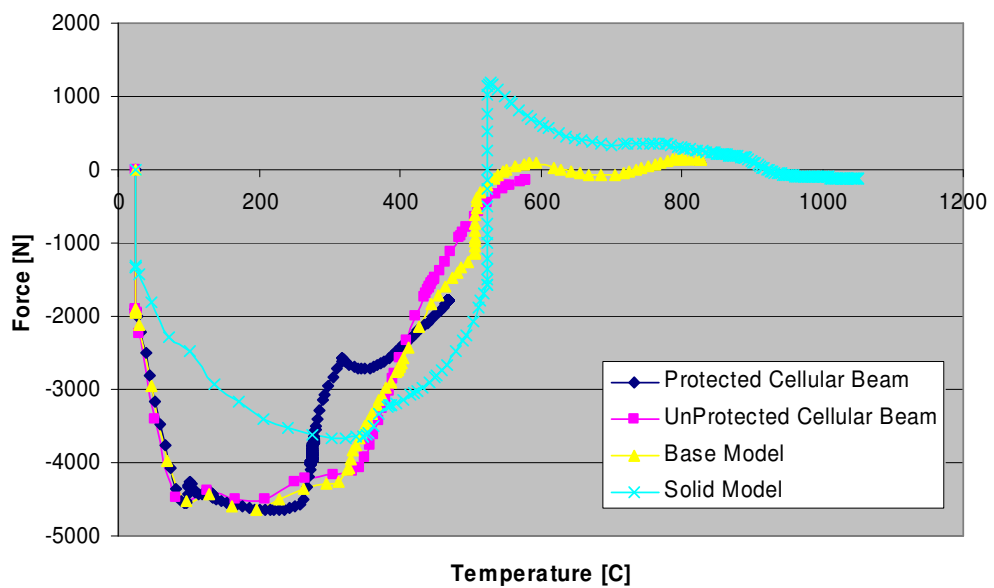


Figure 134 – Axial forces vs. temperature for beams with web temperatures hotter than the flanges.

4.3 Summary of Results and General Observations

The structural model as described above was evaluated from several perspectives to determine its sensitivity to different parameters. For the purpose of this paper, only general trends in buckling behavior, axial forces, and midspan displacements were presented as they related to variations in cellular beam section geometry and an equivalent solid beam. These trends provide an insight into the parameters that govern the local response of cellular beams in fire, as well as the implications they have for the surrounding structure.

4.3.1 *General Buckling Behavior*

Table 11 indicates the observed trends in buckling behavior with respect to buckling/yielding events, buckling mode, and buckling/yielding temperatures for each parameter analyzed in this study. In all the cellular beam cases listed in Table 11, two buckling events were observed, where the first event was buckling or yielding of the bottom flange, and the second event was either buckling of the web post, end post or overall lateral torsional buckling (LTB) of the beam member (See Fig. 135). This response differs from the single buckling event witnessed in the solid beam tests at Cardington.[33] In these tests, the lower flange buckled near the supports at approximately 120-150°C resulting in an increased rate of deflection and an unloading of the axial forces in the beam (towards tension).

However, in this study, the buckling/yielding of the bottom flange in the cellular beams occurs at around 95-105°C but does not result in an increased rate of deflection or load reversal, as will be discussed in detail

later (See Figure 138). It is not until a second buckling event – the limiting event – that an increased rate of displacement and a trend toward catenary action is observed. This behavior may be attributed to the increased depth of the beams in this study (690 mm), which allow the high compressive axial forces to redistribute into the web and temporarily stabilize the beam response. This critical buckling event, as indicated in Table 11, seems to occur at around 300 °C, which is significantly lower than that typically cited as the limiting temperature for load bearing structural steel members (~600-650 °C)[5,6,7,44]. This lower temperature is likely the result of the realistic end conditions coupled with the increased slenderness of long span cellular beams relative to the shorter span beam configurations tested in standard fire tests.

Table 11: Trends in observed buckling behavior

| Scenario | Case | Parameter Tested | Buckling Events | | | |
|------------|------|-----------------------|------------------------|----------------|------------------------|----------------|
| | | | 1st Event | | 2nd Event | |
| | | | Description | Temperature °C | Description | Temperature °C |
| Solid Beam | | | Overall buckling | ~350 | n/a | |
| I | a | Diameter =150mm | Bottom flange buckling | 95-100 | Overall LTB | 327 |
| | | Diameter =300mm | | | Overall LTB | 321 |
| | | Diameter =450mm | | | web post + end post | 319 |
| | | Diameter =500mm | | | web post | 257 |
| | b | Endpost = 100 | | 95-100 | end post | 329 |
| | | Endpost = 400 | | 130 | end post | 319 |
| | | Endpost = 900 | | 95-100 | web post + end post | 319 |
| | | Endpost = 1400 | | 95-100 | web post | 285 |
| | c | No. of Holes = 12 | | 95-100 | end post + overall LTB | 287 |
| | | No. of Holes = 24 | | | web post + end post | 319 |
| | | No. of Holes = 30 | | | web post | 202 |
| | d | Web Thickness = 8mm | | 70 | web post | 191 |
| | | Web Thickness = 12 mm | | 95-100 | web post + end post | 319 |

| | | | | | | |
|-----|---|---|------------------------|--------|---------------------|---------|
| | | Web Thickness = 20 mm | | 130 | Overall LTB | 314 |
| | e | Flange Thickness = 12 mm | | 95-100 | Local bottom flange | 215-365 |
| | | Flange Thickness = 24 mm | | | web post + end post | 319 |
| | | Flange Thickness = 48 mm | | | web post | 260 |
| | f | Bottom Flange Width = 270 mm | | 95-100 | web post | 260-353 |
| | | Bottom Flange Width = 370 mm | | | web post + end post | 319 |
| | | Bottom Flange Width = 470 mm | | | web post | 357 |
| | g | Span = 6150 mm | | 207 | Overall LTB | 411 |
| | | Span = 12000 mm | | 139 | Overall LTB | 292 |
| | | Span = 18000 mm | | 95-100 | web post + end post | 319 |
| II | 1 | $T_{\max} = 1200^{\circ}\text{C}$, $\alpha = 0.005$ | Bottom flange buckling | 95-100 | End post + web post | 328 |
| | 2 | $T_{\max} = 1000^{\circ}\text{C}$, $\alpha = 0.005$ | | | Bottom flange* | 309 |
| | 3 | $T_{\max} = 800^{\circ}\text{C}$, $\alpha = 0.005$ | | | End post + web post | 316 |
| | 4 | $T_{\max} = 1000^{\circ}\text{C}$, $\alpha = 0.0015$ | | | End post + web post | 312 |
| | 5 | $T_{\max} = 1000^{\circ}\text{C}$, $\alpha = 0.0007$ | | | End post + web post | 297 |
| | | | | | | |
| III | 1 | Protected beam | Bottom flange buckling | 95-100 | End post + web post | 307-354 |
| | 2 | Unprotected beam | | | End post + web post | 345 |

* In this scenario, the bottom flange appears to be the dominant buckling mode. Additional analysis should be conducted to determine the cause of this mode, and if it is significant.

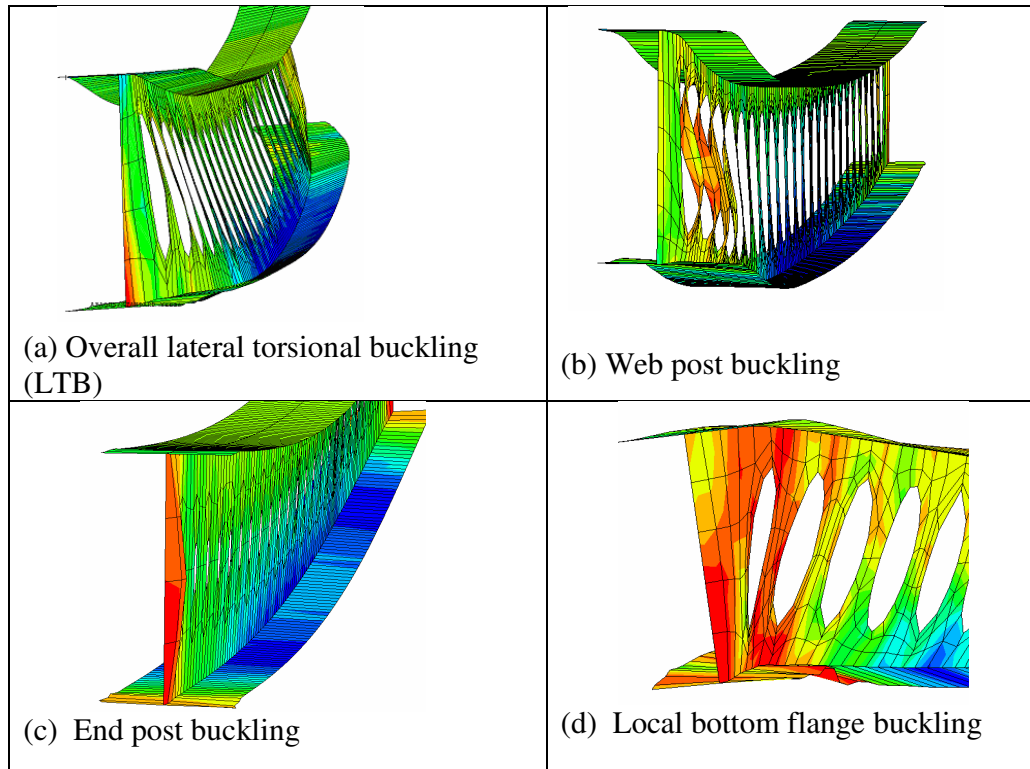


Figure 135 - Modes of behavior of cellular beams at fire limit state

As indicated in Table 11, the mode of buckling in cellular beams appears to occur in the web particularly the posts between the openings. This buckling mode is expected due to the reduced shear capacity as a result of the web openings and Vierendeel effects inherent in cellular beams. Therefore, parameters that increase web stiffness and/or strength (such as cases a-d in Table 2) have a more significant affect on the local buckling mode and overall beam response in the early stages of the analysis. In cases e-f, where the flange width and thickness were varied, little to no change was observed in the buckling mode because the limiting factor continued to be the local web stiffness and strength. So, increasing the flange width or thickness will have little benefit on local buckling modes, where the controlling parameter will still be the web stiffness. While increasing flange thickness or width may have little influence on pre-buckling response, there

may be some benefit in the post-buckling region where catenary action dominates the overall structural behavior.

The web post buckling observed for the cellular beams differs to the solid beam, which experienced overall lateral torsional buckling – a more ductile/stable buckling mode [45]. Unlike the solid beams tested in Cardington, the solid beam in this study does not appear to have a distinct localized buckling event. The solid beam is seen to undergo overall lateral buckling initiating at approximately 350°C. This behavior may also be attributed to the increased depth of the member studied. Unlike the cellular beams, the solid beam has the full depth of its web to transfer forces, thereby reducing the likelihood of force localization at the bottom flange.

4.3.2 Cellular Beam Axial Forces And Midspan Displacements

Figure 136 illustrates the axial forces against temperature near the column of the cellular beams with varying web opening diameter. Initially at 20°C, there is a local concentration of compressive forces at the bottom flange of the beam due to an initial hogging moment from the load. As the temperature in the compartment increases, the compressive forces in the beam further increase due to restrained thermal elongation and thermal bowing. This compressive force increases until local buckling of the lower flange occurs and is typically observed for solid beams at 120-150°C, as described in the literature [33]. However, in Figure 136 and Table 11 this local buckling of the bottom flange appears to occur much earlier in the fire for the long span cellular beams - at around 90-100°C. This could be the result of shear forces from Vierendeel bending causing a local increase in

stress concentrations in the bottom flange near the support. For the solid beam model, this local buckling of the bottom flange is not evident until 350 °C. This may be a result of the increased depth (690 mm) of the solid beam in this study which may be causing the axial forces to be distributed more evenly in the web and bottom flange.

After the local buckling event, the axial forces at the column appear to stabilize as the thermal expansion induces increased deflections instead of compression. As the beam continues to heat, the deflection rate is seen to increase and a second buckling event is observed at around 350 °C. At this point, the web posts are starting to buckle as the local web stiffness and shear capacity is overcome by the high shear forces near the supports (Fig 135b). After this point, the deflection rate grows at a higher rate and $P-\Delta$ moments increase rapidly as subsequent web-posts buckle along the length of the beam towards its center and the material properties degrade with increased temperature. These buckling events are also evident in the displacement vs. temperature plots, such as those in Figures 138 and 139. The conventional composite flexure mechanism is now replaced by tensile (catenary) mechanisms [33]. It is interesting to note, that the system completely changes to catenary action at around 500 °C. In previous tests such as those at Cardington, this event occurred much later [33]. However, the Cardington tests incorporated a composite deck with universal beam sections at a maximum span of 9m, where tensile membrane action of the slab contributed to the performance of the structural system.

As indicated in Figure 136, the axial forces in the cellular beams do not appear to be particularly sensitive to the diameter of the web openings in the pre-buckling region of the response history. However, once buckling has occurred the larger hole diameter beam (500 mm) appears to unload (change from compression to tension) at a greater rate than the smaller diameter cases. This response is likely due to the reduced web flexural stiffness of the beam with larger holes relative to the beams with the smaller holes. The buckling of the 500 mm case occurs more rapidly and the beam transitions from a flexural mechanism to a tensile mechanism, as seen in the graph. These observations were also apparent in the displacement histories, where the 500 mm case resulted in larger displacements. Similar trends occurred for the other parameters tested.

The variation in different aspects of the section geometry, except for the web thickness (Figure 137), had little affect on the pre-buckling forces in the beams. The post-buckling behavior, as discussed above for various hole diameters (Fig 136), was also observed in the other parameters studied. That is, the beams with reduced web flexural stiffness (longer end posts*, more holes*, thinner webs) experienced a more rapid transition into tensile mechanisms than the flexurally stiffer beams. (*Note: The variation of these parameters affected the dimension of the web post length, so the beams with longer end posts and the ones with more holes had shorter web posts. These web post characteristics dominated the beam behavior and were the controlling parameter for these beams.)

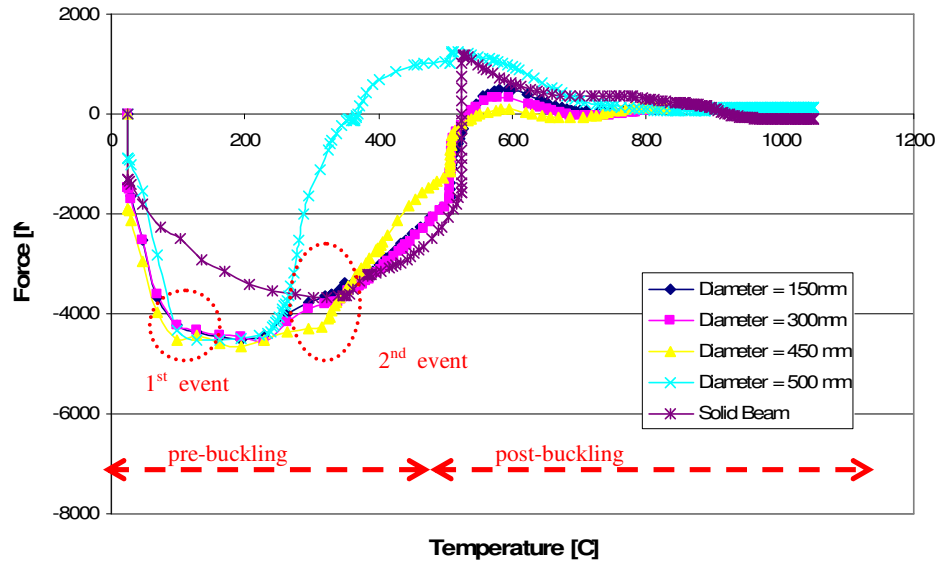


Figure 136 - Connection forces of cellular beams with various web opening diameters

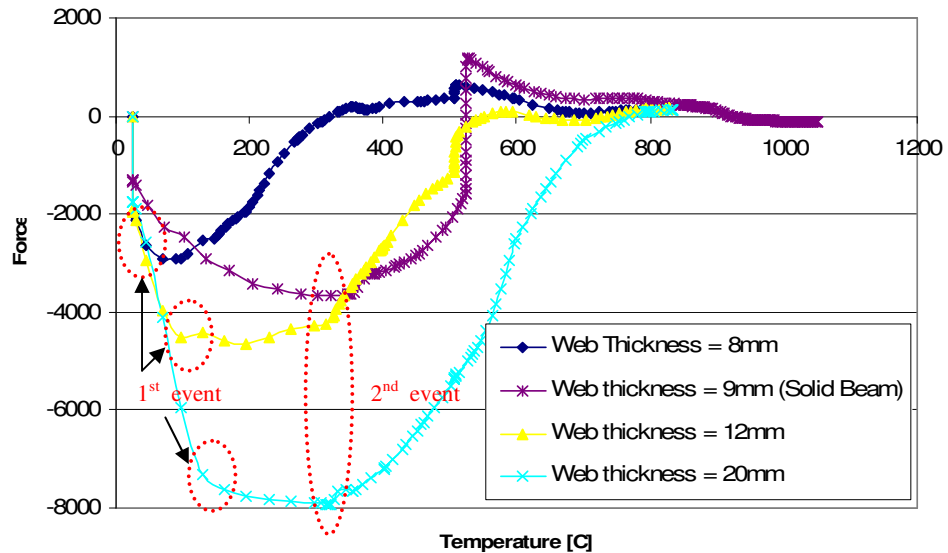


Figure 137 - Connection forces for cellular beams with various web thicknesses

Figure 137 illustrates the significant affect that increasing web thickness plays on the magnitude of the axial forces in the cellular beam. As to be expected, increasing the web thickness increases the axial force in the beam due to the increase in axial stiffness. Although increasing web thickness has resulted in increased axial forces, the buckling mode changes from web post buckling to overall lateral torsional buckling (See

Fig 135.c and Table 11). This may prove to be beneficial, as lateral torsional buckling tends to be a more ductile buckling mechanism [45]. Further investigation however is needed.

In Figures 136 and 137, the solid beam axial forces appear to be less than those of the cellular beams tested. One would anticipate that the solid beam axial forces would be greater due to its increased axial stiffness relative to the cellular beams. However, in this study the solid beam was selected to achieve a similar load ratio to that of the “base” cellular beam. This resulted in a solid beam that is slightly smaller than the “base” cellular beam. This is likely the cause of the discrepancy in the axial force comparison.

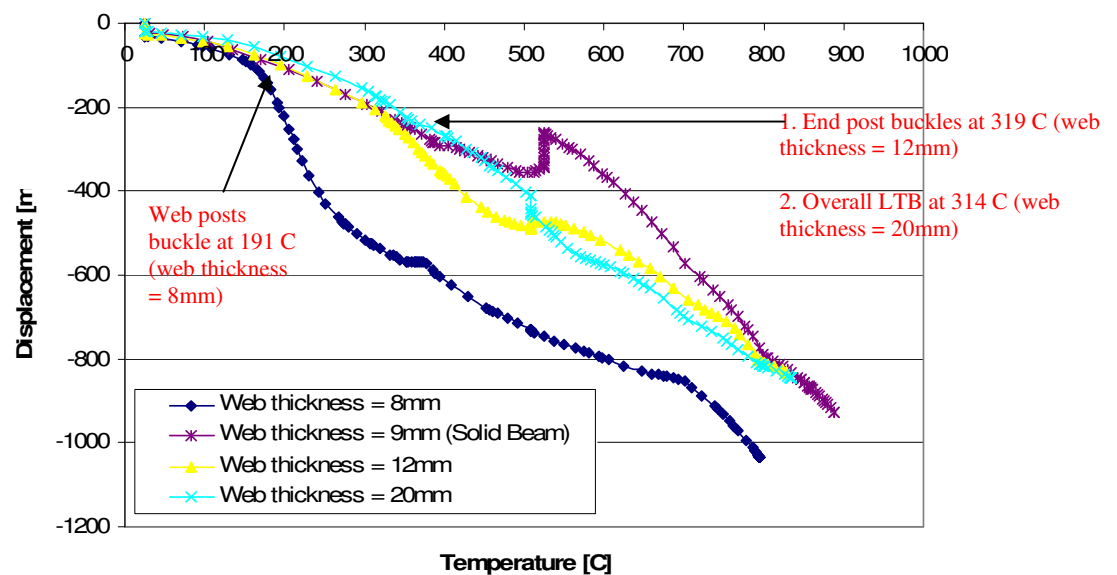


Figure 138 - Displacement versus temperature for varying web thicknesses

As described earlier, the displacement history is closely linked with the overall behavior of the structural system. Figure 138 illustrates the vertical displacement of cellular beams of varying web thicknesses with respect to

temperature. Figure 139 plots the displacements versus temperature for cellular beams with varying bottom flange width. These figures reveal not only the initiation of buckling events, but also, the implications of different buckling modes on structural behavior. That is, the type of buckling mode appears to affect the displacement response of the beams.

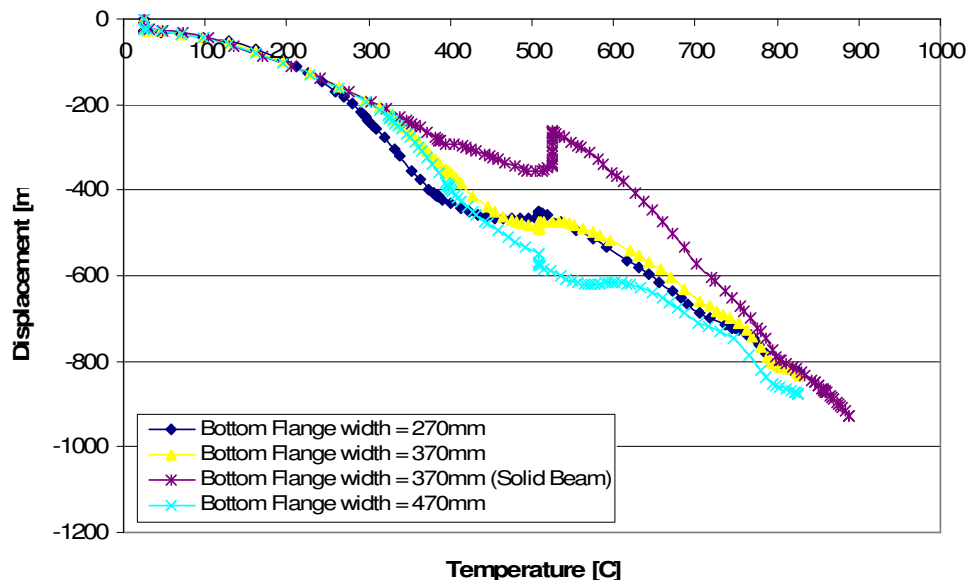


Figure 139 - Displacement versus temperature for varying bottom flange widths

The thinner webbed cellular beams had web post buckling at around 191°C and subsequently experienced greater displacements than the thicker webbed beams that underwent end post and/or overall lateral torsional buckling modes (Fig 138). The latter buckling modes are typically more stable/ductile as evident by the lower displacement rates. The displacement vs. temperature plots from the varying diameter, number of holes, and end post simulations revealed similar results – the simulations that experienced web post buckling tended to have increased displacement relative to those that underwent more stable buckling modes (i.e. overall lateral buckling, end post buckling, etc.) As seen in Figure 139, the

displacement histories of the cellular beams with varying bottom flange widths had similar responses. In these simulations, all the scenarios experienced web post buckling. Similar trends were also observed for the cellular beams with varying bottom flange thickness.

These observations coupled with the axial force plots seem to suggest a strong correlation between buckling mode and displacement response initially after a buckling event has occurred. This correlation may alter as the simulation continues further into the post-buckling region, where catenary action becomes the dominating structural mechanism. This trend can already be seen in Figures 138 and 139, where the displacement histories are beginning to coincide. The full displacement history (up to the global failure of the structure) should be investigated.

4.3.3 Affect of Various Heating Curves and Thermal Profiles

In Scenario II and Scenario III, different time-temperature curves and thermal gradients were applied to the same cellular beam model. As discussed earlier, the response of the cellular beam is largely influenced by the temperature. Therefore, the models with higher maximum temperatures experienced larger displacements; and the models that experienced higher heating rates, experienced larger displacements sooner than those that experienced lower heating rates. In most of the cases, the local buckling mode and axial forces were similar.

In Scenario III, higher web temperatures were artificially created and applied to one of the cellular beam models to simulate the data observed in

recent cellular beam fire tests. From this analysis, the hotter web temperatures appeared to influence the behavior of the cellular beam immediately after the 2nd local buckling event. As observed in Figures 133, the displacement of the “protected” beam (the beam with hotter web temperatures) appears to initially have higher displacements immediately after the 2nd buckling event. However, as the simulation continues the response begins to coincide with the other simulations. Similarly, in the axial force plot (Figure 134) , the “protected” beam appears to unload at a slightly greater rate than the other beams tested. This behavior is a more unstable response, and is indicative a more sudden event in the response history. Further research should be conducted to determine if the hotter web temperatures affect the structural response in the post-buckling region.

Chapter 5: Conclusions

A long span cellular beam model is evaluated from several perspectives in this study to determine its sensitivity to different parameters. The displacements, local buckling modes and connection forces of each case study were compared with a solid beam model, and general trends were observed. These details indicate the effects varying parameters have not only on global response, but local response of the cellular beam.

This study suggests that the characteristics of a cellular beam's web play a more significant role in the structural fire behavior not only in terms of the local beam response but ultimately on the surrounding structure. While other parameters do influence the structural response, it appears that the cellular beam web characteristics dominate the beam behavior, connection forces, and displacements particularly after a buckling event has occurred. While the web characteristics appear to markedly affect the pre-buckling behavior, they may not have much of a significant role in the post-buckling region where catenary action dominates the global structural response.

Additional work should be conducted on these long span cellular beams to determine how these parameters affect the post-buckling response where catenary action becomes the dominant structural mechanism. The parameters that influence pre-buckling behavior may have little to no influence in the post-buckling region. Various spans (12-20m) should be tested, in addition, to various locations in the building (such as an external bay, or a bay near the core). Building location can play a significant role, not only, on the local response of the cellular beam, but also on the surrounding structure (i.e. external columns will have not have lateral support from the surrounding structure).

The affects on the surrounding structure will be markedly different, than that presented here.

More realistic fire scenarios should also be tested/analyzed. This study only observed the influence of the heating regime. Additional work should include the cooling phase, as well.

APPENDIX A: Heat Transfer Calculations

Scenario I – Heat Transfer (Matlab script file)

```
%%%%%%%%%%%%%%%%%%%%%%%%%%%%%%%%%%%%%%%%%%%%%%%%%%%%%%%%%%%%%%%%%%%%%%%%%%%%%%
%%%%%%%%%%%%%%%%%%%%%%%%%%%%%%%%%%%%%%%%%%%%%%%%%%%%%%%%%%%%%%%%%%%%%%%%%%%%%%
% Case 1 - STANDARD TIME TEMPERATURE CURVE
%%%%%%%%%%%%%%%%%%%%%%%%%%%%%%%%%%%%%%%%%%%%%%%%%%%%%%%%%%%%%%%%%%%%%%%%%%%%%%
%%%%%%%%%%%%%%%%%%%%%%%%%%%%%%%%%%%%%%%%%%%%%%%%%%%%%%%%%%%%%%%%%%%%%%%%%%%%%%

clear all;
clc;
%%%%%%%%%%%%%%%%%%%%%%%%%%%%%%%%%%%%%%%%%%%%%%%%%%%%%%%%%%%%%%%%%%%%%%%%%%%%%%
%%%%%%%%%%%%%%%%%%%%%%%%%%%%%%%%%%%%%%%%%%%%%%%%%%%%%%%%%%%%%%%%%%%%%%%%%%%%%%
% PROPERTIES
%%%%%%%%%%%%%%%%%%%%%%%%%%%%%%%%%%%%%%%%%%%%%%%%%%%%%%%%%%%%%%%%%%%%%%%%%%%%%%
%%%%%%%%%%%%%%%%%%%%%%%%%%%%%%%%%%%%%%%%%%%%%%%%%%%%%%%%%%%%%%%%%%%%%%%%%%%%%%
% Steel Properties - constant
% Physical properties
rho_a = 7850;      % Density of steel [kg/m^3]

% Thermal Properties
% Convection Coefficients
alpha_c = 25;      % [W/m^2-K]
gamma_hc = 1;

% Radiation Coefficients
eps_f = 0.8;
eps_m = 0.7;
eps_res = 0.56;
gamma_hr = 1;
PHI = 1;
stef_bolz = 5.67e-8;

% Hp/A Values (Section Factors)

% Total Section Factor Value or Hp/A Value(whole section)
% Cellular Beam
sf_cell = 96.843;   % Total Heated Perimeter [m]/ Total x-sectional area [m^2]

% Solid Beam Hp/A
sf_beam = 104.119;

% Column Hp/A
sf_col = 53.7;

%Section Factor Matrix
sf=[sf_cell;sf_beam;sf_col];
```

```

%%%%%%%%%%%%%%%%%%%%%%%%%%%%%%%%%%%%%%%%%%%%%%%%%%%%%%%%%%%%%%%%%%%%%%%%
%%%%%%%%%%%%%%%%%%%%%%%%%%%%%%%%%%%%%%%%%%%%%%%%%%%%%%%%%%%%%%%%%%%%%%%%
% CALCULATION FOR STEEL TEMPERATURE CURVES

```

```

%%%%%%%%%%%%%%%%%%%%%%%%%%%%%%%%%%%%%%%%%%%%%%%%%%%%%%%%%%%%%%%%%%%%%%%%
%%%%%%%%%%%%%%%%%%%%%%%%%%%%%%%%%%%%%%%%%%%%%%%%%%%%%%%%%%%%%%%%%%%%%%%%

```

```

%%%%%%%%%%%%%%%%%%%%%%%%%%%%%%%%%%%%%%%%%%%%%%%%%%%%%%%%%%%%%%%%%%%%%%%%
%%%%%%%%%%%%%%%%%%%%%%%%%%%%%%%%%%%%%%%%%%%%%%%%%%%%%%%%%%%%%%%%%%%%%%%% UnProtected Steel %%%%%%%%%%%%%%%%%%%%%%%%%%%%%%%%%%%%%%%%%%%%%%%%%%%%%%%%%%%%%%%%%%%%%%%%%

```

```

% In this portion of the analysis, the only unprotected member is
% the cellular beam and solid beam of study. The edge beams, columns,
% and slab will always be protected throughout the study.

```

```

% Number of element in this section to be calc
ne= 2;          %cellular and solid

```

```

%Section factors used
sf=[sf_cell;sf_beam];

```

```

% The unprotected steel temperatures were derived from
% Eurocode 3: Part 1-2 Equation 4.21

```

```

% Extract Gas Temperatures from TT_Asif file
[T, Tg_2, Tg, To, t, dt] = Temps;

```

```

% Calculate Unprotected steel temperatures

```

```

T = T + 273;          % Gas temperature [K]
Ts_u(1,1:ne) = To+273; % Initial Temperature of Steel [C]
i=1;
j=1;
hc(1,1:ne)= 0;
hr(1,1:ne) = 0;
hnet(1,1:ne) = 0;
for j=1:ne
    for i=1:length(t)-1
        if Ts_u(i,j) < 873
            c_a(i,j) = 425 + (7.73e-1)*Ts_u(i,j) - 1.69e-3*(Ts_u(i,j)^2) + 2.22e-6*(Ts_u(i,j)^3);
            hc(i+1,j) = alpha_c*(T(i+1)-Ts_u(i,j));
            hr(i+1,j) = PHI*eps_res*stef_bolz*(T(i+1)^4-(Ts_u(i,j))^4);
            hnet(i+1,j) = gamma_hc*hc(i+1,j)+gamma_hr*hr(i+1,j);
            dTs_u(i,j) = sf(j)/c_a(i,j)/rho_a*hnet(i+1,j)*dt;
        elseif Ts_u(i,j)>=873 & Ts_u(i,j)<1008
            c_a(i,j) = 666+ (13002/(738-Ts_u(i,j)));
            hc(i+1,j) = alpha_c*(T(i+1)-Ts_u(i,j));
            hr(i+1,j) = PHI*eps_res*stef_bolz*(T(i+1)^4-(Ts_u(i,j))^4);
            hnet(i+1,j) = gamma_hc*hc(i+1,j)+gamma_hr*hr(i+1,j);
            dTs_u(i,j) = sf(j)/c_a(i,j)/rho_a*hnet(i+1,j)*dt;
        elseif Ts_u(i,j)>=1008 & Ts_u(i,j)<1173
            c_a(i,j) = 545 + (17820/ (Ts_u(i,j) - 731));
            hc(i+1,j) = alpha_c*(T(i+1)-Ts_u(i,j));
            hr(i+1,j) = PHI*eps_res*stef_bolz*(T(i+1)^4-(Ts_u(i,j))^4);
            hnet(i+1,j) = gamma_hc*hc(i+1,j)+gamma_hr*hr(i+1,j);
            dTs_u(i,j) = sf(j)/c_a(i,j)/rho_a*hnet(i+1,j)*dt;
        else
            c_a(i,j) = 650;

```

```

        hc(i+1,j) = alpha_c*(T(i+1)-Ts_u(i,j));
        hr(i+1,j) = PHI*eps_res*stef_bolz*(T(i+1)^4-(Ts_u(i,j))^4);
        hnet(i+1,j) = gamma_hc*hc(i+1,j)+gamma_hr*hr(i+1,j);
        dTs_u(i,j) = sf(j)/c_a(i)/rho_a*hnet(i+1,j)*dt;
    end
    Ts_u(i+1,j)= dTs_u(i,j) + Ts_u(i,j);
    i=i+1;
end
j=j+1;
end
Ts_u = Ts_u - 273;

%%%%%%%%%%%%%%%%%%%%%%%%%%%%%%%%%%%%%%%%%%%%%%%%%%%%%%%%%%%%%%%%%%%%%%%%%%%%%%
%%%%%%%%%%%%%%%%%%%%%%%%%%%%%%%%%%%%%%%%%%%%%%%%%%%%%%%%%%%%%%%%%%%%%%%%%% Protected Steel %%%%%%%%%%%%%%%%%%%%%%%%%%%%%%%%%%%%%%%%%%%%%%%%%%%%%%%%%%%%%%%%%%%%%%%%%%
%%%%%%%%%%%%%%%%%%%%%%%%%%%%%%%%%%%%%%%%%%%%%%%%%%%%%%%%%%%%%%%%%%%%%%%%%%
% Number of element in this section to be calc
ne= 2;          %cellular and column

%Section factors used
sf=[sf_cell;sf_col];

% Fire Protection Material Properties: Firetex FB120
% Note: Properties given by ARUP & Partners
dp = 0.02;      % Thickness of material [m]
c_p = 900;      % Specific Heat [J/kg-K]
rho_p = 700;    % Density [kg/m^3]
lamda_p = 0.17; % Thermal conductivity [W/m-K]

% Calculate Protected steel temperatures
Ts_p(1,1:ne) = To+273; % Initial Temperature of Steel [C]
i=1;
j=1;
for j=1:ne
    for i=1:length(t)-1
        if Ts_p(i,j) < 873
            c_a(i,j) = 425 + 7.73e-1*Ts_p(i,j) - 1.69e-3*Ts_p(i,j)^2 + 2.22e-6*Ts_p(i,j)^3;
            phi(i,j) = (c_p*rho_p)/(c_a(i,j)*rho_a)*dp*sf(j);
            dTs_p(i,j) = ((lamda_p*sf(j))/(dp*c_a(i,j)*rho_a)*(T(i)-Ts_p(i,j))/(1+phi(i,j)/3)*dt)-
            (exp(phi(i,j)/10)-1)*(T(i+1)-(T(i)));
        elseif Ts_p(i,j)>=873 & Ts_p(i,j)<1008
            c_a(i,j) = 666+ (13002/(738-Ts_p(i,j)));
            phi(i,j) = (c_p*rho_p)/(c_a(i,j)*rho_a)*dp*sf(j);
            dTs_p(i,j) = ((lamda_p*sf(j))/(dp*c_a(i,j)*rho_a)*(T(i)-Ts_p(i,j))/(1+phi(i,j)/3)*dt)-
            (exp(phi(i,j)/10)-1)*(T(i+1)-(T(i)));
        elseif Ts_p(i,j)>=1008 & Ts_p(i,j)<1173
            c_a(i,j) = 545 + (17820/ (Ts_p(i,j) - 731));
            phi(i,j) = (c_p*rho_p)/(c_a(i,j)*rho_a)*dp*sf(j);
            dTs_p(i,j) = ((lamda_p*sf(j))/(dp*c_a(i,j)*rho_a)*(T(i)-Ts_p(i,j))/(1+phi(i,j)/3)*dt)-
            (exp(phi(i,j)/10)-1)*(T(i+1)-(T(i)));
        else
            c_a(i,j) = 650;
            phi(i,j) = (c_p*rho_p)/(c_a(i,j)*rho_a)*dp*sf(j);
            dTs_p(i,j) = ((lamda_p*sf(j))/(dp*c_a(i,j)*rho_a)*(T(i)-Ts_p(i,j))/(1+phi(i,j)/3)*dt)-
            (exp(phi(i,j)/10)-1)*(T(i+1)-(T(i)));
        end
    end
end

```

```

end
if dTs_p(i,j) < 0
    dTs_p(i,j) = 0;
    Ts_p(i+1,j)=dTs_p(i,j)+Ts_p(i,j);
    i=i+1;
else
    Ts_p(i+1,j)= dTs_p(i,j) + Ts_p(i,j);
    i=i+1;
end
end
j=j+1;
end
Ts_p = Ts_p -273;
T = T-273;

figure
plot(t,T,t,Ts_u(:,1),'--',t,Ts_u(:,2),'-.',t,Ts_p(:,1),t,Ts_p(:,2))
xlabel('Time [s]','FontSize',16)
ylabel('Temperature [C]','FontSize',16)
title('Scenario I - Protected and UnProtected Steel Temperatures, Standard Curve','FontSize',18)
legend('Standard Curve','Unprotected - Cellular Beam','Unprotected - Solid Beam','Protected - Edge Beams','Protected - Column',0)

[success]=xlswrite('N:myhome/Thesis/Calcs/Matlab/Scenario I/UnProtected Steel Temps.xls',Ts_u,'Sheet1','B4:C1445')
[success]=xlswrite('N:myhome/Thesis/Calcs/Matlab/Scenario I/Protected Steel Temps.xls',Ts_p,'Sheet1','B4:C1445')

```

Scenario II – Heat Transfer (Matlab script file)

```
%%%%%%%%%%%%%%%%%%%%%%%%%%%%%%%%%%%%%%%%%%%%%%%%%%%%%%%%%%%%%%%%%%%%%%%%%%
%%%%%%%%%%%%%%%%%%%%%%%%%%%%%%%%%%%%%%%%%%%%%%%%%%%%%%%%%%%%%%%%%%%%%%%%%
% Scenario II - GENERALIZED EXPONENTIAL CURVE
%%%%%%%%%%%%%%%%%%%%%%%%%%%%%%%%%%%%%%%%%%%%%%%%%%%%%%%%%%%%%%%%%%%%%%%%%
% Case B - Rate of heating: 0.005, 0.0015, 0.0007 with Tmax=1000C
%
%%%%%%%%%%%%%%%%%%%%%%%%%%%%%%%%%%%%%%%%%%%%%%%%%%%%%%%%%%%%%%%%%%%%%%%%%
%%%%%%%%%%%%%%%%%%%%%%%%%%%%%%%%%%%%%%%%%%%%%%%%%%%%%%%%%%%%%%%%%%%%%%%%%

clear all;
clc;
%%%%%%%%%%%%%%%%%%%%%%%%%%%%%%%%%%%%%%%%%%%%%%%%%%%%%%%%%%%%%%%%%%%%%%%%%
%%%%%%%%%%%%%%%%%%%%%%%%%%%%%%%%%%%%%%%%%%%%%%%%%%%%%%%%%%%%%%%%%%%%%%%%%
%%%%%%%%%%%%%%%%%%%%%%%%%%%%%%%%%%%%%%%%%%%%%%%%%%%%%%%%%%%%%%%%%%%%%%%%%
% PROPERTIES
%%%%%%%%%%%%%%%%%%%%%%%%%%%%%%%%%%%%%%%%%%%%%%%%%%%%%%%%%%%%%%%%%%%%%%%%%
%%%%%%%%%%%%%%%%%%%%%%%%%%%%%%%%%%%%%%%%%%%%%%%%%%%%%%%%%%%%%%%%%%%%%%%%%

% Steel Properties - constant
% Physical properties
rho_a = 7850; % Density of steel [kg/m^3]

% Thermal Properties
% Convection Coefficients
alpha_c = 25; % [W/m^2-K]
gamma_hc = 1;

% Radiation Coefficients
eps_f = 0.8;
eps_m = 0.7;
eps_res = 0.56;
gamma_hr = 1;
PHI = 1;
stef_bolz = 5.67e-8;

% Hp/A Values (Section Factors)

% Total Section Factor Value or Hp/A Value(whole section)
% Cellular Beam
sf_cell = 96.843; % Total Heated Perimeter [m]/ Total x-sectional area [m^2]

% Solid Beam Hp/A
sf_beam = 104.119;

% Column Hp/A
sf_col = 53.7;

%Section Factor Matrix
sf=[sf_cell;sf_beam;sf_col];

%%%%%%%%%%%%%%%%%%%%%%%%%%%%%%%%%%%%%%%%%%%%%%%%%%%%%%%%%%%%%%%%%%%%%%%%%
%%%%%%%%%%%%%%%%%%%%%%%%%%%%%%%%%%%%%%%%%%%%%%%%%%%%%%%%%%%%%%%%%%%%%%%%%
% CALCULATION FOR STEEL TEMPERATURE CURVES
```

```
%%%%%%%%%%%%%%%%%%%%%%%%%%%%%%%%%%%%%%%%%%%%%%%%%%%%%%%%%%%%%%%%%%%%%%%%%
```

```
%%%%%%%%%%%%%%%%%%%%%%%%%%%%%%%%%%%%%%%%%%%%%%%%%%%%%%%%%%%%%%%%%%%%%%%%%  
%%%%%%%%%%%%%%%%%%%%%%%%%%%%%%%%%%%%%%%%%%%%%%%%%%%%%%%%%%%%%%%%%%%%%%%%% Gas Temperatures 1 - alpha = 0.005, Tmax = 1000C %%%%%%%%%%  
%%%%%%%%%%%%%%%%%%%%%%%%%%%%%%%%%%%%%%%%%%%%%%%%%%%%%%%%%%%%%%%%%%%%%%%%%
```

```
%%%%%%%%%%%%%%%%%%%%%%%%%%%%%%%%%%%%%%%%%%%%%%%%%%%%%%%%%%%%%%%%%%%%%%%%%  
%%%%%%%%%%%%%%%%%%%%%%%%%%%%%%%%%%%%%%%%%%%%%%%%%%%%%%%%%%%%%%%%%%%%%%%%% UnProtected Steel %%%%%%%%%%  
%%%%%%%%%%%%%%%%%%%%%%%%%%%%%%%%%%%%%%%%%%%%%%%%%%%%%%%%%%%%%%%%%%%%%%%%%  
% In this portion of the analysis, the only unprotected member is  
% the cellular beam and solid beam of study. The edge beams, columns,  
% and slab will always be protected throughout the study.
```

```
% Number of element in this section to be calc  
ne= 2; %cellular and solid
```

```
%Section factors used  
sf=[sf_cell;sf_beam];
```

```
% The unprotected steel temperatures were derived from  
% Eurocode 3: Part 1-2 Equation 4.21
```

```
% Extract Gas Temperatures from TT_Asif file  
[T, Tg_2, Tg, To, t, dt] = Temps;
```

```
% Calculate Unprotected steel temperatures
```

```
Tg = Tg + 273; % Gas temperature [K]  
Ts_u(1,1:ne) = To+273; % Initial Temperature of Steel [C]  
i=1;  
j=1;  
hc(1,1:ne)= 0;  
hr(1,1:ne) = 0;  
hnet(1,1:ne) = 0;  
for j=1:ne  
    for i=1:length(t)-1  
        if Ts_u(i,j) < 873  
            c_a(i,j) = 425 + (7.73e-1)*Ts_u(i,j) - 1.69e-3*(Ts_u(i,j)^2) + 2.22e-6*(Ts_u(i,j)^3);  
            hc(i+1,j) = alpha_c*(Tg(i+1,1)-Ts_u(i,j));  
            hr(i+1,j) = PHI*eps_res*stef_bolz*(Tg(i+1,1)^4-(Ts_u(i,j))^4);  
            hnet(i+1,j) = gamma_hc*hc(i+1,j)+gamma_hr*hr(i+1,j);  
            dTs_u(i,j) = sf(j)/c_a(i,j)/rho_a*hnet(i+1,j)*dt;  
        elseif Ts_u(i,j)>=873 & Ts_u(i,j)<1008  
            c_a(i,j) = 666+ (13002/(738-Ts_u(i,j)));  
            hc(i+1,j) = alpha_c*(Tg(i+1,1)-Ts_u(i,j));  
            hr(i+1,j) = PHI*eps_res*stef_bolz*(Tg(i+1,1)^4-(Ts_u(i,j))^4);  
            hnet(i+1,j) = gamma_hc*hc(i+1,j)+gamma_hr*hr(i+1,j);  
            dTs_u(i,j) = sf(j)/c_a(i,j)/rho_a*hnet(i+1,j)*dt;  
        elseif Ts_u(i,j)>=1008 & Ts_u(i,j)<1173  
            c_a(i,j) = 545 + (17820/ (Ts_u(i,j) - 731));  
            hc(i+1,j) = alpha_c*(Tg(i+1,1)-Ts_u(i,j));  
            hr(i+1,j) = PHI*eps_res*stef_bolz*(Tg(i+1,1)^4-(Ts_u(i,j))^4);  
            hnet(i+1,j) = gamma_hc*hc(i+1,j)+gamma_hr*hr(i+1,j);  
            dTs_u(i,j) = sf(j)/c_a(i,j)/rho_a*hnet(i+1,j)*dt;
```



```

else
    c_a(i,j) = 650;
    hc(i+1,j) = alpha_c*(Tg(i+1,1)-Ts_u(i,j));
    hr(i+1,j) = PHI*eps_res*stef_bolz*(Tg(i+1,1)^4-(Ts_u(i,j))^4);
    hnet(i+1,j) = gamma_hc*hc(i+1,j)+gamma_hr*hr(i+1,j);
    dTs_u(i,j) = sf(j)/c_a(i)/rho_a*hnet(i+1,j)*dt;
end
Ts_u(i+1,j)= dTs_u(i,j) + Ts_u(i,j);
i=i+1;
end
j=j+1;
end
Ts_u = Ts_u - 273;

%%%%%%%%%%%%%%%%%%%%%%%%%%%%%%%%%%%%%%%%%%%%%%%%%%%%%%%%%%%%%%%%%%%%%%%%%%%%%%
%%
%%%%%%%%%%%%%%%%%%%%%%%%%%%%%%%%%%%%%%%%%%%%%%%%%%%%%%%%%%%%%%%%%%%%%%%%%%%%%% Protected Steel %%%%%%%%%%%%%%%%%%%%%%%%%%%%%%%%%%%%%%%%%%%%%%%%%%%%%%%%%%%%%%%%%%%%%%%%%%%%%%%
%%%%%%%%%%%%%%%%%%%%%%%%%%%%%%%%%%%%%%%%%%%%%%%%%%%%%%%%%%%%%%%%%%%%%%%%%%%%%%
%% Number of element in this section to be calc
ne= 2;          %cellular and column

%Section factors used
sf=[sf_cell;sf_col];

% Fire Protection Material Properties: Firetex FB120
% Note: Properties given by ARUP & Partners
dp = 0.02;      % Thickness of material [m]
c_p = 900;      % Specific Heat [J/kg-K]
rho_p = 700;    % Density [kg/m^3]
lamda_p = 0.17; % Thermal conductivity [W/m-K]

% Calculate Protected steel temperatures
Ts_p(1,1:ne) = To+273; % Initial Temperature of Steel [C]
i=1;
j=1;
for j=1:ne
    for i=1:length(t)-1
        if Ts_p(i,j) < 873
            c_a(i,j) = 425 + 7.73e-1*Ts_p(i,j) - 1.69e-3*Ts_p(i,j)^2 + 2.22e-6*Ts_p(i,j)^3;
            phi(i,j) = (c_p*rho_p)/(c_a(i,j)*rho_a)*dp*sf(j);
            dTs_p(i,j) = ((lamda_p*sf(j))/(dp*c_a(i,j)*rho_a)*(Tg(i,1)-Ts_p(i,j))/(1+phi(i,j)/3)*dt)-
            (exp(phi(i,j)/10)-1)*(Tg(i+1,1)-(Tg(i,1)));
            elseif Ts_p(i,j)>=873 & Ts_p(i,j)<1008
                c_a(i,j) = 666+ (13002/(738-Ts_p(i,j)));
                phi(i,j) = (c_p*rho_p)/(c_a(i,j)*rho_a)*dp*sf(j);
                dTs_p(i,j) = ((lamda_p*sf(j))/(dp*c_a(i,j)*rho_a)*(Tg(i,1)-Ts_p(i,j))/(1+phi(i,j)/3)*dt)-
                (exp(phi(i,j)/10)-1)*(Tg(i+1,1)-(Tg(i,1)));
            elseif Ts_p(i,j)>=1008 & Ts_p(i,j)<1173
                c_a(i) = 545 + (17820/ (Ts_p(i,j) - 731));
                phi(i,j) = (c_p*rho_p)/(c_a(i,j)*rho_a)*dp*sf(j);
                dTs_p(i,j) = ((lamda_p*sf(j))/(dp*c_a(i,j)*rho_a)*(Tg(i,1)-Ts_p(i,j))/(1+phi(i,j)/3)*dt)-
                (exp(phi(i,j)/10)-1)*(Tg(i+1,1)-(Tg(i,1)));
            else

```

```

        c_a(i,j) = 650;
        phi(i,j) = (c_p*rho_p)/(c_a(i,j)*rho_a)*dp*sf(j);
        dTs_p(i,j) = ((lamda_p*sf(j))/(dp*c_a(i,j)*rho_a)*(Tg(i,1)-Ts_p(i,j))/(1+phi(i,j)/3)*dt)-
        (exp(phi(i,j)/10)-1)*(Tg(i+1,1)-(Tg(i,1)));
    end
    if dTs_p(i,j) < 0
        dTs_p(i,j) = 0;
        Ts_p(i+1,j)=dTs_p(i,j)+Ts_p(i,j);
        i=i+1;
    else
        Ts_p(i+1,j)= dTs_p(i,j) + Ts_p(i,j);
        i=i+1;
    end
end
end
j=j+1;
end
Ts_p = Ts_p -273;
Tg = Tg-273;

```

```

figure
plot(t,Tg(:,1),'--',t,Ts_u(:,1),'--',t,Ts_u(:,2),'-',t,Ts_p(:,1),t,Ts_p(:,2))
xlabel('Time [s]','FontSize',12)
ylabel('Temperature [C]','FontSize',12)
title('Steel Temperatures, Generalized Exponential Curve alpha = 0.005, Tmax =
1000C','FontSize',12)
legend('Generalized Curve, Tmax=1000C, alpha=0.005','Unprotected - Cellular
Beam','Unprotected - Solid Beam','Protected - Edge Beams','Protected - Column',0)

```

```

%%%%%%%%%%%%%%%%%%%%%%%%%%%%%%%%%%%%%%%%%%%%%%%%%%%%%%%%%%%%%%%%%%%%%%%%
%%%%%%%%%%%%%%%%%%%%%%%%%%%%%%%%%%%%%%%%%%%%%%%%%%%%%%%%%%%%%%%%%%%%%%%%
%%%%%%%%%%%%%%%%%%%%%%%%%%%%%%%%%%%%%%%%%%%%%%%%%%%%%%%%%%%%%%%%%%%%%%%% Gas Temperatures 2 - alpha = 0.0015, Tmax = 1000C %%%%%%%%%
%%%%%%%%%%%%%%%%%%%%%%%%%%%%%%%%%%%%%%%%%%%%%%%%%%%%%%%%%%%%%%%%%%%%%%%%
%%%%%%%%%%%%%%%%%%%%%%%%%%%%%%%%%%%%%%%%%%%%%%%%%%%%%%%%%%%%%%%%%%%%%%%%

```

```

%%%%%%%%%%%%%%%%%%%%%%%%%%%%%%%%%%%%%%%%%%%%%%%%%%%%%%%%%%%%%%%%%%%%%%%%
%%%%%%%%
%%%%%%%% UnProtected Steel %%%%%%%%%
%%%%%%%%
%%%%%%%%

```

```

% In this portion of the analysis, the only unprotected member is
% the cellular beam and solid beam of study. The edge beams, columns,
% and slab will always be protected throughout the study.

```

```

% Number of element in this section to be calc
ne= 2;          %cellular and solid

```

```

%Section factors used
sf=[sf_cell;sf_beam];

```

```

% The unprotected steel temperatures were derived from
% Eurocode 3: Part 1-2 Equation 4.21

```

```

% Extract Gas Temperatures from TT_Asif file

```

```
[T, Tg_2, Tg, To, t, dt] = Temps;
```

```
% Calculate Unprotected steel temperatures
```

```
Tg = Tg + 273; % Gas temperature [K]
Ts_u(1,1:ne) = To+273; % Initial Temperature of Steel [C]
```

```
i=1;
```

```
j=1;
```

```
hc(1,1:ne)= 0;
```

```
hr(1,1:ne) = 0;
```

```
hnet(1,1:ne) = 0;
```

```
for j=1:ne
```

```
for i=1:length(t)-1
```

```
if Ts_u(i,j) < 873
```

```
c_a(i,j) = 425 + (7.73e-1)*Ts_u(i,j) - 1.69e-3*(Ts_u(i,j)^2) + 2.22e-6*(Ts_u(i,j)^3);
```

```
hc(i+1,j) = alpha_c*(Tg(i+1,2)-Ts_u(i,j));
```

```
hr(i+1,j) = PHI*eps_res*stef_bolz*(Tg(i+1,2)^4-(Ts_u(i,j))^4);
```

```
hnet(i+1,j) = gamma_hc*hc(i+1,j)+gamma_hr*hr(i+1,j);
```

```
dTs_u(i,j) = sf(j)/c_a(i,j)/rho_a*hnet(i+1,j)*dt;
```

```
elseif Ts_u(i,j)>=873 & Ts_u(i,j)<1008
```

```
c_a(i,j) = 666+ (13002/(738-Ts_u(i,j)));
```

```
hc(i+1,j) = alpha_c*(Tg(i+1,2)-Ts_u(i,j));
```

```
hr(i+1,j) = PHI*eps_res*stef_bolz*(Tg(i+1,2)^4-(Ts_u(i,j))^4);
```

```
hnet(i+1,j) = gamma_hc*hc(i+1,j)+gamma_hr*hr(i+1,j);
```

```
dTs_u(i,j) = sf(j)/c_a(i,j)/rho_a*hnet(i+1,j)*dt;
```

```
elseif Ts_u(i,j)>=1008 & Ts_u(i,j)<1173
```

```
c_a(i,j) = 545 + (17820/ (Ts_u(i,j) - 731));
```

```
hc(i+1,j) = alpha_c*(Tg(i+1,2)-Ts_u(i,j));
```

```
hr(i+1,j) = PHI*eps_res*stef_bolz*(Tg(i+1,2)^4-(Ts_u(i,j))^4);
```

```
hnet(i+1,j) = gamma_hc*hc(i+1,j)+gamma_hr*hr(i+1,j);
```

```
dTs_u(i,j) = sf(j)/c_a(i,j)/rho_a*hnet(i+1,j)*dt;
```

```
else
```

```
c_a(i,j) = 650;
```

```
hc(i+1,j) = alpha_c*(Tg(i+1,2)-Ts_u(i,j));
```

```
hr(i+1,j) = PHI*eps_res*stef_bolz*(Tg(i+1,2)^4-(Ts_u(i,j))^4);
```

```
hnet(i+1,j) = gamma_hc*hc(i+1,j)+gamma_hr*hr(i+1,j);
```

```
dTs_u(i,j) = sf(j)/c_a(i,j)/rho_a*hnet(i+1,j)*dt;
```

```
end
```

```
Ts_u(i+1,j)= dTs_u(i,j) + Ts_u(i,j);
```

```
i=i+1;
```

```
end
```

```
j=j+1;
```

```
end
```

```
Ts_u = Ts_u - 273;
```

```
%%%%%%%%%%%%%%%%%%%%%%%%%%%%%%%%%%%%%%%%%%%%%%%%%%%%%%%%%%%%%%%%%%%%%%%%%
```

```
%%%%%%%%%%%%%%%%%%%%%%%%%%%%%%%%%%%%%%%%%%%%%%%%%%%%%%%%%%%%%%%%%%%%%%%%% Protected Steel %%%%%%%%%%%%%%%%%%%%%%%%%%%%%%%%%%%%%%%%%%%%%%%%%%%%%%%%%%%%%%%%%%%%%%%%%%
```

```
%%%%%%%%%%%%%%%%%%%%%%%%%%%%%%%%%%%%%%%%%%%%%%%%%%%%%%%%%%%%%%%%%%%%%%%%%
```

```
% Number of element in this section to be calc
```

```
ne= 2; %cellular and column
```

```
%Section factors used
```

```
sf=[sf_cell;sf_col];
```

```
% Fire Protection Material Properties: Firetex FB120
```

```

% Note: Properties given by ARUP & Partners
dp = 0.02;      % Thickness of material [m]
c_p = 900;      % Specific Heat [J/kg-K]
rho_p = 700;    % Density [kg/m^3]
lamda_p = 0.17; % Thermal conductivity [W/m-K]

% Calculate Protected steel temperatures
Ts_p(1,1:ne) = To+273; % Initial Temperature of Steel [C]
i=1;
j=1;
for j=1:ne
    for i=1:length(t)-1
        if Ts_p(i,j) < 873
            c_a(i,j) = 425 + 7.73e-1*Ts_p(i,j) - 1.69e-3*Ts_p(i,j)^2 + 2.22e-6*Ts_p(i,j)^3;
            phi(i,j) = (c_p*rho_p)/(c_a(i,j)*rho_a)*dp*sf(j);
            dTs_p(i,j) = ((lamda_p*sf(j))/(dp*c_a(i,j)*rho_a)*(Tg(i,2)-Ts_p(i,j))/(1+phi(i,j)/3)*dt)-
            (exp(phi(i,j)/10)-1)*(Tg(i+1,2)-(Tg(i,2)));
            elseif Ts_p(i,j)>=873 & Ts_p(i,j)<1008
                c_a(i,j) = 666+ (13002/(738-Ts_p(i,j)));
                phi(i,j) = (c_p*rho_p)/(c_a(i,j)*rho_a)*dp*sf(j);
                dTs_p(i,j) = ((lamda_p*sf(j))/(dp*c_a(i,j)*rho_a)*(Tg(i,2)-Ts_p(i,j))/(1+phi(i,j)/3)*dt)-
                (exp(phi(i,j)/10)-1)*(Tg(i+1,2)-(Tg(i,2)));
            elseif Ts_p(i,j)>=1008 & Ts_p(i,j)<1173
                c_a(i,j) = 545 + (17820/(Ts_p(i,j) - 731));
                phi(i,j) = (c_p*rho_p)/(c_a(i,j)*rho_a)*dp*sf(j);
                dTs_p(i,j) = ((lamda_p*sf(j))/(dp*c_a(i,j)*rho_a)*(Tg(i,2)-Ts_p(i,j))/(1+phi(i,j)/3)*dt)-
                (exp(phi(i,j)/10)-1)*(Tg(i+1,2)-(Tg(i,2)));
            else
                c_a(i,j) = 650;
                phi(i,j) = (c_p*rho_p)/(c_a(i,j)*rho_a)*dp*sf(j);
                dTs_p(i,j) = ((lamda_p*sf(j))/(dp*c_a(i,j)*rho_a)*(Tg(i,2)-Ts_p(i,j))/(1+phi(i,j)/3)*dt)-
                (exp(phi(i,j)/10)-1)*(Tg(i+1,2)-(Tg(i,2)));
            end
            if dTs_p(i,j) < 0
                dTs_p(i,j) = 0;
                Ts_p(i+1,j)=dTs_p(i,j)+Ts_p(i,j);
                i=i+1;
            else
                Ts_p(i+1,j)= dTs_p(i,j) + Ts_p(i,j);
                i=i+1;
            end
        end
        j=j+1;
    end
end
Ts_p = Ts_p -273;
Tg = Tg-273;

figure
plot(t,Tg(:,2),'--',t,Ts_u(:,1),'--',t,Ts_u(:,2),'-.',t,Ts_p(:,1),t,Ts_p(:,2))
xlabel('Time [s]','FontSize',12)
ylabel('Temperature [C]','FontSize',12)
title('Scenario II - Steel Temperatures, Generalized Exponential Curve alpha = 0.0015, Tmax = 1000C','FontSize',12)
legend('Generalized Curve, Tmax=1000C, alpha=0.0015','Unprotected - Cellular Beam','Unprotected - Solid Beam','Protected - Edge Beams','Protected - Column',0)

```

```
[success]=xlswrite('N:\myhome\Thesis\Calcs\Matlab\Scenario II\UnProtected Steel  
Temps_Case4.xls',Ts_u,'Sheet1','B4:C1445')  
[success]=xlswrite('N:\myhome\Thesis\Calcs\Matlab\Scenario II\Protected Steel  
Temps_Case4.xls',Ts_p,'Sheet1','B4:C1445')
```

UnProtected Steel

In this portion of the analysis, the only unprotected member is the cellular beam and solid beam of study. The edge beams, columns, and slab will always be protected throughout the study.

```
%Section factors used
sf=[sf_cell;sf_beam];
```

```
% Extract Gas Temperatures from TT_Asf file
[T, Tg_2, Tg, To, t, dt] = Temps;
```

```
Tg = Tg + 273; % Gas temperature [K]
Ts_u(1,1:ne) = To+273; % Initial Temperature of Steel [C]
i=1;
j=1;
hc(1,1:ne)= 0;
hr(1,1:ne) = 0;
hnet(1,1:ne) = 0;
for j=1:ne
    for i=1:length(t)-1
        if Ts_u(i,j) < 873
            c_a(i,j) = 425 + (7.73e-1)*Ts_u(i,j) - 1.69e-3*(Ts_u(i,j)^2) + 2.22e-6*(Ts_u(i,j)^3);
            hc(i+1,j) = alpha_c*(Tg(i+1,3)-Ts_u(i,j));
            hr(i+1,j) = PHI*eps_res*stef_bolz*(Tg(i+1,3)^4-(Ts_u(i,j))^4);
            hnet(i+1,j) = gamma_hc*hc(i+1,j)+gamma_hr*hr(i+1,j);
            dTs_u(i,j) = sf(j)/c_a(i,j)/rho_a*hnet(i+1,j)*dt;
        elseif Ts_u(i,j)>=873 & Ts_u(i,j)<1008
            c_a(i,j) = 666+ (13002/(738-Ts_u(i,j)));
            hc(i+1,j) = alpha_c*(Tg(i+1,3)-Ts_u(i,j));
            hr(i+1,j) = PHI*eps_res*stef_bolz*(Tg(i+1,3)^4-(Ts_u(i,j))^4);
            hnet(i+1,j) = gamma_hc*hc(i+1,j)+gamma_hr*hr(i+1,j);
            dTs_u(i,j) = sf(j)/c_a(i,j)/rho_a*hnet(i+1,j)*dt;
        elseif Ts_u(i,j)>=1008 & Ts_u(i,j)<1173
```

```

c_a(i,j) = 545 + (17820/ (Ts_u(i,j) - 731));
hc(i+1,j) = alpha_c*(Tg(i+1,3)-Ts_u(i,j));
hr(i+1,j) = PHI*eps_res*stef_bolz*(Tg(i+1,3)^4-(Ts_u(i,j))^4);
hnet(i+1,j) = gamma_hc*hc(i+1,j)+gamma_hr*hr(i+1,j);
dTsu_u(i,j) = sf(j)/c_a(i)/rho_a*hnet(i+1,j)*dt;
else
c_a(i,j) = 650;
hc(i+1,j) = alpha_c*(Tg(i+1,3)-Ts_u(i,j));
hr(i+1,j) = PHI*eps_res*stef_bolz*(Tg(i+1,3)^4-(Ts_u(i,j))^4);
hnet(i+1,j) = gamma_hc*hc(i+1,j)+gamma_hr*hr(i+1,j);
dTsu_u(i,j) = sf(j)/c_a(i)/rho_a*hnet(i+1,j)*dt;
end
Ts_u(i+1,j)= dTsu_u(i,j) + Ts_u(i,j);
i=i+1;
end
j=j+1;
end
Ts_u = Ts_u - 273;

%%%%%%%%%%%%%%%%%%%%%%%%%%%%%%%%%%%%%%%%%%%%%%%%%%%%%%%%%%%%%%%%%%%%%%%%%%%%%%
%%%%%%%%%%%%%%%%%%%%%%%%%%%%%%%%%%%%%%%%%%%%%%%%%%%%%%%%%%%%%%%%%%%%%%%%%%%%%% Protected Steel %%%%%%%%%%%%%%%%%%%%%%%%%%%%%%%%%%%%%%%%%%%%%%%%%%%%%%%%%%%%%%%%%%%%%%%%%%%%%%%
%%%%%%%%%%%%%%%%%%%%%%%%%%%%%%%%%%%%%%%%%%%%%%%%%%%%%%%%%%%%%%%%%%%%%%%%%%%%%%
% Number of element in this section to be calc
ne= 2;          %cellular and column

%Section factors used
sf=[sf_cell;sf_col];

% Fire Protection Material Properties: Firetex FB120
% Note: Properties given by ARUP & Partners
dp = 0.02;      % Thickness of material [m]
c_p = 900;      % Specific Heat [J/kg-K]
rho_p = 700;    % Density [kg/m^3]
lamda_p = 0.17; % Thermal conductivity [W/m-K]

% Calculate Protected steel temperatures
Ts_p(1,1:ne) = To+273; % Initial Temperature of Steel [C]
i=1;
j=1;
for j=1:ne
    for i=1:length(t)-1
        if Ts_p(i,j) < 873
            c_a(i,j) = 425 + 7.73e-1*Ts_p(i,j) - 1.69e-3*Ts_p(i,j)^2 + 2.22e-6*Ts_p(i,j)^3;
            phi(i,j) = (c_p*rho_p)/(c_a(i,j)*rho_a)*dp*sf(j);
            dTs_p(i,j) = ((lamda_p*sf(j))/(dp*c_a(i,j)*rho_a)*(Tg(i,3)-Ts_p(i,j))/(1+phi(i,j)/3)*dt)-
            (exp(phi(i,j)/10)-1)*(Tg(i+1,3)-(Tg(i,3)));
        elseif Ts_p(i,j)>=873 & Ts_p(i,j)<1008
            c_a(i,j) = 666+ (13002/(738-Ts_p(i,j)));
            phi(i,j) = (c_p*rho_p)/(c_a(i,j)*rho_a)*dp*sf(j);
            dTs_p(i,j) = ((lamda_p*sf(j))/(dp*c_a(i,j)*rho_a)*(Tg(i,3)-Ts_p(i,j))/(1+phi(i,j)/3)*dt)-
            (exp(phi(i,j)/10)-1)*(Tg(i+1,3)-(Tg(i,3)));
        elseif Ts_p(i,j)>=1008 & Ts_p(i,j)<1173
            c_a(i) = 545 + (17820/ (Ts_p(i,j) - 731));
            phi(i,j) = (c_p*rho_p)/(c_a(i,j)*rho_a)*dp*sf(j);

```

```

        dTs_p(i,j) = ((lamda_p*sf(j))/(dp*c_a(i,j)*rho_a)*(Tg(i,3)-Ts_p(i,j))/(1+phi(i,j)/3)*dt)-
        (exp(phi(i,j)/10)-1)*(Tg(i+1,3)-(Tg(i,3)));
    else
        c_a(i,j) = 650;
        phi(i,j) = (c_p*rho_p)/(c_a(i,j)*rho_a)*dp*sf(j);
        dTs_p(i,j) = ((lamda_p*sf(j))/(dp*c_a(i,j)*rho_a)*(Tg(i,3)-Ts_p(i,j))/(1+phi(i,j)/3)*dt)-
        (exp(phi(i,j)/10)-1)*(Tg(i+1,3)-(Tg(i,3)));
    end
    if dTs_p(i,j) < 0
        dTs_p(i,j) = 0;
        Ts_p(i+1,j)=dTs_p(i,j)+Ts_p(i,j);
        i=i+1;
    else
        Ts_p(i+1,j)= dTs_p(i,j) + Ts_p(i,j);
        i=i+1;
    end
end
j=j+1;
end
Ts_p = Ts_p - 273;
Tg = Tg - 273;

```

```

figure
plot(t,Tg(:,3),'--',t,Ts_u(:,1),'--',t,Ts_u(:,2),'-',t,Ts_p(:,1),t,Ts_p(:,2))
xlabel('Time [s]','FontSize',12)
ylabel('Temperature [C]','FontSize',12)
title('Steel Temperatures, Generalized Exponential Curve alpha = 0.0007,
Tmax=1000C','FontSize',12)
legend('Generalized Curve, Tmax=1000C, alpha=0.0007','Unprotected - Cellular
Beam','Unprotected - Solid Beam','Protected - Edge Beams','Protected - Column',0)

```

% Output to excel files

```

[success]=xlswrite('N:\myhome\Thesis\Calcs\Matlab\Scenario II\UnProtected Steel
Temps_Case5.xls',Ts_u,'Sheet1','B4:C1445')
[success]=xlswrite('N:\myhome\Thesis\Calcs\Matlab\Scenario II\Protected Steel
Temps_Case5.xls',Ts_p,'Sheet1','B4:C1445')

```

```

%%%%%%%%%%%%%%%%%%%%%%%%%%%%%%%%%%%%%%%%%%%%%%%%%%%%%%%%%%%%%%%%%%%%%%%%
% Scenario 2- GENERALIZED EXPONENTIAL CURVE  %%%%%%%%%
% Case A - 800C<Tmax<1200C with rate of heating = 0.005
%
%%%%%%%%%%%%%%%%%%%%%%%%%%%%%%%%%%%%%%%%%%%%%%%%%%%%%%%%%%%%%%%%%%%%%%%%

```

clear all;

clc;

```

%%%%%%%%%%%%%%%%%%%%%%%%%%%%%%%%%%%%%%%%%%%%%%%%%%%%%%%%%%%%%%%%%%%%%%%%
%%%%%%%%%%%%%%%%%%%%%%%%%%%%%%%%%%%%%%%%%%%%%%%%%%%%%%%%%%%%%%%%%%%%%%%%
% PROPERTIES
%%%%%%%%%%%%%%%%%%%%%%%%%%%%%%%%%%%%%%%%%%%%%%%%%%%%%%%%%%%%%%%%%%%%%%%%
%%%%%%%%%%%%%%%%%%%%%%%%%%%%%%%%%%%%%%%%%%%%%%%%%%%%%%%%%%%%%%%%%%%%%%%%
%%%%%%%%%%%%%%%%%%%%%%%%%%%%%%%%%%%%%%%%%%%%%%%%%%%%%%%%%%%%%%%%%%%%%%%%

```

% Steel Properties - constant

% Physical properties

```

rho_a = 7850;          % Density of steel [kg/m^3]

% Thermal Properties
% Convection Coefficients
alpha_c = 25;          % [W/m^2-K]
gamma_hc = 1;

% Radiation Coefficients
eps_f = 0.8;
eps_m = 0.7;
eps_res = 0.56;
gamma_hr = 1;
PHI = 1;
stef_bolz = 5.67e-8;

% Hp/A Values (Section Factors)

% Total Section Factor Value or Hp/A Value(whole section)
% Cellular Beam
sf_cell = 96.843;      % Total Heated Perimeter [m]/ Total x-sectional area [m^2]

% Solid Beam Hp/A
sf_beam = 104.119;

% Column Hp/A
sf_col = 53.7;

%Section Factor Matrix
sf=[sf_cell;sf_beam;sf_col];

%%%%%%%%%%%%%%%%%%%%%%%%%%%%%%%%%%%%%%%%%%%%%%%%%%%%%%%%%%%%%%%%%%%%%%%%
% CALCULATION FOR STEEL TEMPERATURE CURVES
%%%%%%%%%%%%%%%%%%%%%%%%%%%%%%%%%%%%%%%%%%%%%%%%%%%%%%%%%%%%%%%%%%%%%%%%

%%%%%%%%%%%%%%%%%%%%%%%%%%%%%%%%%%%%%%%%%%%%%%%%%%%%%%%%%%%%%%%%%%%%%%%%
% Gas Temperatures 1 - Tmax = 1200C
%%%%%%%%%%%%%%%%%%%%%%%%%%%%%%%%%%%%%%%%%%%%%%%%%%%%%%%%%%%%%%%%%%%%%%%%

%%%%%%%%%%%%%%%%%%%%%%%%%%%%%%%%%%%%%%%%%%%%%%%%%%%%%%%%%%%%%%%%%%%%%%%%
% UnProtected Steel
%%%%%%%%%%%%%%%%%%%%%%%%%%%%%%%%%%%%%%%%%%%%%%%%%%%%%%%%%%%%%%%%%%%%%%%%
% In this portion of the analysis, the only unprotected member is
% the cellular beam and solid beam of study. The edge beams, columns,
% and slab will always be protected throughout the study.

% Number of element in this section to be calc
ne= 2;                %cellular and solid

%Section factors used
sf=[sf_cell;sf_beam];

```


% The unprotected steel temperatures were derived from
 % Eurocode 3: Part 1-2 Equation 4.21

% Extract Gas Temperatures from TT_Asif file
 [T, Tg_2, Tg, To, t, dt] = Temps;

% Calculate Unprotected steel temperatures

```
Tg_2 = Tg_2 + 273;          % Gas temperature [K]
Ts_u(1,1:ne) = To+273;     % Initial Temperature of Steel [C]
i=1;
j=1;
hc(1,1:ne)= 0;
hr(1,1:ne) = 0;
hnet(1,1:ne) = 0;
for j=1:ne
  for i=1:length(t)-1
    if Ts_u(i,j) < 873
      c_a(i,j) = 425 + (7.73e-1)*Ts_u(i,j) - 1.69e-3*(Ts_u(i,j)^2) + 2.22e-6*(Ts_u(i,j)^3);
      hc(i+1,j) = alpha_c*(Tg_2(i+1,1)-Ts_u(i,j));
      hr(i+1,j) = PHI*eps_res*stef_bolz*(Tg_2(i+1,1)^4-(Ts_u(i,j))^4);
      hnet(i+1,j) = gamma_hc*hc(i+1,j)+gamma_hr*hr(i+1,j);
      dTs_u(i,j) = sf(j)/c_a(i,j)/rho_a*hnet(i+1,j)*dt;
    elseif Ts_u(i,j)>=873 & Ts_u(i,j)<1008
      c_a(i,j) = 666+ (13002/(738-Ts_u(i,j)));
      hc(i+1,j) = alpha_c*(Tg_2(i+1,1)-Ts_u(i,j));
      hr(i+1,j) = PHI*eps_res*stef_bolz*(Tg_2(i+1,1)^4-(Ts_u(i,j))^4);
      hnet(i+1,j) = gamma_hc*hc(i+1,j)+gamma_hr*hr(i+1,j);
      dTs_u(i,j) = sf(j)/c_a(i,j)/rho_a*hnet(i+1,j)*dt;
    elseif Ts_u(i,j)>=1008 & Ts_u(i,j)<1173
      c_a(i,j) = 545 + (17820/ (Ts_u(i,j) - 731));
      hc(i+1,j) = alpha_c*(Tg_2(i+1,1)-Ts_u(i,j));
      hr(i+1,j) = PHI*eps_res*stef_bolz*(Tg_2(i+1,1)^4-(Ts_u(i,j))^4);
      hnet(i+1,j) = gamma_hc*hc(i+1,j)+gamma_hr*hr(i+1,j);
      dTs_u(i,j) = sf(j)/c_a(i,j)/rho_a*hnet(i+1,j)*dt;
    else
      c_a(i,j) = 650;
      hc(i+1,j) = alpha_c*(Tg_2(i+1,1)-Ts_u(i,j));
      hr(i+1,j) = PHI*eps_res*stef_bolz*(Tg_2(i+1,1)^4-(Ts_u(i,j))^4);
      hnet(i+1,j) = gamma_hc*hc(i+1,j)+gamma_hr*hr(i+1,j);
      dTs_u(i,j) = sf(j)/c_a(i,j)/rho_a*hnet(i+1,j)*dt;
    end
    Ts_u(i+1,j)= dTs_u(i,j) + Ts_u(i,j);
    i=i+1;
  end
  j=j+1;
end
Ts_u = Ts_u - 273;
```

%%
 %%% Protected Steel %%%
 %%%
 % Number of element in this section to be calc
 ne= 2; %cellular and column

%Section factors used

sf=[sf_cell;sf_col];

% Fire Protection Material Properties: Firetex FB120

% Note: Properties given by ARUP & Partners

dp = 0.02; % Thickness of material [m]

c_p = 900; % Specific Heat [J/kg-K]

rho_p = 700; % Density [kg/m^3]

lamda_p = 0.17; % Thermal conductivity [W/m-K]

% Calculate Protected steel temperatures

Ts_p(1,1:ne) = To+273; % Initial Temperature of Steel [C]

i=1;

j=1;

for j=1:ne

for i=1:length(t)-1

if Ts_p(i,j) < 873

c_a(i,j) = 425 + 7.73e-1*Ts_p(i,j) - 1.69e-3*Ts_p(i,j)^2 + 2.22e-6*Ts_p(i,j)^3;

phi(i,j) = (c_p*rho_p)/(c_a(i,j)*rho_a)*dp*sf(j);

dTs_p(i,j) = ((lamda_p*sf(j))/(dp*c_a(i,j)*rho_a)*(Tg_2(i,1)-Ts_p(i,j))/(1+phi(i,j)/3)*dt)-
(exp(phi(i,j)/10)-1)*(Tg_2(i+1,1)-(Tg_2(i,1))));

elseif Ts_p(i,j)>=873 & Ts_p(i,j)<1008

c_a(i,j) = 666+ (13002/(738-Ts_p(i,j)));

phi(i,j) = (c_p*rho_p)/(c_a(i,j)*rho_a)*dp*sf(j);

dTs_p(i,j) = ((lamda_p*sf(j))/(dp*c_a(i,j)*rho_a)*(Tg_2(i,1)-Ts_p(i,j))/(1+phi(i,j)/3)*dt)-
(exp(phi(i,j)/10)-1)*(Tg_2(i+1,1)-(Tg_2(i,1))));

elseif Ts_p(i,j)>=1008 & Ts_p(i,j)<1173

c_a(i,j) = 545 + (17820/ (Ts_p(i,j) - 731));

phi(i,j) = (c_p*rho_p)/(c_a(i,j)*rho_a)*dp*sf(j);

dTs_p(i,j) = ((lamda_p*sf(j))/(dp*c_a(i,j)*rho_a)*(Tg_2(i,1)-Ts_p(i,j))/(1+phi(i,j)/3)*dt)-
(exp(phi(i,j)/10)-1)*(Tg_2(i+1,1)-(Tg_2(i,1))));

else

c_a(i,j) = 650;

phi(i,j) = (c_p*rho_p)/(c_a(i,j)*rho_a)*dp*sf(j);

dTs_p(i,j) = ((lamda_p*sf(j))/(dp*c_a(i,j)*rho_a)*(Tg_2(i,1)-Ts_p(i,j))/(1+phi(i,j)/3)*dt)-
(exp(phi(i,j)/10)-1)*(Tg_2(i+1,1)-(Tg_2(i,1))));

end

if dTs_p(i,j) < 0

dTs_p(i,j) = 0;

Ts_p(i+1,j)=dTs_p(i,j)+Ts_p(i,j);

i=i+1;

else

Ts_p(i+1,j)= dTs_p(i,j) + Ts_p(i,j);

i=i+1;

end

end

j=j+1;

end

Ts_p = Ts_p -273;

Tg_2 = Tg_2-273;

figure

plot(t,Tg_2(:,1),t,Ts_u(:,1),'--',t,Ts_u(:,2),'-',t,Ts_p(:,1),t,Ts_p(:,2))

xlabel('Time [s]', 'FontSize', 12)

ylabel('Temperature [C]', 'FontSize', 12)

```
title('Scenario II - Steel Temperatures, Generalized Exponential Curve Tmax = 1200 C,  
alpha=0.005','FontSize',12)
```

```
legend('Generalized Curve, Tmax=1200C, alpha =0.005','Unprotected - Cellular  
Beam','Unprotected - Solid Beam','Protected - Edge Beams','Protected - Column',0)
```

```
% Output to excel files
```

```
[success]=xlswrite('N:\myhome\Thesis\Calcs\Matlab\Scenario II\UnProtected Steel  
Temps_Case1.xls',Ts_u,'Sheet1','B4:C1445')
```

```
[success]=xlswrite('N:\myhome\Thesis\Calcs\Matlab\Scenario II\Protected Steel  
Temps_Case1.xls',Ts_p,'Sheet1','B4:C1445')
```

```
%%%%%%%%%%%%%%%%%%%%%%%%%%%%%%%%%%%%%%%%%%%%%%%%%%%%%%%%%%%%%%%%%%%%%%%%  
%%%%%%%%%%%%%%%%%%%%%%%%%%%%%%%%%%%%%%%%%%%%%%%%%%%%%%%%%%%%%%%%%%%%%%%% Gas Temperatures 2 - Tmax = 1000C %%%%%%%%%  
%%%%%%%%%%%%%%%%%%%%%%%%%%%%%%%%%%%%%%%%%%%%%%%%%%%%%%%%%%%%%%%%%%%%%%%%
```

```
%%%%%%%%%%%%%%%%%%%%%%%%%%%%%%%%%%%%%%%%%%%%%%%%%%%%%%%%%%%%%%%%%%%%%%%%  
%%%%%%%%%%%%%%%%%%%%%%%%%%%%%%%%%%%%%%%%%%%%%%%%%%%%%%%%%%%%%%%%%%%%%%%% UnProtected Steel %%%%%%%%%  
%%%%%%%%%%%%%%%%%%%%%%%%%%%%%%%%%%%%%%%%%%%%%%%%%%%%%%%%%%%%%%%%%%%%%%%%  
%%%%%%%%%%%%%%%%%%%%%%%%%%%%%%%%%%%%%%%%%%%%%%%%%%%%%%%%%%%%%%%%%%%%%%%%  
% In this portion of the analysis, the only unprotected member is  
% the cellular beam and solid beam of study. The edge beams, columns,  
% and slab will always be protected throughout the study.
```

```
% Number of element in this section to be calc  
ne= 2; %cellular and solid
```

```
%Section factors used  
sf=[sf_cell;sf_beam];
```

```
% The unprotected steel temperatures were derived from  
% Eurocode 3: Part 1-2 Equation 4.21
```

```
% Extract Gas Temperatures from TT_Asif file  
[T, Tg_2, Tg, To, t, dt] = Temps;
```

```
% Calculate Unprotected steel temperatures
```

```
Tg_2 = Tg_2 + 273; % Gas temperature [K]  
Ts_u(1,1:ne) = To+273; % Initial Temperature of Steel [C]  
i=1;  
j=1;  
hc(1,1:ne)= 0;  
hr(1,1:ne) = 0;  
hnet(1,1:ne) = 0;  
for j=1:ne  
for i=1:length(t)-1  
if Ts_u(i,j) < 873  
c_a(i,j) = 425 + (7.73e-1)*Ts_u(i,j) - 1.69e-3*(Ts_u(i,j)^2) + 2.22e-6*(Ts_u(i,j)^3);  
hc(i+1,j) = alpha_c*(Tg_2(i+1,2)-Ts_u(i,j));  
hr(i+1,j) = PHI*eps_res*stef_bolz*(Tg_2(i+1,2)^4-(Ts_u(i,j))^4);  
hnet(i+1,j) = gamma_hc*hc(i+1,j)+gamma_hr*hr(i+1,j);  
dTs_u(i,j) = sf(j)/c_a(i,j)/rho_a*hnet(i+1,j)*dt;  
elseif Ts_u(i,j)>=873 & Ts_u(i,j)<1008  
c_a(i,j) = 666+ (13002/(738-Ts_u(i,j)));  
hc(i+1,j) = alpha_c*(Tg_2(i+1,2)-Ts_u(i,j));
```

```

hr(i+1,j) = PHI*eps_res*stef_bolz*(Tg_2(i+1,2)^4-(Ts_u(i,j))^4);
hnet(i+1,j) = gamma_hc*hc(i+1,j)+gamma_hr*hr(i+1,j);
dTs_u(i,j) = sf(j)/c_a(i)/rho_a*hnet(i+1,j)*dt;
elseif Ts_u(i,j)>=1008 & Ts_u(i,j)<1173
c_a(i,j) = 545 + (17820/ (Ts_u(i,j) - 731));
hc(i+1,j) = alpha_c*(Tg_2(i+1,2)-Ts_u(i,j));
hr(i+1,j) = PHI*eps_res*stef_bolz*(Tg_2(i+1,2)^4-(Ts_u(i,j))^4);
hnet(i+1,j) = gamma_hc*hc(i+1,j)+gamma_hr*hr(i+1,j);
dTs_u(i,j) = sf(j)/c_a(i)/rho_a*hnet(i+1,j)*dt;
else
c_a(i,j) = 650;
hc(i+1,j) = alpha_c*(Tg_2(i+1,2)-Ts_u(i,j));
hr(i+1,j) = PHI*eps_res*stef_bolz*(Tg_2(i+1,2)^4-(Ts_u(i,j))^4);
hnet(i+1,j) = gamma_hc*hc(i+1,j)+gamma_hr*hr(i+1,j);
dTs_u(i,j) = sf(j)/c_a(i)/rho_a*hnet(i+1,j)*dt;
end
Ts_u(i+1,j)= dTs_u(i,j) + Ts_u(i,j);
i=i+1;
end
j=j+1;
end
Ts_u = Ts_u - 273;

```

```

%%%%%%%%%%%%%%%%%%%%%%%%%%%%%%%%%%%%%%%%%%%%%%%%%%%%%%%%%%%%%%%%%%%%%%%%%%%%%%
%%%%%%%%%%%%%%%%%%%%%%%%%%%%%%%%%%%%%%%%%%%%%%%%%%%%%%%%%%%%%%%%%%%%%%%%%% Protected Steel %%%%%%%%%%%%%%%%%%%%%%%%%%%%%%%%%%%%%%%%%%%%%%%%%%%%%%%%%%%%%%%%%%%%%%%%%%
%%%%%%%%%%%%%%%%%%%%%%%%%%%%%%%%%%%%%%%%%%%%%%%%%%%%%%%%%%%%%%%%%%%%%%%%%% Number of element in this section to be calc
ne= 2;          %cellular and column

```

```

%Section factors used
sf=[sf_cell;sf_col];

```

```

% Fire Protection Material Properties: Firetex FB120
% Note: Properties given by ARUP & Partners
dp = 0.02;      % Thickness of material [m]
c_p = 900;      % Specific Heat [J/kg-K]
rho_p = 700;    % Density [kg/m^3]
lamda_p = 0.17; % Thermal conductivity [W/m-K]

```

```

% Calculate Protected steel temperatures
Ts_p(1,1:ne) = To+273; % Initial Temperature of Steel [C]
i=1;
j=1;
for j=1:ne
for i=1:length(t)-1
if Ts_p(i,j) < 873
c_a(i,j) = 425 + 7.73e-1*Ts_p(i,j) - 1.69e-3*Ts_p(i,j)^2 + 2.22e-6*Ts_p(i,j)^3;
phi(i,j) = (c_p*rho_p)/(c_a(i,j)*rho_a)*dp*sf(j);
dTs_p(i,j) = ((lamda_p*sf(j))/(dp*c_a(i,j)*rho_a)*(Tg_2(i,2)-Ts_p(i,j))/(1+phi(i,j)/3)*dt)-
(exp(phi(i,j)/10)-1)*(Tg_2(i+1,2)-(Tg_2(i,2)));
elseif Ts_p(i,j)>=873 & Ts_p(i,j)<1008
c_a(i,j) = 666+ (13002/(738-Ts_p(i,j)));
phi(i,j) = (c_p*rho_p)/(c_a(i,j)*rho_a)*dp*sf(j);

```

```

        dTs_p(i,j) = ((lamda_p*sf(j))/(dp*c_a(i,j)*rho_a)*(Tg_2(i,2)-Ts_p(i,j))/(1+phi(i,j)/3)*dt)-
        (exp(phi(i,j)/10)-1)*(Tg_2(i+1,2)-(Tg_2(i,2)));
    elseif Ts_p(i,j)>=1008 & Ts_p(i,j)<1173
        c_a(i) = 545 + (17820/ (Ts_p(i,j) - 731));
        phi(i,j) = (c_p*rho_p)/(c_a(i,j)*rho_a)*dp*sf(j);
        dTs_p(i,j) = ((lamda_p*sf(j))/(dp*c_a(i,j)*rho_a)*(Tg_2(i,2)-Ts_p(i,j))/(1+phi(i,j)/3)*dt)-
        (exp(phi(i,j)/10)-1)*(Tg_2(i+1,2)-(Tg_2(i,2)));
    else
        c_a(i,j) = 650;
        phi(i,j) = (c_p*rho_p)/(c_a(i,j)*rho_a)*dp*sf(j);
        dTs_p(i,j) = ((lamda_p*sf(j))/(dp*c_a(i,j)*rho_a)*(Tg_2(i,2)-Ts_p(i,j))/(1+phi(i,j)/3)*dt)-
        (exp(phi(i,j)/10)-1)*(Tg_2(i+1,2)-(Tg_2(i,2)));
    end
    if dTs_p(i,j) < 0
        dTs_p(i,j) = 0;
        Ts_p(i+1,j)=dTs_p(i,j)+Ts_p(i,j);
        i=i+1;
    else
        Ts_p(i+1,j)= dTs_p(i,j) + Ts_p(i,j);
        i=i+1;
    end
end
j=j+1;
end
Ts_p = Ts_p -273;
Tg_2 = Tg_2-273;

figure
plot(t,Tg_2(:,2),t,Ts_u(:,1),'--',t,Ts_u(:,2),'-',t,Ts_p(:,1),t,Ts_p(:,2))
xlabel('Time [s]','FontSize',12)
ylabel('Temperature [C]','FontSize',12)
title('Scenario II - Steel Temperatures, Generalized Exponential Curve Tmax = 1000 C, alpha =
0.005','FontSize',12)
legend('Generalized Curve, Tmax=1000C, alpha =0.005 ','Unprotected - Cellular
Beam','Unprotected - Solid Beam','Protected - Edge Beams','Protected - Column',0)

% Output to excel files
[success]=xlswrite('N:myhome/Thesis/Calcs/Matlab/Scenario II/UnProtected Steel
Temps_Case2.xls',Ts_u,'Sheet1','B4:C1445')
[success]=xlswrite('N:myhome/Thesis/Calcs/Matlab/Scenario II/Protected Steel
Temps_Case2.xls',Ts_p,'Sheet1','B4:C1445')

```

%%%%%%%%%% Gas Temperatures 1 - Tmax = 800C %%%%%%%%%%

%%%%%%%%%% UnProtected Steel %%%%%%%%%%
 %%%%%%%%%% In this portion of the analysis, the only unprotected member is
 % the cellular beam and solid beam of study. The edge beams, columns,
 % and slab will always be protected throughout the study.

% Number of element in this section to be calc

```
ne= 2;          %cellular and solid
```

```
%Section factors used  
sf=[sf_cell;sf_beam];
```

```
% The unprotected steel temperatures were derived from  
% Eurocode 3: Part 1-2 Equation 4.21
```

```
% Extract Gas Temperatures from TT_Asif file  
[T, Tg_2, Tg, To, t, dt] = Temps;
```

```
% Calculate Unprotected steel temperatures
```

```
Tg_2 = Tg_2 + 273;          % Gas temperature [K]  
Ts_u(1,1:ne) = To+273;     % Initial Temperature of Steel [C]
```

```
i=1;  
j=1;  
hc(1,1:ne)= 0;  
hr(1,1:ne) = 0;  
hnet(1,1:ne) = 0;  
for j=1:ne  
    for i=1:length(t)-1  
        if Ts_u(i,j) < 873  
            c_a(i,j) = 425 + (7.73e-1)*Ts_u(i,j) - 1.69e-3*(Ts_u(i,j)^2) + 2.22e-6*(Ts_u(i,j)^3);  
            hc(i+1,j) = alpha_c*(Tg_2(i+1,3)-Ts_u(i,j));  
            hr(i+1,j) = PHI*eps_res*stef_bolz*(Tg_2(i+1,3)^4-(Ts_u(i,j))^4);  
            hnet(i+1,j) = gamma_hc*hc(i+1,j)+gamma_hr*hr(i+1,j);  
            dTs_u(i,j) = sf(j)/c_a(i,j)/rho_a*hnet(i+1,j)*dt;  
        elseif Ts_u(i,j)>=873 & Ts_u(i,j)<1008  
            c_a(i,j) = 666+ (13002/(738-Ts_u(i,j)));  
            hc(i+1,j) = alpha_c*(Tg_2(i+1,3)-Ts_u(i,j));  
            hr(i+1,j) = PHI*eps_res*stef_bolz*(Tg_2(i+1,3)^4-(Ts_u(i,j))^4);  
            hnet(i+1,j) = gamma_hc*hc(i+1,j)+gamma_hr*hr(i+1,j);  
            dTs_u(i,j) = sf(j)/c_a(i,j)/rho_a*hnet(i+1,j)*dt;  
        elseif Ts_u(i,j)>=1008 & Ts_u(i,j)<1173  
            c_a(i,j) = 545 + (17820/ (Ts_u(i,j) - 731));  
            hc(i+1,j) = alpha_c*(Tg_2(i+1,3)-Ts_u(i,j));  
            hr(i+1,j) = PHI*eps_res*stef_bolz*(Tg_2(i+1,3)^4-(Ts_u(i,j))^4);  
            hnet(i+1,j) = gamma_hc*hc(i+1,j)+gamma_hr*hr(i+1,j);  
            dTs_u(i,j) = sf(j)/c_a(i,j)/rho_a*hnet(i+1,j)*dt;  
        else  
            c_a(i,j) = 650;  
            hc(i+1,j) = alpha_c*(Tg_2(i+1,3)-Ts_u(i,j));  
            hr(i+1,j) = PHI*eps_res*stef_bolz*(Tg_2(i+1,3)^4-(Ts_u(i,j))^4);  
            hnet(i+1,j) = gamma_hc*hc(i+1,j)+gamma_hr*hr(i+1,j);  
            dTs_u(i,j) = sf(j)/c_a(i,j)/rho_a*hnet(i+1,j)*dt;  
        end  
        Ts_u(i+1,j)= dTs_u(i,j) + Ts_u(i,j);  
        i=i+1;  
    end  
    j=j+1;  
end  
Ts_u = Ts_u - 273;
```

```
%%%%%%%%%%%%%%%%%%%%%%%%%%%%%%%%%%%%%%%%%%%%%%%%%%%%%%%%%%%%%%%%%%%%%%%%
```

```

%%%%%%%%%% Protected Steel %%%%%%%%%%%
%%%%%%%%%%
% Number of element in this section to be calc
ne= 2;          %cellular and column

%Section factors used
sf=[sf_cell;sf_col];

% Fire Protection Material Properties: Firetex FB120
% Note: Properties given by ARUP & Partners
dp = 0.02;      % Thickness of material [m]
c_p = 900;      % Specific Heat [J/kg-K]
rho_p = 700;    % Density [kg/m^3]
lamda_p = 0.17; % Thermal conductivity [W/m-K]

% Calculate Protected steel temperatures
Ts_p(1,1:ne) = To+273; % Initial Temperature of Steel [C]
i=1;
j=1;
for j=1:ne
    for i=1:length(t)-1
        if Ts_p(i,j) < 873
            c_a(i,j) = 425 + 7.73e-1*Ts_p(i,j) - 1.69e-3*Ts_p(i,j)^2 + 2.22e-6*Ts_p(i,j)^3;
            phi(i,j) = (c_p*rho_p)/(c_a(i,j)*rho_a)*dp*sf(j);
            dTs_p(i,j) = ((lamda_p*sf(j))/(dp*c_a(i,j)*rho_a)*(Tg_2(i,3)-Ts_p(i,j))/(1+phi(i,j)/3)*dt)-
            (exp(phi(i,j)/10)-1)*(Tg_2(i+1,3)-(Tg_2(i,3)));
        elseif Ts_p(i,j)>=873 & Ts_p(i,j)<1008
            c_a(i,j) = 666+ (13002/(738-Ts_p(i,j)));
            phi(i,j) = (c_p*rho_p)/(c_a(i,j)*rho_a)*dp*sf(j);
            dTs_p(i,j) = ((lamda_p*sf(j))/(dp*c_a(i,j)*rho_a)*(Tg_2(i,3)-Ts_p(i,j))/(1+phi(i,j)/3)*dt)-
            (exp(phi(i,j)/10)-1)*(Tg_2(i+1,3)-(Tg_2(i,3)));
        elseif Ts_p(i,j)>=1008 & Ts_p(i,j)<1173
            c_a(i) = 545 + (17820/ (Ts_p(i,j) - 731));
            phi(i,j) = (c_p*rho_p)/(c_a(i,j)*rho_a)*dp*sf(j);
            dTs_p(i,j) = ((lamda_p*sf(j))/(dp*c_a(i,j)*rho_a)*(Tg_2(i,3)-Ts_p(i,j))/(1+phi(i,j)/3)*dt)-
            (exp(phi(i,j)/10)-1)*(Tg_2(i+1,3)-(Tg_2(i,3)));
        else
            c_a(i,j) = 650;
            phi(i,j) = (c_p*rho_p)/(c_a(i,j)*rho_a)*dp*sf(j);
            dTs_p(i,j) = ((lamda_p*sf(j))/(dp*c_a(i,j)*rho_a)*(Tg_2(i,3)-Ts_p(i,j))/(1+phi(i,j)/3)*dt)-
            (exp(phi(i,j)/10)-1)*(Tg_2(i+1,3)-(Tg_2(i,3)));
        end
        if dTs_p(i,j) < 0
            dTs_p(i,j) = 0;
            Ts_p(i+1,j)=dTs_p(i,j)+Ts_p(i,j);
            i=i+1;
        else
            Ts_p(i+1,j)= dTs_p(i,j) + Ts_p(i,j);
            i=i+1;
        end
    end
    j=j+1;
end
Ts_p = Ts_p -273;
Tg_2 = Tg_2-273;

```

```
figure
plot(t,Tg_2(:,3),t,Ts_u(:,1),'--',t,Ts_u(:,2),'-',t,Ts_p(:,1),t,Ts_p(:,2))
xlabel('Time [s]','FontSize',12)
ylabel('Temperature [C]','FontSize',12)
title('Scenario II - Steel Temperatures, Generalized Exponential Curve Tmax = 800 C,
alpha=0.005','FontSize',12)
legend('Generalized Curve, Tmax=800C, alpha =0.005','Unprotected - Cellular
Beam','Unprotected - Solid Beam','Protected - Edge Beams','Protected - Column',0)
```

% Output to excel files

```
[success]=xlswrite('N:myhome/Thesis/Calcs/Matlab/Scenario II/UnProtected Steel
Temps_Case3.xls',Ts_u,'Sheet1','B4:C1445')
[success]=xlswrite('N:myhome/Thesis/Calcs/Matlab/Scenario II/Protected Steel
Temps_Case3.xls',Ts_p,'Sheet1','B4:C1445')
```

Scenario III – Heat Transfer (Matlab script file)

```
function [O,P,bf_T,avg_web,tf_T,time]=caseA()
%%%%%%%%%%%%%%%%%%%%%%%%%%%%%%%%%%%%%%%%%%%%%%%%%%%%%%%%%%%%%%%%%%%%%%%%%%%%%%
% SCENARIO III - STANDARD TIME TEMPERATURE CURVE %%%%%%%%%%%%%%%
% %%%%%%%%% Case A - Vary Temperatures across depth %%%%%%%%%
% %%%%%%%%%%%%%%%
```

```
clear all;
```

```
clc;
```

```
%%%%%%%%%%%%%%%%%%%%%%%%%%%%%%%%%%%%%%%%%%%%%%%%%%%%%%%%%%%%%%%%%%%%%%%%%%%%%%
% %%%%%%%%% PROPERTIES %%%%%%%%%
% %%%%%%%%%%%%%%%
% %%%%%%%%%%%%%%%
```

```
% Steel Properties - constant
```

```
% Physical properties
```

```
rho_a = 7850; % Density of steel [kg/m^3]
```

```
% Thermal Properties
```

```
% Convection Coefficients
```

```
alpha_c = 25; % [W/m^2-K]
```

```
gamma_hc = 1;
```

```
% Radiation Coefficients
```

```
eps_f = 0.8;
```

```
eps_m = 0.7;
```

```
eps_res = 0.56;
```

```
gamma_hr = 1;
```

```
PHI = 1;
```

```
stef_bolz = 5.67e-8;
```

```
% Hp/A Values (Section Factors)
```

```
% Heated Perimeter [m]/ Total x-sectional area [m^2]
```



```

% Section Factors by parts
% Bottom Flange Hp/A
sf_bf = 87.387;

%Web Hp/A
sf_w = 166.667;

%Top Flange
sf_tf = 45.721;

%Section Factor Matrix
sf=[sf_bf;sf_w;sf_tf];

% Number of elements
ne= 3;           %bottom flange, web, top fl

%%%%%%%%%%%%%%%%%%%%%%%%%%%%%%%%%%%%%%%%%%%%%%%%%%%%%%%%%%%%%%%%%%%%%%%%%%%%%%
%%%%%%%%%%%%%%%%%%%%%%%%%%%%%%%%%%%%%%%%%%%%%%%%%%%%%%%%%%%%%%%%%%%%%%%%%%%%%%
% CALCULATION FOR STEEL TEMPERATURE CURVES
%%%%%%%%%%%%%%%%%%%%%%%%%%%%%%%%%%%%%%%%%%%%%%%%%%%%%%%%%%%%%%%%%%%%%%%%%%%%%%
%%%%%%%%%%%%%%%%%%%%%%%%%%%%%%%%%%%%%%%%%%%%%%%%%%%%%%%%%%%%%%%%%%%%%%%%%%%%%%

%%%%%%%%%%%%%%%%%%%%%%%%%%%%%%%%%%%%%%%%%%%%%%%%%%%%%%%%%%%%%%%%%%%%%%%%%%%%%%
%%%%%%%%%%%%%%%%%%%%%%%%%%%%%%%%%%%%%%%%%%%%%%%%%%%%%%%%%%%%%%%%%%%%%%%%%%%%%%
% UnProtected Steel %%%%%%%%%%%%%%%%%%%%%%%%%%%%%%%%%%%%%%%%%%%%%%%%%%%%%%%%%%%%%%%%%%%%%%%%%%%%%%%
%%%%%%%%%%%%%%%%%%%%%%%%%%%%%%%%%%%%%%%%%%%%%%%%%%%%%%%%%%%%%%%%%%%%%%%%%%%%%%
% In this portion of the analysis, the only unprotected member is
% the cellular beam and solid beam of study. The edge beams, columns,
% and slab will always be protected throughout the study.

%%%%%%%%%%%%%%%%%%%%%%%%%%%%%%%%%%%%%%%%%%%%%%%%%%%%%%%%%%%%%%%%%%%%%%%%%%%%%%
%%%%%%%%%%%%%%%%%%%%%%%%%%%%%%%%%%%%%%%%%%%%%%%%%%%%%%%%%%%%%%%%%%%%%%%%%%%%%%
% The unprotected steel temperatures were derived from
% Eurocode 3: Part 1-2 Equation 4.21

% Extract Gas Temperatures from TT_Asif file
[T, Tg_2, Tg, To, t, dt] = Temps;

% Calculate Unprotected steel temperatures
T = T + 273;           % Gas temperature [K]
Ts_u(1,1:ne) = To+273; % Initial Temperature of Steel [C]
i=1;
j=1;
hc(1,1:ne)= 0;
hr(1,1:ne) = 0;
hnet(1,1:ne) = 0;
for j=1:ne
    for i=1:length(t)-1
        if Ts_u(i,j) < 873
            c_a(i,j) = 425 + (7.73e-1)*Ts_u(i,j) - 1.69e-3*(Ts_u(i,j)^2) + 2.22e-6*(Ts_u(i,j)^3);
            hc(i+1,j) = alpha_c*(T(i+1)-Ts_u(i,j));
            hr(i+1,j) = PHI*eps_res*stef_bolz*(T(i+1)^4-(Ts_u(i,j))^4);
            hnet(i+1,j) = gamma_hc*hc(i+1,j)+gamma_hr*hr(i+1,j);
            dTs_u(i,j) = sf(j)/c_a(i,j)/rho_a*hnet(i+1,j)*dt;
        elseif Ts_u(i,j)>=873 & Ts_u(i,j)<1008
            c_a(i,j) = 666+ (13002/(738-Ts_u(i,j)));

```

```

        hc(i+1,j) = alpha_c*(T(i+1)-Ts_u(i,j));
        hr(i+1,j) = PHI*eps_res*stef_bolz*(T(i+1)^4-(Ts_u(i,j))^4);
        hnet(i+1,j) = gamma_hc*hc(i+1,j)+gamma_hr*hr(i+1,j);
        dTs_u(i,j) = sf(j)/c_a(i)/rho_a*hnet(i+1,j)*dt;
    elseif Ts_u(i,j)>=1008 & Ts_u(i,j)<1173
        c_a(i,j) = 545 + (17820/ (Ts_u(i,j) - 731));
        hc(i+1,j) = alpha_c*(T(i+1)-Ts_u(i,j));
        hr(i+1,j) = PHI*eps_res*stef_bolz*(T(i+1)^4-(Ts_u(i,j))^4);
        hnet(i+1,j) = gamma_hc*hc(i+1,j)+gamma_hr*hr(i+1,j);
        dTs_u(i,j) = sf(j)/c_a(i)/rho_a*hnet(i+1,j)*dt;
    else
        c_a(i,j) = 650;
        hc(i+1,j) = alpha_c*(T(i+1)-Ts_u(i,j));
        hr(i+1,j) = PHI*eps_res*stef_bolz*(T(i+1)^4-(Ts_u(i,j))^4);
        hnet(i+1,j) = gamma_hc*hc(i+1,j)+gamma_hr*hr(i+1,j);
        dTs_u(i,j) = sf(j)/c_a(i)/rho_a*hnet(i+1,j)*dt;
    end
    Ts_u(i+1,j)= dTs_u(i,j) + Ts_u(i,j);
    i=i+1;
end
j=j+1;
end
Ts_u = Ts_u - 273;

```

```

%%%%%%%%%%%%%%%%%%%%%%%%%%%%%%%%%%%%%%%%%%%%%%%%%%%%%%%%%%%%%%%%%%%%%%%%%%%%%%
%%%%%%%%%%%%%%%%%%%%%%%%%%%%%%%%%%%%%%%%%%%%%%%%%%%%%%%%%%%%%%%%%%%%%%%%%%%%%% Protected Steel %%%%%%%%%%%%%%%%%%%%%%%%%%%%%%%%%%%%%%%%%%%%%%%%%%%%%%%%%%%%%%%%%%%%%%%%%%%%%%%
%%%%%%%%%%%%%%%%%%%%%%%%%%%%%%%%%%%%%%%%%%%%%%%%%%%%%%%%%%%%%%%%%%%%%%%%%%%%%%
% Fire Protection Material Properties: Firetex FB120
% Note: Properties given by ARUP & Partners
dp = 0.02;      % Thickness of material [m]
c_p = 900;      % Specific Heat [J/kg-K]
rho_p = 700;    % Density [kg/m^3]
lamda_p = 0.17; % Thermal conductivity [W/m-K]

```

```

% Calculate Protected steel temperatures
Ts_p(1,1:ne) = To+273; % Initial Temperature of Steel [C]
i=1;
j=1;
for j=1:ne
    for i=1:length(t)-1
        if Ts_p(i,j) < 873
            c_a(i,j) = 425 + 7.73e-1*Ts_p(i,j) - 1.69e-3*Ts_p(i,j)^2 + 2.22e-6*Ts_p(i,j)^3;
            phi(i,j) = (c_p*rho_p)/(c_a(i,j)*rho_a)*dp*sf(j);
            dTs_p(i,j) = ((lamda_p*sf(j))/(dp*c_a(i,j)*rho_a)*(T(i)-Ts_p(i,j))/(1+phi(i,j)/3)*dt)-
            (exp(phi(i,j)/10)-1)*(T(i+1)-(T(i)));
        elseif Ts_p(i,j)>=873 & Ts_p(i,j)<1008
            c_a(i,j) = 666+ (13002/(738-Ts_p(i,j)));
            phi(i,j) = (c_p*rho_p)/(c_a(i,j)*rho_a)*dp*sf(j);
            dTs_p(i,j) = ((lamda_p*sf(j))/(dp*c_a(i,j)*rho_a)*(T(i)-Ts_p(i,j))/(1+phi(i,j)/3)*dt)-
            (exp(phi(i,j)/10)-1)*(T(i+1)-(T(i)));
        elseif Ts_p(i,j)>=1008 & Ts_p(i,j)<1173
            c_a(i) = 545 + (17820/ (Ts_p(i,j) - 731));
            phi(i,j) = (c_p*rho_p)/(c_a(i,j)*rho_a)*dp*sf(j);

```

```

        dTs_p(i,j) = ((lamda_p*sf(j))/(dp*c_a(i,j)*rho_a)*(T(i)-Ts_p(i,j))/(1+phi(i,j)/3)*dt)-
        (exp(phi(i,j)/10)-1)*(T(i+1)-(T(i)));
    else
        c_a(i,j) = 650;
        phi(i,j) = (c_p*rho_p)/(c_a(i,j)*rho_a)*dp*sf(j);
        dTs_p(i,j) = ((lamda_p*sf(j))/(dp*c_a(i,j)*rho_a)*(T(i)-Ts_p(i,j))/(1+phi(i,j)/3)*dt)-
        (exp(phi(i,j)/10)-1)*(T(i+1)-(T(i)));
    end
    if dTs_p(i,j) < 0
        dTs_p(i,j) = 0;
        Ts_p(i+1,j)=dTs_p(i,j)+Ts_p(i,j);
        i=i+1;
    else
        Ts_p(i+1,j)= dTs_p(i,j) + Ts_p(i,j);
        i=i+1;
    end
end
j=j+1;
end
Ts_p = Ts_p -273;
T = T-273;

figure
plot(t,T,t,Ts_u(:,1),'-','t,Ts_u(:,2),'-','t,Ts_u(:,3),'-','t,Ts_p(:,1),t,Ts_p(:,2),t,Ts_p(:,3))
xlabel('Time [s]','FontSize',12)
ylabel('Temperature [C]','FontSize',12)
title('Scenario III - Steel Temperatures for top/bottom flange & web, Standard Curve','FontSize',12)
legend('Standard Curve','Unprotected - Bottom Flange','Unprotected - Web','Unprotected - Top
Flange','Protected - Bottom Flange','Protected - Web','Protected - Top Flange',0)
hold on

O = Ts_u;
P = Ts_p;

[success]=xlswrite('N:\myhome\Thesis\Calcs\Matlab\Scenario III\UnProtected Steel
Temps.xls',Ts_u,'Sheet1','B4:D1445')
[success]=xlswrite('N:\myhome\Thesis\Calcs\Matlab\Scenario III\Protected Steel
Temps.xls',Ts_p,'Sheet1','B4:D1445')

%%%%%%%%%%%%%%%%%%%%%%%%%%%%%%%%%%%%%%%%%%%%%%%%%%%%%%%%%%%%%%%%%%%%%%%%
%%%%%%%%%%%%%%%%%%%%%%%%%%%%%%%%%%%%%%%%%%%%%%%%%%%%%%%%%%%%%%%%%%%%%%%%
%%%%%%%% COMPARISON WITH FABSEC TEMPERATURES
%%%%%%%%%%%%%%%%%%%%%%%%%%%%%%%%%%%%%%%%%%%%%%%%%%%%%%%%%%%%%%%%%%%%%%%%
%%%%%%%%%%%%%%%%%%%%%%%%%%%%%%%%%%%%%%%%%%%%%%%%%%%%%%%%%%%%%%%%%%%%%%%%

% Bottom Flange Temperatures
bf_T = [25,350, 427, 628, 829];

% Web Temperatures
web_bot_T = [336, 478.5, 663, 810];
web_edgebot_T = [385, 522, 723.6, 887.8];
web_edgetop_T = [385, 478.5, 663.3,849.2];
web_top_T = [350, 435, 603, 772];

```

```

avg_web_T =
[25;(web_bot_T(1)+web_edgebot_T(1)+web_edgetop_T(1)+web_top_T(1))/4;(web_bot_T(2)+we
b_edgebot_T(2)+web_edgetop_T(2)+web_top_T(2))/4;(web_bot_T(3)+web_edgebot_T(3)+web_
edgetop_T(3)+web_top_T(3))/4;(web_bot_T(4)+web_edgebot_T(4)+web_edgetop_T(4)+web_top
_T(4))/4];

```

```

% Top Flange Temperatures
tf_T = [25,350,400,562,722];

```

```

% Time (Defined by Fabsec output)
time = [0,1800, 3600, 5400,7200];

```

```

figure
plot(time,bf_T,time,avg_web_T,'-.',time,tf_T,':')
xlabel('Time [s]','FontSize',12)
ylabel('Temperature [C]','FontSize',12)
title('Protected Cellular Beam Temperatures from FABSEC','FontSize',12)
legend('Bottom Flange Temperature','Avg. Web Temperature','Top Flange Temperature')

```

```

%%%%%%%%%%%%%%%%%%%%%%%%%%%%%%%%%%%%%%%%%%%%%%%%%%%%%%%%%%%%%%%%%%%%%%%%
%%%%%%%%%%%%%%%%%%%%%%%%%%%%%%%%%%%%%%%%%%%%%%%%%%%%%%%%%%%%%%%%%%%%%%%%
% COMPARISON WITH BAILEY TEMPERATURES
%%%%%%%%%%%%%%%%%%%%%%%%%%%%%%%%%%%%%%%%%%%%%%%%%%%%%%%%%%%%%%%%%%%%%%%%
%%%%%%%%%%%%%%%%%%%%%%%%%%%%%%%%%%%%%%%%%%%%%%%%%%%%%%%%%%%%%%%%%%%%%%%%

```

```

% Cellular beams protected with 0.8mm water based intumescent
web_wb=[25,230,720,930,1050];
bf_wb = [25,230,990];
t1=[0,5,48,78,90]*60;
t2 = [0,5,90]*60;
% Cellular beams protected with 0.8mm solvent based intumescent
web_sb=[25,240,430,670,830,1000];
bf_sb = [25,280,350,670,710,830,980];
t3=[0,5,20,40,60,90]*60;
t4=[0,10,20,40,60,70,90]*60;

```

```

% Cellular beams protected with 2.1 mm solvent based intumescent
web_2=[25,220,250,340,400,590,990];
bf_2 = [25,250,305,400,805];
t5=[0,5,10,20,30,40,90]*60;
t6=[0,10,20,40,90]*60;

```

```

figure
plot(t1,web_wb,t2, bf_wb,t3,web_sb,t4, bf_sb,t5,web_2,t6, bf_2)
xlabel('Time [s]','FontSize',14)
ylabel('Temperature [C]','FontSize',14)
title('Protected Cellular Beam Temperatures from Bailey','FontSize',14)
legend('Web Temp 0.8mm water based','Bottom Flange 0.8 water-based','Web Temp 0.8mm
solvent','Bottom Flange 0.8 water-based','Web Temp 2.1mm solvent','Bottom Flange 2.1 solvent

```

APPENDIX B: Structural Design Sheets (FABSEC)

| | | |
|--|--|--|
|  Fabsec Limited | **FBEAM3 ENHANCED FIRE** Ver. 3. 2. 234 | Job No: Serial No: |
|  Prepared By: Arup | JOB REF.: BEAM REF.: COMPANY: CLIENT: | Calcs.: Checked.: Date: 10/11/2005 Time: 17:35:23 |

LONG OUTPUT

DISCLAIMER :

The core FBEAM design software is written by The Steel Construction Institute on behalf of Fabsec Ltd. It is provided to specifiers of plated fabricated sections for use in the analysis and design of composite and non-composite Fabsec beams, as used in general building construction.

This core software by The SCI has been augmented by Fabsec's in-house Software Development Team. The main additions are the Beam WizardTM optimiser (for normal and fire engineering), PC Units, end moments, the new toolbar for opening generation and editing, an improved user interface and the 'save as PDF' function.

Care has been taken to ensure that the information herein is accurate, but neither Fabsec Limited nor The Steel Construction Institute accept responsibility for errors due to misinterpretation of the input data or of output information by the user. Queries relating to the use of this software should be directed to Fabsec Limited - Tel: 0113 272 7586, Fax: 0113 272 7587 or e-mail sales@fabsec.co.uk

CONDITIONS OF USE

1. FBEAM computer software, the associated data files and documentation are the property of Fabsec Limited. Reproduction of any kind, in whole or in part in any form, without prior written consent is strictly prohibited. Fabsec Limited has various patents pending in the UK and selected overseas markets. Patent applications encompass the FBEAM software and the fabrication of any structural element designed with it.
2. The fire engineering module permits engineers to design Fabsec's Firebeam product range. These designs require the use of Firetex FB120 intumescent coating from Leigh's Paints. FIREBEAM has been proven through loaded full-scale fire tests. No other coating or method of fire protection may be substituted when FBEAM is used for the design of the Firebeam product range.
3. As a result of patent applications the fabrication of beams designed using FBEAM eg Fabsec and Firebeam product ranges must be carried out in the UK by one of two licensed fabricators:

Severfield – Rowen plc
 William Hare Ltd.

Fabrication of Fabsec beams in the UK and overseas territories, shall only be carried out by fabricators licensed by Fabsec Ltd. Unlicensed fabrication will result in legal action to both halt production, and seek damages for patent infringement.

**DESIGN CRITERIA : NORMAL DESIGN - [ADEQUATE]****FIRE DESIGN - [ADEQUATE]**

| Design Stage | Design Criteria | Max. Unity Factor | Remarks |
|-------------------------------|---|-------------------|---------|
| Normal Condition (NS) | Vertical shear check | 0.20 | |
| | Interaction of bending moment and vertical shear | 0.42 | |
| | Lateral torsional buckling check | N/A | |
| | Concrete longitudinal shear check | 0.21 | |
| | Vertical shear check @ opening(s) | 0.51 | |
| | Interaction of bending moment & vertical shear @ opening(s) | 0.51 | |
| | Vierendeel bending check | 0.30 | |
| | Web buckling around opening(s) | 0.42 | |
| | Web post horizontal shear check between opening(s) | 0.50 | |
| | Web post flexural strength check between opening(s) | 0.40 | |
| Construction Condition (CS) | Interaction of bending moment and vertical shear | 0.25 | |
| | Lateral torsional buckling check | 0.98 | |
| | Vertical shear check @ opening(s) | 0.26 | |
| | Interaction of bending moment & vertical shear @ opening(s) | 0.28 | |
| | Vierendeel bending check | 0.16 | |
| | Web buckling around opening(s) | 0.21 | |
| | Web post horizontal shear check between opening(s) | 0.22 | |
| | Web post flexural strength check between opening(s) | 0.18 | |
| Serviceability Condition (SS) | Concrete compressive stress check | 0.15 | |
| | Steel tensile stress check | 0.37 | |
| | Steel compressive stress check | 0.21 | |
| | Vibration check | 0.87 | |
| | Imposed load deflection | 0.43 | |

FIRE DESIGN :

Specified and recommended thicknesses of FB120 for 120 minutes fire resistance.

Maximum unity factor = 1.00 (relative to the user specified protection thickness).

| Section | User specified (mm) | Recommended (mm) |
|---------------|---------------------|------------------|
| Top flange | 1.90 | 1.90 |
| Web | 1.90 | 1.90 |
| Bottom flange | 1.90 | 1.90 |

NOTE :

For beams with unfilled voids, the guidance for fire protection thickness given in 'Fire protection for structural steel in buildings' should be followed.

BEAM SPECIFICATION :

FIREBEAM 690 x 370/370 x 179.9kg/m S355 FB120 x 1.90 R120

C40NWC, A252 Mesh + 489 mm²/m additional reinforcement required, 234 No. 19 dia. x 95 mm shear studs.

DIMENSIONS :

| | | | |
|----------------------|------------|-------------------------|-----------------------|
| Depth | 690.0 mm | Web thickness | 12.0 mm |
| Top flange width | 370.0 mm | Bottom flange width | 370.0 mm |
| Top flange thickness | 24.0 mm | Bottom flange thickness | 24.0 mm |
| Beam mass (Gross) | 199.9 kg/m | Beam mass (Net) | 179.9 kg/m |
| Steel grade | S355 | Design strength | 355 N/mm ² |



FILLET WELD(s) :
5mm double-sided FW required

MAXIMUM DEFLECTIONS :

Dead = 34.3mm
Super Dead = 2.1mm
Imposed = 21.3mm (Limit = SPAN/360 i.e 50.0mm)
Total = 57.7mm (Limit = SPAN/200 i.e 90.0mm) (**< SPAN / 200 = 90.0 mm**) **SATISFACTORY**

NOTES :

1. The components of total deflection are the values at the position of maximum total deflection, not always the sum of the individual critical components

REACTIONS (UNFACTORED & FACTORED):

| REACTION | ---CONSTRUCTION--- | | ----- FINAL CONDITION ----- | | |
|---------------------|--------------------|---------|-----------------------------|------------|---------|
| | DEAD | IMPOSED | DEAD | SUPER DEAD | IMPOSED |
| LHS UNFACTORED (kN) | 86.5 | 11.3 | 85.1 | 11.3 | 112.5 |
| RHS UNFACTORED (kN) | 86.5 | 11.3 | 85.1 | 11.3 | 112.5 |
| LHS FACTORED (kN) | 121.1 | 18.0 | 119.1 | 15.8 | 180.0 |
| RHS FACTORED (kN) | 121.1 | 18.0 | 119.1 | 15.8 | 180.0 |

INTELLECTUAL PROPERTY RIGHT INFORMATION :

This design is protected in the UK and throughout the European Community by unregistered design right owned by Fabsec Ltd.

Copyright © Fabsec Ltd, 2004



Prepared By: Anup

BEAM DETAILS AND DIMENSIONS :**DETAILS :**

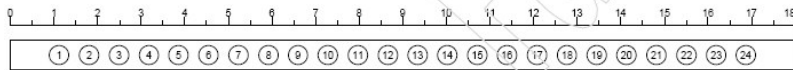
| | | | |
|--------------------------|------------------------|-----------------------|------------------|
| Beam type: | Prismatic | Top flange (mm): | 370 x 24 |
| Construction type: | Composite [Floor beam] | Bottom flange (mm): | 370 x 24 |
| Beam span (m): | 18.00 | Web thickness (mm): | 12 |
| Beam mass Gross (kg/m): | 199.89 | Beam mass Net (kg/m): | 179.92 |
| Number of change points: | 0 | Weld size: | 5mm double-sided |
| Beam depth (mm): | 690 | Steel grade: | S355 |

PRECAMBER NOTES :

If preamber is specified the minimum recommended camber is L/250 or 20mm whichever is greater.
Camber tolerance is +/- L/500.

WEB OPENINGS

| No. | Length (mm) | Depth (mm) | Dia. (mm) | x (mm) | dt (mm) | db (mm) |
|-----|----------------|---------------|--------------|-----------|------------|------------|
| 1 | - | - | 450 | 1125 | 00 | 00 |
| 2 | - | - | 450 | 1210 | 00 | 00 |
| 3 | - | - | 450 | 2405 | 00 | 00 |
| 4 | - | - | 450 | 3179 | 00 | 00 |
| 5 | - | - | 450 | 3864 | 00 | 00 |
| 6 | - | - | 450 | 4549 | 00 | 00 |
| 7 | - | - | 450 | 5234 | 00 | 00 |
| 8 | - | - | 450 | 5918 | 00 | 00 |
| 9 | - | - | 450 | 6603 | 00 | 00 |
| 10 | - | - | 450 | 7288 | 00 | 00 |
| 11 | - | - | 450 | 7973 | 00 | 00 |
| 12 | - | - | 450 | 8658 | 00 | 00 |
| 13 | - | - | 450 | 9342 | 00 | 00 |
| 14 | - | - | 450 | 10027 | 00 | 00 |
| 15 | - | - | 450 | 10712 | 00 | 00 |
| 16 | - | - | 450 | 11397 | 00 | 00 |
| 17 | - | - | 450 | 12082 | 00 | 00 |
| 18 | - | - | 450 | 12766 | 00 | 00 |
| 19 | - | - | 450 | 13451 | 00 | 00 |
| 20 | - | - | 450 | 14136 | 00 | 00 |
| 21 | - | - | 450 | 14821 | 00 | 00 |
| 22 | - | - | 450 | 15505 | 00 | 00 |
| 23 | - | - | 450 | 16190 | 00 | 00 |
| 24 | - | - | 450 | 16875 | 00 | 00 |



File Name:

FBEAM3 V 3. 2. 234

INPUT DATA (LONG OUTPUT)

GENERAL :

COMPOSITE construction with solid slab

Beam will NOT be propped in construction

Floor slab will NOT be propped in construction

Floor slab PERPENDICULAR to beam (SIDE 1)

Floor slab PERPENDICULAR to beam (SIDE 2)

FLOOR PLAN DATA (INTERNAL BEAM) :

Beam span 18.00 m

Beam spacing (SIDE 1) 2.50 m

Beam spacing (SIDE 2) 2.50 m

TOP FLANGE BEAM RESTRAINT DATA :

Beam laterally unrestrained during construction

BOTTOM FLANGE BEAM RESTRAINT DATA :

Beam laterally unrestrained during construction

CONCRETE SLAB (Normal Weight Concrete - NWC) :Characteristic strength 40 N/mm²Wet density 2400 kg/m³

Modular ratio 10

Design strength of mesh reinf't 460 N/mm²

Overall slab depth 130 mm

Dry density 2350 kg/m³

Mesh reinforcement A252

No screed

BEAM DATA :

Depth 690.0 mm

Top flange width 370.0 mm

Top flange thickness 24.0 mm

Beam mass (Gross) 199.9 kg/m

Steel grade S355

Web thickness 12.0 mm

Bottom flange width 370.0 mm

Bottom flange thickness 24.0 mm

Beam mass (Net) 179.9 kg/m

Design strength 355 N/mm²**STEEL SECTION PROPERTIES :**

Top flange classification COMPACT

Web classification PLASTIC

Elastic neutral axis is in WEB (345.0 mm from beam top flange)

Plastic neutral axis is in WEB (345.0 mm from beam top flange)

2nd moment of area $I_{xx} = 223485.0 \text{ cm}^4$ Elastic modulus (top) $Z_t = 6477.8 \text{ cm}^3$ Radius of gyration $r_x = 29.6 \text{ cm}$ Plastic modulus - unreduced $S_x = 7150.6 \text{ cm}^3$ Cross section area $A = 254.6 \text{ cm}^2$ 2nd moment of area $I_{yy} = 20270.5 \text{ cm}^4$ Elastic modulus (btm) $Z_b = 6477.8 \text{ cm}^3$ Radius of gyration $r_y = 8.9 \text{ cm}$ Elastic modulus (minor axis) $Z_y = 1095.7 \text{ cm}^3$ **COMPOSITE SECTION PROPERTIES :**

| No. / Dist.(m) | Web Clas. | Flange Clas. | beff (mm) | dc (mm) | ye (mm) | yp (mm) | lxx (cm ⁴) | lyy (cm ⁴) | Zt (cm ³) | Zb (cm ³) | Zc (cm ³) | Sx (cm ³) |
|-------------------|--------------|-----------------|--------------|------------|------------|------------|---------------------------|---------------------------|--------------------------|--------------------------|--------------------------|--------------------------|
| 1 / 0.00 | 1 | 2 | 0 | 0.0 | 345.0 | 345.0 | 223485 | 20270 | 6478 | 6478 | 0 | 7151 |
| 2 / 0.36 | 1 | 2 | 100 | 0.0 | 345.0 | 345.0 | 223485 | 20270 | 6478 | 6478 | 0 | 7151 |
| 3 / 0.72 | 2 | 1 | 200 | 130.0 | 245.1 | 418.5 | 468067 | 1712979 | 40660 | 8142 | 190957 | 7668 |
| 4 / 1.08 | 3 | 1 | 300 | 130.0 | 245.1 | 390.2 | 468067 | 1712979 | 40660 | 8142 | 190957 | 7899 |
| 5 / 1.44 | 3 | 1 | 400 | 130.0 | 245.1 | 362.0 | 468067 | 1712979 | 40660 | 8142 | 190957 | 8110 |
| 6 / 1.80 | 3 | 1 | 500 | 130.0 | 245.1 | 333.7 | 468067 | 1712979 | 40660 | 8142 | 190957 | 8301 |
| 7 / 2.16 | 3 | 1 | 600 | 130.0 | 245.1 | 305.4 | 468067 | 1712979 | 40660 | 8142 | 190957 | 8474 |
| 8 / 2.52 | 3 | 1 | 700 | 130.0 | 245.1 | 277.2 | 468067 | 1712979 | 40660 | 8142 | 190957 | 8628 |
| 9 / 2.88 | 3 | 1 | 800 | 130.0 | 245.1 | 248.9 | 468067 | 1712979 | 40660 | 8142 | 190957 | 8762 |
| 10 / 3.24 | 3 | 1 | 900 | 130.0 | 245.1 | 220.7 | 468067 | 1712979 | 40660 | 8142 | 190957 | 8877 |
| 11 / 3.60 | 3 | 1 | 1000 | 130.0 | 245.1 | 192.4 | 468067 | 1712979 | 40660 | 8142 | 190957 | 8973 |
| 12 / 3.96 | 3 | 1 | 1100 | 130.0 | 245.1 | 164.1 | 468067 | 1712979 | 40660 | 8142 | 190957 | 9050 |
| 13 / 4.32 | 1 | 1 | 1200 | 130.0 | 245.1 | 153.4 | 468067 | 1712979 | 40660 | 8142 | 190957 | 9111 |
| 14 / 4.68 | 1 | 1 | 1300 | 130.0 | 245.1 | 152.5 | 468067 | 1712979 | 40660 | 8142 | 190957 | 9171 |
| 15 / 5.04 | 1 | 1 | 1400 | 130.0 | 245.1 | 151.6 | 468067 | 1712979 | 40660 | 8142 | 190957 | 9230 |

File Name:

FBEM3 V 3. 2. 234

| No. / Dist.(m) | Web Clas. | Flange Clas. | b _{eff} (mm) | d _c (mm) | y _e (mm) | y _p (mm) | I _{xx} (cm ⁴) | I _{yy} (cm ⁴) | Z _t (cm ³) | Z _b (cm ³) | Z _c (cm ³) | S _x (cm ³) |
|-------------------|--------------|-----------------|--------------------------|------------------------|------------------------|------------------------|---------------------------------------|---------------------------------------|--------------------------------------|--------------------------------------|--------------------------------------|--------------------------------------|
| 16 / 5.40 | 1 | 1 | 1500 | 130.0 | 245.1 | 150.7 | 468067 | 1712979 | 40660 | 8142 | 190957 | 9288 |
| 17 / 5.76 | 1 | 1 | 1600 | 130.0 | 245.1 | 149.7 | 468067 | 1712979 | 40660 | 8142 | 190957 | 9346 |
| 18 / 6.12 | 1 | 1 | 1700 | 130.0 | 245.1 | 148.8 | 468067 | 1712979 | 40660 | 8142 | 190957 | 9403 |
| 19 / 6.48 | 1 | 1 | 1800 | 130.0 | 245.1 | 147.9 | 468067 | 1712979 | 40660 | 8142 | 190957 | 9460 |
| 20 / 6.84 | 1 | 1 | 1900 | 130.0 | 245.1 | 147.0 | 468067 | 1712979 | 40660 | 8142 | 190957 | 9516 |
| 21 / 7.20 | 1 | 1 | 2000 | 130.0 | 245.1 | 146.1 | 468067 | 1712979 | 40660 | 8142 | 190957 | 9571 |
| 22 / 7.56 | 1 | 1 | 2100 | 130.0 | 245.1 | 145.2 | 468067 | 1712979 | 40660 | 8142 | 190957 | 9626 |
| 23 / 7.92 | 1 | 1 | 2200 | 130.0 | 245.1 | 144.2 | 468067 | 1712979 | 40660 | 8142 | 190957 | 9680 |
| 24 / 8.28 | 1 | 1 | 2300 | 130.0 | 245.1 | 143.3 | 468067 | 1712979 | 40660 | 8142 | 190957 | 9733 |
| 25 / 8.64 | 1 | 1 | 2400 | 130.0 | 245.1 | 142.4 | 468067 | 1712979 | 40660 | 8142 | 190957 | 9786 |
| 26 / 9.00 | 1 | 1 | 2500 | 130.0 | 245.1 | 141.5 | 468067 | 1712979 | 40660 | 8142 | 190957 | 9838 |
| 27 / 9.36 | 1 | 1 | 2400 | 130.0 | 245.1 | 142.4 | 468067 | 1712979 | 40660 | 8142 | 190957 | 9786 |
| 28 / 9.72 | 1 | 1 | 2300 | 130.0 | 245.1 | 143.3 | 468067 | 1712979 | 40660 | 8142 | 190957 | 9733 |
| 29 / 10.08 | 1 | 1 | 2200 | 130.0 | 245.1 | 144.2 | 468067 | 1712979 | 40660 | 8142 | 190957 | 9680 |
| 30 / 10.44 | 1 | 1 | 2100 | 130.0 | 245.1 | 145.2 | 468067 | 1712979 | 40660 | 8142 | 190957 | 9626 |
| 31 / 10.80 | 1 | 1 | 2000 | 130.0 | 245.1 | 146.1 | 468067 | 1712979 | 40660 | 8142 | 190957 | 9571 |
| 32 / 11.16 | 1 | 1 | 1900 | 130.0 | 245.1 | 147.0 | 468067 | 1712979 | 40660 | 8142 | 190957 | 9516 |
| 33 / 11.52 | 1 | 1 | 1800 | 130.0 | 245.1 | 147.9 | 468067 | 1712979 | 40660 | 8142 | 190957 | 9460 |
| 34 / 11.88 | 1 | 1 | 1700 | 130.0 | 245.1 | 148.8 | 468067 | 1712979 | 40660 | 8142 | 190957 | 9403 |
| 35 / 12.24 | 1 | 1 | 1600 | 130.0 | 245.1 | 149.7 | 468067 | 1712979 | 40660 | 8142 | 190957 | 9346 |
| 36 / 12.60 | 1 | 1 | 1500 | 130.0 | 245.1 | 150.7 | 468067 | 1712979 | 40660 | 8142 | 190957 | 9288 |
| 37 / 12.96 | 1 | 1 | 1400 | 130.0 | 245.1 | 151.6 | 468067 | 1712979 | 40660 | 8142 | 190957 | 9230 |
| 38 / 13.32 | 1 | 1 | 1300 | 130.0 | 245.1 | 152.5 | 468067 | 1712979 | 40660 | 8142 | 190957 | 9171 |
| 39 / 13.68 | 1 | 1 | 1200 | 130.0 | 245.1 | 153.4 | 468067 | 1712979 | 40660 | 8142 | 190957 | 9111 |
| 40 / 14.04 | 3 | 1 | 1100 | 130.0 | 245.1 | 164.1 | 468067 | 1712979 | 40660 | 8142 | 190957 | 9050 |
| 41 / 14.40 | 3 | 1 | 1000 | 130.0 | 245.1 | 192.4 | 468067 | 1712979 | 40660 | 8142 | 190957 | 8973 |
| 42 / 14.76 | 3 | 1 | 900 | 130.0 | 245.1 | 220.7 | 468067 | 1712979 | 40660 | 8142 | 190957 | 8877 |
| 43 / 15.12 | 3 | 1 | 800 | 130.0 | 245.1 | 248.9 | 468067 | 1712979 | 40660 | 8142 | 190957 | 8762 |
| 44 / 15.48 | 3 | 1 | 700 | 130.0 | 245.1 | 277.2 | 468067 | 1712979 | 40660 | 8142 | 190957 | 8628 |
| 45 / 15.84 | 3 | 1 | 600 | 130.0 | 245.1 | 305.4 | 468067 | 1712979 | 40660 | 8142 | 190957 | 8474 |
| 46 / 16.20 | 3 | 1 | 500 | 130.0 | 245.1 | 333.7 | 468067 | 1712979 | 40660 | 8142 | 190957 | 8301 |
| 47 / 16.56 | 3 | 1 | 400 | 130.0 | 245.1 | 362.0 | 468067 | 1712979 | 40660 | 8142 | 190957 | 8110 |
| 48 / 16.92 | 3 | 1 | 300 | 130.0 | 245.1 | 390.2 | 468067 | 1712979 | 40660 | 8142 | 190957 | 7899 |
| 49 / 17.28 | 2 | 1 | 200 | 130.0 | 245.1 | 418.5 | 468067 | 1712979 | 40660 | 8142 | 190957 | 7668 |
| 50 / 17.64 | 1 | 2 | 100 | 0.0 | 345.0 | 345.0 | 223485 | 20270 | 6478 | 6478 | 0 | 7151 |
| 51 / 18.00 | 1 | 2 | 0 | 0.0 | 345.0 | 345.0 | 223485 | 20270 | 6478 | 6478 | 0 | 7151 |

NOTE :

Section properties at the location of openings are given in the openings part of this output

SHEAR CONNECTOR DATA :

| | | | |
|------------------------|---------|-----------------------------|--------|
| Diameter | 19 mm | Height | 95 mm |
| No. of studs per group | 2 | Total No. of studs provided | 234 |
| Stud resistance | 87.2 kN | | |
| Minimum stud clearance | 20 mm | Stud spacing | 150 mm |

NOTES :

1. The clearance between the edge of the shear connector and the edge of the top flange must be checked by an engineer to ensure it conforms to the appropriate standard
2. The spacing between shear connectors in pairs measured transverse to the beam should not be less than 4 times the stud diameter

WEB OPENINGS DETAILS :

| Opening No. | Type | Length (mm) | Depth (mm) | Dia. (mm) | x (mm) | dt (mm) | db (mm) | Stiffened | Centred |
|-------------|------|-------------|------------|-----------|---------|---------|---------|-----------|---------|
| 1 | C | - | - | 450 | 1125.0 | 96 | 96 | N | Y |
| 2 | C | - | - | 450 | 1810.0 | 96 | 96 | N | Y |
| 3 | C | - | - | 450 | 2495.0 | 96 | 96 | N | Y |
| 4 | C | - | - | 450 | 3179.0 | 96 | 96 | N | Y |
| 5 | C | - | - | 450 | 3864.0 | 96 | 96 | N | Y |
| 6 | C | - | - | 450 | 4549.0 | 96 | 96 | N | Y |
| 7 | C | - | - | 450 | 5234.0 | 96 | 96 | N | Y |
| 8 | C | - | - | 450 | 5918.0 | 96 | 96 | N | Y |
| 9 | C | - | - | 450 | 6603.0 | 96 | 96 | N | Y |
| 10 | C | - | - | 450 | 7288.0 | 96 | 96 | N | Y |
| 11 | C | - | - | 450 | 7973.0 | 96 | 96 | N | Y |
| 12 | C | - | - | 450 | 8658.0 | 96 | 96 | N | Y |
| 13 | C | - | - | 450 | 9342.0 | 96 | 96 | N | Y |
| 14 | C | - | - | 450 | 10027.0 | 96 | 96 | N | Y |
| 15 | C | - | - | 450 | 10712.0 | 96 | 96 | N | Y |
| 16 | C | - | - | 450 | 11397.0 | 96 | 96 | N | Y |
| 17 | C | - | - | 450 | 12082.0 | 96 | 96 | N | Y |
| 18 | C | - | - | 450 | 12766.0 | 96 | 96 | N | Y |
| 19 | C | - | - | 450 | 13451.0 | 96 | 96 | N | Y |
| 20 | C | - | - | 450 | 14136.0 | 96 | 96 | N | Y |
| 21 | C | - | - | 450 | 14821.0 | 96 | 96 | N | Y |
| 22 | C | - | - | 450 | 15505.0 | 96 | 96 | N | Y |
| 23 | C | - | - | 450 | 16190.0 | 96 | 96 | N | Y |
| 24 | C | - | - | 450 | 16875.0 | 96 | 96 | N | Y |

NOTES :

Distance to first opening from LHS = 900.0 mm

Distance to last opening from RHS = 900.0 mm

R = Rectangular C = Circular E = Elongated

x = Distance to opening from LHS

dt = Distance from top of opening to btm of top flange

db = Distance from btm of opening to top of btm flange

WEB STIFFENER DETAILS :

None

TRANSVERSE BEAM DETAILS :

None

LOADS ACTING ON BEAM :Occupancy imposed loads 4.0 kN/m²Ceilings, services and finishes 0.5 kN/m²

Natural frequency limit 4.0 Hz

BS 6399 imposed load reduction is NOT considered

Partition loads

1.0 kN/m²

Construction load

0.5 kN/m²**ADDITIONAL POINT LOADS :**

None

ADDITIONAL DISTRIBUTED LOADS :

None

END MOMENTS :

None

**PARTIAL SAFETY FACTORS :**

| | | | |
|--|-----|---------|-----|
| Dead (self weight) | 1.4 | Imposed | 1.6 |
| Super imposed dead | 1.4 | | |
| FIRE : | | | |
| Dead | 1.0 | Imposed | 0.8 |
| Proportion of imposed load considered as non-permanent in fire | | | 1.0 |

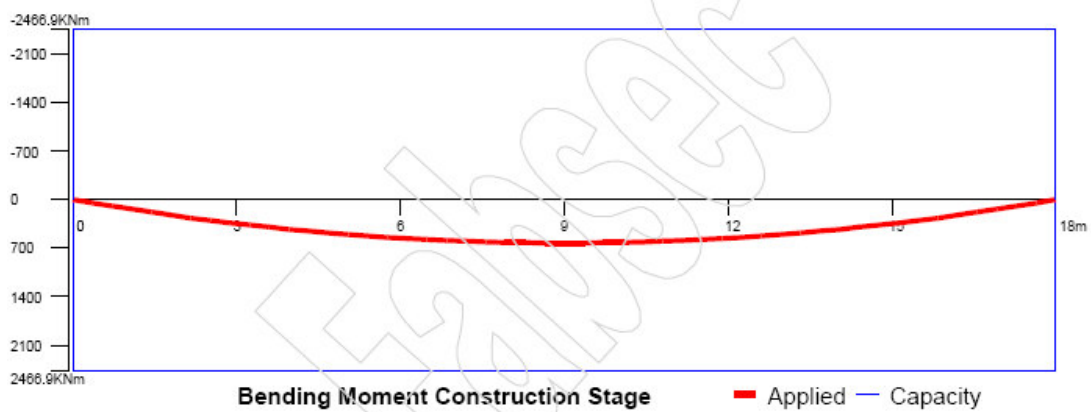
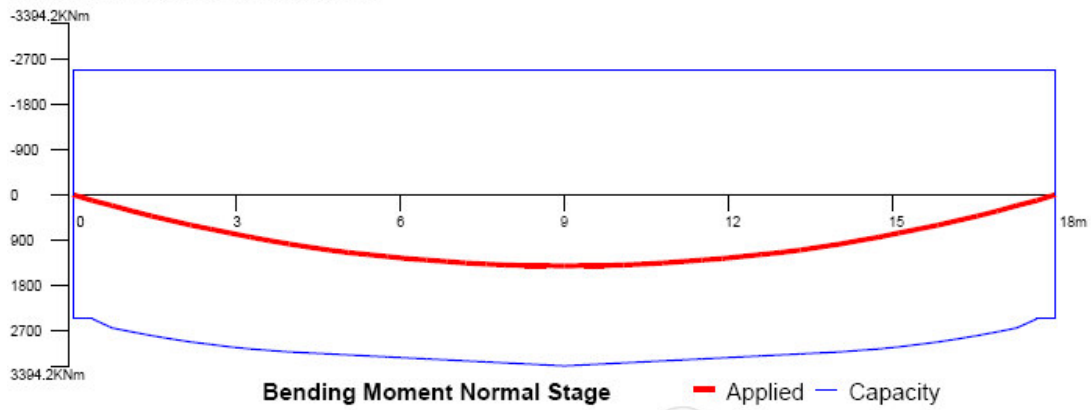
FIRE ENGINEERING DATA :

Fire resistance 120 mins

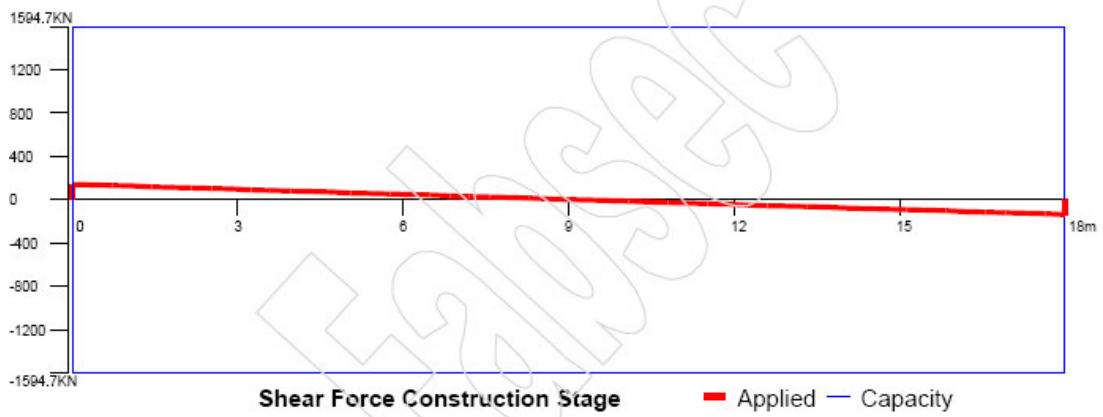
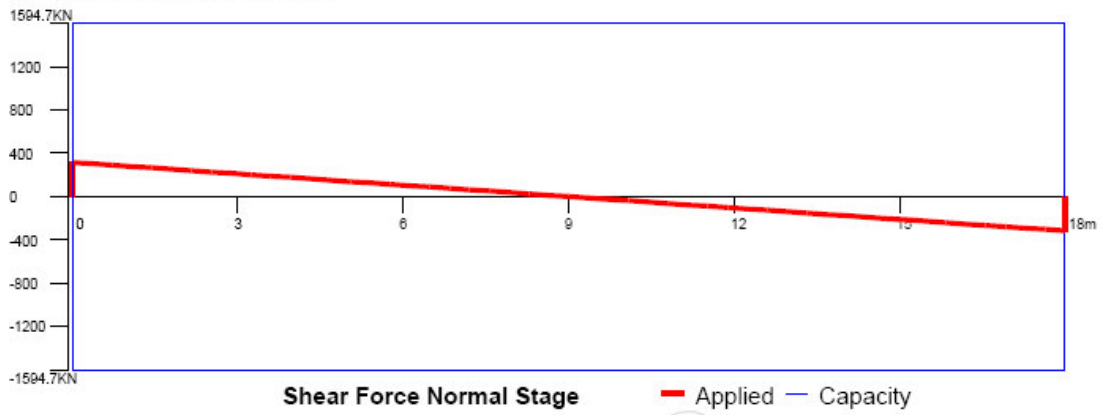
SPECIFIED THICKNESS OF FIRE PROTECTION :

| | | | |
|---------------|--------|-----|--------|
| Top flange | 1.9 mm | Web | 1.9 mm |
| Bottom flange | 1.9 mm | | |

BMD, SFD AND DEFLECTION PROFILES :
BENDING MOMENT DIAGRAMS :

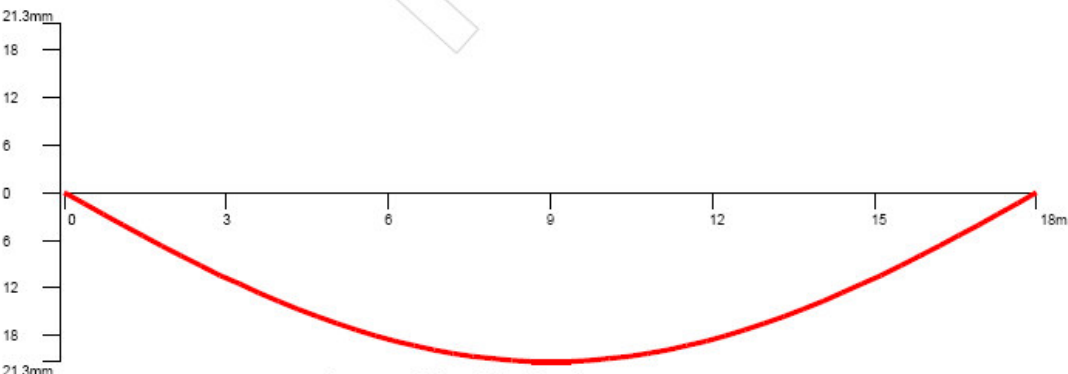
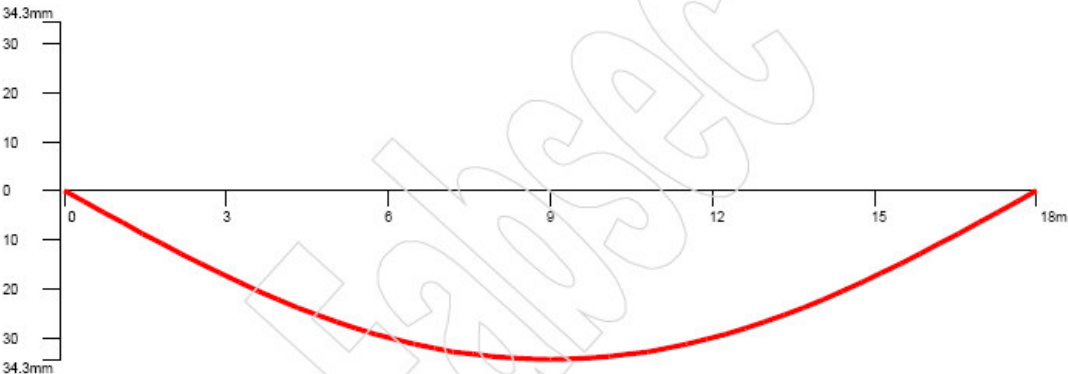
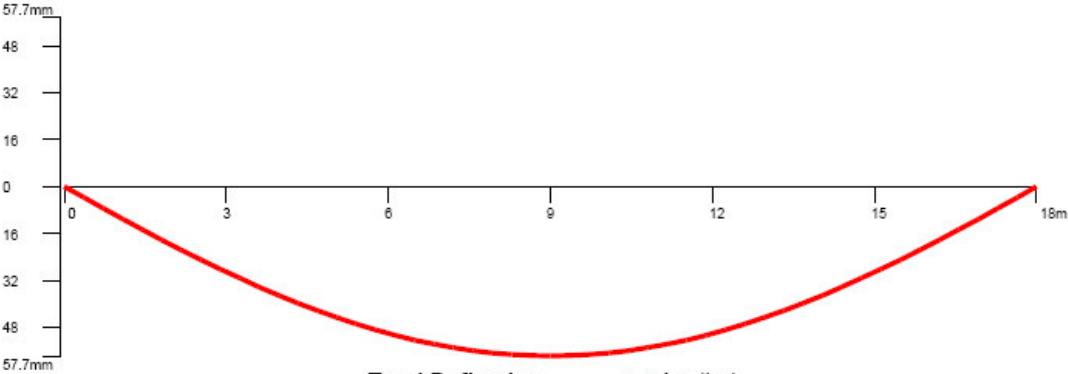


SHEAR FORCE DIAGRAMS :





DEFLECTION PROFILES :



NORMAL STAGE - ULTIMATE LIMIT STATE CHECKS (LONG OUTPUT)

FLOOR LOADS (UNFACTORED) :

DEAD :

Self weight of beam = $199.9 \times 9.81 / 2.5 / 1000$
= 0.78 kN/m²
Self weight of in-situ concrete = $9.81 \times 130.0 \times 2350 / 10^6$
= 3.00 kN/m²

LIVE :

Occupancy load = 4.00 kN/m²
Partitions = 1.00 kN/m²
Total imposed load = 5.00 kN/m² (no BS6399 imposed load reduction)

SUPER-IMPOSED DEAD :

Ceilings and services = 0.50 kN/m²

NS: DEGREE OF SHEAR CONNECTION :

*** check at maximum moment position :

Maximum moment is at mid-span

No. of shear connectors = 116 (to maximum moment position)
Degree of shear connection = 100% (***FULL SHEAR CONNECTION)
Minimum degree of shear connection = 100% (***SATISFACTORY)

NS: SECTION SHEAR CHECK :

| No. / Dist.(m) | d (mm) | t (mm) | d/t | Critical Mode | Applied Shear (kN) | Shear Capacity (kN) | Shear Stress (N/mm ²) | Unity Factor | Remarks |
|----------------|--------|--------|------|---------------|--------------------|---------------------|-----------------------------------|--------------|---------|
| 1 / 0.00 | 642.0 | 12 | 53.5 | Yielding | 315 | 1595 | 207.0 | 0.197 | |
| 2 / 0.36 | 642.0 | 12 | 53.5 | Yielding | 302 | 1595 | 207.0 | 0.190 | |
| 3 / 0.72 | 642.0 | 12 | 53.5 | Yielding | 290 | 1595 | 207.0 | 0.182 | |
| 4 / 1.08 | 642.0 | 12 | 53.5 | Yielding | 277 | 1595 | 207.0 | 0.174 | |
| 5 / 1.44 | 642.0 | 12 | 53.5 | Yielding | 264 | 1595 | 207.0 | 0.166 | |
| 6 / 1.80 | 642.0 | 12 | 53.5 | Yielding | 252 | 1595 | 207.0 | 0.158 | |
| 7 / 2.16 | 642.0 | 12 | 53.5 | Yielding | 239 | 1595 | 207.0 | 0.150 | |
| 8 / 2.52 | 642.0 | 12 | 53.5 | Yielding | 227 | 1595 | 207.0 | 0.142 | |
| 9 / 2.88 | 642.0 | 12 | 53.5 | Yielding | 214 | 1595 | 207.0 | 0.134 | |
| 10 / 3.24 | 642.0 | 12 | 53.5 | Yielding | 202 | 1595 | 207.0 | 0.126 | |
| 11 / 3.60 | 642.0 | 12 | 53.5 | Yielding | 189 | 1595 | 207.0 | 0.118 | |
| 12 / 3.96 | 642.0 | 12 | 53.5 | Yielding | 176 | 1595 | 207.0 | 0.111 | |
| 13 / 4.32 | 642.0 | 12 | 53.5 | Yielding | 164 | 1595 | 207.0 | 0.103 | |
| 14 / 4.68 | 642.0 | 12 | 53.5 | Yielding | 151 | 1595 | 207.0 | 0.095 | |
| 15 / 5.04 | 642.0 | 12 | 53.5 | Yielding | 139 | 1595 | 207.0 | 0.087 | |
| 16 / 5.40 | 642.0 | 12 | 53.5 | Yielding | 126 | 1595 | 207.0 | 0.079 | |
| 17 / 5.76 | 642.0 | 12 | 53.5 | Yielding | 113 | 1595 | 207.0 | 0.071 | |
| 18 / 6.12 | 642.0 | 12 | 53.5 | Yielding | 101 | 1595 | 207.0 | 0.063 | |
| 19 / 6.48 | 642.0 | 12 | 53.5 | Yielding | 88 | 1595 | 207.0 | 0.055 | |
| 20 / 6.84 | 642.0 | 12 | 53.5 | Yielding | 76 | 1595 | 207.0 | 0.047 | |
| 21 / 7.20 | 642.0 | 12 | 53.5 | Yielding | 63 | 1595 | 207.0 | 0.039 | |
| 22 / 7.56 | 642.0 | 12 | 53.5 | Yielding | 50 | 1595 | 207.0 | 0.032 | |
| 23 / 7.92 | 642.0 | 12 | 53.5 | Yielding | 38 | 1595 | 207.0 | 0.024 | |
| 24 / 8.28 | 642.0 | 12 | 53.5 | Yielding | 25 | 1595 | 207.0 | 0.016 | |
| 25 / 8.64 | 642.0 | 12 | 53.5 | Yielding | 13 | 1595 | 207.0 | 0.008 | |
| 26 / 9.00 | 642.0 | 12 | 53.5 | Yielding | 0 | 1595 | 207.0 | 0.000 | |
| 27 / 9.36 | 642.0 | 12 | 53.5 | Yielding | 13 | 1595 | 207.0 | 0.008 | |
| 28 / 9.72 | 642.0 | 12 | 53.5 | Yielding | 25 | 1595 | 207.0 | 0.016 | |
| 29 / 10.08 | 642.0 | 12 | 53.5 | Yielding | 38 | 1595 | 207.0 | 0.024 | |
| 30 / 10.44 | 642.0 | 12 | 53.5 | Yielding | 50 | 1595 | 207.0 | 0.032 | |
| 31 / 10.80 | 642.0 | 12 | 53.5 | Yielding | 63 | 1595 | 207.0 | 0.039 | |
| 32 / 11.16 | 642.0 | 12 | 53.5 | Yielding | 76 | 1595 | 207.0 | 0.047 | |

File Name :

FBEAM3 V 3. 2. 234

| No. / Dist.(m) | d (mm) | t (mm) | d/t | Critical Mode | Applied Shear (kN) | Shear Capacity (kN) | Shear Stress (N/mm ²) | Unity Factor | Remarks |
|----------------|--------|--------|------|---------------|--------------------|---------------------|-----------------------------------|--------------|---------|
| 33 / 11.52 | 642.0 | 12 | 53.5 | Yielding | 88 | 1595 | 207.0 | 0.055 | |
| 34 / 11.88 | 642.0 | 12 | 53.5 | Yielding | 101 | 1595 | 207.0 | 0.063 | |
| 35 / 12.24 | 642.0 | 12 | 53.5 | Yielding | 113 | 1595 | 207.0 | 0.071 | |
| 36 / 12.60 | 642.0 | 12 | 53.5 | Yielding | 126 | 1595 | 207.0 | 0.079 | |
| 37 / 12.96 | 642.0 | 12 | 53.5 | Yielding | 139 | 1595 | 207.0 | 0.087 | |
| 38 / 13.32 | 642.0 | 12 | 53.5 | Yielding | 151 | 1595 | 207.0 | 0.095 | |
| 39 / 13.68 | 642.0 | 12 | 53.5 | Yielding | 164 | 1595 | 207.0 | 0.103 | |
| 40 / 14.04 | 642.0 | 12 | 53.5 | Yielding | 176 | 1595 | 207.0 | 0.111 | |
| 41 / 14.40 | 642.0 | 12 | 53.5 | Yielding | 189 | 1595 | 207.0 | 0.118 | |
| 42 / 14.76 | 642.0 | 12 | 53.5 | Yielding | 202 | 1595 | 207.0 | 0.126 | |
| 43 / 15.12 | 642.0 | 12 | 53.5 | Yielding | 214 | 1595 | 207.0 | 0.134 | |
| 44 / 15.48 | 642.0 | 12 | 53.5 | Yielding | 227 | 1595 | 207.0 | 0.142 | |
| 45 / 15.84 | 642.0 | 12 | 53.5 | Yielding | 239 | 1595 | 207.0 | 0.150 | |
| 46 / 16.20 | 642.0 | 12 | 53.5 | Yielding | 252 | 1595 | 207.0 | 0.158 | |
| 47 / 16.56 | 642.0 | 12 | 53.5 | Yielding | 264 | 1595 | 207.0 | 0.166 | |
| 48 / 16.92 | 642.0 | 12 | 53.5 | Yielding | 277 | 1595 | 207.0 | 0.174 | |
| 49 / 17.28 | 642.0 | 12 | 53.5 | Yielding | 290 | 1595 | 207.0 | 0.182 | |
| 50 / 17.64 | 642.0 | 12 | 53.5 | Yielding | 302 | 1595 | 207.0 | 0.190 | |
| 51 / 18.00 | 642.0 | 12 | 53.5 | Yielding | 315 | 1595 | 207.0 | 0.197 | |

NOTES :

All distance measurements from LHS

Web slenderness limit ($d/t = 62 \times \epsilon$) = 55.4**NS: INTERACTION OF BENDING MOMENT AND VERTICAL SHEAR/BUCKLING :**

| No. / Dist.(m) | Applied Shear (kN) | te (mm) | Applied Moment (kNm) | Stud No. | Shear Deg. (%) | dc (mm) | yp (mm) | Modulus (cm ⁴) | Moment Capacity (kNm) | Unity Factor | Remarks |
|----------------|--------------------|---------|----------------------|----------|----------------|---------|---------|----------------------------|-----------------------|--------------|---------|
| 1 / 0.00 | 315 (L) | 12.0 | 0 | - | - | - | 345.0 | 7151 | 2467 | 0.000 | |
| 2 / 0.36 | 302 (L) | 12.0 | 111 | - | - | - | 345.0 | 7151 | 2467 | 0.045 | |
| 3 / 0.72 | 290 (L) | 12.0 | 218 | 6 | 100 (F) | 130.0 | 418.5 | 7668 | 2646 | 0.082 | |
| 4 / 1.08 | 277 (L) | 12.0 | 320 | 10 | 100 (F) | 130.0 | 390.2 | 7899 | 2725 | 0.117 | |
| 5 / 1.44 | 264 (L) | 12.0 | 417 | 16 | 100 (F) | 130.0 | 362.0 | 8110 | 2798 | 0.149 | |
| 6 / 1.80 | 252 (L) | 12.0 | 510 | 20 | 100 (F) | 130.0 | 333.7 | 8301 | 2864 | 0.178 | |
| 7 / 2.16 | 239 (L) | 12.0 | 598 | 24 | 100 (F) | 130.0 | 305.4 | 8474 | 2924 | 0.205 | |
| 8 / 2.52 | 227 (L) | 12.0 | 682 | 30 | 100 (F) | 130.0 | 277.2 | 8628 | 2977 | 0.229 | |
| 9 / 2.88 | 214 (L) | 12.0 | 762 | 34 | 100 (F) | 130.0 | 248.9 | 8762 | 3023 | 0.252 | |
| 10 / 3.24 | 202 (L) | 12.0 | 837 | 40 | 100 (F) | 130.0 | 220.7 | 8877 | 3063 | 0.273 | |
| 11 / 3.60 | 189 (L) | 12.0 | 907 | 44 | 100 (F) | 130.0 | 192.4 | 8973 | 3096 | 0.293 | |
| 12 / 3.96 | 176 (L) | 12.0 | 973 | 48 | 100 (F) | 130.0 | 164.1 | 9050 | 3122 | 0.311 | |
| 13 / 4.32 | 164 (L) | 12.0 | 1034 | 54 | 100 (F) | 130.0 | 153.4 | 9111 | 3143 | 0.329 | |
| 14 / 4.68 | 151 (L) | 12.0 | 1090 | 58 | 100 (F) | 130.0 | 152.5 | 9171 | 3164 | 0.345 | |
| 15 / 5.04 | 139 (L) | 12.0 | 1143 | 64 | 100 (F) | 130.0 | 151.6 | 9230 | 3184 | 0.359 | |
| 16 / 5.40 | 126 (L) | 12.0 | 1190 | 68 | 100 (F) | 130.0 | 150.7 | 9288 | 3205 | 0.371 | |
| 17 / 5.76 | 113 (L) | 12.0 | 1233 | 72 | 100 (F) | 130.0 | 149.7 | 9346 | 3224 | 0.382 | |
| 18 / 6.12 | 101 (L) | 12.0 | 1272 | 78 | 100 (F) | 130.0 | 148.8 | 9403 | 3244 | 0.392 | |
| 19 / 6.48 | 88 (L) | 12.0 | 1306 | 82 | 100 (F) | 130.0 | 147.9 | 9460 | 3264 | 0.400 | |
| 20 / 6.84 | 76 (L) | 12.0 | 1335 | 88 | 100 (F) | 130.0 | 147.0 | 9516 | 3283 | 0.407 | |
| 21 / 7.20 | 63 (L) | 12.0 | 1360 | 92 | 100 (F) | 130.0 | 146.1 | 9571 | 3302 | 0.412 | |
| 22 / 7.56 | 50 (L) | 12.0 | 1381 | 96 | 100 (F) | 130.0 | 145.2 | 9626 | 3321 | 0.416 | |
| 23 / 7.92 | 38 (L) | 12.0 | 1396 | 102 | 100 (F) | 130.0 | 144.2 | 9680 | 3340 | 0.418 | |
| 24 / 8.28 | 25 (L) | 12.0 | 1408 | 106 | 100 (F) | 130.0 | 143.3 | 9733 | 3358 | 0.419 | |
| 25 / 8.64 | 13 (L) | 12.0 | 1415 | 112 | 100 (F) | 130.0 | 142.4 | 9786 | 3376 | 0.419 | |
| 26 / 9.00 | 0 (L) | 12.0 | 1417 | 116 | 100 (F) | 130.0 | 141.5 | 9838 | 3394 | 0.417 | |
| 27 / 9.36 | 13 (L) | 12.0 | 1415 | 112 | 100 (F) | 130.0 | 142.4 | 9786 | 3376 | 0.419 | |
| 28 / 9.72 | 25 (L) | 12.0 | 1408 | 106 | 100 (F) | 130.0 | 143.3 | 9733 | 3358 | 0.419 | |
| 29 / 10.08 | 38 (L) | 12.0 | 1396 | 102 | 100 (F) | 130.0 | 144.2 | 9680 | 3340 | 0.418 | |
| 30 / 10.44 | 50 (L) | 12.0 | 1381 | 96 | 100 (F) | 130.0 | 145.2 | 9626 | 3321 | 0.416 | |
| 31 / 10.80 | 63 (L) | 12.0 | 1360 | 92 | 100 (F) | 130.0 | 146.1 | 9571 | 3302 | 0.412 | |
| 32 / 11.16 | 76 (L) | 12.0 | 1335 | 88 | 100 (F) | 130.0 | 147.0 | 9516 | 3283 | 0.407 | |
| 33 / 11.52 | 88 (L) | 12.0 | 1306 | 82 | 100 (F) | 130.0 | 147.9 | 9460 | 3264 | 0.400 | |
| 34 / 11.88 | 101 (L) | 12.0 | 1272 | 78 | 100 (F) | 130.0 | 148.8 | 9403 | 3244 | 0.392 | |
| 35 / 12.24 | 113 (L) | 12.0 | 1233 | 72 | 100 (F) | 130.0 | 149.7 | 9346 | 3224 | 0.382 | |
| 36 / 12.60 | 126 (L) | 12.0 | 1190 | 68 | 100 (F) | 130.0 | 150.7 | 9288 | 3205 | 0.371 | |
| 37 / 12.96 | 139 (L) | 12.0 | 1143 | 64 | 100 (F) | 130.0 | 151.6 | 9230 | 3184 | 0.359 | |
| 38 / 13.32 | 151 (L) | 12.0 | 1090 | 58 | 100 (F) | 130.0 | 152.5 | 9171 | 3164 | 0.345 | |
| 39 / 13.68 | 164 (L) | 12.0 | 1034 | 54 | 100 (F) | 130.0 | 153.4 | 9111 | 3143 | 0.329 | |

| No. / Dist.(m) | Applied Shear (kN) | te (mm) | Applied Moment (kNm) | Stud No. | Shear Deg. (%) | dc (mm) | yp (mm) | Modulus (cm ²) | Moment Capacity (kNm) | Unity Factor | Remarks |
|----------------|--------------------|---------|----------------------|----------|----------------|---------|---------|----------------------------|-----------------------|--------------|---------|
| 40 / 14.04 | 176 (L) | 12.0 | 973 | 48 | 100 (F) | 130.0 | 164.1 | 9050 | 3122 | 0.311 | |
| 41 / 14.40 | 189 (L) | 12.0 | 907 | 44 | 100 (F) | 130.0 | 192.4 | 8973 | 3096 | 0.293 | |
| 42 / 14.76 | 202 (L) | 12.0 | 837 | 40 | 100 (F) | 130.0 | 220.7 | 8877 | 3063 | 0.273 | |
| 43 / 15.12 | 214 (L) | 12.0 | 762 | 34 | 100 (F) | 130.0 | 248.9 | 8762 | 3023 | 0.252 | |
| 44 / 15.48 | 227 (L) | 12.0 | 682 | 30 | 100 (F) | 130.0 | 277.2 | 8628 | 2977 | 0.229 | |
| 45 / 15.84 | 239 (L) | 12.0 | 598 | 24 | 100 (F) | 130.0 | 305.4 | 8474 | 2924 | 0.205 | |
| 46 / 16.20 | 252 (L) | 12.0 | 510 | 20 | 100 (F) | 130.0 | 333.7 | 8301 | 2864 | 0.178 | |
| 47 / 16.56 | 264 (L) | 12.0 | 417 | 16 | 100 (F) | 130.0 | 362.0 | 8110 | 2798 | 0.149 | |
| 48 / 16.92 | 277 (L) | 12.0 | 320 | 10 | 100 (F) | 130.0 | 390.2 | 7899 | 2725 | 0.117 | |
| 49 / 17.28 | 290 (L) | 12.0 | 218 | 6 | 100 (F) | 130.0 | 418.5 | 7668 | 2646 | 0.082 | |
| 50 / 17.64 | 302 (L) | 12.0 | 111 | - | - | - | 345.0 | 7151 | 2467 | 0.045 | |
| 51 / 18.00 | 315 (L) | 12.0 | 0 | - | - | - | 345.0 | 7151 | 2467 | 0.000 | |

NOTES:

(L) = Low shear (H) = High shear (*) = Web contribution to bending capacity neglected

te = Effective web thickness

yp = Depth to Plastic Neutral Axis

(P) = Partial shear connection (F) = Full shear connection

dc = Depth of concrete in compression

NS: CONCRETE LONGITUDINAL SHEAR RESISTANCE CHECK :

Design longitudinal shear force (plane a - a) = $0.42 * 67 / 116 * 2 * 87.2 / 150 / 2 * 1000$
 = 140.77 kN/m
 Concrete shear area = $130.0 * 1000$
 = 130000 mm²/m
 Longitudinal shear capacity = $0.8 * 1.0 * 130000.00 * (40.0)^{0.5} / 1000$
 = 657.75 kN/m
 UNITY FACTOR = $140.77 / 657.75$
 = 0.214

PASS

Design longitudinal shear force (plane b - b) = $0.42 * 67 / 116 * 2 * 87.2 / 150 / 1000$
 = 281.54 kN/m
 Concrete shear area = $(2 * 95.0 + 5 * 19.0 + 12) * 1000$
 = 297000 mm²/m
 Longitudinal shear capacity = $0.8 * 1.0 * 297000.00 * (40.0)^{0.5} / 1000$
 = 1502.71 kN/m
 UNITY FACTOR = $281.54 / 1502.71$
 = 0.187

PASS**NOTE:**

For the concrete shear check, the longitudinal shear force is reduced by the ratio of the applied factored moment to the moment capacity of the section for the actual degree of shear connection

NS: TRANSVERSE REINFORCEMENT CHECK :**SHEAR PLANE a - a :**

Maximum shear force on plane = $67 / 116 * 2 * 87.2 / 150 / 2 * 1000$
 = 335.77 kN/m
 Shear area = $130000.0 \text{ mm}^2/\text{m}$
 Transverse resistance (concrete & mesh) = 237.14 kN/m
 Additional reinforcement required = $1000 * (335.8 - 237.1) / (0.7 * 460.0)$
 = 306 mm²/m

NOTE :

For the transverse reinforcement check, the longitudinal shear force is reduced if more connectors than that needed for full shear connection have been provided

**SHEAR PLANE b - b :**

Shear force on plane $= 67 / 116 * 2 * 87.2 / 150 * 1000$
 $= 671.54 \text{ kN/m}$

Shear area $= (2 * 95.0 + 5 * 19.0 + 12) * 1000$
 $= 297000.0 \text{ mm}^2/\text{m}$

Transverse resistance (concrete only) $= (0.03 * 1.0 * 297000 * 40.0) / 1000$
 $= 356.40 \text{ kN/m}$

Additional bar reinforcement required $= 1000 * (671.5 - 356.4) / (0.7 * 460.0) / 2$
 $= 489 \text{ mm}^2/\text{m}$

NOTE :

1. Lateral torsional buckling check is performed using the 'm' factor approach, as in BS 5950 : Part 1 : 2000, modified for the varying level of stresses at different sections of a tapered beam

NS: WELD DESIGN :**STUD SHEAR FLOW :**

Stud shear flow $= 67 / 116 * 2 * 87.2 / 150$
 $= 0.67 \text{ kN/mm}$

MOMENT SHEAR FLOW :

Critical location is at Left Hand Support

Flange forces

T1 $= 0.00 * 370.0 * 24.0 * 345.0$
 $= 0.00 \text{ kN/mm}$

T2 $= 0.05 * 370.0 * 24.0 * 345.0$
 $= 137.95 \text{ kN/mm}$

Moment shear flow $= \text{ABS}(137.95 - 0.00) / 360.00$
 $= 0.38 \text{ kN/mm}$

Weld force $= \text{MAX}(0.67, 0.38)$
 $= 0.67 \text{ kN/mm}$

Weld size $= (0.67 / 0.250) / 0.7$
 $= 4 \text{ mm (total weld required)}$

Therefore, use 5 mm fillet weld on both sides

NOTES :

Uniform and continuous FW along whole length of beam i.e no intermittent welds

Same size welds assumed top and bottom

Weld sizes based on electrode Class 42 to BS EN 756

NS: LOCAL CHECKS AT CHANGE POINTS :

None required

NS: ADDITIONAL CHECKS AT OPENINGS :**NS: SECTION PROPERTIES AT CENTRELINE OF OPENINGS :**

| No. / Dist.(m) | Web Clas. | b _{eff} (mm) | d _c (mm) | y _e (mm) | y _p (mm) | I _{xx} (cm ⁴) | Z _c (cm ³) | Z _t (cm ³) | Z _b (cm ³) | S _x (cm ³) |
|-------------------|--------------|--------------------------|------------------------|------------------------|------------------------|---------------------------------------|--------------------------------------|--------------------------------------|--------------------------------------|--------------------------------------|
| 1 / 1.13 | 2 | 312.5 | 130.0 | 406.0 | 161.7 | 271736 | 66936 | 9847 | 6563 | 6842 |
| 2 / 1.81 | 2 | 502.8 | 130.0 | 374.3 | 152.5 | 298168 | 79669 | 12207 | 6689 | 6956 |
| 3 / 2.50 | 2 | 693.1 | 130.0 | 347.9 | 150.8 | 320161 | 92015 | 14690 | 6782 | 7068 |
| 4 / 3.18 | 2 | 883.1 | 130.0 | 325.8 | 149.0 | 338734 | 103974 | 17301 | 6854 | 7178 |
| 5 / 3.86 | 2 | 1073.3 | 130.0 | 306.8 | 147.3 | 354683 | 115598 | 20058 | 6912 | 7285 |
| 6 / 4.55 | 2 | 1263.6 | 130.0 | 290.4 | 145.5 | 368516 | 126885 | 22970 | 6959 | 7390 |
| 7 / 5.23 | 2 | 1453.9 | 130.0 | 276.1 | 143.8 | 380637 | 137851 | 26049 | 6999 | 7493 |
| 8 / 5.92 | 2 | 1643.9 | 130.0 | 263.5 | 142.0 | 391338 | 148495 | 29306 | 7033 | 7593 |
| 9 / 6.60 | 2 | 1834.2 | 130.0 | 252.4 | 140.3 | 400887 | 158861 | 32765 | 7062 | 7691 |
| 10 / 7.29 | 2 | 2024.4 | 130.0 | 242.4 | 138.6 | 409455 | 168945 | 36442 | 7088 | 7787 |
| 11 / 7.97 | 2 | 2214.7 | 130.0 | 233.4 | 136.8 | 417190 | 178761 | 40355 | 7112 | 7881 |
| 12 / 8.66 | 2 | 2405.0 | 130.0 | 225.3 | 135.1 | 424214 | 188318 | 44530 | 7133 | 7973 |
| 13 / 9.34 | 2 | 2405.0 | 130.0 | 225.3 | 135.1 | 424214 | 188318 | 44530 | 7133 | 7973 |
| 14 / 10.03 | 2 | 2214.7 | 130.0 | 233.4 | 136.8 | 417190 | 178761 | 40355 | 7112 | 7881 |
| 15 / 10.71 | 2 | 2024.4 | 130.0 | 242.4 | 138.6 | 409455 | 168945 | 36442 | 7088 | 7787 |

File Name:

FBEAM3 V 3. 2. 234

**NS: DETAILED CALCULATION AT THE CRITICAL OPENING (NO.12) :****NS: VERTICAL SHEAR CHECK :**

| | |
|-----------------------------|--|
| Applied shear | = 11.96 kN |
| Shear capacity (top tee) | = $0.6 * 345.0 * 96.00 * 12.00 / 1000$ |
| | = 238.46 kN |
| Shear capacity (bottom tee) | = $0.6 * 345.0 * 96.00 * 12.00 / 1000$ |
| | = 238.46 kN |
| Concrete Shear Stress | = 0.62 N/mm ² |
| Concrete Shear Capacity | = 61.71 kN |
| Total Shear Capacity | = 538.64 kN |
| UNITY FACTOR | = 11.96 / 538.64 |
| | = 0.088 |

PASS**NS: INTERACTION OF BENDING MOMENT AND VERTICAL SHEAR :**

| | |
|-------------------|---------------|
| Applied moment | = 1414.73 kNm |
| Co-existent shear | = 11.96 kN |

CHECK VERTICAL SHEAR CAPACITY :

| | |
|--------------------------------|---|
| Shear capacity (steel section) | = 476.93 kN |
| Concrete shear stress | = 0.62 N/mm ² |
| Concrete shear capacity | = $0.62 * (130.0 * (370.0 + 3 * 130.0)) / 1000$ |
| | = 61.71 kN |
| Total shear capacity | = 476.93 + 61.71 |
| | = 538.64 kN |
| UNITY FACTOR | = $11.96 / (476.93 + 61.71)$ |
| | = 0.022 (low shear) |

No reduction in moment capacity of section due to shear

CHECK BENDING CAPACITY :

| | |
|---|---|
| Concrete in compression | = 130.0 mm |
| Effective width of slab | = 2405.0 mm |
| Plastic modulus (composite section) | = 7972.9 cm ³ (includes effective web thickness) |
| Plastic neutral axis is 135.1 mm from top of slab | |
| Section bending capacity | = $7972.9 * 345.0 / 1000$ |
| | = 2750.64 kNm |

| | |
|--------------|---------------------|
| UNITY FACTOR | = 1414.73 / 2750.64 |
| | = 0.514 |

PASS

CONSTRUCTION STAGE - ULTIMATE LIMIT STATE CHECKS (LONG OUTPUT)

FLOOR LOADS (UNFACTORED) :

DEAD :

See normal stage load calculations for details.

 Self weight of beam = 0.78 kN/m²

Self weight of in-situ concrete = 3.00 * 2400.00 / 2350.00

 = 3.06 kN/m²

 Construction load = 0.50 kN/m²

CS: INTERACTION OF BENDING MOMENT AND VERTICAL SHEAR/BUCKLING :

| No. / Dist.(m) | Web Clas. | Flange Clas. | Applied Shear (kN) | Applied Moment (kNm) | te (mm) | Moment Capacity (kNm) | Unity Factor | Remarks |
|----------------|-----------|--------------|--------------------|----------------------|---------|-----------------------|--------------|---------|
| 1 / 0.00 | 1 | 2 | 139 (L) | 0 | 12.00 | 2467 | 0.000 | |
| 2 / 0.36 | 1 | 2 | 134 (L) | 49 | 12.00 | 2467 | 0.020 | |
| 3 / 0.72 | 1 | 2 | 128 (L) | 96 | 12.00 | 2467 | 0.039 | |
| 4 / 1.08 | 1 | 2 | 122 (L) | 141 | 12.00 | 2467 | 0.057 | |
| 5 / 1.44 | 1 | 2 | 117 (L) | 184 | 12.00 | 2467 | 0.075 | |
| 6 / 1.80 | 1 | 2 | 111 (L) | 225 | 12.00 | 2467 | 0.091 | |
| 7 / 2.16 | 1 | 2 | 106 (L) | 264 | 12.00 | 2467 | 0.107 | |
| 8 / 2.52 | 1 | 2 | 100 (L) | 302 | 12.00 | 2467 | 0.122 | |
| 9 / 2.88 | 1 | 2 | 95 (L) | 337 | 12.00 | 2467 | 0.136 | |
| 10 / 3.24 | 1 | 2 | 89 (L) | 370 | 12.00 | 2467 | 0.150 | |
| 11 / 3.60 | 1 | 2 | 83 (L) | 401 | 12.00 | 2467 | 0.162 | |
| 12 / 3.96 | 1 | 2 | 78 (L) | 430 | 12.00 | 2467 | 0.174 | |
| 13 / 4.32 | 1 | 2 | 72 (L) | 457 | 12.00 | 2467 | 0.185 | |
| 14 / 4.68 | 1 | 2 | 67 (L) | 482 | 12.00 | 2467 | 0.195 | |
| 15 / 5.04 | 1 | 2 | 61 (L) | 505 | 12.00 | 2467 | 0.205 | |
| 16 / 5.40 | 1 | 2 | 56 (L) | 526 | 12.00 | 2467 | 0.213 | |
| 17 / 5.76 | 1 | 2 | 50 (L) | 545 | 12.00 | 2467 | 0.221 | |
| 18 / 6.12 | 1 | 2 | 45 (L) | 562 | 12.00 | 2467 | 0.228 | |
| 19 / 6.48 | 1 | 2 | 39 (L) | 577 | 12.00 | 2467 | 0.234 | |
| 20 / 6.84 | 1 | 2 | 33 (L) | 590 | 12.00 | 2467 | 0.239 | |
| 21 / 7.20 | 1 | 2 | 28 (L) | 601 | 12.00 | 2467 | 0.244 | |
| 22 / 7.56 | 1 | 2 | 22 (L) | 610 | 12.00 | 2467 | 0.247 | |
| 23 / 7.92 | 1 | 2 | 17 (L) | 617 | 12.00 | 2467 | 0.250 | |
| 24 / 8.28 | 1 | 2 | 11 (L) | 622 | 12.00 | 2467 | 0.252 | |
| 25 / 8.64 | 1 | 2 | 6 (L) | 625 | 12.00 | 2467 | 0.253 | |
| 26 / 9.00 | 1 | 2 | 0 (L) | 626 | 12.00 | 2467 | 0.254 | |
| 27 / 9.36 | 1 | 2 | 6 (L) | 625 | 12.00 | 2467 | 0.253 | |
| 28 / 9.72 | 1 | 2 | 11 (L) | 622 | 12.00 | 2467 | 0.252 | |
| 29 / 10.08 | 1 | 2 | 17 (L) | 617 | 12.00 | 2467 | 0.250 | |
| 30 / 10.44 | 1 | 2 | 22 (L) | 610 | 12.00 | 2467 | 0.247 | |
| 31 / 10.80 | 1 | 2 | 28 (L) | 601 | 12.00 | 2467 | 0.244 | |
| 32 / 11.16 | 1 | 2 | 33 (L) | 590 | 12.00 | 2467 | 0.239 | |
| 33 / 11.52 | 1 | 2 | 39 (L) | 577 | 12.00 | 2467 | 0.234 | |
| 34 / 11.88 | 1 | 2 | 45 (L) | 562 | 12.00 | 2467 | 0.228 | |
| 35 / 12.24 | 1 | 2 | 50 (L) | 545 | 12.00 | 2467 | 0.221 | |
| 36 / 12.60 | 1 | 2 | 56 (L) | 526 | 12.00 | 2467 | 0.213 | |
| 37 / 12.96 | 1 | 2 | 61 (L) | 505 | 12.00 | 2467 | 0.205 | |
| 38 / 13.32 | 1 | 2 | 67 (L) | 482 | 12.00 | 2467 | 0.195 | |
| 39 / 13.68 | 1 | 2 | 72 (L) | 457 | 12.00 | 2467 | 0.185 | |
| 40 / 14.04 | 1 | 2 | 78 (L) | 430 | 12.00 | 2467 | 0.174 | |
| 41 / 14.40 | 1 | 2 | 83 (L) | 401 | 12.00 | 2467 | 0.162 | |
| 42 / 14.76 | 1 | 2 | 89 (L) | 370 | 12.00 | 2467 | 0.150 | |
| 43 / 15.12 | 1 | 2 | 95 (L) | 337 | 12.00 | 2467 | 0.136 | |
| 44 / 15.48 | 1 | 2 | 100 (L) | 302 | 12.00 | 2467 | 0.122 | |
| 45 / 15.84 | 1 | 2 | 106 (L) | 264 | 12.00 | 2467 | 0.107 | |
| 46 / 16.20 | 1 | 2 | 111 (L) | 225 | 12.00 | 2467 | 0.091 | |
| 47 / 16.56 | 1 | 2 | 117 (L) | 184 | 12.00 | 2467 | 0.075 | |
| 48 / 16.92 | 1 | 2 | 122 (L) | 141 | 12.00 | 2467 | 0.057 | |
| 49 / 17.28 | 1 | 2 | 128 (L) | 96 | 12.00 | 2467 | 0.039 | |
| 50 / 17.64 | 1 | 2 | 134 (L) | 49 | 12.00 | 2467 | 0.020 | |
| 51 / 18.00 | 1 | 2 | 139 (L) | 0 | 12.00 | 2467 | 0.000 | |

**NOTES :**

(L) = Low shear (H) = High shear (*) = Web contribution to bending capacity neglected
 te = reduced web thickness due to high shear

CS: TOP FLANGE LTB CHECK :

Effective length = 1.00 * 18.00
 = 18.00 m
 Maximum applied moment = 626.04 kNm
 Buckling moment Mbar = 0.93 * 626.04
 = 579.09 kNm
 Buckling Capacity = 590.48 kNm
 UNITY FACTOR = 579.09 / 590.48
 = 0.981

PASS**NOTE :**

1. Lateral torsional buckling check is performed using the 'm' factor approach, as in BS 5950 : Part 1 : 2000, modified for the varying level of stresses at different sections of a tapered beam

ADDITIONAL CHECKS AT OPENINGS :**CS: SECTION PROPERTIES AT CENTRELINE OF OPENINGS :**

| No. / Dist.(m) | Web Clas. | rx (cm) | ry (cm) | A (cm ²) | ye (mm) | yp (mm) | Ixx (cm ⁴) | Zt (cm ³) | Zb (cm ³) | Sx (cm ³) |
|-------------------|--------------|------------|------------|-------------------------|------------|------------|---------------------------|--------------------------|--------------------------|--------------------------|
| 1 / 1.13 | 2 | 32.7 | 10.0 | 200.6 | 345.0 | 345.0 | 214372.5 | 6213.7 | 6213.7 | 6543.1 |
| 2 / 1.81 | 2 | 32.7 | 10.0 | 200.6 | 345.0 | 345.0 | 214372.5 | 6213.7 | 6213.7 | 6543.1 |
| 3 / 2.50 | 2 | 32.7 | 10.0 | 200.6 | 345.0 | 345.0 | 214372.5 | 6213.7 | 6213.7 | 6543.1 |
| 4 / 3.18 | 2 | 32.7 | 10.0 | 200.6 | 345.0 | 345.0 | 214372.5 | 6213.7 | 6213.7 | 6543.1 |
| 5 / 3.86 | 2 | 32.7 | 10.0 | 200.6 | 345.0 | 345.0 | 214372.5 | 6213.7 | 6213.7 | 6543.1 |
| 6 / 4.55 | 2 | 32.7 | 10.0 | 200.6 | 345.0 | 345.0 | 214372.5 | 6213.7 | 6213.7 | 6543.1 |
| 7 / 5.23 | 2 | 32.7 | 10.0 | 200.6 | 345.0 | 345.0 | 214372.5 | 6213.7 | 6213.7 | 6543.1 |
| 8 / 5.92 | 2 | 32.7 | 10.0 | 200.6 | 345.0 | 345.0 | 214372.5 | 6213.7 | 6213.7 | 6543.1 |
| 9 / 6.60 | 2 | 32.7 | 10.0 | 200.6 | 345.0 | 345.0 | 214372.5 | 6213.7 | 6213.7 | 6543.1 |
| 10 / 7.29 | 2 | 32.7 | 10.0 | 200.6 | 345.0 | 345.0 | 214372.5 | 6213.7 | 6213.7 | 6543.1 |
| 11 / 7.97 | 2 | 32.7 | 10.0 | 200.6 | 345.0 | 345.0 | 214372.5 | 6213.7 | 6213.7 | 6543.1 |
| 12 / 8.66 | 2 | 32.7 | 10.0 | 200.6 | 345.0 | 345.0 | 214372.5 | 6213.7 | 6213.7 | 6543.1 |
| 13 / 9.34 | 2 | 32.7 | 10.0 | 200.6 | 345.0 | 345.0 | 214372.5 | 6213.7 | 6213.7 | 6543.1 |
| 14 / 10.03 | 2 | 32.7 | 10.0 | 200.6 | 345.0 | 345.0 | 214372.5 | 6213.7 | 6213.7 | 6543.1 |
| 15 / 10.71 | 2 | 32.7 | 10.0 | 200.6 | 345.0 | 345.0 | 214372.5 | 6213.7 | 6213.7 | 6543.1 |
| 16 / 11.40 | 2 | 32.7 | 10.0 | 200.6 | 345.0 | 345.0 | 214372.5 | 6213.7 | 6213.7 | 6543.1 |
| 17 / 12.08 | 2 | 32.7 | 10.0 | 200.6 | 345.0 | 345.0 | 214372.5 | 6213.7 | 6213.7 | 6543.1 |
| 18 / 12.77 | 2 | 32.7 | 10.0 | 200.6 | 345.0 | 345.0 | 214372.5 | 6213.7 | 6213.7 | 6543.1 |
| 19 / 13.45 | 2 | 32.7 | 10.0 | 200.6 | 345.0 | 345.0 | 214372.5 | 6213.7 | 6213.7 | 6543.1 |
| 20 / 14.14 | 2 | 32.7 | 10.0 | 200.6 | 345.0 | 345.0 | 214372.5 | 6213.7 | 6213.7 | 6543.1 |
| 21 / 14.82 | 2 | 32.7 | 10.0 | 200.6 | 345.0 | 345.0 | 214372.5 | 6213.7 | 6213.7 | 6543.1 |
| 22 / 15.51 | 2 | 32.7 | 10.0 | 200.6 | 345.0 | 345.0 | 214372.5 | 6213.7 | 6213.7 | 6543.1 |
| 23 / 16.19 | 2 | 32.7 | 10.0 | 200.6 | 345.0 | 345.0 | 214372.5 | 6213.7 | 6213.7 | 6543.1 |
| 24 / 16.88 | 2 | 32.7 | 10.0 | 200.6 | 345.0 | 345.0 | 214372.5 | 6213.7 | 6213.7 | 6543.1 |

CS: VERTICAL SHEAR CHECK :

| No. / Dist.(m) | Applied Shear (kN) | Shear Cap. TOP (kN) | Shear Cap. BOTTOM (kN) | Shear Cap. Total (kN) | Unity Factor | Remarks |
|-------------------|--------------------------|---------------------------|------------------------------|-----------------------------|-----------------|---------|
| 1 / 1.13 | 122 | 238 | 238 | 477 | 0.255 | |
| 2 / 1.81 | 111 | 238 | 238 | 477 | 0.233 | |
| 3 / 2.50 | 101 | 238 | 238 | 477 | 0.211 | |
| 4 / 3.18 | 90 | 238 | 238 | 477 | 0.189 | |
| 5 / 3.86 | 79 | 238 | 238 | 477 | 0.166 | |
| 6 / 4.55 | 69 | 238 | 238 | 477 | 0.144 | |
| 7 / 5.23 | 58 | 238 | 238 | 477 | 0.122 | |
| 8 / 5.92 | 48 | 238 | 238 | 477 | 0.100 | |
| 9 / 6.60 | 37 | 238 | 238 | 477 | 0.078 | |
| 10 / 7.29 | 35 | 238 | 238 | 477 | 0.073 | |
| 11 / 7.97 | 35 | 238 | 238 | 477 | 0.073 | |
| 12 / 8.66 | 35 | 238 | 238 | 477 | 0.073 | |
| 13 / 9.34 | 35 | 238 | 238 | 477 | 0.073 | |

File Name :

FB3EAM3 V 3. 2. 234

| No. / Dist.(m) | Applied Shear (kN) | Shear Cap. TOP (kN) | Shear Cap. BOTTOM (kN) | Shear Cap. Total (kN) | Unity Factor | Remarks |
|----------------|--------------------|---------------------|------------------------|-----------------------|--------------|---------|
| 14 / 10.03 | 35 | 238 | 238 | 477 | 0.073 | |
| 15 / 10.71 | 35 | 238 | 238 | 477 | 0.073 | |
| 16 / 11.40 | 37 | 238 | 238 | 477 | 0.078 | |
| 17 / 12.08 | 48 | 238 | 238 | 477 | 0.100 | |
| 18 / 12.77 | 58 | 238 | 238 | 477 | 0.122 | |
| 19 / 13.45 | 69 | 238 | 238 | 477 | 0.144 | |
| 20 / 14.14 | 79 | 238 | 238 | 477 | 0.166 | |
| 21 / 14.82 | 90 | 238 | 238 | 477 | 0.189 | |
| 22 / 15.51 | 101 | 238 | 238 | 477 | 0.211 | |
| 23 / 16.19 | 111 | 238 | 238 | 477 | 0.233 | |
| 24 / 16.88 | 122 | 238 | 238 | 477 | 0.255 | |

CS: INTERACTION OF BENDING MOMENT AND VERTICAL SHEAR :

| No. / Dist.(m) | Applied Shear (kN) | Shear Capacity (kN) | te (mm) | Modulus (cm ³) | Applied Moment (kNm) | Moment Capacity (kNm) | Unity Factor | Remarks |
|----------------|--------------------|---------------------|---------|----------------------------|----------------------|-----------------------|--------------|---------|
| 1 / 1.13 | 122 (L) | 477 | 12.0 | 6543.1 | 146.6 | 2257.4 | 0.065 | |
| 2 / 1.81 | 111 (L) | 477 | 12.0 | 6543.1 | 226.5 | 2257.4 | 0.100 | |
| 3 / 2.50 | 101 (L) | 477 | 12.0 | 6543.1 | 298.9 | 2257.4 | 0.132 | |
| 4 / 3.18 | 90 (L) | 477 | 12.0 | 6543.1 | 364.0 | 2257.4 | 0.161 | |
| 5 / 3.86 | 79 (L) | 477 | 12.0 | 6543.1 | 422.0 | 2257.4 | 0.187 | |
| 6 / 4.55 | 69 (L) | 477 | 12.0 | 6543.1 | 472.7 | 2257.4 | 0.209 | |
| 7 / 5.23 | 58 (L) | 477 | 12.0 | 6543.1 | 516.2 | 2257.4 | 0.229 | |
| 8 / 5.92 | 48 (L) | 477 | 12.0 | 6543.1 | 552.4 | 2257.4 | 0.245 | |
| 9 / 6.60 | 37 (L) | 477 | 12.0 | 6543.1 | 581.4 | 2257.4 | 0.258 | |
| 10 / 7.29 | 26 (L) | 477 | 12.0 | 6543.1 | 603.2 | 2257.4 | 0.267 | |
| 11 / 7.97 | 16 (L) | 477 | 12.0 | 6543.1 | 617.8 | 2257.4 | 0.274 | |
| 12 / 8.66 | 5 (L) | 477 | 12.0 | 6543.1 | 625.1 | 2257.4 | 0.277 | |
| 13 / 9.34 | 5 (L) | 477 | 12.0 | 6543.1 | 625.1 | 2257.4 | 0.277 | |
| 14 / 10.03 | 16 (L) | 477 | 12.0 | 6543.1 | 617.8 | 2257.4 | 0.274 | |
| 15 / 10.71 | 26 (L) | 477 | 12.0 | 6543.1 | 603.2 | 2257.4 | 0.267 | |
| 16 / 11.40 | 37 (L) | 477 | 12.0 | 6543.1 | 581.4 | 2257.4 | 0.258 | |
| 17 / 12.08 | 48 (L) | 477 | 12.0 | 6543.1 | 552.4 | 2257.4 | 0.245 | |
| 18 / 12.77 | 58 (L) | 477 | 12.0 | 6543.1 | 516.2 | 2257.4 | 0.229 | |
| 19 / 13.45 | 69 (L) | 477 | 12.0 | 6543.1 | 472.7 | 2257.4 | 0.209 | |
| 20 / 14.14 | 79 (L) | 477 | 12.0 | 6543.1 | 422.0 | 2257.4 | 0.187 | |
| 21 / 14.82 | 90 (L) | 477 | 12.0 | 6543.1 | 364.0 | 2257.4 | 0.161 | |
| 22 / 15.51 | 101 (L) | 477 | 12.0 | 6543.1 | 298.9 | 2257.4 | 0.132 | |
| 23 / 16.19 | 111 (L) | 477 | 12.0 | 6543.1 | 226.5 | 2257.4 | 0.100 | |
| 24 / 16.88 | 122 (L) | 477 | 12.0 | 6543.1 | 146.6 | 2257.4 | 0.065 | |

CS: VIERENDEEL BENDING CHECK :

| No. / Dist.(m) | leff (mm) | Applied Shear (kN) | Vierendeel Moment (kNm) | Vierendeel Capacity (kNm) | Unity Factor | Remarks |
|----------------|-----------|--------------------|-------------------------|---------------------------|--------------|---------|
| 1 / 1.13 | 225.0 | 121.7 | 27.4 | 167.0 | 0.164 | |
| 2 / 1.81 | 225.0 | 111.1 | 25.0 | 166.0 | 0.151 | |
| 3 / 2.50 | 225.0 | 100.6 | 22.6 | 164.7 | 0.137 | |
| 4 / 3.18 | 225.0 | 90.0 | 20.2 | 163.3 | 0.124 | |
| 5 / 3.86 | 225.0 | 79.4 | 17.9 | 161.8 | 0.110 | |
| 6 / 4.55 | 225.0 | 68.8 | 15.5 | 160.3 | 0.097 | |
| 7 / 5.23 | 225.0 | 58.2 | 13.1 | 158.9 | 0.082 | |
| 8 / 5.92 | 225.0 | 47.6 | 10.7 | 157.6 | 0.068 | |
| 9 / 6.60 | 225.0 | 37.1 | 8.3 | 156.6 | 0.053 | |
| 10 / 7.29 | 225.0 | 26.5 | 7.8 | 155.7 | 0.050 | |
| 11 / 7.97 | 225.0 | 15.9 | 7.8 | 155.1 | 0.050 | |
| 12 / 8.66 | 225.0 | 5.3 | 7.8 | 154.8 | 0.051 | |
| 13 / 9.34 | 225.0 | 5.3 | 7.8 | 154.8 | 0.051 | |
| 14 / 10.03 | 225.0 | 15.9 | 7.8 | 155.1 | 0.050 | |
| 15 / 10.71 | 225.0 | 26.5 | 7.8 | 155.7 | 0.050 | |
| 16 / 11.40 | 225.0 | 37.1 | 8.3 | 156.6 | 0.053 | |
| 17 / 12.08 | 225.0 | 47.6 | 10.7 | 157.6 | 0.068 | |
| 18 / 12.77 | 225.0 | 58.2 | 13.1 | 158.9 | 0.082 | |
| 19 / 13.45 | 225.0 | 68.8 | 15.5 | 160.3 | 0.097 | |
| 20 / 14.14 | 225.0 | 79.4 | 17.9 | 161.8 | 0.110 | |
| 21 / 14.82 | 225.0 | 90.0 | 20.2 | 163.3 | 0.124 | |

| No. / Dist.(m) | leff (mm) | Applied Shear (kN) | Vierendeel Moment (kNm) | Vierendeel Capacity (kNm) | Unity Factor | Remarks |
|----------------|-----------|--------------------|-------------------------|---------------------------|--------------|---------|
| 22 / 15.51 | 225.0 | 100.6 | 22.6 | 164.7 | 0.137 | |
| 23 / 16.19 | 225.0 | 111.1 | 25.0 | 166.0 | 0.151 | |
| 24 / 16.88 | 225.0 | 121.7 | 27.4 | 167.0 | 0.164 | |

CS: WEB BUCKLING AROUND OPENINGS :

| No. / Dist.(m) | Applied Shear (kN) | Buckling Stress (N/mm ²) | Buckling Capacity (kN) | Unity Factor | Remarks |
|----------------|--------------------|--------------------------------------|------------------------|--------------|---------|
| 1 / 1.13 | 60.0 | 203.7 | 287.2 | 0.209 | |
| 2 / 1.81 | 56.4 | 203.7 | 287.2 | 0.197 | |
| 3 / 2.50 | 51.1 | 203.7 | 287.2 | 0.178 | |
| 4 / 3.18 | 45.9 | 203.9 | 286.2 | 0.160 | |
| 5 / 3.86 | 40.6 | 203.7 | 287.2 | 0.141 | |
| 6 / 4.55 | 35.3 | 203.7 | 287.2 | 0.123 | |
| 7 / 5.23 | 30.0 | 203.7 | 287.2 | 0.104 | |
| 8 / 5.92 | 24.7 | 203.9 | 286.2 | 0.086 | |
| 9 / 6.60 | 19.4 | 203.7 | 287.2 | 0.068 | |
| 10 / 7.29 | 17.4 | 203.7 | 287.2 | 0.061 | |
| 11 / 7.97 | 17.4 | 203.7 | 287.2 | 0.061 | |
| 12 / 8.66 | 17.4 | 203.9 | 286.2 | 0.061 | |
| 13 / 9.34 | 17.4 | 203.9 | 286.2 | 0.061 | |
| 14 / 10.03 | 17.4 | 203.7 | 287.2 | 0.061 | |
| 15 / 10.71 | 17.4 | 203.7 | 287.2 | 0.061 | |
| 16 / 11.40 | 19.4 | 203.7 | 287.2 | 0.068 | |
| 17 / 12.08 | 24.7 | 203.9 | 286.2 | 0.086 | |
| 18 / 12.77 | 30.0 | 203.7 | 287.2 | 0.104 | |
| 19 / 13.45 | 35.3 | 203.7 | 287.2 | 0.123 | |
| 20 / 14.14 | 40.6 | 203.7 | 287.2 | 0.141 | |
| 21 / 14.82 | 45.9 | 203.9 | 286.2 | 0.160 | |
| 22 / 15.51 | 51.1 | 203.7 | 287.2 | 0.178 | |
| 23 / 16.19 | 56.4 | 203.7 | 287.2 | 0.197 | |
| 24 / 16.88 | 60.0 | 203.7 | 287.2 | 0.209 | |

CS: WEB POST HORIZONTAL SHEAR :

| Web Post | Pitch (mm) | Horizontal Force (kN) | Horz. Shear Capacity (kN) | Unity Factor | Remarks |
|----------|------------|-----------------------|---------------------------|--------------|---------|
| 0 / 1 | 1125 | N/A | N/A | N/A | N/A |
| 1 / 2 | 685 | 116 | 525 | 0.220 | |
| 2 / 3 | 685 | 105 | 525 | 0.200 | |
| 3 / 4 | 684 | 94 | 523 | 0.181 | |
| 4 / 5 | 685 | 84 | 525 | 0.160 | |
| 5 / 6 | 685 | 74 | 525 | 0.140 | |
| 6 / 7 | 685 | 63 | 525 | 0.120 | |
| 7 / 8 | 684 | 52 | 523 | 0.100 | |
| 8 / 9 | 685 | 42 | 525 | 0.080 | |
| 9 / 10 | 685 | 36 | 525 | 0.068 | |
| 10 / 11 | 685 | 35 | 525 | 0.066 | |
| 11 / 12 | 685 | 35 | 525 | 0.066 | |
| 12 / 13 | 684 | 34 | 523 | 0.066 | |
| 13 / 14 | 685 | 35 | 525 | 0.066 | |
| 14 / 15 | 685 | 35 | 525 | 0.066 | |
| 15 / 16 | 685 | 36 | 525 | 0.068 | |
| 16 / 17 | 685 | 42 | 525 | 0.080 | |
| 17 / 18 | 684 | 52 | 523 | 0.100 | |
| 18 / 19 | 685 | 63 | 525 | 0.120 | |
| 19 / 20 | 685 | 74 | 525 | 0.140 | |
| 20 / 21 | 685 | 84 | 525 | 0.160 | |
| 21 / 22 | 684 | 94 | 523 | 0.181 | |
| 22 / 23 | 685 | 105 | 525 | 0.200 | |
| 23 / 24 | 685 | 116 | 525 | 0.220 | |

CS: WEB POST FLEXURAL CHECK :

| Web Post | Pitch (mm) | Applied Moment (kNm) | Moment Capacity (kNm) | Unity Factor | Remarks |
|----------|------------|----------------------|-----------------------|--------------|---------|
| 0 / 1 | 1125 | N/A | N/A | N/A | N/A |
| 1 / 2 | 685 | 26 | 146 | 0.178 | |
| 2 / 3 | 685 | 24 | 146 | 0.162 | |
| 3 / 4 | 684 | 21 | 145 | 0.146 | |
| 4 / 5 | 685 | 19 | 146 | 0.130 | |
| 5 / 6 | 685 | 17 | 146 | 0.113 | |
| 6 / 7 | 685 | 14 | 146 | 0.097 | |
| 7 / 8 | 684 | 12 | 145 | 0.081 | |
| 8 / 9 | 685 | 9 | 146 | 0.065 | |
| 9 / 10 | 685 | 8 | 146 | 0.055 | |
| 10 / 11 | 685 | 8 | 146 | 0.053 | |
| 11 / 12 | 685 | 8 | 146 | 0.053 | |
| 12 / 13 | 684 | 8 | 145 | 0.053 | |
| 13 / 14 | 685 | 8 | 146 | 0.053 | |
| 14 / 15 | 685 | 8 | 146 | 0.053 | |
| 15 / 16 | 685 | 8 | 146 | 0.055 | |
| 16 / 17 | 685 | 9 | 146 | 0.065 | |
| 17 / 18 | 684 | 12 | 145 | 0.081 | |
| 18 / 19 | 685 | 14 | 146 | 0.097 | |
| 19 / 20 | 685 | 17 | 146 | 0.113 | |
| 20 / 21 | 685 | 19 | 146 | 0.130 | |
| 21 / 22 | 684 | 21 | 145 | 0.146 | |
| 22 / 23 | 685 | 24 | 146 | 0.162 | |
| 23 / 24 | 685 | 26 | 146 | 0.178 | |

CS: DETAILED CALCULATION AT THE CRITICAL OPENING (NO.12) :**CS: VERTICAL SHEAR CHECK :**

Applied shear = 34.78 kN
 Shear capacity (top tee) = $0.6 * 345.0 * 96.00 * 12.00 / 1000$
 = 238.46 kN
 Shear capacity (btm tee) = $0.6 * 345.0 * 96.00 * 12.00 / 1000$
 = 238.46 kN
 Total Shear Capacity = 476.93 kN
 UNITY FACTOR = $34.78 \text{ kN} / 476.93$
 = 0.073

PASS**CS: INTERACTION OF BENDING MOMENT AND VERTICAL SHEAR :**

Applied moment = 625.09 kNm
 Co-existent shear = 5.29 kN

CHECK VERTICAL SHEAR CAPACITY :

Shear capacity (steel section) = 476.93 kN
 UNITY FACTOR = $5.29 / 476.93$
 = 0.011 (**low shear)
 No reduction in moment capacity of section due to shear

FIREBEAM 690 x 370/370 x 179.9kg/m S355 FB120 x 1.90 R120

Page 25



ARUP
Prepared By: Arup

CHECK BENDING CAPACITY :

Plastic modulus (steel section) = 6543.1 cm³ (includes effective web thickness)

Plastic neutral axis is 345.0 mm from beam top flange

Section bending capacity = 6543.1 * 345.0 / 1000

= 2257.36 kNm

UNITY FACTOR = 625.09 / 2257.36

= 0.277

PASS

SERVICEABILITY LIMIT STATE CHECKS

SS: CONCRETE COMPRESSIVE STRESS CHECK :

| | |
|--|----------------------------|
| Critical location is at mid-span | |
| Applied moment (major axis) | = 556.88 kNm (at mid-span) |
| Elastic neutral axis is in WEB (245.1 mm from top of slab) | |
| Moment of inertia (cracked section) | = 468067 cm ⁴ |
| Concrete modulus | = 190957 cm ³ |
| Concrete compressive stress | = 556.9 / 190957.2 * 1000 |
| | = 2.92 N/mm ² |
| UNITY FACTOR | = 2.92 / (0.5 * 40.0) |
| | = 0.146 |

PASS

SS: STEEL STRESSES :

SS: CONSTRUCTION STAGE (stresses due to self weight) :

| | |
|---|----------------------------|
| Critical location is at mid-span | |
| Applied moment | = 382.86 kNm (at mid-span) |
| Elastic neutral axis is in WEB (345.0mm from beam top flange) | |
| Moment of inertia (steel section) | = 223485 cm ⁴ |
| Steel modulus (top) | = 6478 cm ³ |
| Compression (top) | = 382.9 / 6477.8 * 1000 |
| | = 59.1 N/mm ² |
| Steel modulus (btm) | = 6478 cm ³ |
| Tension (btm) | = 382.9 / 6477.8 * 1000 |
| | = 59.1 N/mm ² |

SS: NORMAL STAGE :

| | |
|--|----------------------------|
| Applied moment (major axis) | = 556.88 kNm (at mid-span) |
| Elastic neutral axis is in WEB (245.1 mm from top of slab) | |
| Steel modulus (top) | = 40660 cm ³ |
| Steel stress (top - compression) | = 556.9 / 40660.5 * 1000 |
| | = 13.70 N/mm ² |
| Steel modulus (btm) | = 8142 cm ³ |
| Steel stress (btm - tension) | = 556.9 / 8141.9 * 1000 |
| | = 68.4 N/mm ² |

SS: STEEL TENSILE STRESS CHECK :

Tension (at bottom of beam) = $59.10 + 68.40$
 = 127.50 N/mm^2
 UNITY FACTOR = $127.50 / 345.0$
 = 0.370

PASS

SS: STEEL COMPRESSIVE STRESS CHECK:

Compression (at top of beam) = $59.10 + 13.70$
 = 72.80 N/mm^2
 UNITY FACTOR = $72.80 / 345.0$
 = 0.211

PASS



SS: VIBRATION CHECK :

SS: DYNAMIC SENSITIVITY :

| | |
|-------------------------------------|--|
| Dynamic inertia (uncracked section) | = 522283 cm ⁴ (at mid-span) |
| Maximum deflection | = 15.27 mm |
| Frequency | = 18 / SQR(15.27) |
| | = 4.61 Hz (greater than 4.00 Hz) |

SATISFACTORY

NOTES :

Loads are dead + super-imposed dead + 10% imposed

A more rigorous approach based on energy principles gives the natural frequency of the beam as 4.91 Hz. Refer to program HELP for details.

**SS: DEFLECTION CHECKS :****SS: SELF WEIGHT DEFLECTION (CS) :**

Critical location is at mid-span
 Inertia (steel section) = 223485 cm⁴
 Maximum deflection = 28.69 mm
 Additional deflection = 5.61 mm (due to openings)
 Total deflection = 28.69 + 5.61
 = 34.30 mm

SS: DEFLECTION DUE TO IMPOSED LOADS (NS) :

Critical location is at mid-span
 Inertia (uncracked section) = 468067 cm⁴
 Maximum deflection = 17.82 mm
 Additional deflection = 3.49 mm (due to openings)
 Total deflection = 17.82 + 3.49
 = 21.30 mm (< SPAN / 360 i.e 50.0 mm)

SATISFACTORY**SS: DEFLECTION DUE TO SUPERIMPOSED DEAD LOADS (NS) :**

Critical location is at mid-span
 Inertia (uncracked section) = 468067 cm⁴
 Maximum deflection = 1.78 mm
 Additional deflection = 0.35 mm (due to openings)
 Total deflection = 1.78 + 0.35
 = 2.13 mm

SS: TOTAL DEFLECTION CHECK :

Critical location is at mid-span
 Total deflection = 34.30 + 21.30 + 2.13
 = 57.74 mm (< SPAN / 200 = 90.0 mm)

SATISFACTORY**NOTES :**

1. The components of total deflection are the values at the position of maximum total deflection, not always the sum of the individual critical components.
2. If precamber is specified the minimum recommended camber is L/250 or 20mm whichever is greater.
 Camber tolerance is +/- L/500

FIRE LIMIT STATE CHECKS (LONG OUTPUT)

FIRE PROTECTION :

FB120. (Data Version No. 4, 14 January 02).

FIRE: GENERAL NOTES :

1. All deck voids must be filled for the fire analysis results to be valid
2. All distance measurements from LHS
3. For section dimensions see normal design checks
4. All unity factors are calculated relative to the user specified protection thickness
5. The thickness of fire protection is the required thickness
6. Where t is given as > 2.2 then the required protection exceeds the maximum protection thickness available.

FIRE: CHECKS ON FULL SECTION (PLAIN BEAM):

| No. / Dist.(m) | Applied Shear / Shear Capacity (kN) | Unity Factor | Applied Moment / Bending Resistance (kNm) | Unity Factor | Protection Thickness (mm) |
|----------------|-------------------------------------|--------------|---|--------------|---------------------------|
| 1 / 0.00 | 191 / 842 | 0.227 | 0 / 874 | 0.000 | 0.90 |
| 2 / 0.36 | 183 / 711 | 0.258 | 67 / 806 | 0.084 | 1.00 |
| 3 / 0.72 | 176 / 580 | 0.303 | 132 / 798 | 0.165 | 1.05 |
| 4 / 1.08 | 168 / 569 | 0.295 | 194 / 827 | 0.234 | 1.05 |
| 5 / 1.44 | 160 / 569 | 0.282 | 253 / 868 | 0.291 | 1.10 |
| 6 / 1.80 | 153 / 569 | 0.268 | 309 / 900 | 0.343 | 1.10 |
| 7 / 2.16 | 145 / 569 | 0.255 | 363 / 931 | 0.389 | 1.15 |
| 8 / 2.52 | 137 / 569 | 0.241 | 414 / 964 | 0.429 | 1.20 |
| 9 / 2.88 | 130 / 569 | 0.228 | 462 / 992 | 0.465 | 1.30 |
| 10 / 3.24 | 122 / 569 | 0.215 | 507 / 1013 | 0.500 | 1.35 |
| 11 / 3.60 | 114 / 569 | 0.201 | 550 / 1030 | 0.533 | 1.40 |
| 12 / 3.96 | 107 / 569 | 0.188 | 589 / 1044 | 0.565 | 1.45 |
| 13 / 4.32 | 99 / 569 | 0.174 | 627 / 1056 | 0.594 | 1.45 |
| 14 / 4.68 | 92 / 569 | 0.161 | 661 / 1065 | 0.620 | 1.50 |
| 15 / 5.04 | 84 / 569 | 0.148 | 692 / 1074 | 0.645 | 1.50 |
| 16 / 5.40 | 76 / 569 | 0.134 | 721 / 1081 | 0.667 | 1.55 |
| 17 / 5.76 | 69 / 569 | 0.121 | 747 / 1087 | 0.687 | 1.55 |
| 18 / 6.12 | 61 / 569 | 0.107 | 771 / 1093 | 0.705 | 1.60 |
| 19 / 6.48 | 53 / 569 | 0.094 | 791 / 1098 | 0.721 | 1.60 |
| 20 / 6.84 | 46 / 569 | 0.080 | 809 / 1102 | 0.734 | 1.60 |
| 21 / 7.20 | 38 / 569 | 0.067 | 824 / 1106 | 0.745 | 1.65 |
| 22 / 7.56 | 31 / 569 | 0.054 | 837 / 1110 | 0.754 | 1.65 |
| 23 / 7.92 | 23 / 569 | 0.040 | 846 / 1113 | 0.760 | 1.65 |
| 24 / 8.28 | 15 / 569 | 0.027 | 853 / 1116 | 0.764 | 1.65 |
| 25 / 8.64 | 8 / 569 | 0.013 | 857 / 1119 | 0.766 | 1.65 |
| 26 / 9.00 | 0 / 569 | 0.000 | 859 / 1121 | 0.766 | 1.65 |
| 27 / 9.36 | 8 / 569 | 0.013 | 857 / 1119 | 0.766 | 1.65 |
| 28 / 9.72 | 15 / 569 | 0.027 | 853 / 1116 | 0.764 | 1.65 |
| 29 / 10.08 | 23 / 569 | 0.040 | 846 / 1113 | 0.760 | 1.65 |
| 30 / 10.44 | 31 / 569 | 0.054 | 837 / 1110 | 0.754 | 1.65 |
| 31 / 10.80 | 38 / 569 | 0.067 | 824 / 1106 | 0.745 | 1.65 |
| 32 / 11.16 | 46 / 569 | 0.080 | 809 / 1102 | 0.734 | 1.60 |
| 33 / 11.52 | 53 / 569 | 0.094 | 791 / 1098 | 0.721 | 1.60 |
| 34 / 11.88 | 61 / 569 | 0.107 | 771 / 1093 | 0.705 | 1.60 |
| 35 / 12.24 | 69 / 569 | 0.121 | 747 / 1087 | 0.687 | 1.55 |
| 36 / 12.60 | 76 / 569 | 0.134 | 721 / 1081 | 0.667 | 1.55 |
| 37 / 12.96 | 84 / 569 | 0.148 | 692 / 1074 | 0.645 | 1.50 |
| 38 / 13.32 | 92 / 569 | 0.161 | 661 / 1065 | 0.620 | 1.50 |
| 39 / 13.68 | 99 / 569 | 0.174 | 627 / 1056 | 0.594 | 1.45 |
| 40 / 14.04 | 107 / 569 | 0.188 | 589 / 1044 | 0.565 | 1.45 |
| 41 / 14.40 | 114 / 569 | 0.201 | 550 / 1030 | 0.533 | 1.40 |
| 42 / 14.76 | 122 / 569 | 0.215 | 507 / 1013 | 0.500 | 1.35 |
| 43 / 15.12 | 130 / 569 | 0.228 | 462 / 992 | 0.465 | 1.30 |
| 44 / 15.48 | 137 / 569 | 0.241 | 414 / 964 | 0.429 | 1.20 |
| 45 / 15.84 | 145 / 569 | 0.255 | 363 / 931 | 0.389 | 1.15 |
| 46 / 16.20 | 153 / 569 | 0.268 | 309 / 900 | 0.343 | 1.10 |
| 47 / 16.56 | 160 / 569 | 0.282 | 253 / 868 | 0.291 | 1.10 |
| 48 / 16.92 | 168 / 569 | 0.295 | 194 / 827 | 0.234 | 1.05 |
| 49 / 17.28 | 176 / 580 | 0.303 | 132 / 798 | 0.165 | 1.05 |

File Name:

FBEAM3 V 3. 2. 234

| No. / Dist.(m) | Applied Shear / Shear Capacity (kN) | Unity Factor | Applied Moment / Bending Resistance (kNm) | Unity Factor | Protection Thickness (mm) |
|----------------|-------------------------------------|--------------|---|--------------|---------------------------|
| 50 / 17.64 | 183 / 711 | 0.258 | 67 / 806 | 0.084 | 1.00 |
| 51 / 18.00 | 191 / 842 | 0.227 | 0 / 874 | 0.000 | 0.90 |

FIRE: ADDITIONAL CHECKS AT OPENINGS :

| No. / Dist.(m) | Vertical Shear (kN) | | Global Moment (kNm) | | Vierendeel Moment (kNm) | | Web Buckling (kN) | | Horizontal Shear (kN) | | t (mm) |
|----------------|---------------------|--------------|---------------------|--------------|-------------------------|--------------|--------------------|--------------|-----------------------|--------------|--------|
| | Applied / Capacity | Unity Factor | Applied / Capacity | Unity Factor | Applied / Capacity | Unity Factor | Applied / Capacity | Unity Factor | Applied / Capacity | Unity Factor | |
| 1 / 1.13 | 167 / 242 | 0.689 | 201 / 650 | 0.309 | 38 / 80 | 0.468 | 73 / 79 | 0.918 | 250 / 466 | 0.535 | 1.85 |
| 2 / 1.81 | 152 / 242 | 0.629 | 311 / 604 | 0.515 | 34 / 69 | 0.500 | - | - | - | - | 1.75 |
| 3 / 2.50 | 138 / 240 | 0.574 | 410 / 687 | 0.597 | 31 / 80 | 0.389 | - | - | - | - | 1.60 |
| 4 / 3.18 | 123 / 234 | 0.528 | 499 / 735 | 0.679 | 28 / 67 | 0.417 | - | - | - | - | 1.70 |
| 5 / 3.86 | 109 / 228 | 0.478 | 579 / 775 | 0.747 | 25 / 65 | 0.375 | - | - | - | - | 1.80 |
| 6 / 4.55 | 94 / 223 | 0.424 | 648 / 815 | 0.796 | 21 / 76 | 0.279 | - | - | - | - | 1.80 |
| 7 / 5.23 | 80 / 218 | 0.366 | 708 / 853 | 0.830 | 18 / 63 | 0.284 | - | - | - | - | 1.85 |
| 8 / 5.92 | 65 / 215 | 0.305 | 758 / 862 | 0.879 | 15 / 74 | 0.198 | - | - | - | - | 1.85 |
| 9 / 6.60 | 51 / 212 | 0.240 | 798 / 868 | 0.918 | 11 / 62 | 0.185 | - | - | - | - | 1.85 |
| 10 / 7.29 | 36 / 210 | 0.173 | 827 / 874 | 0.947 | 8 / 73 | 0.112 | - | - | - | - | 1.90 |
| 11 / 7.97 | 22 / 208 | 0.105 | 847 / 878 | 0.965 | 5 / 61 | 0.080 | - | - | - | - | 1.90 |
| 12 / 8.66 | 7 / 208 | 0.035 | 857 / 882 | 0.972 | 2 / 61 | 0.027 | - | - | - | - | 1.90 |
| 13 / 9.34 | 7 / 208 | 0.035 | 857 / 882 | 0.972 | 2 / 61 | 0.027 | - | - | - | - | 1.90 |
| 14 / 10.03 | 22 / 208 | 0.105 | 847 / 878 | 0.965 | 5 / 61 | 0.080 | - | - | - | - | 1.90 |
| 15 / 10.71 | 36 / 210 | 0.173 | 827 / 874 | 0.947 | 8 / 73 | 0.112 | - | - | - | - | 1.90 |
| 16 / 11.40 | 51 / 212 | 0.240 | 798 / 868 | 0.918 | 11 / 62 | 0.185 | - | - | - | - | 1.85 |
| 17 / 12.08 | 65 / 215 | 0.305 | 758 / 862 | 0.879 | 15 / 74 | 0.198 | - | - | - | - | 1.85 |
| 18 / 12.77 | 80 / 218 | 0.366 | 708 / 853 | 0.830 | 18 / 63 | 0.284 | - | - | - | - | 1.85 |
| 19 / 13.45 | 94 / 223 | 0.424 | 648 / 815 | 0.796 | 21 / 76 | 0.279 | - | - | - | - | 1.80 |
| 20 / 14.14 | 109 / 228 | 0.478 | 579 / 775 | 0.747 | 25 / 65 | 0.375 | - | - | - | - | 1.80 |
| 21 / 14.82 | 123 / 234 | 0.528 | 499 / 735 | 0.679 | 28 / 67 | 0.417 | - | - | - | - | 1.70 |
| 22 / 15.51 | 138 / 240 | 0.574 | 410 / 687 | 0.597 | 31 / 80 | 0.389 | - | - | - | - | 1.60 |
| 23 / 16.19 | 152 / 242 | 0.629 | 311 / 604 | 0.515 | 34 / 69 | 0.500 | - | - | - | - | 1.75 |
| 24 / 16.88 | 167 / 242 | 0.689 | 201 / 650 | 0.309 | 38 / 80 | 0.468 | 73 / 79 | 0.918 | 250 / 466 | 0.535 | 1.85 |

FIRE: WEB POSTS :

| Web Post | Shear Connection (kN) | | Shear Buckling of Web Posts (kN) | | Resistance of Bottom Tee (kN) | | Resistance of Top Tee (kN) | | t (mm) |
|----------|-----------------------|--------------|----------------------------------|--------------|-------------------------------|--------------|----------------------------|--------------|--------|
| | Applied / Capacity | Unity Factor | Applied / Capacity | Unity Factor | Applied / Capacity | Unity Factor | Applied / Capacity | Unity Factor | |
| LH End | 359 / 1161 | 0.309 | - | - | 250 / 807 | 0.309 | 109 / 1855 | 0.059 | 1.85 |
| 1 : 2 | 636 / 774 | 0.822 | 84 / 84 | 1.000 | 333 / 812 | 0.410 | 662 / 1861 | 0.356 | 1.75 |
| 2 : 3 | 531 / 967 | 0.549 | 80 / 80 | 1.000 | 413 / 816 | 0.507 | 1113 / 1865 | 0.597 | 1.60 |
| 3 : 4 | 230 / 774 | 0.297 | 75 / 75 | 1.000 | 487 / 817 | 0.597 | 1268 / 1867 | 0.679 | 1.70 |
| 4 : 5 | 195 / 967 | 0.202 | 69 / 69 | 1.000 | 556 / 817 | 0.681 | 1394 / 1867 | 0.747 | 1.80 |
| 5 : 6 | 155 / 774 | 0.201 | 64 / 64 | 1.000 | 620 / 817 | 0.759 | 1486 / 1867 | 0.796 | 1.80 |
| 6 : 7 | 120 / 967 | 0.124 | 57 / 92 | 0.622 | 678 / 817 | 0.830 | 1549 / 1867 | 0.830 | 1.85 |
| 7 : 8 | 133 / 774 | 0.172 | 40 / 92 | 0.440 | 718 / 817 | 0.879 | 1641 / 1867 | 0.879 | 1.85 |
| 8 : 9 | 105 / 967 | 0.109 | 32 / 92 | 0.346 | 750 / 817 | 0.918 | 1714 / 1867 | 0.918 | 1.85 |
| 9 : 10 | 77 / 967 | 0.079 | 23 / 92 | 0.252 | 774 / 817 | 0.947 | 1768 / 1867 | 0.947 | 1.90 |
| 10 : 11 | 48 / 774 | 0.062 | 15 / 92 | 0.158 | 788 / 817 | 0.965 | 1801 / 1867 | 0.965 | 1.90 |
| 11 : 12 | 19 / 967 | 0.020 | 6 / 92 | 0.064 | 794 / 817 | 0.972 | 1814 / 1867 | 0.972 | 1.90 |
| 12 : 13 | 0 / 967 | 0.000 | 0 / 92 | 0.000 | 794 / 817 | 0.972 | 1814 / 1867 | 0.972 | 1.90 |
| 13 : 14 | 19 / 967 | 0.020 | 6 / 92 | 0.064 | 794 / 817 | 0.972 | 1814 / 1867 | 0.972 | 1.90 |
| 14 : 15 | 48 / 774 | 0.062 | 15 / 92 | 0.158 | 788 / 817 | 0.965 | 1801 / 1867 | 0.965 | 1.90 |
| 15 : 16 | 77 / 967 | 0.079 | 23 / 92 | 0.252 | 774 / 817 | 0.947 | 1768 / 1867 | 0.947 | 1.90 |
| 16 : 17 | 105 / 967 | 0.109 | 32 / 92 | 0.346 | 750 / 817 | 0.918 | 1714 / 1867 | 0.918 | 1.85 |
| 17 : 18 | 133 / 774 | 0.172 | 40 / 92 | 0.440 | 718 / 817 | 0.879 | 1641 / 1867 | 0.879 | 1.85 |
| 18 : 19 | 120 / 967 | 0.124 | 57 / 92 | 0.622 | 678 / 817 | 0.830 | 1549 / 1867 | 0.830 | 1.85 |
| 19 : 20 | 155 / 774 | 0.201 | 64 / 64 | 1.000 | 620 / 817 | 0.759 | 1486 / 1867 | 0.796 | 1.80 |
| 20 : 21 | 195 / 967 | 0.202 | 69 / 69 | 1.000 | 556 / 817 | 0.681 | 1394 / 1867 | 0.747 | 1.80 |
| 21 : 22 | 230 / 774 | 0.297 | 75 / 75 | 1.000 | 487 / 817 | 0.597 | 1268 / 1867 | 0.679 | 1.70 |
| 22 : 23 | 531 / 967 | 0.549 | 80 / 80 | 1.000 | 413 / 816 | 0.507 | 1113 / 1865 | 0.597 | 1.60 |
| 23 : 24 | 636 / 774 | 0.822 | 84 / 84 | 1.000 | 333 / 812 | 0.410 | 662 / 1861 | 0.356 | 1.75 |
| RH End | 359 / 1161 | 0.309 | - | - | 250 / 807 | 0.309 | 109 / 1855 | 0.059 | 1.85 |

FIRE: Opening Temperatures:

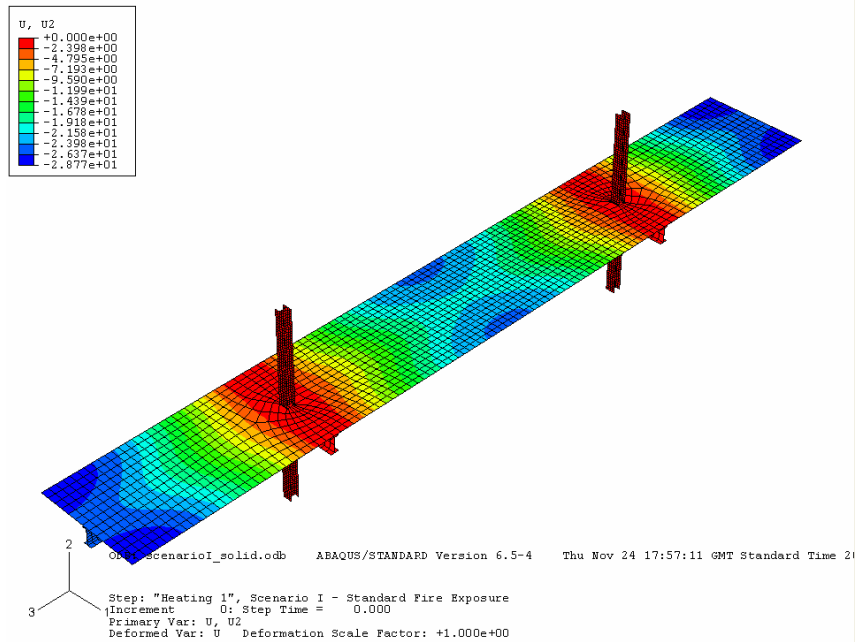
| No. / Dist.(m) | Top Flange | Web Top | Web Edge Top | Web Edge Bottom | Web Bottom | Bottom Flange | Stiffener Top | Stiffener Bottom |
|-------------------|---------------|------------|--------------------|-----------------------|---------------|------------------|------------------|---------------------|
| 1 / 1.13 | 564.000 | 704.000 | 774.400 | 809.600 | 739.200 | 694.000 | - | - |
| 2 / 1.81 | 564.000 | 704.000 | 774.400 | 809.600 | 739.200 | 694.000 | - | - |
| 3 / 2.50 | 564.000 | 704.000 | 774.400 | 809.600 | 739.200 | 694.000 | - | - |
| 4 / 3.18 | 564.000 | 704.000 | 774.400 | 809.600 | 739.200 | 694.000 | - | - |
| 5 / 3.86 | 564.000 | 704.000 | 774.400 | 809.600 | 739.200 | 694.000 | - | - |
| 6 / 4.55 | 564.000 | 704.000 | 774.400 | 809.600 | 739.200 | 694.000 | - | - |
| 7 / 5.23 | 564.000 | 704.000 | 774.400 | 809.600 | 739.200 | 694.000 | - | - |
| 8 / 5.92 | 564.000 | 704.000 | 774.400 | 809.600 | 739.200 | 694.000 | - | - |
| 9 / 6.60 | 564.000 | 704.000 | 774.400 | 809.600 | 739.200 | 694.000 | - | - |
| 10 / 7.29 | 564.000 | 704.000 | 774.400 | 809.600 | 739.200 | 694.000 | - | - |
| 11 / 7.97 | 564.000 | 704.000 | 774.400 | 809.600 | 739.200 | 694.000 | - | - |
| 12 / 8.66 | 564.000 | 704.000 | 774.400 | 809.600 | 739.200 | 694.000 | - | - |
| 13 / 9.34 | 564.000 | 704.000 | 774.400 | 809.600 | 739.200 | 694.000 | - | - |
| 14 / 10.03 | 564.000 | 704.000 | 774.400 | 809.600 | 739.200 | 694.000 | - | - |
| 15 / 10.71 | 564.000 | 704.000 | 774.400 | 809.600 | 739.200 | 694.000 | - | - |
| 16 / 11.40 | 564.000 | 704.000 | 774.400 | 809.600 | 739.200 | 694.000 | - | - |
| 17 / 12.08 | 564.000 | 704.000 | 774.400 | 809.600 | 739.200 | 694.000 | - | - |
| 18 / 12.77 | 564.000 | 704.000 | 774.400 | 809.600 | 739.200 | 694.000 | - | - |
| 19 / 13.45 | 564.000 | 704.000 | 774.400 | 809.600 | 739.200 | 694.000 | - | - |
| 20 / 14.14 | 564.000 | 704.000 | 774.400 | 809.600 | 739.200 | 694.000 | - | - |
| 21 / 14.82 | 564.000 | 704.000 | 774.400 | 809.600 | 739.200 | 694.000 | - | - |
| 22 / 15.51 | 564.000 | 704.000 | 774.400 | 809.600 | 739.200 | 694.000 | - | - |
| 23 / 16.19 | 564.000 | 704.000 | 774.400 | 809.600 | 739.200 | 694.000 | - | - |
| 24 / 16.88 | 564.000 | 704.000 | 774.400 | 809.600 | 739.200 | 694.000 | - | - |

APPENDIX C: Sample Input File (upon request)

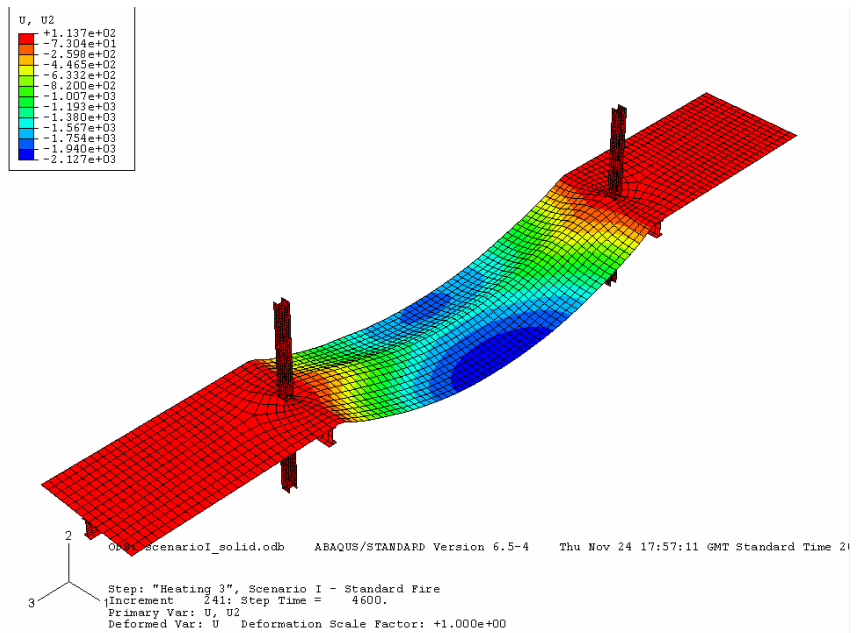
APPENDIX D: ABAQUS Structural Fire Analysis Data For Each Case Study

Solid Beam Model

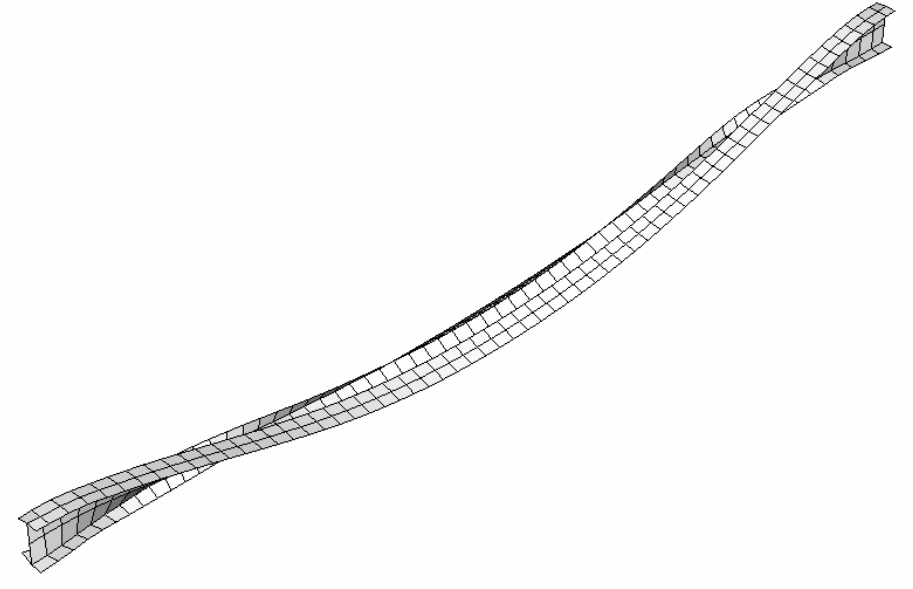
Displacement after Loading



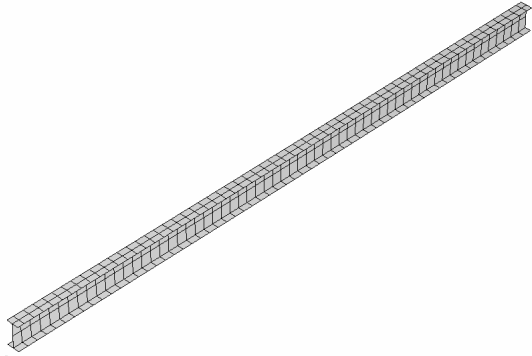
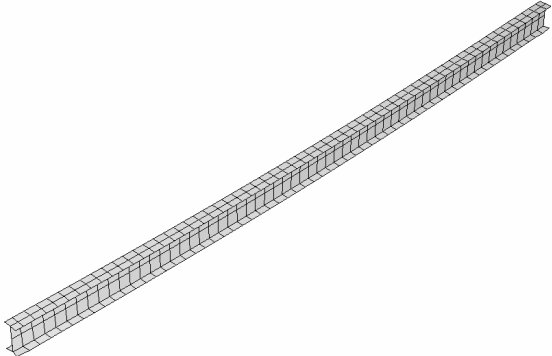
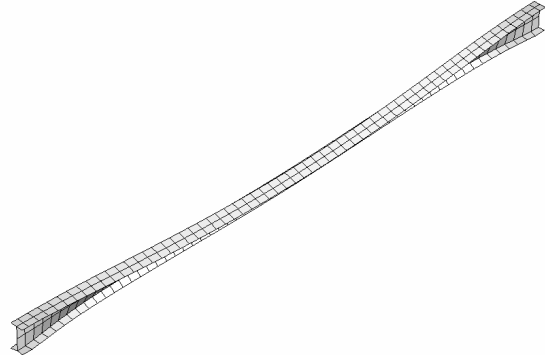
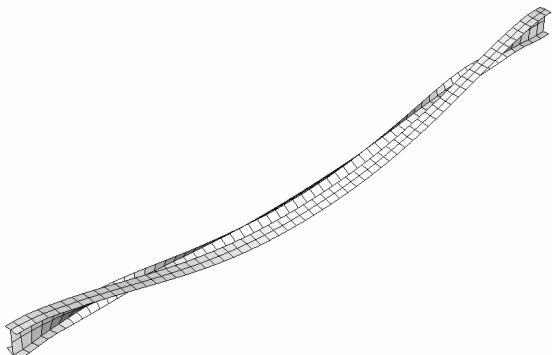
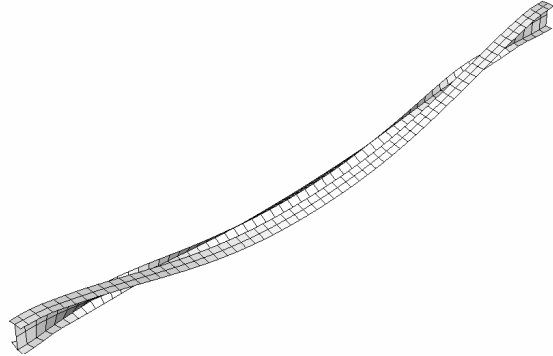
Displacement at end of simulation (time = 7200s)

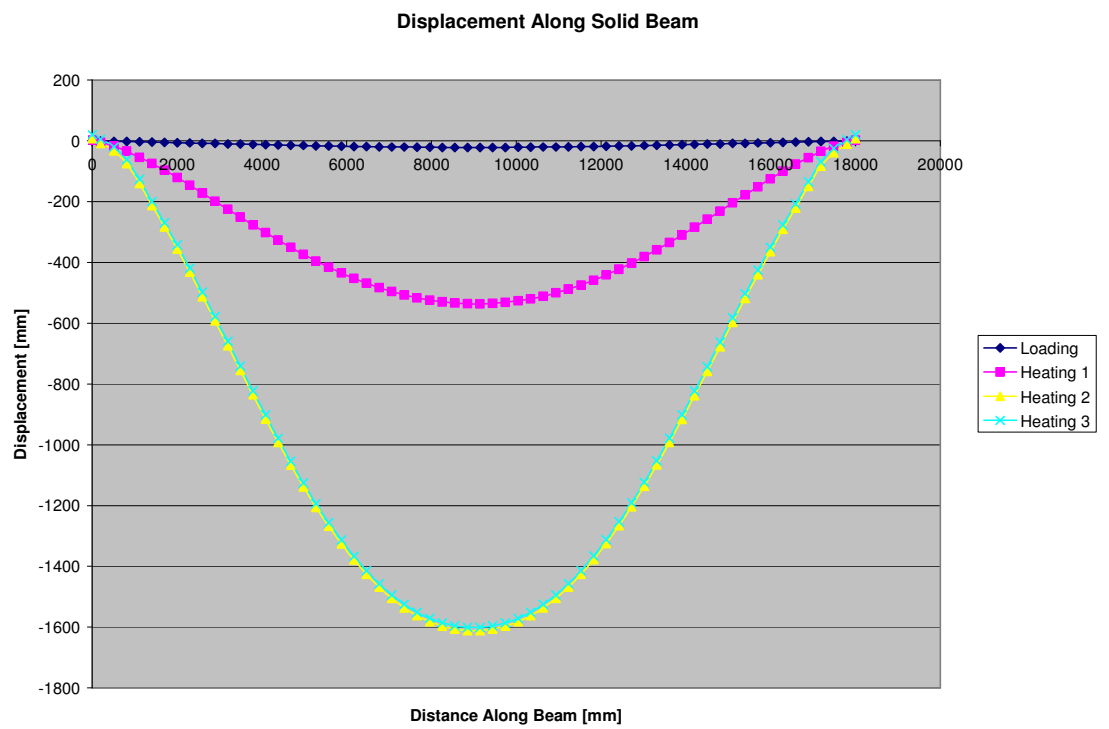
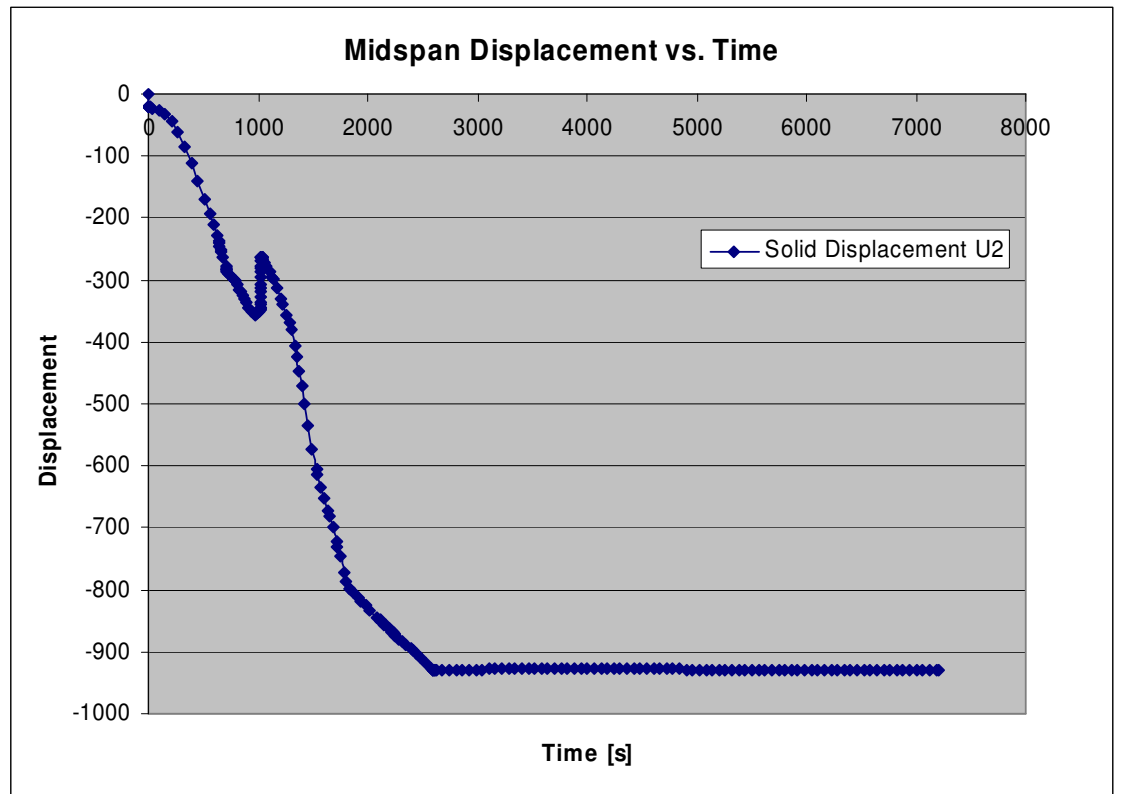


Deformation of solid beam at end of simulation (time = 7200s)

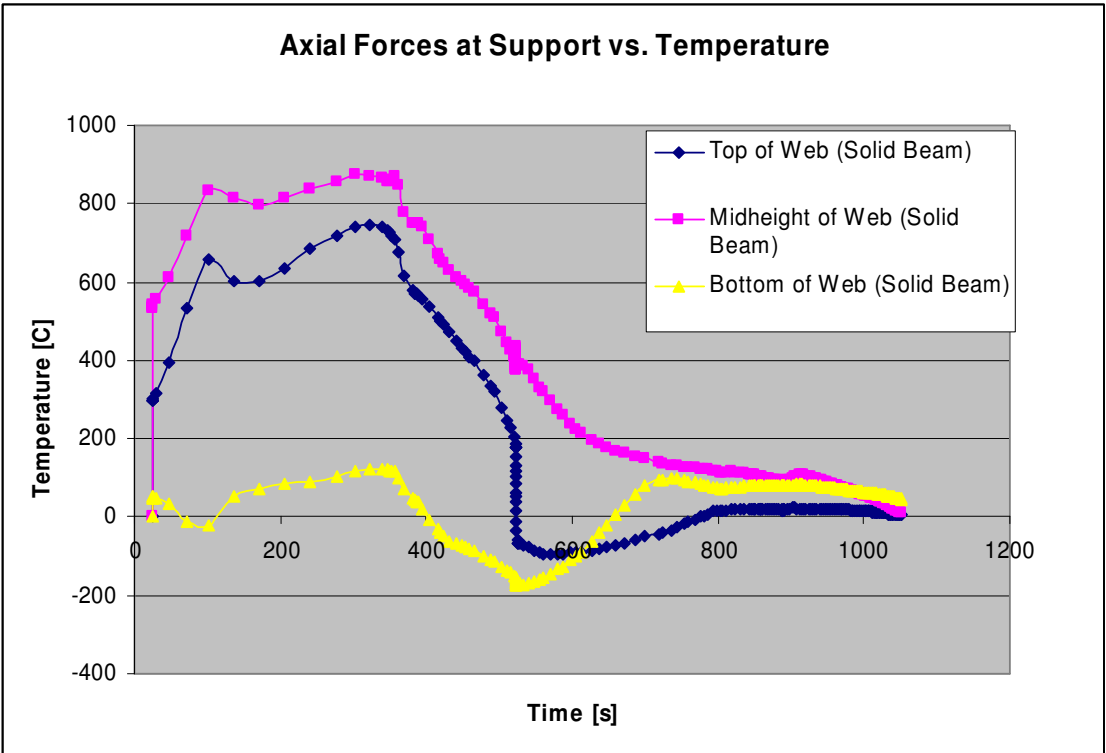
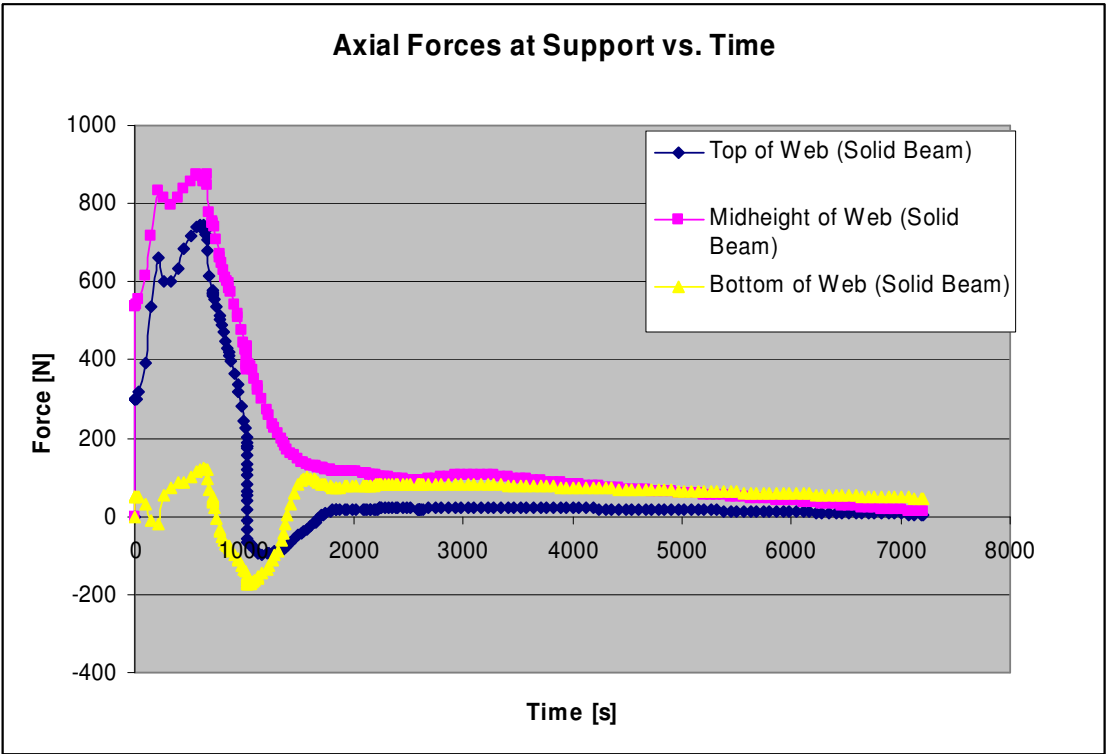


DEFORMATIONS: Solid Beam Model

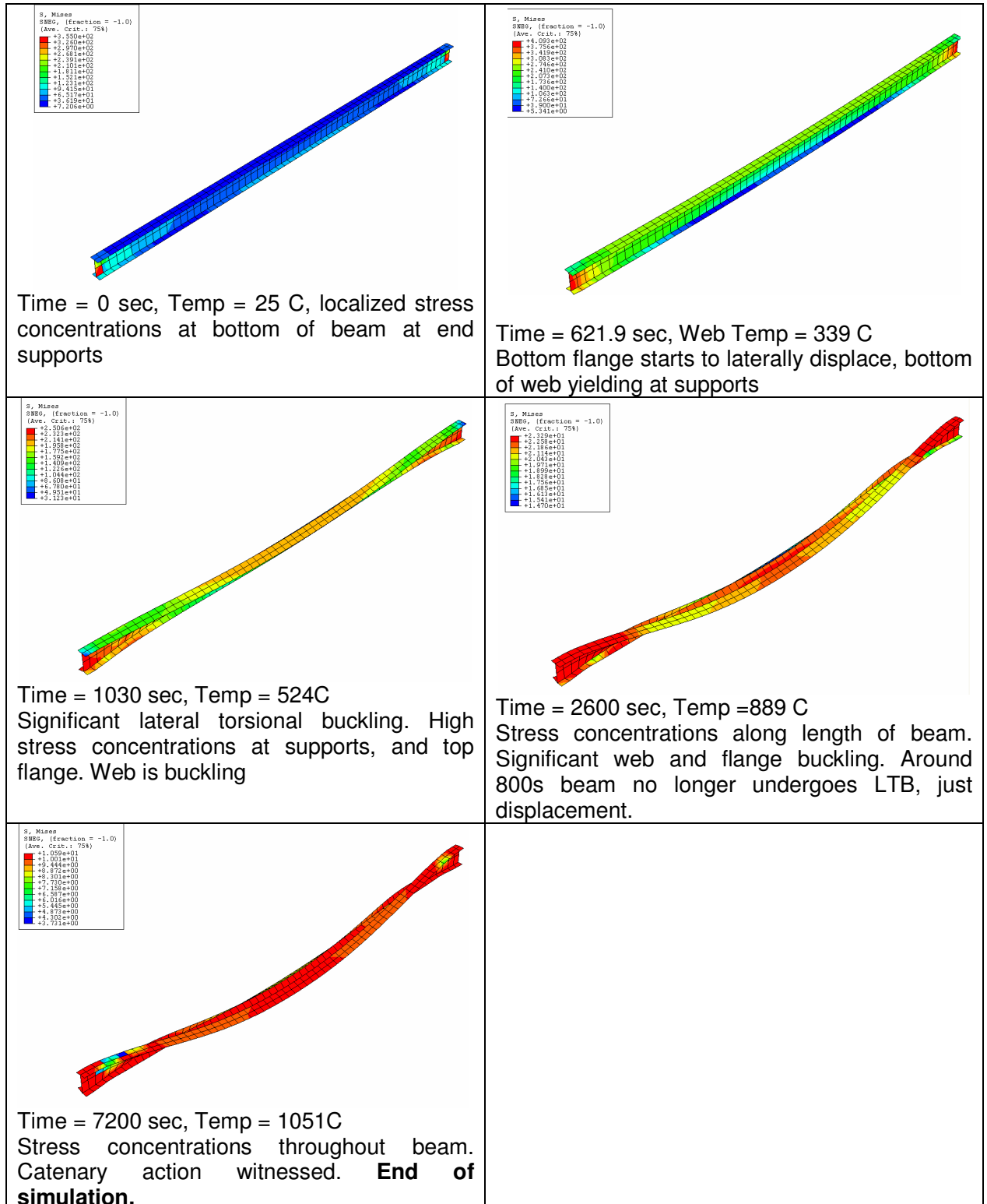
| | |
|--|--|
|  <p>Time = 0 sec, Temp = 25 C, localized stress concentrations at bottom of beam at end supports</p> |  <p>Time = 621.9 sec, Web Temp = 339 C Bottom flange starts to laterally displace, bottom of web yielding at supports</p> |
|  <p>Time = 1030 sec, Temp = 524C Significant lateral torsional buckling. High stress concentrations at supports, and top flange. Web is buckling</p> |  <p>Time = 2600 sec, Temp = 889 C Stress concentrations along length of beam. Significant web and flange buckling. Around 800s beam no longer undergoes LTB, just displacement.</p> |
|  <p>Time = 7200 sec, Temp = 1051C Stress concentrations throughout beam. Catenary action witnessed. End of simulation.</p> | |



Forces at Supports



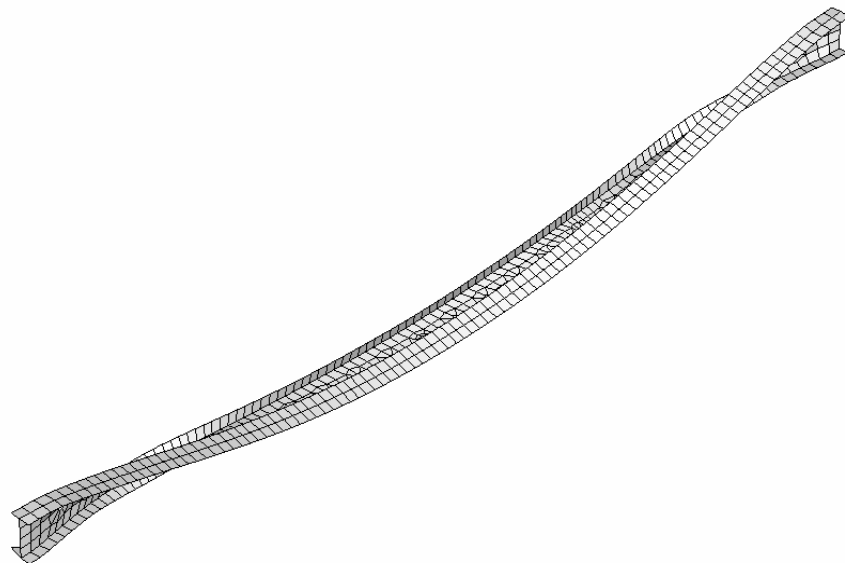
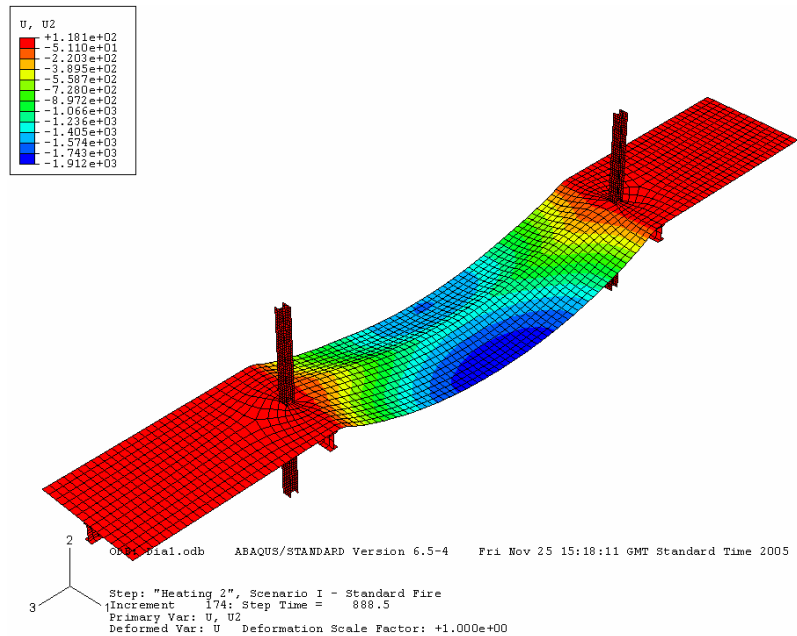
Solid Beam Case – Von Mises stresses



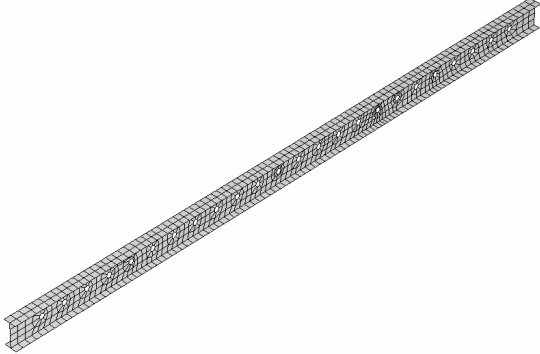
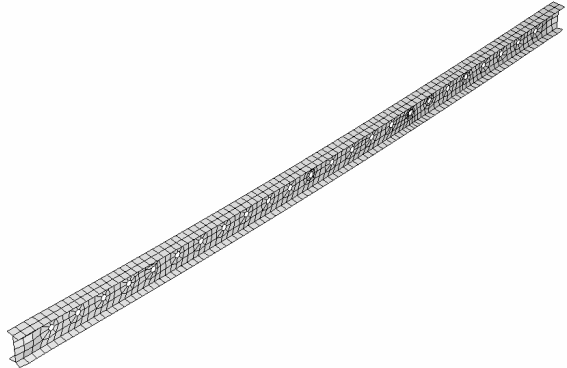
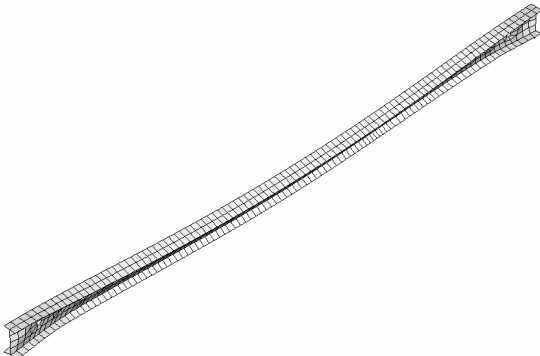
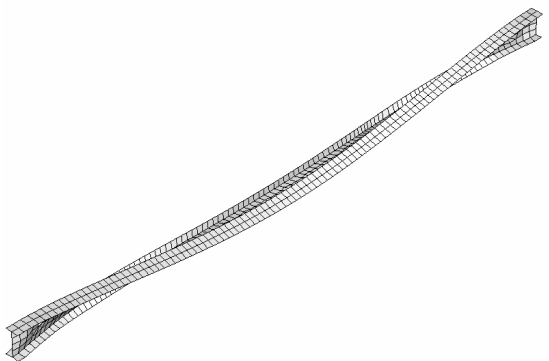
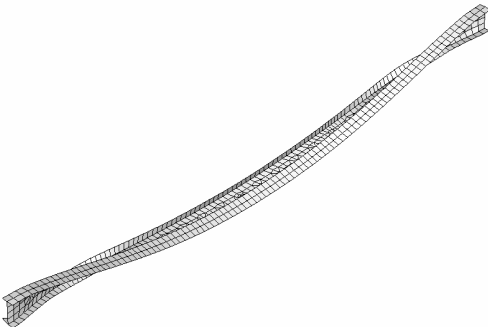
Scenario I – Case a.1

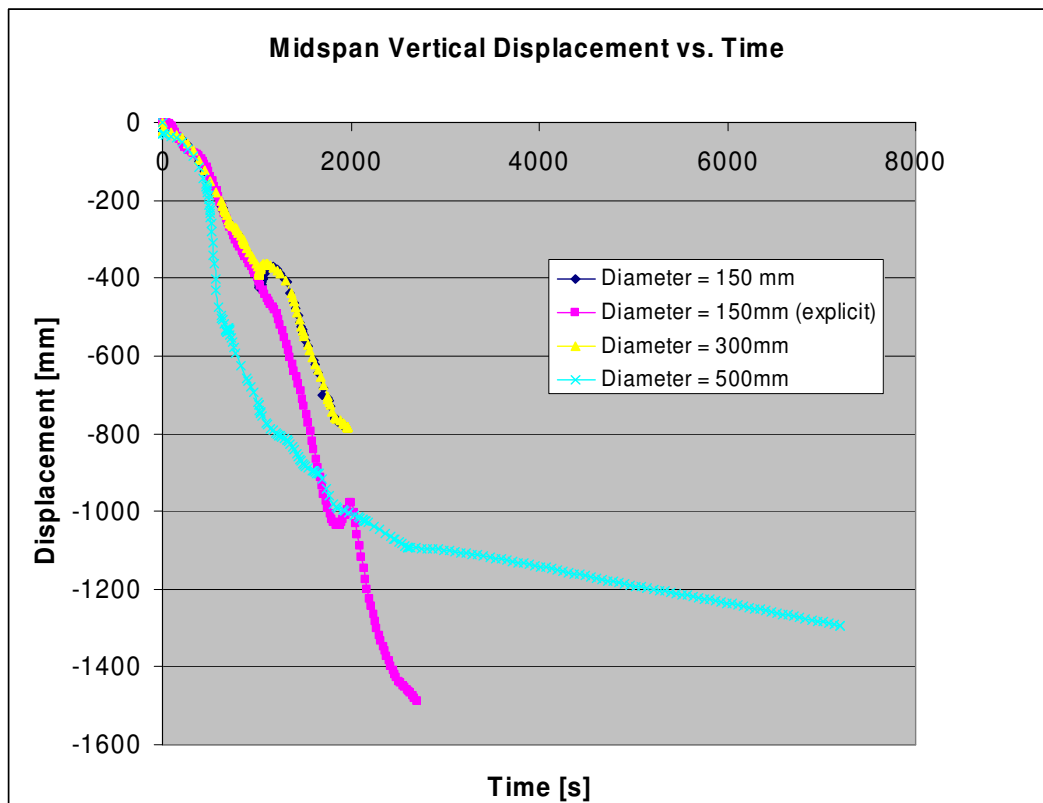
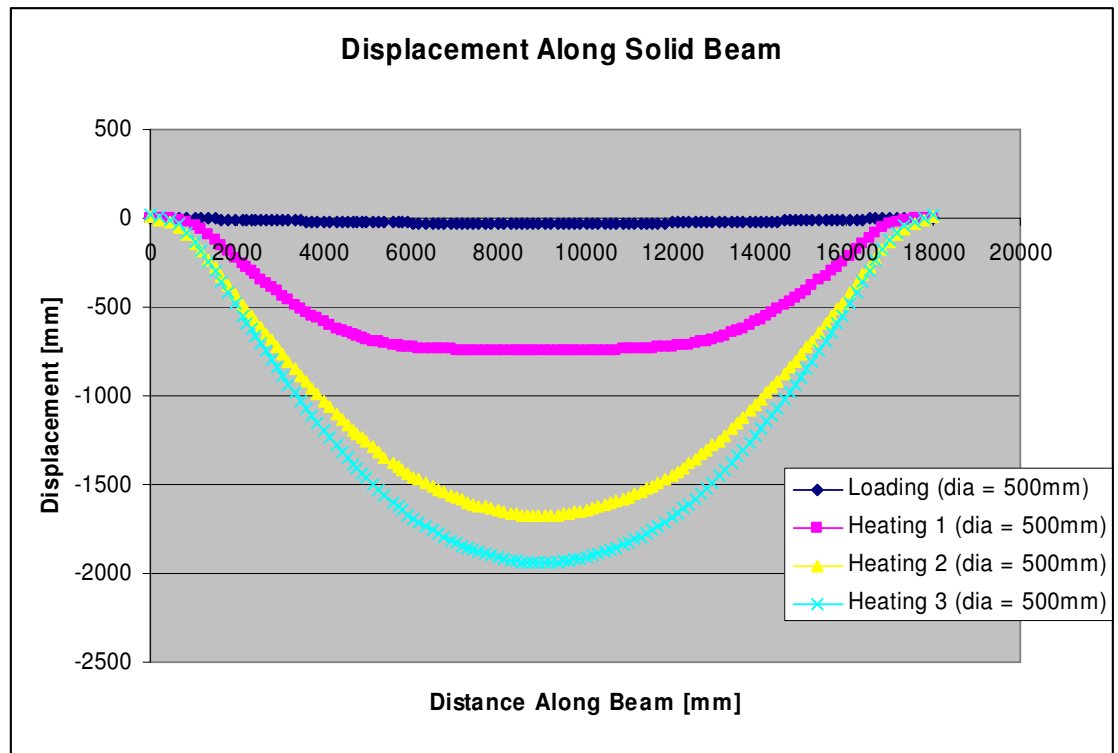
Case a.1 – Hole Diameter=150mm

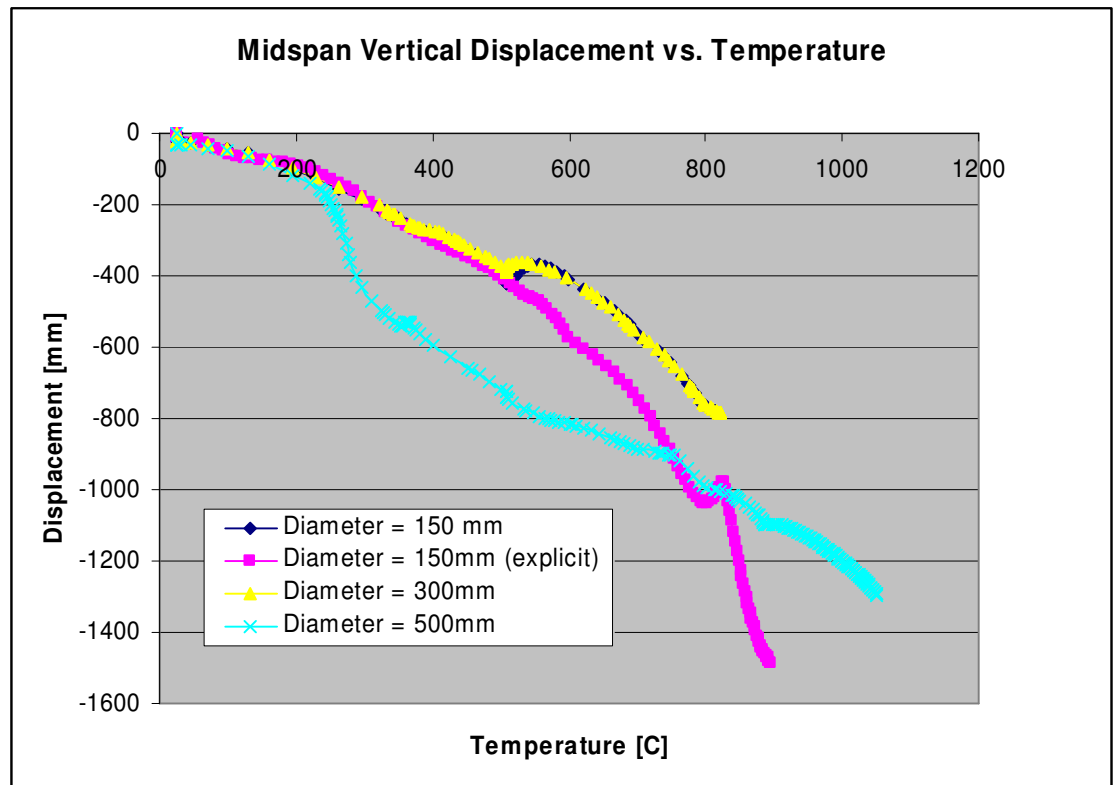
Displacement at end of simulation (t = 1918s, Temp = 812 C)



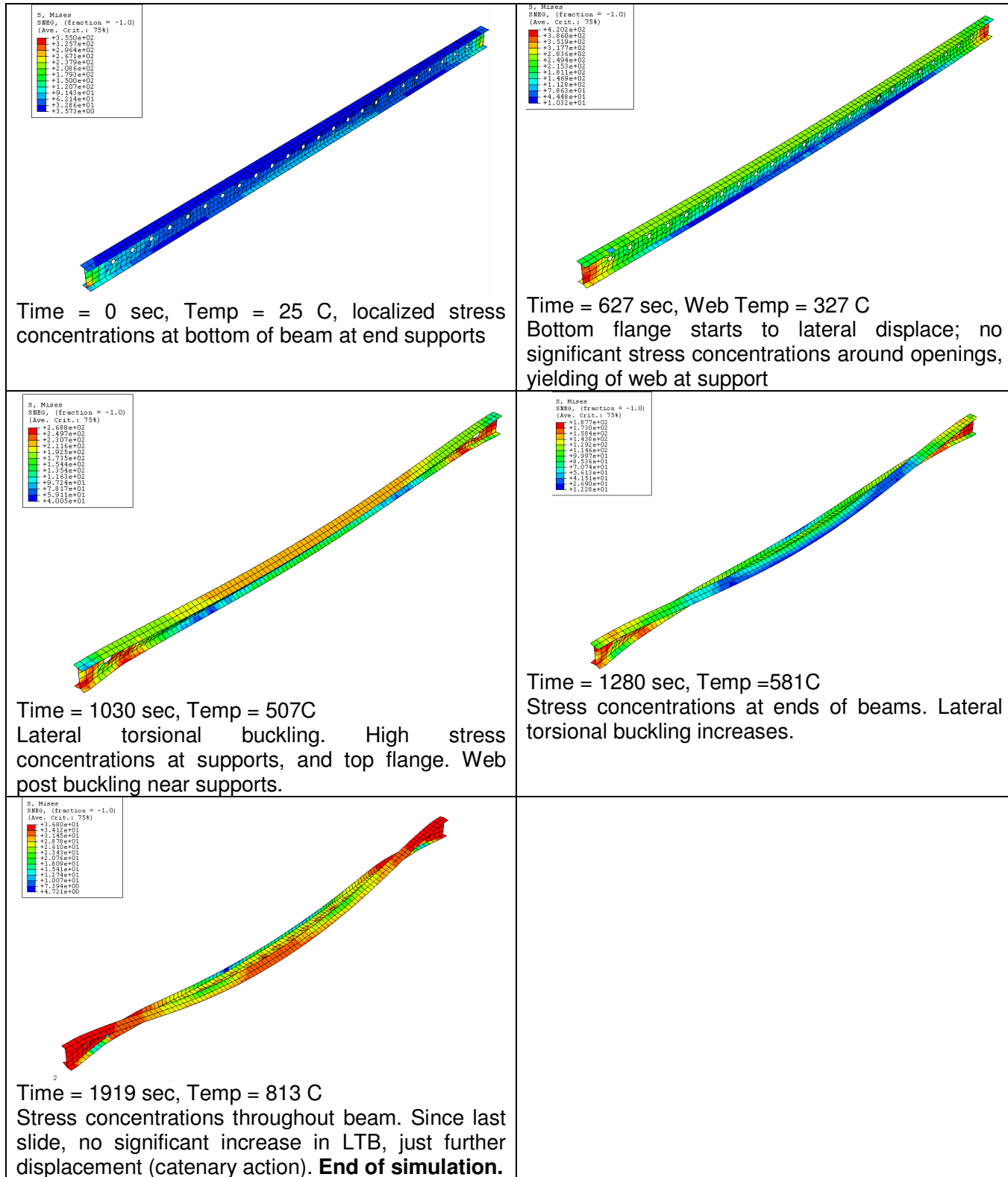
DEFORMATIONS: Case a.1 – Hole Diameter=150mm

| | |
|---|---|
|  <p>Time = 0 sec, Temp = 25C</p> |  <p>Time = 627 sec, Web Temp = 327 C Bottom flange starts to lateral displace; no significant stress concentrations around openings, yielding of web at support</p> |
|  <p>Time = 1030 sec, Temp = 507C Lateral torsional buckling. High stress concentrations at supports, and top flange. Web buckling near supports.</p> |  <p>Time = 1280 sec, Temp = 581C Stress concentrations at ends of beams. Lateral torsional buckling increases.</p> |
|  <p>Time = 1919 sec, Temp = 813 C Stress concentrations throughout beam. Since last slide, no significant increase in LTB, just further displacement (catenary action). End of simulation. No convergence</p> | |





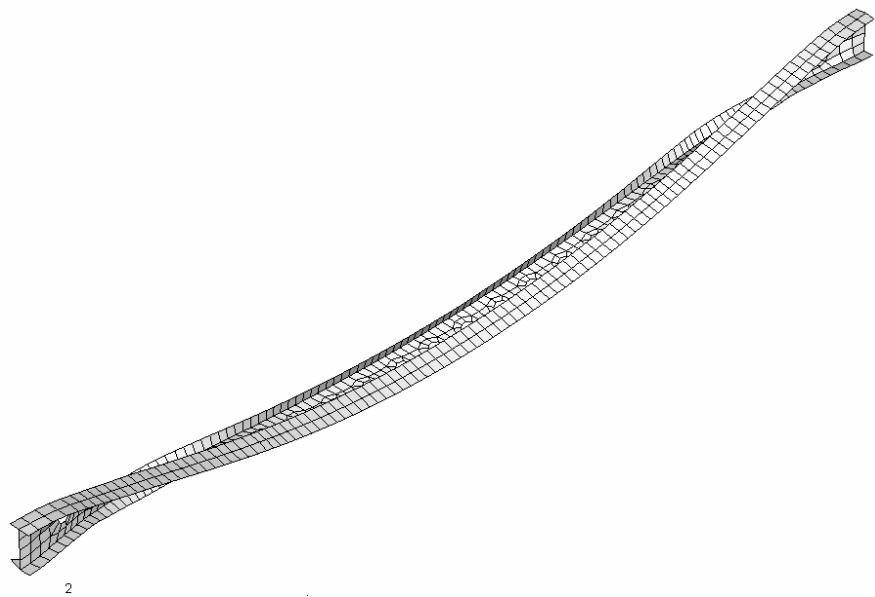
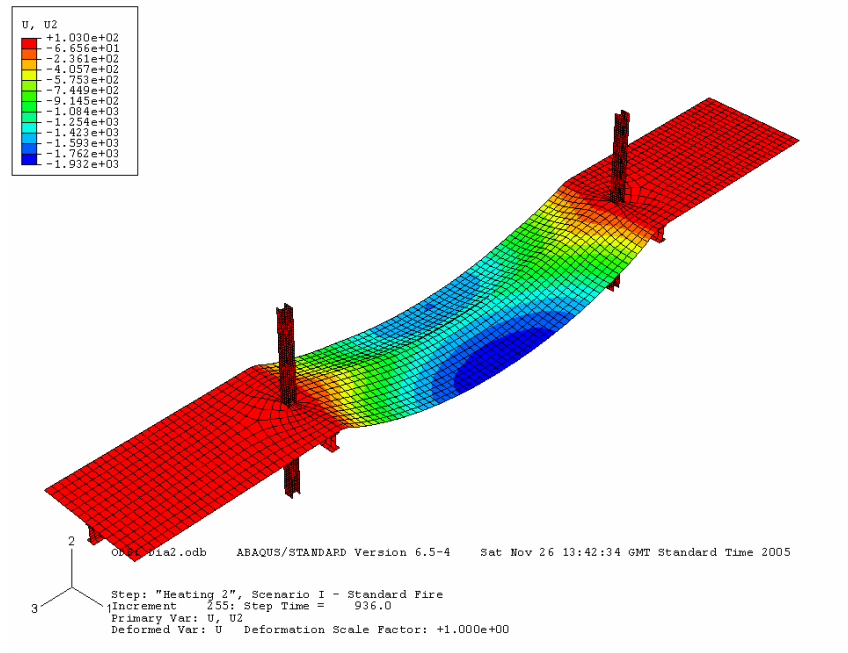
Case a.1 – Von Mises stresses



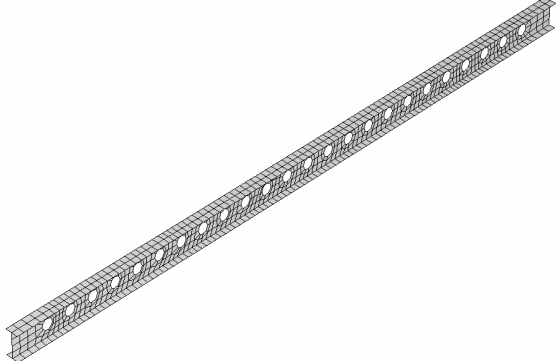
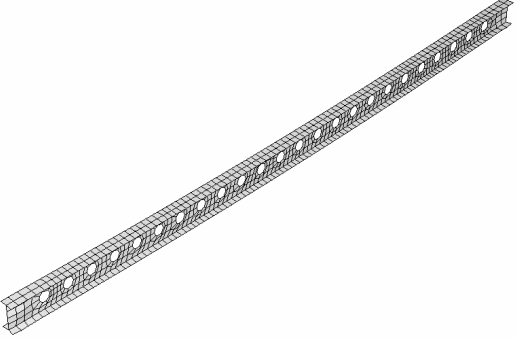
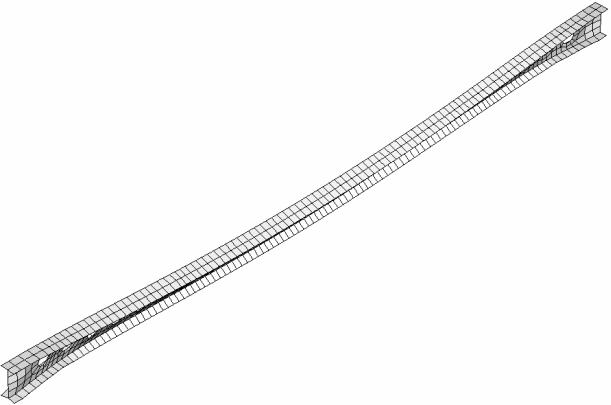
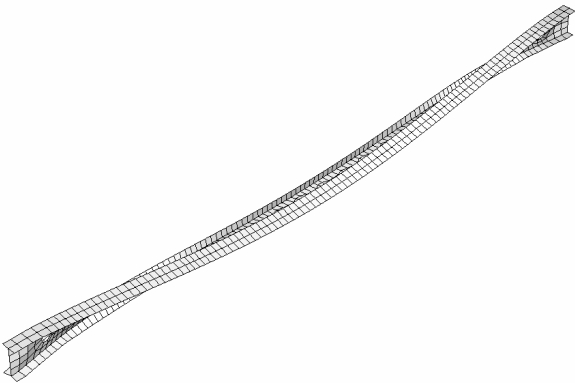
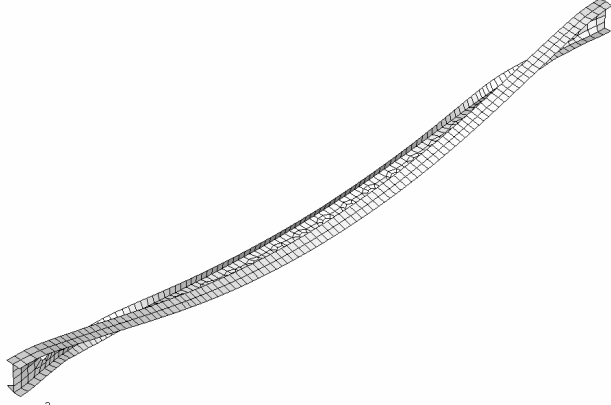
Scenario I – Case a.2

Case a.2 – Hole Diameter=300 mm

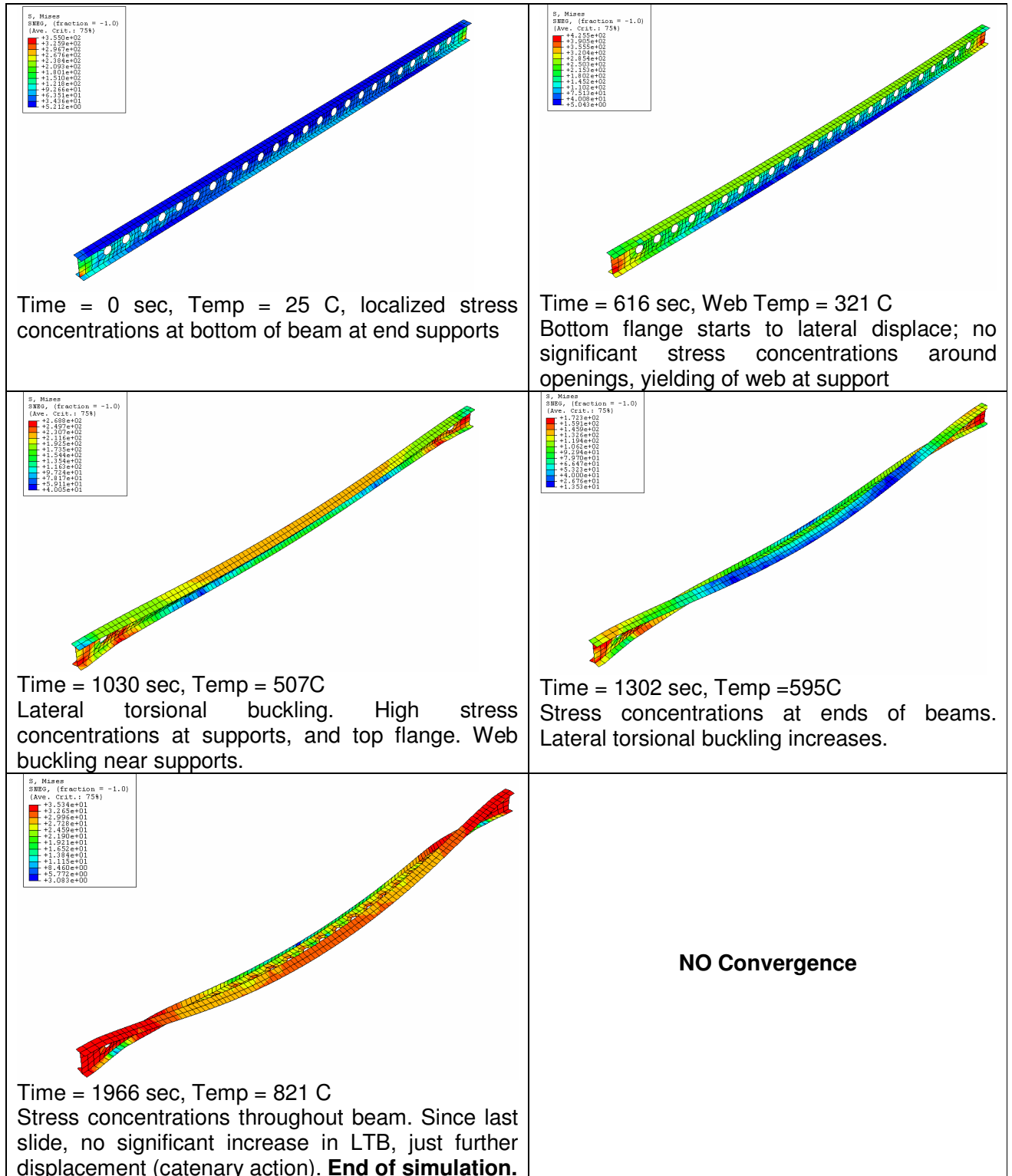
Displacement at end of simulation (t = 1966s), Temp = 821C



DEFORMATIONS: Case a.2 – Hole Diameter=300 mm

| | |
|---|---|
|  <p>Time = 0 sec, Temp = 25 C, localized stress concentrations at bottom of beam at end supports</p> |  <p>Time = 616 sec, Web Temp = 321 C Bottom flange starts to lateral displace; no significant stress concentrations around openings, yielding of web at support</p> |
|  <p>Time = 1030 sec, Temp = 507C Lateral torsional buckling. High stress concentrations at supports, and top flange. Web buckling near supports.</p> |  <p>Time = 1302 sec, Temp = 595C Stress concentrations at ends of beams. Lateral torsional buckling increases.</p> |
|  <p>Time = 1966 sec, Temp = 821 C Stress concentrations throughout beam. Since last slide, no significant increase in LTB, just further displacement (catenary action). End of simulation. No convergence</p> | |

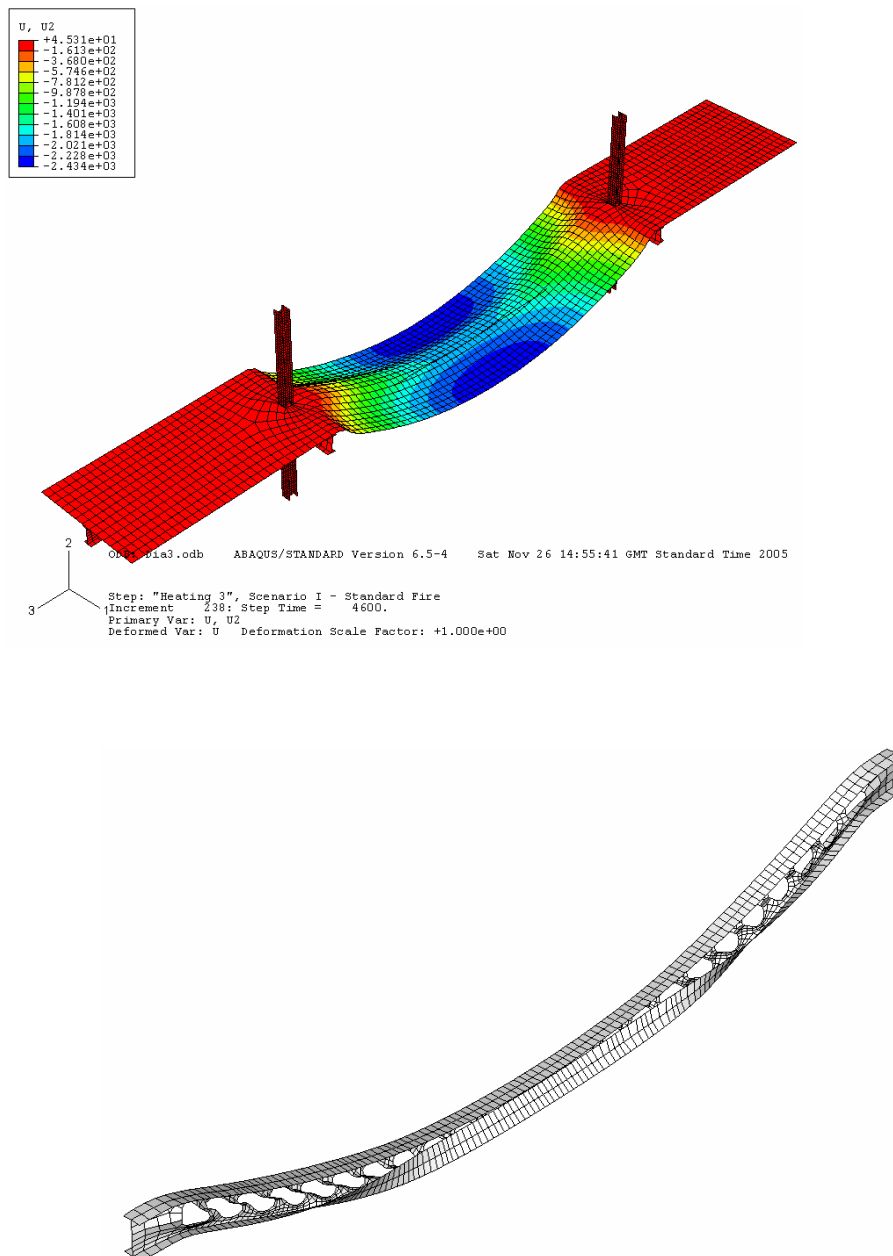
Case a.2 – Von Mises stresses



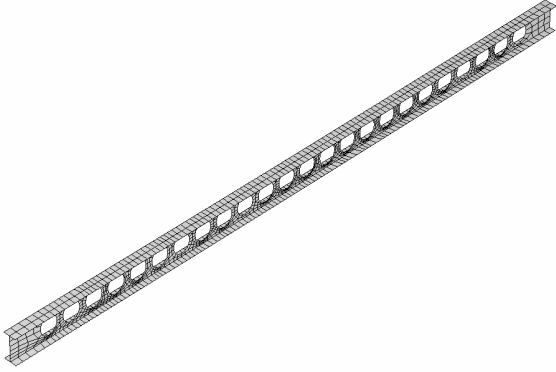
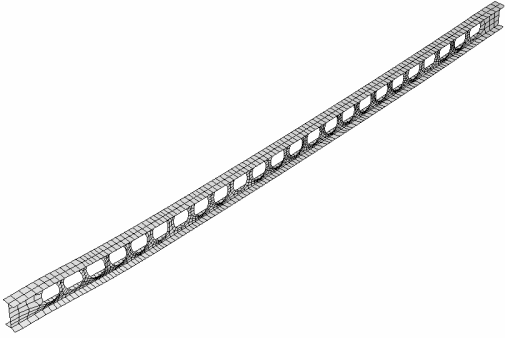
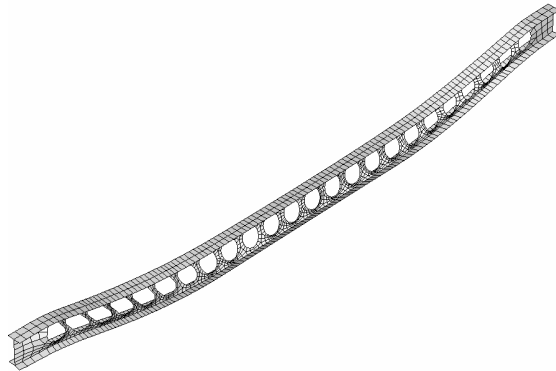
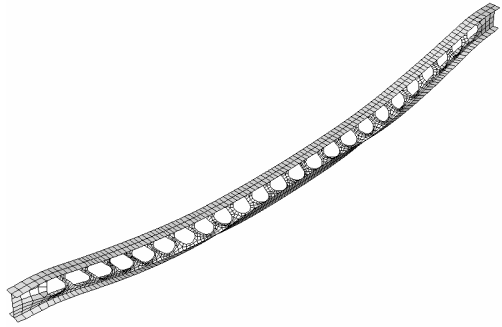
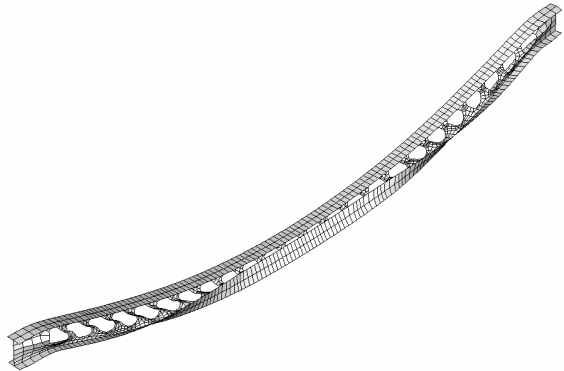
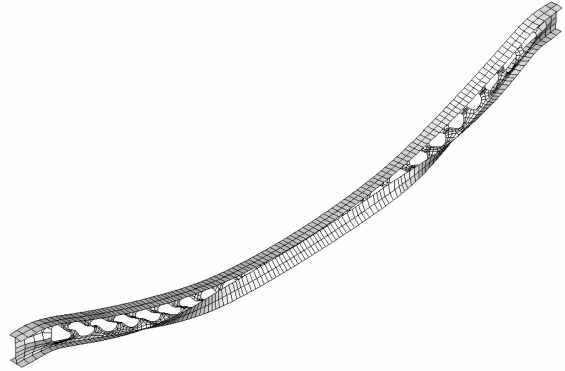
Scenario I – Case a.3

Case a.3 – Hole Diameter = 500 mm

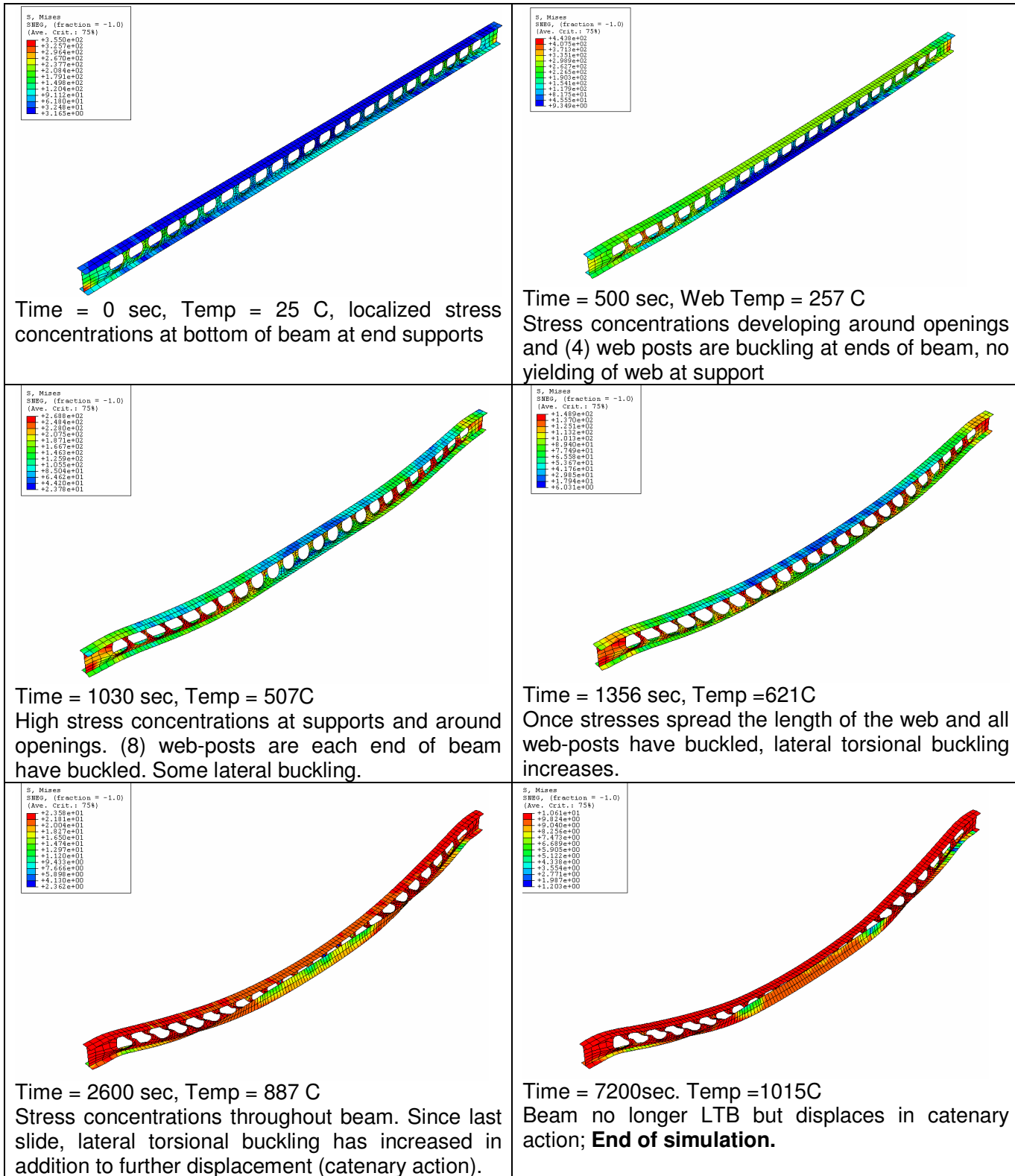
Displacement at end of simulation (t = 7200s), Temp = 1051 C



DEFORMATIONS: Case a.3 – Hole Diameter = 500 mm

| | |
|---|---|
|  <p>Time = 0 sec, Temp = 25 C, localized stress concentrations at bottom of beam at end supports</p> |  <p>Time = 500 sec, Web Temp = 257 C Stress concentrations developing around openings and (4) web posts are buckling at ends of beam, no yielding of web at support</p> |
|  <p>Time = 1030 sec, Temp = 507C High stress concentrations at supports and around openings. (8) web-posts are each end of beam have buckled. Some lateral buckling.</p> |  <p>Time = 1356 sec, Temp = 621C Once stresses spread the length of the web and all web-posts have buckled, lateral torsional buckling increases.</p> |
|  <p>Time = 2600 sec, Temp = 887 C Stress concentrations throughout beam. Since last slide, lateral torsional buckling has increased in addition to further displacement (catenary action).</p> |  <p>Time = 7200sec. Temp = 1015C Beam no longer LTB but displaces in catenary action; End of simulation.</p> |

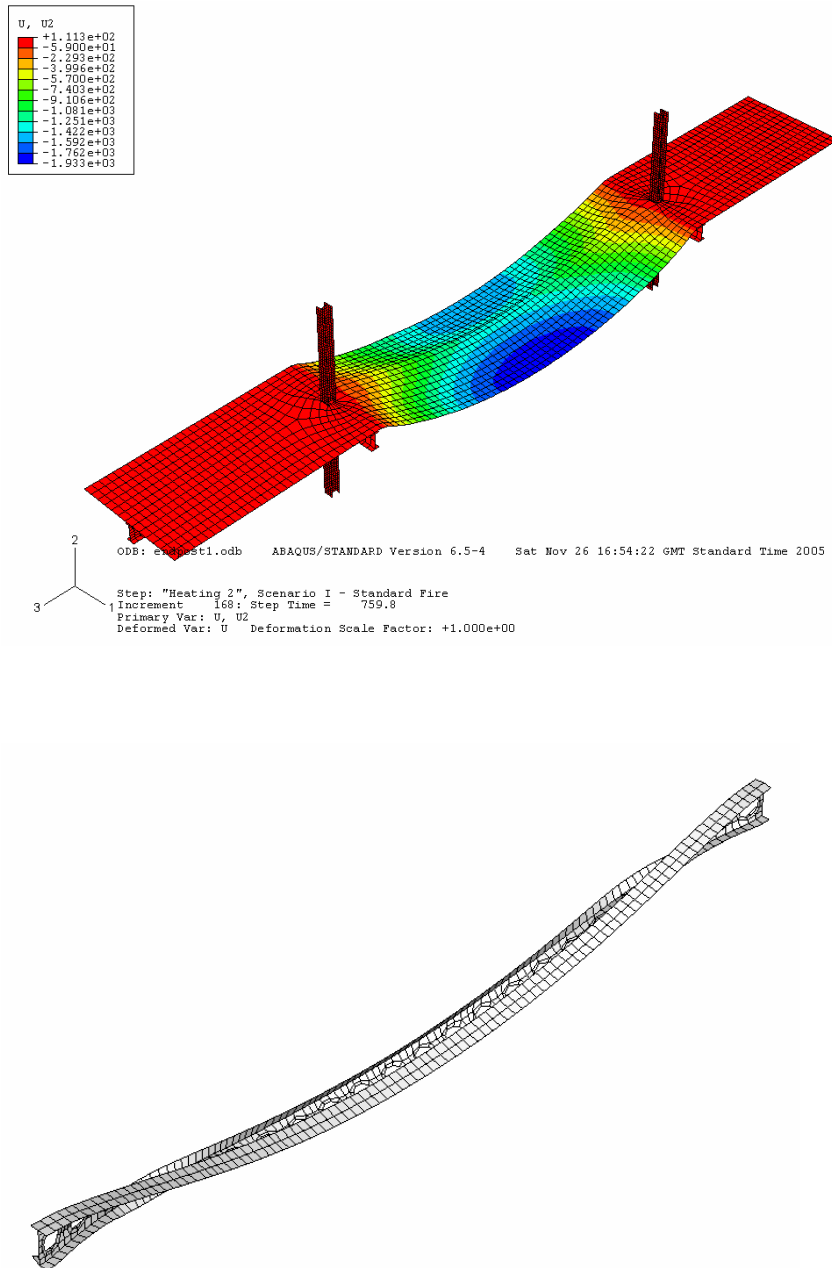
Case a.3 – Von Mises stresses



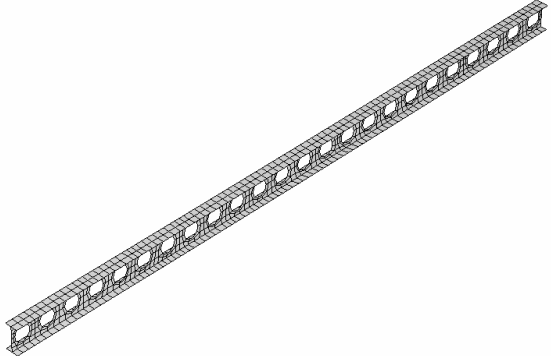
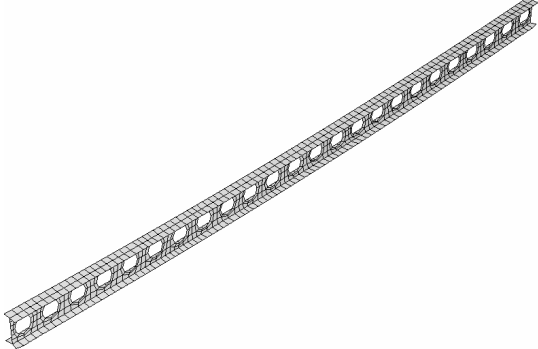
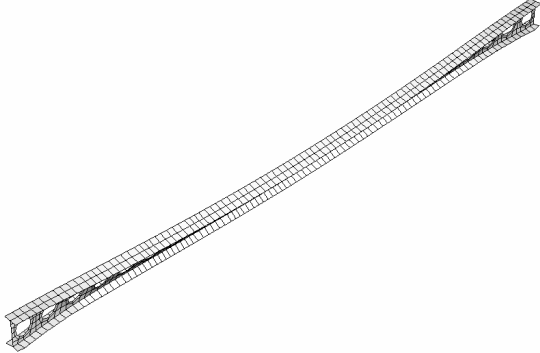
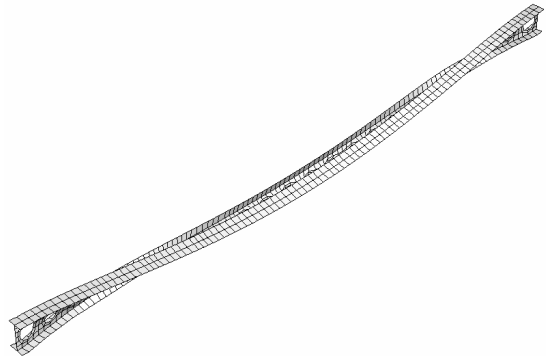
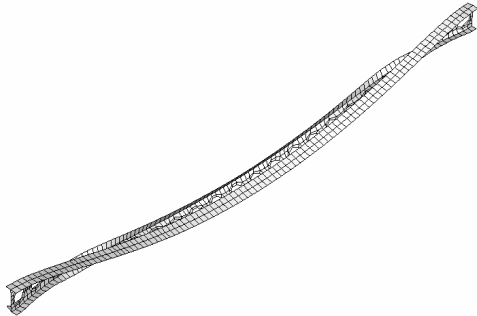
Scenario I – Case b.1

Case b.1 – End Post Length = 100 mm

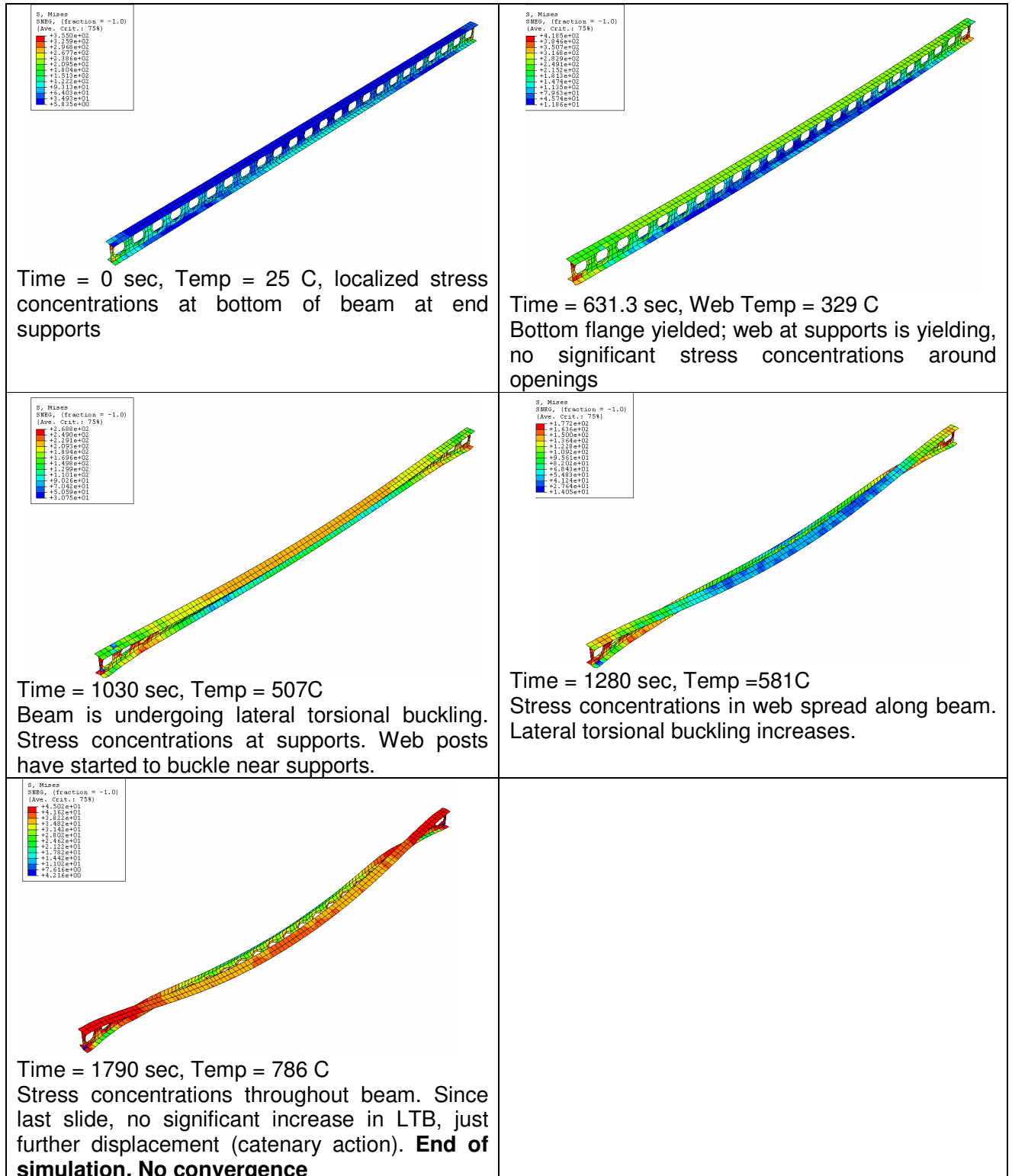
Displacement at end of simulation (t = 1790s, Temp = 786 C)

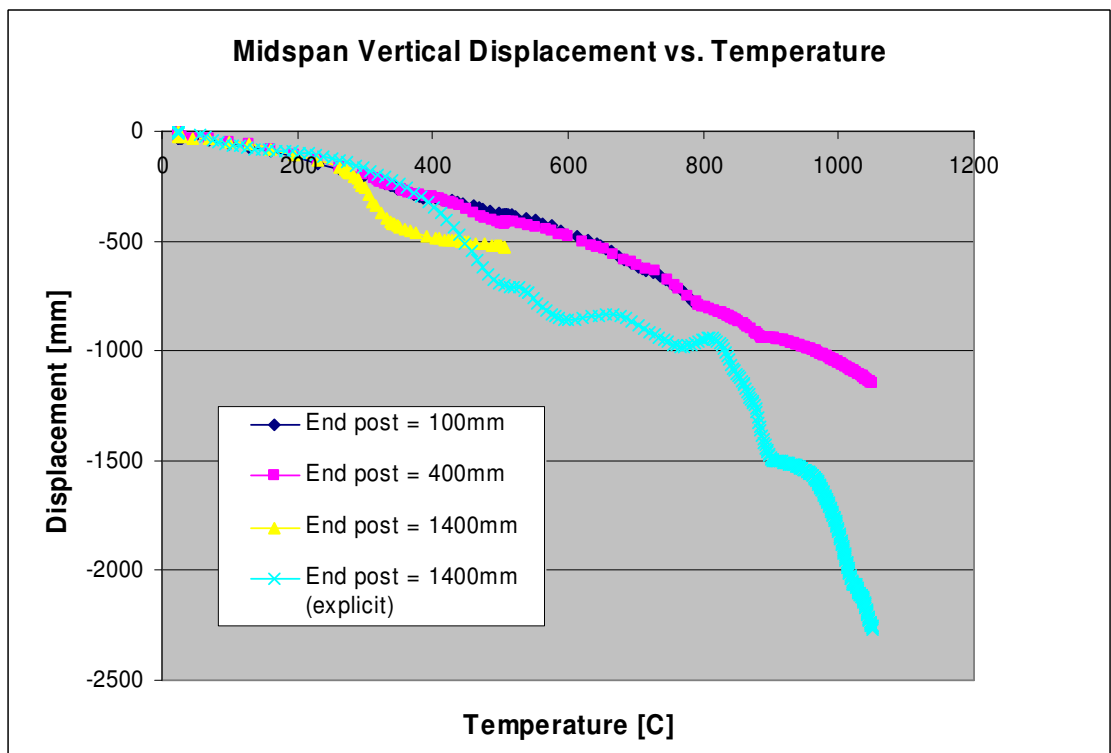
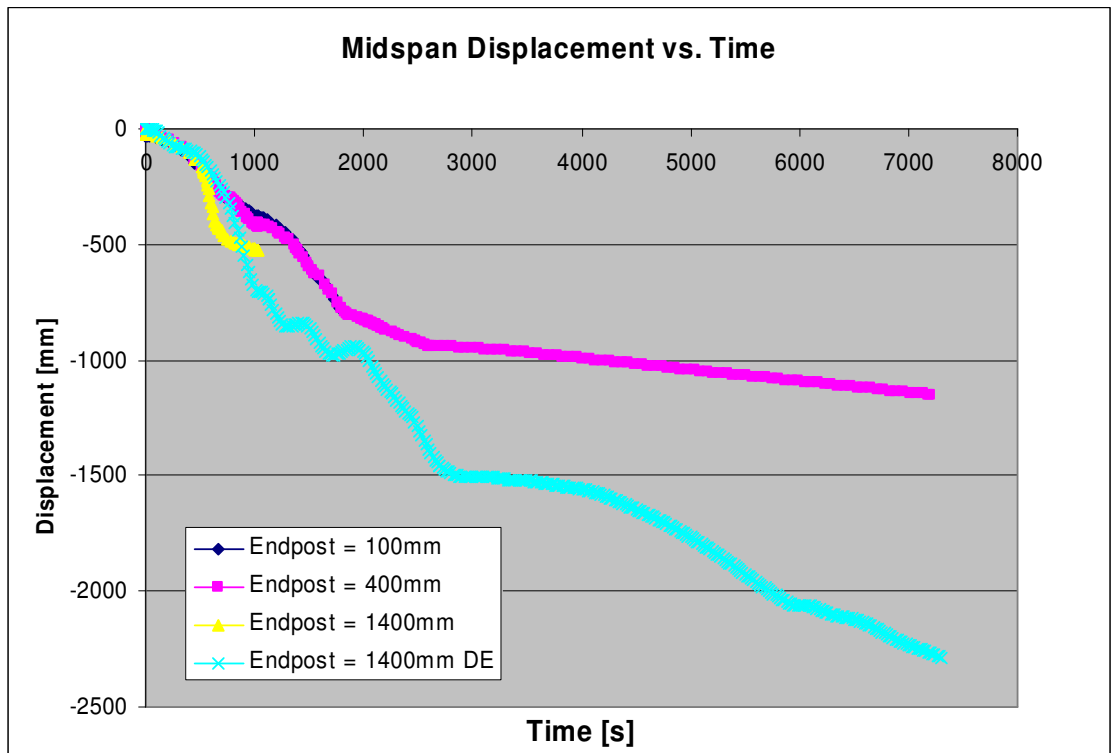


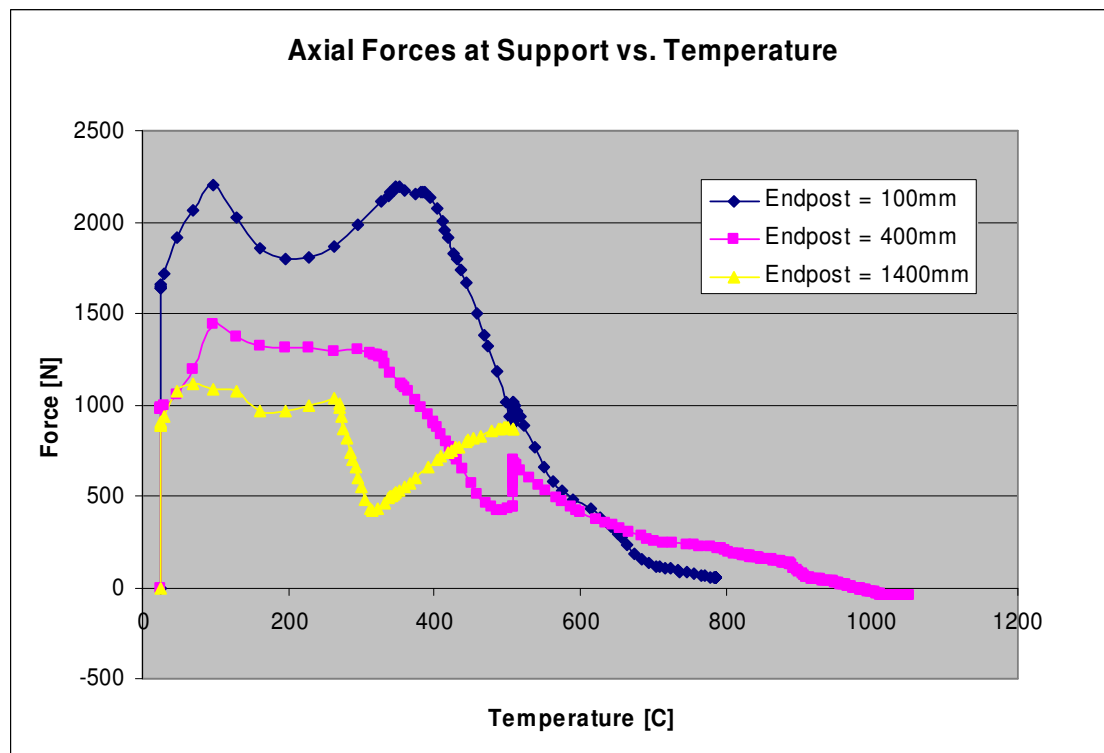
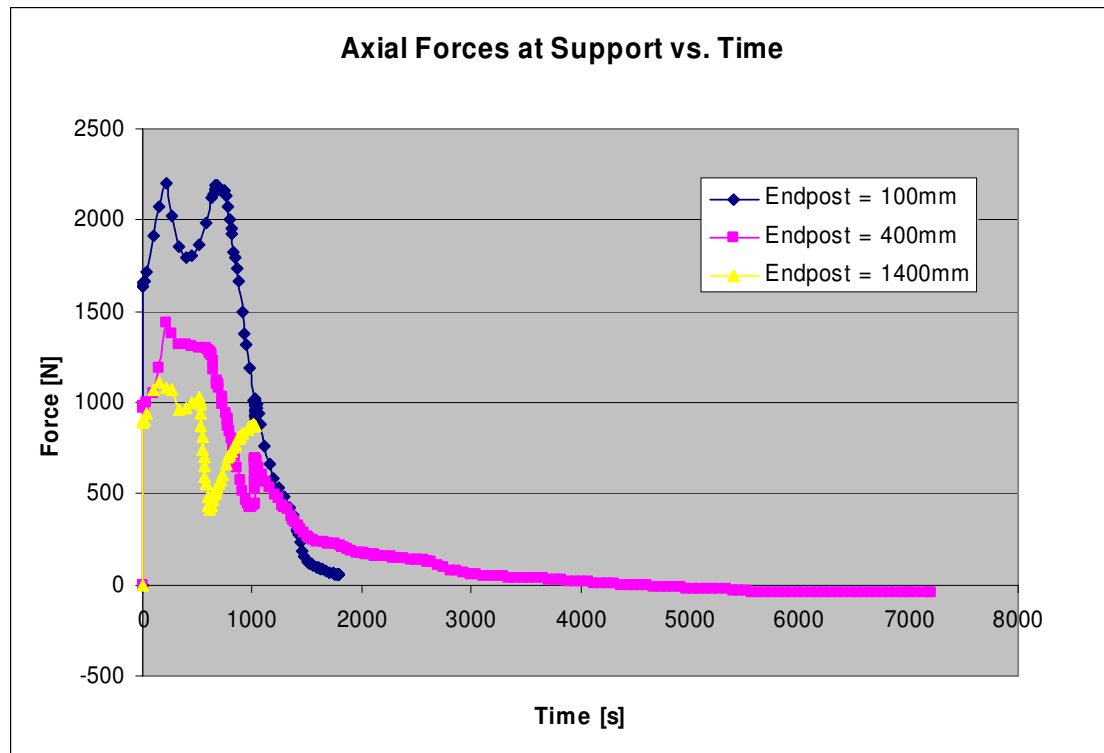
DEFORMATIONS: Case b.1 – End Post Length = 100 mm

| | |
|---|---|
|  <p>Time = 0 sec, Temp = 25 C, localized stress concentrations at bottom of beam at end supports</p> |  <p>Time = 631.3 sec, Web Temp = 329 C Bottom flange yielded; web at supports is yielding, no significant stress concentrations around openings</p> |
|  <p>Time = 1030 sec, Temp = 507C Beam is undergoing lateral torsional buckling. Stress concentrations at supports. Web posts have started to buckle near supports.</p> |  <p>Time = 1280 sec, Temp = 581C Stress concentrations in web spread along beam. Lateral torsional buckling increases.</p> |
|  <p>Time = 1790 sec, Temp = 786 C Stress concentrations throughout beam. Since last slide, no significant increase in LTB, just further displacement (catenary action). End of simulation. No convergence</p> | |

Case b.1 – Von Mises stresses



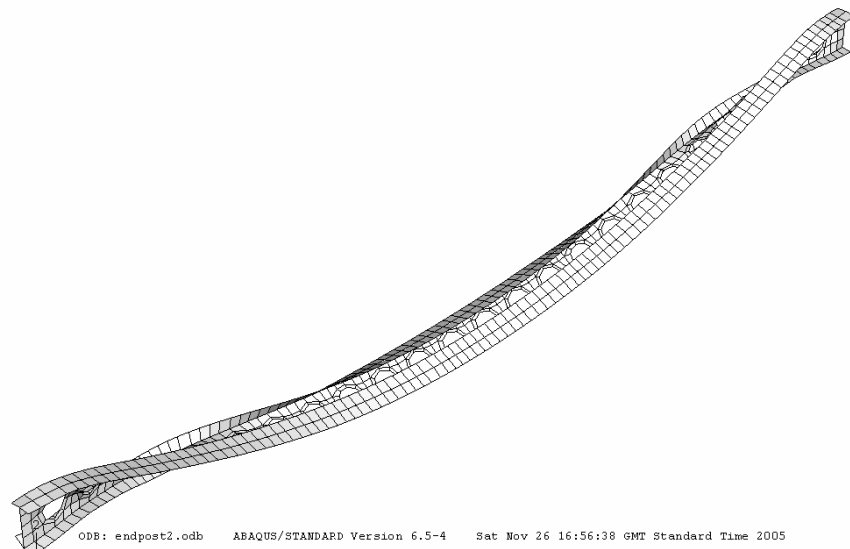
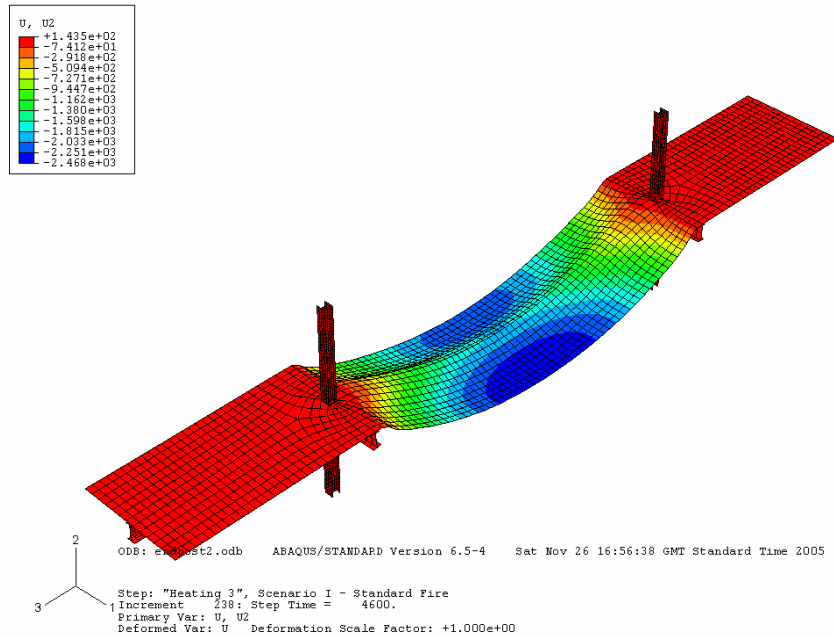




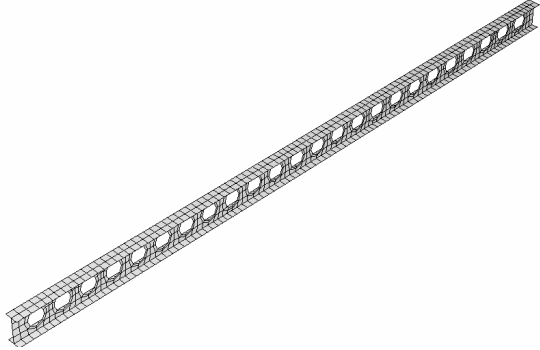
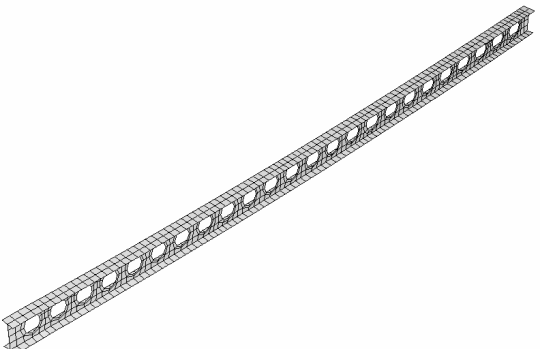
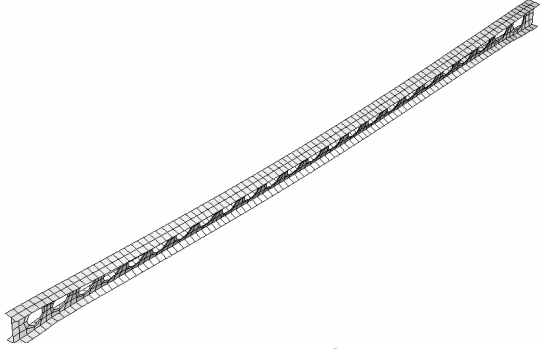
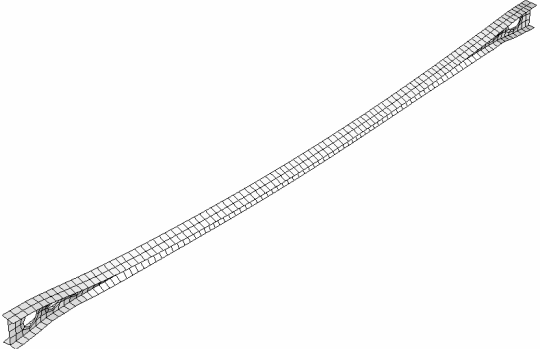
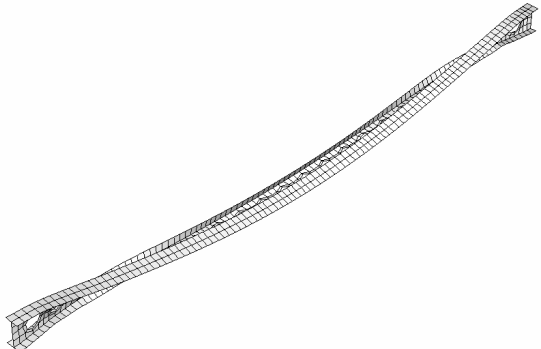
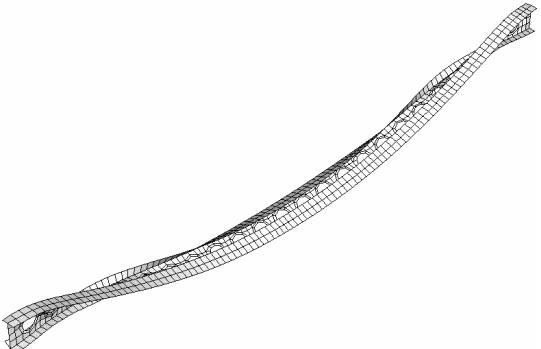
Scenario I – Case b.2

Case b.2 – End Post Length = 400 mm

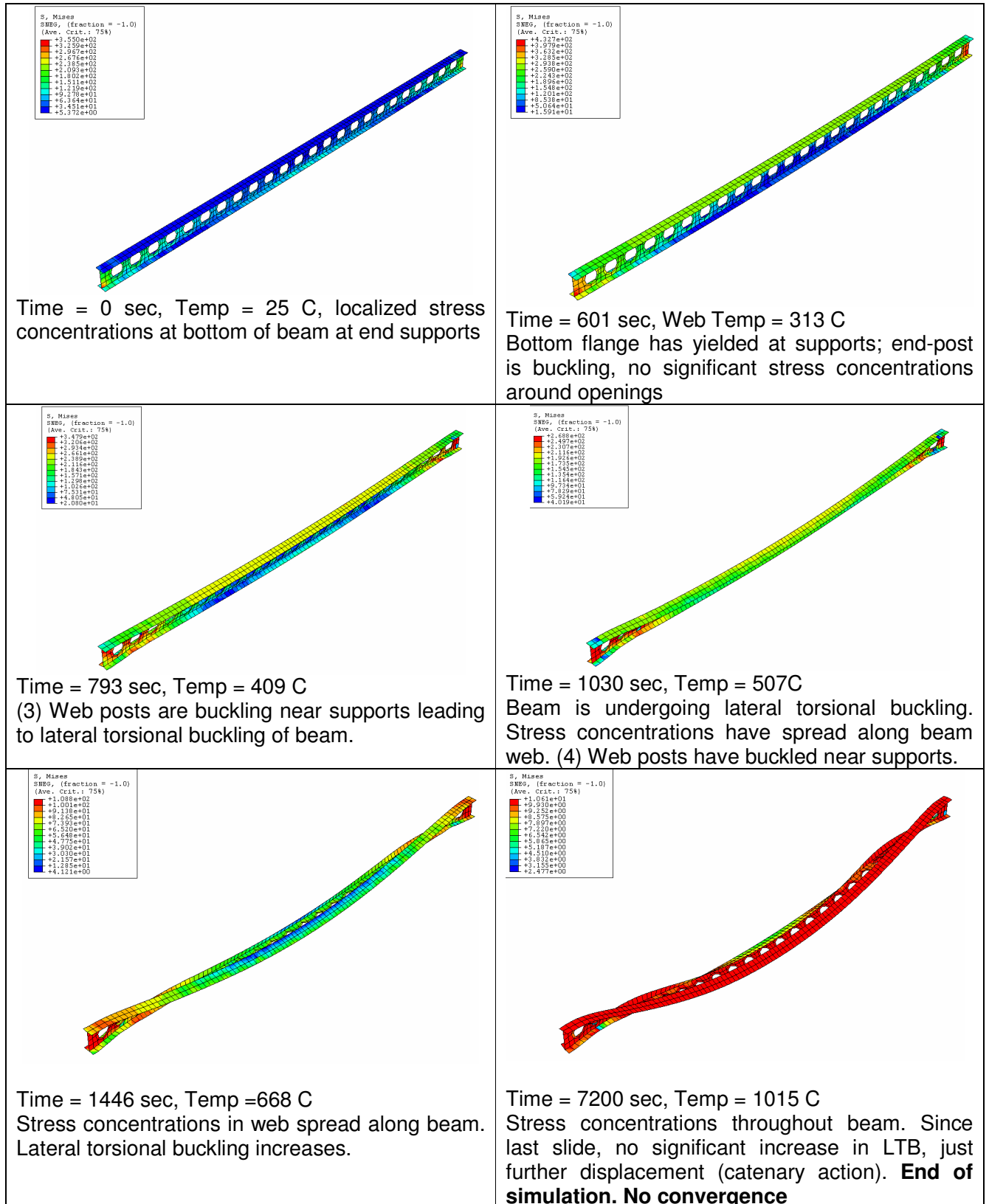
Displacement at end of simulation (t = 7200s, Temp = C)



DEFORMATIONS: Case b.2 – End Post Length = 400 mm

| | |
|--|---|
|  <p>Time = 0 sec, Temp = 25 C, localized stress concentrations at bottom of beam at end supports</p> |  <p>Time = 601 sec, Web Temp = 313 C Bottom flange has yielded at supports; end-post is buckling, no significant stress concentrations around openings</p> |
|  <p>Time = 793 sec, Temp = 409 C (3) Web posts are buckling near supports leading to lateral torsional buckling of beam.</p> |  <p>Time = 1030 sec, Temp = 507C Beam is undergoing lateral torsional buckling. Stress concentrations have spread along beam web. (4) Web posts have buckled near supports.</p> |
|  <p>Time = 1446 sec, Temp = 668 C Stress concentrations in web spread along beam. Lateral torsional buckling increases.</p> |  <p>Time = 7200 sec, Temp = 1015 C Stress concentrations throughout beam. Since last slide, no significant increase in LTB, just further displacement (catenary action). End of simulation. No convergence</p> |

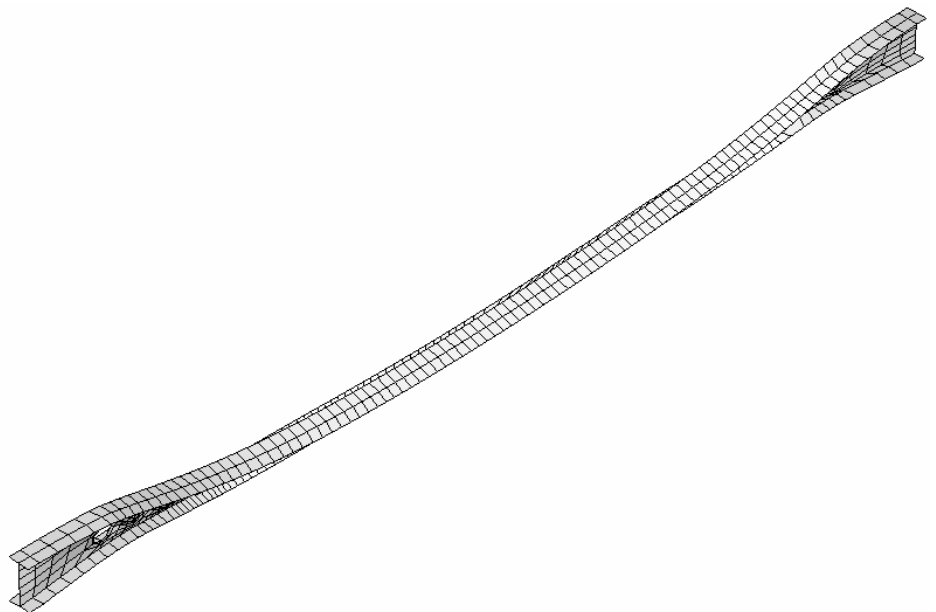
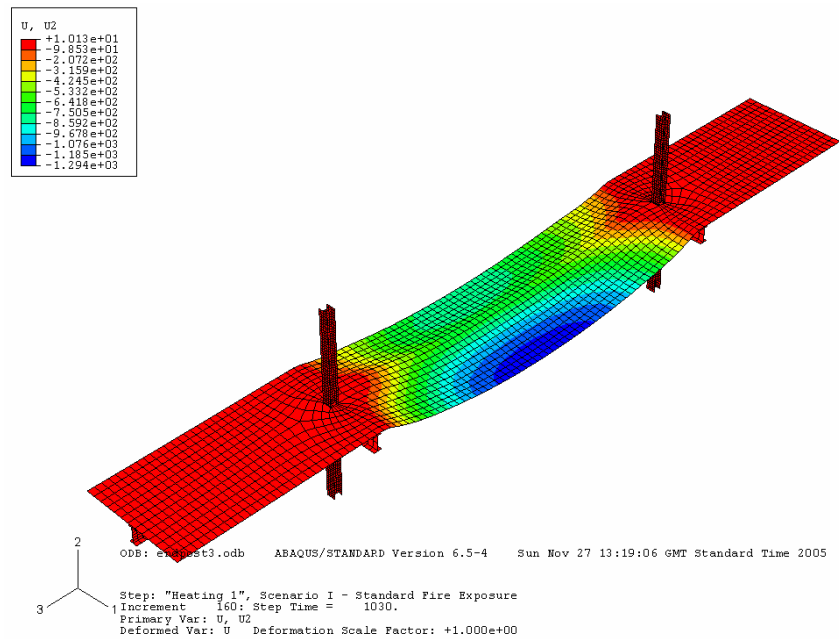
Case b.2 – Von Mises stresses



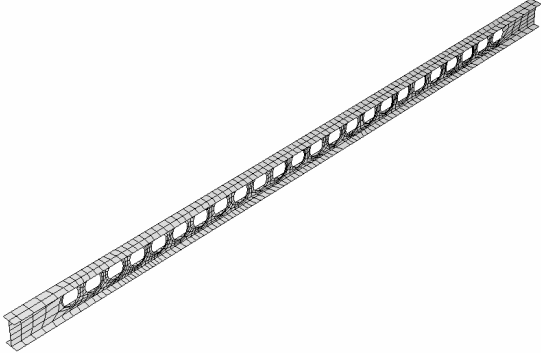

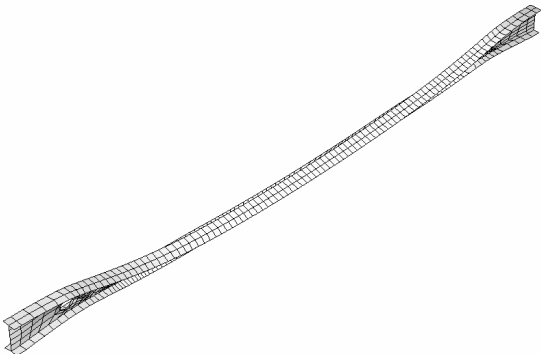
Scenario I – Case b.3

Case b.3 – End Post Length = 1400 mm

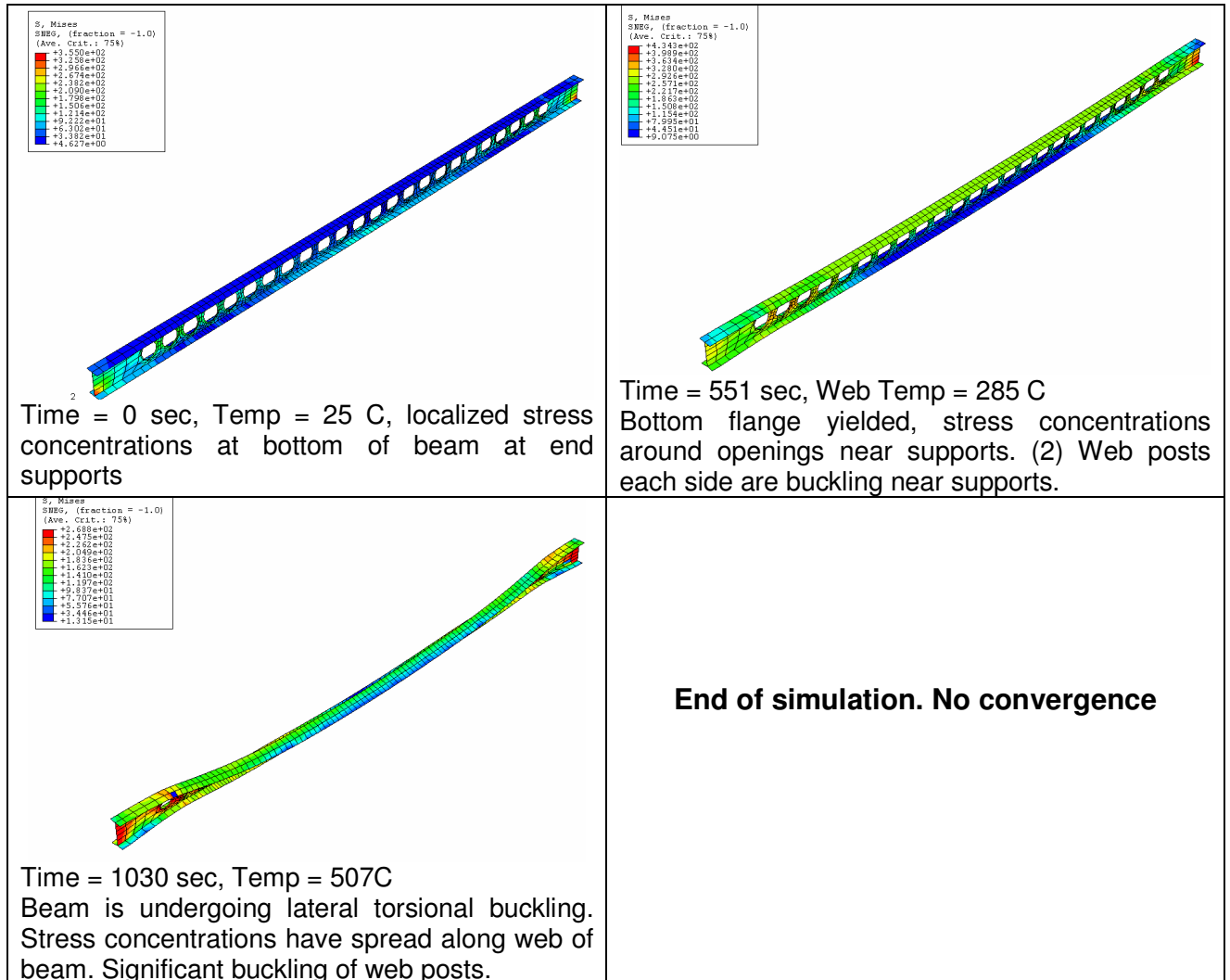
Displacement at end of simulation (t = 1030s, Temp = 507 C)



DEFORMATIONS: Case b.3 – End Post Length = 1400 mm

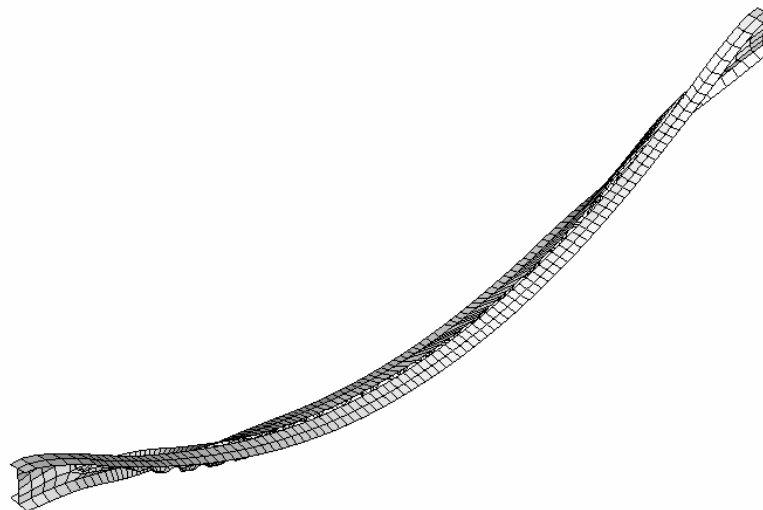
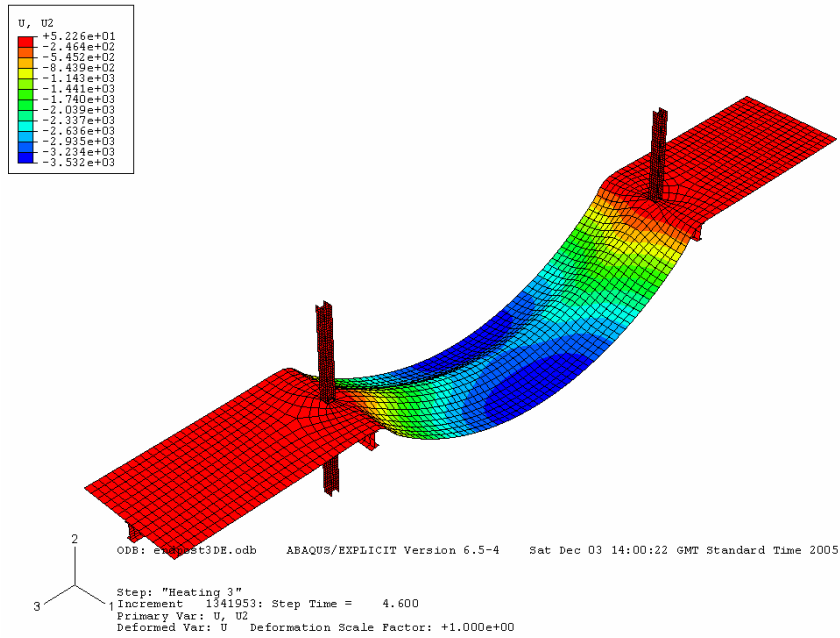
| | |
|---|--|
|  <p>Time = 0 sec, Temp = 25 C, localized stress concentrations at bottom of beam at end supports</p> |  <p>Time = 551 sec, Web Temp = 285 C Bottom flange yielded, stress concentrations around openings near supports. (2) Web posts each side are buckling near supports.</p> |
|  <p>Time = 1030 sec, Temp = 507C Beam is undergoing lateral torsional buckling. Stress concentrations have spread along web of beam. Significant buckling of web posts.</p> | <p>End of simulation. No convergence</p> |

Case b.3 – Von Mises stresses

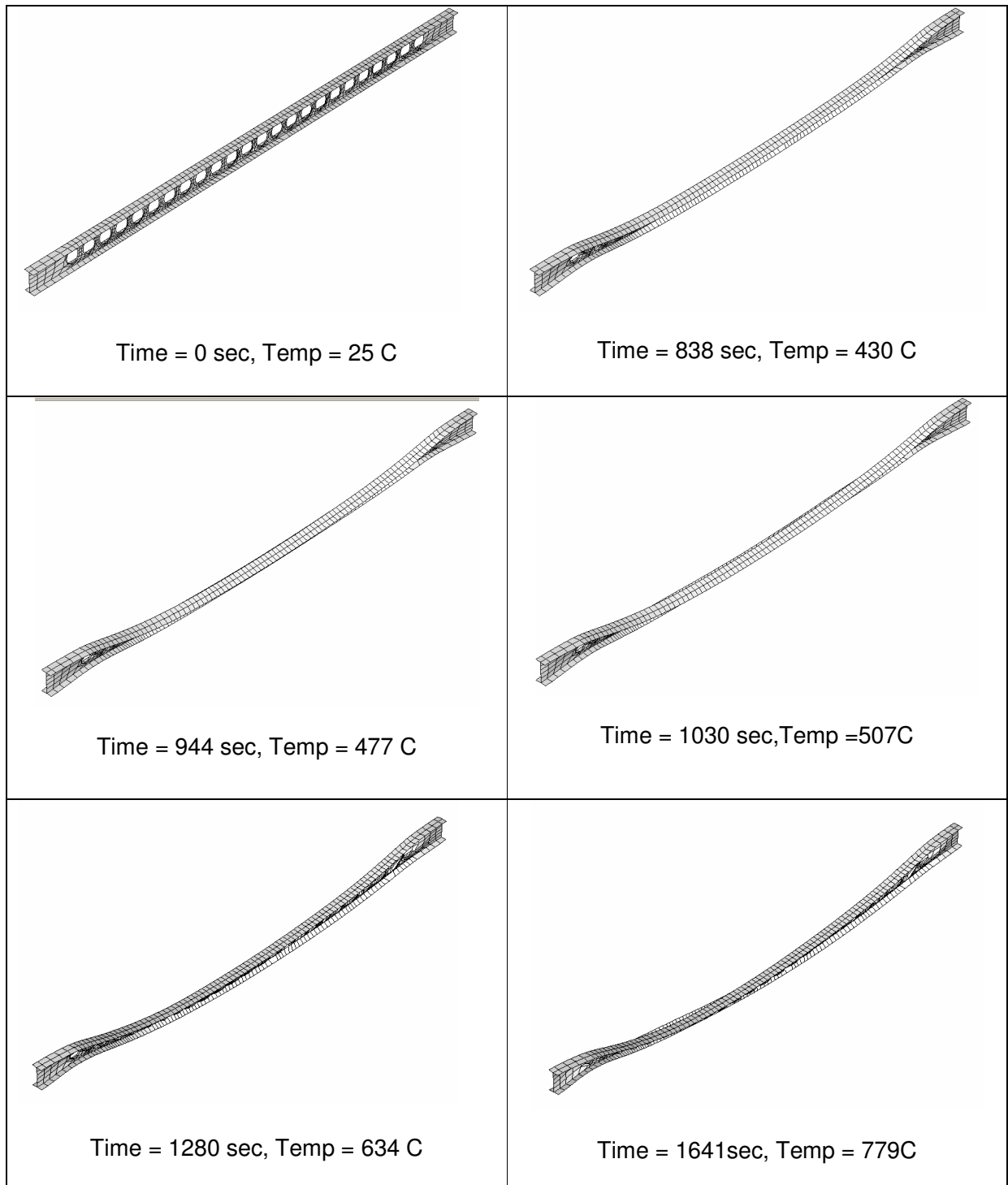


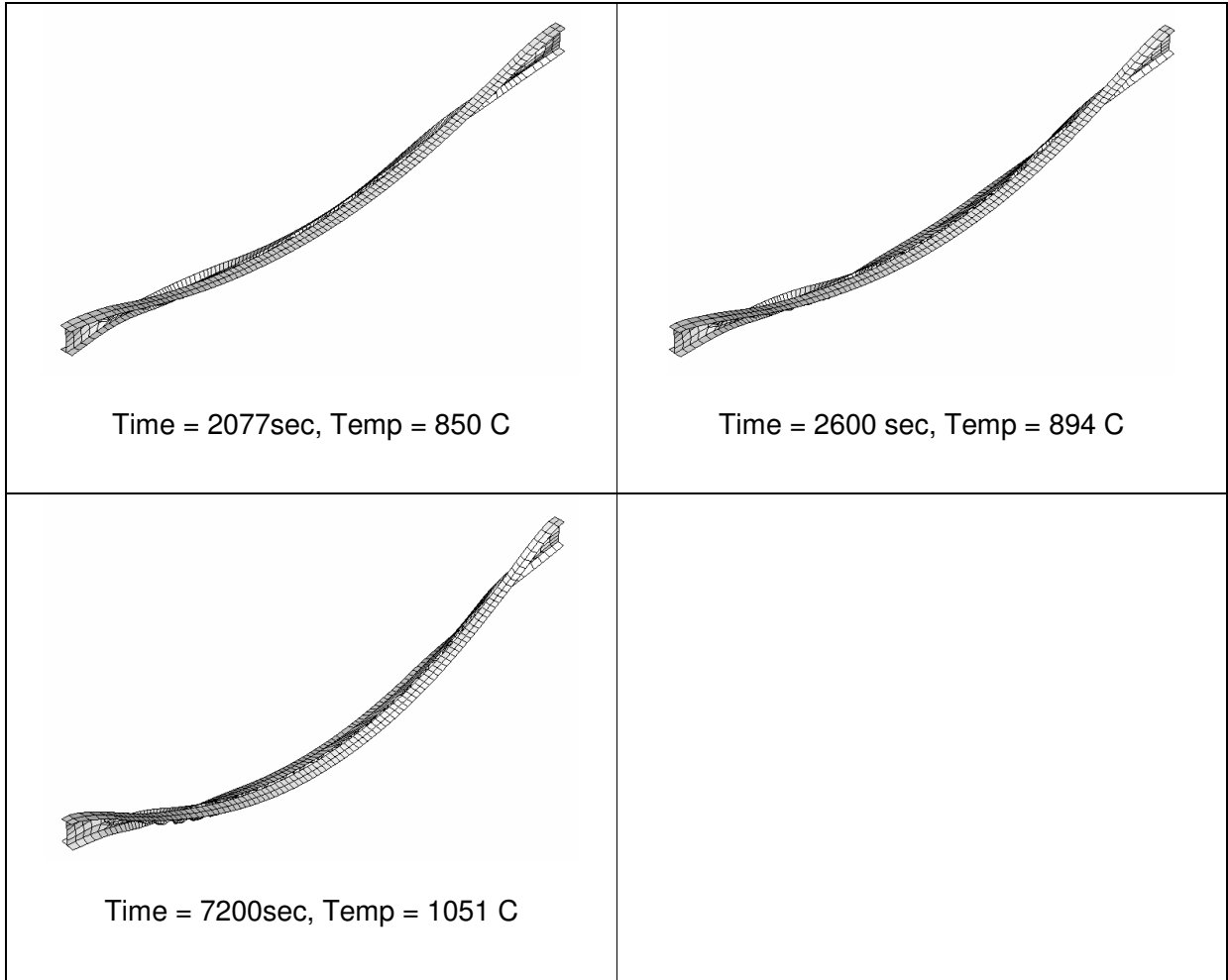
Case b.3 (EXPLICIT Model) – End Post Length = 1400 mm

Displacement at end of simulation (t = 1030s, Temp = 507 C)

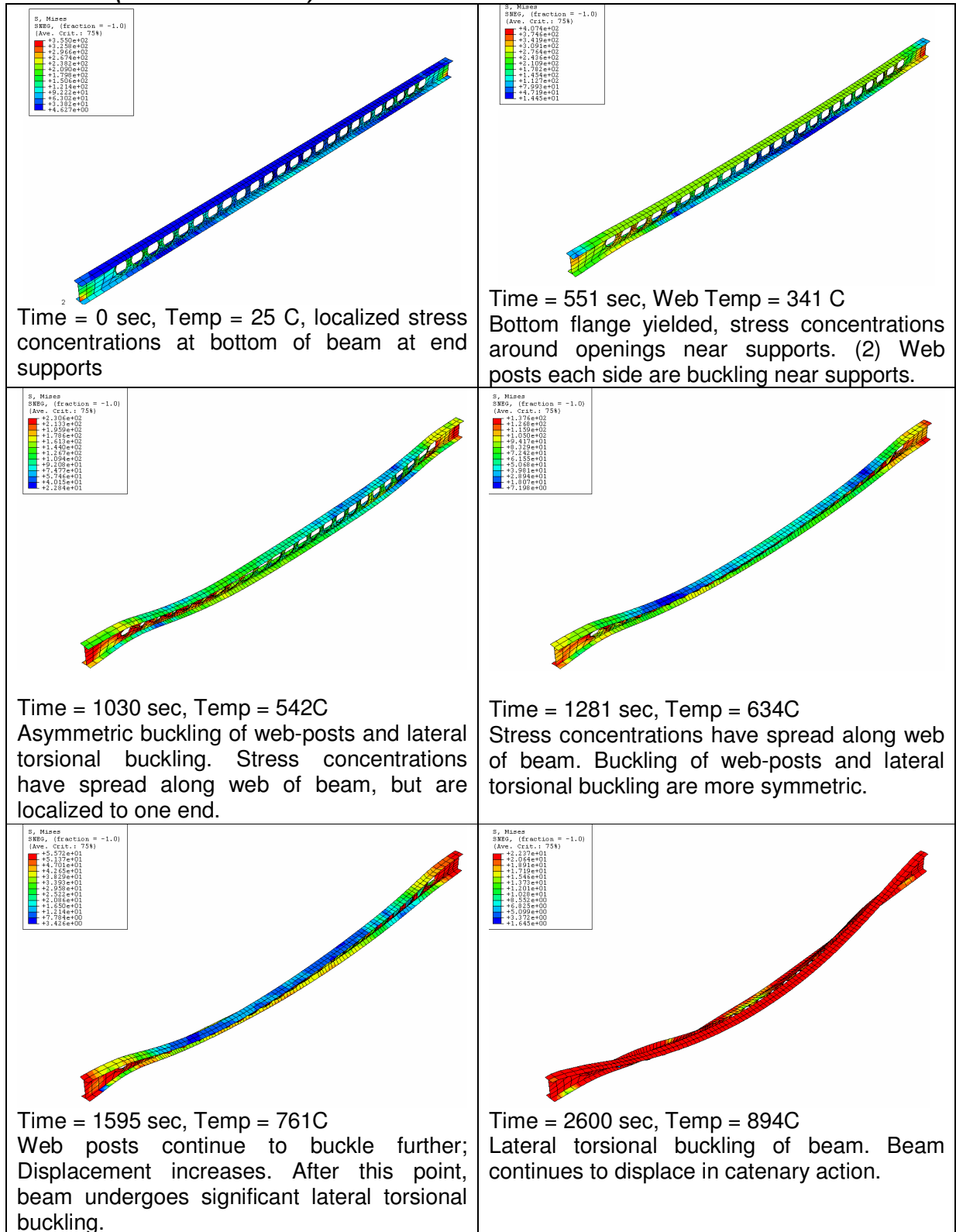


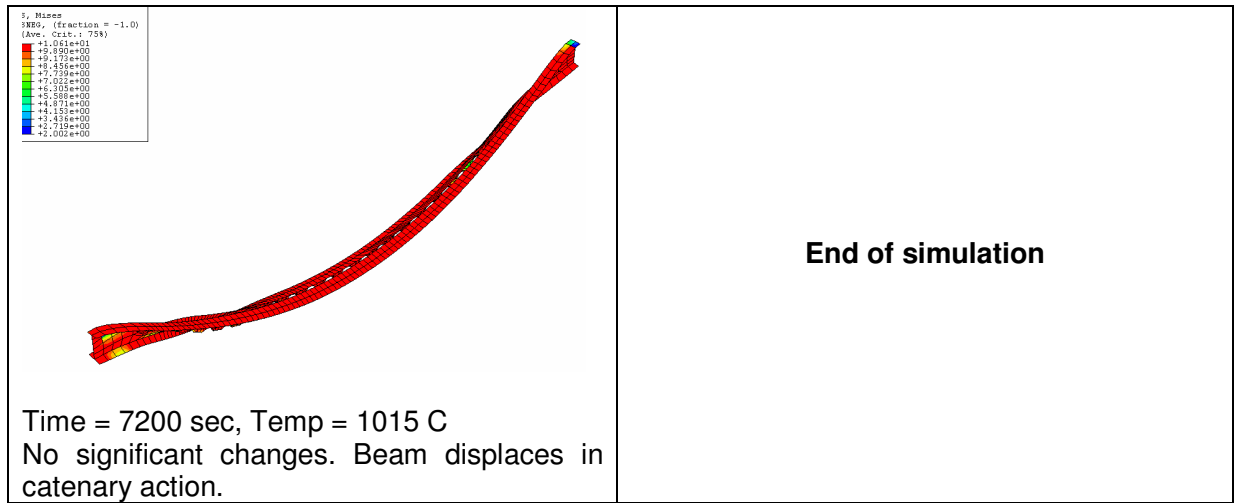
DEFORMATIONS: Case b.3 (EXPLICIT Model) – End Post Length = 1400 mm





Case b.3 (EXPLICIT MODEL) – Von Mises stresses

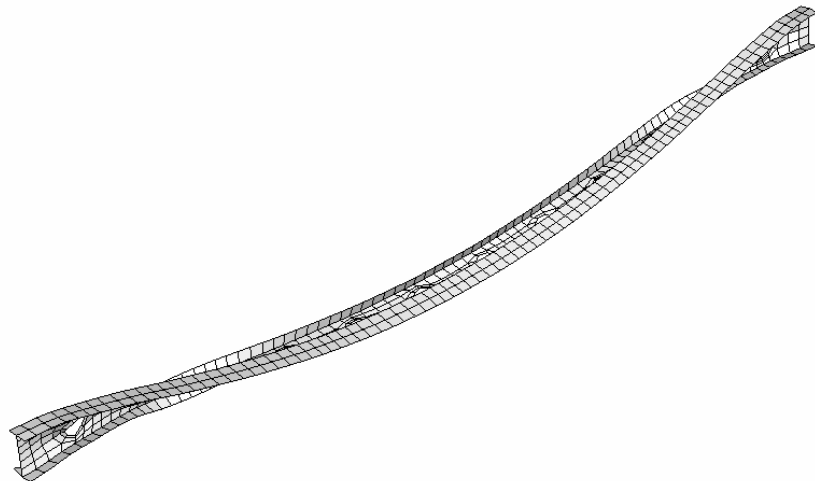
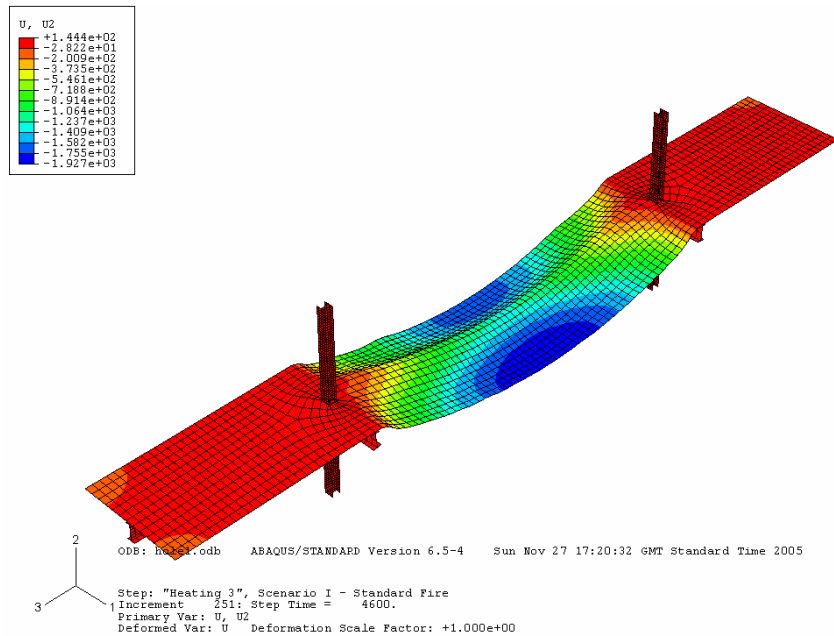




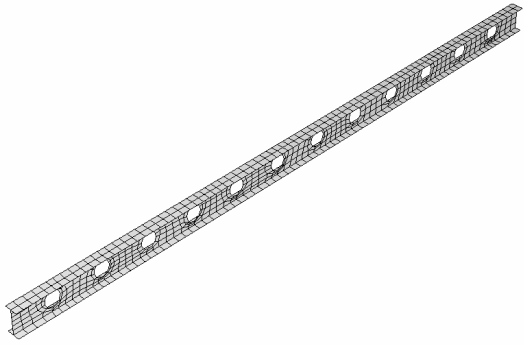
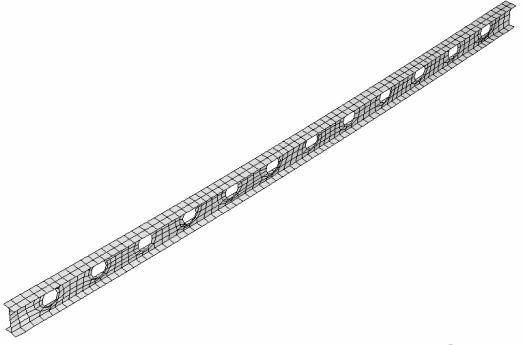
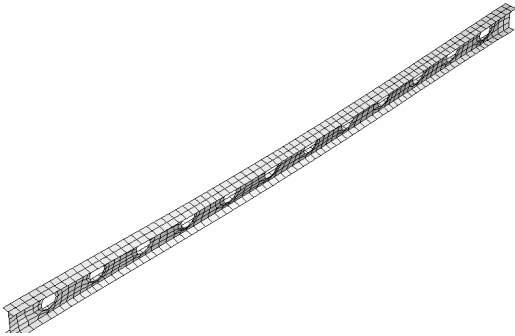
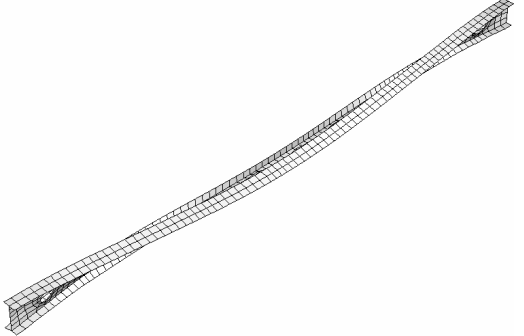
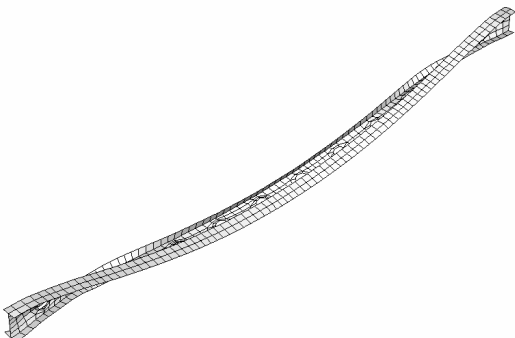
Scenario I – Case c.1

Case c.1 – Number of web openings = 12

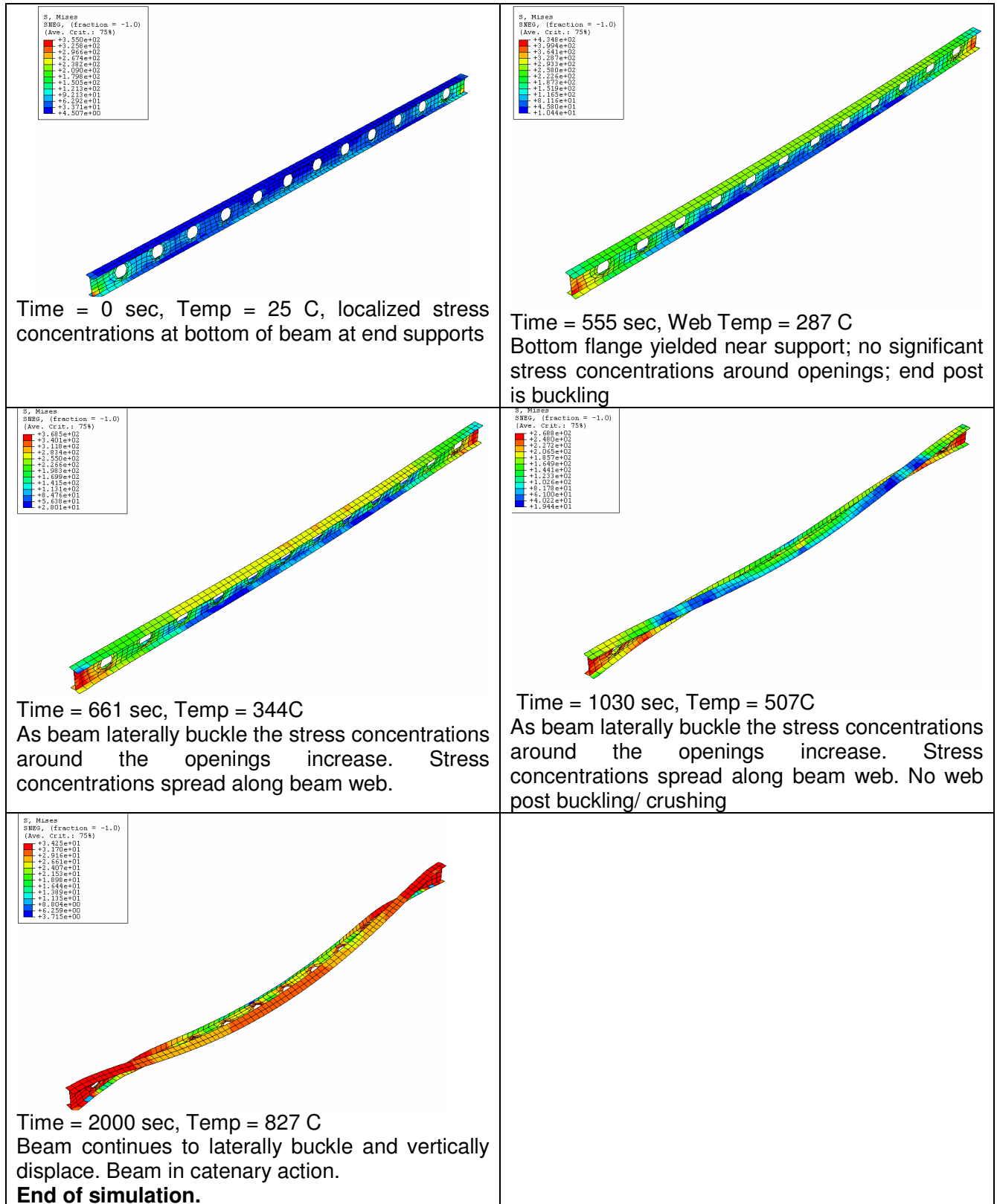
Displacement at end of simulation (t = 2000s, Temp = 827 C)



DEFORMATIONS: Case c.1 – Number of web openings = 12

| | |
|---|--|
|  <p>Time = 0 sec, Temp = 25 C, localized stress concentrations at bottom of beam at end supports</p> |  <p>Time = 555 sec, Web Temp = 287 C Bottom flange yielded near support; no significant stress concentrations around openings; end post is buckling</p> |
|  <p>Time = 661 sec, Temp = 344C As beam laterally buckle the stress concentrations around the openings increase. Stress concentrations spread along beam web.</p> |  <p>Time = 1030 sec, Temp = 507C As beam laterally buckle the stress concentrations around the openings increase. Stress concentrations spread along beam web. No web post buckling/ crushing</p> |
|  <p>Time = 2000 sec, Temp = 827 C Beam continues to laterally buckle and vertically displace. Beam in catenary action. End of simulation.</p> | |

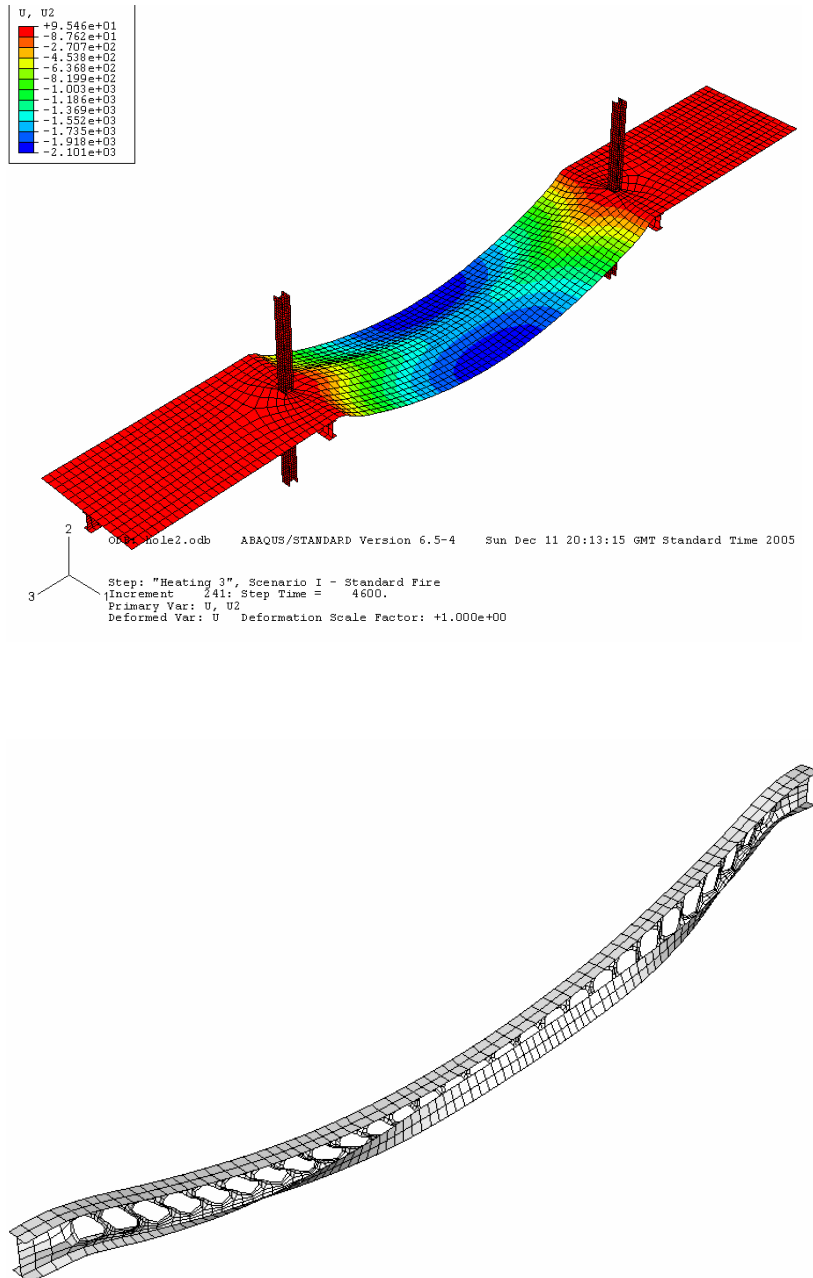
Case c.1 – Von Mises stresses



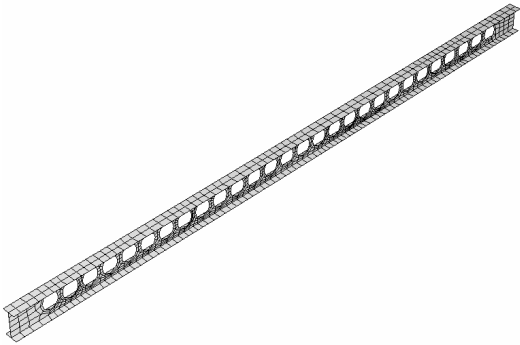
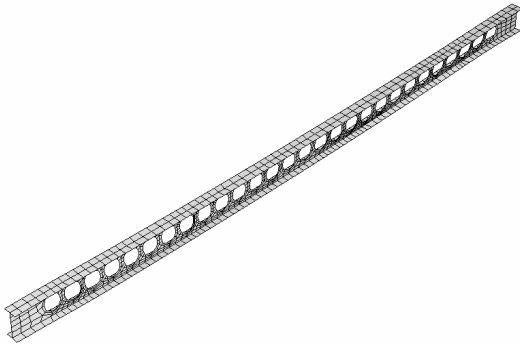
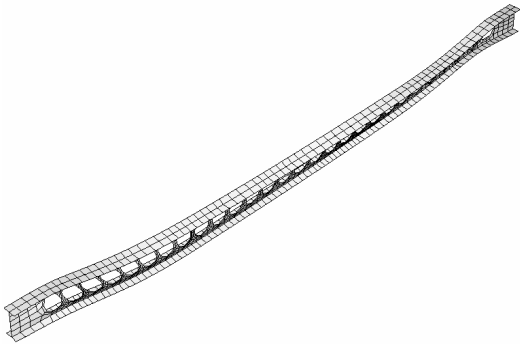
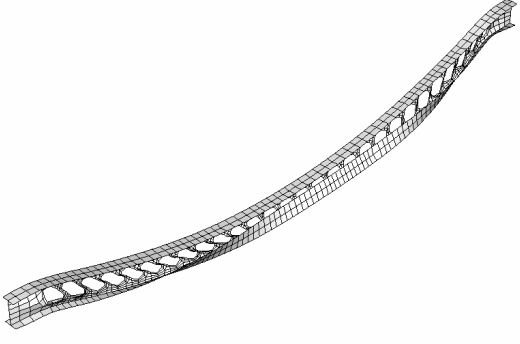
Scenario I – Case c.2

Case c.2 – Number of web openings = 28

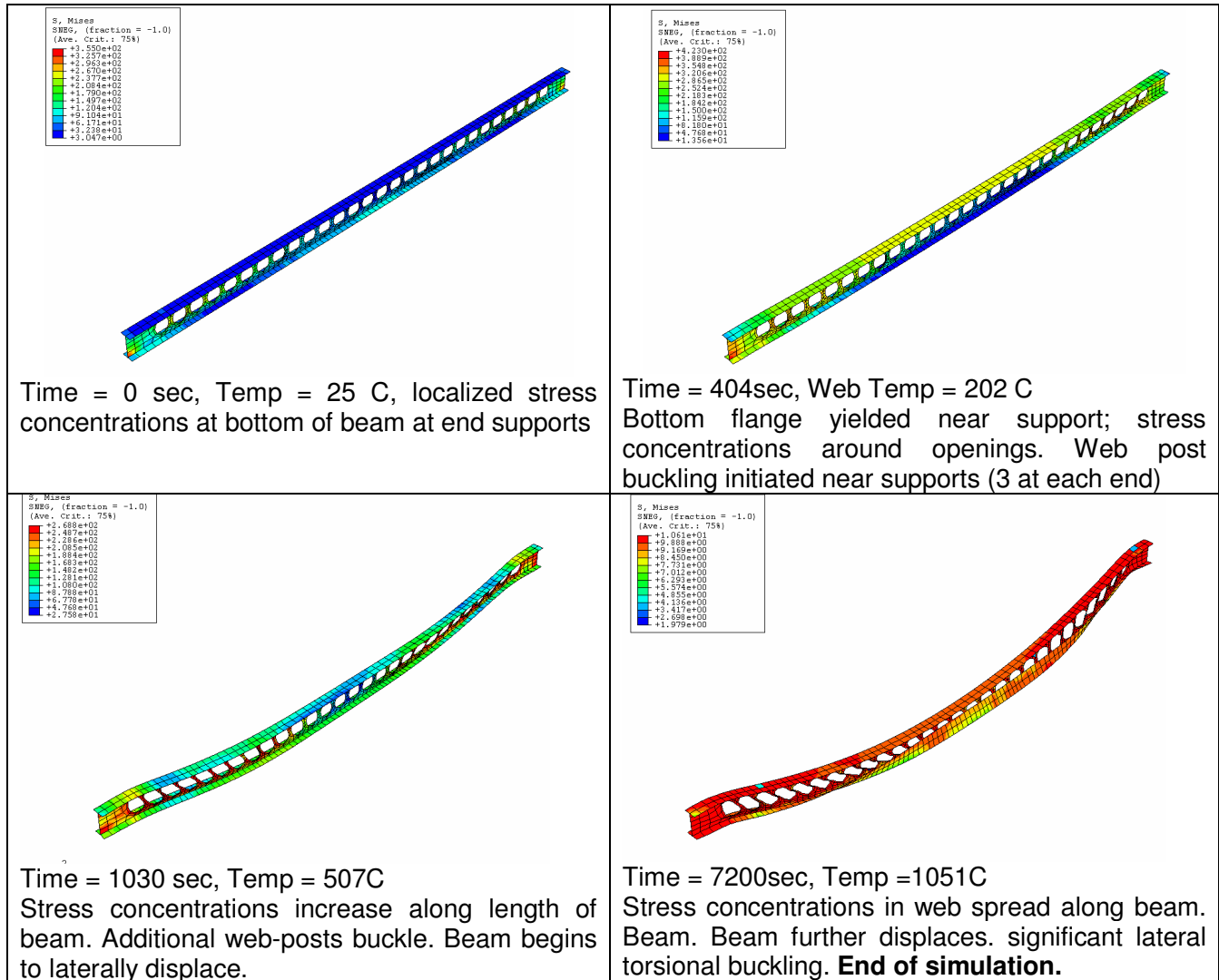
Displacement at end of simulation (t = 7200s, Temp =1051 C)



DEFORMATIONS: Case c.2 – Number of web openings = 28

| | |
|---|---|
|  <p>Time = 0 sec, Temp = 25 C, localized stress concentrations at bottom of beam at end supports</p> |  <p>Time = 553 sec, Web Temp = 286 C Bottom flange yielded near support; stress concentrations around openings. Web post buckling initiated near supports (3 at each end)</p> |
|  <p>Time = 1030 sec, Temp = 507C Stress concentrations increase along length of beam. Additional web-posts buckle. Beam begins to laterally displace.</p> |  <p>Time = 1979 sec, Temp = 823C Stress concentrations in web spread along beam. Beam further displaces. No significant lateral torsional buckling. End of simulation. No convergence</p> |

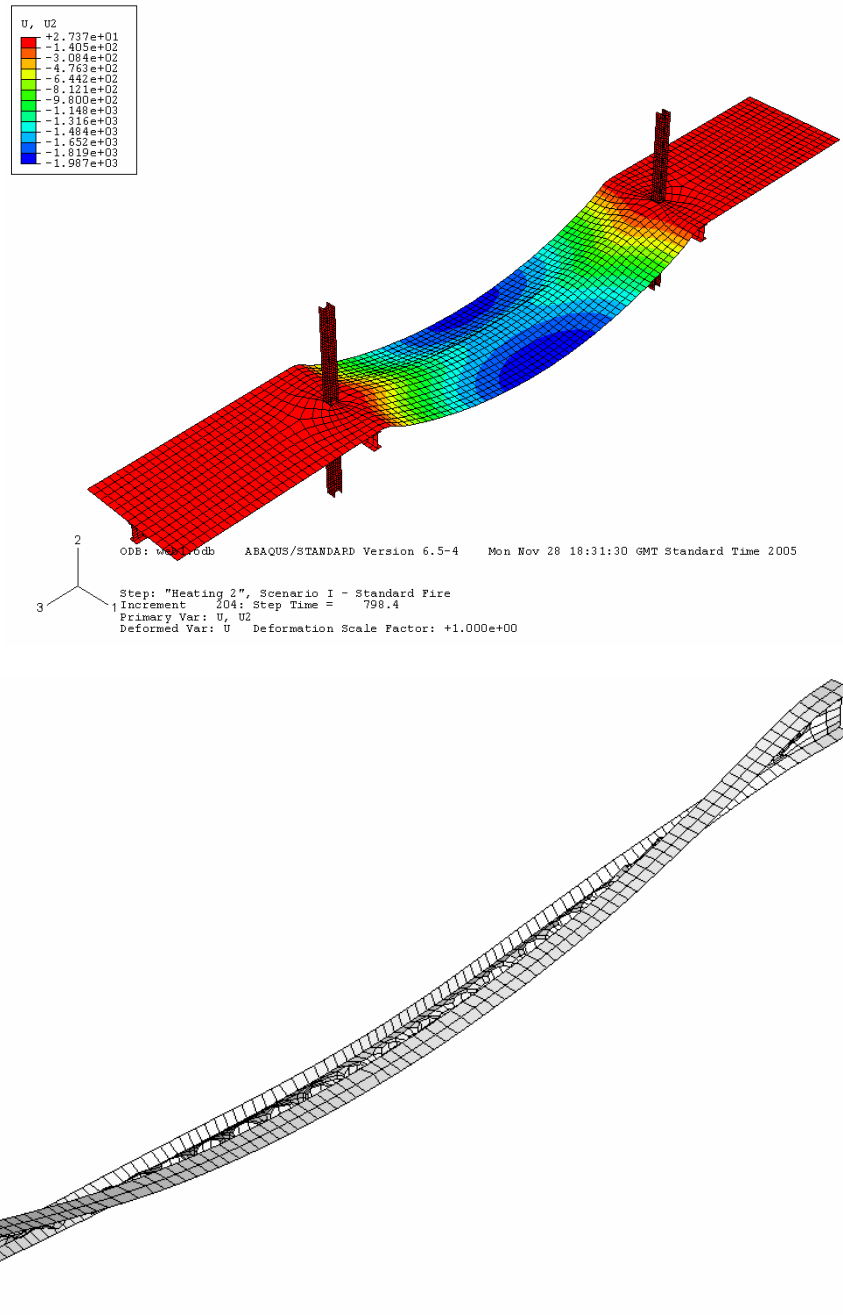
Case c.2 – Von Mises stresses



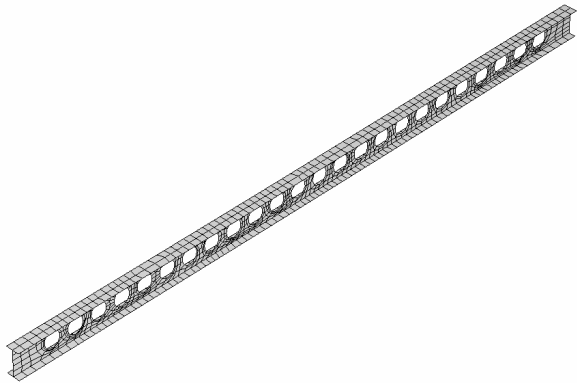
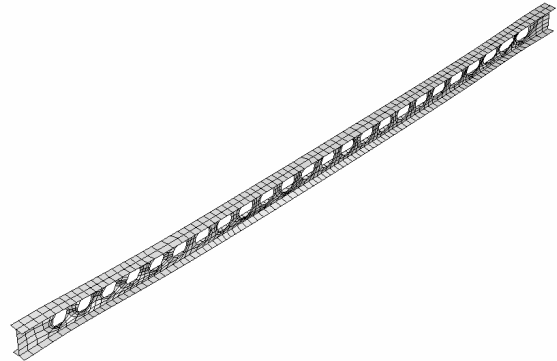
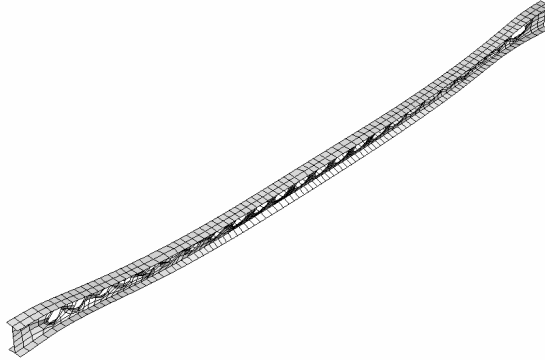
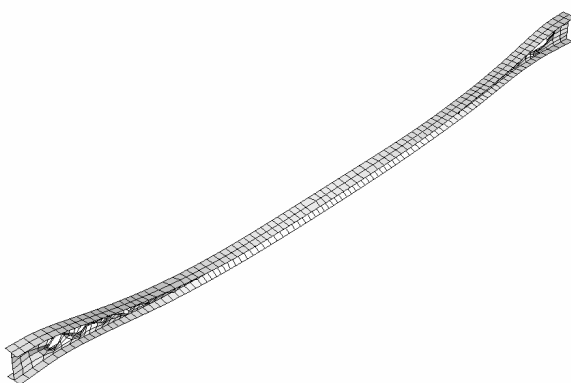
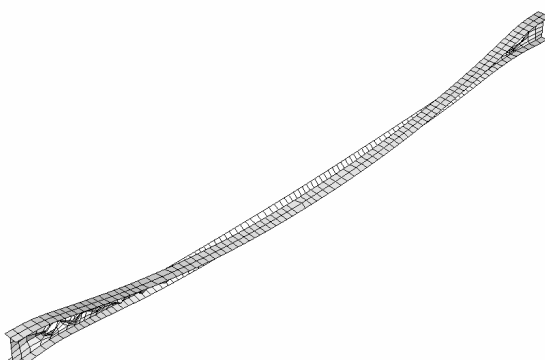
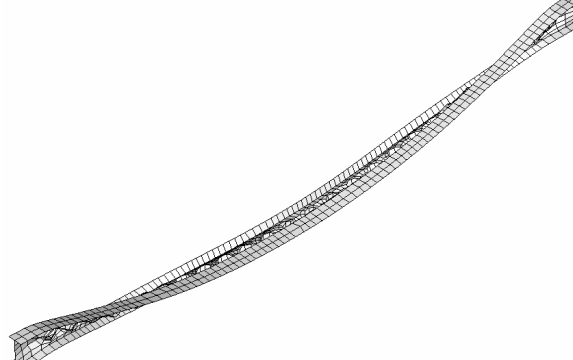
Scenario I – Case d.1

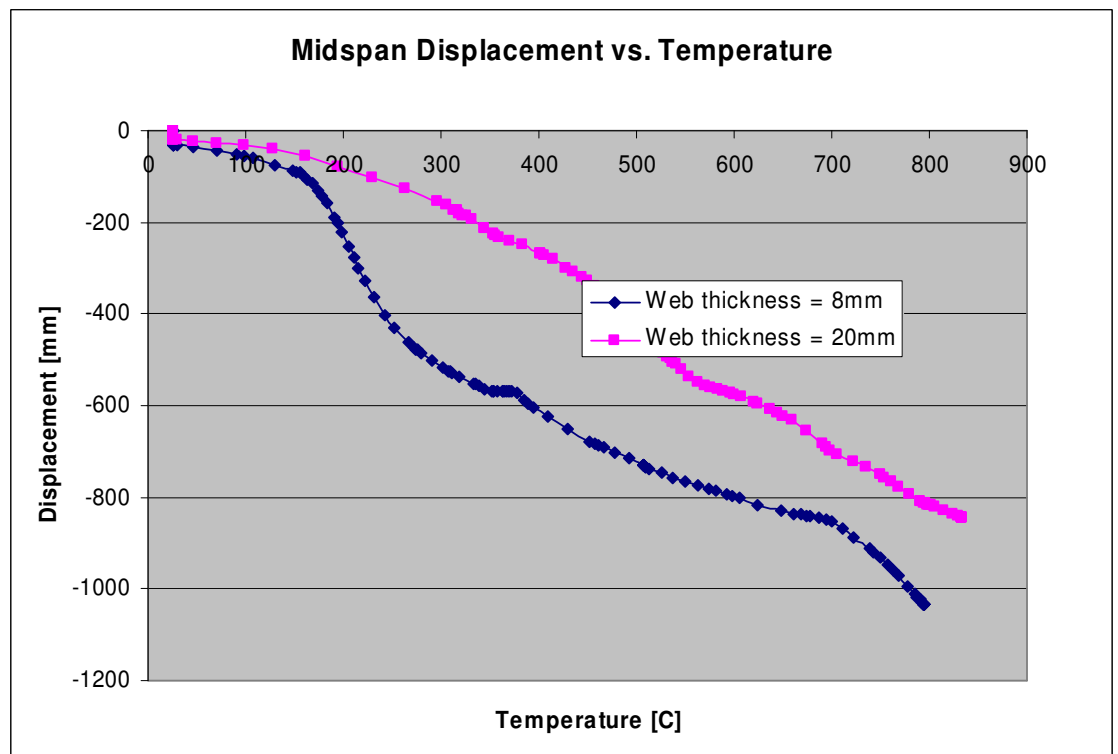
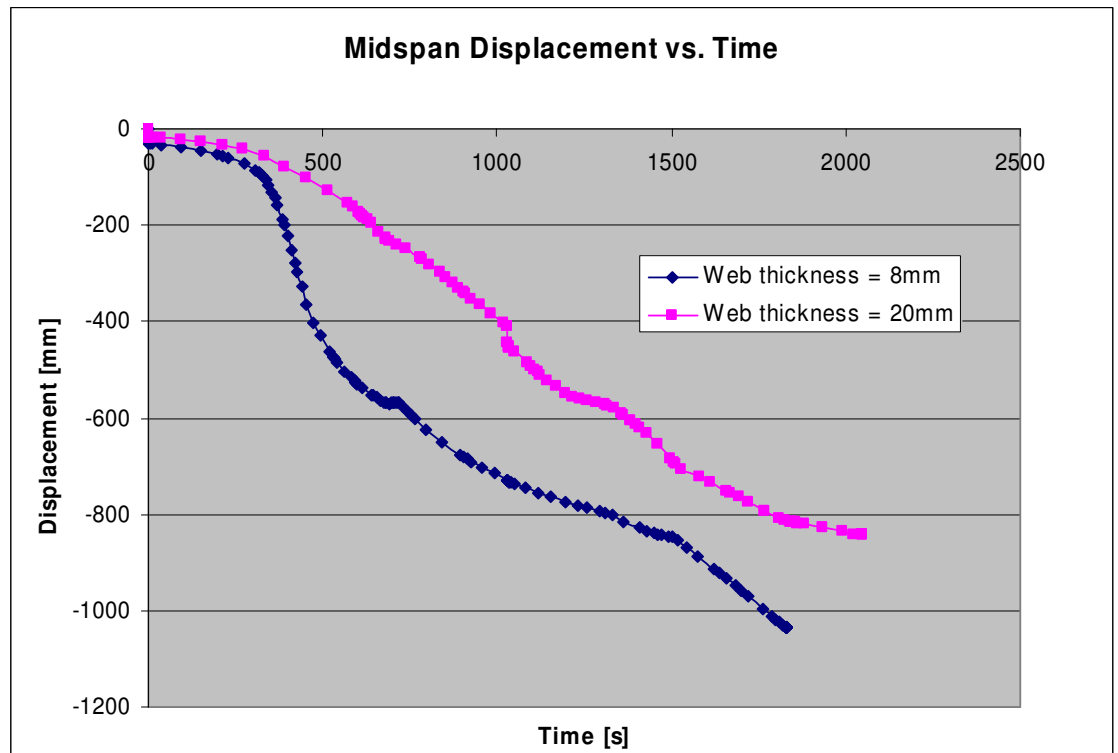
Case d.1 – web thickness = 8mm

Displacement at end of simulation (t = 1828s, Temp = 795C)

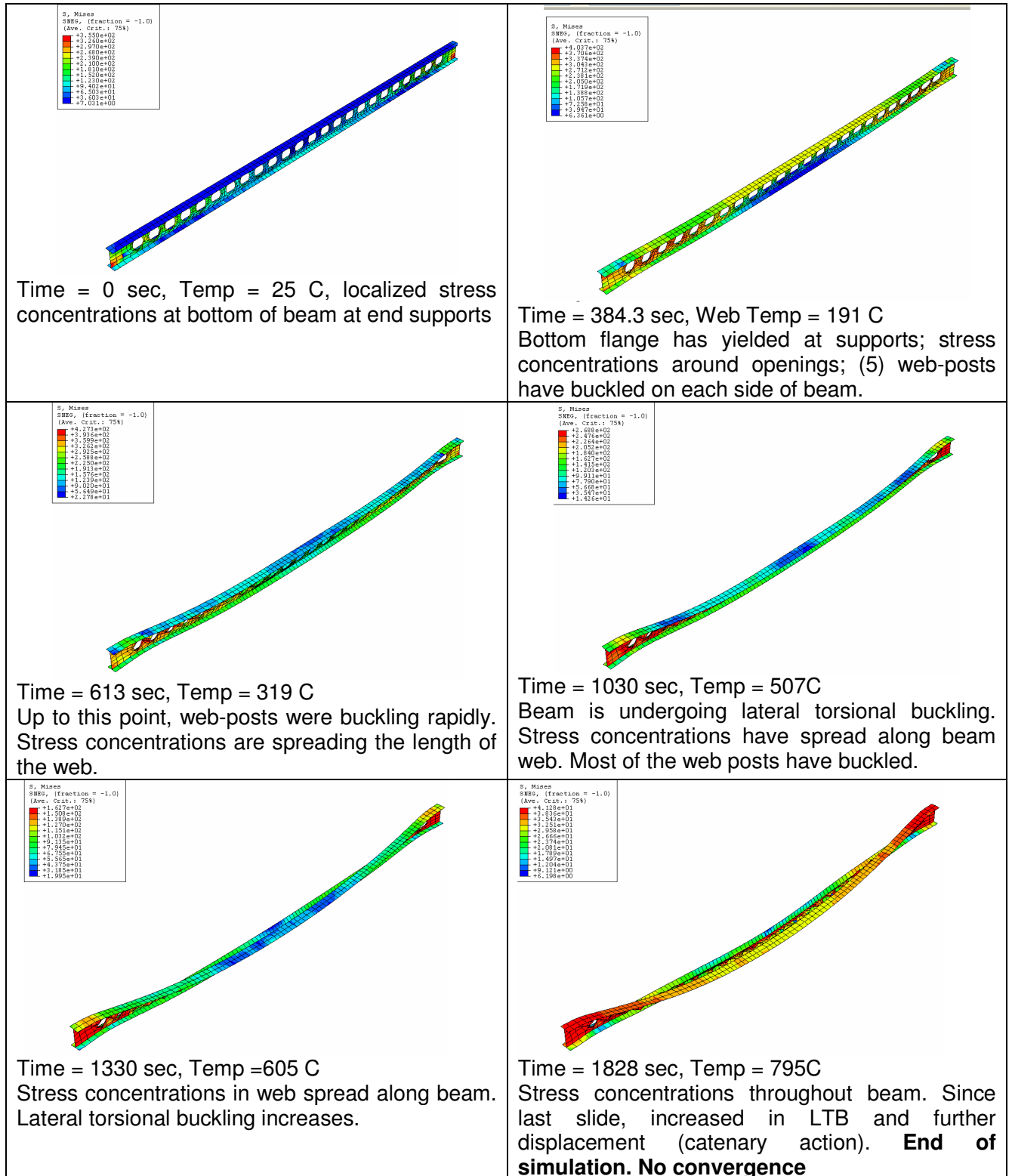


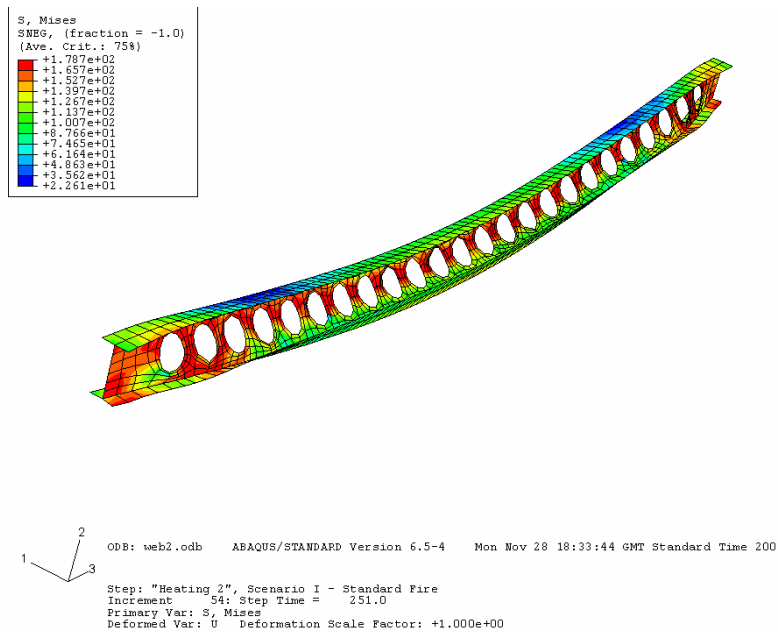
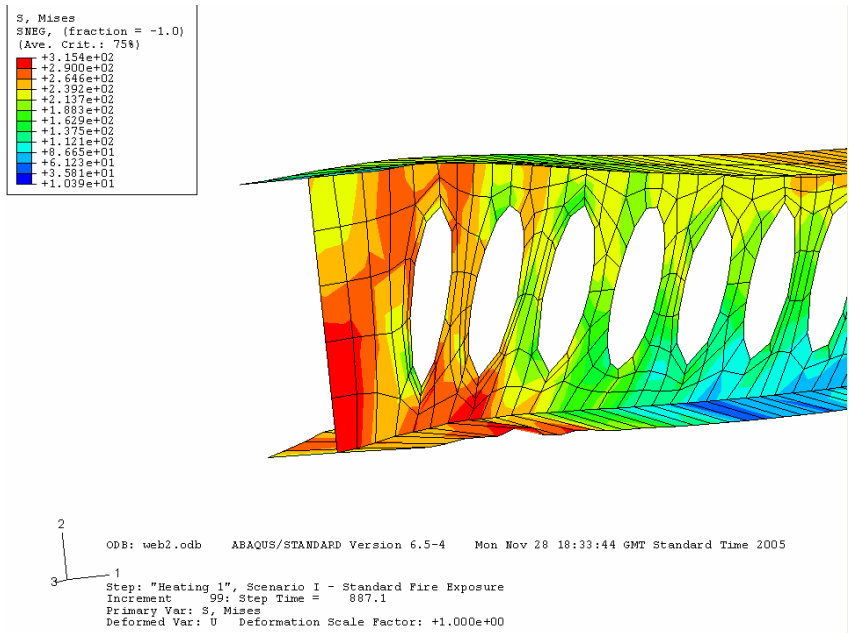
DEFORMATIONS: Case d.1 – Web thickness = 8mm

| | |
|--|---|
|  <p>Time = 0 sec, Temp = 25 C, localized stress concentrations at bottom of beam at end supports</p> |  <p>Time = 384.3 sec, Web Temp = 191 C Bottom flange has yielded at supports; stress concentrations around openings; (5) web-posts have buckled on each side of beam.</p> |
|  <p>Time = 613 sec, Temp = 319 C Up to this point, web-posts were buckling rapidly. Stress concentrations are spreading the length of the web.</p> |  <p>Time = 1030 sec, Temp = 507C Beam is undergoing lateral torsional buckling. Stress concentrations have spread along beam web. Most of the web posts have buckled.</p> |
|  <p>Time = 1330 sec, Temp = 605 C Stress concentrations in web spread along beam. Lateral torsional buckling increases.</p> |  <p>Time = 1828 sec, Temp = 795C Stress concentrations throughout beam. Since last slide, increased in LTB and further displacement (catenary action). End of simulation. No convergence</p> |



Case d.1 – Von Mises stresses

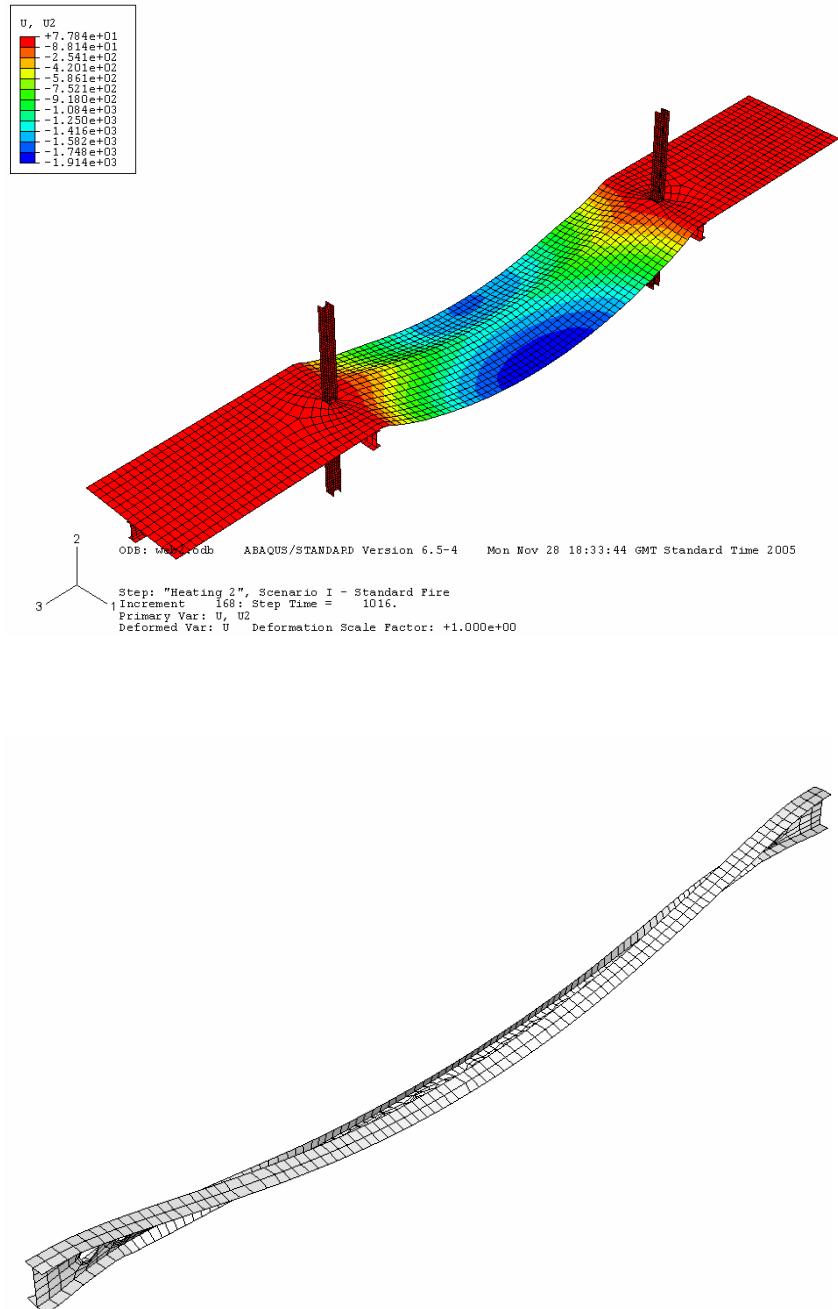




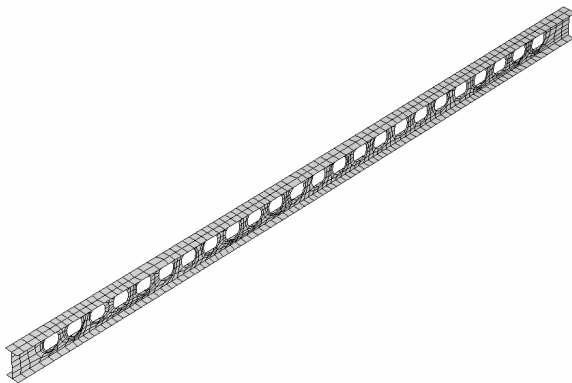
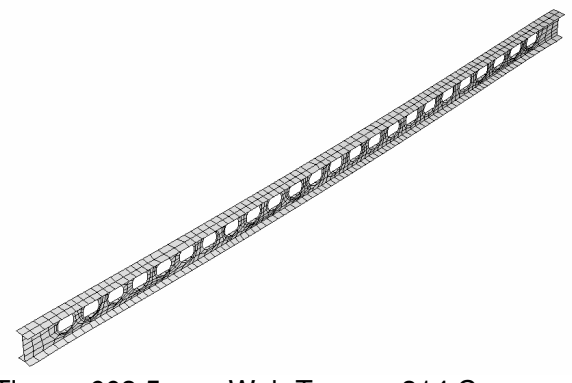
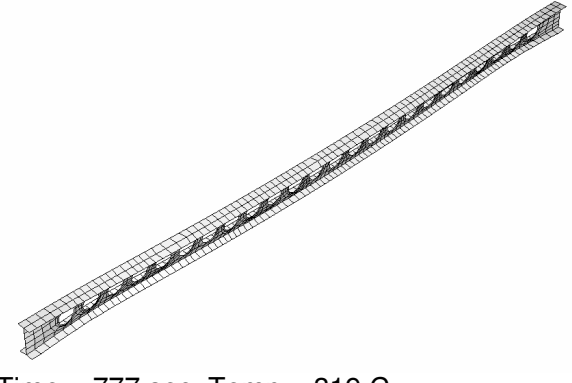
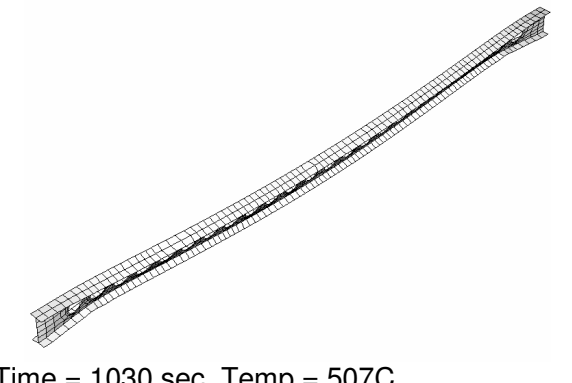
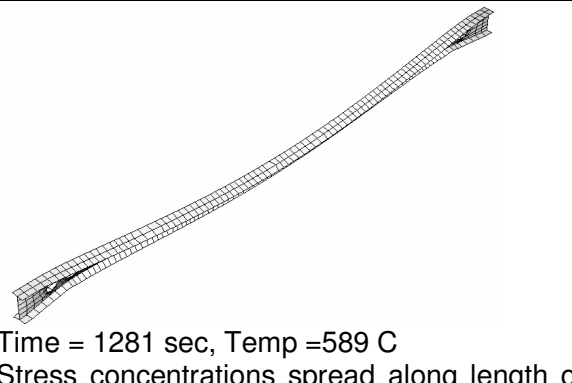
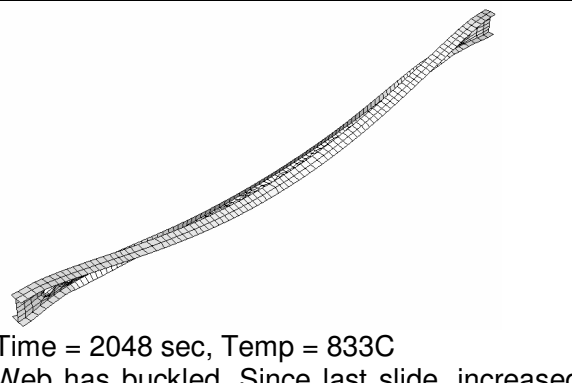
Scenario I – Case d.2

Case d.2 – Web thickness = 20 mm

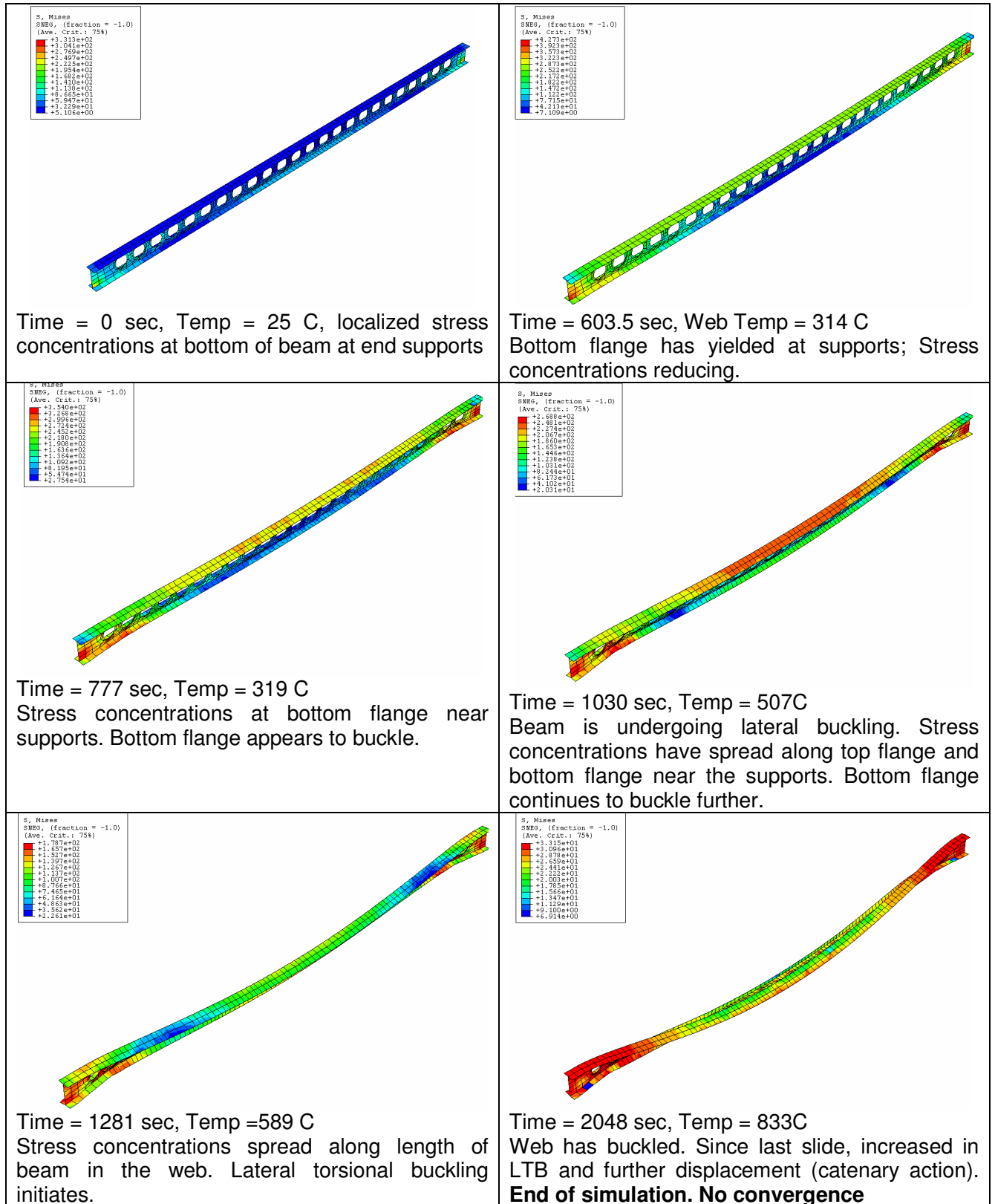
Displacement at end of simulation (t = 2046s, Temp =795 C)



DEFORMATIONS: Case d.2 – Web thickness = 20 mm

| | |
|--|---|
|  <p>Time = 0 sec, Temp = 25 C, localized stress concentrations at bottom of beam at end supports</p> |  <p>Time = 603.5 sec, Web Temp = 314 C Bottom flange has yielded at supports; Stress concentrations reducing.</p> |
|  <p>Time = 777 sec, Temp = 319 C Stress concentrations at bottom flange near supports. Bottom flange appears to buckle.</p> |  <p>Time = 1030 sec, Temp = 507C Beam is undergoing lateral buckling. Stress concentrations have spread along top flange and bottom flange near the supports. Bottom flange continues to buckle further.</p> |
|  <p>Time = 1281 sec, Temp = 589 C Stress concentrations spread along length of beam in the web. Lateral torsional buckling initiates.</p> |  <p>Time = 2048 sec, Temp = 833C Web has buckled. Since last slide, increased in LTB and further displacement (catenary action). End of simulation. No convergence</p> |

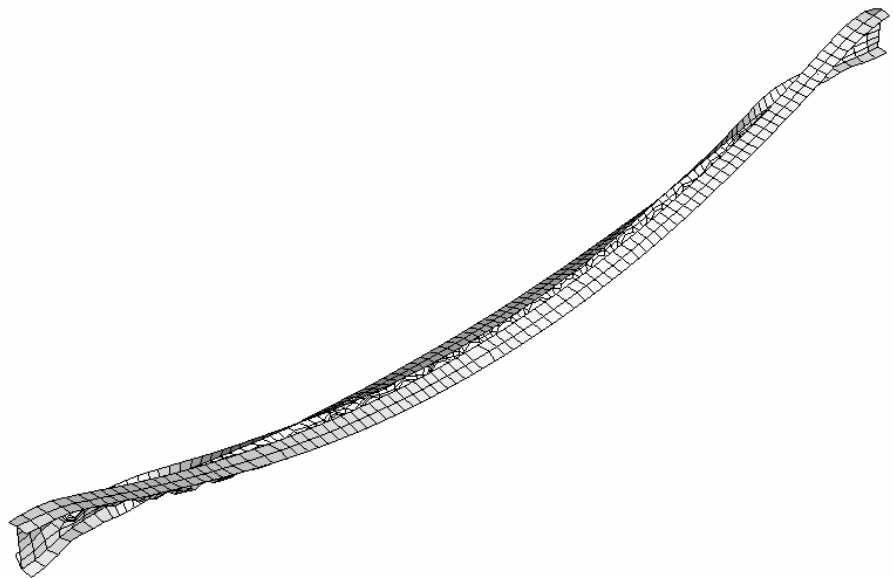
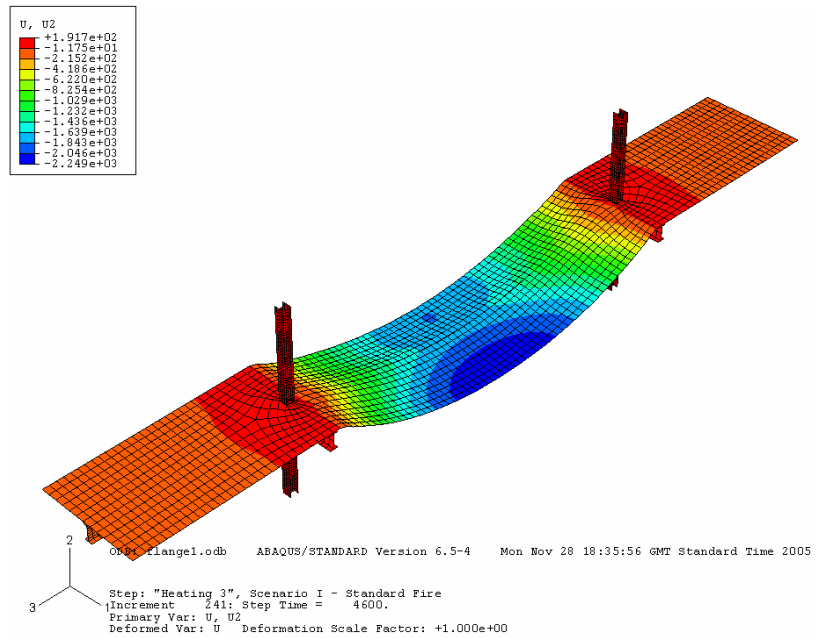
Case d.2 – Von Mises stresses



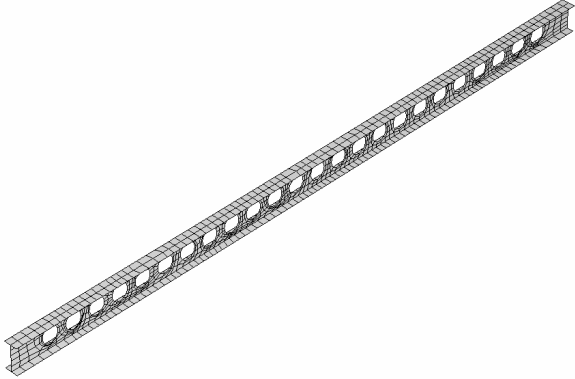
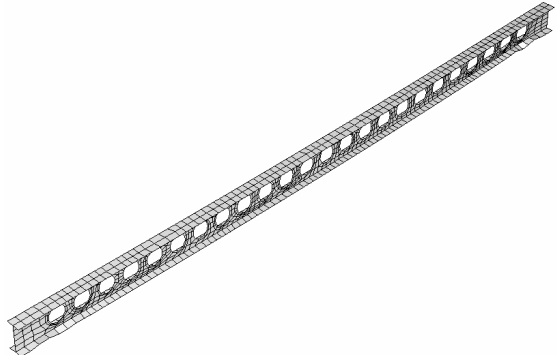
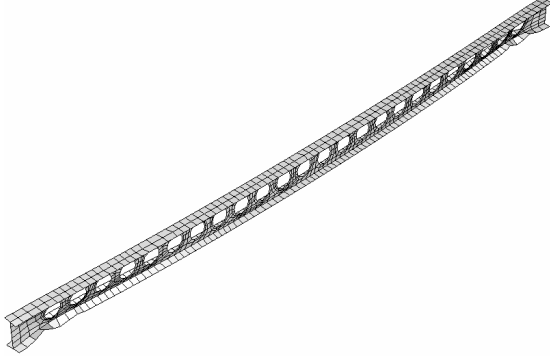
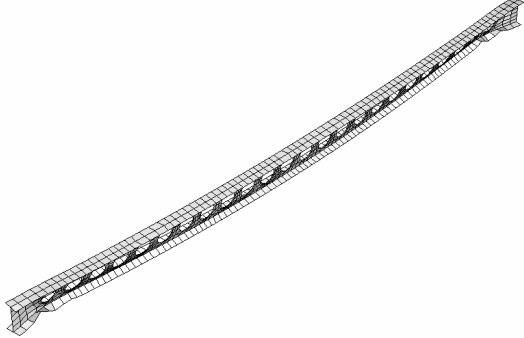
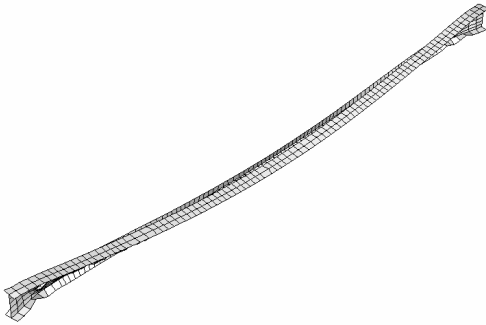
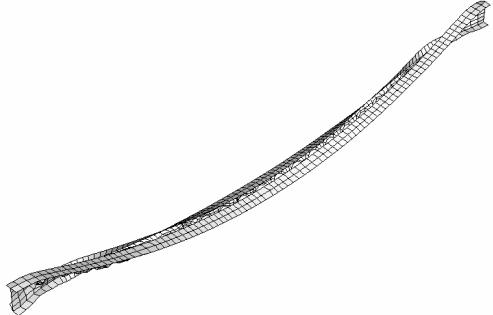
Scenario I – Case e.1

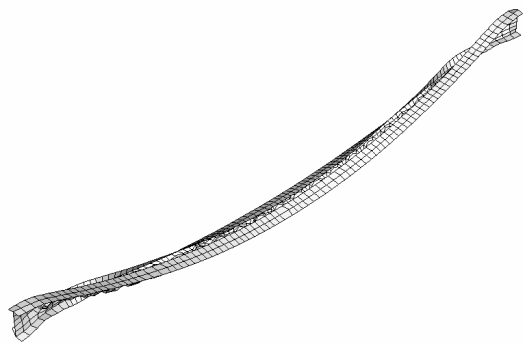
Case e.1 – Flange thickness = 12mm

Displacement at end of simulation (t = 7200s, Temp = 1015C)



DEFORMATIONS: Case e.1 – Flange thickness = 12mm

| | |
|--|---|
|  <p>Time = 0 sec, Temp = 25 C, localized stress concentrations at bottom of beam at end supports</p> |  <p>Time = 427 sec, Web Temp = 215 C Bottom flange has yielded near supports; stress concentrations near buckling flanges.</p> |
|  <p>Time = 701 sec, Temp = 365 C Bottom flange buckles further. Stress concentrations localized in these areas.</p> |  <p>Time = 1030 sec, Temp = 507C End-post and web-post near supports have buckled. Stresses concentrated near supports. Beam is laterally displacing more.</p> |
|  <p>Time = 1286 sec, Temp = 591 C Since last slide, stress concentrations spread rapidly in web along beam. Lateral torsional buckling increases quickly.</p> |  <p>Time = 2600 sec, Temp = 887C Stress concentrations throughout beam. Since last slide, increased in LTB and further displacement (catenary action).</p> |



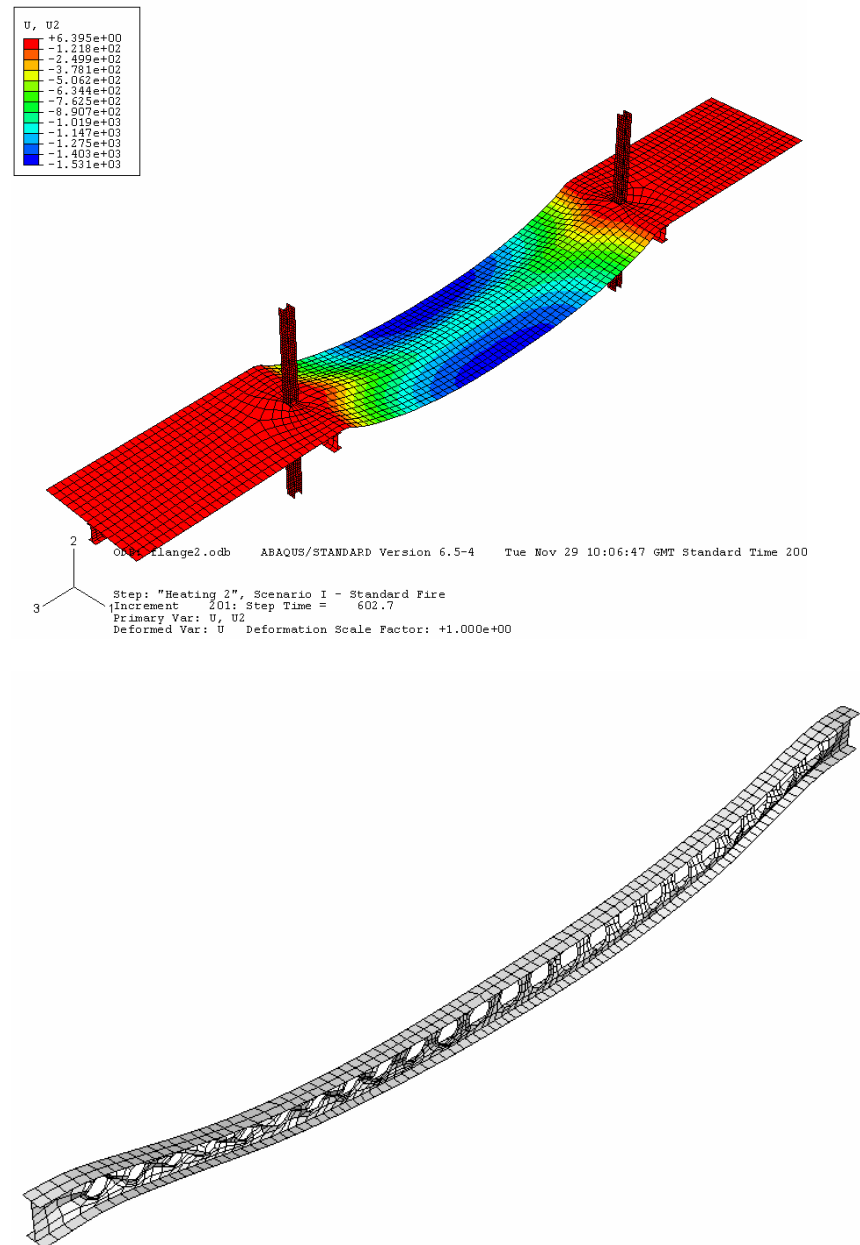
Time = 7200 sec, Temp = 1015 C
Stress concentrations throughout beam.
Beam undergoes catenary action >>> further
displaces.

END OF SIMULATION

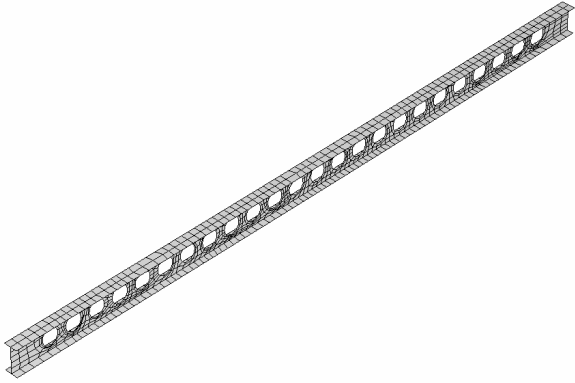
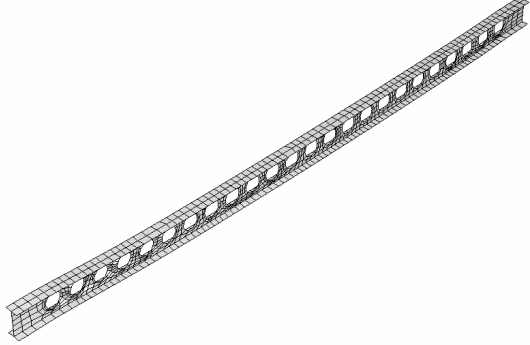
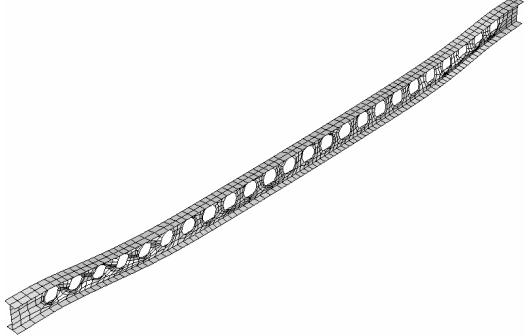
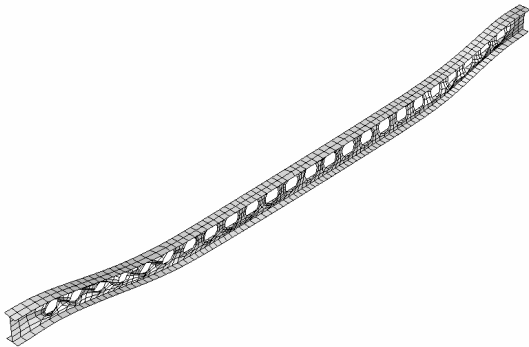
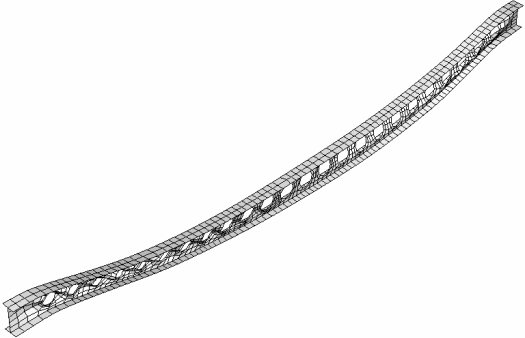
Scenario I – Case e.2

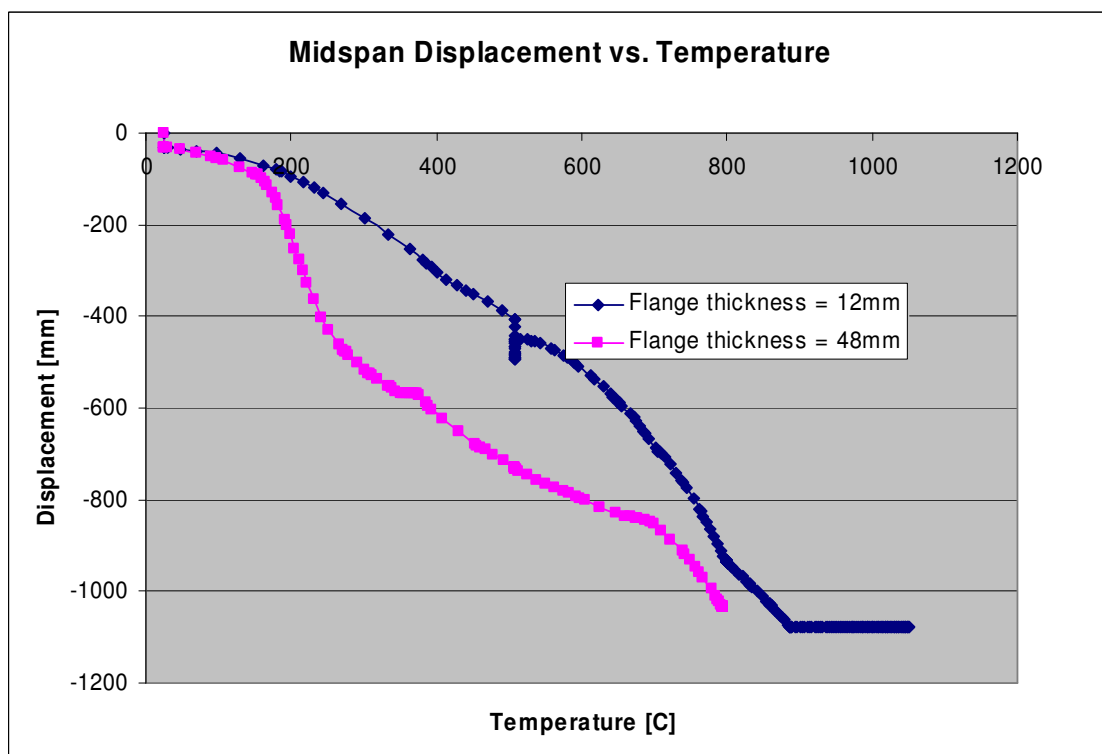
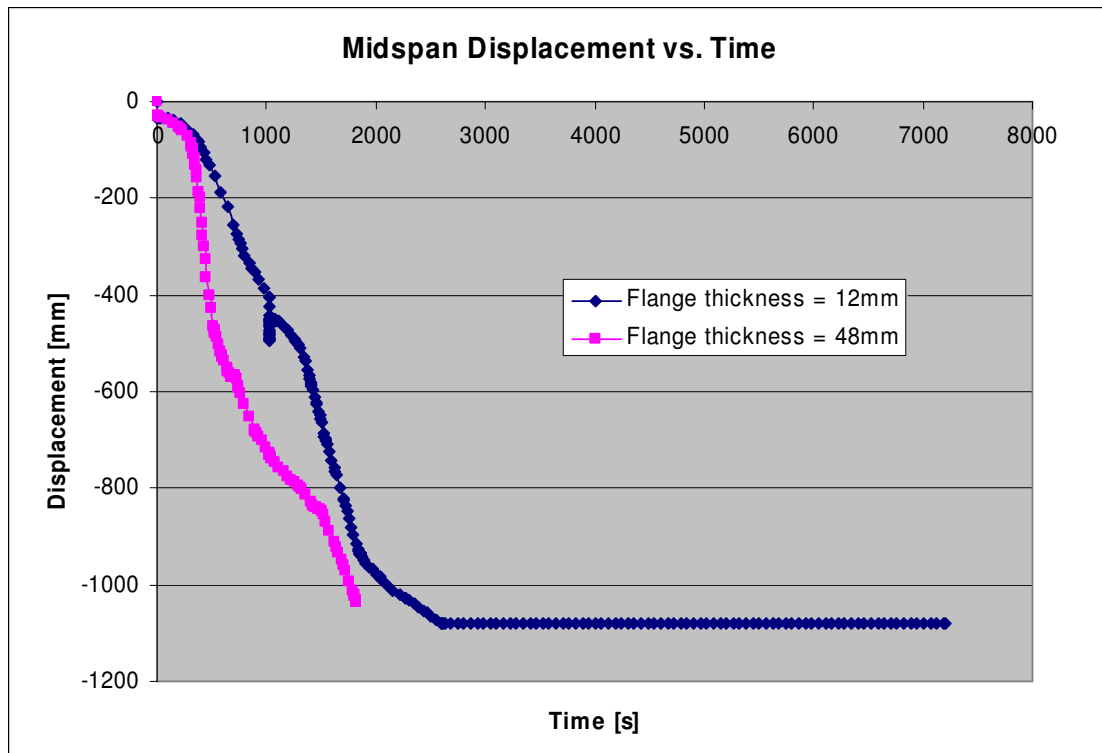
Case e.2 – Flange thickness = 48mm

Displacement at end of simulation (t = 1633s, Temp = 742C)

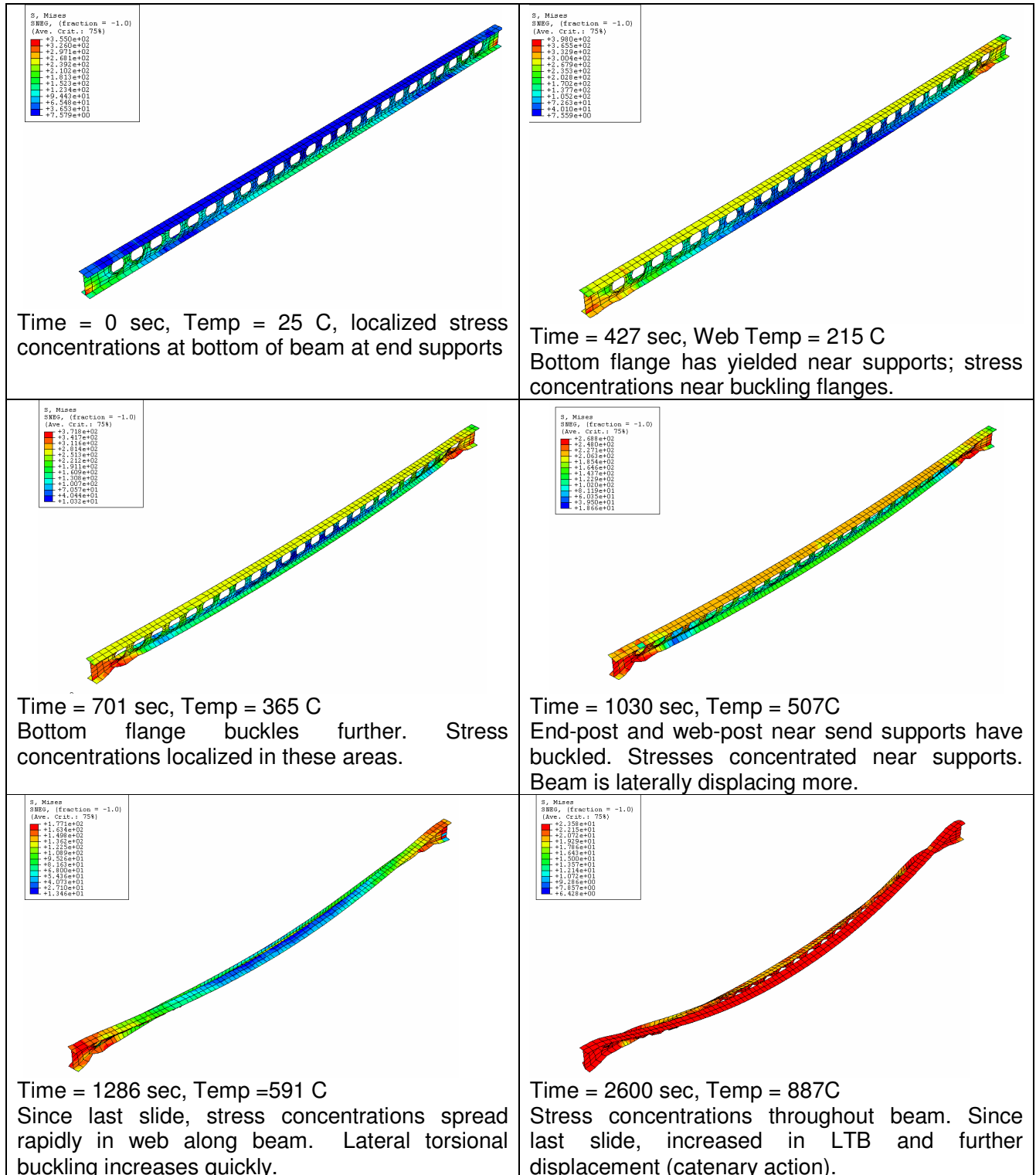


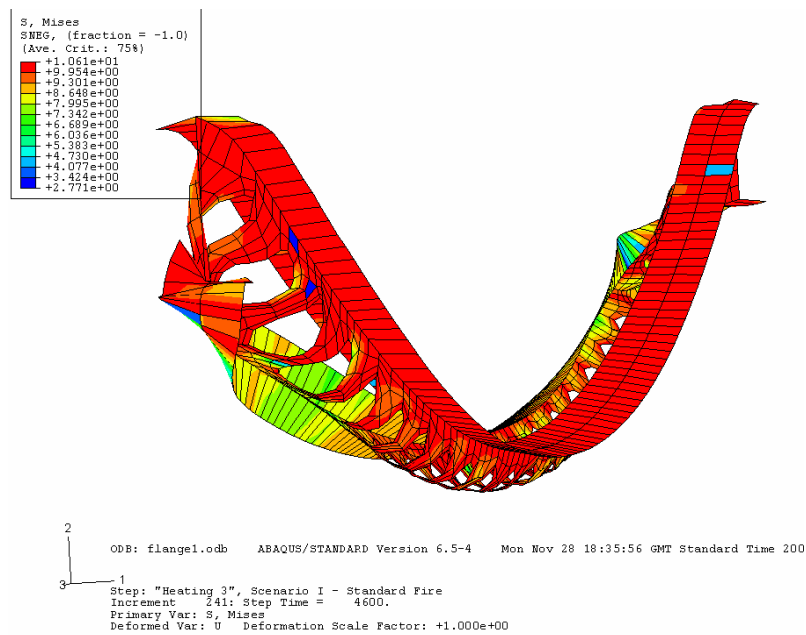
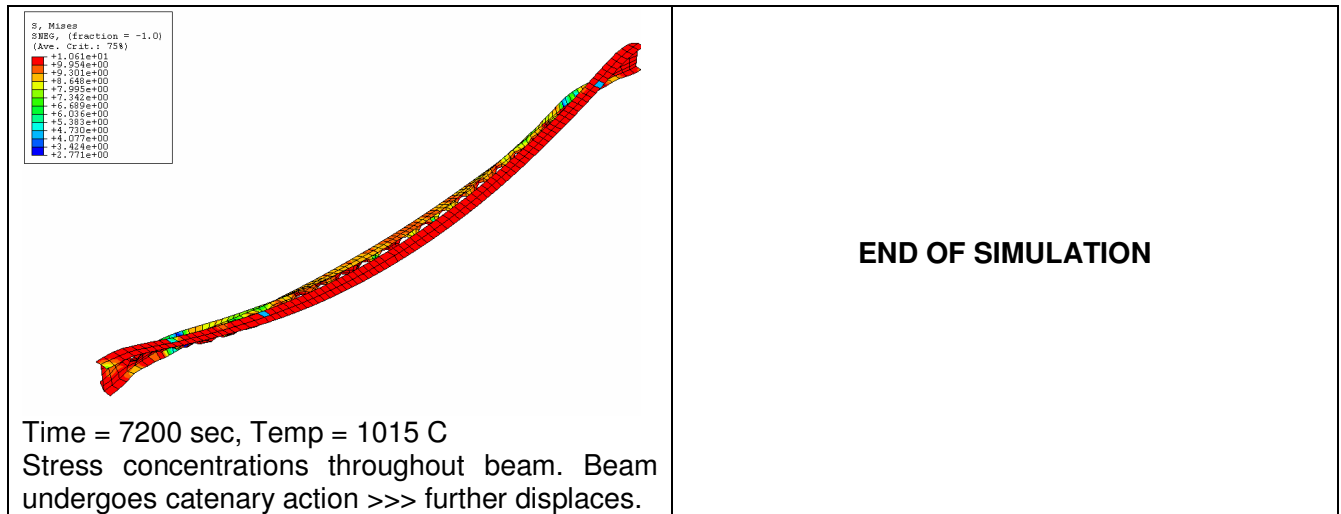
DEFORMATIONS: Case e.2 – Flange thickness = 48mm

| | |
|--|---|
|  <p>Time = 0 sec, Temp = 25 C, localized stress concentrations at bottom of beam at end supports</p> |  <p>Time = 505 sec, Web Temp = 260 C Stress concentrations around web openings near supports. Web posts start buckling (4) on each end.</p> |
|  <p>Time = 575 sec, Temp = 365 C Stress concentrations spread along web. Beam stabilizes slightly.</p> |  <p>Time = 1030 sec, Temp = 507C Stress concentrations spread further. Web posts buckle more as beam displaces downward. Minimal LTB</p> |
|  <p>Time = 1632 sec, Temp = 742 C Since last slide, stress concentrations spread rapidly in web along beam. Beam displaces further. Minimal lateral torsional buckling.</p> | <p>END OF SIMULATION NO CONVERGENCE</p> |

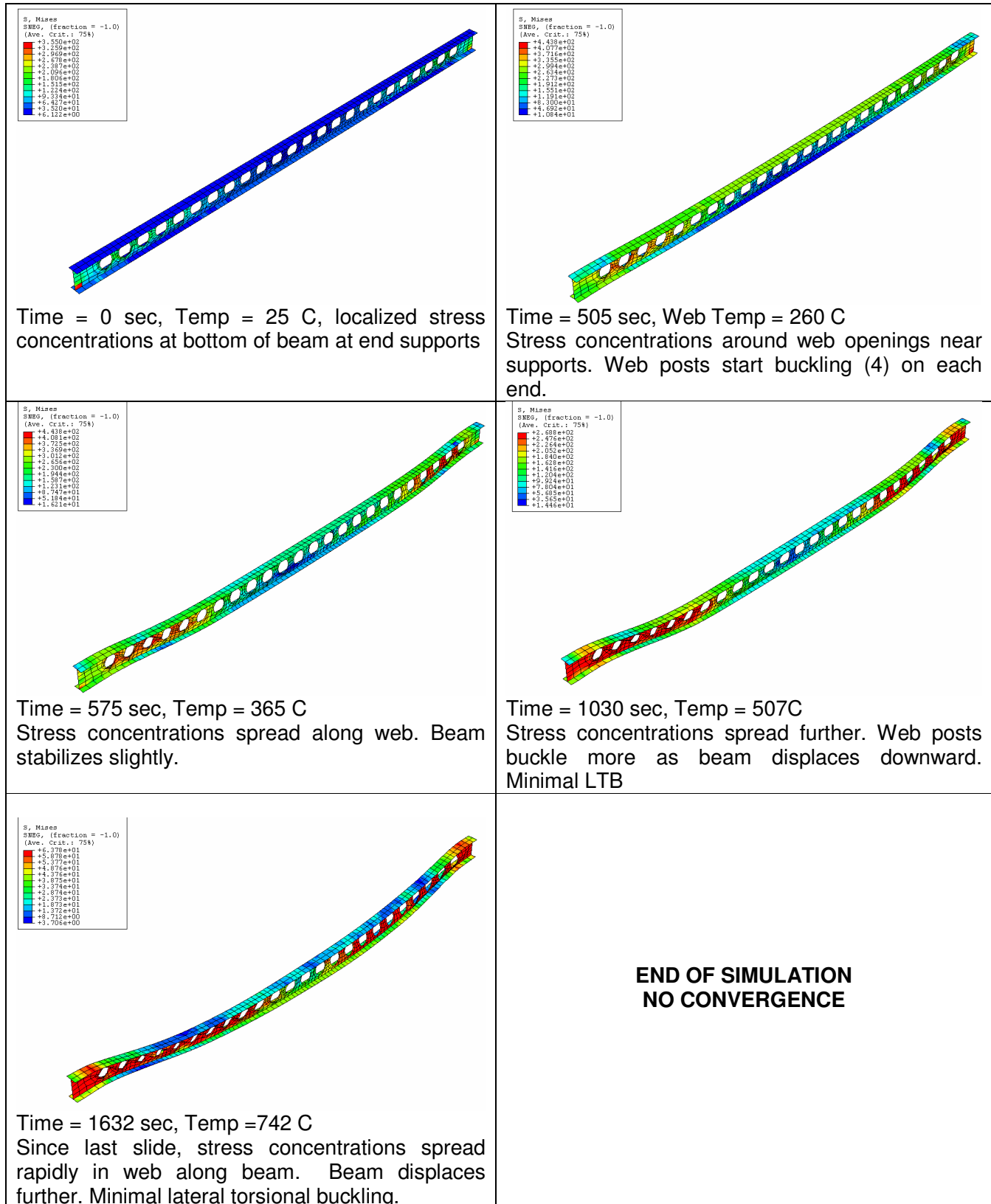


Case e.1 – Von Mises stresses





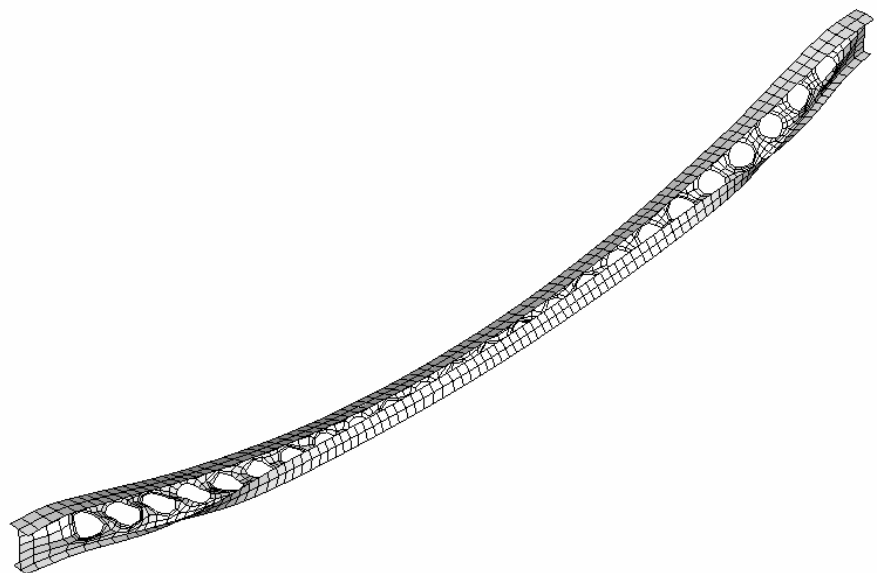
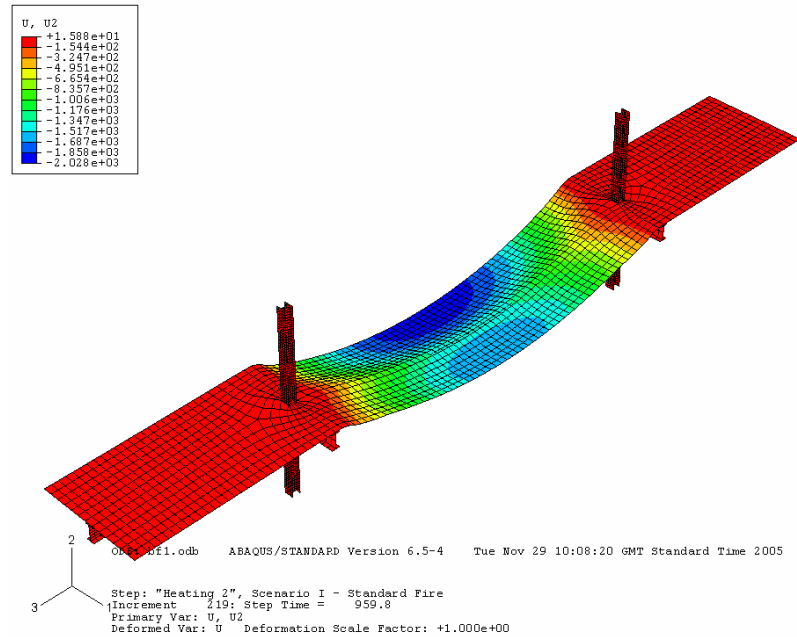
Case e.2 – Von Mises stresses



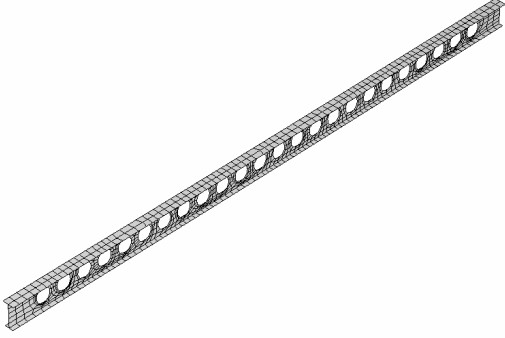
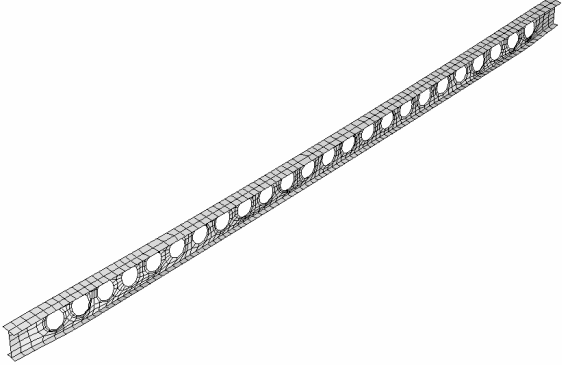
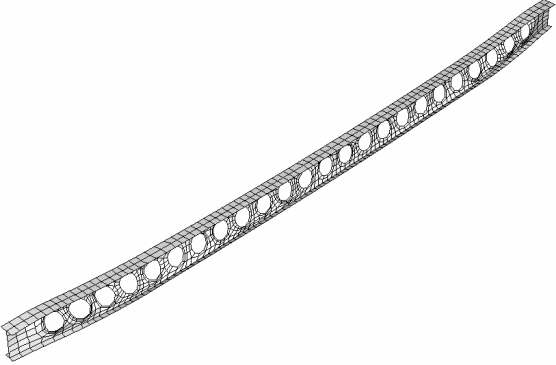
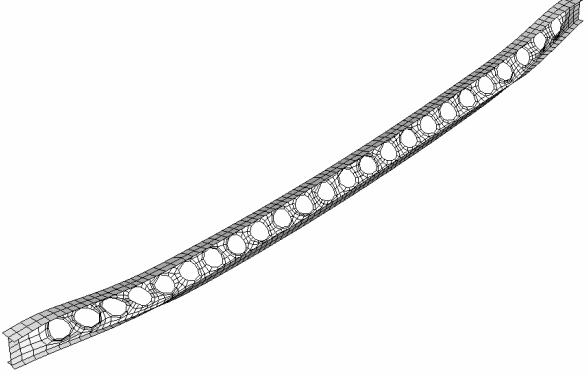
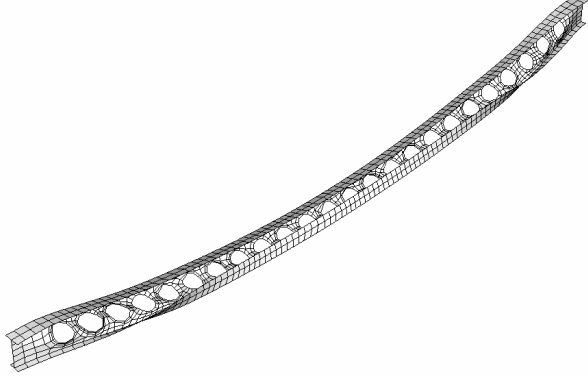
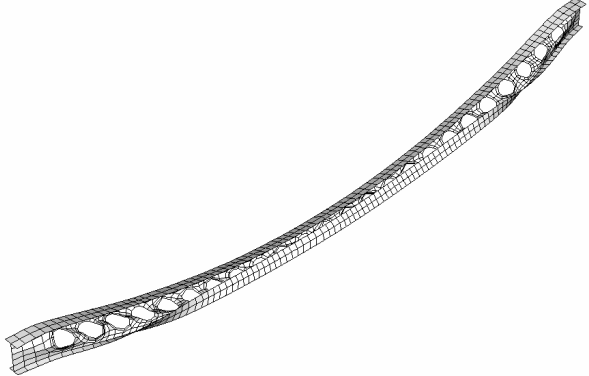
Scenario I – Case f.1 and Case f.2

Case f.1 – Bottom flange width = 270mm

Displacement at end of simulation (t = 1990s, Temp = 825C)

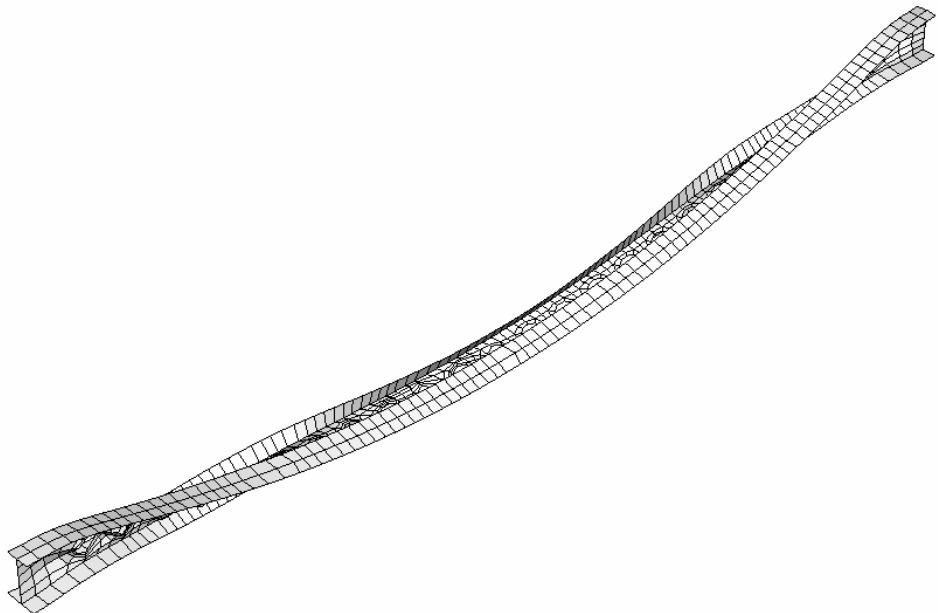
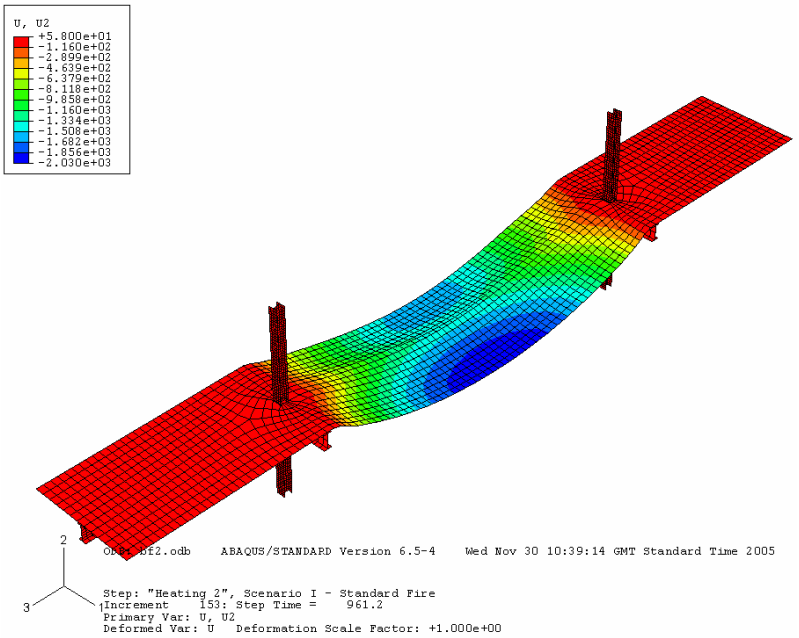


DEFORMATIONS: Case f.1 – Bottom flange width = 270mm

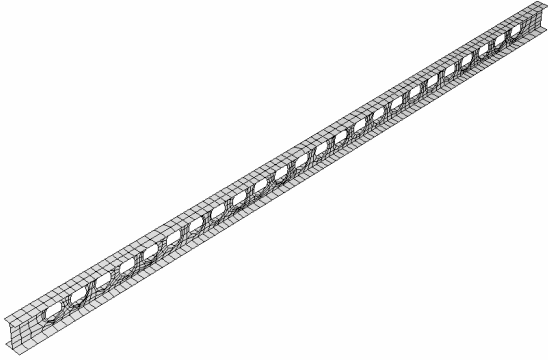
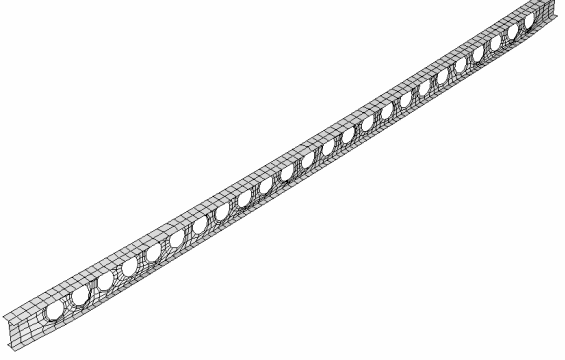
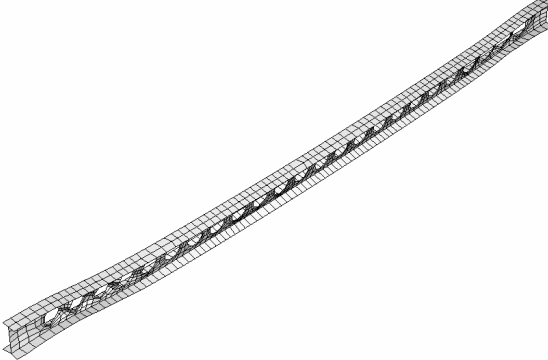
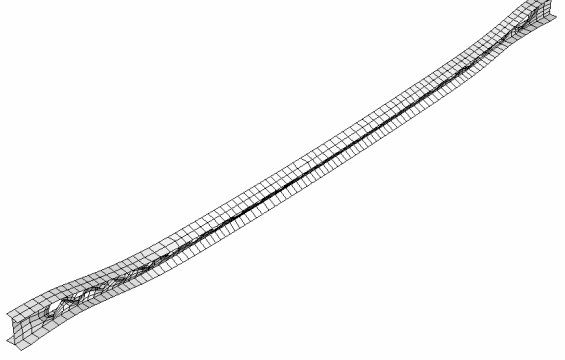
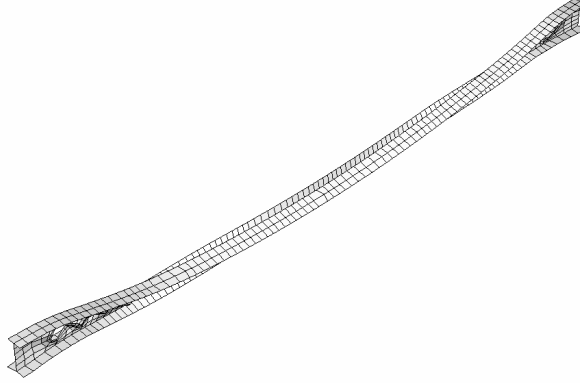
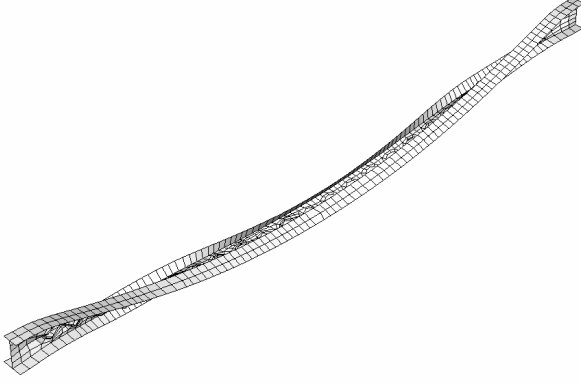
| | |
|--|---|
|  <p>Time = 0 sec, Temp = 25 C</p> |  <p>Time = 506 sec, Temp = 260 C Lateral torsional buckling starts</p> |
|  <p>Time = 679 sec, Temp = 353 C (3) Web posts at each ending are starting to buckle, stress concentrations around holes of buckling web posts</p> |  <p>Time = 1030 sec, Temp = 570 C Stress concentrations along beam around holes, more lateral buckling</p> |
|  <p>Time = 1397 sec, Temp = 644 C Beam buckles lateral more and then goes into catenary action</p> |  <p>Time = 1990 sec. Temp = 825 C End of simulation; catenary action</p> |

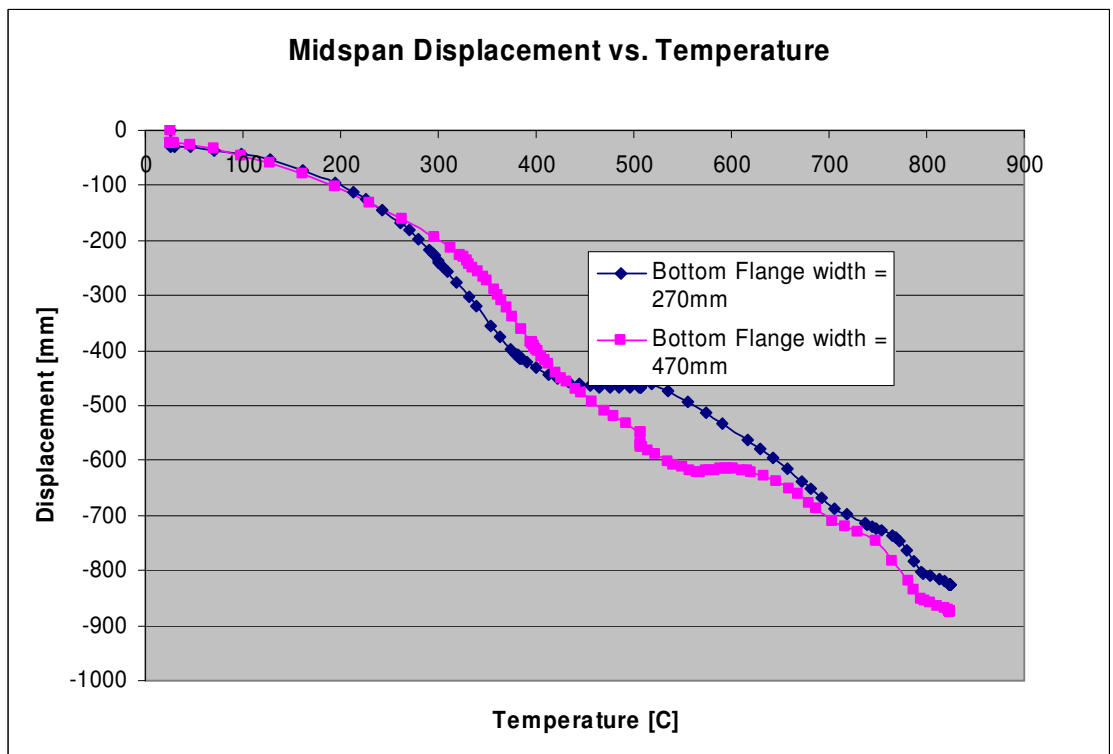
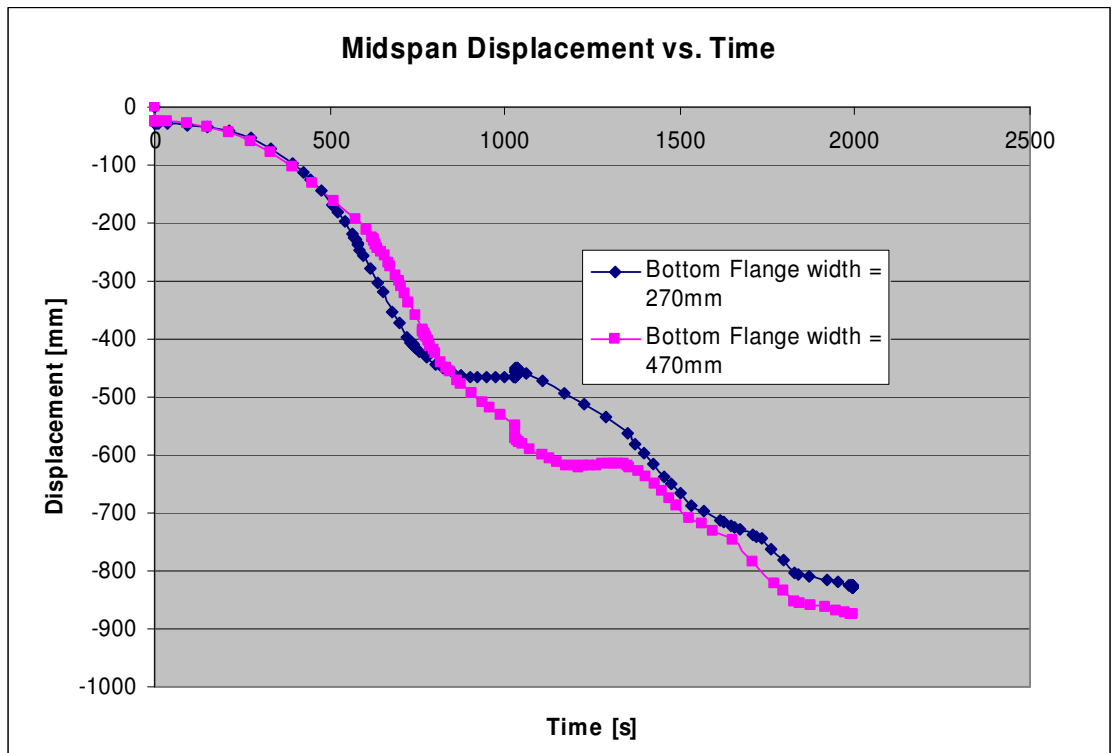
Case f.2 – Bottom flange width = 470mm

Displacement at end of simulation (t = 1991s, Temp = 825 C)

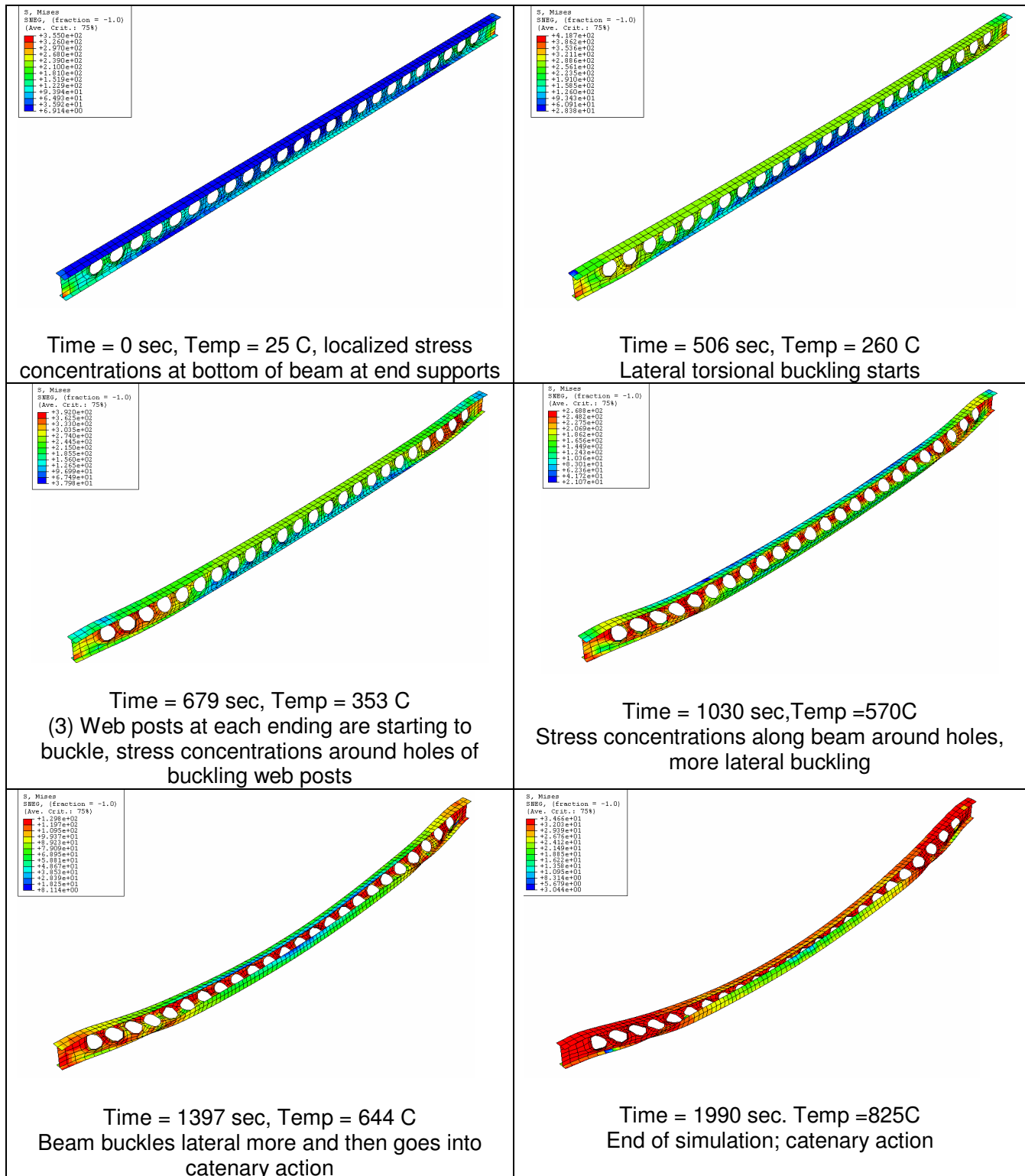


DEFORMATIONS: Case f.2 – Bottom flange width = 470mm

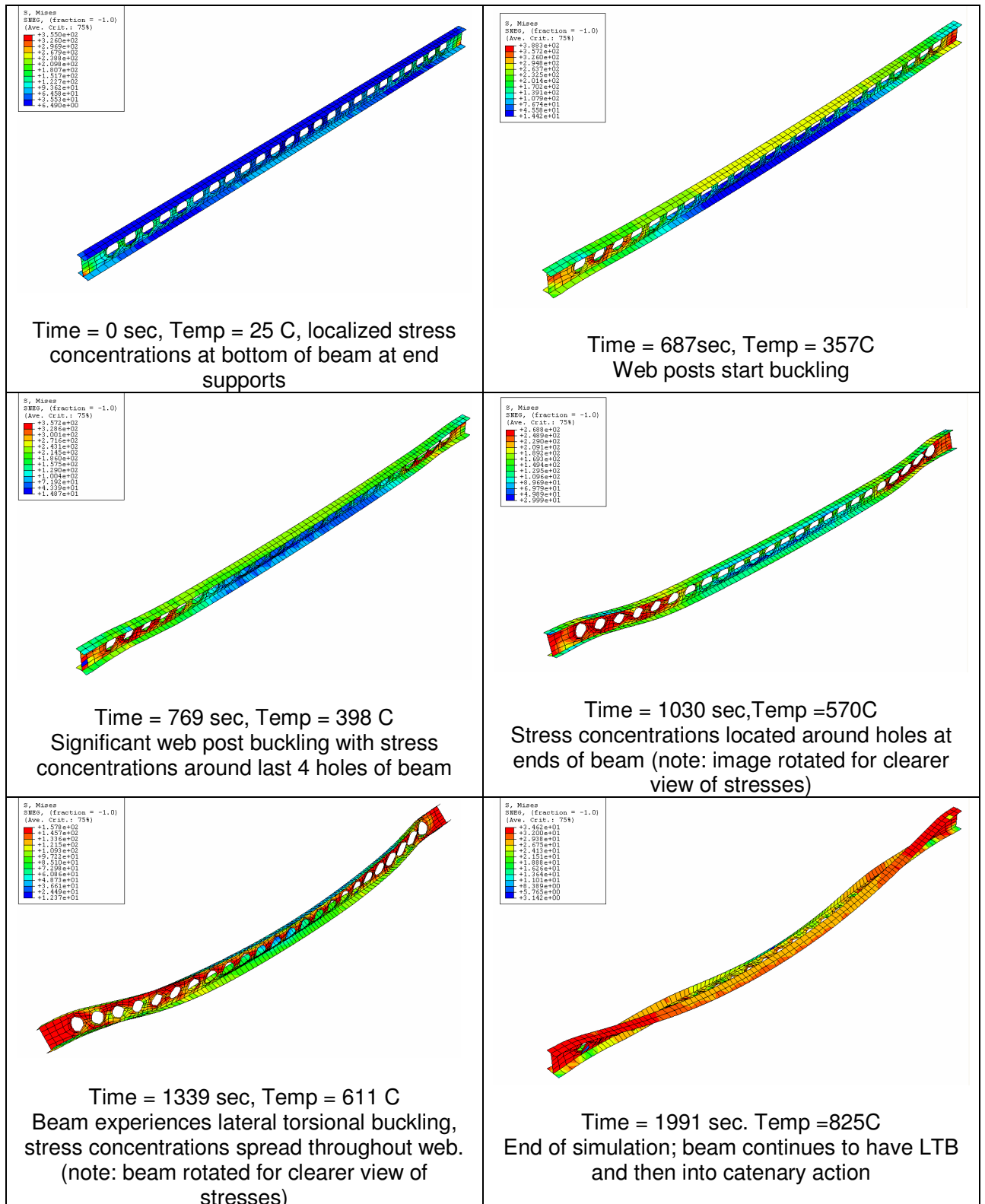
| | |
|---|---|
|  <p>Time = 0 sec, Temp = 25 C</p> |  <p>Time = 687 sec, Temp = 357C Web posts begin buckling</p> |
|  <p>Time = 769 sec, Temp = 398 C Significant web post buckling with stress concentrations around last 4 holes of beam</p> |  <p>Time = 1030 sec, Temp = 570C Beam displaces more, stress concentrations located around holes at ends of beam</p> |
|  <p>Time = 1339 sec, Temp = 611 C Beam experiences lateral torsional buckling, stress concentrations spread throughout web</p> |  <p>Time = 1991 sec, Temp = 825C End of simulation; beam continues to have LTB and then into catenary action</p> |



Case f.1 – Von Mises stresses



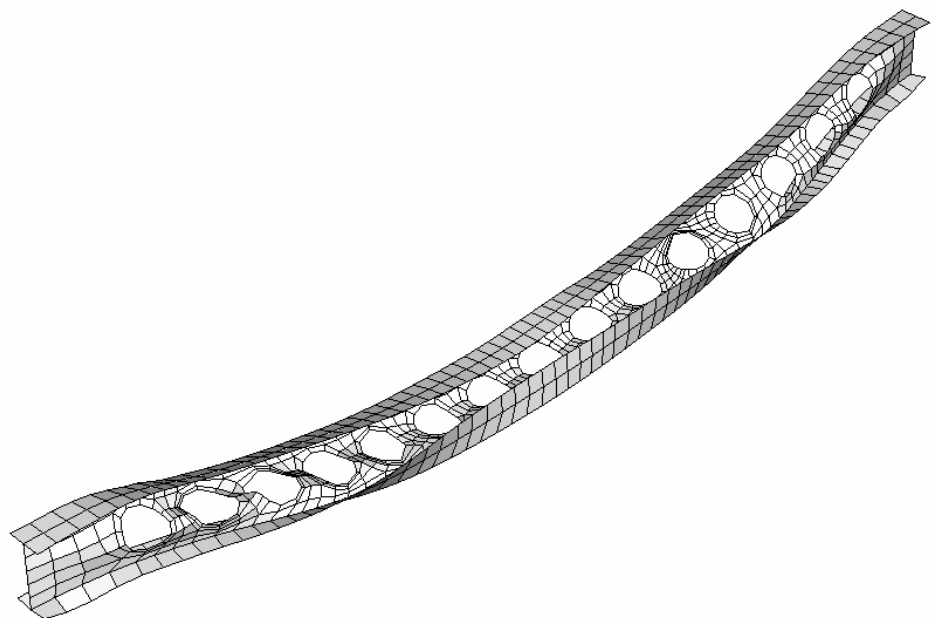
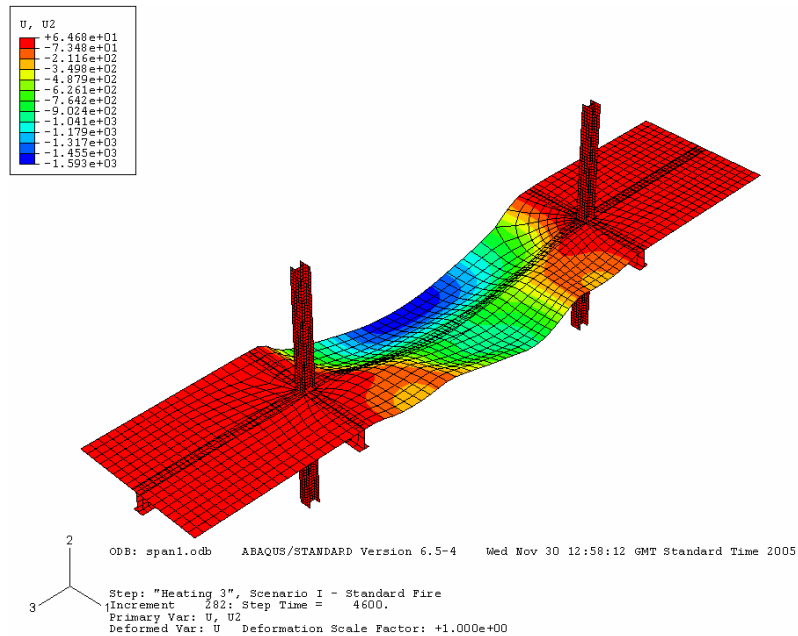
Case f.2 – Von Mises stresses



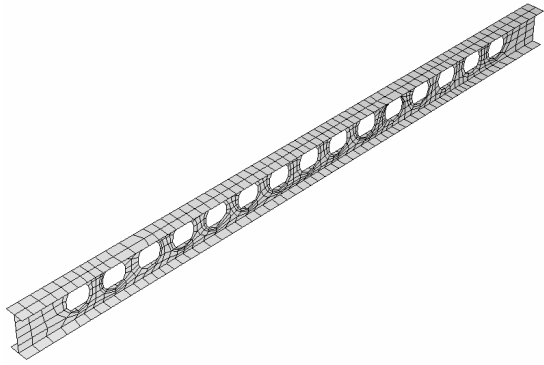
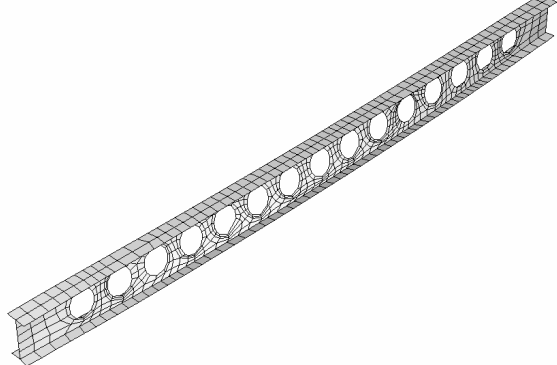
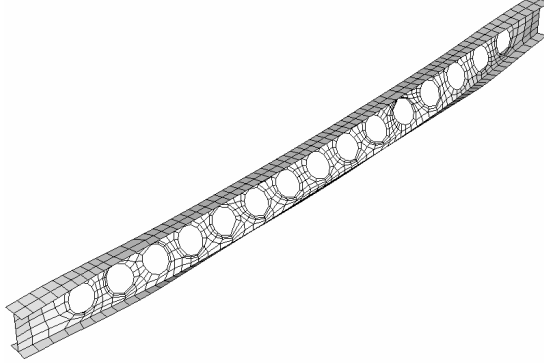
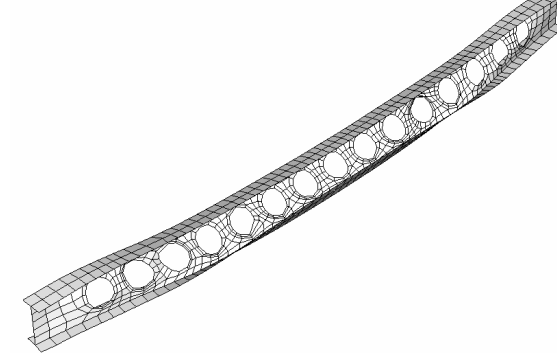
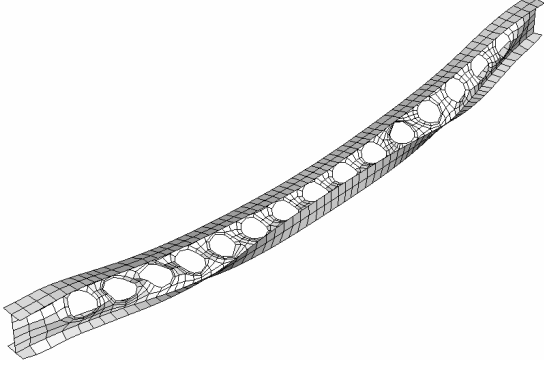
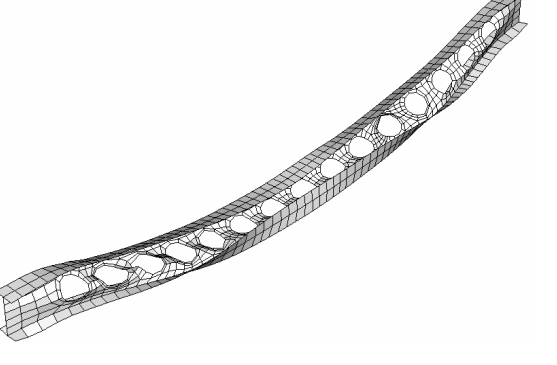
Scenario I – Case q.1 and Case q.2

Case g.1 – Span = 6150mm

Displacement at end of simulation (t = 7200s, Temp = 1015C)

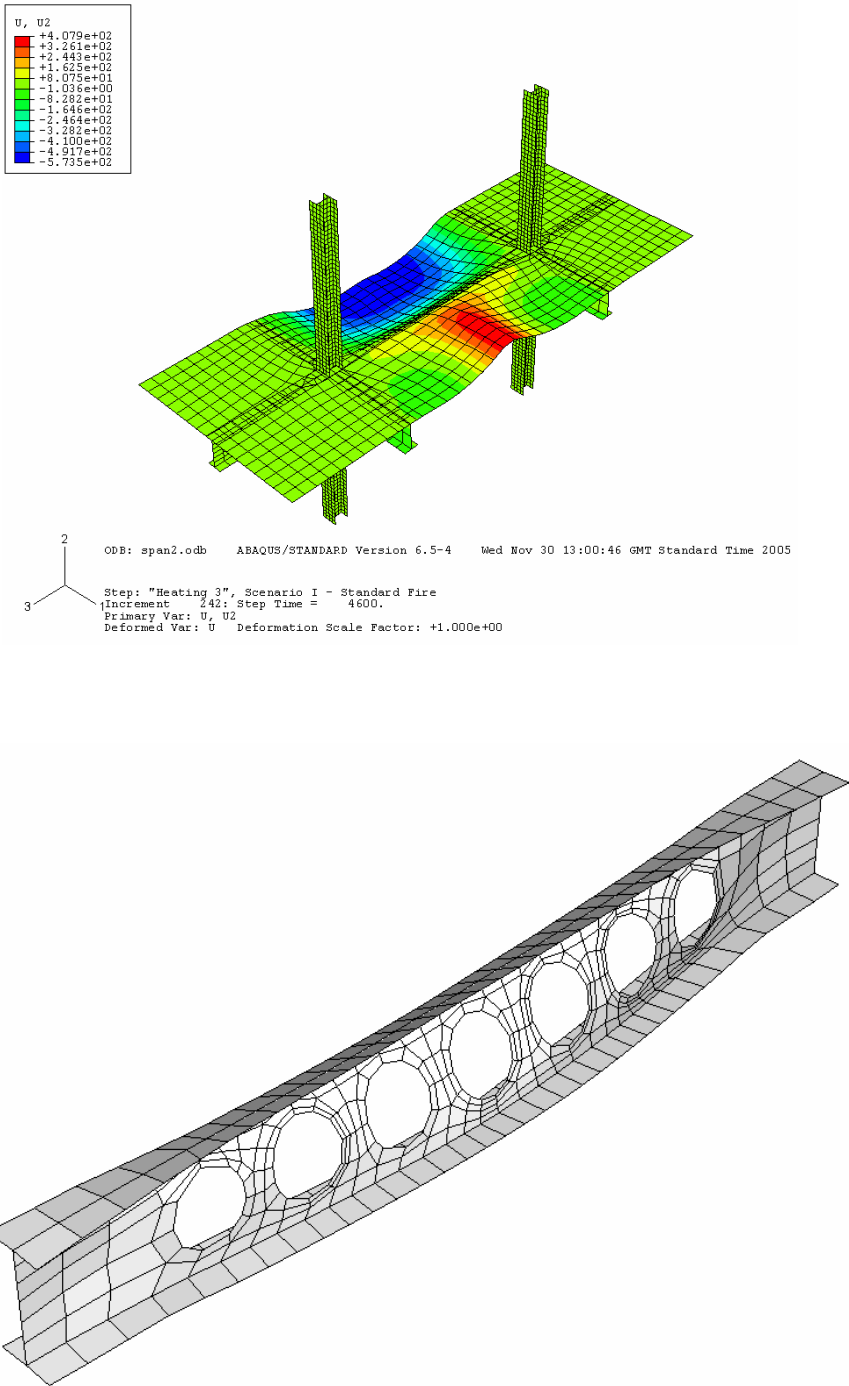


DEFORMATIONS: Case g.1 – Span = 6150mm

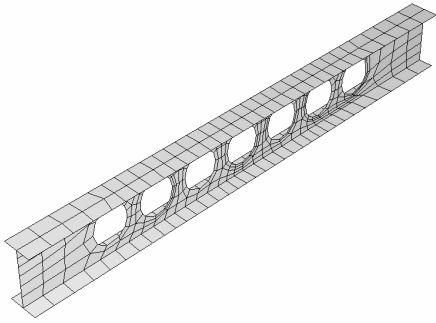
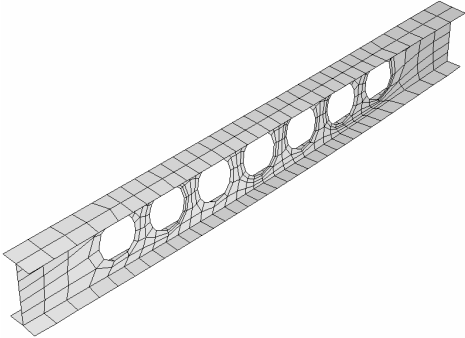
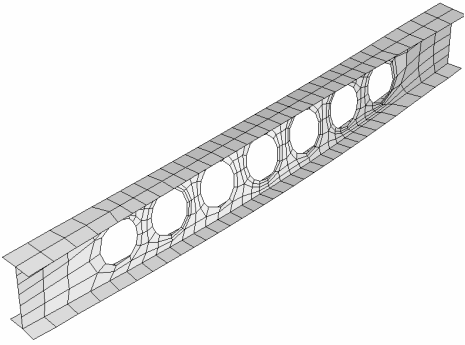
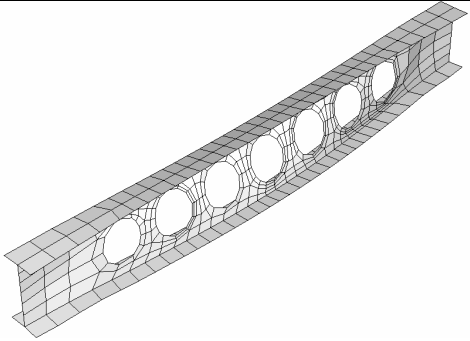
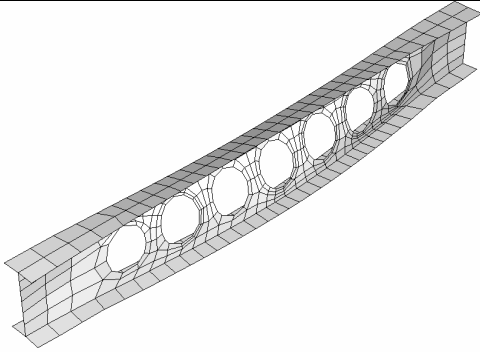
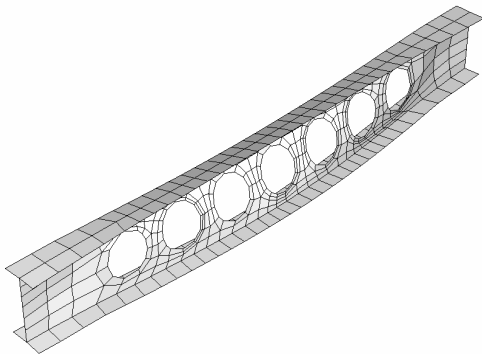
| | |
|--|--|
|  <p>Time = 0 sec, Temp = 25 C</p> |  <p>Time = 650 sec, Temp = 336C Lateral torsional buckling starts, bottom flange</p> |
|  <p>Time = 1030 sec, Temp = 570C 1st time web posts begin to buckle. stress concentrations around holes of buckling web posts (2)</p> |  <p>Time = 1219 sec, Temp = 571 C Stress concentrations spread along beam, after this point beam displaces and laterally rotates rapidly.</p> |
|  <p>Time = 1570 sec, Temp = 887 C Beam buckles lateral more and then goes into catenary action</p> |  <p>Time = 7200sec. Temp = 1015C Beam in catenary action; End of simulation, no convergence</p> |

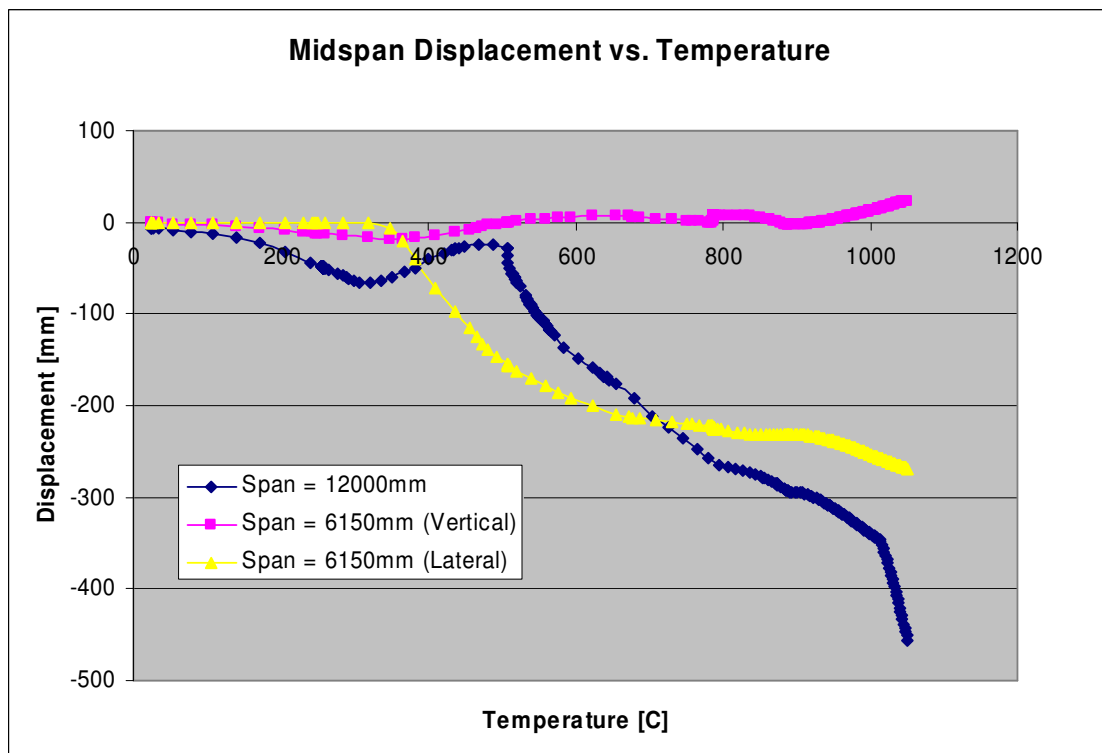
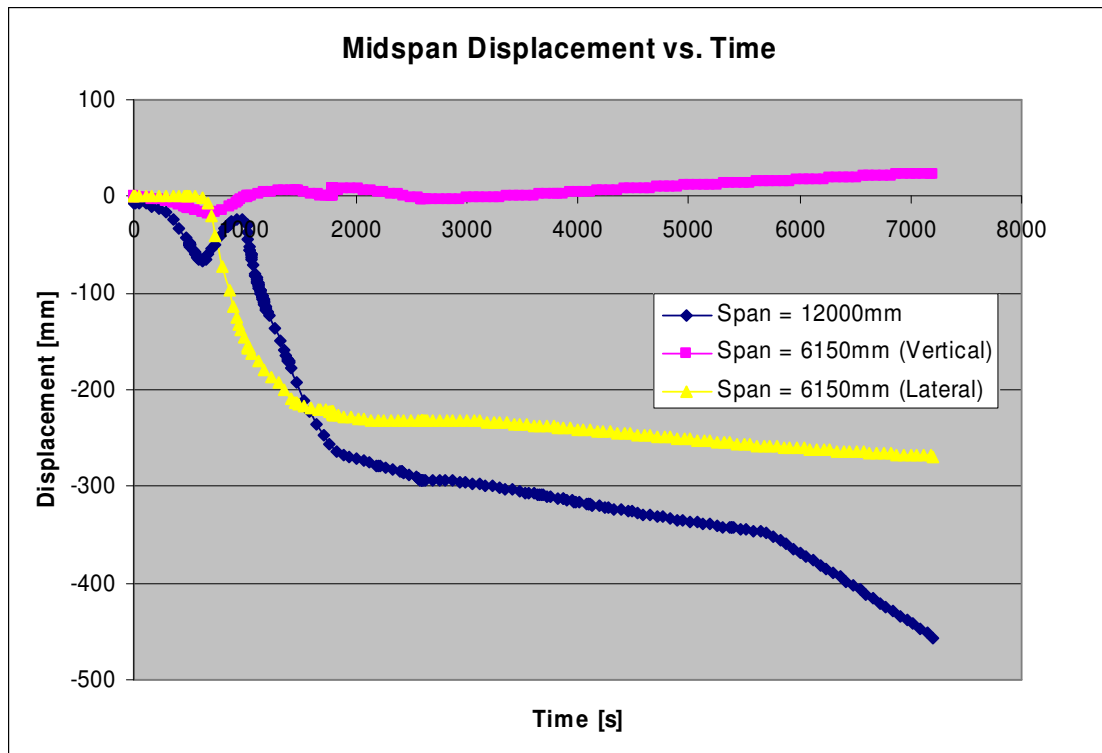
Case g.2 – Span = 12000mm

Displacement at end of simulation (t = 7200s, Temp = 1015C)

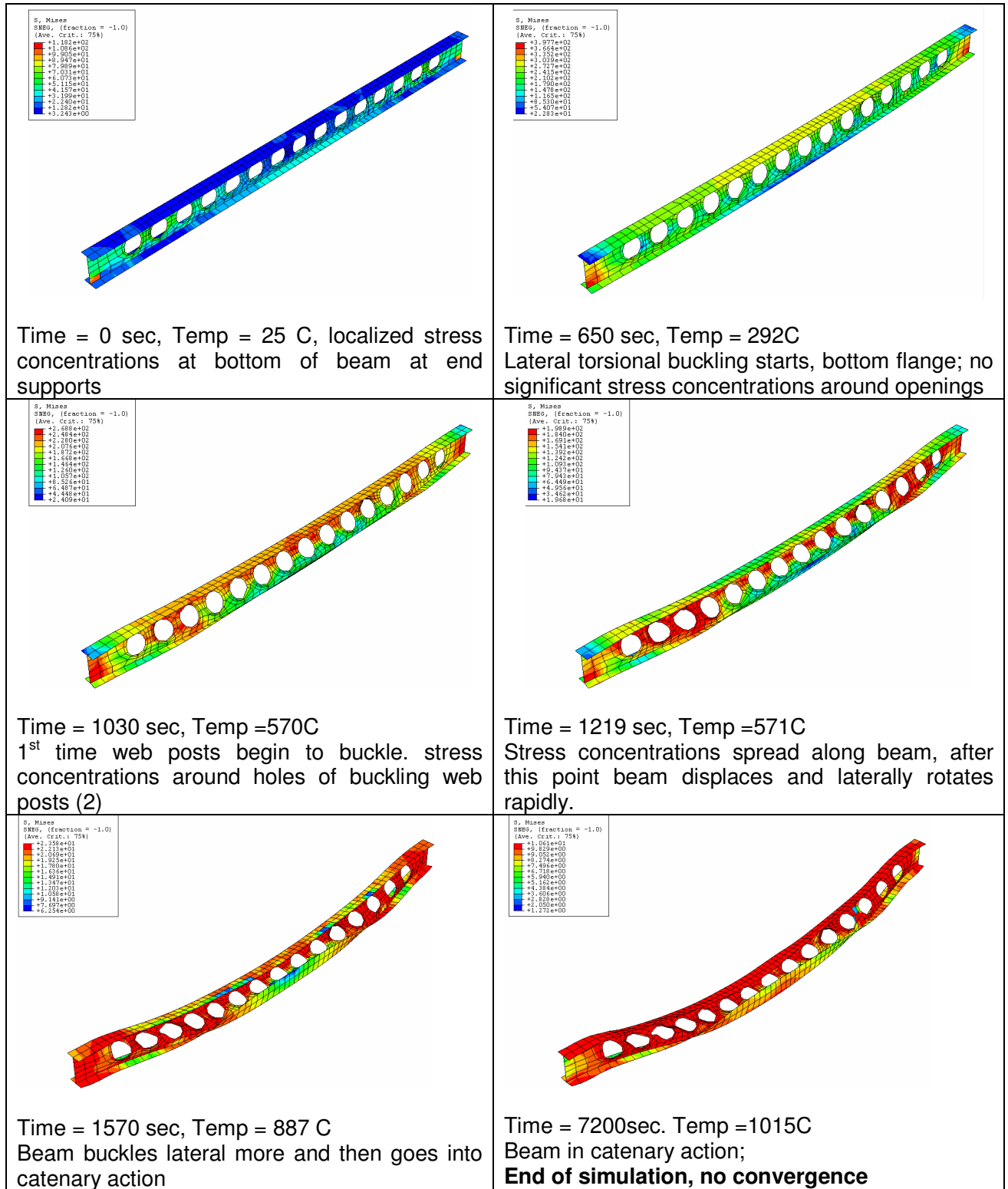


DEFORMATIONS: Case g.2 – Span = 12000mm

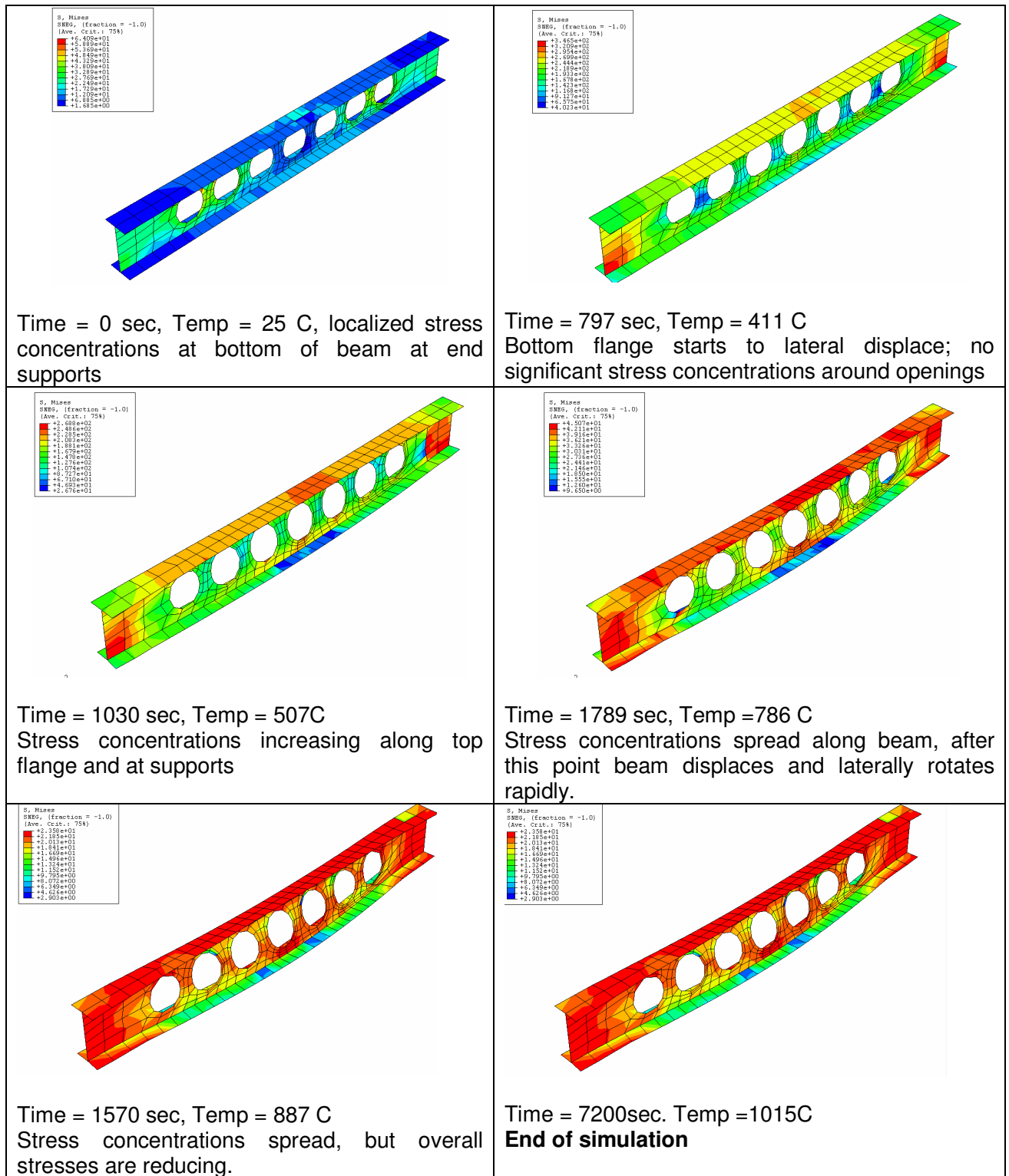
| | |
|---|--|
|  <p>Time = 0 sec, Temp = 25 C</p> |  <p>Time = 797 sec, Temp = C Bottom flange starts to lateral displace; no significant stress concentrations around openings</p> |
|  <p>Time = 1030 sec, Temp = C Stress concentrations increasing along top flange and at supports</p> |  <p>Time = 1789 sec, Temp = C Stress concentrations spread along beam, after this point beam displaces and laterally rotates rapidly.</p> |
|  <p>Time = 1570 sec, Temp = 887 C Stress concentrations spread, but overall stresses are reducing.</p> |  <p>Time = 7200sec. Temp = 1015C End of simulation</p> |



Case g.1 – Von Mises stresses

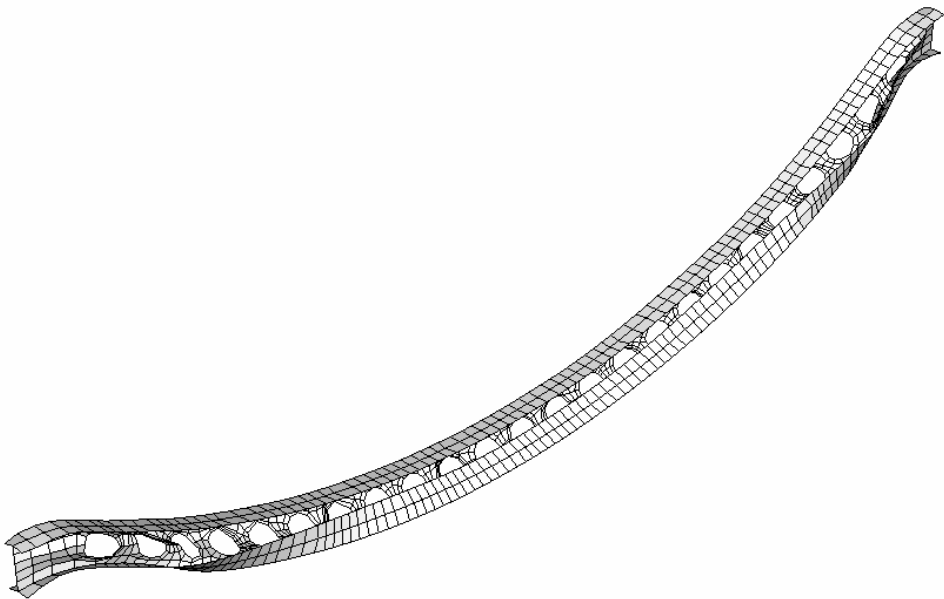
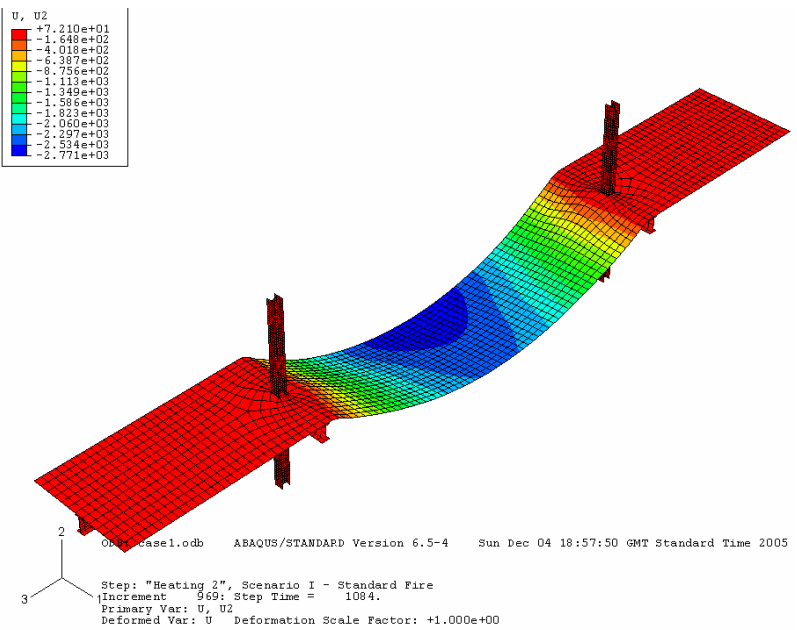


Case g.2 – Von Mises stresses

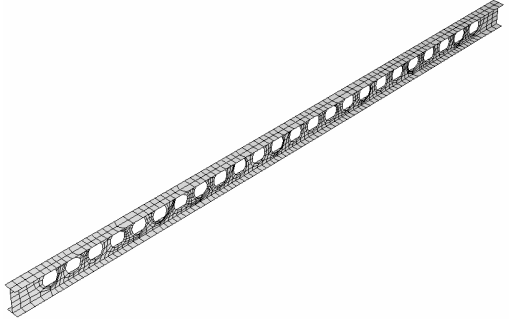
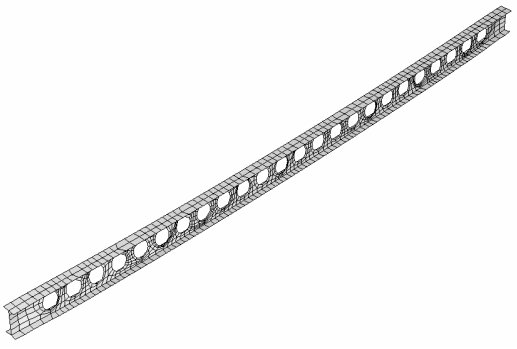
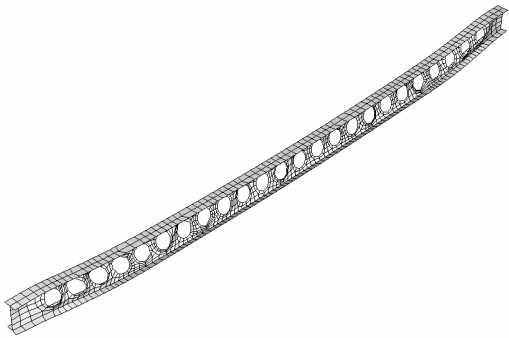
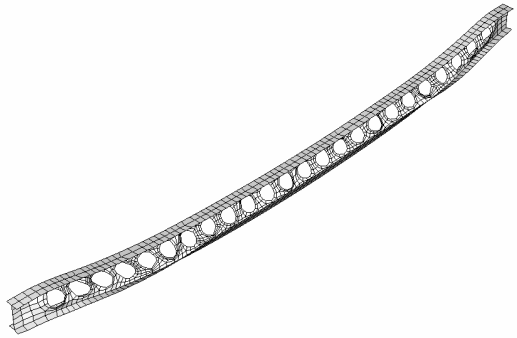
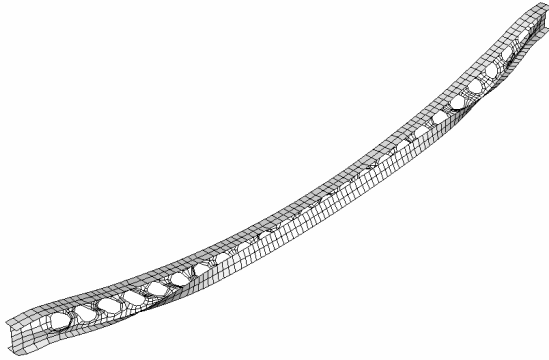
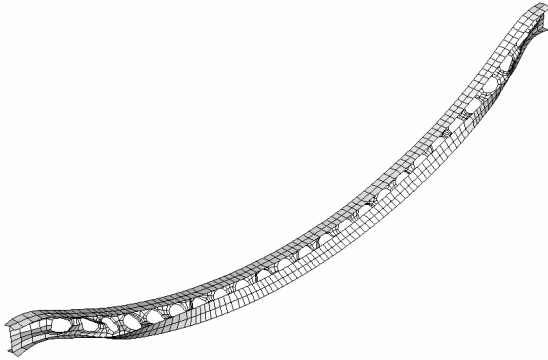


Scenario II – Case 1

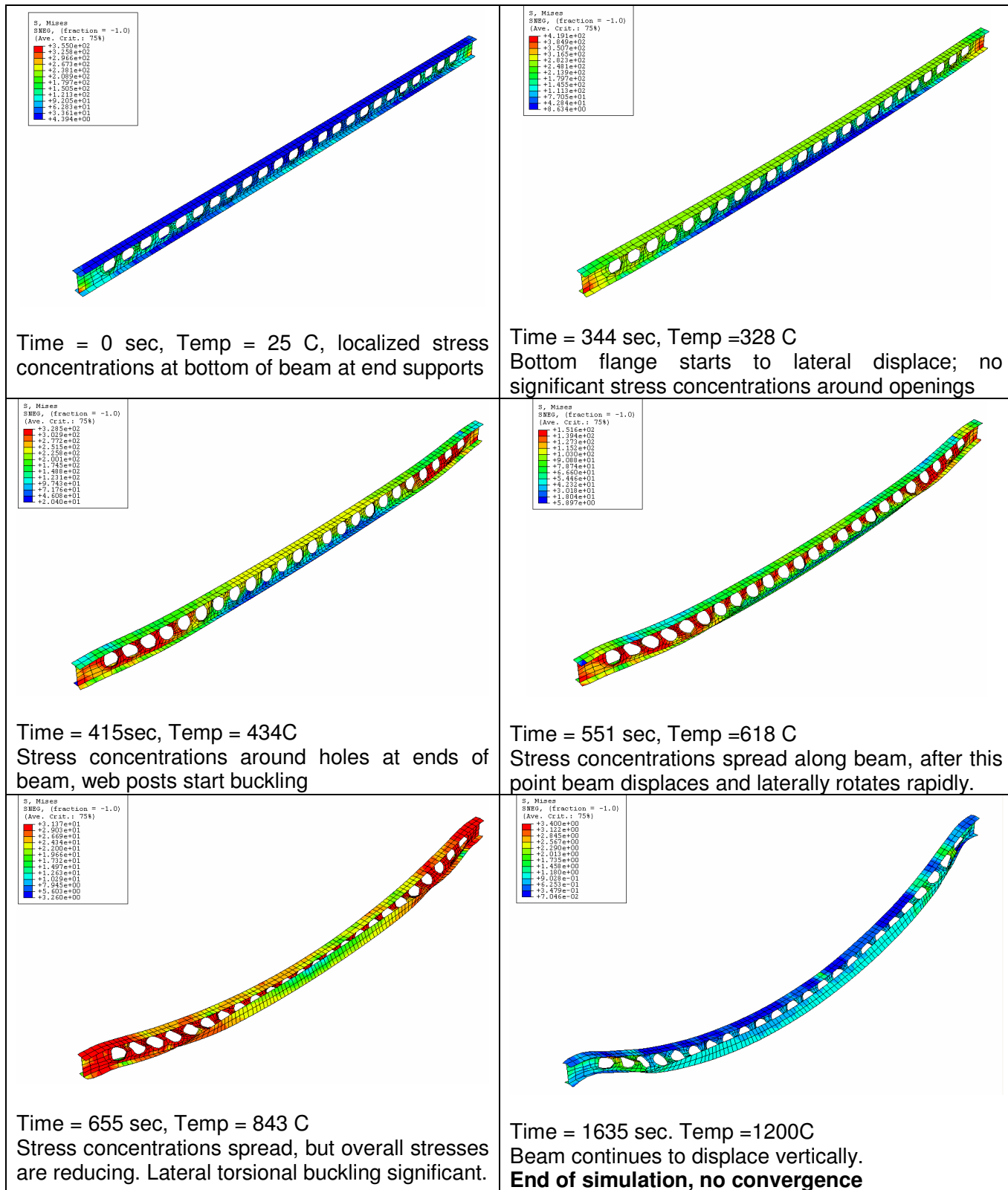
Displacement at end of simulation (t = 1635s, Temp = 1200C)



DEFORMATIONS: Case 1 – $T_{max}=1200^{\circ}\text{C}$, $\alpha = 0.005$

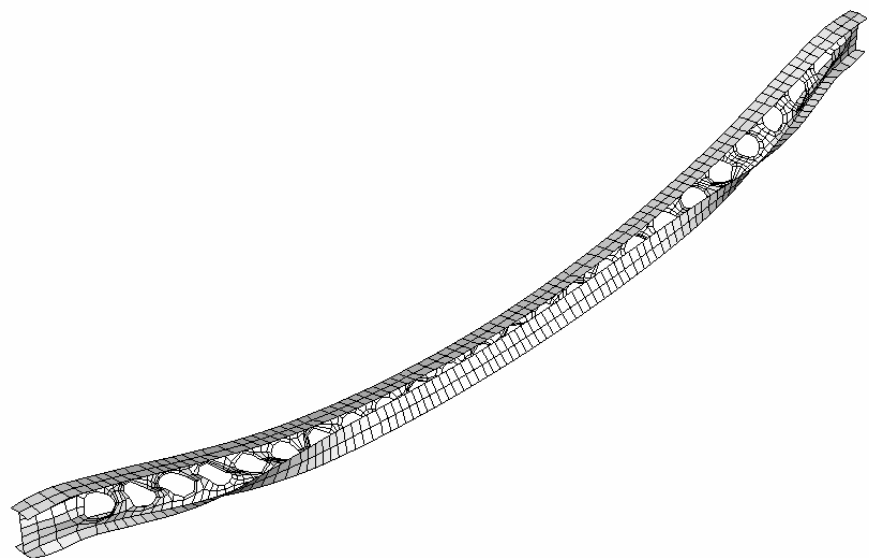
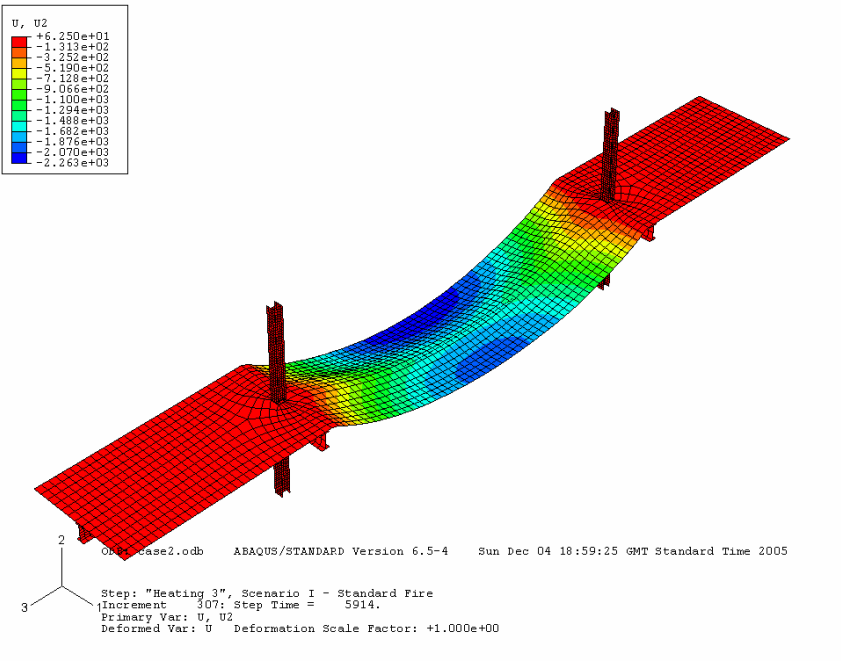
| | |
|--|--|
|  <p>Time = 0 sec, Temp = 25 C</p> |  <p>Time = 344 sec, Temp = 328 C Bottom flange starts to lateral displace; no significant stress concentrations around openings</p> |
|  <p>Time = 415sec, Temp = 434C Stress concentrations around holes at ends of beam, web posts start buckling</p> |  <p>Time = 1789 sec, Temp = C Stress concentrations spread along beam, after this point beam displaces and laterally rotates rapidly.</p> |
|  <p>Time = 655 sec, Temp = 843 C Stress concentrations spread, but overall stresses are reducing. Lateral torsional buckling significant.</p> |  <p>Time = 1635 sec. Temp = 1200C Beam continues to displace vertically. End of simulation, no convergence</p> |

Von Mises stresses

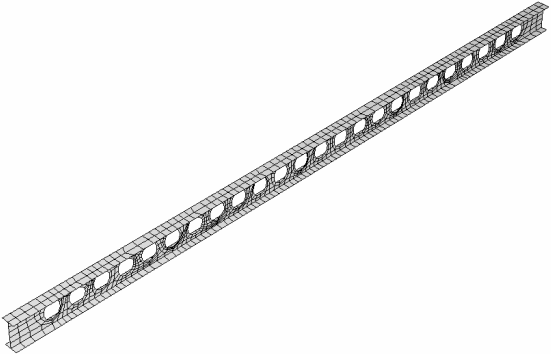
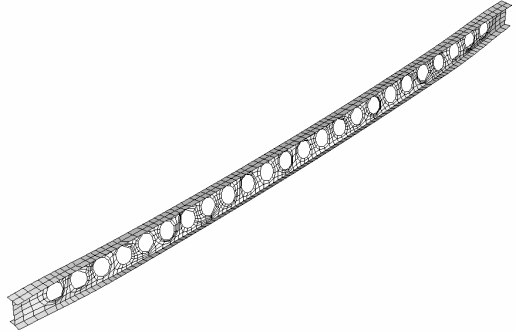
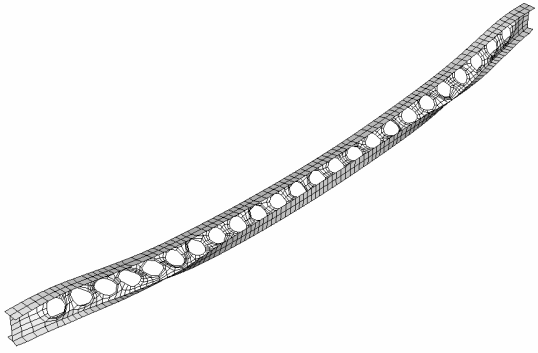
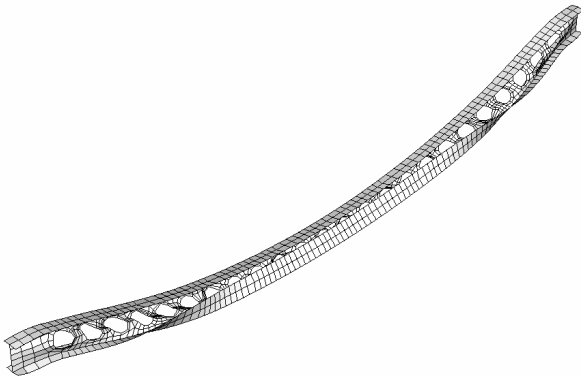
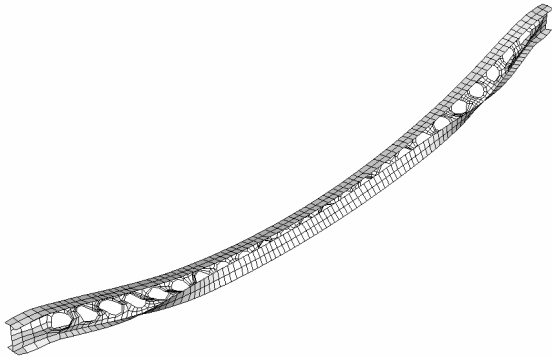


Scenario II – Case 2

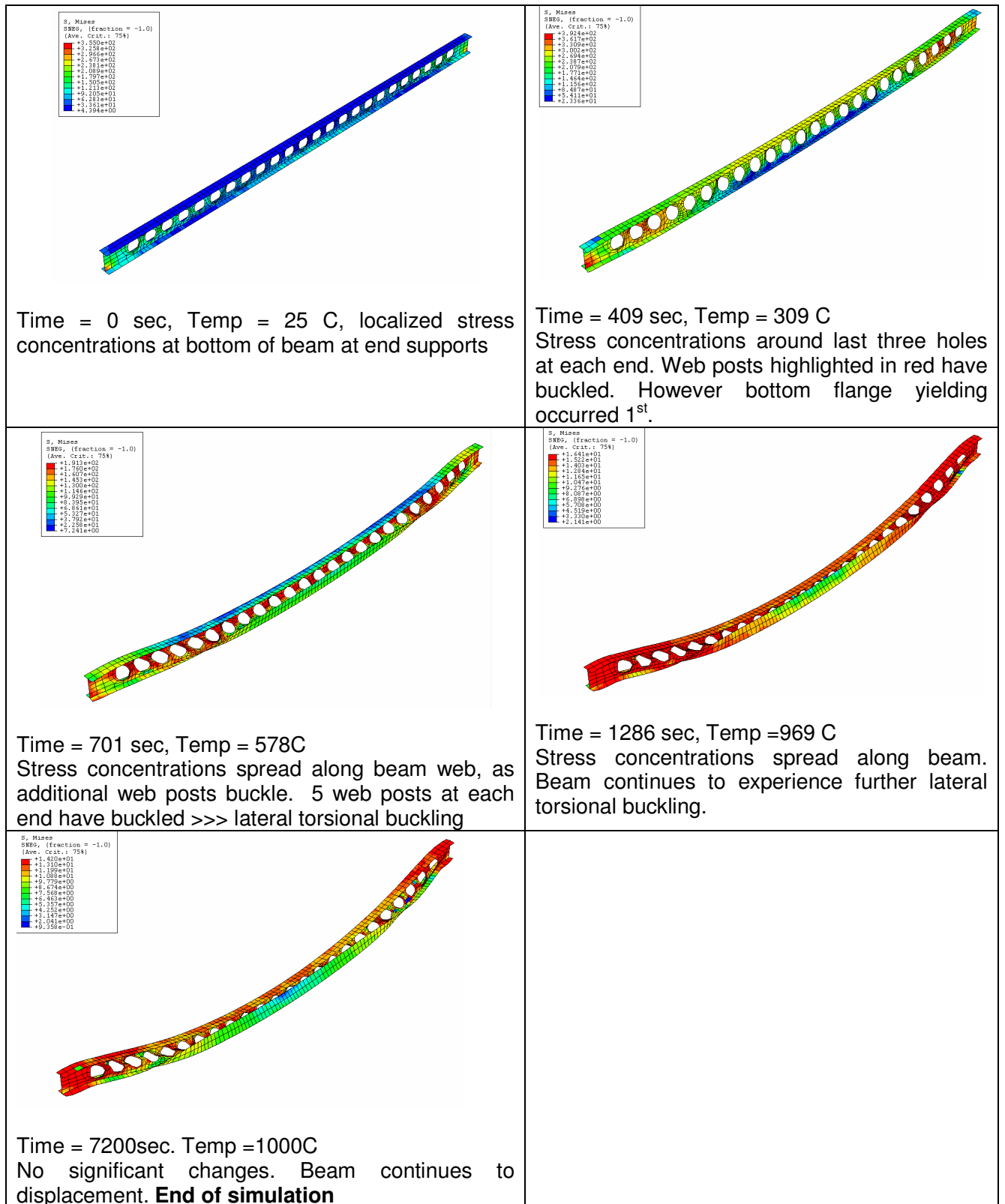
Displacement at end of simulation (t = 7200s, Temp = 1000C)



DEFORMATIONS: Case 2 (Scenario II)

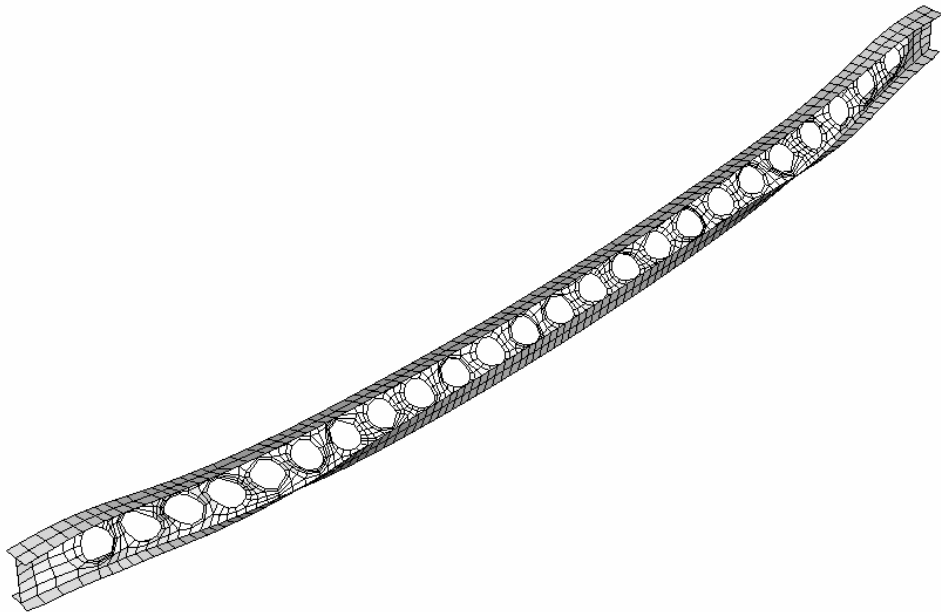
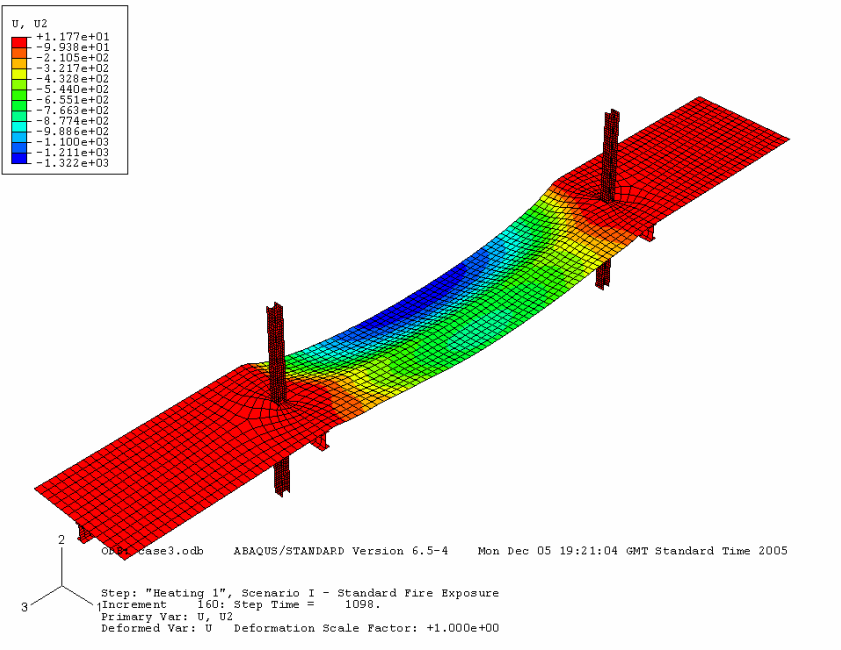
| | |
|---|---|
|  <p>Time = 0 sec, Temp = 25 C</p> |  <p>Time = 409 sec, Temp = 309 C Stress concentrations around last three holes at each end. Web post buckling observed at ends of beams. (last three holes)</p> |
|  <p>Time = 701 sec, Temp = 578C Stress concentrations spread along beam web, as additional web posts buckle. 5 web posts at each end have buckled >>> lateral torsional buckling</p> |  <p>Time = 1286 sec, Temp =969 C Stress concentrations spread along beam. Beam continues to experience further lateral torsional buckling.</p> |
|  <p>Time = 7200sec. Temp =1000C No significant changes. Beam continues to displacement. End of simulation</p> | |

Stresses

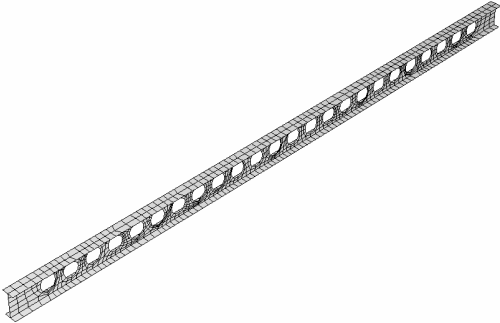
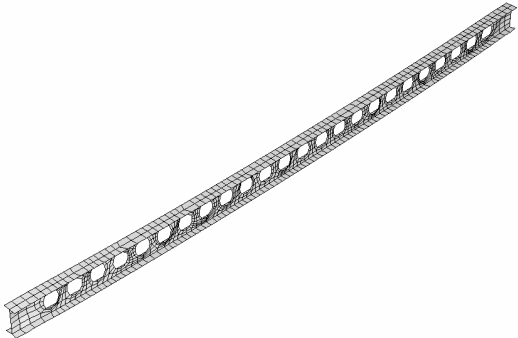
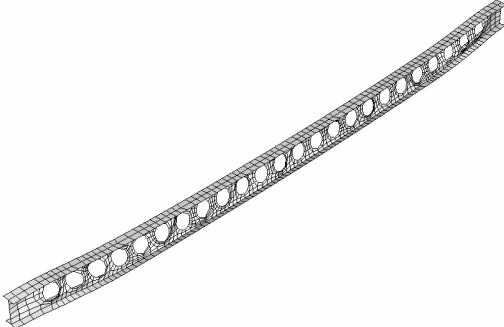
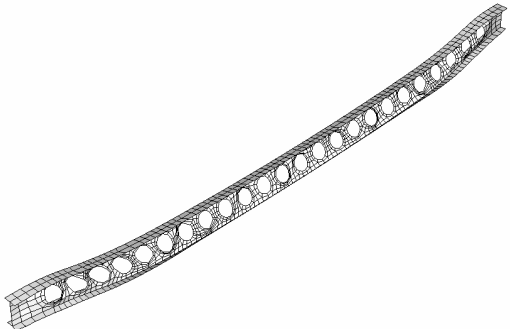
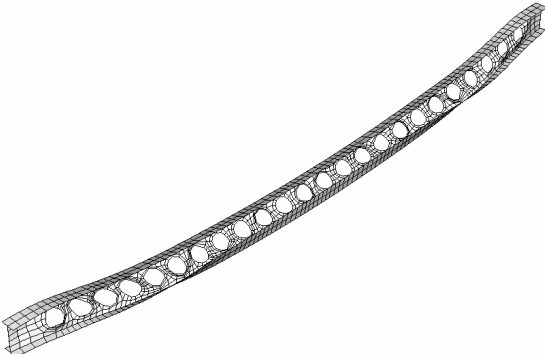


Scenario II – Case 3

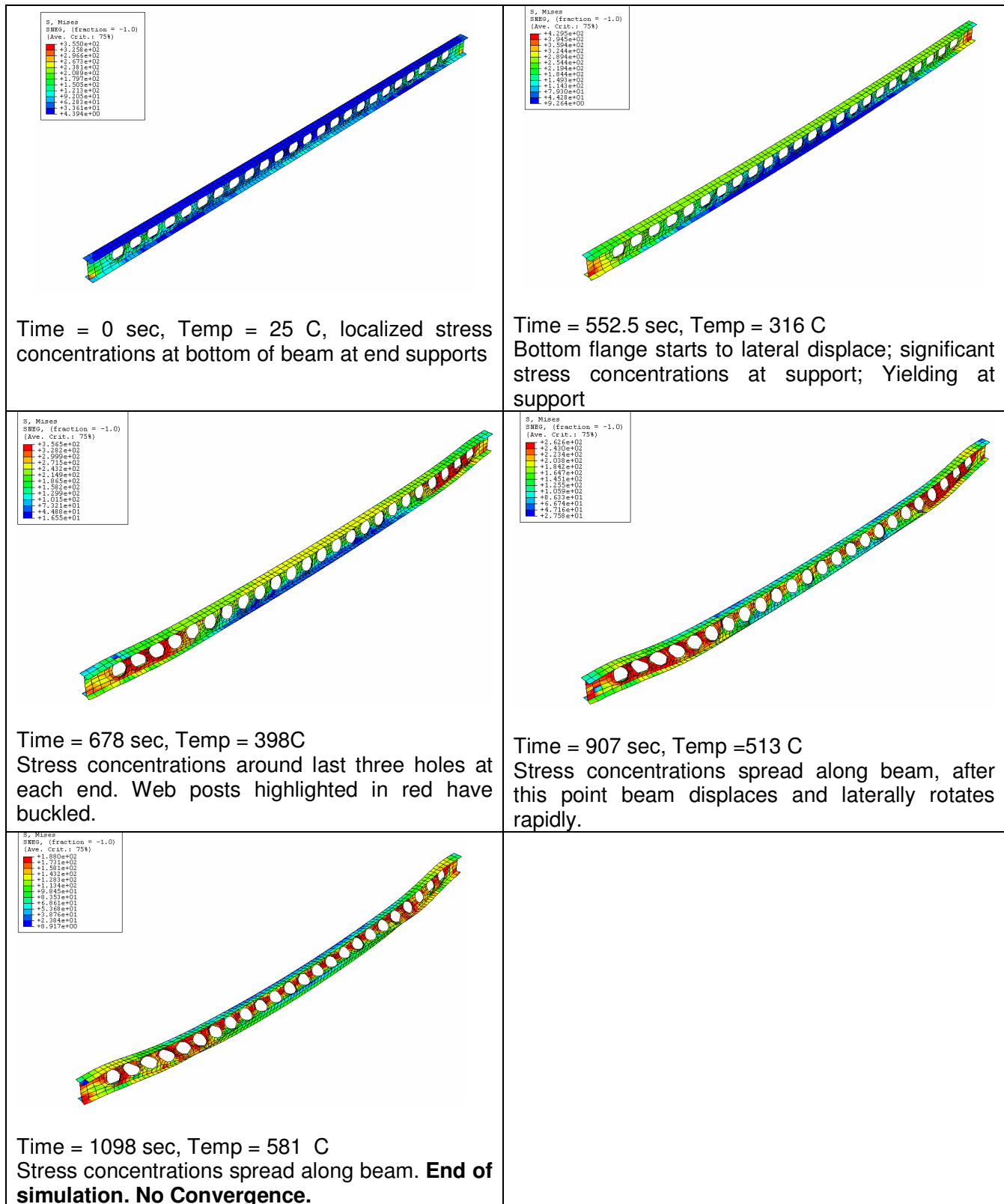
Displacement at end of simulation (t = 1098s, Temp = 581C)



DEFORMATIONS: Case 3 (Scenario II)

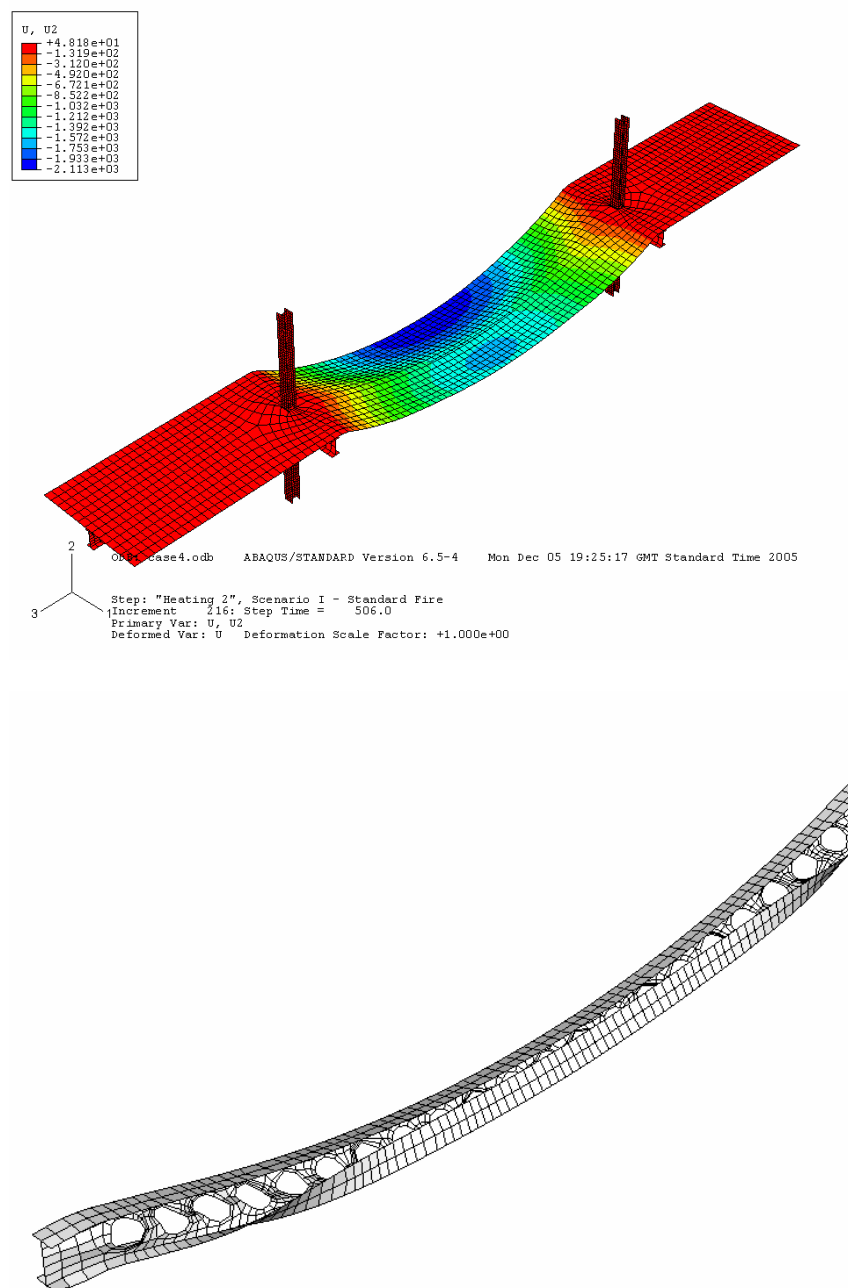
| | |
|---|--|
|  <p>Time = 0 sec, Temp = 25 C</p> |  <p>Time = 552.5 sec, Temp = 316 C Bottom flange starts to lateral displace; significant stress concentrations at support; Yielding at support</p> |
|  <p>Time = 678 sec, Temp = 398C Stress concentrations around last three holes at each end. Web posts highlighted in red have buckled.</p> |  <p>Time = 907 sec, Temp = 513 C Stress concentrations spread along beam, after this point beam displaces and laterally rotates rapidly.</p> |
|  <p>Time = 1098 sec, Temp = 581 C Stress concentrations spread along beam. End of simulation. No Convergence.</p> | |

Stresses

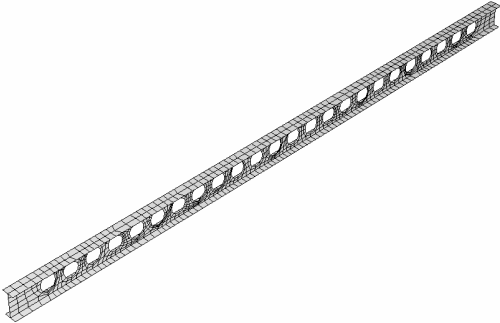
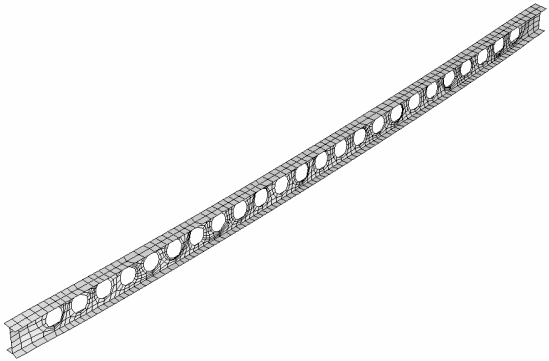
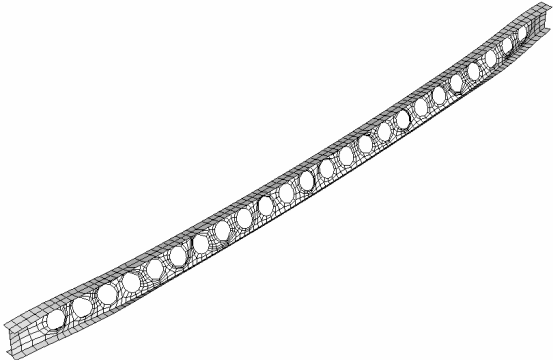
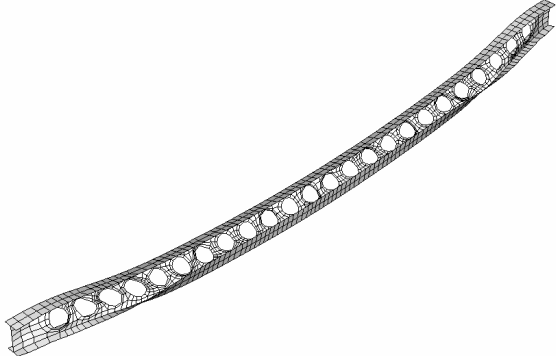
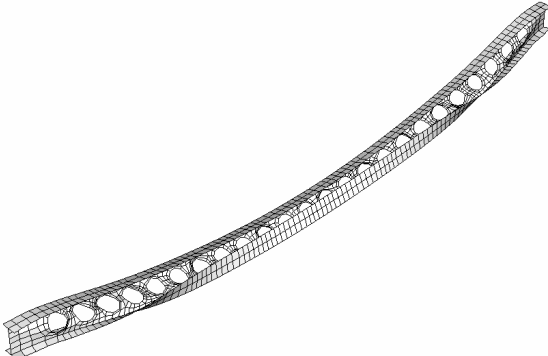
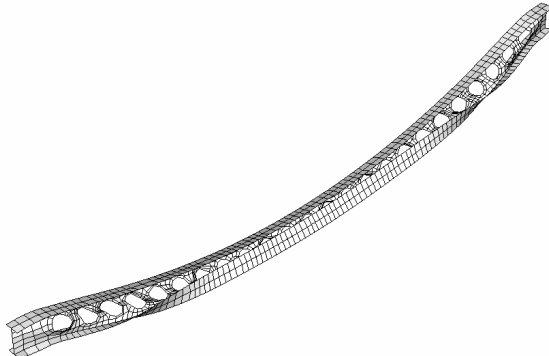


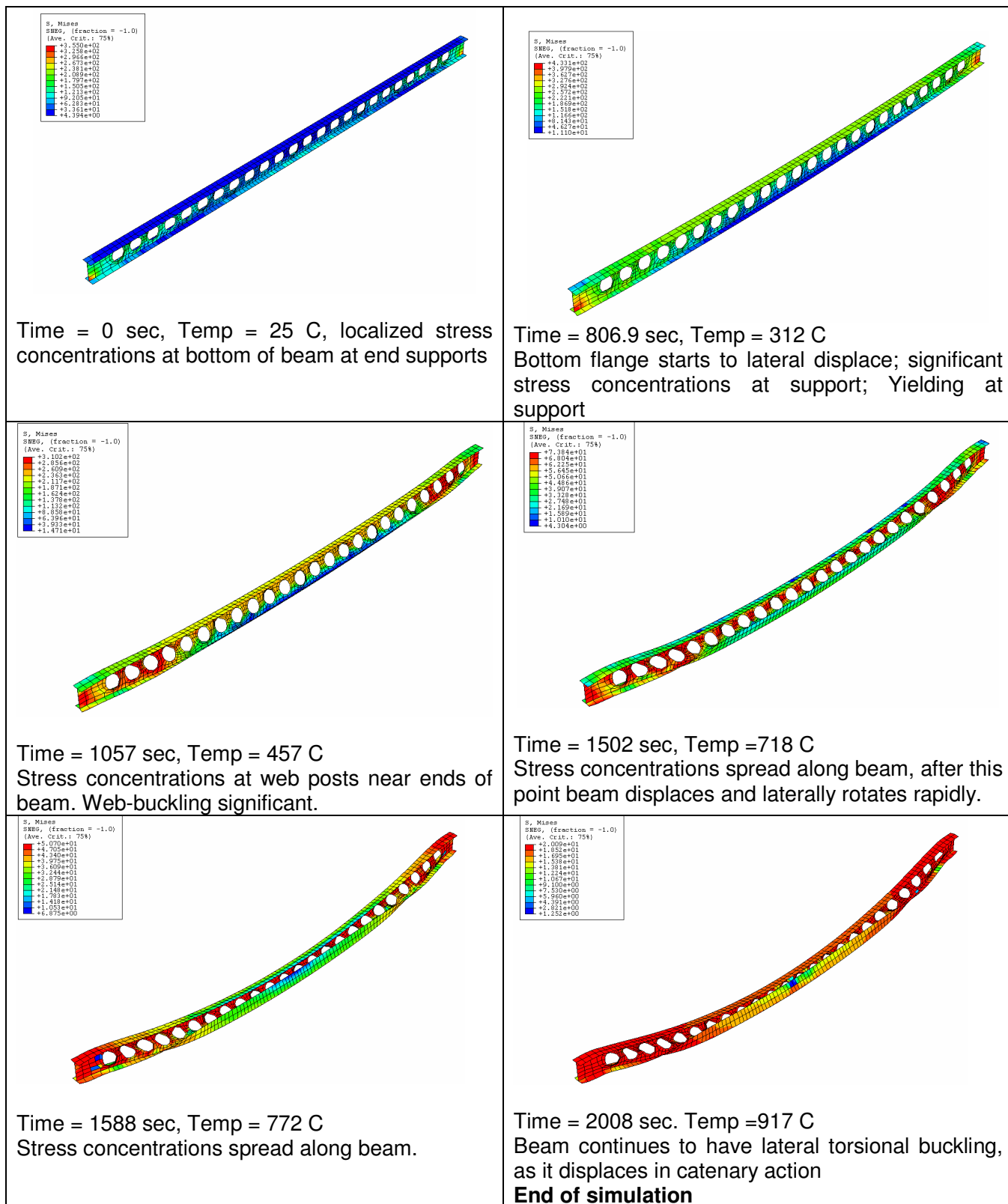
Scenario II – Case 4

Displacement at end of simulation (t = 2008s, Temp = 917C)



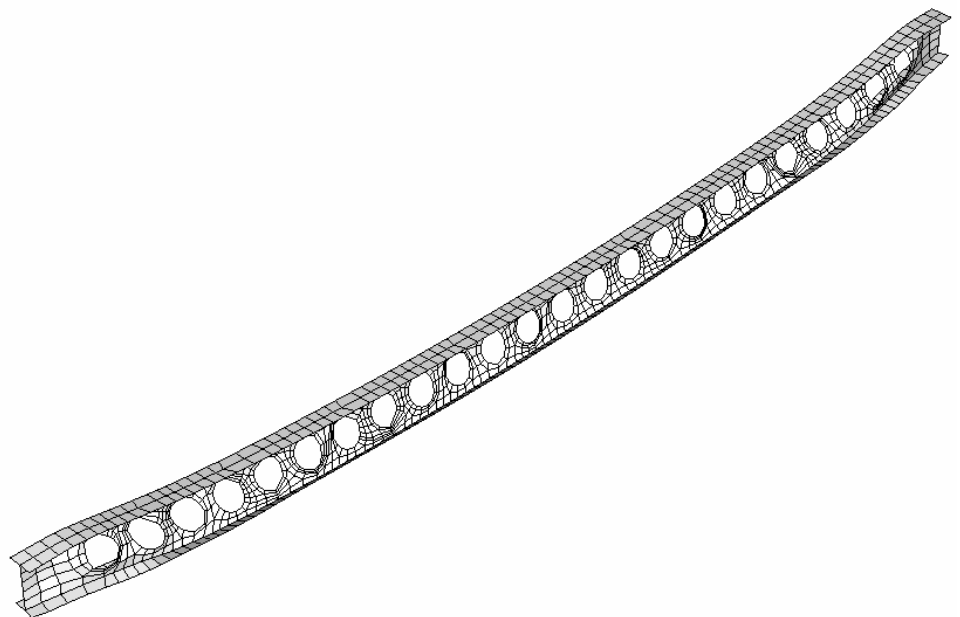
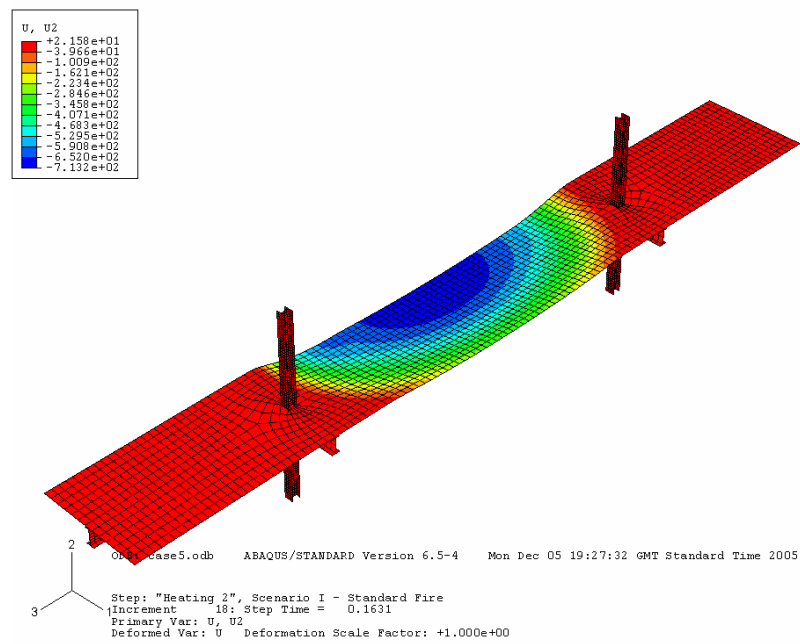
DEFORMATIONS: Case 4 (Scenario II)

| | |
|---|--|
|  <p>Time = 0 sec, Temp = 25 C</p> |  <p>Time = 806.9 sec, Temp = 312 C Bottom flange starts to lateral displace; significant stress concentrations at support; Yielding at support</p> |
|  <p>Time = 1057 sec, Temp = 457 C Stress concentrations at web posts near ends of beam. Web-buckling significant.</p> |  <p>Time = 1789 sec, Temp = C Stress concentrations spread along beam, after this point beam displaces and laterally rotates rapidly.</p> |
|  <p>Time = 1588 sec, Temp = 772 C Stress concentrations spread along beam.</p> |  <p>Time = 2008 sec. Temp = 917 C Beam continues to have lateral torsional buckling, as it displaces in catenary action End of simulation</p> |

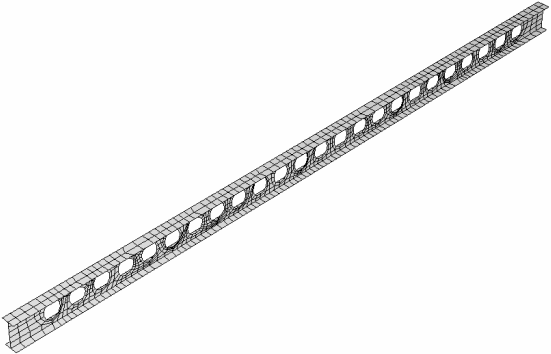
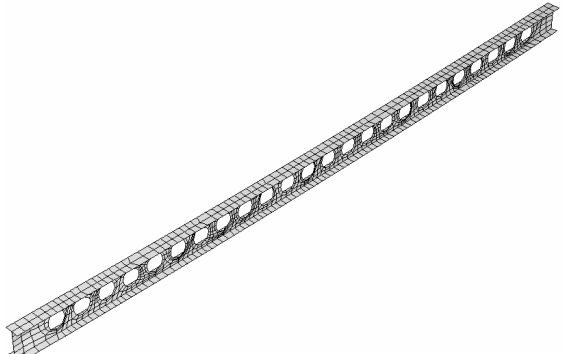
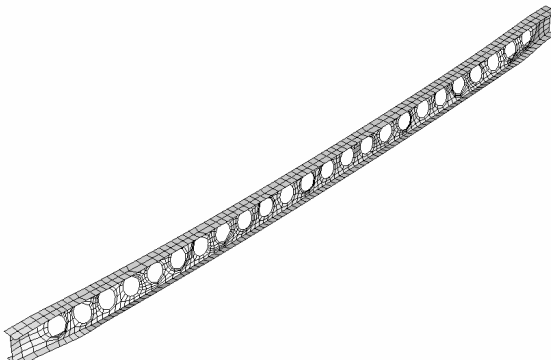
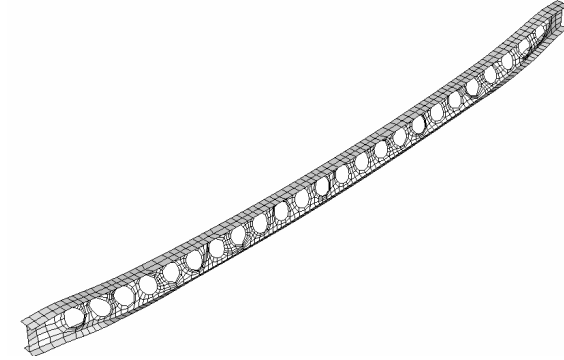


Scenario II – Case 5

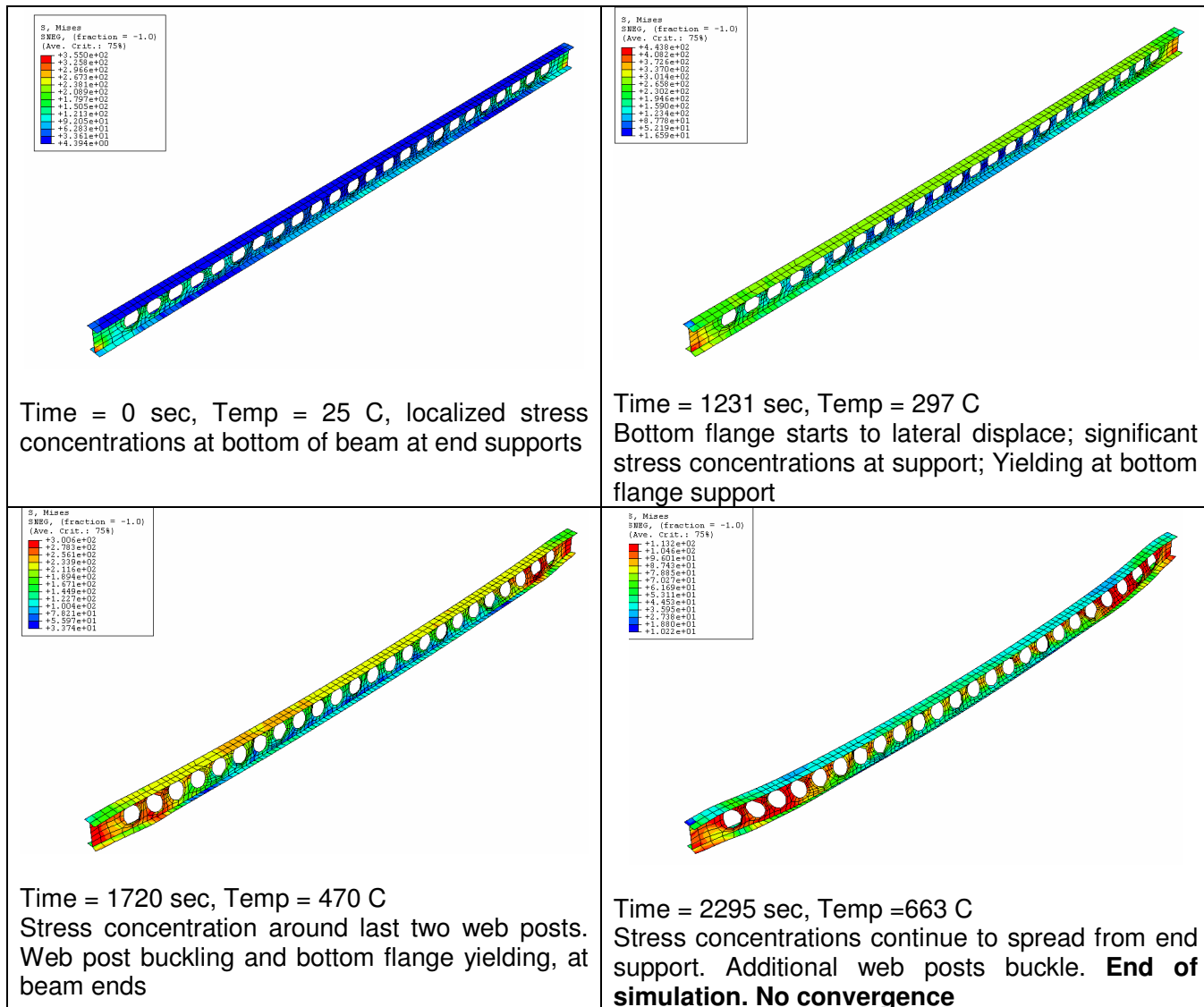
Displacement at end of simulation (t = 2295s, Temp = 663C)

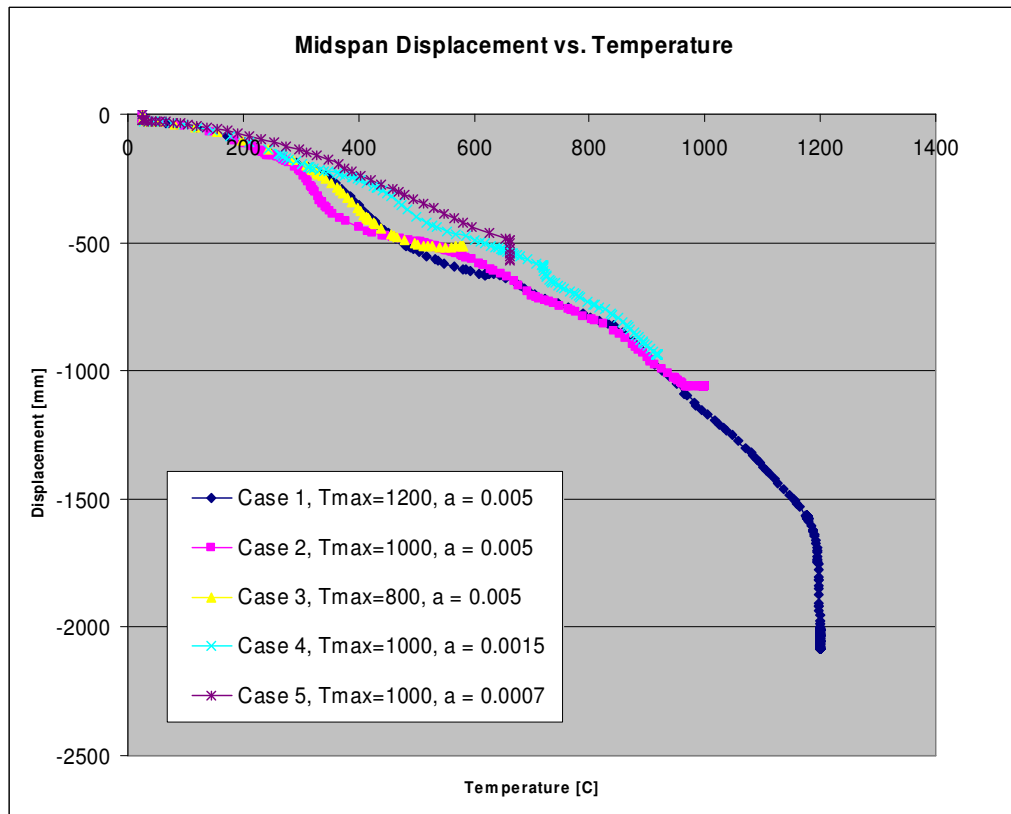
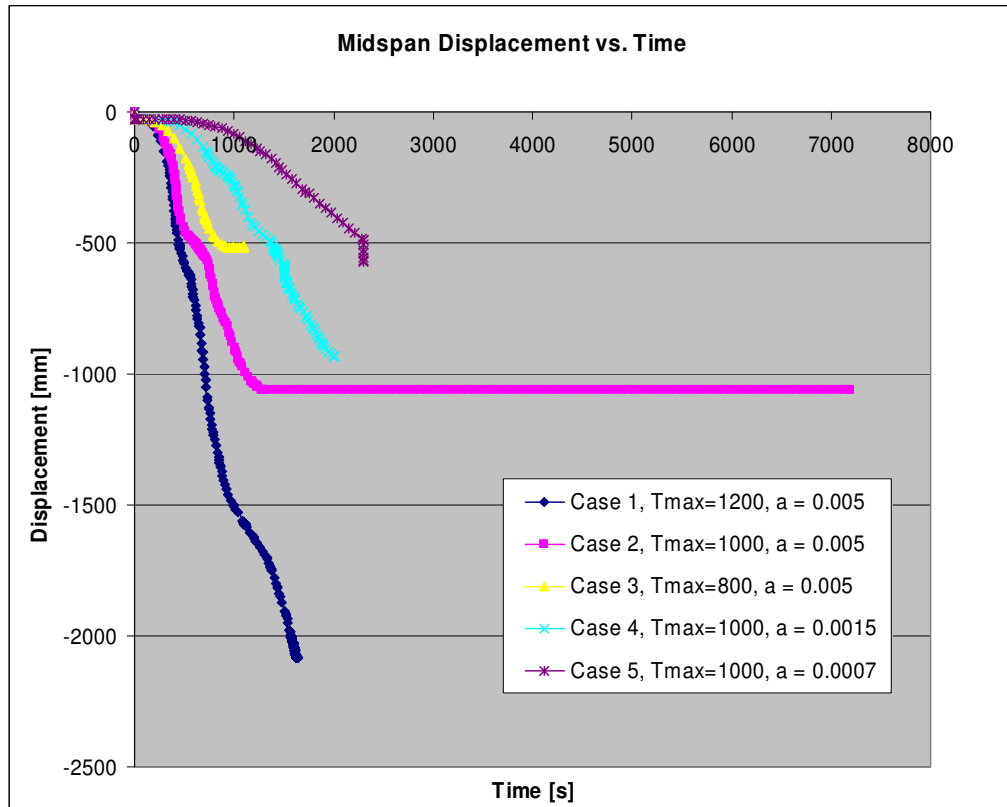


DEFORMATIONS: Case 5 (Scenario II)

| | |
|--|---|
|  <p>Time = 0 sec, Temp = 25 C</p> |  <p>Time = 1231 sec, Temp = 297 C Bottom flange starts to lateral displace; significant stress concentrations at support; Yielding at bottom flange support</p> |
|  <p>Time = 1720 sec, Temp = 470 C Stress concentration around last two web posts. Web post buckling and bottom flange yielding, at beam ends</p> |  <p>Time = 2295 sec, Temp = 663 C Stress concentrations continue to spread from end support. Additional web posts buckle. End of simulation. No convergence</p> |

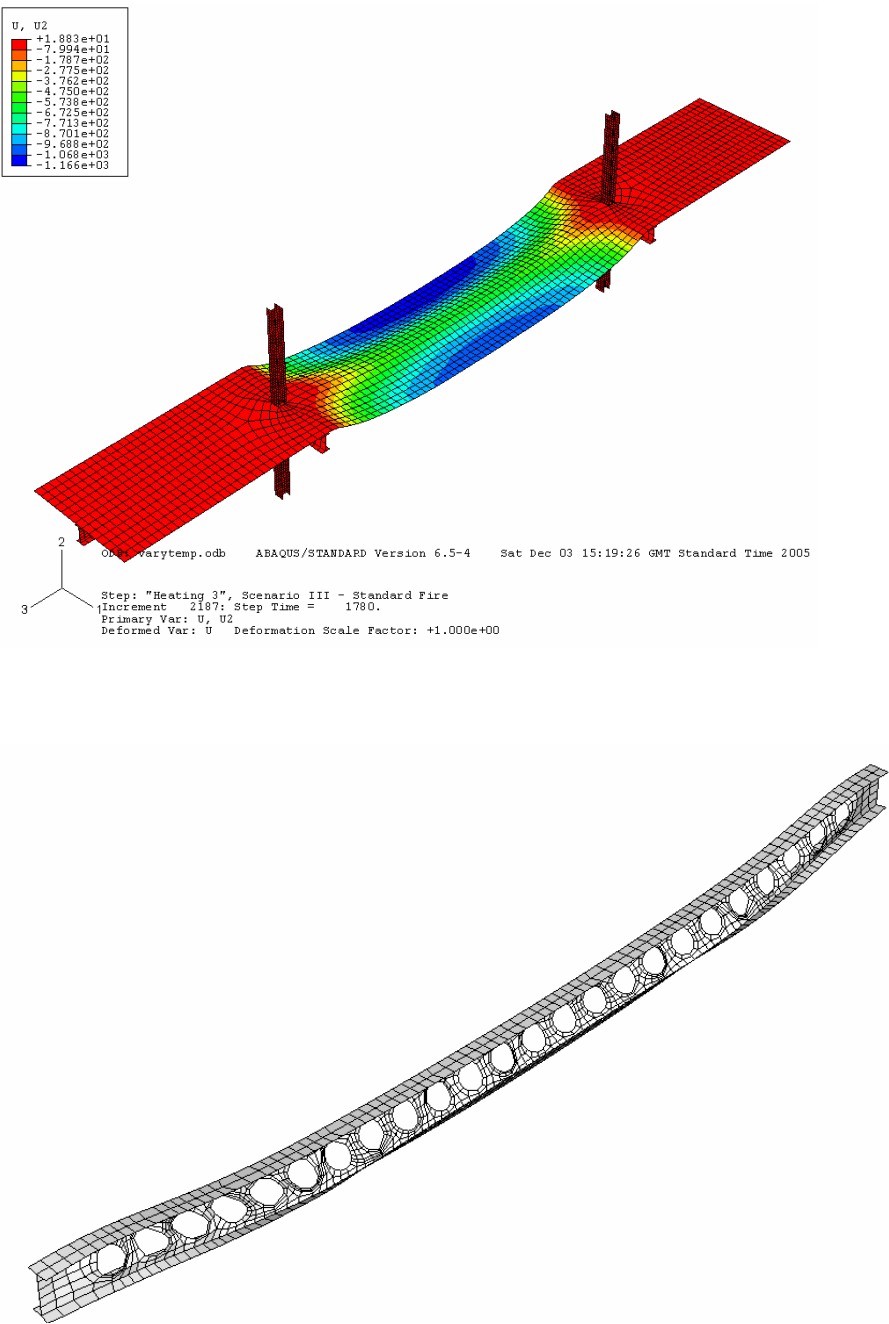
Von Mises Stresses



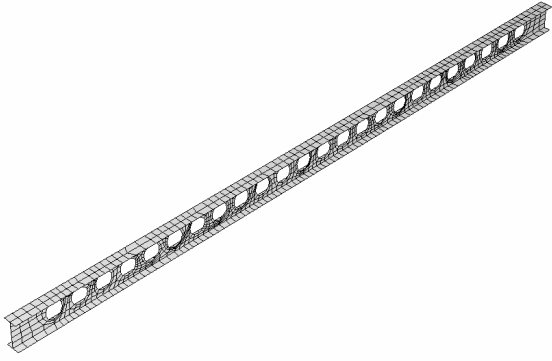
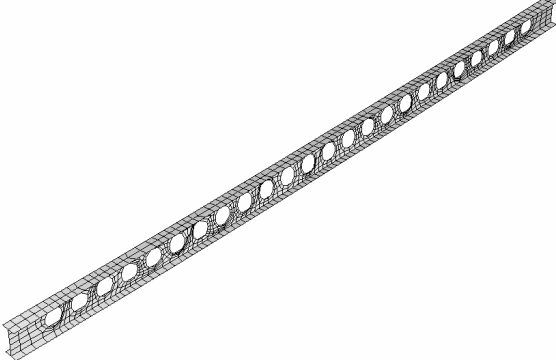
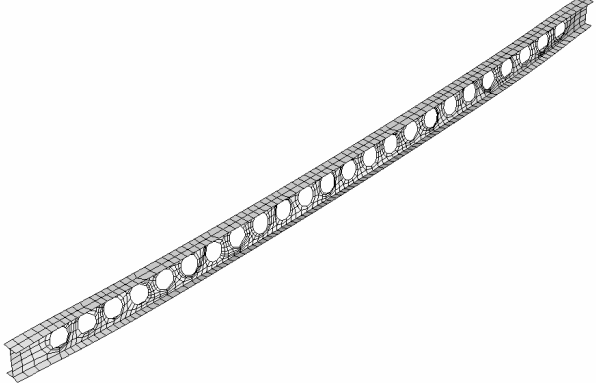
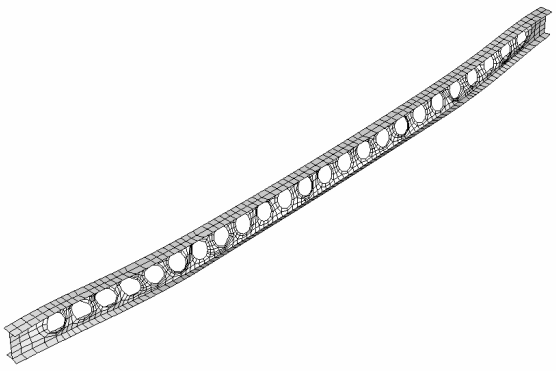
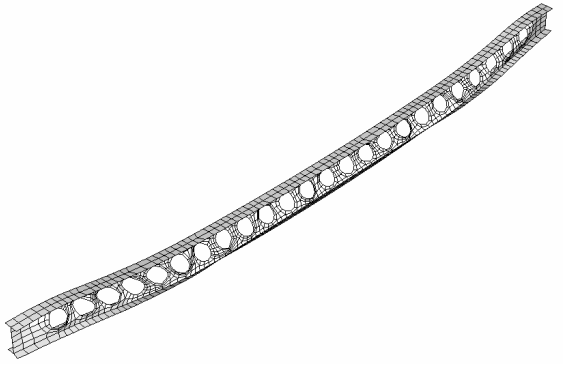


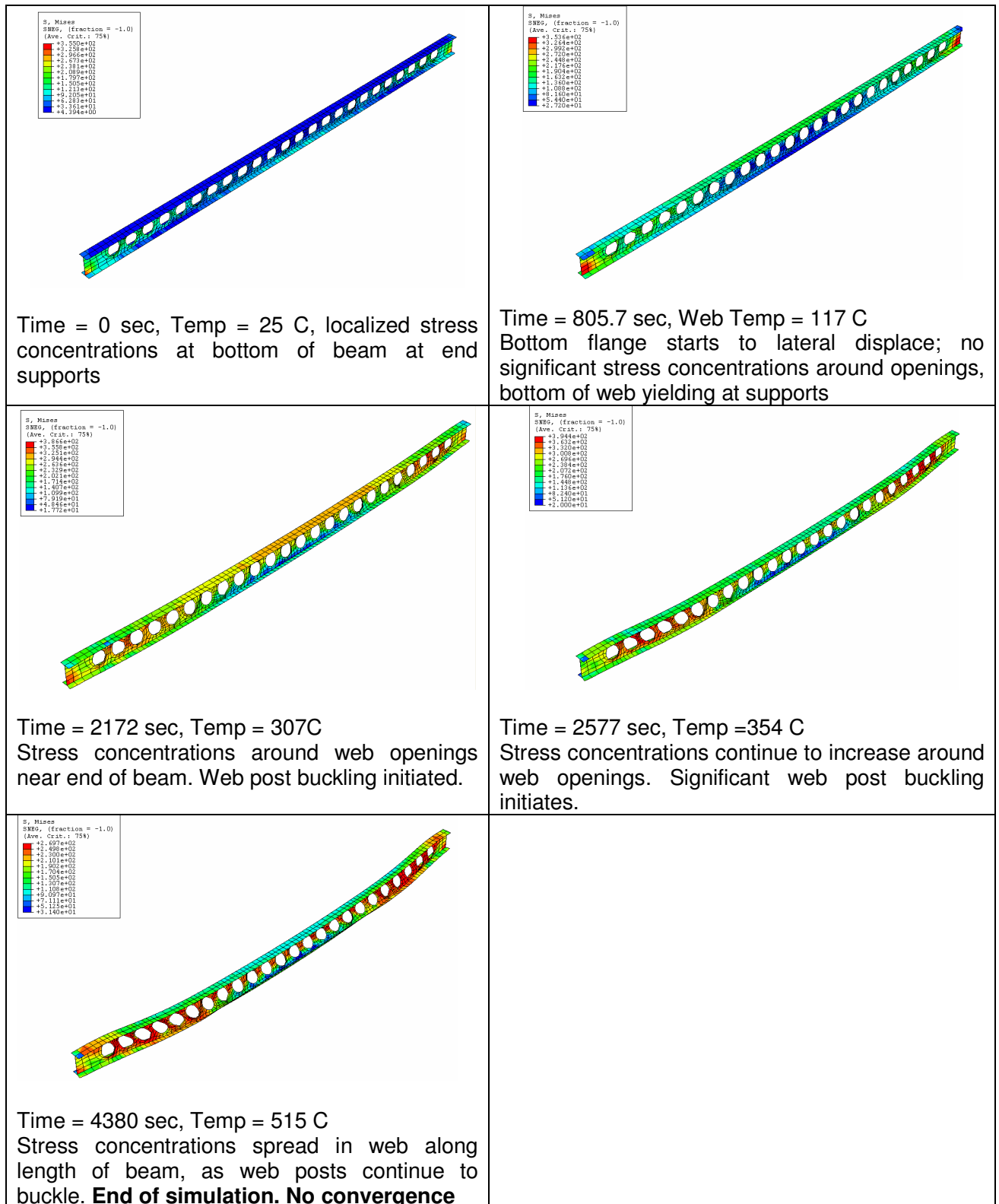
Scenario III – Protected Cellular Beam

Displacement at end of simulation (t = 4380s, Temp = 663C)



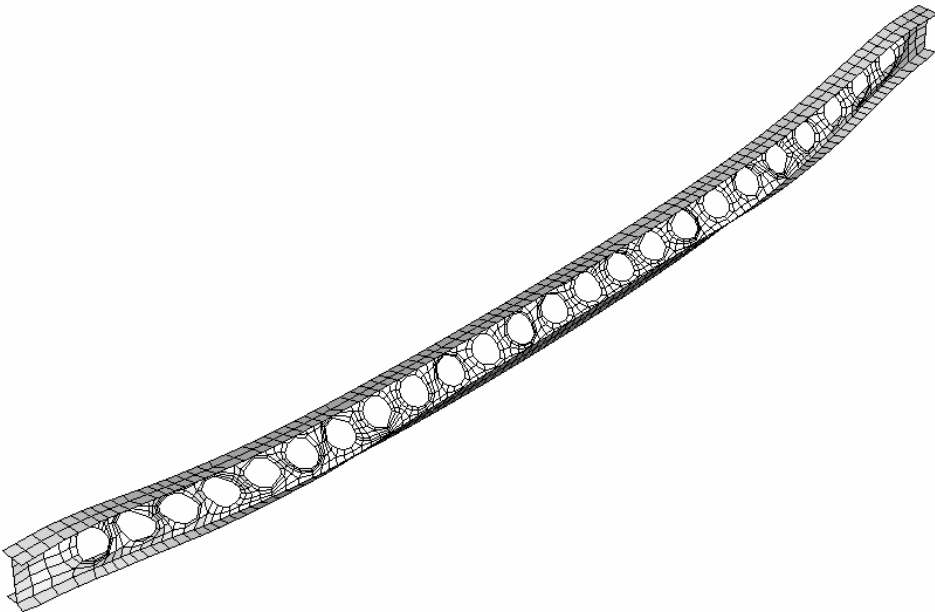
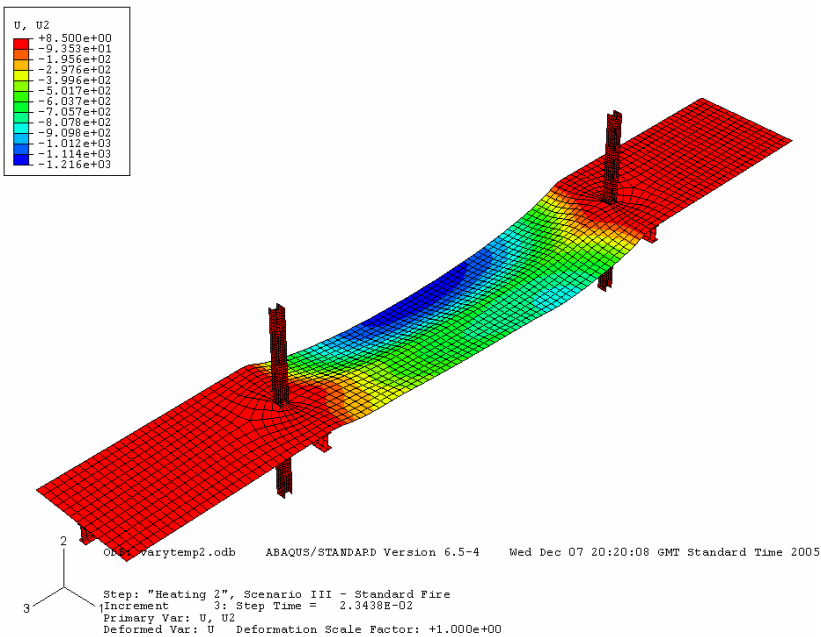
DEFORMATIONS: Case 1, Scenario III, Protected Cellular Beam

| | |
|--|---|
|  <p>Time = 0 sec, Temp = 25 C</p> |  <p>Time = 805.7 sec, Web Temp = 117 C Bottom flange starts to lateral displace; no significant stress concentrations around openings, bottom of web yielding at supports</p> |
|  <p>Time = 2172 sec, Temp = 307C Stress concentrations around web openings near end of beam. Web post buckling initiated.</p> |  <p>Time = 2577 sec, Temp = 354 C Stress concentrations continue to increase around web openings. Significant web post buckling initiates.</p> |
|  <p>Time = 4380 sec, Temp = 515 C Stress concentrations spread in web along length of beam, as web posts continue to buckle. End of simulation. No convergence</p> | |

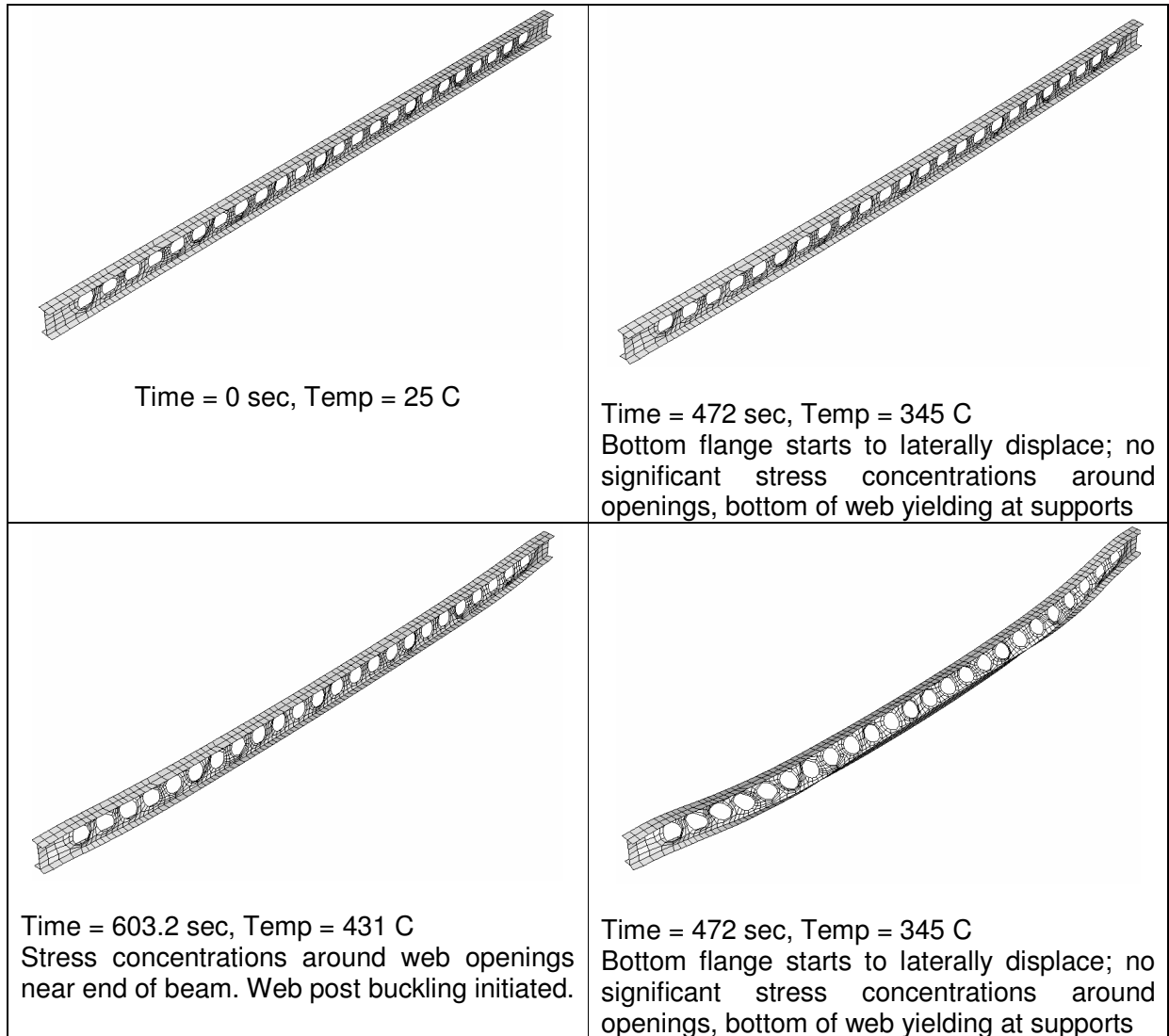


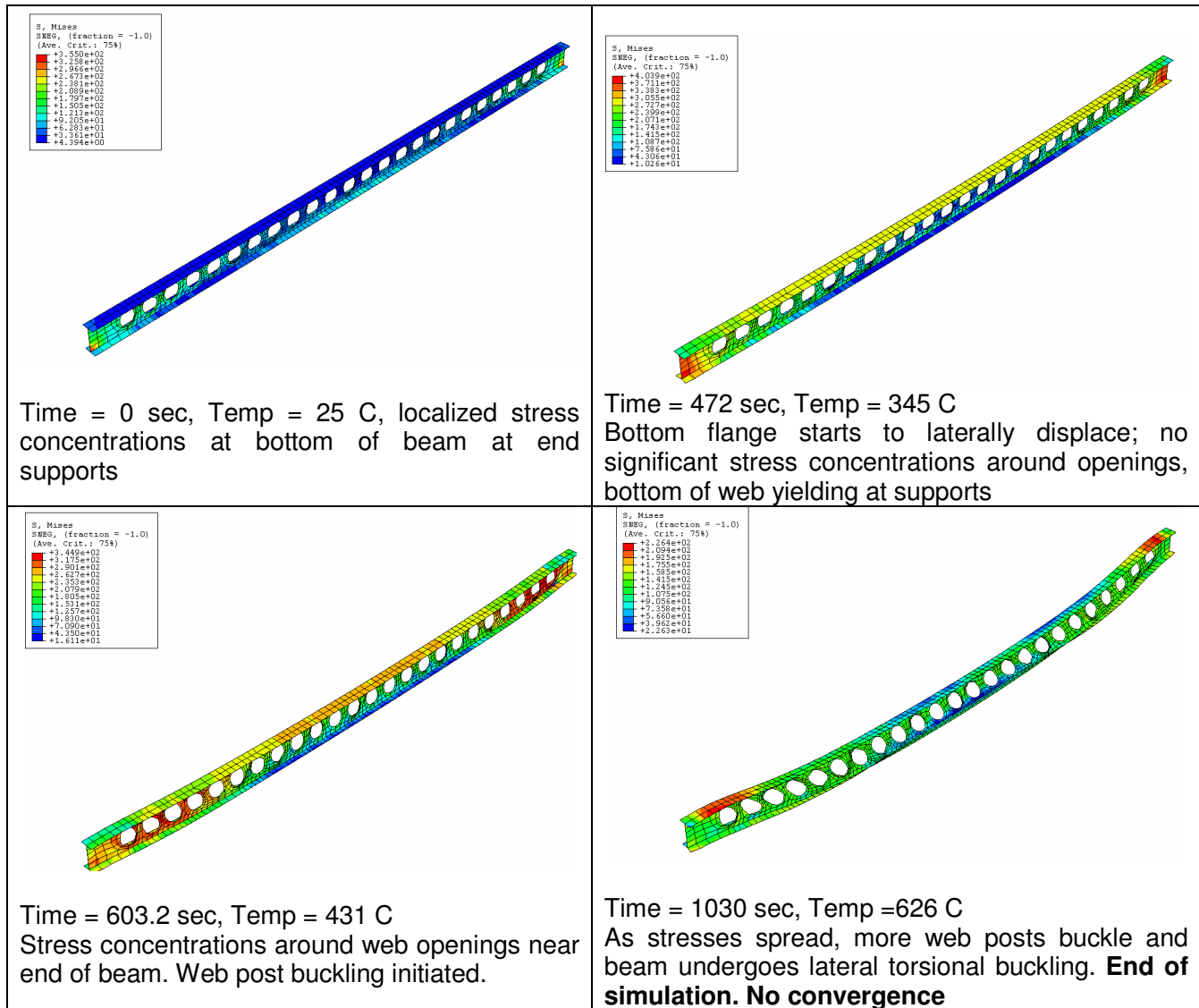
Scenario III – Unprotected Cellular Beam

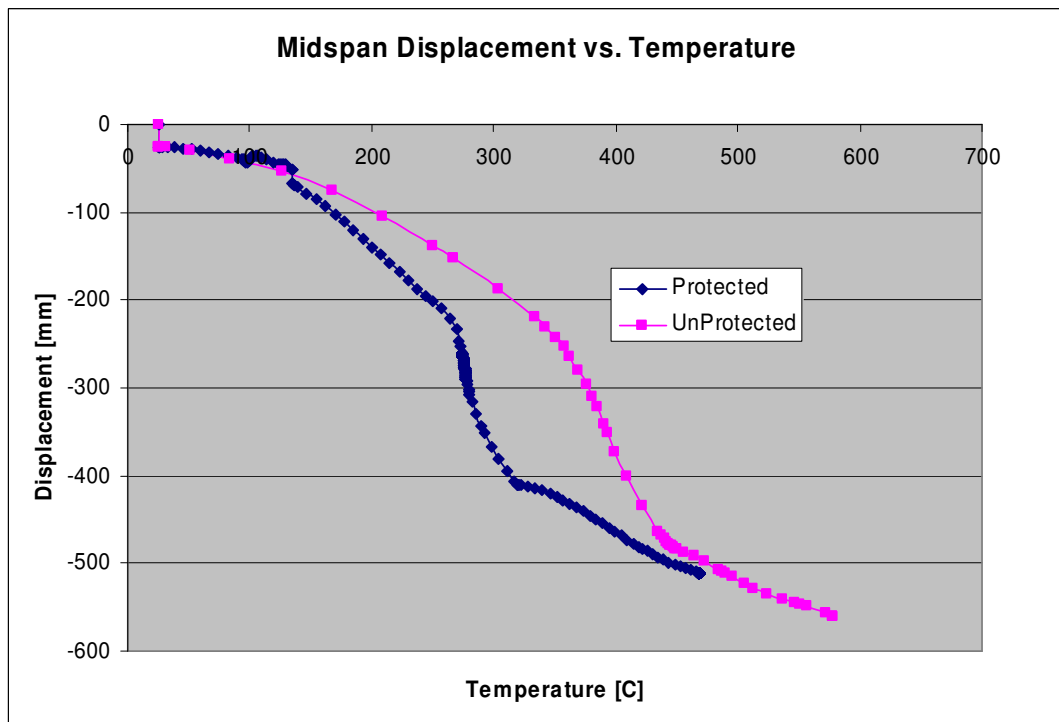
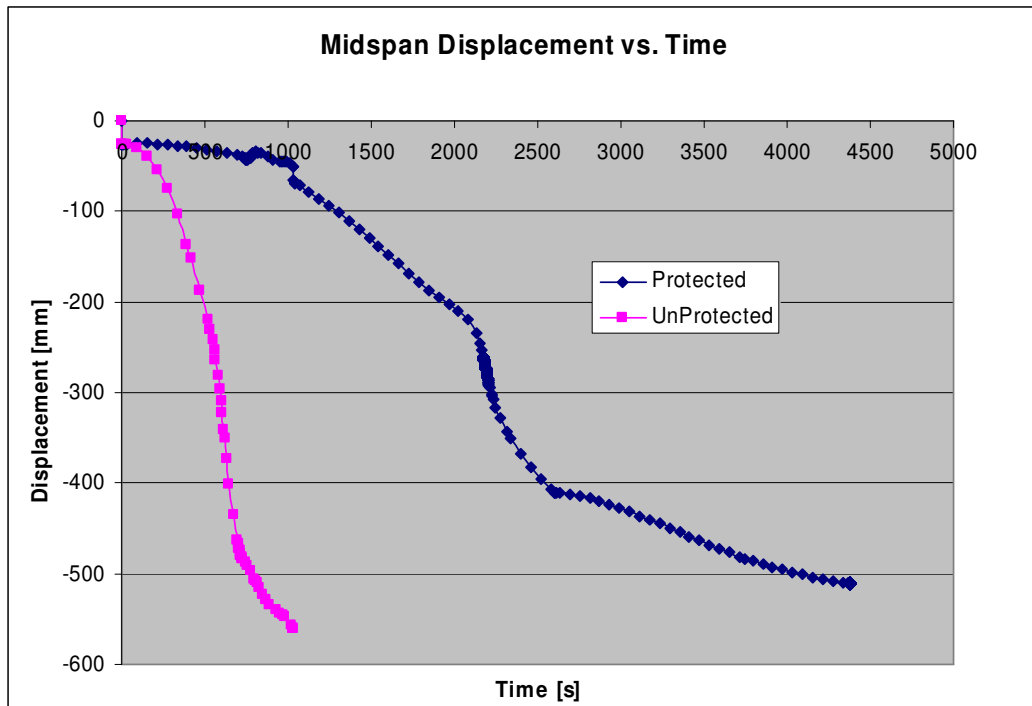
Displacement at end of simulation (t = 1030s, Temp = 663C)



DEFORMATIONS: Case 2, Scenario III, UnProtected Cellular Beam

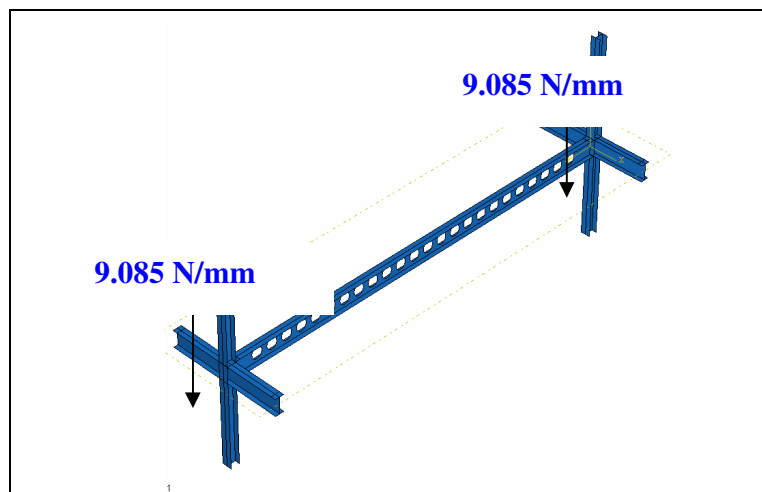


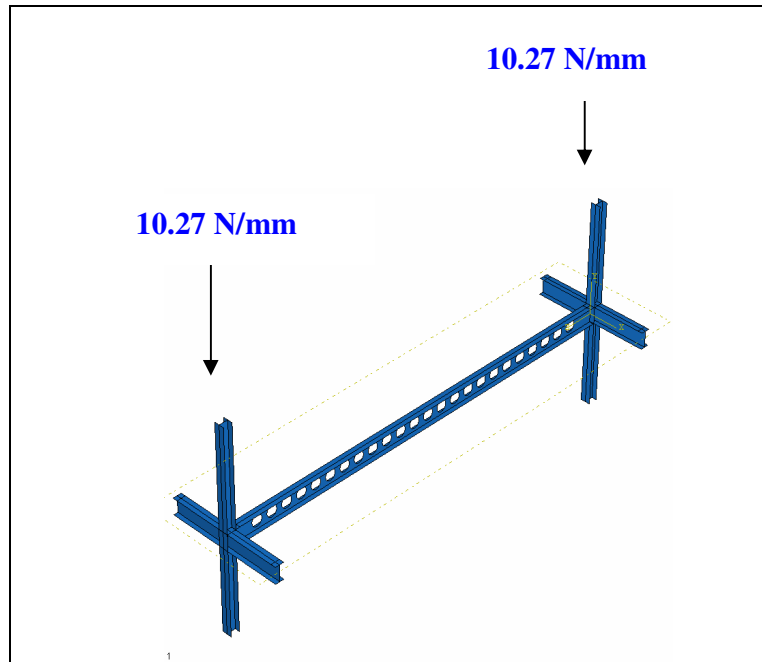




4.2.1.1 Case h – Vary Column Load (Weak Column Scenario)

In this case study, a weak column scenario was studied. Due to geometric constraints, a weak column was simulated by increasing the column loads by 15% and 30%, respectively. The actual column loads tested included: 9.085 N/mm and 10.27N/mm. The column loads were applied as shell line loads to the top ends of the columns; therefore, the actual point loads applied to the columns (given the cross-sectional length of the column) were 10.9kN and 12.34kN. The base cellular beam model had a column shell line load of 7.9N/mm (or a 9.5kN point load equivalent). All other aspects of the structural system and geometry were maintained. Both trials were run using implicit analysis. **As seen in Table Y, both the 15% increase and 30% increase cases had simulation times of 7200s (entire fire duration).** No additional models were run using an explicit analysis. Figure Y is a visual representation of each case analyzed.

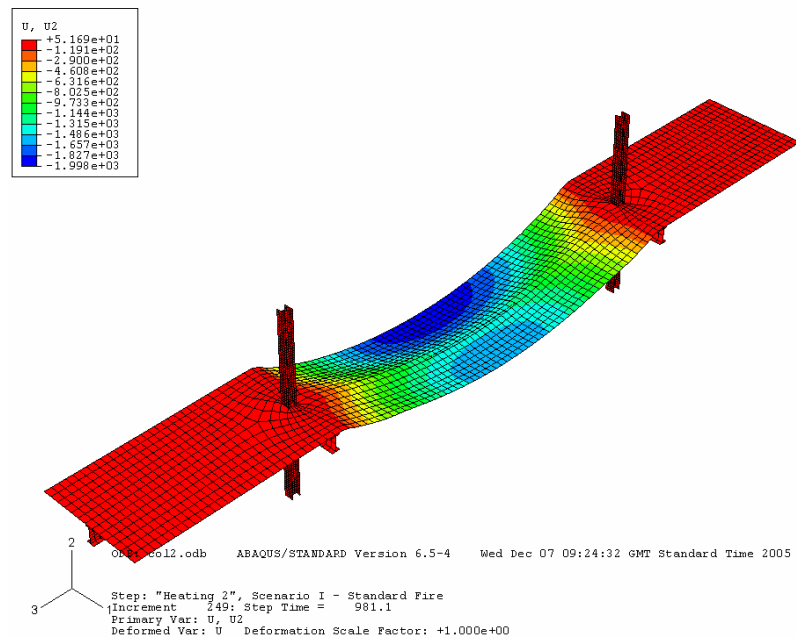


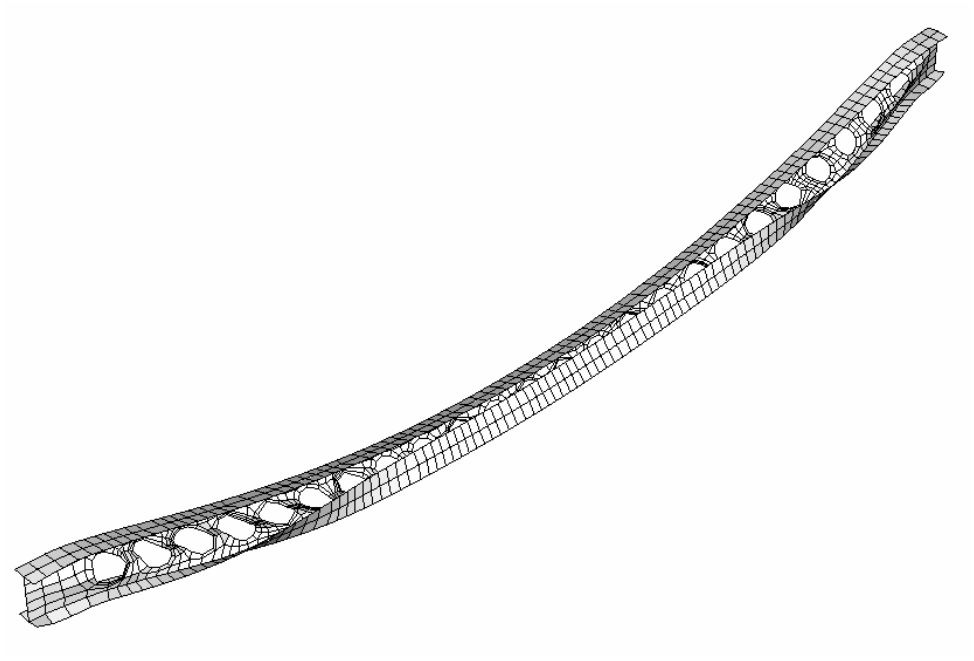


4.2.1.1.1 Displacements

Case h.1 – Column Load = 9.085mm

Displacement at end of simulation (t = 7200s, Temp = 1015C)





REFERENCES

1. ENV 1991-2-2:1995, Basis of design and actions on structures, Part 2-2: Actions on structures exposed to fire, British Standard Institute, 2000.
2. Macsteel Service Centres SA. Retrieved: December, 12, 2005, from <http://www.macsteel.co.za>.
3. BS 476, Fire tests on building materials and structures, Part 21 Methods for determination of the fire resistance of load bearing elements of construction, British Standard Institute
4. Bailey, C.G. "Indicative fire tests to investigate the behaviour of cellular beams protected with intumescent coatings." *Fire Safety Journal*, 39:689-709, 2004.
5. Technical note – 'Fire engineering of cellular beams using intumescent coatings', The Structural Engineer, pp 24-25, October 2002.
6. "Interim Guidance on the Use of Intumescent Coatings for the Fire Protection of Beams with Web Openings." SCI Document RT983. The Steel Construction Institute, Ascot, November, 2003.
7. AD269: The steel use of intumescent coatings for the fire protection of beams with circular web openings. New Steel Construction 2003: 33-4.
8. ABAQUS/Standard and ABAQUS/Explicit. Hibbit, Karlsson, & Sorensen, Inc. Pawtucket, RI.
9. ENV 1993-1-2:1995, Design of steel structures, Part 1-2: Structural fire design, British Standard Institute, 1995.
10. Westok Limited. Hobury Junction Industrial Estate, Horbury Junction, Wakefield, England WF4 5ER
11. Lawson, R.M, Oshatogbe, D., and Newman, G.M. *Design of FABSEC Beams in Non-Composite and Composite Applications (including Fire)*. Retrieved: April 23, 2002, from <http://fabsec.co.uk>.
12. Fire protection for structural steel in buildings. "Yellow Book". Third Edition. Association for Specialist Fire Protection. Steel Construction Institute. Fire Test Study Group. 2002.
13. Buchanan, A.H., Structural Design for Fire Safety, John Wiley & Sons, Ltd. Chichester. 2001

14. Swinden Technology Centre British Steel plc. The behavior of multi-storey steel framed buildings in fire. Technical report, European Joint Research Program Report...British Steel plc (now CORUS), 1999.
15. S.C.I. Investigation of Broadgate Phase 8 Fire. Structural fire engineering. Steel Construction Institute, Ascot, Berkshire, 1991.
16. A.S. Usmani, J.M. Rotter, S. Lamont, A.M. Sanad, M. Gillie. Fundamental principles of structural behavior under thermal effects. *Fire Safety Journal*, 36:721-744, 2001.
17. ASTM E119-00a, Standard Test Methods for Fire Tests of Building Construction and Materials, ASTM International, West Conshohocken, PA 19428-2959
18. Mowrer, Fred. Introduction and Overview of Fire Modeling. Module 1 – Notes. 2005.
19. Interstate Bank Building Fire – Technical Report Series. United States Fire Administration. Report 022. 1998
20. High-rise Office Building Fire, One Meridian Plaza – Technical Report Series. United States Fire Administration. Report 049. 1991
21. Gewain, R.G., Iwankiw, N.R., Alfawakhiri, F. “Facts for Steel Buildings – Fire.” American Institute of Steel Construction, Inc. October 2003.
22. ENV 1993-1-2:1995, Design of steel structures, Part 1-2: Structural fire design, British Standard Institute, 1995.
23. Iwankiw, N. and Beitel, J. (2002). “Analysis of Needs and Existing Capabilities for Full-Scale Fire Resistance Testing”, Huges Associates, Report NIST GCR 02-843, December, 2002.
24. Malhotra, H.L. (1984). “Spalling of concrete in fires.” CIRIA Technical Note No. 118. Construction Industry Research and information Association, London, UK.
25. Phan, L.T. (1996). “ Fire performance of high-strength concrete: a report of the state of the art”. NISTIR 5934. National Institute of Standards and Technology.
26. ENV 1992-1-2:1993, Design of concrete structures, Part 1-2: Structural fire design, British Standard Institute, 1993
27. Schneider, U. (1988). “concrete at high temperatures – a general review”. *Fire Safety Journal*, **13**, 55-68.

28. Khoury, G.A., Grainger, B.N., and Sullivan, P.J.E. (1985). "Strain of concrete during first heating to 600C." *Magazine of Concrete Research*, **37**, 195-215.
29. BS 8110, Structural use of concrete - Part 2 Code of practice for special circumstances, British Standard Institute. 1985.
30. Inwood, M. (1999). "Review of NZS 3101 for high strength concrete and lightweight concrete exposed to fire." Fire Engineering Research Report 99/10. University of Canterbury, New Zealand.
31. Rotter, JM, Sanad AM, Usmani AS, Gillie M. Structural performance of redundant structures under local fires. Proceedings of the Interflam '99, Eighth International Fire Science and Engineering Conference, Edinburgh, Scotland, 29 June-1 July 1999. P. 1069-80.
32. Sanad AM, Rotter JM, Usmani AS, O'Connor M. Composite beam in buildings under fire. *Fire Safety Journal* 2000; 35:165-88.
33. Usmani, A.S., Lamont, S. "Key events in the Structural Response of a Composite Steel Frame Structure in Fire." *Fire and Materials*. **28** (2004) p. 281-297.
34. Gillie, M., Usmani, A., Rotter, M, O'Connor, M. "Modelling of Heated Composite Floor Slabs with Reference to the Cardington Experiments." *Fire Safety Journal*. 36 (2001) p 745-767.
35. Usmani, A.S., Cameron, N.J.K. "Limit capacity of laterally restrained reinforced concrete floor slabs in fire." *Cement & Concrete Composites*. 26 (2004) p 127-140.
36. Bailey, C.G., White, D.S, and Moore, D.B. "The tensile membrane action of unrestrained composite slabs simulated under fire conditions." *Engineering Structures*, 22:1583-1595, 2000.
37. Guice, L.K. and Rhomberg, E.J. "Membrane action in partially restrained slabs. *ACI Structural Journal*, (85):365-373, 1988.
38. Usmani, A.S, Chung, Y.C., Torero, J.L. "How did the WTC towers collapse: a new theory." p. 513
39. Passive material properties came from Kevin Hart at Cafco International (www.cafcointl.com) Test carried out on 11th June 1981.
40. ENV 1991-1-2:1995, Actions on structures, Part 1-2: General actions – Actions on structures exposed to fire, British Standard Institute, 1995
41. Fabsec Ltd. Brooklands Courst, Tunstall Road. Leeds LS11 5HL.

42. British Standards Institution. *The structural use of steelwork in buildings*. BS 5980. Part 1:2000.
43. British Standards Institution. *The structural use of steelwork in buildings: fire resistant design*. BS 5980. Part 8: 1990.
44. Liu, T.C.H and Liew, K.H. "Behaviour of cellular steel beams in fire." Interflam Proceedings, 2004. pp157-169.
45. Astaneh-Asl, Abolhassan. Behavior and Design of Steel and Composite Structures. Chapter 6 - Notes. 2004.
46. Anderberg. Y. (1976). " Fire exposed hyperstatic concrete structures – an experimental and theoretical study." Division of Structural Mechanics and Concrete Construction, Lund Institute of Technology, Lund, Sweden.
47. Toczek, P., The maturing structure of the cellular beam market, Steel Construction Yearbook 2002, McMillan-Scott, 2002, pp. 125-127.